

Characterization of the immune microenvironment in gliomas and its potential clinical value

Sørensen, Mia Dahl

DOI:
10.21996/c38d-bv21

Publication date:
2023

Document version:
Forlagets udgivne version

Citation for published version (APA):
Sørensen, M. D. (2023). *Characterization of the immune microenvironment in gliomas and its potential clinical value*. [Ph.d.-afhandling, SDU]. Syddansk Universitet. Det Sundhedsvidenskabelige Fakultet.
<https://doi.org/10.21996/c38d-bv21>

Go to publication entry in University of Southern Denmark's Research Portal

Terms of use

This work is brought to you by the University of Southern Denmark.
Unless otherwise specified it has been shared according to the terms for self-archiving.
If no other license is stated, these terms apply:

- You may download this work for personal use only.
- You may not further distribute the material or use it for any profit-making activity or commercial gain
- You may freely distribute the URL identifying this open access version

If you believe that this document breaches copyright please contact us providing details and we will investigate your claim.
Please direct all enquiries to puresupport@bib.sdu.dk

PhD Thesis

**Characterization of the immune microenvironment
in gliomas and its potential clinical value**

Mia Dahl Sørensen, MD

Department of Pathology,
Odense University Hospital

Department of Clinical Research,
Faculty of Health Sciences,
University of Southern Denmark

Odense,
February 2023



University of
Southern Denmark

"Vi kan øve os i at gå på vandet" siger Pippi
"Ej, det kan man da ikke", siger Tommy
"Selvfølgelig kan man da det" siger Pippi, "Man kan da i hvert fald prøve."
(Afsnit 13, 24:32-24:39, Pippi går ombord).



Pippilotta Viktualia Rullgardinia Krusemynta Efraimsdotter Långstrump, Astrid Lindgren

Table of contents

1. Preface	3
1.1 Acknowledgements	3
1.2 Manuscripts included in this thesis	4
1.3 Related publications not included in this thesis	5
1.4 Supervisors.....	8
1.5 Funding	8
2. English summary	9
3. Dansk resumé	12
4. The thesis at a glance	15
5. Glossary of abbreviations	16
6. Introduction and aims	19
7. Background	23
7.1 Gliomas – epidemiology and etiology	23
7.2 Gliomas – classification, grading, biomarkers, and prognosis.....	25
7.2.1 Biomarkers in gliomas	26
7.2.2 The 2016 WHO classification of diffuse gliomas	29
7.2.3 Prognostic factors in diffuse gliomas	36
7.2.4 The 2021 WHO classification of diffuse gliomas	37
7.3 Treatment of gliomas	39
7.3.1 First-line treatment.....	39
7.3.2 Recurrence	41
7.3.3 Novel therapies	41
7.4 The tumor microenvironment	42
7.4.1 Neovascularization and hypoxia.....	44
7.4.2 Cancer stem cells and intratumoral heterogeneity	45
7.5 The tumor immune microenvironment	48
7.5.1 The complement system	50
7.5.2 Tumor-associated microglia/macrophages	50
7.5.3 T cells and immune checkpoint markers	55
7.6 Applied research methodologies and methods.....	59
7.6.1 Immunohistochemistry	59
7.6.2 Multiplex immunohistochemistry and immunofluorescence.....	62
7.6.3 Digital image analysis.....	64
7.6.4 NanoString.....	65
8. Methods	69
8.1 Patient tissue (manuscripts I-IV).....	69
8.2 Glioma reclassification (manuscripts I-IV).....	70
8.2.1 Next-generation sequencing (manuscripts I, III, and IV)	70
8.2.2 Fluorescent in situ hybridization analysis (manuscripts I, III, and IV)	71

Table of contents

8.2.3	DNA methylation profiling (manuscripts I, III, and IV)	72
8.3	Immunohistochemistry and immunofluorescence (manuscripts I-IV)	73
8.3.1	Conventional immunohistochemistry (manuscripts I-IV)	73
8.3.2	Double immunohistochemistry (manuscripts II and III)	74
8.3.3	Chromogenic multiplex immunohistochemistry (manuscript IV)	74
8.3.4	Double immunofluorescence (manuscripts I, III, and IV)	75
8.4	Digital image acquisition and analysis (manuscripts I-IV)	79
8.4.1	Digital automated image analysis (manuscripts I, II, and IV)	80
8.4.2	Pathological scoring (manuscripts I and III)	81
8.4.3	Stereology (manuscripts II, III, and IV)	82
8.5	NanoString gene expression panel (manuscript II)	83
8.6	<i>In silico</i> analyses (manuscripts I, II, and IV)	84
8.7	Statistics (manuscripts I-IV)	85
8.8	Ethics (manuscripts I-IV)	85
9.	Results	86
9.1	Manuscript I	86
9.2	Manuscript II	89
9.3	Manuscript III	92
9.4	Manuscript IV	94
10.	General discussion	97
10.1	The prognostic value of M2-like TAMs in diffuse gliomas	97
10.2	The heterogeneity of TAMs in diffuse glioma	99
10.3	The possible biological role(s) of CD204 in glioblastoma	101
10.4	The impact of IDH mutation on the immune microenvironment in diffuse glioma	104
10.5	Profiling the immune landscape in diffuse glioma	107
11.	Conclusions and perspectives	109
12.	References	111
13.	Appendix	139
13.1	Manuscript I	139
13.2	Manuscript II	179
13.3	Manuscript III	239
13.4	Manuscript IV	261

1. Preface

1.1 Acknowledgements

The work presented in this PhD thesis was performed at the Department of Pathology, Odense University Hospital, and the Department of Clinical Research, University of Southern Denmark.

Firstly, I would like to thank my main supervisor Bjarne W. Kristensen for introducing me to the fields of brain cancer pathology and scientific research. Thank you for letting me pursue my ideas and for including me in various collaboration and side projects. I also thank you for providing the laboratory facilities and economical funding to make this thesis possible. Thank you to my co-supervisors Kate L. Lambertsen, Bente Finsen, and Justin D. Lathia for your interest in the project and input during my time as a PhD student.

A special thanks also goes to the Department of Clinical Genetics (Mark Burton, Stephanie Kavan, Mads Thomassen, and Torben A. Kruse) and to Dorte Lyholmer and Morten Meyer from Neurobiology Research, University of Southern Denmark, for your help and guidance in various experimental techniques.

I am thankful to the Department of Pathology for providing the setting to carry out my research. A special thanks to the late senior histotechnician Ole Nielsen as well as histotechnicians Lisbet Mortensen, Lone Christiansen, and Tanja D. Højgaard for their invaluable assistance with immunohistochemical stainings. Also cheers to all the members of the Chromosome and PCR laboratories for their contribution to the project.

I am very grateful to technician Helle Wohlleben. This thesis would not have been possible without your continued help and expertise in tissue sectioning and immunostainings.

Thank you to past members of the “BWK group”, especially Charlotte Aaberg-Poulsen, Rikke H. Dahlrot, Sune Munthe, Jakob Klitkou, and Henning B. Boldt for introducing me to the art of cell culturing and animal experiments, immunostainings, statistics, and/or molecular diagnostics. A special thanks to my colleague and former office buddy Ann Mari Rosager for all our talks and laughs about work- and non-work-related matters.

Thank you to my former office buddies Louise Kristensen, Eva K. Hejbøl, Lise K. H. Hansen, and Maj Rabjerg for making the office a great place to be.

To my former colleagues and partners in crime Stine A. Petterson and Michael F. B. Nielsen: thank you for your friendship and support, for tolerating my bad jokes and silly comments, and for making the office a happy place.

Finally, and most of all, I would like to thank my friends and family; especially my mom Birgit, dad Flemming, and big brother Michael, for putting up with my babbling about the immunostainings, cell cultures, little laboratory mice, and microglia/macrophages. None of this would have been possible without your continued support, patience, and words of encouragement.

Mia Sørensen
Odense, February, 2023

1.2 Manuscripts included in this thesis

The thesis is based on the manuscripts listed below. The full-length manuscripts are available in the *Appendix*.

- I. Sørensen MD, Dahlrot RH, Boldt HB, Hansen S, Kristensen BW. **Tumour-associated microglia/macrophages predict poor prognosis in high-grade gliomas and correlate with an aggressive tumour subtype.** *Neuropathol Appl Neurobiol.* 2017 Aug 2. doi: 10.1111/nan.12428.
- II. Sørensen MD, Kristensen BW. **Tumour-associated CD204+ microglia/macrophages accumulate in perivascular and perinecrotic niches and correlate with an interleukin-6-enriched inflammatory profile in glioblastoma.** *Neuropathol Appl Neurobiol.* 2022 Feb;48(2):e12772. doi: 10.1111/nan.12772.
- III. Zhang L, Sørensen MD, Kristensen BW, Reifenberger G, McIntyre TM, Lin F. **D-2-Hydroxyglutarate Is an Intercellular Mediator in IDH-Mutant Gliomas Inhibiting Complement and T Cells.** *Clin Cancer Res.* 2018 Nov 1;24(21):5381-5391. doi: 10.1158/1078-0432.CCR-17-3855.
- IV. Sørensen MD, Nielsen O, Reifenberger G, Kristensen BW. **The presence of TIM-3 positive cells in WHO grade III and IV astrocytic gliomas correlates with isocitrate dehydrogenase mutation status.** *Brain Pathol.* 2020 Nov 26;e12921. doi: 10.1111/bpa.12921.

1.3 Related publications not included in this thesis

1. Petterson SA, Sørensen MD, Burton M, Thomassen M, Kruse TA, Michaelsen SR, Kristensen BW. **Differential expression of checkpoint markers in the normoxic and hypoxic microenvironment of glioblastomas.** Brain Pathol. 2022 Sep 12;e13111. doi: 10.1111/bpa.13111.
2. Rosager AM, Dahlrot RH, Sørensen MD, Bangsø JA, Hansen S, Kristensen BW. **The Epigenetic Regulator Jumonji Domain-Containing Protein 6 (JMJD6) Is Highly Expressed but Not Prognostic in IDH-Wildtype Glioblastoma Patients.** J Neuropathol Exp Neurol. 2021 Dec 7:nlab124. doi: 10.1093/jnen/nlab124.
3. Dahlrot RH, Bangsø JA, Petersen JK, Rosager AM, Sørensen MD, Reifenberger G, Hansen S, Kristensen BW. **Prognostic role of Ki-67 in glioblastomas excluding contribution from non-neoplastic cells.** Sci Rep. 2021 Sep 9;11(1):17918. doi: 10.1038/s41598-021-95958
4. Knudsen AM, Rudkjøbing SJ, Sørensen MD, Dahlrot RH, Kristensen BW. **Expression and Prognostic Value of the Immune Checkpoints Galectin-9 and PD-L1 in Glioblastomas.** J Neuropathol Exp Neurol. 2021 Jun 4;80(6):541-551. doi: 10.1093/jnen/nlab041.
5. Schmidt SI, Bogetofte H, Ritter L, Agergaard JB, Hammerich D, Kabiljagic AA, Wlodarczyk A, Lopez SG, Sørensen MD, Jørgensen ML, Okarmus J, Serrano AM, Kristensen BW, Freude K, Owens T, Meyer M. **Microglia-Secreted Factors Enhance Dopaminergic Differentiation of Tissue- and iPSC-Derived Human Neural Stem Cells.** Stem Cell Reports. 2021 Jan 6;S2213-6711(20)30506-3. doi: 10.1016/j.stemcr.2020.12.011.
6. Petterson SA, Sørensen MD, Kristensen BW. **Expression Profiling of Primary and Recurrent Glioblastomas Reveals a Reduced Level of Pentraxin 3 in Recurrent Glioblastomas.** J Neuropathol Exp Neurol. 2020 Sep 1;79(9):975-985. doi: 10.1093/jnen/nlaa088.
7. Petersen JK, Boldt HB, Sørensen MD, Blach S, Dahlrot RH, Hansen S, Burton M, Thomassen M, Kruse T, Poulsen FR, Andreasen L, Hager H, Ulhøi BP, Lukacova S, Reifenberger G, Kristensen BW. **Targeted next-generation sequencing of adult gliomas for retrospective prognostic evaluation and up-front diagnostics.** Neuropathol Appl Neurobiol. 2020;10.1111/nan.12645. doi:10.1111/nan.12645
8. Knudsen AM, Eilertsen I, Kielland S, Pedersen MW, Sørensen MD, Dahlrot RH, Boldt HB, Munthe S, Poulsen FR, Kristensen BW. **Expression and prognostic value of the transcription factors EGR1 and EGR3 in gliomas.** Sci Rep. 2020 Jun 9;10(1):9285. doi: 10.1038/s41598-020-66236-x.
9. Bayik D, Zhou Y, Park C, Hong C, Vail D, Silver DJ, Lauko A, Roversi G, Watson DC, Lo A, Alban TJ, McGraw M, Sørensen M, Grabowski M, Otvos B, Vogelbaum MA, Horbinski C, Kristensen BW, Khalil AM, Hwang TH, Ahluwalia MS, C Feixiong, Lathia JD. **Myeloid-derived suppressor cell subsets drive glioblastoma growth in a sex-specific manner.** Cancer Discov. 2020 Apr 16;CD-19-1355. doi: 10.1158/2159-8290.CD-19-1355.
10. Bömers JP, Danielsen ME, Schulz MK, Halle B, Kristensen BW, Sørensen MD, Poulsen FR, Pedersen CB. **Sodium fluorescein shows high surgeon-reported usability in glioblastoma surgery.** Surgeon. 2020 Feb 7;S1479-666X(20)30014-7. doi: 10.1016/j.surge.2020.01.003.

11. Ferreira MSV, Sørensen MD, Pusch S, Beier D, Bouillon A, Kristensen BW, Brümmendorf TH, Beier CP, Beier F. **Alternative lengthening of telomeres is the major telomere maintenance mechanism in astrocytoma with isocitrate dehydrogenase 1 mutation.** J Neurooncol. 2020 Mar;147(1):1-14. doi: 10.1007/s11060-020-03394-y.
12. Alban TJ, Alvarado AG, Sorensen MD, Bayik D, Volovetz J, Serbinowski E, Mulkearns-Hubert EE, Sinyuk M, Hale JS, Onzi GR, McGraw M, Huang P, Grabowski MM, Wathen CA, Ahluwalia MS, Radivoyevitch T, Kornblum H, Kristensen BW, Vogelbaum MA, Lathia JD. **Global immune fingerprinting in glioblastoma patient peripheral blood reveals immune-suppression signatures associated with prognosis.** JCI insight. 2018;3(21). doi: 10.1172/jci.insight.122264
13. Beier CP, Rasmussen T, Dahlrot RH, Tenstad HB, Aaro JS, Sorensen MF, Heimisdóttir SB, Sørensen MD, Svenningsen P, Riemenschneider MJ, Beier D, Kristensen BW. **Aberrant neuronal differentiation is common in glioma but is associated neither with epileptic seizures nor with better survival.** Scientific reports. 2018;8(1):14965. doi: 10.1038/s41598-018-33282-5.
14. Aaberg-Jessen C*, Sørensen MD*, Matos A, Moreira JM, Brunner N, Knudsen A, Kristensen BW. **Co-expression of TIMP-1 and its cell surface binding partner CD63 in glioblastomas.** BMC cancer. 2018;18(1):270. doi: 10.1186/s12885-018-4179-y.
15. Sorensen MF, Heimisdottir SB, Sørensen MD, Mellegaard CS, Wohlleben H, Kristensen BW, Beier CP. **High expression of cystine-glutamate antiporter xCT (SLC7A11) is an independent biomarker for epileptic seizures at diagnosis in glioma.** Journal of neuro-oncology. 2018;138(1):49-53. doi: 10.1007/s11060-018-2785-9.
16. Verano-Braga T, Gorshkov V, Munthe S, Sørensen MD, Kristensen BW, Kjeldsen F. **SuperQuant-assisted comparative proteome analysis of glioblastoma subpopulations allows for identification of potential novel therapeutic targets and cell markers.** Oncotarget. 2018;9(10):9400-14. doi: 10.18632/oncotarget.24321.
17. Hermansen SK*, Sørensen MD*, Hansen A, Knudsen S, Alvarado AG, Lathia JD, Kristensen BW. **A 4-miRNA signature to predict survival in glioblastomas.** PloS one. 2017;12(11):e0188090. doi: 10.1371/journal.pone.0188090.
18. Aaberg-Jessen C, Fogh L, Sørensen MD, Halle B, Brunner N, Kristensen BW. **Overexpression of TIMP-1 and Sensitivity to Topoisomerase Inhibitors in Glioblastoma Cell Lines.** Pathology oncology research: POR. 2019;25(1):59-69. doi: 10.1007/s12253-017-0312-5.
19. Rosager AM*, Sørensen MD*, Dahlrot RH, Boldt HB, Hansen S, Lathia JD, Kristensen BW. **Expression and prognostic value of JAM-A in gliomas.** Journal of neuro-oncology. 2017;135(1):107-17. doi: 10.1007/s11060-017-2555-0.
20. Rosager AM, Sørensen MD, Dahlrot RH, Hansen S, Schonberg DL, Rich JN, Lathia JD, Kristensen BW. **Transferrin receptor-1 and ferritin heavy and light chains in astrocytic brain tumors: Expression and prognostic value.** PloS one. 2017;12(8):e0182954. doi: 10.1371/journal.pone.0182954.

21. Fosmark S, Hellwege S, Dahlrot RH, Jensen KL, Derand H, Lohse J, Sørensen MD, Hansen S, Kristensen BW. **APNG as a prognostic marker in patients with glioblastoma**. PloS one. 2017;12(6):e0178693. doi: 10.1371/journal.pone.0178693.
22. Dahlrot RH, Dowsett J, Fosmark S, Malmstrom A, Henriksson R, Boldt H, de Stricker K, Sørensen MD, Poulsen HS, Lysiak M, Söderkvist P, Rosell J, Hansen S, Kristensen BW. **Prognostic value of O-6-methylguanine-DNA methyltransferase (MGMT) protein expression in glioblastoma excluding nontumour cells from the analysis**. Neuropathol Appl Neurobiol. 2018;44(2):172-84. doi: 10.1111/nan.12415.
23. Ramachandran RK*, Sørensen MD*, Aaberg-Jessen C, Hermansen SK, Kristensen BW. **Expression and prognostic impact of matrix metalloproteinase-2 (MMP-2) in astrocytomas**. PloS one. 2017;12(2):e0172234. 10.1371/journal.pone.0172234.
24. Krogh Petersen J, Jensen P, Dahl Sørensen M, Winther Kristensen B. **Expression and Prognostic Value of Oct-4 in Astrocytic Brain Tumors**. PloS one. 2016;11(12):e0169129. doi: 10.1371/journal.pone.0169129.
25. Munthe S, Sørensen MD, Thomassen M, Burton M, Kruse TA, Lathia JD, Poulsen FR, Kristensen BW. **Migrating glioma cells express stem cell markers and give rise to new tumors upon xenografting**. Journal of neuro-oncology. 2016;130(1):53-62. doi: 10.1007/s11060-016-2221-y.
26. Otvos B, Silver DJ, Mulkearns-Hubert EE, Alvarado AG, Turaga SM, Sørensen MD, Rayman P, Flavahan WA, Hale JS, Stoltz K, Sinyuk M, Wu Q, Jarrar A, Kim SH, Fox PL, Nakano I, Rich JN, Ransohoff RM, Finke J, Kristensen BW, Vogelbaum MA, Lathia JD. **Cancer Stem Cell-Secreted Macrophage Migration Inhibitory Factor Stimulates Myeloid Derived Suppressor Cell Function and Facilitates Glioblastoma Immune Evasion**. Stem cells (Dayton, Ohio). 2016;34(8):2026-39. doi: 10.1002/stem.2393.
27. Halle B, Thomassen M, Venkatesan R, Kaimal V, Marcusson EG, Munthe S, Sørensen MD, Aaberg-Jessen C, Jensen SS, Meyer M, Kruse TA, Christiansen H, Schmidt S, Mollenhauer J, Schulz MK, Andersen C, Kristensen BW. **Shift of microRNA profile upon orthotopic xenografting of glioblastoma spheroid cultures**. Journal of neuro-oncology. 2016;128(3):395-404. doi: 10.1007/s11060-016-2125-x.

* Shared 1st authorship

1.4 Supervisors

Main supervisor:

- Bjarne W. Kristensen, professor, MD, PhD. Institute for Clinical Medicine and Biotech Research and Innovation Center (BRIC), Copenhagen University, and senior consultant neuropathologist, Department of Pathology, Bartholin Institute, Rigshospitalet, DK.

Co-supervisors:

- Bente Finsen, professor, professor, MD, dr. med. Neurobiology Research, Department of Molecular Medicine, University of Southern Denmark, Odense, DK
- Kate L. Lambertsen, professor, cand. scient., PhD. Neurobiology Research, Department of Molecular Medicine, University of Southern Denmark, Odense, DK
- Justin D. Lathia, associate professor, PhD. Department of Molecular Medicine, Cleveland Clinic, Lerner College of Medicine, Cleveland, Ohio, USA

1.5 Funding

The PhD study was funded by the foundations listed below, and I gratefully acknowledge their contributions:

- The Danish Council for Independent Research (4183-00183)
- Odense University Hospital Research Funds, University of Southern Denmark
- Danish Cancer Research Foundation
- Oda og Hans Svenningsens Fond
- Krista og Viggo Petersens Fond
- Brødrene Hartmanns Fond
- Knud og Edith Eriksens Mindefond
- Eva og Henry Frænkels Mindefond
- Aase og Ejner Danielsens Fond
- Dagmar Marshall Fond
- Lily Benthine Lunds Fond af 1.6.1978
- Else og Aage Grønbeck-Olsens Legat
- A.P. Møller Fonden til Lægevidenskabens Fremme
- Fabrikant Einar Willumsens Mindelegat
- Familien Erichsens Mindefond
- Købmand M. Kristjan Kjær og hustru Margrethe Kjær, født la Cour-Holmes Fond
- Thora og Viggo Groves Mindelegat
- Harboefonden
- A.J. Andersen og Hustrus Fond
- Torben og Alice Frimodts Fond
- Marie og Børge Kroghs Fond
- Arkitekt Holger Hjortenbergs og Hustru Dagmar Hjortenbergs Fond

2. English summary

Diffuse gliomas constitute the most frequent malignant primary brain tumors in adults. Every year ~600 adults are diagnosed with diffuse glioma in Denmark. Diffuse gliomas are graded into World Health Organization (WHO) malignancy grades II-IV based on histomolecular features. Glioblastomas, grade IV, account for ~60% of all gliomas and remain one of the deadliest cancer types. Despite standard-of-care treatment with surgery, radiation, and chemotherapy, only 5-10% of patients are alive five years after diagnosis. Especially glioblastomas are very heterogeneous and plastic in nature, presenting a cellular and molecular diversity both among tumors and within the same tumor, and some glioblastoma subtypes and cellular subpopulations are described as exceptionally aggressive and treatment resistant. Until recently most therapeutic strategies have focused on the tumor cells. However, over the past decade accumulating data suggest that the tumor immune microenvironment plays a crucial role in tumor progression. This has led to the introduction of immunotherapy, such as checkpoint inhibitors, as a strategy to treat and even cure cancer.

The predominant immune cell population in glioma is the tumor-associated microglia/macrophages (TAMs). Traditionally, TAMs are categorized into two phenotypes: the M1 phenotype which promotes immunity and inhibits tumor growth, and the M2 phenotype which is immunosuppressive and promotes tumor progression. The pattern recognition/scavenger receptor cluster of differentiation 204 (CD204) is a relatively novel marker of M2-like TAMs. CD204 has been reported to negatively influence patient outcome in many cancer types including glioma, making it a possible target for anti-cancer therapy, however; little knowledge exists on its independent prognostic value. To date, studies of glioblastomas have unveiled a high level of resistance to immunotherapy, most likely caused by a lymphocyte-depleted and an immunosuppressive microenvironment with deficient immune recognition of tumor cells due to low neoantigen burden. The most common neoantigen in diffuse glioma is mutant isocitrate dehydrogenase (IDH), and increasing evidence suggests that D-2-hydroxyglutarate produced by neomorphic IDH mutations may suppress the immune microenvironment. The overall aim of this PhD thesis was to characterize the immune landscape in gliomas focusing on 1) the possible clinical value of CD204⁺ TAMs in glioblastoma and 2) the association between IDH mutation and different components of the immune system in diffuse glioma.

In manuscript I, the prognostic influence of TAMs and CD204⁺ TAMs in gliomas was investigated. Tissue samples from 240 patients with primary glioma were stained using an automated quantitative double immunofluorescence techniques with antibodies against ionized calcium-binding adaptor molecule-1 (IBA1) and CD204 to detect all TAMs and M2-like TAMs, respectively. A pixel-based algorithm was developed to quantify individual expression signals of the makers and their co-expression pattern. We found that the amount of IBA1 and CD204 increased with malignancy grade. In grade III–IV gliomas, high CD204 levels independently predicted shorter survival when adjusting for clinico-pathological parameters, while high staining intensity of IBA1 was associated with better outcome. TAMs were heterogeneously dispersed in gliomas at both an intra- and intertumoral level. The density of TAMs was highest in the tumor core, but CD204⁺ TAMs were also present at the invasive front, indicating a potential involvement in promotion of tumor migration/invasion. TAMs also accumulated in perivascular and perinecrotic areas where glioblastoma

cells with stem-like cell properties are known to reside, and necrosis was more prominent in glioblastomas with high CD204 expression. We therefore investigated the possible crosstalk between these two cell populations by performing double immunohistochemistry using IBA1, CD204 and panel of stem cell-related markers, e.g. podoplanin and CD133. We found that especially podoplanin⁺ glioblastoma cells and CD204⁺ TAMs were in close proximity to each other in perinecrotic regions. Additionally, we subtyped a cohort of glioma using immunohistochemistry and observed that particularly CD204⁺ TAMs were more abundant in tumors with the aggressive mesenchymal phenotype. Immunofluorescent phenotyping of CD204⁺ TAMs showed conjunctional expression of proteins related to the M1 and M2 polarization, and CD204⁺ TAMs also co-expressed markers related to tumor aggressiveness. Collectively, these results indicate that CD204⁺ TAMs may favor tumor progression by stimulating formation of more aggressive and invasive tumors.

In manuscript II, we explored the possible biological role of CD204 more comprehensively using myeloid transcriptome profiling. Profiling showed that CD204-enriched glioblastomas had a distinct signature with upregulation of genes related to hypoxia, angiogenesis and invasion, including interleukin-6, interleukin-8, programmed death-ligand 1, podoplanin, and CD44. The gene profile correlated with poor prognosis, but was not a stronger prognosticator of survival than CD204. Cluster and network analyses of the upregulated genes revealed that interleukin-6 formed an epicenter with the highest number of gene-gene interactions, and pathway analyses demonstrated an overrepresentation of terms related to e.g. immune activation and extracellular matrix organization, including the tumor necrosis factor (TNF) and interferon signaling pathways.

In manuscript III, we investigated the potential role of IDH mutation and its oncometabolite D-2-hydroxyglutarate as an intercellular regulator of the innate and adaptive immune system in glioma. We evaluated the level of complement deposition and T cell infiltration using immunohistochemistry and a patient cohort with 72 astrocytic gliomas, grade III-IV, stratified according to IDH mutation status. We found that IDH-mutant tumors had reduced complement activation and decreased numbers of CD4⁺ T helper cells, CD8⁺ cytotoxic T cells, and forkhead box P3⁺ regulatory T cells compared to IDH-wildtype gliomas. *Ex vivo* experiments demonstrated that D-2-hydroxyglutarate impaired complement-mediated destruction of both erythrocytes and a glioblastoma cell line by inhibiting effective cell lysis and by reducing the level of opsonization-mediated phagocytosis. In contrast, D-2-hydroxyglutarate neither affected the differentiation of dendritic cells nor their ability to present antigens. The proliferation, cytokine secretion, and migration of T helper cells as well as the migration of cytotoxic T cells were inhibited by D-2-hydroxyglutarate. Notably, the differentiation of regulatory T cells was stimulated by exposure to D-2-hydroxyglutarate, while their proliferation and secretion of interleukin-10 was inhibited.

In manuscript IV, we explored the association between IDH mutation and presence of cells expressing the co-inhibitory immune checkpoint proteins galectin-9 and/or T cell immunoglobulin and mucin-domain containing-3 (TIM3). We established a chromogenic 3-plex immunohistochemistry protocol with antibodies against galectin-9, TIM3, and the tumor marker oligodendrocyte transcription factor 2 (OLIG2) and stained tumor sections from the patient cohort of 72 astrocytic gliomas described above. Quantification was done using stereological-based cell counting. We found that the number of TIM3⁺ cells was significantly lower in IDH-mutant compared to IDH-wildtype tumors. In contrast, the number of galectin-9⁺ cells did not significantly

differ. Using double immunofluorescence, most TIM3⁺ and galectin-9⁺ cells were found to be IBA1⁺ TAMs. OLIG2⁺ tumor cells accounted for ~45-50% of the cells in both IDH-mutant and IDH-wildtype tumors, and OLIG2⁺ cells rarely co-expressed galectin-9 and TIM3. The presence of TIM3⁺ galectin-9⁻ cells were infrequent, and these cells morphologically resembled TAMs and T cells. Double immunofluorescence showed that only ~10% of the CD3⁺ T cell population expressed TIM3. IDH-mutant tumors had lower frequency of TIM3⁺ T cells than wildtype tumors, and only 50% of these T cells interacted with galectin-9⁺ TAMs compared to the ~85-100% interaction rate observed in IDH-wildtype tumors. In contrast, almost no crosstalk occurred between TIM3⁺ T cells and galectin-9⁺ OLIG2⁺ tumor cells. We employed an *in silico* dataset from to screen for transcriptional changes comparing the glioblastomas with the highest and lowest *TIM3* mRNA levels. A total of 75 genes were differentially upregulated in glioblastomas with the highest *TIM3* mRNA expression, while no genes were differentially downregulated. Many of the upregulated genes were associated with leukocyte regulation, and chemotaxis. Among the upregulated genes were *CD204* and interleukin-6 whose expression levels were significantly reduced in IDH-mutant astrocytic gliomas. The upregulated genes were enriched in various signaling pathways including TNF, complement, and the phagosome pathways.

In conclusion, this thesis demonstrates that the prognostic value of TAMs in gliomas does not depend on the total amount of TAMs, but on the acquired phenotype, as only high levels of CD204⁺ TAMs predicted shorter survival in patients with grade III-IV glioma. Profiling CD204⁺ TAMs and CD204-enriched glioblastomas revealed that CD204 is associated with an inflamed and immunosuppressive milieu with high expression of several pro-tumorigenic factors especially interleukin-6. These findings suggest that CD204 and/or interleukin-6 could serve as targets for reprogramming of TAMs as a means of potentiating the anti-glioma response of current and future treatment strategies including other immunotherapies. The results of this thesis support the hypothesis that the neomorphic activity of IDH mutations conveys a global glioma-associated immunosuppression affecting innate and adaptive immune responses as well as immune checkpoint signaling. This aspect underlines that IDH mutation status could serve as a useful tool for selecting patients more likely to respond to immunotherapy, but also indicates that mutant IDH may be an immunotherapeutic target, and combining immunotherapy with mutation-specific IDH inhibitors/vaccines could be clinically relevant.

3. Dansk resumé

Den hyppigst forekommende maligne primære hjernetumor er diffust gliom. Hvert år bliver omkring 600 voksne danskere diagnosticeret med diffust gliom. Diffuse gliomer inddeles i malignitetsgrad II-IV ud fra Verdenssundhedsorganisationens (WHO) retningslinjer, og klassifikationen er baseret på histomolekylære karakteristika. Glioblastomet, grad IV, er den hyppigste og mest aggressive type af diffust gliom. Glioblastom er en af de mest dødelige kræftformer. Kun 5-10% af patienterne med glioblastom er i live 5 år efter diagnosetidspunktet trods behandling med resektion, stråle- og kemoterapi. Glioblastomer er meget heterogene, og flere subtyper og subpopulationer af celler eksisterer både i den samme tumor og mellem forskellige tumorer, hvilket vanskeliggør målrettet kræftbehandling. Nogle af disse subtyper og subpopulationer er kendetegnet ved at være særligt aggressive og modstandsdygtige over for behandling. Indtil for nyligt har de fleste behandlingsstrategier fokuseret på selve tumorcellerne, men adskillige forskningsresultater gennem de sidste årtier har vist, at særligt immuncellerne i tumorens mikromiljø fremmer progression af kræft. Dette har medført, at immunterapi fx immun-checkpoint hæmmere indgår som en del af kræftbehandlingsstrategien.

Vævsundersøgelser har vist, at tumor-associerede mikroglia/makrofager (TAMs) er den dominerende type af immunceller i gliomer. Ud af deres aktiveringsstatus kategoriseres TAMs oftest som 1) tumor-hæmmende og pro-inflammatorisk (M1 fænotype) eller 2) tumor-fremmende og immunsupprimerende (M2 fænotype). Scavenger-receptoren CD204 er en relativt ny markør for M2-polariserede TAMs, og ifølge flere studier er CD204 forbundet med en dårlig prognose i mange kræftformer inklusiv diffust gliom. CD204 kunne derfor være et fremtidigt mål for kræftbehandling, men yderligere forskning er påkrævet for bl.a. at afdække dens uafhængige prognostiske værdi. Indtil videre har patienter med glioblastom haft sparsom effekt af immunterapi, hvilket kan skyldes dets immunsupprimerende mikromiljø med få T-celler og svækket immunogenicitet pga. lavt udtryk af neoantigener. Det hyppigst forekommende neoantigen i diffust gliom er muteret isocitrat dehydrogenase (IDH). Nyere forskning indikerer, at IDH-mutationer og dens onkometabolit D-2-hydroxyglutarat undertrykker immun-mikromiljøet i gliomer. Det overordnede formål med denne PhD afhandling var at karakterisere immun-landskabet i gliom med to primære fokuspunkter: 1) den kliniske værdi af CD204⁺ TAMs i glioblastom og 2) IDH-mutationers betydning for immun-mikromiljøet i diffust gliom.

I manuskript I undersøgte vi den prognostiske værdi af TAMs og CD204⁺ TAMs i gliomer. Vævsprøver fra 240 gliompatienter blev analyseret ved dobbelt immunfluorescens-farvninger med antistoffer rettet mod ionized calcium-binding adaptor molecule-1 (IBA1) og CD204 for at detektere hhv. alle TAMs og M2-polariserede TAMs. En pixel-baseret algoritme blev udviklet til at kvantificere niveauet af de individuelle markører og deres koekspression. Resultaterne viste, at udtrykket af både IBA1 og CD204 steg med malignitetsgraden. CD204 havde en uafhængig prognostisk værdi i grad III-IV gliomer og var associeret med kortere overlevelsestid. Omvendt var høj IBA1 intensitet associeret med en bedre prognose. TAMs var heterogent fordelt i gliomer på et intra- og intertumoral niveau og ophobede sig især centralt i tumorvævet. CD204⁺ TAMs var dog også tilstede i invasionszone og har derfor en mulig betydning for tumorens evne til at migrere og invadere. Tætheden af TAMs var særligt høj i perivaskulære og perinekrotiske områder, hvor

glioblastomceller med stamcelle egenskaber er kendt for at opholde sig. Nekrotiske områder viste sig også at være mere udpræget i glioblastomer med højt CD204 udtryk. Vi undersøgte derfor, om der var en interaktion mellem TAMs og glioblastomceller med stamcelle egenskaber vha. dobbelt immunhistokemiske farvninger med antistoffer rettet mod IBA1, CD204 og et panel af stamcelle-relaterede markører bl.a. podoplanin og CD133. Vi observerede, at navnligt podoplanin⁺ glioblastomceller og CD204⁺ TAMs var i tæt kontakt med hinanden i perinekrotiske områder. Vi subtypebestemte en gliomkohorte vha. immunohistokemi og observerede, at især andelen af CD204⁺ TAMs var signifikant højere i tumorer med den aggressive mesenkymale fænotype. Immunfluorescens-baseret subtypering viste, at CD204⁺ TAMs udtrykte både M1- og M2-relaterede proteiner samt tumor-faciliterende proteiner. Vores resultater tyder således på, at CD204⁺ TAMs fremmer tumor progression ved at inducere en aggressiv og invasiv subtype af gliom/glioblastom.

I manuskript II udforskede vi den mulige biologiske betydning af CD204 nærmere vha. myeloid transkriptom-profilering på en selekteret glioblastom-kohorte. Denne profilering afslørede, at glioblastomer med højt CD204 udtryk havde en unik signatur med opregulering af gener relateret til hypoksi, angiogenese og invasion. Blandt disse gener var interleukin-6, interleukin-8, programmed death-ligand 1, podoplanin og CD44. Gen-signaturen var associeret med dårlig prognose, men var ikke en stærkere prognostisk markør end CD204. Klynge- og netværksanalyser af de opregulerede gener afslørede, at interleukin-6 formede et epicenter og havde det højeste antal gen-gen-interaktioner. Pathway-analyser demonstrerede en overrepræsentation af termer relateret til fx immunaktivering og ekstracellulær matrix organisering herunder tumor necrosis factor (TNF) and interferon signaleringsvejene.

I manuskript III undersøgte vi, om IDH-mutation og D-2-hydroxyglutarat havde en indvirkning på det medfødte og adaptive immunsystem i diffust gliom. Vi analyserede niveauet af komplement aflejring og T-celle infiltration ved at lave immunhistokemiske farvninger på en patientkohorte bestående af 72 astrocytære gliomer, grad III-IV, som var stratificeret ud fra IDH-mutationsstatus. Analyserne viste, at IDH-muterede tumorer havde signifikant mindre aflejret komplement samt færre CD4⁺ T-hjælpeceller, CD8⁺ cytotoxiske T-celler og forkhead box P3⁺ regulatoriske T-celler ift. IDH-vildtype tumorer. *Ex vivo* eksperimenter med D-2-hydroxyglutarat demonstrerede, at D-2-hydroxyglutarat hæmmede komplement-medieret destruktion af både erythrocytter og en glioblastom-cellelinje ved at hindre cellelysering og opsonin-medieret fagocytose. D-2-hydroxyglutarat influerede derimod ikke dendritcellers evne til at differentiere eller præsentere antigen. D-2-hydroxyglutarat svækkede T-hjælpecellers proliferation, cytokin sekretion og migration samt cytotoxiske T-cellers migration. Eksponering for D-2-hydroxyglutarat stimulerede differentiering af regulatoriske T-celler, men hæmmede samtidig de regulatoriske T-cellers evne til at proliferere og secernere interleukin-10.

I manuskript IV undersøgte vi sammenhængen mellem IDH-mutation og forekomsten af de inhibitoriske immun-checkpoint proteiner galectin-9 og/eller T cell immunoglobulin and mucin-domain containing-3 (TIM3). Vi implementerede en 3-plex kromogen immunhistokemisk protokol bestående af antistoffer rettet mod galectin-9, TIM3 og tumor-markøren oligodendrocyte transcription factor 2 (OLIG2) og brugte protokollen til at farve vævsprøver fra den etablerede patientkohorte, som er beskrevet ovenfor. Farvningen blev kvantificeret ved brug af celletælling og stereologiske principper. Data viste, at antallet af TIM3⁺ celler var signifikant lavere i IDH-muterede tumorer sammenlignet med IDH-vildtype tumorer. Derimod så vi ingen

signifikant forskel i antallet af galectin-9⁺ celler. Dobbelt immunfluorescens-farvninger demonstrerede, at hovedparten af de TIM3⁺ og galectin-9⁺ celler var IBA1⁺ TAMs. OLIG2⁺ tumorceller udgjorde ~45-50% af alle celler i både IDH-muterede og IDH-vildtype tumorer, og disse tumorceller udtrykte kun undtagelsesvist galectin-9 og TIM3. Forekomsten af TIM3⁺ galectin-9⁻ var lav, og morfologisk lignede disse celler TAMs eller T-celler. Dobbelt immunfluorescens-farvninger fastslog, at TIM3 blev udtrykt af kun ~10% af CD3⁺ T-celler. IDH-muterede tumorer havde færre TIM3⁺ T-celler, og kun 50% af disse T-celler interagerede med galectin-9⁺ TAMs. Derimod blev en ~85-100% interaktionsrate påvist i IDH-vildtype tumorer. Stort set ingen interaktion blev observeret mellem TIM3⁺ T-celler og OLIG2⁺ tumorceller. Ved brug af et *in silico* datasæt påviste vi, at 75 gener var differentielt opreguleret i glioblastomer med den højeste TIM3 ekspresion sammenlignet med glioblastomer med den laveste TIM3 ekspresion. Ingen gener var differentielt nedreguleret. Størstedelen af de opregulerede gener var associeret med regulering og kemotaksi af leukocytter. CD204 og interleukin-6 var blandt de opregulerede gener, og deres ekspressionsniveauer var signifikant lavere i IDH-muterede astrocytære gliomer. Pathway-analyser viste, at de opregulerede gener bl.a. var involveret i TNF, komplement og fagosom signaleringsvejene.

Samlet set viser resultaterne i denne afhandling, at den prognostiske værdi af TAMs afhænger af deres fænotype frem for det samlede antal af TAMs, idet kun CD204⁺ TAMs korrelerede med en dårlig prognose hos patienter med grad III-IV gliom. Karakterisering af CD204⁺ TAMs og glioblastomer med højt CD204 udtryk demonstrerede, at CD204 er associeret med et inflammatorisk og immunsupprimerende tumor-mikromiljø, som har en høj ekspresion af multiple tumor-fremmende faktorer herunder interleukin-6. En lovende immunterapeutisk strategi kunne derfor være hæmning af CD204 og/eller interleukin-6 med det formål at reprogrammere TAMs til en tumor-bekæmpende fænotype og øge effekten af standard kræftbehandling inkl. immunterapi. Vores resultater understøtter ideen om, at IDH-mutationer inducerer en global immunsuppression i diffuse gliomer, som påvirker det medfødte og adaptive immunsystem samt immun-checkpoint signalering. Dette fund indikerer, at forskere og klinikere bør tage højde for IDH-mutationsstatus, når immunterapi overvejes som en behandlingsform. Muteret IDH kunne ligeledes være et attraktivt immunterapeutisk mål i sig selv, og kombinationsbehandling med fx immun-checkpoint hæmmere sammen med mutationspecifikke IDH-inhibitorer/vacciner kunne være klinisk relevant.

4. The thesis at a glance

I	<p>Aim To investigate the prognostic value of alternatively activated (M2) CD204⁺ tumor-associated microglia/macrophages (TAMs) in gliomas.</p> <p>Study design Descriptive study</p> <p>Methods Immunohistochemistry, double immunofluorescence, <i>in silico</i> analyses</p> <p>Conclusions CD204⁺ TAMs</p> <ul style="list-style-type: none"> - hold an unfavorable prognostic value in grade III-IV gliomas. - may contribute to treatment resistance in glioblastoma. - are associated with more aggressive tumor subtypes. - express proteins that are related to matrix remodeling, angiogenesis, and tumor growth. - may enable tumor progression.
II	<p>Aims To investigate the association between cancer stem-like cells and TAMs in glioblastoma tissue and to characterize the tumor immune microenvironment in CD204-enriched glioblastomas.</p> <p>Study design Descriptive study</p> <p>Methods Transcriptome profiling, immunohistochemistry/double immunohistochemistry, <i>in silico</i> analyses</p> <p>Conclusions</p> <ul style="list-style-type: none"> - TAMs including CD204⁺ TAMs accumulate in cancer stem-like cell niches in close relation to especially podoplanin⁺ glioblastoma stem-like cells. - Glioblastomas with high CD204 levels display a unique gene expression profile related to immune system pathways, including the tumor necrosis factor (TNF), interferon (IFN), nucleotide-binding and oligomerization domain-like (NOD-like) receptor signaling, and overexpress markers associated with tumor aggressiveness e.g. interleukin-6.
III	<p>Aim To investigate the association between immune activation and mutation in the isocitrate dehydrogenase (<i>IDH</i>) genes and the oncometabolite, D-2-hydroxyglutarate (D-2-HG), produced due to the neomorph activity of IDH-mutant tumor cells.</p> <p>Study design Descriptive and experimental <i>ex vivo</i> study</p> <p>Methods Immunohistochemistry/double immunohistochemistry, functional experiments</p> <p>Conclusions</p> <ul style="list-style-type: none"> - In grade III-IV astrocytic glioma, IDH-mutant tumors display decreased levels of complement deposition and contain fewer tumor-infiltrating CD4⁺ T helper cells, CD8⁺ cytotoxic cells, and forkhead box P3⁺ regulatory T cells (Tregs) relative to IDH-wildtype tumors. - D-2-HG inhibited the activation of complement cascades, reduced complement-mediated glioma cell damage and the complement-mediated phagocytic ability of macrophages. - D-2-HG inhibited proliferation of Th1 and Th17 cells and diminished their production IFNγ. - D-2-HG promoted differentiation of Treg, but inhibited their proliferation and IL10 production. - D-2-HG attenuated migration of CD4⁺ and CD8⁺ T cells. - D-2-HG did not influence dendritic cell function.
IV	<p>Aim To investigate the association between mutation in the <i>IDH</i> genes and the expression of the immune checkpoint markers, T cell immunoglobulin and mucin-domain containing-3 (TIM3) and galectin-9, in grade III-IV astrocytic gliomas.</p> <p>Study design Descriptive study</p> <p>Methods Chromogenic multiplex immunohistochemistry, double immunofluorescence, <i>in silico</i> analyses</p> <p>Conclusions</p> <ul style="list-style-type: none"> - TIM3 and galectin-9 were primarily expressed and co-expressed by TAMs. - IDH-mutant tumors had fewer TIM3⁺ cells relative to their IDH-wildtype counterparts. - Fewer TIM-3⁺ T cells and interactions between TIM-3⁺ T cells and galectin-9⁺ TAMs were observed in IDH-mutant relative to IDH-wildtype tumors. - <i>In silico</i> analyses showed that glioblastomas with high TIM3 mRNA levels had upregulation of several genes, including interleukin-6, complement component 3, and CD204, and the upregulated genes were involved in various immune-related and cytokine pathways including the TNF and NOD-like receptor signaling pathways.

5. Glossary of abbreviations

A

Ab	Antibody
AC-like	Astrocyte-like
ADCC	Antibody-dependent cellular cytotoxicity
ADCP	Antibody-dependent cellular phagocytosis
Ag	Antigen
AIF1	Allograft inflammatory factor 1
Akt	Protein kinase B/serine/threonine kinase
ALDH1A1	Aldehyde dehydrogenase 1 family member A1
ALT	Alternative lengthening of telomeres
ANGPT1	Angiotensinogen 1
AMP	Amplification
AP	Alkaline phosphatase
AQUA	Automated quantitative analysis
ASMA	Alpha smooth muscle actin
ATRX	Alpha thalassemia/mental retardation X-linked syndrome
α -C-GalCer	Alpha-C-galactosylceramide
α -GalCer	Alpha-galactosylceramide;
α -KG	Alpha-ketoglutarate

B

α -KG	α -ketoglutarate
BAM	Border-associated macrophage
BBB	Blood-brain barrier
BID	BH3 Interacting domain death agonist
BIRC3	Baculoviral IAP repeat containing 3
BMI1	BMI1 proto-oncogene, polycomb ring finger
BRAF	B-Raf proto-oncogene, serine/threonine kinase
BST2	Bone marrow stromal cell antigen 2
BTG2	B-cell translocation gene 2
BTLA	B- and T-lymphocyte attenuator
B7-H-	Receptor from the B7 family

C

CAR-T	Chimeric antigen receptor T cells
CCL/R	C-C motif chemokine ligand/receptor
CC1/2	Cell conditioning solution 1/2
CD	Cluster of differentiation
CDK	Cyclin-dependent kinase
CDKN2A/B	Cyclin-dependent kinase inhibitor 2A/B
Ceacam-1	Carcinoembryonic antigen-related cell adhesion molecule 1
CHI3L1	Chitinase 3-like
Chr	Chromosome
CI	Confidence interval
CIC	Capicua transcriptional repressor
cIMPACT	The Consortium to Inform Molecular and Practical Approaches to CNS Tumor Taxonomy
CNS	Central nervous system
CNV	Copy number variation
CR	Complement receptor
CSA	Catalyzed Signal Amplification
CSC	Cancer stem cell
CSF	Colony stimulating factor
CTL	Cytotoxic T lymphocyte
CTLA4	Cytotoxic T-lymphocyte-associated protein 4

CTSG	Cathepsin G
CXCL/R	C-X-C motif chemokine ligand/receptor
CyTOF	Cytometry by time of flight
Cy5	Cyanine 5
C3/5	Complement component 3/5

D

CSC	Cancer stem cell
CSF	Colony stimulating factor
DAB	3,3'-diaminobenzidine
DAPI	4',6-diamidino-2-phenylindole
DEL	Deletion
DLBCL	Diffuse large B cell lymphoma
DLL3	Delta-like 3
DISCO	DISCOVERY
DNA	Deoxyribonucleic acid
DNAM1	DNAX accessory molecule 1
DSP	Digital spatial profiling
(D-)-2-HG	D-2-hydroxyglutarate

E

(D-)-2-HG	D-2-hydroxyglutarate
EDTA	Ethylene-diamine-tetraacetic acid
EGF(R)	Epidermal growth factor (receptor)
ELISA	Enzyme-linked immunosorbent assay
EnV	EnVision

F

F	Fraction
FABP4	Fatty acid-binding protein 4
FAM	6-carboxyfluorescein
FAS	Fas cell surface death receptor
FBXO3	F-Box Protein 3
Fc γ R	Fragment crystallizable gamma receptor
FDR	False Discovery Rate
FFPE	Formalin-fixed paraffin-embedded
FGL1	Fibrinogen-like protein 1
FITC	Fluorescein isothiocyanate
FISH	Fluorescent in situ hybridization
FOXP3	Forkhead box P3
FUBP1	Far upstream element-binding protein 1
FYN	FYN Proto-Oncogene, Src Family Tyrosine Kinase

G

GABRA1	Gamma-aminobutyric acid type a receptor subunit alpha 1
GAL	Galectin
GAPDH	Glyceraldehyde-3-Phosphate Dehydrogenase
GATA3	GATA binding protein 3
G-CIMP	Glioma CpG island methylator phenotype
GFAP	Glial fibrillary acidic protein
GITR(L)	Glucocorticoid-induced TNFR family related protein (ligand)
GM-CSF	Granulocyte macrophage colony-stimulating factor
GO	Gene ontology
GWAS	Genome-wide association studies

Glossary of abbreviations

H

HAVCR2	Hepatitis A virus cellular receptor 2
HDAC	Histone deacetylase
HER2	Human epidermal growth factor receptor 2
HIER	Heat-induced epitope retrieval
HLA	Human leukocyte antigen
HIF	Hypoxia-inducible factor
HMGB1	High-mobility group protein B1
HR	Hazard ratios
HRP	Horseradish peroxidase
HVEM	Herpes virus entry mediator
H3F3A	H3 histone, family 3A
H&E	Hematoxylin-eosin

I

IBA1	Ionized calcium-binding adaptor molecule 1
ICAM1	Intercellular adhesion molecule 1
ICOS(L)	Inducible T cell co-stimulator (ligand)
IDH	Isocitrate dehydrogenase
IDO	Indoleamine 2,3-dioxygenase
IFI	
IFN	Interferon
IHC	Immunohistochemistry
IL	Interleukin
IL1RA	Interleukin 1 receptor antagonist
IMC	Imaging mass cytometry
IRF	Interferon regulatory factor
ISH	In situ hybridization
ITGAM/6	Integrin subunit alpha M/6

J

JAK	Janus kinase
-----	--------------

K

KEGG	Kyoto Encyclopedia of Genes and Genomes
KIR	Killer cell immunoglobulin-like receptors

L

LAG3	Lymphocyte activation gene 3
LGALS3/9	Galectin-3/9
LOH	Loss of heterozygosity
LSECtin	Liver and lymph node sinusoidal endothelial cell C-type lectin

M

mAb	Monoclonal antibody
MAC	Membrane attack complex
MAFF	V-maf avian musculoaponeurotic fibrosarcoma oncogene homolog F
MAGE-1	Melanoma-associated antigen 1
MAPK	Mitogen-activated protein kinase
MAP2	Microtubule-associated protein 2
MASP	MBL-associated serine protease
MBL	Mannose-binding lectin
MBP	Maltose-binding protein
MCM5	Minichromosome maintenance complex component 5
MDM2	Murine double minute 2 homolog
MDM4	Murine double minute 4 regulator of P53
MDSC	Myeloid-derived suppressor cells

Mes	Mesenchymal
MES-like	Mesenchymal-like
MET	Tyrosine protein kinase Met
MGMT	O6-methylguanine-DNA methyltransferase
MIBI-TOF	Multiplex ion beam imaging, by time of flight
MICSSS	Multiplexed immunohistochemical consecutive staining on single slide
MLH1	MutL homolog 1
MMP	Matrix metalloproteinase/metalloproteinase
MSH2/6	MutS homolog 2/6
mTOR	Mammalian target of rapamycin
MR	Mannose receptor
MRI	Magnetic resonance imaging
Ms	Mouse
MSR1	Macrophage scavenger receptor 1 (CD204)
mTOR	Mammalian target of rapamycin
MUT	Mutation
MVP	Microvascular proliferation
MWO	Microwave oven
MX1/2	MX dynamin like GTPase 1/2
m-MGMT	Methylated MGMT promoter

N

NAD(P)	Nicotinamide adenine dinucleotide (phosphate)
NAMPT	Nicotinamide phosphoribosyltransferase
NANOG	Nanog Homeobox
Ne	Necrosis
NEC	Not elsewhere classified
NES	Nestin
NeuN	Neuronal nuclei
NF1/2	Neurofibromin 1/2
NGS	Next generation sequencing
NFAT	Nuclear factor of activated T cells
NFκB	Nuclear factor kappa-light-chain-enhancer of activated B cells
NK cell	Natural killer cell
NKG2A	NK group 2 member A
NOD	Nucleotide-binding oligomerization domain
NOD2	Nucleotide-binding oligomerization domain-containing protein 2
NOS	Not otherwise specified
NOTCH1	Notch homolog 1, translocation-associated
NP	Nitroprazole
NPC-like	Neural progenitor-like
NSCLC	Non-small cell lung cancer

O

OCT4	Octamer-binding transcription factor 4
OLIG2	Oligodendrocyte transcription factor 2
OPC	Oligodendrocyte progenitor cell
OPC-like	Oligodendrocyte progenitor-like
OV	OptiView

P

pAb	Polyclonal antibody
PAMPs	Pathogen-associated molecular patterns
PARP	Poly (ADP-ribose) polymerase
PCR	Polymerase chain reaction
PCV	Procarbazine-lomustine-vincristine
PDGFRA	Platelet-derived growth factor receptor alpha
PD1	Programmed cell death protein 1

Glossary of abbreviations

PD-L1/2	Programmed death ligand 1/2
PDPN	Podoplanin
PGE2	Prostaglandin E2
PIK3	Phosphoinositide 3-kinase
PI3KCA	PIK3 catalytic, alpha polypeptide
PIK3R1	PIK3 regulatory subunit 1
PMS2	PMS1 homolog 2, mismatch repair system component
POT1	Protection of telomeres protein 1
POU5F1	POU Class 5 Homeobox 1
PROM1	Prominin 1 (CD133)
PS	Performance status
PTEN	Phosphatase and tensin homolog
PTGS2	Prostaglandin-endoperoxide synthase
PTX3	Pentraxin 3
PV	PowerVision
PVR	Poliovirus receptor
PVRL	Poliovirus receptor-related
P2RY12	Purinergic receptor P2Y12

Q

R

Rb	Rabbit
RNI	Reactive nitrogen intermediates receiver operating characteristic
ROC	Receiver operating characteristic
ROI	Reactive oxygen intermediates
ROI(s)	Region(s) of interest
RPL13A	Ribosomal protein L13a
RSAD2	Radical S-adenosyl methionine domain containing 2
RT	Radiotherapy or room temperature
(RT-)qPCR	Reverse transcription quantitative real-time PCR
RTU	Ready-to-use
RTK I/II	Receptor tyrosine kinase I/II

S

SALL1	Spalt Like Transcription Factor 1
Sarc	Sarcomatous
SIPR α	Signal regulatory protein alpha
SOX2	Sex determining region Y-box 2
SNCG	Gamma-synuclein
SNPs	Single-nucleotide polymorphisms
SOCS1	Suppressor of cytokine signaling 1
SRA/B	Scavenger receptor class A/B
STAT	Signal transducer and activator of transcription

STING	Stimulator of interferon genes
SURS	Systemic uniform random sampling

T

TAMs	Tumor-associated microglia/macrophages
TCF12	Transcription factor 12
TCGA	The Cancer Genome Atlas
TCR	T cell receptor
TERT	Telomerase reverse transcriptase
TERTp	Telomerase reverse transcriptase promoter
TGF β	Transforming growth factor beta
Th cell	T helper cell
Tie2	Tunica interna endothelial cell kinase 2
TIGIT	T cell immunoreceptor with immunoglobulin and ITIM domains
TIME	Tumor immune microenvironment
TIM3	T cell immunoglobulin and mucin-domain containing-3
TLR	Toll-like receptor
TMA	Tissue microarray
TME	Tumor microenvironment
TMZ	Temozolomide
TNF	Tumor necrosis factor
TNFAIP3	TNF, alpha-induced protein 3
TNM	Tumor-node-metastasis
TP53	Tumor protein p53
TRAIL-R	TNF-related apoptosis-inducing ligand receptor
Treg	Regulatory T cell
TREM119	Transmembrane protein 119
TRITC	Tetramethylrhodamine
TSA	Tyramide Signal Amplification
TSC1/2	Tuberous sclerosis 1/2
TTFIELDS	Tumor-treating fields

U

UV	ultraView
u-MGMT	Unmethylated MGMT promoter

V

VEGF(R)	Vascular endothelial growth factor (receptor)
VISTA	V-domain immunoglobulin suppressor of T cell activation

W

WHO	World Health Organization
-----	---------------------------

6. Introduction and aims

Diffuse gliomas are the most common malignant primary neoplasms of the central nervous system (CNS) in adults. Glioblastoma, World Health Organization (WHO) grade IV, is the most frequent and fatal type of diffuse glioma [1, 2]. Despite extensive treatment with surgery and adjuvant radio-chemotherapy, glioblastoma remains incurable with a median overall survival between 13-15 months [3-5]. Glioblastomas are very infiltrative in nature and display significant intra- [6-9] and intertumoral heterogeneity [9-13]. The heterogeneous tumor milieu is a consequence of both intrinsic [7, 9, 12] and extrinsic factors such as the tumor microenvironment (TME) including non-neoplastic cells including immune cells [14], and these factors is thought to favor tumor growth and contribute to treatment inefficiency, eventually leading to tumor recurrence and poor patient outcome [15-20]. In recent years, the interest in targeting the TME, particularly the tumor immune microenvironment (TIME), has intensified with the goal of augmenting the efficacy of anti-cancer therapies (**Figure 1**) [21-24]. The immune landscape in glioblastoma is highly diverse and dynamic, and several studies have shown that the composition of the immune infiltrate in cancer including glioma may predict the response to immunotherapy including checkpoint inhibitors [22, 25-28].

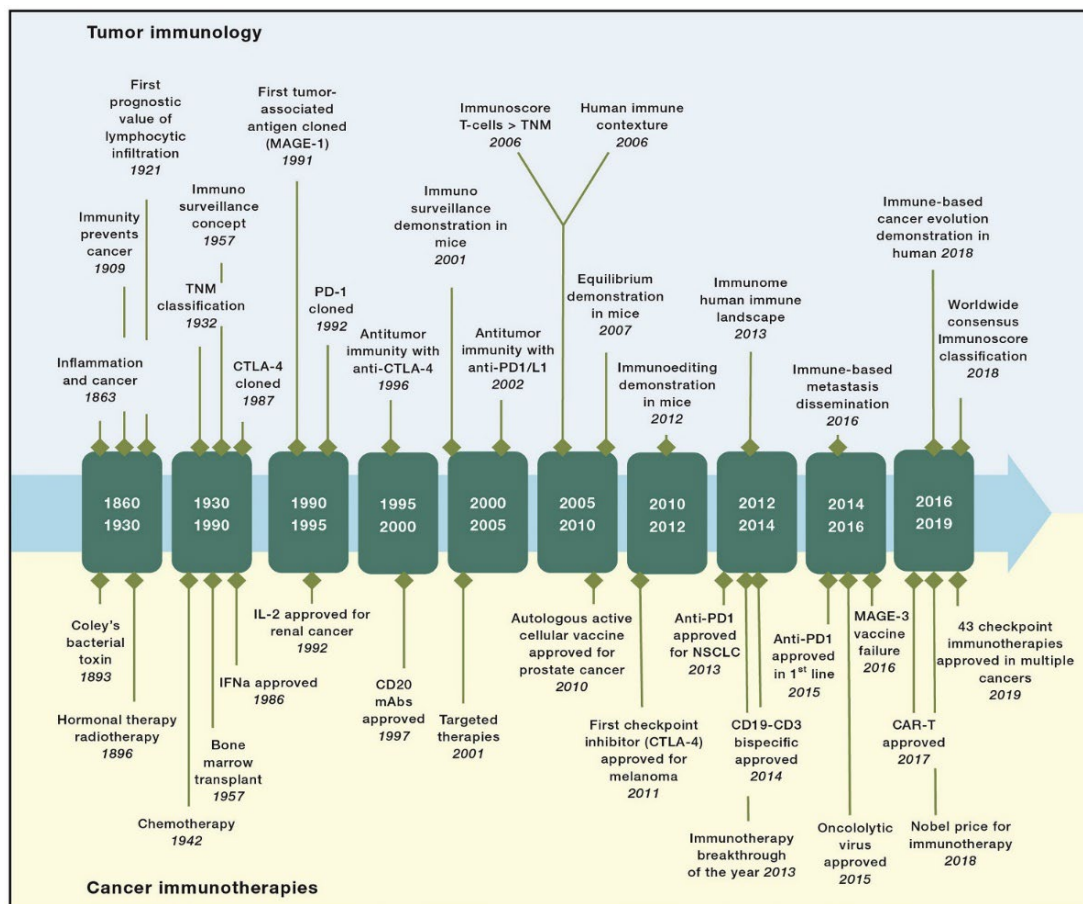


Figure 1 | History of Tumor-Immunology and Cancer (Immuno)therapy. The key milestones of tumor immunology (top) and of cancer therapy and immunotherapy (bottom) are highlighted. Reprinted from Galon *et al.* [21] under the terms and conditions provided by Elsevier and the Copyright Clearance Center.

The aim of the first part of this thesis was to characterize the immune microenvironment in gliomas focusing on the tumor-associated microglia/macrophages (TAMs). In glioblastoma tissue, TAMs comprise up to 30% or more of the cellular content [29-31] making it the most predominant immune cell population in glioma [32-35]. TAMs are innate immune cells and can exert several functions dependent on their polarization state. Numerous studies indicate that TAMs are a mixed cell population consisting of the pro-inflammatory and tumor-suppressive M1 phenotype, the anti-inflammatory and tumor-supportive M2 phenotype as well as the more undifferentiated M0 phenotype [36-42], and that high levels of TAMs correlate with tumor malignancy and have a detrimental effect on patient prognosis [43-50]. The aim of manuscript I was to explore the independent prognostic value of TAMs and especially M2-like TAMs in a large population-based patient cohort, which, to our knowledge, had not been done comprehensively in previous studies. An automated quantitative immunofluorescence approach [51, 52] was used to measure the expression and co-expression levels of the general microglial/macrophage marker, ionized calcium-binding adaptor molecule-1 (IBA1) [53, 54], and of the M2 marker, cluster of differentiation 204 (CD204) [31]. One of the first observations in the project was that especially glioblastomas exhibited a heterogeneous distribution of TAMs (**Figure 2**). The aim was therefore also to investigate the relation between TAMs and two features associated with tumor aggressiveness: glioblastoma subtype [10, 17] and gemistocytic tumor cell content [55-58]. Using double immunofluorescence, the phenotype of CD204⁺ TAMs was examined with a set of markers related to immune activation and tumor aggressiveness. Due to the findings in manuscript I, the aim in manuscript II was to explore the possible biological role of CD204 in glioblastoma as high levels of CD204⁺ TAMs had an unfavorable impact on patient survival and co-expressed proteins related to both M1 and M2 polarization as well as proteins that favor tumor resilience. Concurrently, CD204⁺ TAMs seemed to accumulate in perivascular and perinecrotic/hypoxic niches where the aggressive cancer stem cells (CSCs) reportedly reside and thrive [59-62]. The possible cellular interaction between TAMs and glioblastoma cells with stem cell properties was therefore investigated using double immunohistochemistry. Additionally, CD204-enriched glioblastoma was profiled more thoroughly using the validated NanoString nCounter technology [63] and a customized version of the myeloid innate immunity gene expression panel. Immunohistochemistry and bioinformatics databases were employed to confirm the gene expression profile.

The immune microenvironment in glioma is often described as immunologically quiet/lymphocyte-depleted [64], ‘cold’ [22, 28], or immunosuppressive due to tumor extrinsic and intrinsic mechanisms, including genetic changes and low levels of immunogenic tumor-specific antigens/neoantigens [26, 28, 65, 66]. One of the most prominent genetic alterations in diffuse gliomas is gain-of-function mutations in the isocitrate dehydrogenase (*IDH*) genes, which results in production of the oncometabolite D-2-hydroxyglutarate [2, 67, 68]. D-2-hydroxyglutarate modifies cellular energetics as well as epigenetics, and increasing evidence suggests that it may alter the microenvironment in glioma including the function of the innate and adaptive immune system [48, 49, 64, 66, 69-74], impeding the immunosurveillance and immune-mediated destruction of tumor cells.

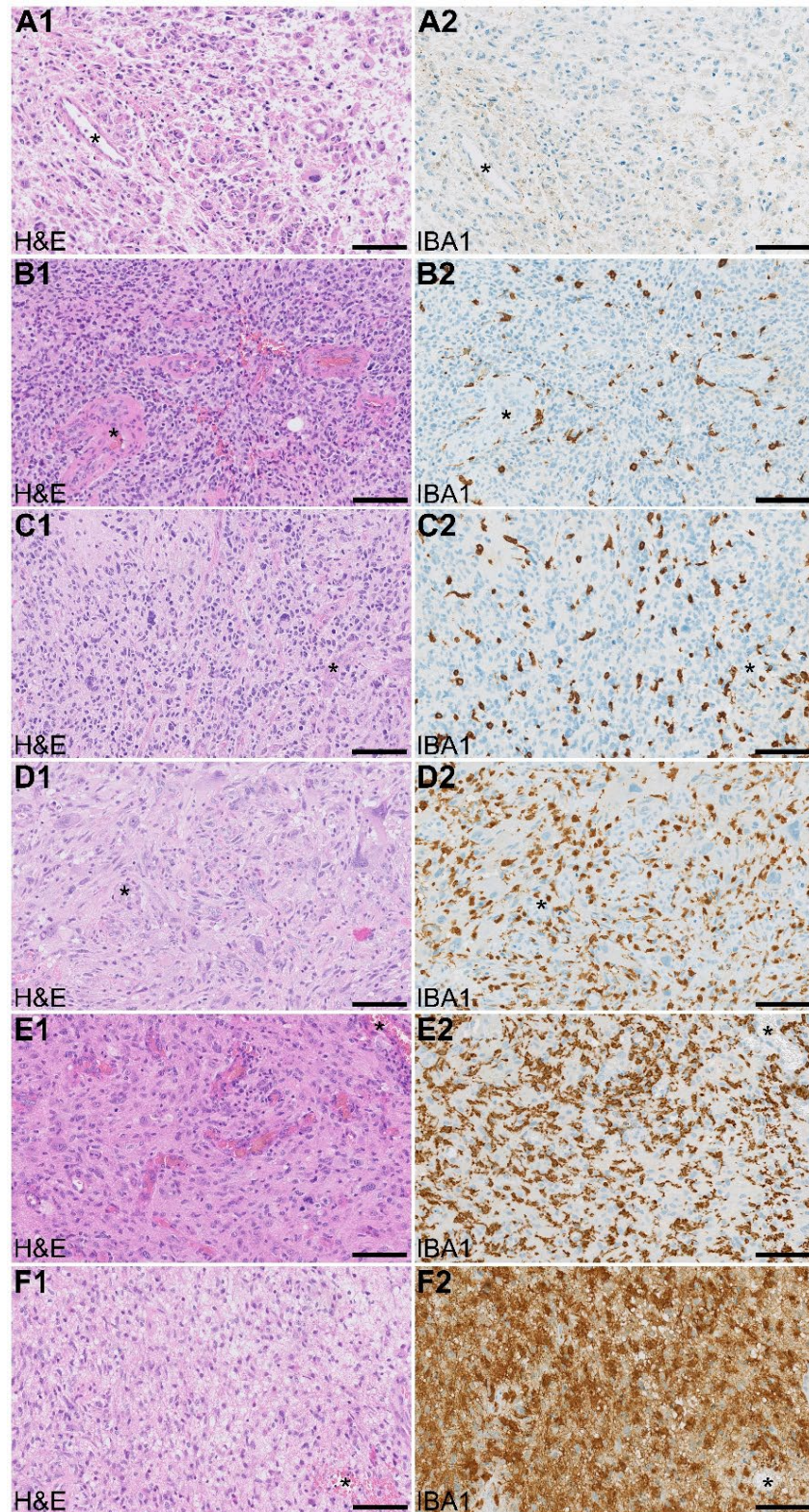


Figure 2 | Glioblastoma heterogeneity and distribution of TAMs. (A1-F1) Glioblastomas are highly heterogeneous as illustrated in the hematoxylin-eosin (H&E) stains. Microglia/macrophages are not readily identified on an H&E stain resulting in a possible underestimation of their contribution to the tumor microenvironment. (A2-F2). Immunostainings using an antibody against the microglia/macrophage marker IBA1 reveals a significant intertumoral heterogeneity. *Scale bar* 100 μ M. *Asterisks* signify microvascular proliferations in the pairwise serial sections.

The objective of the second part of the thesis was to examine the association between IDH mutation and activation of the immune system using primarily immunohistochemistry and glioma tissue samples from a patient cohort with WHO grade III-IV astrocytic gliomas stratified according to IDH mutation status.

In manuscript III, the aim was to investigate the potential role of IDH mutation and D-2-hydroxyglutarate as an intercellular immune regulator in gliomas focusing on the complement system and T cells. While T cells constitute a major component of the adaptive immune system, complement is a key component of the innate immune system that acts as a first line of defense against pathogens, clears cellular debris, apoptotic cells, and immune complexes, and orchestrates the innate and adaptive immunological and inflammatory processes [75, 76]. Using the established patient cohort, protein expression levels of complement component 3 (C3) and different T cell subsets were evaluated. Further, *ex vivo* experiments with D-2-hydroxyglutarate were performed to investigate its inhibitory effects on complement activation, antigen presentation, and T cells.

Immune responses are tuned by a dynamic system of co-stimulatory and co-inhibitory immune checkpoints, which adjusts the duration and amplitude of the immune activation thereby averting autoimmunity and tissue damage [77]. In cancer, tumor cells can exploit the inhibitory checkpoint pathways to escape immune surveillance. Immunotherapy targeting co-inhibitory checkpoints, especially cytotoxic T lymphocyte antigen 4 (CTLA4) and programmed death receptor 1 (PD1) or its ligand programmed death ligand 1 (PD-L1), has proven effective in several cancers including melanoma and non-small cell lung cancer (NSCLC) [78], but has shown limited effect in patients with glioblastoma [28, 79, 80]. Another inhibitory checkpoint protein of growing interest is T cell immunoglobulin and mucin-domain containing 3 (TIM3) [77, 78, 81] which expression levels reportedly positively correlate with glioma malignancy [82, 83]. Several studies have found low expression levels of both PD1/PD-L1 [72, 84-87] and CTLA4 [88] in IDH-mutant gliomas; however, little knowledge exists about the protein expression patterns of TIM3 and its ligand galectin-9 at a cell type-specific level in glioma tissue and about the association between IDH mutation and expression of this checkpoint signaling pathway. In manuscript IV, the objective was to determine if the galectin-9/TIM3 checkpoint pathway is influenced by IDH mutation status in the glioma cohort described above. A novel chromogenic multiplex immunohistochemistry panel was established, which enabled identification of specific cellular subpopulations within the same tissue section including co-localization and interaction patterns. Validation studies were performed using double immunofluorescence and *in silico* datasets.

7. Background

7.1 Gliomas – epidemiology and etiology

Every year 1,600 adults are diagnosed with a tumor in the brain, meninges, or nerves in Denmark; about 600 of these tumors are diffuse gliomas [89] which mostly arise in the supra-tentorium (i.e. the frontal, temporal, parietal and occipital lobes) [1, 90]. Glioblastoma is the most frequent and malignant type of glioma accounting for 15% of all intracranial neoplasms, 45-50% of all malignant primary brain tumors [1, 90, 91], and ~60% of all gliomas [1, 90]. Even though primary brain tumors are relatively rare in adults compared with metastatic brain tumors [92-95] and more common primary cancers (e.g. lung, breast, prostate, and colorectal cancer) [90], they cause a high level of both morbidity and mortality, and the five-year relative survival rate for patients diagnosed with glioblastoma is only 5-10% [1, 90, 96]. The overall incidence of glioma increases with advancing age, peaking among elderly adults between the ages of 65 and 84 years [90, 97]. Epidemiological studies consistently show that men have both higher incidence rate of glioma, especially glioblastoma, [1, 90, 97, 98] and poorer prognosis [99-102], possibly due to sex-related genetic and immunological factors [99, 103, 104]. Further, incidence rates for gliomas are almost two times greater in Caucasians compared to both African-Americans and Asian/Pacific Islanders [1, 90] suggesting that ethnic, cultural and/or geographic differences influence the risk of glioma.

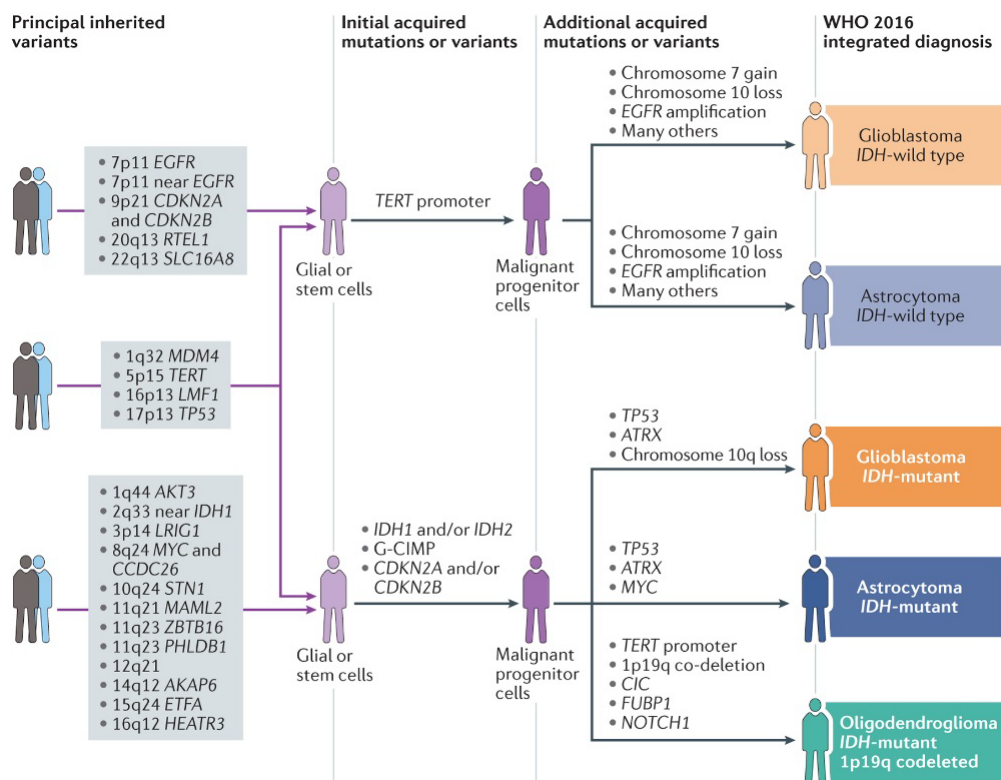


Figure 3 | Hypothesized pathways of glioma development. Our current understanding of gliomagenesis involves an interplay of inherited risk variants and acquired alterations. Reprinted from Molinaro *et al.* [105] under the terms and conditions provided by Springer Nature and the Copyright Clearance Center.

Table 1 | Hereditary syndromes associated with increased risk of glioma

Gene	Syndrome	Inheritance	Features	Associated histology
<i>NF1</i>	Neurofibromatosis 1	Dominant	Neurofibromas, schwannomas, café-au-lait macules	Astrocytoma, optic nerve glioma
<i>NF2</i>	Neurofibromatosis 2	Dominant	Acoustic neuromas, meningiomas, neurofibromas	Spinal ependymoma
<i>TSC1</i> <i>TSC2</i>	Tuberous sclerosis	Dominant	Multisystem non-malignant tumors	Subependymal giant cell astrocytoma
<i>MSH2</i> <i>MLH1</i> <i>MSH6</i> <i>PMS2</i>	Lynch syndrome	Dominant	Gastrointestinal, endometrial, and other cancers	Glioblastoma, astrocytoma
<i>TP53</i>	Li–Fraumeni syndrome	Dominant	Numerous cancers, especially breast, brain, and soft-tissue sarcoma	Glioblastoma, astrocytoma, choroid plexus tumor
<i>POT1</i>	Melanoma-oligodendroglioma susceptibility syndrome	Dominant with reduced penetrance	Predisposition to melanoma and oligodendroglial tumors	Oligodendroglioma, mixed oligoastrocytoma
<i>CDKN2A</i>	Melanoma-neural system tumor syndrome	Dominant	Predisposition to melanoma and astrocytic tumors	Astrocytoma
<i>IDH1/IDH2</i>	Ollier disease/ Maffucci syndrome	Postzygotic, mosaicism / dominant with reduced penetrance	Intraosseous benign cartilaginous tumors, cancer predisposition	Glioma

Reprinted from Walsh *et al.* [97] under the terms and conditions provided by Elsevier and the Copyright Clearance Center. *Abbreviations:* *CDKN2A*, cyclin-dependent kinase inhibitor 2A; *IDH1/2*, isocitrate dehydrogenase 1/2; *MLH1*, MutL homolog 1; *MSH2/6*, MutS homolog 2/6; *NF*, neurofibromin; *PMS2*, PMS1 homolog 2, mismatch repair system component; *POT1*, protection of telomeres protein 1; *TP53*, tumor protein p53; *TSC1/2*, tuberous sclerosis 1/2

Some rare inherited genetic predispositions to glioma have been described (**Table 1**) [106-112], but these monogenic disease syndromes explain less than 5% of the brain tumor incidence [97, 113, 114]. A small proportion (~5-10%) of gliomas occur in familial clusters [115], indicating some level of inherited genetic susceptibility. Recent genome-wide association studies (GWAS) have shown that some genetic variants, also known as single-nucleotide polymorphisms (SNPs), contribute to the heritability of glioma [113, 116-120]. In GWAS, patients with the disease of interest and healthy controls are genotyped at hundreds of thousands of SNPs to discover inherited variants which are significantly more common in patients. A total of 25 strongly glioma-associated SNPs have been identified in adults (**Figure 3**), and most of the SNPs are in or near genes known to be involved in specific signaling pathways, such as tumor protein p53 (TP53/p53), epidermal growth factor receptor (EGFR)-phosphoinositide 3-kinase-Akt as well as nicotinamide adenine dinucleotide (NAD) metabolism and fatty acid metabolism, telomere maintenance, and cell cycle regulation [105] and have to some extent been incorporated into the definition of the different brain tumor entities. These risk variants are neither necessary nor sufficient for gliomagenesis, but might influence susceptibility to glioma in concert with environmental exposures [97]. Several potential environmental risk factors have been examined over the years, including personal history of allergies/atopy, [97, 114, 121], use of aspirin [122] and statin [123, 124] and

estrogen exposure [125, 126] as well as smoking and birth weight, but only moderate-to-high doses of ionizing radiation have consistently been linked to increased glioma risk [97, 98].

Collectively, the etiology of primary brain tumors is most likely multifactorial, and so far the genes and pathways involved in the pathogenesis are not fully understood. However, gliomas are thought to primarily arise through progressive accumulation of genetic (e.g. mutation, amplification, and deletion) and epigenetic (e.g. methylation and demethylation) alterations, permitting the cells to evade normal regulatory mechanisms and escape destruction by the immune system [105, 127, 128].

7.2 Gliomas – classification, grading, biomarkers, and prognosis

Gliomas consist of a very heterogeneous group of primary CNS tumors and were originally classified based on their microscopic resemblance to the supposed glial cell of origin (i.e. astrocyte – astrocytoma; oligodendroglial cell – oligodendroglioma; glioblast – glioblastoma; ependymal cell – ependymoma). Depending on morphologic features of anaplasia (cytological atypia, mitotic activity, microvascular proliferations (MVP), and necrosis), each glioma has additionally been assigned a histologic grade according to a four-tiered WHO grading scheme (grade I-IV) reflecting the range from low to higher grade of malignancy [129, 130]. WHO grades I-II have conventionally been referred to as ‘benign’ or lower-grade gliomas and grades III-IV as malignant or high-grade gliomas. Traditionally, gliomas are characterized as ‘diffuse’ and ‘non-diffuse’ based on their migratory and more circumscribed phenotype, respectively. ‘Non-diffuse’ gliomas include the slow-growing, ‘benign’ pilocytic astrocytoma and the heterogeneous group of ependymomas [131], while ‘diffuse’ gliomas comprise diffusely infiltrating astrocytic and oligodendroglial tumors [129, 132]. Up until the most recent WHO updates in 2016 [91] and 2021 [2], classification of brain tumors was mainly based on light microscopic features in hematoxylin-eosin (H&E) stained sections, immunohistochemical expression patterns, and ultrastructural characterization [129, 133-136]. However, this histopathological classification system held a high level of inter-observer variability [131, 137], and survival varied substantially within the individual grades, overall prompting the need for identification and implementation of more robust diagnostic markers to ensure a more accurate and clinically relevant characterization of the CNS tumor entities. This search has led to the discovery of several diagnostic, prognostic and/or predictive molecular biomarkers to complement the histological classification of gliomas [138-164].

The term ‘biomarker’ has been defined as “a characteristic that is objectively measured and evaluated as an indicator of normal biological processes, pathogenic processes, or pharmacologic responses to a therapeutic intervention” [165]. In cancer research, the terms ‘diagnostic’, ‘prognostic’, and ‘predictive’ biomarker are often employed; a diagnostic biomarker is used to detect or confirm the presence of disease/pathology, while a prognostic biomarker gives information on the likelihood of a clinical event, disease recurrence, or progression in patients regardless of treatment and is measured at baseline. A clinically applicable prognostic biomarker must have an independent significant value and can be useful for selection of patients for a specific treatment, but does not foresee the response to the treatment. A predictive biomarker provides information on the effect of a therapeutic intervention [166]. As mentioned above, several biomarkers have been identified in glioma, and the most significant developments in respect to molecular diagnosis and genetic biomarkers of

CNS tumors were incorporated into the 2016 updated fourth edition [91, 167] and the 2021 fifth edition of the WHO Classification of Tumors of the CNS [2, 168] which introduced the concept of integrated histological and molecular diagnosis of CNS tumors.

The next subsection provides brief overviews of the four most essential biomarkers which were also used throughout this thesis. The subsequent subsections then briefly describe 1) the 2016 WHO classification of diffuse gliomas, 2) the most important prognostic factors in diffuse gliomas, and 3) major changes introduced in the 2021 WHO classification. All manuscripts in this thesis were published prior to the release of the 2021 WHO classification, and the glioma cohorts used in our studies were classified according to the 2016 edition. Thus, the following exposition is mainly based on the 2016 edition.

7.2.1 Biomarkers in gliomas

Isocitrate dehydrogenase mutation

Somatic point mutations in the *IDH1/2* genes were first discovered in 2008 by large scale next-generation sequencing (NGS) in glioblastoma [141] and later in lower-grade diffuse gliomas [144, 155-157]. IDH mutation status has since become the most important diagnostic marker in the classification of diffuse gliomas [91, 167]. The *IDH1* and *IDH2* genes code for enzymes that play important roles in a number of cellular functions, including glucose sensing, glutamine metabolism, lipogenesis, and regulation of cellular redox balance protecting the cell from oxidative stress especially in the brain. IDH1 is located in the cytoplasm and peroxisomes, while IDH2 is found in the mitochondrial matrix. Both IDH enzymes normally catalyze the oxidative carboxylation of isocitrate to α -ketoglutarate, resulting in the reduction of NADP to NADPH. In the event of active site mutations, IDH1/2 acquires a neomorphic enzyme activity that converts the normal product α -ketoglutarate to the oncometabolite D-2-hydroxyglutarate in a NADPH-consuming reduction [67, 68, 169] (**Figure 4A**). In tumors harboring an *IDH* mutation, D-2-hydroxyglutarate accumulates intra- and extracellularly to concentrations that are 100-fold higher than their wildtype counterparts [67, 170, 171]. D-2-hydroxyglutarate in turn deregulates and modifies the cellular energetics and epigenetics including promotion of a hypermethylation phenotype (also known as the glioma CpG island methylator phenotype, G-CIMP) which may promote neoplastic transformation of neural stem/progenitor cells [12, 67, 68, 169, 172-175].

Mutations in the *IDH* genes are found in ~80% of patients with WHO grade II-III gliomas and 'secondary' glioblastomas which are considered to originate from precursor lesions [109, 141, 144, 157, 176]. Mutations occur at codon R132 in the *IDH1* gene or at the homologous residue R172 or R140 in the *IDH2* gene and are considered early events in tumorigenesis [67, 68, 146, 169, 177] that persist during tumor progression [178], but IDH mutation itself is most likely insufficient for induction of tumor growth [179]. Instead, additional genetic alterations are necessary for gliomagenesis, including mutations in the *TP53* and alpha thalassemia/mental retardation X-linked syndrome (*ATRX*) genes in astrocytic tumors or 1p/19q-codeletion and telomerase reverse transcriptase (*TERT*) promoter mutation in oligodendroglial tumors [140, 142, 177, 180]. IDH mutation generally confers superior survival in patients with gliomas [137, 148, 170, 173-179, 181], possibly due to an altered cellular, molecular, and spatial heterogeneity in IDH-mutant tumors [182]

influencing tumor vasculature/angiogenesis [172, 182, 183] and promoting an immunosuppressive microenvironment with few T cells and TAMs [48, 49, 64, 69-73, 84, 184].

Since the mutant IDH protein is a tumor-specific neoantigen, it could be a candidate for targeted therapy [185, 186], especially the IDH1-R132H mutation which is seen in ~90% of the IDH-mutant gliomas [144, 157] (**Figure 4B**). IDH1-R132H is usually detected by immunohistochemistry using a mutation-specific antibody [140, 145, 178, 187]. The remaining IDH mutations can be detected by sequencing methods [144, 156, 188, 189]. Collectively, the discovery of IDH mutations is considered a landmark in the history of gliomas due to its significant diagnostic and prognostic value.

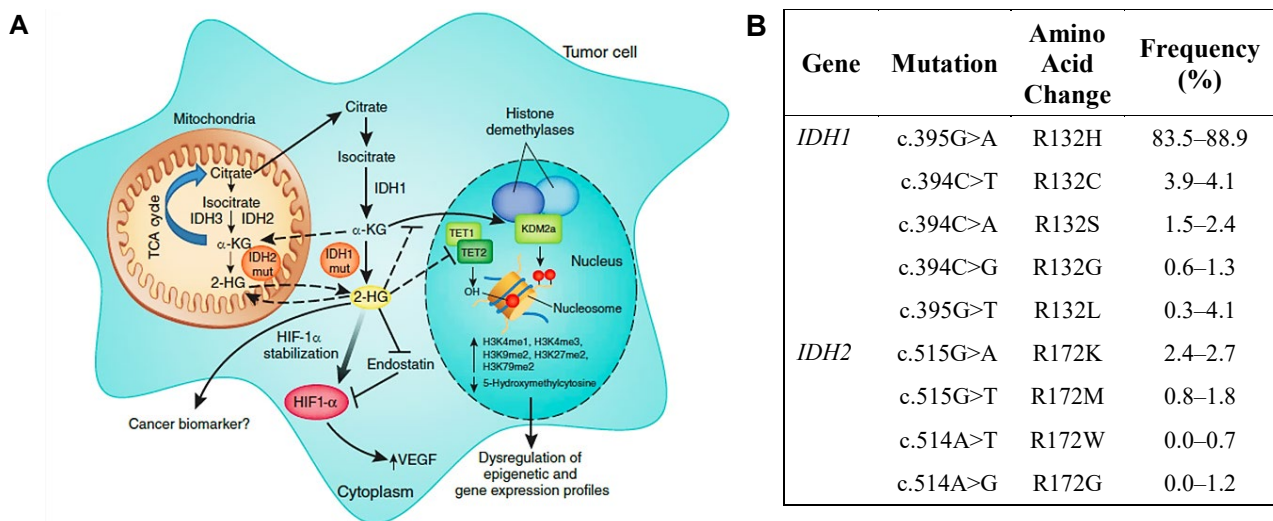


Figure 4 | Mutant IDH enzyme activity and signaling in cancer. **(A)** Wildtype IDH1 (cytoplasmic) and IDH2 (mitochondrial) enzymes convert isocitrate to α -ketoglutarate (α -KG) and carbon dioxide with concomitant production of NADPH from NADP. Tumor-associated mutant IDH1 and IDH2 enzymes neomorphically convert α -KG to the oncometabolite D-2-hydroxyglutarate (2-HG) with concomitant production of NADP from NADPH. The presence of mutant IDH results in increased amounts of 2-HG altering several downstream cellular activities leading to epigenetic dysregulation, hypermethylation and stabilization of hypoxia-inducible factor 1 alpha (HIF1 α) resulting in increased production of the angiogenetic driver, vascular endothelial growth factor (VEGF). **(B)** Frequency of specific IDH mutations in gliomas, represented as the percentage of total *IDH1/2* mutations in glioma patients according to Yan *et al.* [157] and Hartmann *et al.* [144]. (A) is reprinted from Prensner *et al.* [175] under the terms and conditions provided by Springer Nature and the Copyright Clearance Center.

1p/19q-codeletion

In 1994, Reifenberger *et al.* found an association between oligodendroglial tumors and loss of heterozygosity (LOH) for the short arm of chromosome 1 (1p) and the long arm of chromosome 19 (19q) [148]. Since, 1p/19q-codeletion has been found to correlate with higher sensitivity to procarbazine–lomustine–vincristine (PCV) chemotherapy [190] and longer survival in patients with anaplastic oligodendroglioma, WHO grade III [190–192]. Follow-up data from 2013 supported the importance of 1p/19q-codeletion in predicting long-term survival following aggressive multimodal treatment composed of surgical resection followed by adjuvant radio- and chemotherapy with PCV. Patients with IDH-mutant and 1p/19q-codeleted anaplastic

oligodendroglioma had a survival benefit when treated with radiotherapy plus PCV as compared to treatment with radiotherapy alone. In contrast, patients with intact 1p/19q anaplastic gliomas had shorter survival without beneficial effect of adjuvant PCV [193, 194]. The results underline the value of 1p/19q-codeletion as both a diagnostic, prognostic, and predictive biomarker. In the 2016 and 2021 WHO classification, the diagnosis of oligodendroglioma requires demonstration of both IDH mutation and 1p/19q-codeletion. Of note, codeletion refers to whole-arm deletions of both chromosome arms [138] as partial deletions can be detected in other glioma subtypes and may correlate with poorer prognosis [195]. 1p and 19q losses can be detected by (fluorescent) in situ hybridization ((F)ISH), analysis for LOH and/or multiplex ligation-dependent probe amplification [196]. In recent years, DNA microarrays have proven useful for assessment of copy number variations (CNV) including 1p/19q-codeletion [197-200].

ATRX status

The *ATRX* gene was first reported in patients with the X-linked mental retardation syndrome (ATRX syndrome). In cancer, somatic mutations in *ATRX* were first detected in pancreatic neuroendocrine tumors [201] and later reported in glioblastomas [158, 159]. *ATRX* mutation often results in a truncated protein and loss of protein expression [150, 159]. *ATRX* is involved in maintenance of genomic stability, and loss of *ATRX* in gliomas promotes development of non-telomerase-dependent Alternative Lengthening of Telomeres (ALT) phenotype [139, 152, 159, 202-204], resulting in genomic instability through accumulation for genetic alterations. *ATRX* loss has also been linked to DNA damage and replicative stress [203]. *ATRX* expression is highly associated with *TP53* and *IDH* mutations and almost mutually exclusive with 1p/19q-codeletion and *TERT* promoter mutation [142, 149-152, 180, 204], thereby signifying its importance in deciphering between astrocytic and oligodendroglial tumors that also carry an *IDH* mutation. In addition to the diagnostic value of *ATRX*, *ATRX* mutation has been associated with better survival indicating a possible prognostic value [139, 205]. *ATRX* mutation status can be determined using immunohistochemistry or sequencing [140, 178, 204].

O6-methylguanine DNA methyltransferase (MGMT)

O6-methylguanine-DNA methyltransferase (*MGMT*) is a gene located on chromosome 10q26 coding for protein MGMT. In normal non-neoplastic cells, MGMT functions as DNA repair enzyme protecting cells from apoptosis by removing alkyl groups from the O6 position on guanine. In cancer, MGMT unfortunately also counteracts the efficacy of alkylating chemotherapeutic agents (e.g. temozolomide (TMZ) and carmustine) by removing alkylation-induced DNA adducts, in particular methylation at the O6-position of guanine, thereby restoring guanine and preventing chemotherapy-induced DNA damage and apoptosis. High levels of MGMT activity are associated with resistance to the cytotoxic effects of alkylating agents. In ~40% of IDH-wildtype glioblastomas and the vast majority of IDH-mutant and/or hypermethylated gliomas, the *MGMT* gene is transcriptionally silenced by DNA methylation of its 5'-associated CpG-island, an epigenetic aberration known as MGMT promoter methylation [206, 207]. Methylation of the promoter region of MGMT thus results in reduced enzyme activity and increased chemo-sensitivity. Accordingly, promoter methylation of the *MGMT* gene is associated with better treatment response as well as prolonged progression-free and overall survival in

patients who are treated with alkylating agents such as TMZ [96, 160, 208-212], but also has a prognostic value irrespective of postsurgical treatment regime [102, 160, 210, 212-218]. In elderly patients diagnosed with glioblastomas, *MGMT* promoter methylation has emerged as a clinically important predictive biomarker for guiding adjuvant therapy [214, 215, 219-221]. Interestingly, even though most IDH-mutant gliomas (including both astrocytic and oligodendroglial tumors) have methylated *MGMT* promoter, it only predicts benefit from alkylating chemotherapy in patients with IDH-wildtype gliomas. This suggests that the predictive vs. prognostic value of *MGMT* promoter methylation depends on *IDH* mutation status [211]. Collectively, *MGMT* promoter methylation is not a diagnostic biomarker, but is clinically important as a predictive marker for response to alkylating chemotherapy. *MGMT* promoter methylation status is determined using molecular genetic tests, e.g. methylation-specific polymerase chain reaction (PCR), pyrosequencing, or DNA methylation profiling [130, 197, 206, 207].

7.2.2 The 2016 WHO classification of diffuse gliomas

In the 2016 WHO classification of CNS tumors, diffuse astrocytic and oligodendroglial tumors are considered a combined group of neuroepithelial tumors where the common denominator of these tumors is their diffusely infiltrative growth into the brain parenchyma. Gliomas are still graded based on histological features (anaplasia, mitosis/proliferation index, necrosis, and/or MVP), however, four molecular biomarkers are the most central in classifying gliomas: *IDH* mutation, chromosomal 1p/19q-codeletion, *ATRX* status, and *H3-K27M* mutation [91, 130, 132, 167, 221] (**Figure 5**).

Mutation in *H3-K27M* defines an individual tumor entity designated ‘diffuse midline glioma’, which is an aggressive, diffusely infiltrating glial tumor located in midline structures; it is primarily seen in children/young adults and will not be discussed further in this thesis. Other biomarkers are used in the differential diagnostic setting, including mutations in the *TERT* promoter [118, 143, 151, 154, 164, 222, 223], capicua transcriptional repressor (*CIC*) [152, 153], far upstream element-binding protein 1 (*FUBP1*) [152, 153], *TP53* [224, 225], *EGFR* [226, 227], and B-Raf proto-oncogene, serine/threonine kinase (*BRAF*) V600E [228, 229] (**Table 2**). In addition to their diagnostic value some of them may also have prognostic and/or possibly predictive value [10-12, 130, 132, 142, 147, 180].

Based on histological and molecular features, diffuse gliomas in adults include WHO grade II diffuse astrocytomas, WHO grade III anaplastic astrocytomas, WHO grade II oligodendroglioma, WHO grade III anaplastic oligodendroglioma, and WHO grade IV glioblastomas. Each of the entities are supplemented with the addendum of IDH-mutant or IDH-wildtype [91, 130, 167, 221] (**Table 2**).

In some cases diagnostically required molecular pathological examination is not feasible (e.g. due to insufficient amount of available tissue for molecular testing or inconclusive molecular testing), and the final classification may consist solely of the histological diagnosis which can then be supplemented by the note ‘NOS’ (“not otherwise specified”). In other cases, integrated diagnostic results do not fit into any defined WHO entity, and the descriptive diagnosis can be labeled with ‘NEC’ (“not elsewhere classified”) [230].

Background

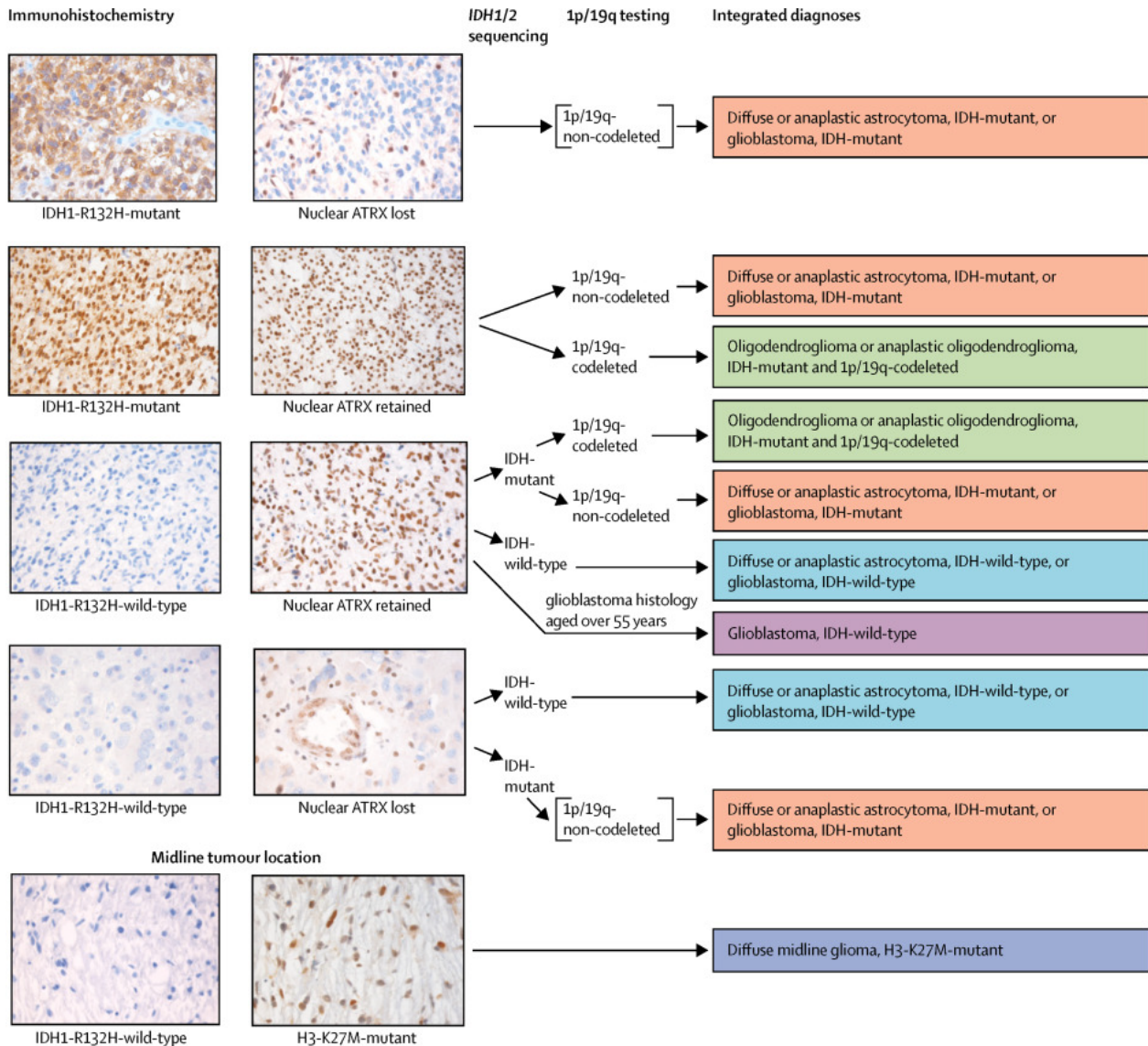


Figure 5 | Diagnostic algorithm for integrated classification of diffuse gliomas according to the WHO classification 2016. Tumor specimens are morphologically evaluated using H&E stains. If the diagnosis ‘diffuse glioma’ is suspected, the tumor is evaluated for the IDH mutation, IDH1-R132H, and loss of nuclear ATRX protein expression using immunohistochemistry. Immunostaining for the histone H3-K27M mutation characterizes diffuse midline glioma, histone H3-K27M-mutant, which is located in midline structures (thalamus, brain stem, and spinal cord) and primarily seen in children/young adults. Depending on the results from the immunohistochemical stainings and patient characteristics, molecular analyses are performed for detection/exclusion of less common *IDH* codon mutations (e.g. by DNA sequencing), and evaluation of possible codeletion of chromosomal arms 1p and 19q (e.g. by FISH or microsatellite PCR-based LOH analyses). IDH mutation and loss of nuclear ATRX expression classify IDH-mutant astrocytic gliomas, and additional molecular testing for 1p/19q-codeletion is not routinely required, but might be performed to further substantiate the diagnosis. Reprinted from Weller *et al.* 2017 [221] under the terms and conditions provided by Elsevier and the Copyright Clearance Center.

Table 2 | Overview of common characteristics of the five 2016 WHO entities of adult diffuse glioma

Glioma entity and WHO grade	Frequent molecular aberrations Genetic (1), epigenetic (2), chromosomal (3)	MGMT promoter methylation (%)	Median age at diagnosis and median overall survival
Oligodendroglial tumors, IDH-mutant and 1p/19q-codeleted, WHO grade II-III	(1) IDH1/2 ^{MUT} , TERT ^p ^{MUT} , CIC ^{MUT} , FUBP1 ^{MUT} , TCF12 ^{MUT} , NOTCH1 ^{MUT} , PIK3 ^{MUT} , CDKN2A ^{DEL} /CDKN2B ^{DEL} (2) G-CIMP (including MGMT promoter methylation) (3) 1p/19q-codeletion	~ 65–100	44 years 17.5 years
Astrocytic tumors, IDH-mutant, WHO grade II-III	(1) IDH1/2 ^{MUT} , TP53 ^{MUT} , ATRX ^{MUT} , heterozygous CDKN2A ^{DEL} /CDKN2B ^{DEL} (2) G-CIMP (including MGMT promoter methylation) (3) Trisomy 7 or 7q gain, LOH 17p	~ 85	36 years 8-12 years
Astrocytic tumors, IDH-wildtype, WHO grade II-III	(1) PTEN ^{DEL} , EGFR ^{AMP} , NF1 ^{DEL} , TP53 ^{MUT} , PIK3CA ^{MUT} , TERT ^p ^{MUT} (2) MGMT promoter methylation (3) Trisomy 7 or 7q gain, monosomy 10	~ 55	52 years 1.5-5 years
Glioblastoma, IDH-mutant, WHO grade IV	(1) IDH1/2 ^{MUT} , TP53 ^{MUT} , ATRX ^{MUT} , homozygous CDKN2A/B ^{DEL} (2) G-CIMP (including MGMT promoter methylation) (3) Trisomy 7 or 7q gain, LOH 17p, 10q deletion	~ 90	44 years 24-31 months
Glioblastoma, IDH-wildtype, WHO grade IV	(1) TERT ^p ^{MUT} , PTEN ^{DEL} , TP53 ^{MUT} , PIK3CA ^{MUT} , PIK3R1 ^{MUT} , NF1 ^{DEL} , H3F3A ^{MUT} , EGFR ^{AMP} , PDGRA ^{AMP} , MET ^{AMP} , CDK4 ^{AMP} , CDK6 ^{AMP} , MDM2 ^{AMP} , MDM4 ^{AMP} , CDKN2A ^{DEL} /CDKN2B ^{DEL} , EGFR ^{vIII} ^{MUT/DEL} (2) MGMT promoter methylation; (3) Trisomy 7 or 7q gain, monosomy 10, 9p loss, double minute chromosomes	~ 40	59 years 9.9-15 months

Based on [91, 105, 130, 231-234]. *Abbreviations:* AMP, amplification; ATRX, alpha thalassemia/mental retardation syndrome X-linked; CDK, cyclin-dependent kinase; CDKN2A/B, cyclin-dependent kinase inhibitor 2A/B; CIC, capicua transcriptional repressor; DEL, deletion; EGFR, epidermal growth factor receptor; FUBP1, far upstream element binding protein 1; G-CIMP; Glioma CpG island methylator phenotype; H3F3A, H3 histone, family 3A; IDH, isocitrate dehydrogenase; LOH, loss of heterozygosity; MDM2, murine double minute 2 homolog; MDM4, murine double minute 4 regulator of P53, MET, Tyrosine-Protein Kinase Met; MGMT, O6-methylguanine-DNA methyltransferase; MUT, mutation; NF1, neurofibromin 1; NOTCH1, Notch homolog 1, translocation-associated; PDGRA, platelet-derived growth factor receptor A; PIK3, phosphoinositide 3-kinase; PI3KCA, PIK3 catalytic, alpha polypeptide; PIK3R1, PIK3 regulatory subunit 1; PTEN, phosphatase and tensin homolog; TCF12, transcription factor 12; TERT^p, telomerase reverse transcriptase promoter; TP53, tumor protein p53

Single-gene/protein analyses can be performed using immunohistochemistry (IDH1-R132H, ATRX, TP53, H3-K27M, BRAF-V600E) or targeted molecular (cyto)genetic methods e.g. FISH, PCR-based techniques, and Sanger or pyrosequencing. In most centers, especially in developed countries, the tissue-based diagnostic process is further refined using newer molecular methods. NGS has already been established as a novel technique suitable for routine diagnostic applications for multiple gene analysis (e.g. gene panels) as well as examination of mutations, copy number changes, and gene fusions [163, 189, 235, 236]. Genome-wide DNA methylation profiling using DNA microarrays has also proven a useful molecular tool for the diagnosis of gliomas and other CNS tumors [198-200, 237-239]. A precise and reproducible classification is obtained by

comparing the DNA methylation profile of the tumor in question with the corresponding profile of several thousand selected reference tumors. Simultaneously, the method allows assessment of MGMT promoter methylation status, DNA CNV (e.g. 1p/19q-codeletion, *EGFR* amplification, the phosphatase and tensin homolog (*PTEN*) loss, cyclin-dependent kinase inhibitor 2A and B (*CDKN2A/B*) deletion), and chromosome 7/10 status [130, 132, 235, 238]. Several reclassification studies have shown that the implementation of the 2016 WHO histomolecular classification of diffuse gliomas improves the accuracy of diagnosis and prognostication of patient outcome [223, 236, 240-242].

The next three paragraphs give brief overviews of the most essential tumor entities included in thesis [91].

Oligodendroglial tumors, WHO grade II-III

Oligodendroglial tumors are defined as IDH-mutant and whole-arm 1p/19q-codeleted. Morphologically these tumors are often characterized by isometric rounded nuclei with perinuclear halos (“fried-egg” appearance) and a branching capillary network. Based on the level of anaplasia, oligodendroglial tumors are subdivided into oligodendrogliomas, WHO grade II, and anaplastic oligodendrogliomas, WHO grade III. MVP, brisk mitotic activity, microcalcifications and/or *CDKN2A* homozygous deletion are typical features for WHO grade III oligodendrogliomas [243]. Oligodendroglial tumors often have mutations in the *CIC* gene [152, 153] and *TERT* gene [244, 245]. A subset of the tumors also carry mutations in e.g. *FUBP1* [152, 153] or the transcription factor 12 (*TCF12*) gene [180, 246] (**Table 2**).

Astrocytic tumors, WHO grade II-III

Astrocytic tumors are classified as diffuse astrocytoma or anaplastic astrocytoma based on morphology and histology. Diffuse astrocytomas, WHO grade II, usually exhibit increased cellularity compared to normal brain tissue and contain moderately pleomorphic, highly-differentiated, and slow-growing cells that have low mitotic activity. Anaplastic astrocytoma, WHO grade III, are characterized by focal or dispersed anaplasia with nuclear atypia, high cellularity, and significant mitotic activity, but without the presence of necrosis and MVP. Anaplastic astrocytomas can arise from grade II astrocytoma, but are often diagnosed without indication of a less-malignant precursor lesion. Astrocytic tumors tend to progress to glioblastomas over time.

Astrocytic tumors are more importantly classified based on IDH mutation status. The diagnosis of IDH-mutant astrocytic tumors is supported by the presence of mutations in *ATRX* (resulting in loss) and *TP53* (resulting in overexpression) as well as absence of 1p/19q-codeletion (**Table 2**). IDH-wildtype diffuse astrocytomas and anaplastic astrocytomas are considered provisional entities and is believed to largely comprise histologically underdiagnosed IDH-wildtype glioblastomas due to their clinical behavior [247]. In fact, in the Consortium to Inform Molecular and Practical Approaches to CNS Tumor Taxonomy (cIMPACT-NOW) updates 3 and 6 from 2018 and 2020 [233, 234], it was concluded that IDH-wildtype astrocytic tumors with *EGFR* amplification, the combination of whole chromosome 7 gain and whole chromosome 10 loss (+7/-10), or *TERT* promoter mutations correspond to WHO grade IV tumors and should be designated as glioblastomas [163, 233, 234, 248-250]. However, some studies show that IDH-wildtype astrocytomas do constitute a diagnosable entity from a histological, molecular, and prognostic standpoint [174, 251, 252].

Table 3 | Transcriptional subtypes and methylation subclasses of glioblastoma

Phillips <i>et al.</i> [10]	Proneural		Proliferative		Mesenchymal
Verhaak <i>et al.</i> [11]	Proneural		Neural §	Classical	Mesenchymal
Neftel <i>et al.</i> [9]	NPC-like and/or OPC-like		-	AC-like	MES-like
Cellular morphology	Astrocytic or oligodendroglial		Astrocytic, oligodendroglial, neural	Astrocytic	Astrocytic
Histological markers	TP53, OLIG2, DLL3, SOX2		MBP, SNCG, FBXO3, GABRA1	EGFR, AKT2, NES	CHI3L1, CD44, VEGF, TLR2/4, MET
Tissue similarities	Adult or fetal brain		Hematopoietic stem cell, lymphoblast		Bone, cartilage, smooth musculature, endothelium, dendritic cells
Biological process	Neurogenesis, cell cycle proliferation		Proliferation and anti-apoptosis		Angiogenesis, inflammation
Signaling pathways	PI3K		EGFR, NOTCH1		Akt, MAPK, mTOR, NFκB, TNF, TGFβ, interleukins
Immune component	Low		Low/intermediate		High
IDH status	Mutant	Wildtype	Wildtype		Wildtype
Necrosis	↓	↓ / -	- / ↑		↑
Evolution of gene expression signature	Arises in lower-grade astrocytoma	Arises in <i>de novo</i> , may persist or convert to mesenchymal	Arises in primary tumors, may persist or convert to mesenchymal		Arises in primary tumors or by conversion from other subtype
Genetic alterations	TP53 ^{MUT} ATRX ^{MUT} CDKN2A/B ^{DEL}	PDGFRA ^{AMP} TP53 ^{MUT} SOX2 ^{AMP} CDK4 ^{AMP}	EGFR ^{AMP} Chr7+ Chr10- CDKN2A ^{DEL}		NF1 ^{DEL}
G-CIMP	Yes	No §§	No		No
Methylation class [253]	IDH	RTK I	RTK II		Mesenchymal
MGMT promoter methylation (%)	~ 90	~ 40	~ 40		~ 40
Age group	Mostly young adults		Mostly older adults		
Median overall survival (months)	~ 30	~ 12-14			

Based on [9-12, 17, 173, 174, 235, 253-258]. § The neural subtype is not well-defined and may be a result of sample contamination by non-malignant tissue/cells (oligodendrocytes and neurons). §§ A few IDH-wildtype proneural glioblastomas may be G-CIMP [173]. *Abbreviations:* AC-like, astrocyte-like; Akt, protein kinase B/serine/threonine kinase; AMP, amplification; ATRX, alpha thalassemia/mental retardation syndrome X-linked; CD, cluster of differentiation; CDK, cyclin-dependent kinase; CDKN2A/B, CDK inhibitor 2A/B; CHI3L1, chitinase 3-like; Chr, chromosome; DLL3, delta-like 3; EGFR, epidermal growth factor receptor; FBXO3, F-Box Protein 3; GABRA1, Gamma-Aminobutyric Acid Type A Receptor Subunit Alpha1; G-CIMP; Glioma CpG island methylator phenotype; IDH, isocitrate dehydrogenase; MAPK, mitogen-activated protein kinase; MBP, maltose-binding protein; MES-like, mesenchymal like; MET, Tyrosine-Protein Kinase Met; mTOR, mammalian target of rapamycin; MUT, mutation; NES, nestin; NF1, neurofibromin 1; NFκB, nuclear factor kappa-light-chain-enhancer of activated B cells; NOTCH1, Notch homolog 1, translocation-associated; NPC-like, neural progenitor-like; OLIG2, oligodendrocyte transcription factor 2; OPC-like, oligodendrocyte progenitor-like; PDGFRA, platelet-derived growth factor receptor A; PIK3, phosphoinositide 3-kinase; RTK, receptor tyrosine kinase; SNCG, Gamma-synuclein; SOX2, sex determining region Y-box 2; TGFβ, transforming growth factor beta; TLR, toll-like receptor; TNF, tumor necrosis factor; TP53, tumor protein p53; VEGF vascular endothelial growth factor

Glioblastoma, WHO grade IV

Glioblastoma is the most common and malignant type of glioma. Glioblastomas are subdivided into two entities based on IDH mutation status, namely the most frequent IDH wildtype glioblastoma, which comprises more than 90% of all glioblastomas, and the less common IDH-mutant glioblastoma which accounts for less than 10%. Most of the IDH-wildtype glioblastomas are primary glioblastomas which are typically seen in elderly patients and develop rapidly *de novo*, i.e. without a pre-existing lower-grade precursor lesion. In contrast, IDH-mutant glioblastomas usually occur in younger adults, and this entity includes the secondary or *evolved* glioblastomas which arise through progression from a pre-existing IDH-mutant grade II-III astrocytoma [161, 177, 259]. From a histopathological viewpoint, IDH-wildtype and IDH-mutant glioblastomas are similar, although, the amount of necrosis is often limited in IDH-mutant glioblastomas [177, 259, 260]. However, the distinction of IDH-wildtype and IDH-mutant glioblastoma is important as these two entities are biologically separate and correlate with different clinical features including age at onset and overall survival (**Tables 2 and 3**) [145, 161, 177, 209, 259, 261].

Histologically, glioblastomas are highly heterogeneous, but usually very cellular tumors with poorly differentiated and sometimes pleomorphic cells with extensive nuclear atypia. Prominent MVP and/or necrosis are hallmarks of glioblastoma and essential diagnostic features (**Figure 6**). Further, brisk mitotic/proliferative activity, especially focally, is often observed. Several cellular morphologies appear in glioblastomas, also within the same tumor (**Figure 6**). Some of the morphologies have been associated with specific genetic alterations, e.g. *BRAF* mutations often are found in epitheloid glioblastomas [228, 229], while small cell glioblastomas frequently have *EGFR* amplification and loss of chromosome 10. In contrast, giant cell glioblastoma and gliosarcomas rarely exhibit *EGFR* amplification, but are instead characterized by frequent mutations in *TP53* and *PTEN*, respectively [91].

Genetically and epigenetically, glioblastomas show a high level of both intra- [6-9, 258, 262-264] and interheterogeneity [9-13, 174, 253, 257, 258, 264], and several genetic aberrations have been reported in glioblastomas (**Table 2**). IDH-wildtype glioblastomas often carry mutations in in the *TERT* promoter and *PTEN* gene. Other frequent alterations are monosomy of chromosome 10, gain of chromosome 7 or 7q, losses on 9p involving the *CDKN2A/B* gene loci, and amplifications of proto-oncogenes e.g. *EGFR*. IDH-mutant glioblastomas rarely exhibit *EGFR* amplification and *PTEN* mutations, but instead show loss of *ATRX* expression and often have mutations in *TP53* [12, 141, 259]. Transcriptomics have identified four subtypes of glioblastoma: proneural, neural, classic and mesenchymal [10, 11] (**Table 3**). The mesenchymal subtype has been linked to radio-resistance [17, 265], poor survival [17, 258, 266], and a higher level of immune infiltration of T cells and myeloid cells [17, 255, 256, 258, 267, 268], whereas the proneural subtype has been associated with a benefit from anti-angiogenic treatment in patients with IDH-wildtype glioblastoma [269]. The classical subtype reportedly is the most sensitive to treatment [11] and is often lost in post-treatment recurrent tumors in favor of especially the mesenchymal subtype [258, 267, 270], suggesting that therapy provides a competitive advantage for non-classical subclones within the glioblastoma. Yet, the clinical relevance of stratifying patients according to these expression signatures is overall limited, as the signature can change as a result of clonal

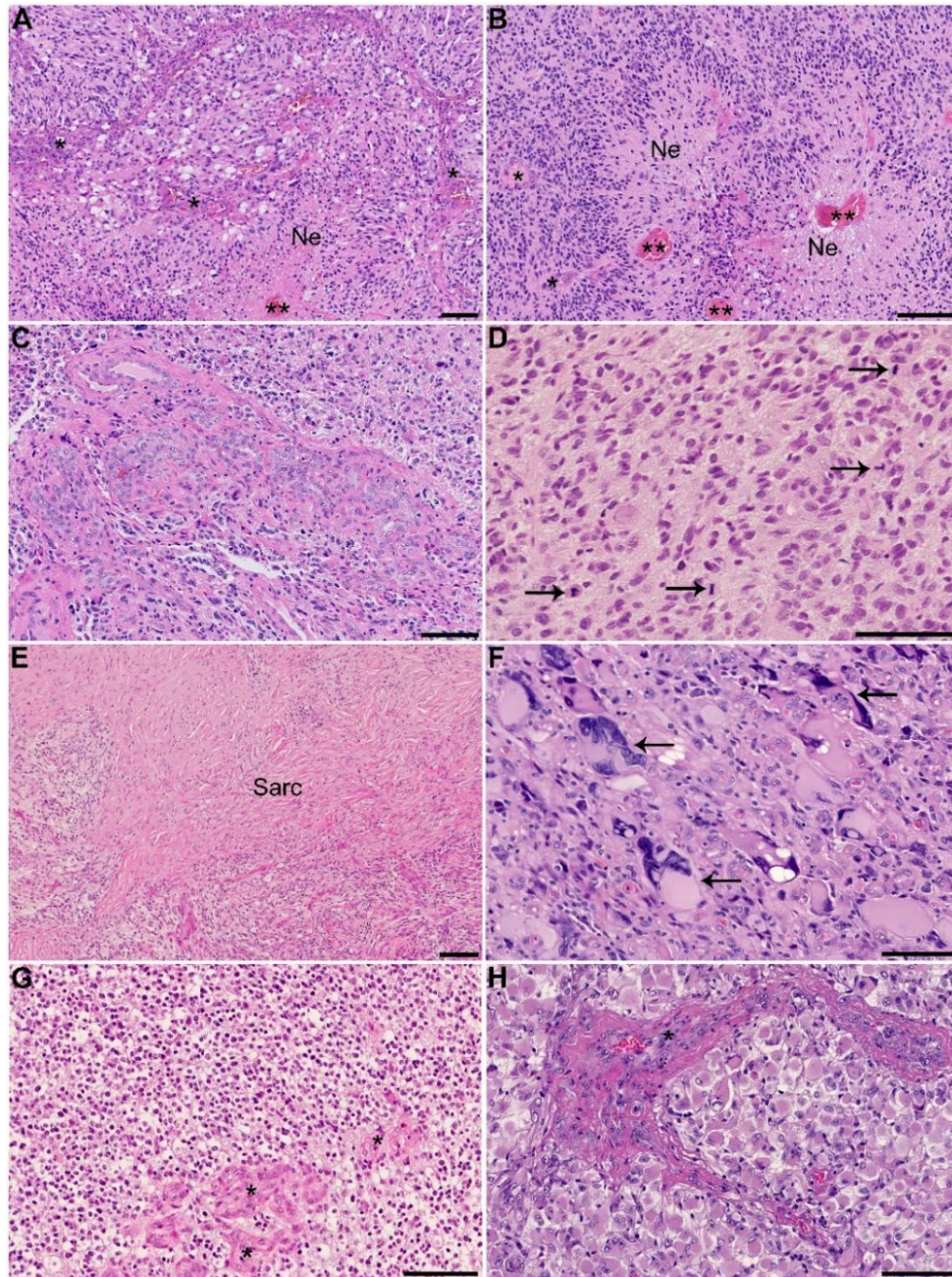


Figure 6 | Examples of histological features of glioblastomas. **(A, B)** Microvascular proliferations (MVP, *) and palisading necrosis (*Ne*) are often observed. Palisade formation is thought to occur due to endothelial injury and intravascular coagulation (**) resulting in perivascular hypoxia, cell migration (= palisading cells), and vascular proliferation. Larger necrotic areas are regularly seen, and the necrotic component can vary from small amounts to more than 80% of the tumor mass. **(C)** Frequently MVP can be seen as glomeruloid tufts which consist of multilayered mitotically active endothelial cells together with smooth muscle cells/pericytes. **(D)** Glioblastomas often exhibit a high mitotic activity (*right arrows* indicate mitosis). **(E)** Glioblastomas with gliosarcoma morphology are characterized by a biphasic tissue pattern with areas displaying glial and mesenchymal (sarcomatous, *Sarc*) differentiation. Gliosarcomas comprise ~2% of all glioblastomas and can present *de novo* or appear during the post-treatment phase. **(F)** Glioblastoma with high degree of anaplasia and multiple multinucleated giant cells (*left arrows*). **(G)** Glioblastoma with a focal oligodendroglioma-like component. **(H)** Glioblastoma consisting primarily of cells with rich cytoplasm and displaced peripheral nuclei, also designated gemistocytic cells. * signifies glomeruloid tufts in **G** and **H**. Scale bar 100 μ M.

evolution [6, 17, 258, 266], and multiple signatures can coexist within the same tumor [6, 7, 9, 258]. Instead DNA methylation profiling has been proven more useful for stratification of glioblastomas based on epigenetic and genetic expression patterns [12, 253]. Four major methylation classes of adult glioblastoma have been identified: an IDH-mutant, G-CIMP/hypermethylated and often MGMT promoter methylated subclass with proneural gene expression profile, and three IDH-wildtype, hypomethylated subclasses (**Table 3**). Among the IDH-wildtype subgroups, the ‘receptor tyrosine kinase I’ (RTK I) subclass is characterized by platelet-derived growth factor receptor A (*PDGFRA*) amplification and a proneural profile, and this type of glioblastoma is mainly detected in adolescents and young adults. The ‘RTK II’ and the ‘mesenchymal’ IDH-wildtype subclasses predominate in older adults (>50 years), are distinguished by different DNA methylation profiles, and correlate with the classical and mesenchymal transcriptional subtypes [12]. However, multiple methylation subclasses also coexist in each tumor [263, 264]. MGMT promoter methylation may also vary within the same tumor [262, 263], indicating that the intratumoral heterogeneity in DNA methylation needs to be taken into account to improve the diagnostic accuracy for glioblastomas.

7.2.3 Prognostic factors in diffuse gliomas

Numerous studies have investigated the prognostic value of both clinical and biological parameters (**Figure 7**) to identify patients who will benefit from treatment and those who will not benefit from treatment.

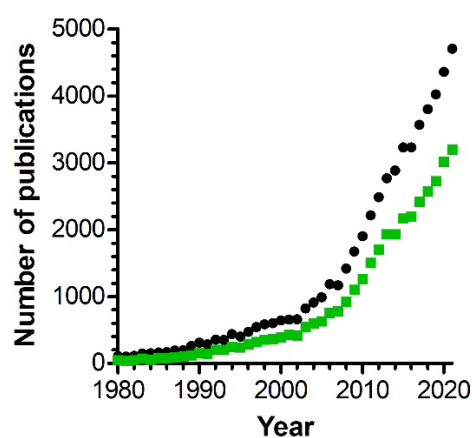


Figure 7 | Timeline of the number of publications related to prognosis and/or biomarkers in gliomas, indexed according to year (1980-2021) in PubMed. The black curve illustrates the number of publications containing the term “(glioma OR glioblastoma OR astrocytoma OR oligodendroglioma) AND (prognosis OR biomarker OR (survival analysis) OR survival)” and the green curve illustrates the number of publications containing the terms “(glioma OR glioblastoma OR astrocytoma OR oligodendroglioma) AND (prognosis OR biomarker)”.

Regarding clinical parameters, younger age and better performance status have consistently been reported as important positive, therapy-independent prognostic factors across glioma entities. Further, a tumor not crossing the midline may also be positive prognostic factor. Extent of resection and post-surgical treatment are important therapy-dependent prognostic factors [143, 221, 261, 271-276]. As mentioned in the previous sections, molecular markers that favor longer survival, e.g. IDH mutation and 1p/19q-codeletion, are now at the core of the WHO classification and define more homogeneous diagnostic and prognostic entities. Thus, prognosis for patients diagnosed with diffuse gliomas now largely depends of IDH mutation, histological entity (i.e. oligodendroglial vs. astrocytic), and WHO grade. IDH-mutant gliomas have superior survival compared to IDH-wildtype also irrespective of WHO grade [137, 148, 170, 173-179, 181]. Similar results were reported for G-CIMP (i.e. hypermethylated) tumors compared to non-G-CIMP- tumors [173]. Patients diagnosed with

oligodendroglial tumors generally have a better prognosis than patients with astrocytic tumors regardless of WHO grade [193, 194, 277]. Patients with grade III oligodendroglioma seem to have a survival detriment compared to patients with grade II oligodendroglioma, suggesting that histological grading has some value in the clinic [236, 242]. Among the IDH-mutant astrocytic tumors including glioblastomas, histological grade has shown some prognostic value as patients with IDH-mutant diffuse astrocytomas, grade II, survive longer than patients with IDH-mutant anaplastic astrocytomas, grade III, and patients with IDH-mutant glioblastomas have the poorest prognosis [145, 232, 236, 242]. In contrast, WHO grade has limited prognostic value in IDH-wildtype astrocytic tumors and glioblastomas; patients with IDH-wildtype diffuse astrocytoma, grade II, without molecular features of glioblastoma show a survival benefit compared to IDH-wildtype anaplastic astrocytomas, grade III, and IDH-wildtype glioblastomas, grade IV, whereas no significant prognostic difference is found between anaplastic astrocytomas and glioblastomas [145, 223, 236, 240-242, 247].

7.2.4 The 2021 WHO classification of diffuse gliomas

The classification of gliomas underwent major changes through the revision of the fourth edition of the WHO classification of Tumors of the CNS in 2016. In the 2021 WHO classification further refinements were made, especially based on the cIMPACT-NOW recommendations [234, 278, 279]. These adjustments involve tumor nomenclature and grading within the tumor types/entities as well as an emphasis on the importance of histomolecular classification. The 2021 edition recognizes the clinical and molecular/biological distinctions between diffuse gliomas that occur primarily in adults (adult-type) and those that occur mostly in children/young adults (pediatric-type). Moreover, the classification of adult-type diffuse gliomas has been simplified and now only comprise three entities: 1) astrocytoma, IDH-mutant, 2) oligodendroglioma, IDH-mutant and 1p/19q codeleted, and 3) glioblastoma, IDH-wildtype. Grading is performed now within the tumor types based on histological *and* molecular features using Arabic numerals (rather than Roman numerals), and modifier terms like “anaplastic” are omitted. The term “glioblastoma” is no longer used to refer to IDH-mutant astrocytic gliomas because these tumors are biologically distinct from IDH-wildtype glioblastomas, even though their histological appearance is similar. Instead, IDH-mutant glioblastoma is now referred to as astrocytoma, IDH-mutant, WHO grade 4 [2, 168, 276]. An overview of the most essential entities of diffuse gliomas in adults is presented in **Figure 8**. Of note, astrocytic gliomas with wildtype status of IDH and histone H3 should be evaluated for glioblastoma-associated genetic alterations in the absence of necrosis or MVP. If one or more of these alterations is found, the glioma can be classified as glioblastoma given their correlation with shorter survival [249]. IDH-wildtype diffuse astrocytomas without any of these alterations, which cannot be assigned to other entities, e.g. on the basis of DNA methylation profiling, are more often seen in pediatric, adolescent, or young adult patients and constitute rare glioma variants that require further molecular assessment [247]. As such, grade 2-3 IDH-wildtype astrocytomas no longer exist as separate tumor entities according to the 2021 WHO classification.

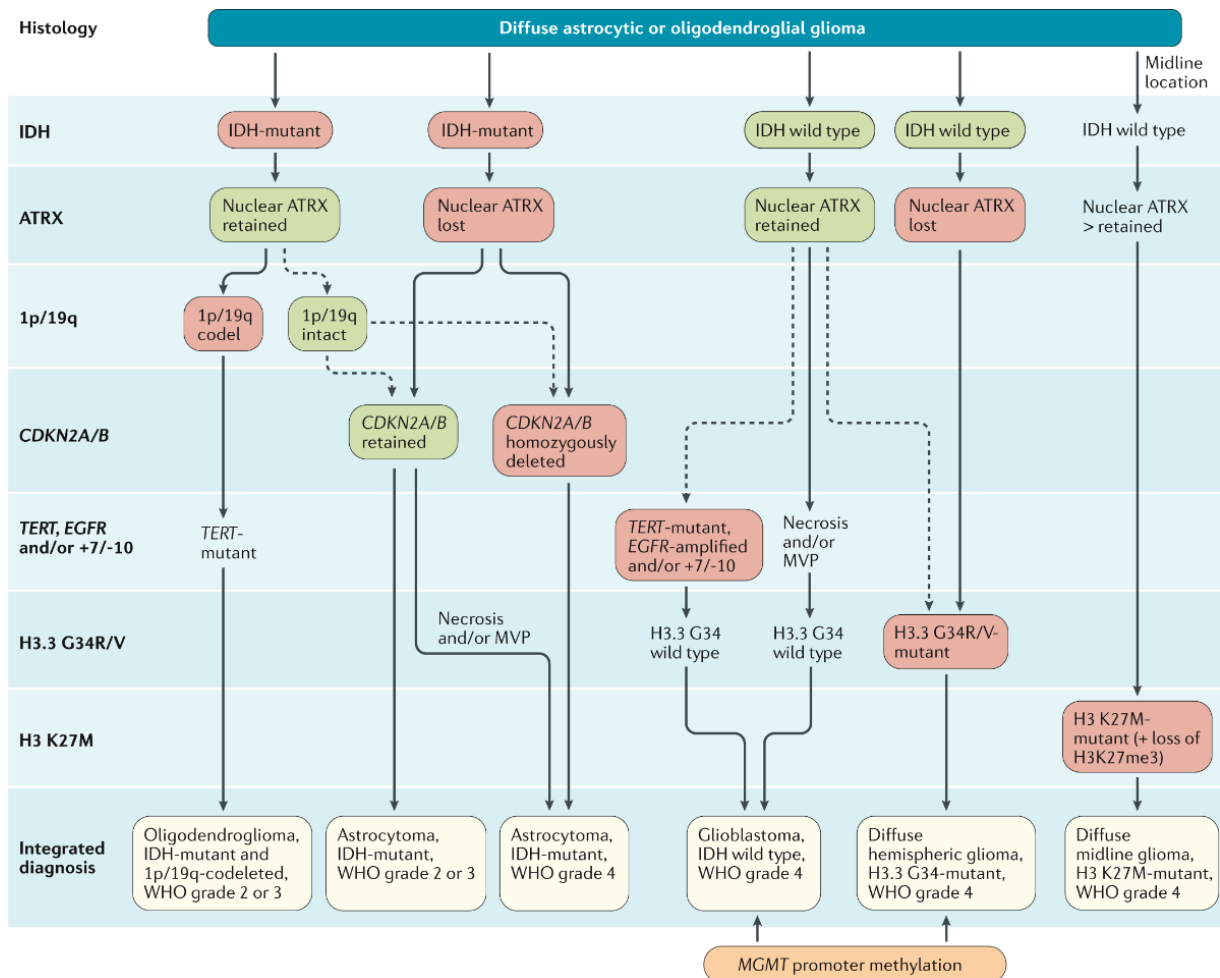


Figure 8 | Diagnostic algorithm for integrated classification of the major diffuse gliomas according to the WHO classification 2021. Tumor specimens are morphologically evaluated using H&E stains. If the diagnosis ‘diffuse glioma’ is suspected, the tumor is evaluated for the isocitrate dehydrogenase mutation, IDH1-R132H, and loss of nuclear ATRX protein expression using immunohistochemistry. IDH1 R132H immuno-negativity is sufficient for the classification as glioblastoma, IDH-wildtype, in patients aged >55 years if following criteria are met: 1) a histologically typical glioblastoma (i.e. presence of necrosis and/or MVP), 2) no pre-existing lower-grade glioma, 3) a non-midline tumor location, and 4) retained nuclear ATRX expression. In all other cases of diffuse glioma, molecular analyses are performed for detection/exclusion of non-canonical *IDH* codon mutations. IDH-wildtype astrocytic gliomas without MVP or necrosis should be tested for *EGFR* amplification, *TERT* promoter mutation and a 7+/-10- cytogenetic signature and then classified as glioblastoma if one or more of these molecular features are present. Additionally, the presence of histone H3.3 G34R/V mutations should be assessed by immunohistochemistry or DNA sequencing to identify H3 G34-mutant diffuse hemispheric gliomas. Diffuse gliomas of the thalamus, brainstem or spinal cord should be evaluated for histone *H3 K27M* mutations. Oligodendrogliomas are still defined as IDH-mutant tumors that harbor 1p/19q-codeletion and are stratified into grade 2 or 3 based on histological features and/or presence of *CDKN2A* homozygous deletion. *IDH* mutation and loss of nuclear ATRX expression classify IDH-mutant astrocytomas, and additional molecular testing for 1p/19q-codeletion is not routinely required, but might be performed to further corroborate the diagnosis. IDH-mutant astrocytomas are stratified into grade 2, 3, or 4 based on histomolecular features including 1) presence of anaplasia, 2) level of mitotic activity, 3) presence of MVP or necrosis, and 4) presence of homozygous deletions of *CDKN2A/B*. Reprinted from Weller *et al.* 2021 [276] under the terms and conditions provided by Springer Nature and the Creative Commons Attribution 4.0 International License.

7.3 Treatment of gliomas

The next subsections provide brief overviews of the most important treatment strategies for diffuse gliomas.

7.3.1 First-line treatment

Surgery

Resection is most common and important initial treatment for gliomas [89, 221, 280-282]. The goal of surgery is maximum safe resection to obtain a histomolecular diagnosis, improve neurological function, provide symptomatic relief, and prolong patient survival. If surgical resection is not feasible, image-guided stereotactic serial biopsy should be performed to obtain a diagnosis. Today, microsurgical techniques are standard, and several useful intraoperative tools are becoming more frequent to increase the extent of resection while minimizing the risk of introducing new neurological deficits. Among these tools are intraoperative neuro-navigation, intraoperative magnetic resonance imaging (MRI), intraoperative functional monitoring using electrophysiological brain mapping, intraoperative ultrasound and ultrasonic aspiration as well as fluorescence-guided surgery with 5-aminolevulinic acid to visualize residual tumor tissue. The extent of surgical resection should be verified by contrast-enhanced MRI within 24-48(72) hours of surgery. A large residual tumor volume is a negative prognostic factor [89, 221, 280-282]. Despite successful gross total resection, some tumor cells are always left behind due to the infiltrative nature of gliomas, especially glioblastomas, and almost all gliomas recur or progress [283]. Treatment of patients with diffuse glioma is hence never curative, but only life-prolonging. To prevent early recurrence/progression, postsurgical treatment consisting of radiation and/or cytotoxic chemotherapy is standard-of-care for most glioma patients (**Table 4**).

Radiotherapy

The goal of radiotherapy is to improve local tumor control, preserve neurological function and increase progression-free and/or overall survival. Indications for timing, dosing, and scheduling of radiotherapy are determined by diagnosis and prognostic factors, including patient age, performance status, and extent of resection [89, 221, 280-282, 284]. Generally, lower-grade diffuse gliomas, WHO grade II, do not receive early radiation unless they have persisting symptoms or residual tumor [221, 285]. Patients with higher-grade gliomas, WHO grade III-IV, often receive radiation. Standard radiotherapy is delivered in 1.8–2 Gy fractions to a total dose of 54–60 Gy. Hypofractionated radiotherapy with higher fraction sizes and lower total dose e.g. 34-40 Gy in 10-15 fractions is a valid option for older patients and for patients poor functional status and is considered biological equivalent of 60 Gy [219]. Radiotherapy can also be withheld in elderly patients or patients with poor performance status if the tumor has methylated MGMT promoter [215]; instead these patients can be treated with chemotherapy alone (i.e. the alkylating chemo agent TMZ) [89, 221, 280-282].

Chemotherapy

For lower-grade diffuse gliomas, WHO grade II, PCV is standard-of-care preceded by radiation if further treatment beyond surgery is necessary [221, 286]. Patients diagnosed with anaplastic oligodendrogliomas are

Table 4 | Current post-surgical treatment regimens for patients with diffuse glioma

WHO glioma entity	Post-surgical treatment	Comment
Oligodendroglioma, IDH-mutant, 1p19q-codeleted, WHO grade II	Observation	Standard-of-care
Diffuse astrocytoma, IDH-mutant, WHO grade II	RT (50.4 Gy / 28 F) + adjuvant PCV	Residual tumor, persisting symptom, or high risk of progression
Diffuse astrocytoma, IDH wildtype, WHO grade II [§]		
Anaplastic oligodendroglioma, IDH-mutant, 1p19q-codeleted, WHO grade III	RT (59.4 Gy / 33 F) + adjuvant PCV	Standard-of-care
Anaplastic astrocytoma, IDH-mutant, WHO grade III	RT (59.4 Gy / 33 F) + adjuvant TMZ	Standard-of-care
Glioblastoma, IDH-mutant, WHO grade IV	RT (60 Gy / 30-33 F) + concomitant TMZ and adjuvant TMZ	Standard-of-care (Stupp regime)
Glioblastoma, IDH-wildtype, WHO grade IV	Hypofractionated RT (34 Gy/10 F or 40 Gy/15F) + concomitant TMZ (possibly adjuvant TMZ)	PS 0-2 with significant comorbidity or age > 70 years ^{§§}
Anaplastic astrocytoma, IDH-wildtype, WHO grade III		
Diffuse astrocytic glioma, IDH-wildtype, with molecular features of glioblastoma	Hypofractionated RT (34 Gy/10 F or 40 Gy/15F) monotherapy (u-MGMT)	

Based on [89, 221, 276, 280, 281, 285]. [§] Without molecular features of glioblastoma (i.e. no *EGFR* amplification, combined 7+/10-, or *TERT* promoter mutation). ^{§§} In elderly patients with good performance status (PS 0-2), standard treatment regime according to Stupp *et al.* [5] can be considered. *Abbreviations:* F, fractions; *IDH*, isocitrate dehydrogenase; *MGMT*, O6-methylguanine DNA methyltransferase; *m-MGMT*, methylated MGMT promoter; *PCV*, procarbazine–lomustine–vincristine; *PS*, performance status; *RT*, radiotherapy; *TMZ*, temozolomide; *u-MGMT*, unmethylated MGMT promoter; *WHO*, World Health Organization

usually offered PVC as adjuvant chemotherapy to resection and radiation [194]. For anaplastic astrocytomas, IDH-mutant, standard post-surgical treatment consists of radiation followed by TMZ [193, 194, 287]. For treatment of glioblastomas, both IDH-mutant and IDH-wildtype, current standard-of-care was introduced in 2005 [5]. Here, Stupp *et al.* published the results from a randomized, multicenter, phase III clinical trial with patients newly diagnosed with glioblastomas, who were treated with either radiation as monotherapy or radiation with concomitant and adjuvant TMZ. Addition of TMZ increased 2-year survival from 10% to 27% and reduced the relative risk of death by 37 % for patients treated with radiotherapy plus TMZ, as compared with those who received radiotherapy alone. The median survival benefit was 2.5 months (14.6 months vs. 12.1) [5]. The benefit of adding TMZ to the postsurgical treatment regime remained significant at the 5-year follow-up [96]. TMZ is an alkylating, small lipophilic drug capable of crossing the blood-brain barrier (BBB) and causes DNA damage mainly by methylation of the O6-position of guanine. The methylation leads to a mismatch with thymine resulting in double-strand breaks and ultimately cell cycle arrest and apoptosis [288]. In normal cells, the DNA damage is mainly repaired through the actions of the MGMT enzyme, as mentioned previously. Hegi *et al.* showed that the response to TMZ in glioblastoma patients depended on the methylation status of MGMT gene promoter region, and a survival benefit of combination therapy with radiation and TMZ was only observed in patients with methylated MGMT promoter which results in an inactivation of the MGMT gene and loss of enzyme expression. In glioblastomas that lack MGMT promoter methylation, TMZ has little

or no benefit [208]. Because MGMT promoter methylation status is predictive of the efficacy of TMZ [208], TMZ can be withheld in patients with poorer functional status and/or elderly patients whose glioblastomas have unmethylated MGMT promoters [215, 219, 281]. No additional survival benefit was found by performing dose-dense TMZ regimens [213], extending the length of adjuvant TMZ treatment beyond 6 cycles [289], or supplementing with anti-angiogenetic vascular endothelial growth factor (VEGF)-targeting antibody bevacizumab (Avastin®) [221, 281, 282, 290-293].

Supportive care

Regardless of performance status, best supportive care is offered to all patients dependent on the symptomatology. Corticosteroids can be prescribed to reduce peritumoral edema relieving neurological deficits and signs of increased intracranial pressure e.g. headaches and drowsiness, but use of corticosteroids should be avoided if possibly as it may worsen clinical outcome in patients by effecting treatment response and inducing an immunosuppressive TME [294-299]. Seizures are frequently seen in especially lower-grade and/or IDH-mutant tumors and can be treated with anti-epileptic drugs [281].

7.3.2 Recurrence

The intrinsic capacity of glioma cells to diffusely infiltrate the normal brain parenchyma impedes surgical eradication, and despite standard-of-care therapy, almost all patients with glioma relapse eventually and require additional treatment. For glioblastoma, well-selected patients in clinical trials have a median overall survival between 15-18 months [5, 213, 290], and a 5-year survival is below 10% [96]. Glioblastomas typically progress after a median interval of less than 7 months [5], and once the tumor recurs, median overall survival is estimated 24-44 weeks. In most cases, the tumor relapses locally within 2-3 cm of the resection cavity [283, 300], but lesions may also manifest in the contralateral hemisphere of the primary tumor as tumor cells migrate along white matter tracts and blood vessels [283, 301]. Treatment of recurrent tumors is less standardized, and clinical decision-making is influenced by prior treatment, age, performance status, and patterns of progression. Resection/surgical debulking or re-irradiation is possible for some patients, but most patients receive second-line systemic therapy with alkylating agents (e.g. TMZ or lomustine) or bevacizumab (possibly in combination with irinotecan) in an attempt to prolong progression-free survival and/or overall survival or to provide symptomatic relief [89, 302-307].

7.3.3 Novel therapies

The standard-of-care treatment in patients with diffuse gliomas has fundamentally remained unchanged since 2005, while advances in targeted therapies and immunotherapies are swiftly improving outcomes in many other cancer types. One of the newest treatment modalities for patients with glioblastoma is tumor-treating fields (TTFields). TTFields are low-intensity, intermediate-frequency (200 kHz) alternating electrical fields, which are applied to the tumor region using specific transducer arrays to ultimately produce antimetabolic effects selective for tumor cells with limited toxicity. Administration of TTFields in patients with recurrent glioblastomas reportedly has limited effect [308]. Inversely, adding TTFields to maintenance TMZ in patients

with newly diagnosed glioblastoma prolonged progression-free survival (6.7 months vs. 4.0) and overall survival (20.9 months vs. 16.0 months) compared with standard treatment alone [309]. Upfront treatment with TTFields may therefore be beneficial to eligible patients [281]. Other therapeutic approaches, including targeted/precision and immunological therapies, are being tested in various clinical trials in both patients with newly diagnosed and recurrent glioblastomas. Targeted therapies (e.g. EGFR and BRAF inhibitors/peptide vaccines) have so far shown limited efficacy, most likely due to the BBB, redundant signaling pathways and tumor plasticity [9, 15, 227, 281, 310, 311]. Until now immunotherapies have proved tolerable and safe in patients with glioblastomas [312, 313], but failed to show any significant and lasting survival benefit [79, 80, 296, 314-316], possibly due to intrinsic, adaptive, and acquired resistance mechanisms [22, 28, 315, 317, 318].

7.4 The tumor microenvironment

Gliomas, and especially glioblastomas, unveil a rich TME with various parenchymal non-neoplastic cell types that all play a part in the shaping and making of the tumor biology (**Figure 9**). Among these cell types are both specialized brain-resident cells (e.g. microglia, brain endothelial cells, astrocytes, oligodendrocytes, oligodendrocyte progenitor cells, and neurons) and infiltrating cells originating from the bone marrow (e.g. lymphocytes, monocytes/macrophages, neutrophils, mast cells, dendritic cells, and endothelial progenitor cells) [14, 319]. These cell types are often distinguished using cell-type specific markers [319, 320]. The TME continuously evolves during tumorigenesis and tumor progression through a complex and dynamic interplay between tumor cells and the non-neoplastic host cells as well as the extracellular matrix components [14] which in concert contribute to the different hallmarks of cancer (**Figure 10**) [321, 322]. Increasing evidence indicates that the non-neoplastic cells of the TME are recruited and then corrupted by the tumor cells to perform tumor-cooperating functions. The reciprocal communication between the cells in the TME is orchestrated by a network of cytokines, chemokines, growth factors, inflammatory factors, and matrix remodeling enzymes in a setting characterized by major disruptions of the physical and chemical properties of the tissue [322]. The evolution, structure and activities of the cells in the TME in many ways resemble the processes of wound healing and inflammation. These processes are partly activated downstream of oncogenic mutations in the tumor cells [321, 323]. The failure of many tumor-targeted therapies has led scientists to explore the potential of targeting the other cells/components within the TME including the vasculature, cancer metabolism, hypoxia, and the TIME [14, 66, 324-326].

----->

Figure 9 | Schematic depiction of the major cellular components of the brain TME. The tumor cells use various modes of communication to hijack the different cell types to support tumor progression. Communication routes include secretion of soluble factors and extracellular vesicles, direct cell-cell contact with gap junctions as well as tunneling nanotubes and microtubes. As the tumor grows, the milieu becomes increasingly hypoxic/necrotic, acidic, and angiogenic, resulting in formation of different niches such as the perinecrotic, perivascular and invasive niches. Within these niches, **cancer stem cells** (CSC) reside, and these cells may be responsible for tumor initiation, progression and resistance [327, 328]. **Endothelial cells** provide oxygen and nutrients to the CNS and play a crucial role in the BBB. **Pericytes** are perivascular cells that support the integrity of the BBB and provide hemodynamic stability. Tumor cells exploit endothelial cells and

pericytes to enable neovascularization and invasion [319, 329, 330]. **Neurons** represent the functional component of the nervous system responsible for information processing and transmission. Neurons may fuel tumor proliferation through secretion of activity-regulatory factors, such as neuroligin-3. In turn, tumor cells secrete neuromodulators, e.g. glutamate, to promote tumor growth/migration [331, 332]. **Oligodendrocytes** arise from oligodendrocyte progenitor cells (OPCs) [333] and are the myelinating cells of the CNS ensuring efficient axonal conduction. Oligodendrocytes also provide metabolic and trophic support to neurons [334]. Little is known about oligodendrocytes/OPCs in brain tumors, however, OPCs co-localize with microglia at the tumor border, possibly contributing to cancer stemness and chemo-radio-resistance [335], and oligodendrocytes promote tumor invasion [336]. **Astrocytes** provide structural and nutritional support to the BBB and neurons and regulate synaptic transmission. During neoplasia, tumor cells activate astrocytes, and these reactive astrocytes may facilitate tumor maintenance and progression [337-342]. **Tumor-associated macrophages (TAM)** and **microglia** are innate immune cells recruited to the site of the tumor through the action of various soluble factors released by especially the tumor cells. In turn, TAMs secrete several pro-tumorigenic molecules to stimulate angiogenesis, tumor proliferation, migration/invasion and niche formation [30, 31]. **Myeloid-derived suppressor cells (MDSC)** are a small group of myeloid progenitors including immature mononuclear and polymorphonuclear cells, which morphologically and phenotypically resemble monocytes and neutrophils, respectively. MDSCs are practically nonexistent in the circulation of healthy individuals, but expand and polarize into highly immunosuppressive cells during tumorigenesis due to growth factors produced in the TME [343]. **T cells** are lymphoid cells of the adaptive immune system. Different T cell populations exist in the TME, including cytotoxic T cells, T helper cells, and regulatory T cells. When entering the TME, T cells are often re-educated into an exhausted, immunosuppressive phenotype [14, 344]. Reprinted from Lauko *et al.* [345] under the terms and conditions provided by Elsevier and the Copyright Clearance Center.

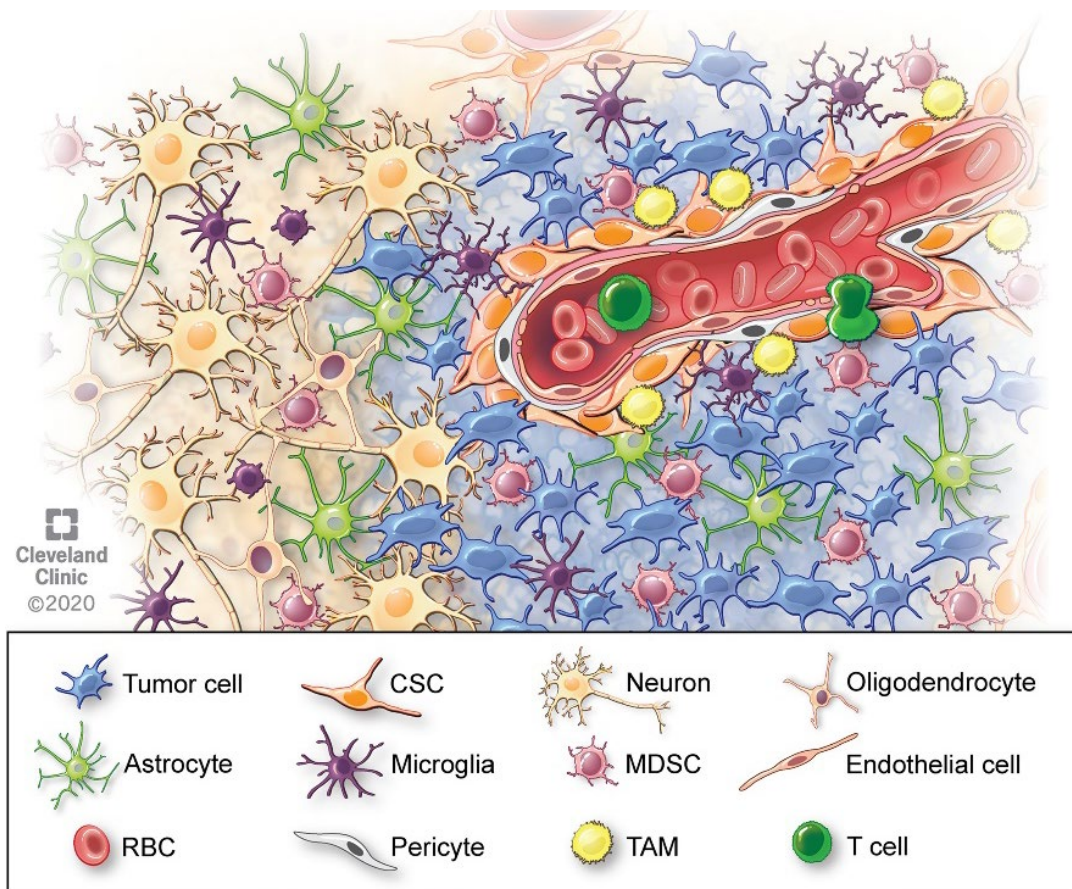




Figure 10 | The *Hallmarks of Cancer* taxonomy. The inner circle signifies the main 10 cancer hallmarks and the outer circles designate the cellular processes associated with each cancer hallmark as described in Hanahan and Weinberg 2011 [321]. Avoiding immune destruction and tumor-promoting inflammation are some of the emerging hallmarks of cancer, and together these hallmarks result in an immunosuppressive milieu within the cancer whereby cancer cells are able to circumvent immune-mediated killing and instead hijack the immune system for tumor progression. Reprinted from Baker *et al.* [346] under the terms of the Creative Commons CC BY license.

7.4.1 Neovascularization and hypoxia

Two prominent environmental features of solid tumors including glioblastomas are hypoxia/necrosis and neovascularization [321, 347, 348]. Like normal tissue, tumors need supplies of oxygen and nutrients as well as clearance of waste products in order to thrive. However, due to the rapid growth of tumor cells, the existing vasculature surrounding the tumor is not able to meet the demands of the tumor cells. To compensate, tumor cells secrete pro-angiogenic factors, such as VEGFs, angiopoietins, and chemokines, which stimulate MVP, especially through sprouting angiogenesis [326, 349]. Others mechanisms of neovascularization include co-option of existing blood [301, 330, 350], postnatal vasculogenesis, intussusception, vascular mimicry [351, 352], and transdifferentiation [319, 326, 349, 353-355]. The normal brain vasculature is highly specialized composed of brain endothelial cell connected by tight junctions and surrounded by a basal lamina shared by pericytes and astrocytic endfeet. Together these cells form, maintain, and regulate the BBB. The BBB is a structure that selectively restricts the molecular and cellular influx/efflux between the intracerebral and extracerebral circulatory system [348, 349]. In contrast, the tumor neovasculature is disorganized, spatiotemporal heterogeneous, and dysfunctional due to aberrations in the endothelial wall, pericyte coverage, and basement membrane. This results in immature, tortuous, fragile, and hyperpermeable blood vessels leading

to abnormal blood flow and poor perfusion [348, 349]. Consequently, the availability of oxygen and nutrients for the cells in the TME rests on their vicinity to a functioning blood vessel. As the tumor progresses, it often outgrows its vascular supply, and hypoxic and necrotic regions arise, and a hypoxic response is initiated by the affected cells in an attempt to restore oxygen availability. Hypoxia regulates a wide range of biological processes, including angiogenesis, metabolism, and extracellular matrix remodeling, and is associated with resistance to radio- and chemotherapy as well as poor outcome in many cancer types [325, 347, 356-358]. Cells adapt to hypoxia by upregulating the expression of hypoxia-inducible factor (HIF) transcription factors, especially HIF1 α that contains an oxygen-sensitive subunit. In normoxia, HIF1 α is targeted for proteasomal degradation. Under hypoxic conditions, HIF1 α is stabilized and able to bind to specific regulatory hypoxia-response elements thereby inducing transcription of numerous target genes, including angiogenic factors, such as VEGF as well as effectors of glycolysis and lactic formation, which are essential for cell survival. Irrespective of oxygen availability, tumor cells show high metabolic adaptability and often rewire their metabolism from oxidative phosphorylation to aerobic glycolysis (a phenomenon known as the Warburg effect) to facilitate rapid proliferation; and this metabolic reprogramming is only augmented by hypoxia. The glycolytic shift leads to increased production of waste products, e.g. lactate acidifying the TME [325, 347].

Hypoxia and acidosis influence the neoplastic and non-neoplastic cells as well as their intercellular communication by altering the secretome of cytokines, chemokines, metabolites, growth factors and exosomes as well the expression of a variety of ligands and cell surface receptors. Multiple studies on glioblastoma have shown that hypoxia and acidosis contribute to progression by favoring tumor proliferation [62, 359], migration/invasion [359-364], mesenchymal phenotype shift [357, 364], and dedifferentiation/stem cell maintenance [62, 360, 365-369]. Further, hypoxia attracts immune cells and may contribute to immune evasion by impairing the anti-tumor function of T cells [325, 370, 371] and promoting a pro-tumorigenic and pro-angiogenic phenotype of myeloid cells [325, 372-375]. The effect of targeting hypoxia and angiogenesis signaling in cancer has been investigated in several preclinical studies and clinical trials as a means to inhibit tumor growth or improve the efficacy of standard therapy by normalizing the vasculature and tissue oxygenation [302, 306, 307, 325, 358]. The most well-known therapeutic agent is bevacizumab, which is a humanized anti-VEGF monoclonal antibody that inhibits VEGF from binding to its receptors VEGFR1 and VEGFR2 expressed on endothelial cells. Bevacizumab is approved for treatment of several cancer types, including metastatic colorectal cancer and advanced NSCLC [376]. In patients with glioblastoma, bevacizumab have shown limited effect on overall survival [290, 292, 302, 307, 377], but may reduce the use of corticosteroid and improve quality of life [292, 378]. In a meta-analysis on patients with newly diagnosed glioblastoma treated with standard-of-care therapy, bevacizumab prolonged progression-free survival with 2.7 months, but did not improve overall survival [307], possibly due to acquired resistance of tumor cells and activation of alternate angiogenic pathways [301, 376].

7.4.2 Cancer stem cells and intratumoral heterogeneity

As mentioned, gliomas, particularly glioblastomas, display cellular heterogeneity and plasticity making development of therapies that eliminate all tumor cells challenging. Tumor initiation, progression, and

heterogeneity have been proposed to rely on clonal evolution and/or the presence of a CSC hierarchy (**Figure 11**), and both models can to some extent explain the level of intratumoral cellular hierarchies observed in gliomas. According to the clonal evolution model, all cells are capable of initiating tumor growth, and heterogeneity arises due genetic instability and clonal selection. In contrast, the CSC model states that only cells with stem cell properties have tumorigenic potential, and heterogeneity occurs due to asymmetrical division [379-381]. CSCs were first described in leukemia in 1997 [382], but was soon after described in brain tumors including diffuse glioma [383-385]. Similar to normal stem cells, including neural stem cells, CSCs represent a small subpopulation of cancer cells defined by their capacities to self-renew, generate to more differentiated progenies, and give rise to tumors *in vivo* that recapitulates the cellular heterogeneity seen in the original tumor [327, 386, 387]. Subsequent studies showed that CSCs exhibit resistant towards radiation [388] as well as anti-angiogenic [20] and chemotherapeutic agents [288, 389, 390].

CSCs reside and flourish in so-called perivascular [60, 61], perinecrotic/hypoxic [62], and invasive niches [335, 391-394]. Here they interact reciprocally with numerous non-neoplastic cell types in the TME [14, 319] including endothelial cells and immune cells [11, 18, 24–27] favoring angiogenesis [330, 354, 355], migration/invasion [339, 395, 396] and an immunosuppressive TME [397-399]. Different markers are used to identity CSCs, including intracellular proteins, e.g. sex determining region Y-box 2 (SOX2) and nestin, and cell surface protein, e.g. CD133, CD44, and CD24 [327, 328, 400, 401]. The numerous, but not necessarily overlapping, markers only begin to describe the immense level of heterogeneity among the CSC population itself [328, 402, 403]. In fact, the hierarchical CSC model has been challenged by increasing evidence suggesting that CSCs are not a defined cellular entity, but rather represent a cellular state driven by genetics and environmental changes, such as nutrient deprivation, hypoxia, and radiation [62, 264, 265, 360, 365, 369, 404-407]. A recent series of studies characterizing gliomas at a single-cell level demonstrated that multiple distinct hierarchical lineages and cellular transcriptional subtypes coexist, interact, and compete with each other to form a complex and diverse tumor ecosystem [6, 9, 369, 408, 409]. Further, these studies showed that the CSC state is not binary, but constitutes a continuous spectrum of stem-like cellular properties, markers and behavior. Therefore, the so-called plasticity model may better explain the observed intratumoral heterogeneity (**Figure 11**). The plasticity model suggests that most tumor cells can reversibly switch between distinct stem cell and differentiated states in response to genetic, microenvironmental, and therapeutic stimuli [345, 379, 387, 407], indicating that phenotypic heterogeneity emerges from non-hierarchical, dynamic cell state transitions. Among the most important single-cell transcriptomic and lineage tracing studies are the reports by Suvà and colleagues, who have evaluated the cellular architectures of IDH-mutant gliomas and IDH-wildtype glioblastomas [9, 408, 409]. These studies show that tumors can be scored based on a neurodevelopmental and cell-cycle program. IDH-mutant tumors exhibit a cancer hierarchy comprised of three main subpopulations; a stem/progenitor-like cells resembling neural progenitor-like (NPC-like) cells and two subpopulations resembling differentiated glial cells, the oligodendrocyte progenitor-like (OPC-like) and the astrocyte-like (AC-like) cells (**Figure 12A**). Proliferation was largely restricted to the NPC-like cells, indicating that cycling NPC-like cells drive the progression of IDH-mutant tumors and give rise to heterogeneity by differentiating into two lineages [408, 409]. In contrast, IDH-wildtype glioblastomas are less hierarchically organized and

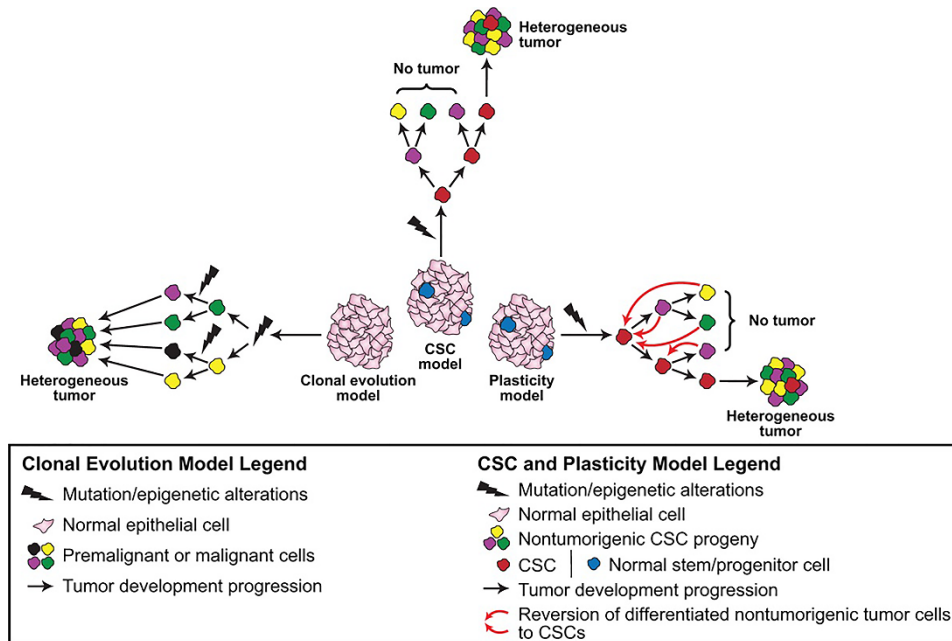


Figure 11 | Different models of tumor evolution. In clonal evolution model (or stochastic model), all cells are able to initiate tumor growth, and mutations accumulate over time due to selection pressure that may be temporally and spatially distinct. In this way, subclones are generated driving tumor progression and heterogeneity. In the cancer stem cell (CSC) model, only stem cells have a tumorigenic potential, while differentiated cells have little or none. CSCs reside at the apex of a hierarchical organization and are able to self-renew by both symmetric and asymmetric cell division. As CSCs divide and produce differentiated cells, a heterogeneous tumor emerges composed of subpopulations of tumorigenic and non-tumorigenic cells. In the plasticity model, differentiation is bidirectional so that differentiated non-tumorigenic tumor cells may convert/dedifferentiate to tumorigenic CSCs. Reprinted from Rich [379] under the terms and conditions provided by Wolters Kluwer Health, Inc. and Copyright Clearance Center.

mainly consist of four cellular states; three with similarities to those observed in IDH-mutant tumors and a fourth, the mesenchymal-like (MES-like), that is not anchored in neurodevelopment [9] (**Figure 12B**). Further, cycling cells were identified in all four cellular states, suggesting that multiple compartments fuel glioblastoma growth. Each of these states were found to coexist in an individual tumor; however, one or two states tended to be predominant in any given tumor [9], possibly explaining the transcriptomic classification for the tumor when profiled in bulk [11, 258]. Interestingly, several CSC markers showed a significant bias toward one of the four cellular states. CD24 was enriched in NPC-like cells, while CD133, nestin, and CD44 were enriched in OPC-like, AC-like, and MES-like cells, respectively [410] (**Figure 12C**). To test the plasticity of the cell state transitions, cells in a specific cellular state were isolated and implanted in mice using a patient-derived xenograft model [9]. At least two of four states (MES-like and NPC-like) had the capacity to propagate tumors and undergo state transition to re-establish the state configuration seen in the parenteral tumor [9, 410]. These results suggest that most glioblastoma cells are highly plastic and can exhibit stem cell-associated capabilities. Taken together, increasing evidence shows that the phenotypic heterogeneity in especially glioblastoma is a result of intrinsic plasticity and that the CSC state is an inducible and transient state, and these dynamic processes need to be considered when developing targeted therapies in the future.

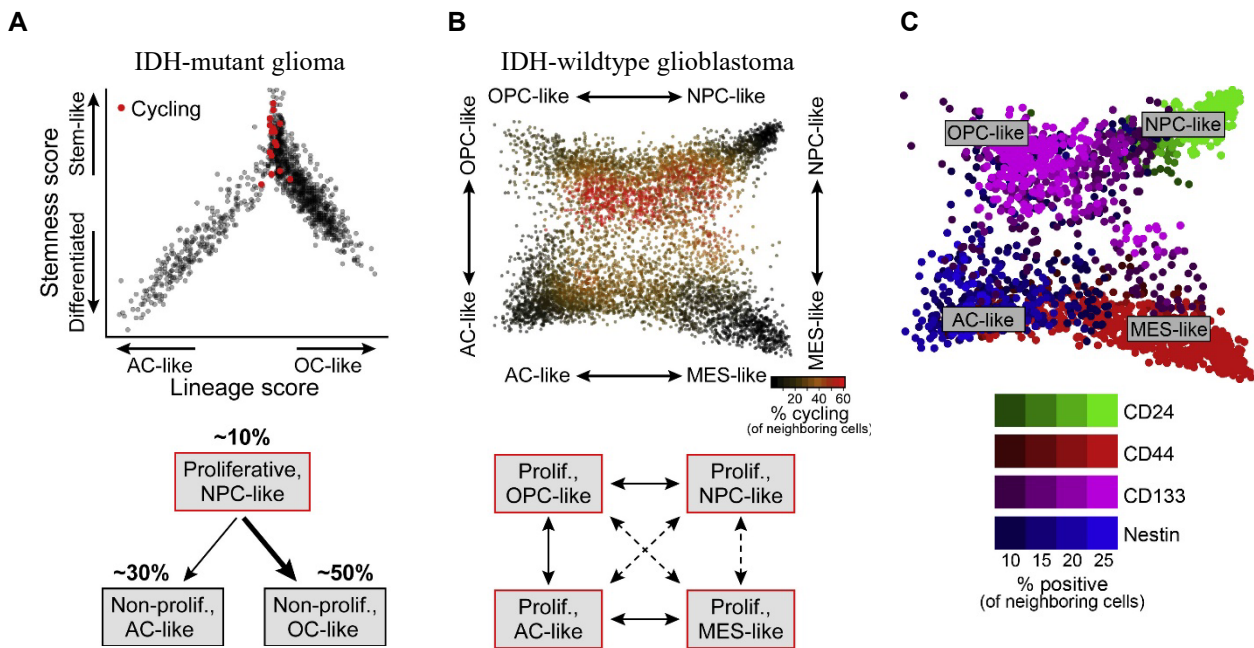


Figure 12 | Cellular hierarchies of glioma and associated CSC markers. **(A, B)** Transcriptional cell states in adult-type diffuse gliomas identified by the single-cell RNA sequencing. The top panel shows cell scores for the stemness/differentiation and proliferation signature in IDH-mutant glioma (A) and IDH-wildtype glioblastoma (B). Bottom panels display the cellular hierarchies and estimated cellular fraction (only in A), with proliferating cell states highlighted in red. Arrows represent the cellular plasticity between the different states. Full arrows reflect cellular transitions supported by literature, and dashed arrows indicate cellular transitions not supported by literature. **(C)** Different CSC markers show a significant bias toward one of the four cellular states identified in IDH-wildtype glioblastomas. CD133 was enriched in oligodendrocyte progenitor-like (OPC-like) cells, CD24 in neural progenitor-like (NPC-like) cells, nestin in astrocyte-like (AC-like) cells, and CD44 in mesenchymal-like (MES-like) cells. Adapted and reprinted from Suvà and Tirosh [410] under the terms and conditions provided by Elsevier and the Copyright Clearance Center.

7.5 The tumor immune microenvironment in glioma

The CNS has long been regarded as an immune-privileged organ due to the blood-brain and blood-cerebrospinal fluid barriers, absence of a classic lymphatic drainage system, infrequency of effector immune cells, and slow adaptive immune responses [411, 412]. However, this viewpoint has been revised based on discoveries showing that a functional lymphatic system exists in the meningeal layers surrounding the brain parenchyma [413-417]. The lymphatic vasculature enables fluid, molecules (including CNS-derived antigens), and immune cells (especially dendritic cells) to drain from the CNS into deep cervical lymph nodes. Here T cells are able to encounter a CNS-antigen loaded dendritic cell and initiate a systemic immune response [411, 415]. Single-cell mapping of the immune landscape in the healthy mouse brain have also demonstrated that multiple immune cell types are present and tissue-resident in the healthy brain, including microglia, border-associated macrophages (BAMs), neutrophils, monocytes/monocyte-derived cells, dendritic cells, T cells, and B cells [412, 418-420]. Microglia and BAMs account for ~ 80% and 10% of all leukocytes, respectively, while the other immune cells contribute with less than 1-3% of the leukocyte population [419]. Ontogenetically, microglia and BAMs derive from myeloid precursors generated in the mesodermal extra-embryonic yolk sac

during early embryogenesis and migrate towards the CNS using blood vessel and white matter tracts as points of orientation [421-424]. In contrast to monocyte-derived macrophages, microglia and most BAMs are long-lived and replenish locally postnatally with a low turnover in steady state, making them a relatively stable population in the CNS [420, 422, 423, 425]. BAMs are localized at the interface between the brain and the periphery lining the meninges, choroid plexus, and perivascular spaces [426] and are phenotypically distinct from microglia [419]. Microglia reside exclusively in the parenchyma comprising ~10% of all cells in the healthy brain parenchyma [423, 424, 427]. Both BAMs and microglia are innate immune cells actively surveilling the CNS to protect it from infectious agents and injury-related products [424, 426]. In fact, microglia actively monitor the brain parenchyma in a territorial manner by constant integration and interpretation of incoming signals, without compromising the neuronal circuitry. They use their branched processes and protrusions to interact with the other CNS cells maintaining homeostasis by immunosurveillance, neurotrophic support, synaptic housekeeping, and phagocytosis upon activation [423, 428]. The CNS is thus immunologically active, but distinct and kept quiescent at baseline. Microglia are the primary watchman in the brain parenchyma, while the BBB and BAMs act as the first lines of defense at the specialized CNS compartments located outside the parenchyma, supported by patrolling, and to some extent tissue-resident, immune cells from the periphery, e.g. T cells [429] and dendritic cells [412, 430].

Pathological damage e.g. brain tumor development attracts the brain-resident microglia and disrupts the integrity of the blood-CNS barriers, resulting in edema formation and recruitment of infiltrating leukocytes through chemokines released by e.g. tumor cells [349, 431], generating a massively inflamed and immune-infiltrated microenvironment [14]. In general, cancer-related inflammation is both capable of eliminating and facilitating tumor development and growth in a complex and dynamic process known as cancer immunoediting. Immunoediting entails that tumor immunogenicity is altered when the immune system attempts to eliminate the genetically unstable tumor cells. This results in selection of tumor cell variants that have acquired abilities to evade the immune system, including loss of tumor antigens, reduced expression of human leukocyte antigen (HLA) class I molecules, and induction of an immunosuppressive TME. Evidence of immunoediting has been reported in several cancer types including glioma [27, 258, 318, 432-434].

Gliomas and especially glioblastomas recruit immune cells to its environs to promote growth, invasion, angiogenesis, and immune evasion [14]. The myeloid cells are the major immune cell determinants of the TME in gliomas, comprising ~60-90% of all leukocytes [32-35, 267, 435-440]. Microglia and macrophages are the most prevalent cell types of myeloid population, while neutrophils, myeloid-derived suppressor cells (MDSCs), mast cells, and dendritic cells are far less abundant [13, 32, 34, 35, 437]. T cells make up the majority of the lymphoid cell population and compose ~10-20% of all leukocytes, while natural killer (NK) cells and B cells are rare [32-34, 435, 438, 440]. During the last decades, it has become increasingly clear that microglia/macrophages and T cells are crucial players in the TME [14]. However, mounting evidence suggests that the less frequent immune cells (e.g., MDSCs [343, 441, 442], monocytes [443], neutrophils [443, 444], dendritic cells [445], and NK cells [446]) also play significant roles in the TME of gliomas and could serve as treatment targets; but their exact functions are still topics of ongoing research. The next three subsections

provide brief overviews of three major immune components in diffuse glioma, especially glioblastomas, which have been the subjects of interest in the present PhD thesis.

7.5.1 The complement system

The complement system is a component of the innate immunity that plays a part in recognition of and response to pathogens. It coordinates immunological and inflammatory processes acting as a surveillance system and first line of defense to discriminate among healthy host tissue, cellular debris, apoptotic cells, invasive pathogens and their pathogen-associated molecular patterns (PAMPs) tuning the collective immune response accordingly. Complement has other versatile functions such as clearance of immune complexes, synapse maturation, tissue regeneration, angiogenesis, and recruitment of hematopoietic stem-progenitor cells [75]. Complement is composed of a range of proteins primarily synthesized in the liver that exists in the plasma and on cell surfaces as zymogens. Complement is a dynamic network triggered by the classical, lectin, or alternative pathways that interact in an amplification loop (**Figure 13**). By sequential cleavage of the proenzymes, activated complement ultimately forms the terminal complement complex, C5b-9, also known membrane attack complex (MAC), resulting in lysis and killing of targeted cells/pathogens. Complement activation also produces the anaphylatoxins C3a and C5a as well as the opsonins C1q and C3b, which activates immune cells and facilitates phagocytosis by binding to receptors on antigen-presenting cells and T cells [75, 447, 448]. The complement cascade can also be activated by extrinsic proteases, e.g. thrombin and plasmin, indicating a significant crosstalk between coagulation and complement [75, 449].

Circulating complement proteins can enter the brain parenchyma when the BBB integrity is disrupted by inflammatory, infectious, malignant, or vascular injury. However, complement proteins are also synthesized in the brain by resident cells such as microglia to regulate brain homeostasis and act as a local defense system [450]. Traditionally, complement was believed to have anti-tumor properties, and in many cancers, including glioma, the expression level of complement proteins is elevated, being produced by both host cells and tumor cells [451, 452]. However, recent studies demonstrate that complement is pathologically activated, promoting tumor growth, migration, cancer stemness, angiogenesis, and an immunosuppressive milieu, overall resulting in tumor progression and poor prognosis [451-454]. Glioma cells and especially glioma cell lines have been reported to upregulate expression of complement inhibitors, e.g. C1-inhibitor, CD59, and CD55, thereby shielding them from complement-mediated attacks [455, 456]. Collectively, growing evidence suggests that complement proteins and receptors could be possible targets for anti-cancer treatment, especially to augment the efficacy of current cancer immunotherapies [454, 457, 458].

7.5.2 Tumor-associated microglia/macrophages

TAMs are a part of the innate immune system and crucial in triggering an adaptive immune response. TAMs contribute with up to 30-50% of the cell content of gliomas, making them the predominant immune cells in glioma [29, 30, 45]. TAMs can originate from brain-resident microglia or peripheral monocyte-derived macrophages recruited from the bone marrow, making them ontogenetically distinct from each other [30, 34, 41, 42, 459-461]. A third source of TAMs in gliomas is the highly immunosuppressive mononuclear MDSCs

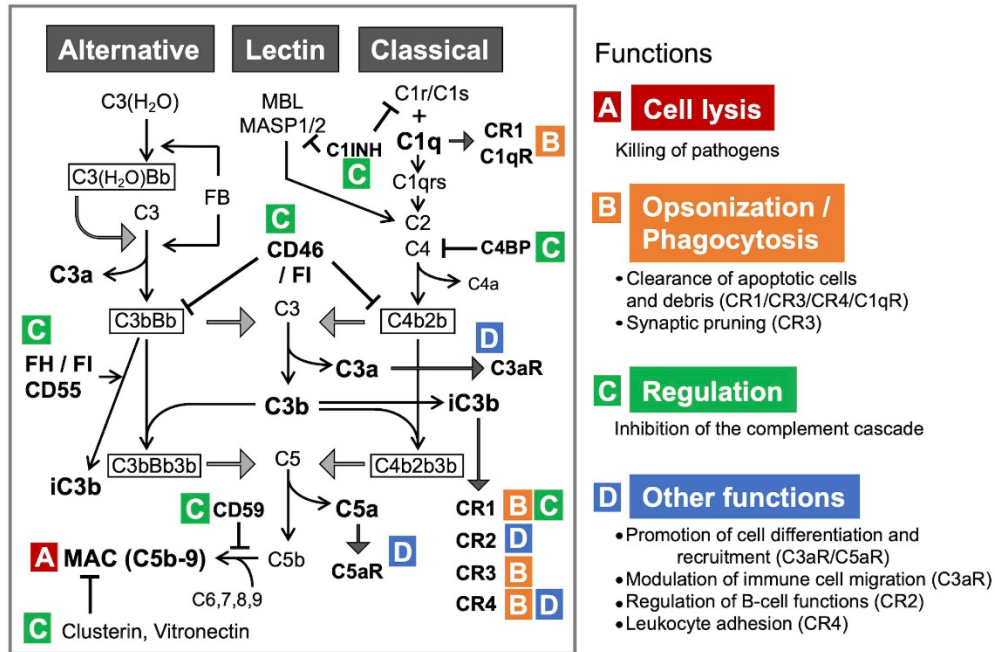


Figure 13 | Schematic diagram of the complement cascade and its functions. The classical pathway is initiated by binding of C1q/C1 complex to distinct structures on microbes or apoptotic cells as well as immune complexes, non-immunoglobulin ligands (e.g. pentraxin-3 and C-reactive protein) and other specific protein motifs (e.g. amyloid). In the lectin pathway, mannose-binding lectin (MBL) and ficolins complexed with the proteolytic MBL-associated serine proteases (MASPs) especially recognize carbohydrate patterns on microorganisms or apoptotic cells. Both the classical and lectin pathways lead to cleavage of C2 and C4 to form the C3 convertase (C4b2b). The alternative pathway begins with spontaneous hydrolysis of C3 and is further triggered by contact with proteins, lipids, or carbohydrate structures on microbes or other foreign surfaces as well as the pattern recognition molecule properdin. Factor B (FB) binds to hydrolyzed C3 and is cleaved by factor D generating the solvent-based C3 convertase (C3(H₂O)Bb) which activates complement by cleavage of C3 into the active fragments C3a and C3b. C3b tags target surfaces covalently, and the initial tagging is propagating on foreign surfaces that lack complement regulators by attracting additional C3b. This results in assembly and stabilization of the C3 convertase (C3bBb). Thus, all three pathways converge at C3, which is then cleaved by the C3 convertases leading to assembly of the C5 convertases (C3bBb3b and C4b2b3b) and formation of MAC (C5b-9) by cleavage of C5. **(A)** MAC forms pores in the lipid bilayers of the cell membranes, which disrupts osmotic regulation and results in lysis. **(B)** C1q and C3b/iC3b activate immune responses via opsonization and promote phagocytosis through binding to their cognate complement receptors (CR). **(C)** Complement is tightly controlled by regulators that inhibit, degrade, prevent assembly, or accelerate decay of the different elements of the complement cascade (e.g. C1-inhibitor (C1-INH), factor 1 (F1), CD59, and CD55, respectively). **(D)** The proteolytic fragments C3a and C5a act as anaphylatoxins through their respective receptors C3aR and C5aR. Reprinted from Shinjyo *et al.* [462] under the terms and conditions provided by the Creative Commons CC BY license.

that are able to differentiate into macrophages under hypoxic conditions [343]. TAMs are attracted to the site of the tumor through the action of signaling molecules secreted by tumor cells and possibly other non-neoplastic cells in the TME. A variety of glioma-derived factors act as chemoattractants for TAMs, especially colony stimulating factor 1/2 (CSF1/-2) [397, 463, 464], C-C motif chemokine ligand 2/5 (CCL2/-5) [45, 465-467], C-X-C motif chemokine ligand 3/14 (CXCL3/14) [468-471], and VEGF [45], which binds to their respective receptors on TAMs [30, 31, 40]. Tumor cells can further secrete numerous molecules that skew the

recruited TAMs into a pro-tumorigenic phenotype (e.g. transforming growth factor beta (TGF β) [397, 472], CCL2 [43], and interleukin-6 (IL6) [473]). This phenotype is characterized by poor antigen presentation, reduced phagocytosis [474], and expression/secretion of immunosuppressive molecules (e.g. IL1 β /-6/-10/-11 [47, 397, 472, 475-477], TGF β [397, 478], PD-L1 [398, 479]) and metalloproteinases (MMPs) [478, 480, 481]. TAMs thereby facilitate tumor proliferation [475], migration/invasion [463, 475, 476, 480, 482], angiogenesis [31, 483], immune evasion [438, 479, 484, 485], and possibly treatment resistance [17, 258, 335, 477, 486-489], ultimately leading to tumor progression [30, 31]. TAMs are identified by immunohistochemistry or flow cytometry using universal microglial/macrophages markers such as IBA1, CD11b, CXCR3, and CD68 [54, 423, 490, 491]. Using immunohistochemistry the amount of TAMs was found to positively correlate with malignancy grade [43-45, 492] and vascular density [408, 493] in gliomas. TAMs often accumulate in the perivascular and perinecrotic niches [37, 41, 45, 440, 470, 494, 495], where they may co-reside with CSC. TAMs are attracted to these areas due to migratory stimulating factors, e.g. VEGF, CCL2 and CXCL12, secreted by the CSCs [45] and as well signals released from necrotic cells [466]. Hypoxia and CSC-derived factors polarize TAMs into an immunosuppressive and pro-invasive phenotype [325, 362, 375, 395, 398].

Myeloid cells are highly plastic and diverse cells adapting their phenotype according to microenvironmental cues to orchestrate a suitable functional response. Like microglia, macrophages are essential in organ development, tissue homeostasis, and host defense against infection under normal physiological conditions; however, microglial and macrophage responses can become maladaptive in numerous diseases and thereby contribute to pathogenesis [40, 490, 496, 497]. Mirroring the T helper cell type 1-T helper cell type 2 (Th1-Th2) polarization, two primary activation states for microglia/macrophages have been recognized: the classically activated (M1) phenotype and the alternatively activated (M2) phenotype. The M1 phenotype is induced by e.g. bacterial moieties and the Th1 cytokine interferon γ (IFN γ), while the M2 phenotype is induced by e.g. Th2 cytokines such as IL4 and IL13. The M1 and M2 phenotypes differ in regards to expression of surface molecules, secretomes, and functional programs (**Figure 14**). M1-polarized cells are characterized by their ability to secrete pro-inflammatory factors (including chemokines/cytokines that drive a Th1 response), higher expression of HLA class II molecules and co-stimulatory molecules (e.g. CD80, CD86), and efficient antigen presentation. In contrast, M2-polarized cells express anti-inflammatory/immunosuppressive factors and are involved in immunoregulation, Th2 responses, extracellular matrix remodeling, and angiogenesis. In terms of cancer, the M1 phenotype is considered anti-tumorigenic, while the M2 phenotype is thought to promote tumorigenesis and prevent an effective anti-tumor immune response [40, 496, 497]. In glioma, the density of TAMs expressing M2 markers has been associated with high malignancy grade and poor prognosis [32, 43, 46-50, 162, 436, 498]. Commonly used M2 markers are the scavenger receptors CD163, CD204, and CD206 that are involved in phagocytosis of e.g. harmful haptoglobin-hemoglobin complexes, apoptotic cells, and mannoseylated glycoproteins, respectively [499]. Emerging evidence using genetic profiling, however, demonstrate that TAMs are mixed cell population that cannot be recapitulated by the simplistic M1-M2 paradigm [33, 36-39]. Instead, TAMs can display several phenotypes along an M1-M2 spectrum including the more undifferentiated M0 state [39]. Single-cell RNA sequencing of TAMs in human tissue have revealed that pro-inflammatory M1 and anti-inflammatory M2 genes are not mutually exclusive and are co-expressed at a

cellular level in several TAM subsets [41, 42, 500]. This is likely due to the unique and dynamic features that shapes the TME, such as hypoxia, nutrient restriction, and opposing inflammatory stimuli [501] from neoplastic and non-neoplastic cells. This creates a complex milieu driving the emergence of myeloid cell phenotypes that cannot be found in normal tissue [496].

As mentioned, increasing evidence indicates that TAMs are central determinants of the immunosuppressive TME hindering T cell infiltration and cytotoxicity, thereby preventing efficient response to immunotherapy. Additionally, TAMs, and myeloid cells in general, fuel resistance towards chemo-, radio-, anti-angiogenic, and targeted therapies [488, 502]. Consequently, TAMs are now being actively pursued as genetically stable targets of immunotherapy to augment the efficacy of standard-of-care treatment or other immunotherapies. A variety of approaches has been explored as means to either eliminate or re-educate TAMs towards a pro-inflammatory,



Figure 14 | Macrophage/microglia polarization, the extremes of a continuum. Exposure to different stimuli polarizes microglia/macrophages into different activation states/phenotypes. The classical phenotype (M1) is induced by type 2 IFN/IFN γ , lipopolysaccharide or TNF and is associated with expression of distinct set of molecules (shown in red). Macrophages can be alternatively activated by different ways resulting in distinct molecular profiles. IL4 and IL13 induce an M2a phenotype (shown in yellow). Immune complexes and lipopolysaccharide in combination with TLR or IL1R ligands induces an M2b phenotype (shown in magenta), while IL10 induces an M2c phenotype (shown in green). Some molecules are common for the M2a and M2c phenotypes as they are induced by both IL4/IL13 and IL10 (shown in blue). Adapted and reprinted from Mantovani *et al.* [40, 497] under the terms and conditions provided by Elsevier and the Copyright Clearance Center.

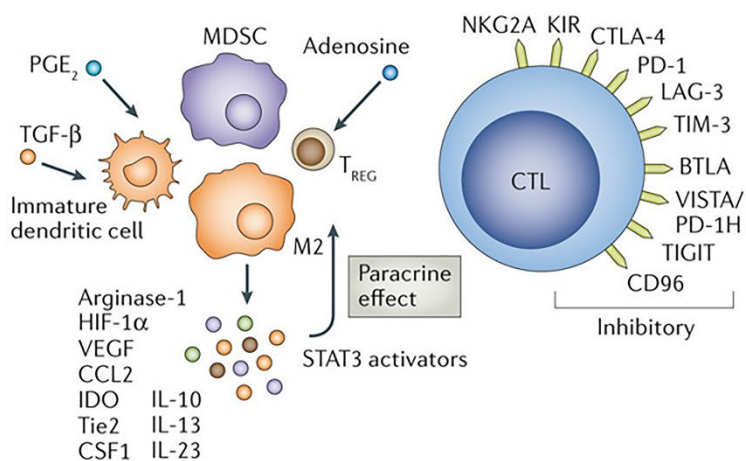
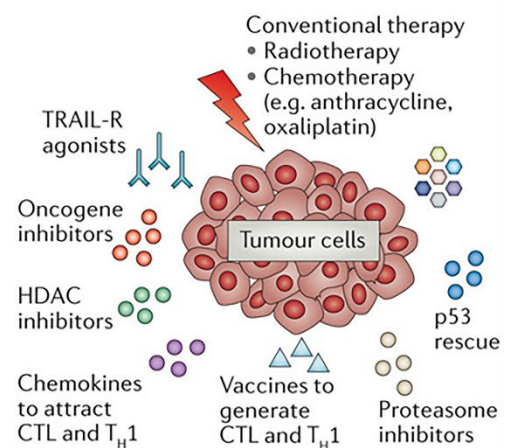
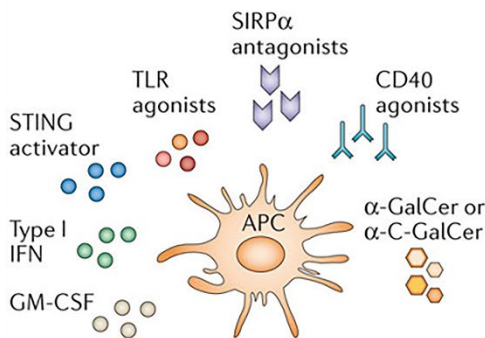
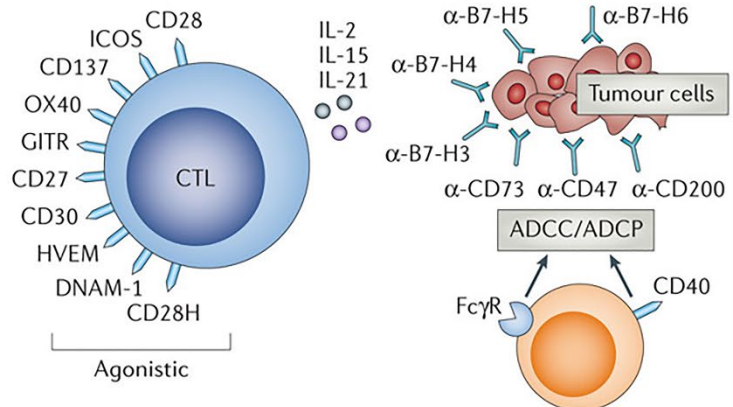
a Node 1: Elimination of immune suppression**b Node 2: Immunogenic cancer cell death****c Node 3: Enhanced APC function/adjuvanticity****d Node 4: Enhanced T/macrophage effector activity**

Figure 15 | Four nodes to target for induction of anti-tumor immunity. Due to the heterogeneity of the TME including the immune milieu, tumors develop resistance to monotherapies, including mono-immunotherapies. Multiple pathways must therefore be co-targeted to achieve an efficient anti-tumor response that mobilizes the myeloid cells and generates effector T cell responses against immunogenic tumor antigens. Different arms of immunity can be targeted to favor an anti-tumor function of the immune system. **(A)** Node 1: Elimination of immune suppression by inhibiting the immunosuppressive cells/mediators/metabolites and through blockade of co-inhibitory checkpoint receptors on the cytotoxic T cell (CTL). **(B)** Node 2: Promotion of immune-mediated cancer cell death using targeted therapies against, e.g. oncogenic signaling pathways and/or vaccines, in combination with conventional therapy. **(C)** Node 3: Stimulation of the function of antigen-presenting cells (e.g., dendritic cells and macrophages/microglia) using immune adjuvants or relevant agonists/antagonists. **(D)** Node 4: Activation of effector T cells and augmentation of macrophage effector function (i.e. M1 polarization) using agonists to promote killing and phagocytosis of tumor cells. Reprinted from Smyth *et al.* [27] under the terms and conditions provided by Springer Nature and the Copyright Clearance Center.

phagocytic, and immunogenic phenotype by inhibiting key factors [502, 503] and signaling pathways [503], including CCL2-CCR2 [459, 461, 504], CXCL2/8-CXCR2 [494], CSF1-CSF1R [461, 484, 485, 505-510], and CD47-signal regulatory protein alpha (SIRP α) [511]. These approaches have shown promising results in preclinical models, but has so far failed to translate to the clinical setting [314]. Administration of the anti-CSF1R antibody PLX3397 had no effect in a phase II clinical trial with recurrent glioblastoma patients [314], possibly due to myeloid recolonization within the TME [461, 508] and acquired resistance mechanisms [508].

However, we are still awaiting the results from a clinical trial assessing whether PLX3397 can improve the efficacy of standard-of-care treatment in patients with newly diagnosed glioblastoma [512]. Results from several preclinical studies and clinical trials, nevertheless, indicate that multiple pathways in the TIME needs to be targeted concomitantly using combination (immuno)therapies to boost anti-tumor immunity and to counteract the heterogeneous and versatile TME [27, 28, 66] (**Figure 15**).

7.5.2 T cells and immune checkpoint markers

T cells constitute the main lymphoid cell population infiltrating gliomas [32-34, 435, 438], and their prevalence increases with malignancy grade [513-516]. However, they are relatively infrequent accounting for only ~1-2% of the total cellular content in glioblastoma [34, 102, 434, 498, 517]. Compared to many other cancer types including metastatic brain cancer, gliomas are often characterized as immunologically cold [25, 28] due to a paucity of lymphocytes and presence immunosuppressive TAMs [32, 33, 64]. Most gliomas are therefore classified as lymphocyte-depleted or immunologically quiet [64].

T cells are the main orchestrators of the adaptive immune system. In contrast to cells of the innate immune system, the cells of the adaptive immune system are able to exert an effective immune response through dramatic clonal expansion of small populations of naïve antigen-specific cells. T cells originate from hematopoietic stem cells in the bone marrow that migrate via the blood to the thymus. In the thymus, the T cells mature undergoing a complex, stepwise selection process in which each T cell acquires a T cell receptor (TCR) that is specific for a particular antigen [76]. Following maturation, the T cells circulate as naïve cells in the blood and lymphatic system or through secondary lymphoid organs (e.g. lymph nodes and the spleen) and peripheral organs, ready to encounter their cognate antigen. The immunological synapses most often occur in lymph nodes where resident or lymph-born dendritic cells present antigens to T cells through their HLA class I/II molecules. This interaction results in T cell activation and clonal expansion of T cells with antigen-specific effector functions, which then migrate to diverse sites to promote pathogen clearance [76]. Two major T cell populations exist: CD4⁺ Th cells and CD8⁺ cytotoxic T cells. CD4⁺ T cells are capable of coordinating and modulating an antigen-specific immune response by differentiating into different subsets characterized by specific cytokine profiles and effectors functions [518]. CD8⁺ T cells can induce selective apoptosis through direct cell-cell interaction with target cells (e.g. virally infected cells or tumor cells) and release of lytic granules, such as perforin and granzymes. CD8⁺ T cells mainly recognize antigenic peptides presented by HLA class I molecules, which are expressed by all nucleated cells and present intracellular antigens. In contrast, CD4⁺ T cells primarily recognize extracellular-derived antigenic peptides presented by HLA class II molecules, which are expressed on antigen-presenting cells (e.g. dendritic cells, macrophages, and microglia) [76]. Upon recognition of an antigen through TCR, full activation of T cells requires additional stimuli from co-signaling receptors (**Table 5**) that functions as a checkpoint system to prevent autoimmunity and minimize tissue damage. Co-stimulatory receptors (e.g. CD28) promote T cell activation through binding to their respective ligands (e.g. CD80/CD86). Co-inhibitory receptors, (e.g. CTLA-4 and PD1), restrict the threshold for activation and modulate the duration and range of the immune response through binding to their ligands (e.g. CD80/CD86 and PD-L1/PD-L2) [77]. A specific subset of CD4⁺ T cells are the forkhead box P3 (FOXP3)⁺

regulatory T cells (Tregs) which are important for maintenance of self-tolerance and homeostasis. Most Tregs derive from the thymus as functionally mature suppressive cells, but can also be induced in the periphery from naïve T cells following antigen encounter under particular conditions, e.g. by exposure to IL10. Tregs exert their immunosuppressive functions e.g. through production of IL10 and TGF β and by suppressing co-stimulation of conventional T cells via CTLA4 [518, 519]. Most activated T cells are short-lived dying when the pathogenic assault has been resolved and the antigen eliminated, but a subset persists as memory T cells and take part in maintaining long-term immunity. Multiple subsets of memory T cells exist including tissue-resident memory T cells, and these subsets differ in terms of their tissue localization, their ability to traffic between peripheral tissues and lymphoid organs, and self-renewal capacities [520, 521].

In gliomas, tumor-infiltrating T cells mainly comprise CD8⁺ T cells, conventional CD4⁺ Th cells, and CD4⁺ FOXP3⁺ Tregs, and these T cells often accumulate in the perivascular areas [434, 435, 515, 522, 523]. Most studies suggest that high levels of CD8⁺ T cells are associated with prolonged survival [32, 513, 516, 524-526], suggesting that these T cells are able to exert direct anti-tumor functions. Meanwhile, the prognostic value of CD4⁺ Th cells is less clear [32, 102, 513], but most data indicate that Treg have a detrimental impact on survival [32, 513, 514, 522, 526-528]. T cells are recruited to the site of the tumor following priming in the deep cervical lymph nodes or through the action of soluble mediators, e.g. CCL2, CCL22 and indolamine 2,3-dioxygenase (IDO), released by tumor cells and TAMs in the TME [31, 527, 529, 530]. Upon arrival to the TME, the T cells encounter a complex array of immunoregulatory mechanisms mediated by a hypoxic environment [325, 370, 371] and cells of the TME, including tumor cells, TAMs, and infiltrating Tregs [14, 31, 523, 531]. Among these mechanisms are exposure to soluble immunosuppressive/-modulatory factors, including IDO, IL10, IL6, TGF β , and VEGF [14, 319, 473, 532, 533], as well as possibly D-2-hydroxyglutarate in IDH-mutant tumors [70, 73]. Other mechanisms include direct cell-cell communication through tolerogenic HLA class I molecules expressed on tumor cells, activation of the apoptosis-inducing receptor CD95/CD95 ligand pathway, and stimulation of co-inhibitory receptors through their cognate ligands expressed on antigen-presenting cells or tumor cells (e.g. PD1-PD-L1/PD-L2 [534], CTLA4-CD80/CD86) [14, 319, 344, 533]. Further, low neoantigen load [26, 535], reduced expression of HLA class II molecules, and co-stimulatory ligands (e.g. CD86 and CD80) by antigen-presenting cells, as well as sequestration of T cells in the bone marrow [536] may result in T cell ignorance, tolerance, anergy, or exhaustion [344]. Together these mechanisms lead to dysfunctional T cells and local expansion of the Treg pool, thereby impairing an effective anti-tumor immune response. A hallmark of T cell dysfunction in cancer is an exhaustion phenotype, which can emerge due to persistent antigen exposure and/or inflammation. The exhaustion state is characterized by loss of effector functions, low cytokine production, reduced proliferative potential, and sustained upregulation and progressive co-expression of multiple co-inhibitory receptors, e.g. PD1, TIM3, lymphocyte activation gene 3 protein (LAG3), T cell immunoreceptor with Ig and ITIM domains (TIGIT), and CTLA4 [532, 537]. Several studies have shown that tumor-infiltrating T cells express high levels of PD1 and other inhibitory receptors, including TIM3, LAG3, and CTLA4 [435, 538-544]. The expression of these receptors is increased in infiltrating T cells compared to peripheral blood T cells from matched patients and/or healthy donors [538-543], supporting the notion that the T cells become dysfunctional upon entry into the TME [542].

Background

Table 5 | Examples of co-stimulatory and co-inhibitory receptor-ligands

Receptor	Ligand	Immunoregulatory effect in T cells
Co-stimulatory immune checkpoints[§]		
CD28 ^[545]	CD80 (B7.1) CD86 (B7.2) (ICOSL)	Constitutively expressed on all T cells. Ligation is required for full T cell activation through TCR. Induces T cell proliferation and survival and stimulates cell metabolism and production of growth cytokines, e.g. IL2 and IFN γ . Competes with CTLA4 for ligand and ligates with lower affinity.
GITR (CD357) ^[546]	GITRL	Constitutively expressed at high levels on Tregs and at low levels on naïve and memory T cells. Upregulated by all T cells upon TCR ligation. Augments effector functions, production of IL2 and IFN γ as well as survival in CD4 ⁺ and CD8 ⁺ T cells. Short-term signaling inhibits the suppressive function of Tregs, while long-term signaling increases their activity and expansion.
CD226 (DNAM1) ^[547]	CD155 (PVR) CD112 (PVRL2)	Constitutively expressed on CD8 ⁺ and CD4 ⁺ T cells including Tregs. Upregulated upon activation through TCR. Suppress Treg function. Expands the effector T cell populations. Competes with TIGIT for ligands and ligates with lower affinity.
Co-inhibitory immune checkpoints[§]		
CTLA4 (CD152) ^[545]	CD80 (B7.1) CD86 (B7.2) (ICOSLG)	Inducibly expressed on all T cells in response to TCR ligation and TCR/CD28 co-stimulation. Increases the threshold for T cell activation. Competes with CD28 for ligand and ligates with higher affinity than CD28. Reduces T cell activation and promotes cell-cycle arrest. Constitutively expressed by Tregs. Enables Tregs to downregulate CD80/CD86 on antigen-presenting cells through CTLA4-mediated trans-endocytosis.
PD1 (CD279) ^[548]	PD-L1 (B7-H1/CD274) PD-L2 (B7-DC/CD273)	Inducibly expressed on all T cells during activation. Inhibits T cell activation, effector functions, and survival by interaction with TCR and CD28 signaling. The extent of PD1-mediated inhibition depends on the strength of the TCR signal. Promotes T cell programming towards Treg differentiation.
TIM3 (HAVR2) ^[549]	Galectin-9 Phosphatidylserine HMGB1 Ceacam-1	Expressed on Tregs and terminally differentiated CD4 ⁺ and CD8 ⁺ T cells. Weakens signal transduction through TCR resulting in T cell anergy, decreased proliferation and possibly apoptosis. Increases the suppressive function of Tregs by stimulating proliferation and production of IL10 and TGF β .
LAG3 (CD223) ^[550, 551]	HLA class II molecules Galectin-3 FGL1 LSECtin	Expressed on activated CD4 ⁺ T cells and CD8 ⁺ T cells as well as Tregs. Upregulated by cytokines IFN γ , IL2, IL12, and IL10 on activated T cells. Inhibits TCR signal transduction by associating with the TCR/CD3 complex upon TCR engagement. Binds to HLA class II molecules with higher affinity than CD4 inhibiting CD4 ⁺ T cell activation, differentiation and effector functions. Inhibits T cell activation/cytotoxicity through ligation to galectin-3, LSECtin, and FGL1 Augments the suppressive function of Tregs.
TIGIT ^[547]	CD155 (PVR) CD112 (PVRL2) CD113 (PVRL3) CD111 (PVRL1) Nectin-4 (PVRL4)	Highly expressed on Tregs and effector/memory CD8 ⁺ and CD4 ⁺ T cells. Dampens TCR signaling by downregulating TCR complex components and/or CD28 expression leading to T anergy/tolerance. Blocks CD226 co-stimulation by binding CD155 with higher affinity and disrupting CD226 homodimerization. Induces IL10 production in Tregs and antigen-presenting cells.

§ Most co-stimulatory and inhibitory receptors are expressed by other cell types than T cells, e.g. natural killer cells and macrophages, and T cells may also express some of the respective ligands upon T cell activation, e.g. PD-L1 and galectin-9. This proves that targeting the checkpoint system is much complex than merely regulating T cell responses.

Abbreviations: *Ceacam-1*, carcinoembryonic antigen-related cell adhesion molecule 1; *CTLA4*; cytotoxic T-lymphocyte antigen 4; *DNAM1*, DNAX accessory molecule-1; *FGL1*, fibrinogen-like protein 1; *GITR(L)*, glucocorticoid-induced TNFR family related protein ligand; *HAVCR2*, Hepatitis A Virus Cellular Receptor 2; *HLA*, human leukocyte antigen; *HMGB1*, High-mobility group protein B1; *ICOSL*, inducible T-cell co-stimulator ligand; *IFN*, interferon; *IL*, interleukin; *LAG3*, lymphocyte activation gene-3/CD223; *LSECtin*, liver and lymph node sinusoidal endothelial cell C-type lectin; *PDI*, programmed cell death protein 1; *PD-L1/PD-L2*, programmed death ligand 1/2; *PVR*, poliovirus receptor; *PVRL*, poliovirus receptor-related; *TCR*, T cell receptor; *TIGIT*, T-cell immunoreceptor with immunoglobulin and ITIM domains; *TIM3*, T-cell immunoglobulin and mucin domain 3



The number of co-inhibitory receptors usually defines the degree of exhaustion, and T cells in glioblastomas display a severely exhausted phenotype compared to grade II-III gliomas [542]. Interestingly, Mohme *et al.* found that these dysfunctional T cells also had an effector and transitional memory phenotype, indicating that the tumor-infiltrating T cells in glioblastoma constitute a population, which has been activated to form a tumor-specific immune response [544].

Reversal of T cell exhaustion/dysfunction using checkpoint inhibition, e.g. anti-PD1/anti-PD-L1 and anti-CTLA4 antibodies, has been successful in patients with melanoma [552-554], NSCLC [554-556] and renal cell carcinoma [557]. However, checkpoint inhibition has so far shown limited effect in patients with both primary and recurrent glioblastomas [23, 79, 80, 296, 316] The clinical inefficacy of checkpoint inhibitors could be attributed to a high level of intrinsic and adaptive resistance hindering initiation of an immune response and deactivating/hijacking the infiltrating immune cells, respectively [27, 28]. Most studies show that efficacy of checkpoint blockade is associated high tumor mutational burden [558-560], high levels of infiltrating CD8⁺ T cells, and checkpoint receptor-ligand expression [27, 28]. Although most glioblastomas contain PD-L1⁺ cells [561-564], the majority of glioblastomas have low T cell count [256], and low mutational burden [26, 535], rendering them immunologically cold. Interestingly, studies using orthotopic, immunocompetent murine glioblastoma models have reported response rates of 40-100% when targeting immune checkpoints with anti-PD1/PD-L1, anti-TIM3, anti-CTLA4, anti-CD137, or anti-IDO1 antibodies either alone or combined and in combination with chemo-/radiotherapy [565-570]. Further, *ex vivo* studies have shown that the infiltrating PD1⁺T cells isolated from glioblastoma tissue are relatively refractory to PD1 blockade dependent on their degree of exhaustion [543], but are revivable to some extent by combined CTLA4 and PD1 blockade. Interestingly, IL2 stimulation and IL10 neutralization of infiltrating T cells isolated from glioblastoma resulted in increased proliferation, while stimulation of CD3 (which complexes with TCR upon antigen recognition) and of the co-stimulatory CD28 had not effect [517]. Further, combined targeting of TIM3 and PD-L1 was able to restore IFN γ production in tumor-infiltrating T cells isolated from a murine colon carcinoma and led to significantly reduced tumor growth [571]. TIM3 has also been linked to acquired resistance to PD1 blockade in a mouse model of lung adenocarcinoma, and subsequent combination therapy with PD1 and TIM3 blockade resulted in a longer survival [572]. Collectively, these results indicate that combination immunotherapies are necessary to overcome the challenge of T cell exhaustion and immunosuppression in the TME. Further, combination strategies will counter the acquired resistance to

checkpoint inhibition, which is observed in several cancer types including glioblastoma, due to e.g. immunoediting, prolonged interferon signaling [573, 574], or upregulation of alternative checkpoint pathways [27, 318, 550, 572]. Numerous ongoing clinical trials are focusing on targeting checkpoint receptors/ligands (both inhibitory and stimulatory), as single agents and in combinations. Other immunotherapies being explored include immune modulators (e.g. cytokines), microenvironment modifiers, vaccines targeting specific antigens or patient tumor lysates, oncolytic viruses, epigenetic modifiers, macrophage-based therapy, and adoptive T cell transfer including chimeric antigen receptor T cells (CAR-T cells) [22, 23, 27, 575] (**Figure 15**).

7.6 Applied research methodologies and methods

In this thesis, four major techniques were used: immunohistochemistry/immunofluorescence, multiplex immunohistochemistry/immunofluorescence, digital image analysis, and NanoString mRNA profiling. Brief overviews of the basic theories behind these techniques are provided in the following subsections, while details regarding the methodologies are provided the *Methods* chapter and in the individual manuscripts.

7.6.1 Immunohistochemistry

Immunohistochemistry is a standard method used in research and in a clinical setting to assess the expression level and cellular localization of an antigen in tissue. Immunohistochemistry remains an integrated diagnostic tool in surgical pathology despite the development of several newer molecular methods, seeing that tumors are still classified based on a combination of phenotypic and genotypic characteristics. This “integrated” diagnostic approach is also employed in the CNS WHO classification as mentioned previously. Immunohistochemistry is a complex and time-consuming process with many steps. Originally all steps were performed manually, but to achieve high quality, reproducibility, and speed, the need for automation arose, and now fully- and semi-automated platforms are available from several vendors and available in most pathological departments [576].

The basic principle behind immunohistochemistry is detection of antigens using specific antibodies. The advantage of immunohistochemistry over other protein detection methods such as flow cytometry, western blotting and enzyme-linked immunosorbent assay (ELISA) is the ability to get a spatial and cellular mapping of the investigated protein in addition to information on its expression level. As indicated by its name, immunohistochemistry involves three major disciplines: immunology, histology, and chemistry. The immunological part is based on the binding of an antibody to its respective antigen/epitope. An antigen is a molecule (often protein or protein structure) that can trigger an antibody production by the immune system, and the epitope is the part of the antigen to which the antibody binds. Antibodies - or immunoglobulins - are glycoproteins made by immunizing animals (e.g. mouse, rabbit, and goat) with purified antigen. Antibodies can be either monoclonal (produced by one clone, specific for a single epitope) or polyclonal (pooled from multiple clones, may identify multiple epitopes) [577]. The histochemical part comprises the micro-anatomical study of cells and tissue. Immunohistochemistry is usually performed on frozen tissue or formalin-fixed paraffin-embedded (FFPE) tissue. The process of tissue fixation followed by dehydration and paraffin-embedding ensures tissue preservation and is widely used in pathology. The most commonly used fixative is

10% neutral-buffered formalin. Formalin immobilizes and stabilizes the antigens by forming cross-links which in turn may result in masking of epitopes by changing the quaternary and tertiary structure of proteins [578, 579]. To increase the immunohistochemical detection of the antigens, the epitopes are unmasked by a process called epitope retrieval which is primarily based on heat-induction in appropriate buffer and/or enzymatic digestion [577, 578, 580-582]. Although the activity of most endogenous enzymes including peroxidase is almost completely destroyed during formalin fixation, enzyme activity may persist in erythrocytes and myeloid cells resulting in unspecific background staining. As most antigen-antibody complexes are detected using horseradish peroxidase (HRP)-based detection systems, endogenous peroxidase activity is quenched by a hydrogen peroxide solution prior to incubation with primary antibody [577, 578, 582]. When implementing an immunohistochemical staining, different epitope retrievals and antibody concentrations should be tested. Different approaches can be used to detect and visualize the antigen-antibody complex, and some of these are briefly described in the next paragraphs.

Chromogenic detection

The simplest type of detection is the direct one-step detection method which involves application of a primary antibody that is directly conjugated to a chromogen. The method is simple and fast, but not very sensitive. A more sensitive approach is the indirect two-step technique where the primary antibody-antigen complex is detected and amplified using a secondary antibody (targeted against the primary antibody) labeled with an enzyme e.g. HRP or alkaline phosphatase (AP). The antigen-antibody complex is invisible under a brightfield microscope, but can be visualized by adding chromogen/substrate. For HRP, 3,3'-diaminobenzidine (DAB) is the most commonly used chromogen. DAB is oxidized by HRP resulting in a brown-colored precipitate forming where the antibody has bound. The sensitivity of this two-step method is higher because the primary antibody is unlabeled, thereby retaining its activity resulting in a stronger signal. Also, the number of labels e.g. HRP per molecule of primary antibody is higher thereby increasing the intensity of the reaction. This overall results in the ability to detect smaller amounts of antigen or to increase the dilution of the primary antibody as at least two labeled immunoglobulins can bind each primary antibody molecule [577, 578]. To prevent the secondary antibody from cross-reacting with endogenous immunoglobulins, the primary antibody should be derived from a different species than that of the tissue. Consequently, the secondary antibody must be against the host species of the primary antibody. Secondary antibodies can be modified for purposes of visualization and/or signal amplification e.g. using a polymer-based approach (e.g. EnVision+ or EnVision FLEX), which comprises a polymer backbone to which multiple molecules of enzyme and secondary antibody are conjugated, or a multimer-based approach (e.g. UltraView or Omnimap) which consists of long-arm linkers that attach the enzymes directly to the secondary antibodies. Another amplification system is the three-step method (e.g. EnVision FLEX+ or PowerVision+) which have an additional layer consisting of a linking antibody which may be tagged with a hapten (e.g. OptiView or DISCOVERY). Tyramide signal amplification (TSA) is a highly sensitive method for detection of low-abundance targets used in especially immunofluorescence and FISH applications, but can also be easily integrated in chromogenic immunostainings. TSA is used to enhance

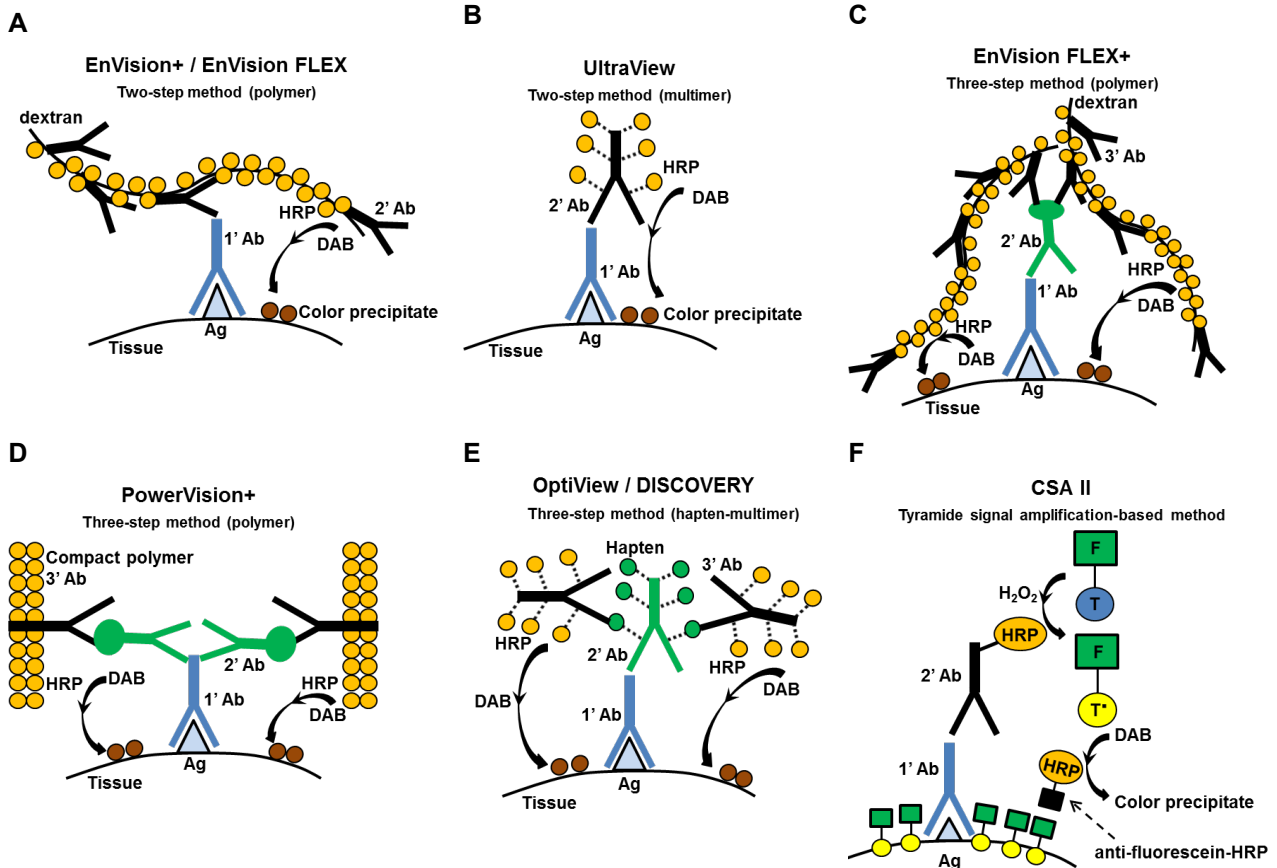


Figure 16 | Examples of different detection systems. (A, B) A two-step indirect detection is used in EnVision+/FLEX and UltraView where the secondary antibody (2' Ab) is conjugated to either a polymer backbone (A) or multimer (B). (C, D) In EnVision FLEX+ and PowerVision+ an additional step is applied between the primary antibody (1' Ab) and the polymer-conjugated antibody (3' Ab) using a linking antibody (2' Ab) resulting signal amplification. (E) In the OptiView/Discovery detection system the linking antibody is conjugated to a hapten which also amplifies the signal. (F) The Catalyzed Signal Amplification (CSA) II detection system is based on the principles of the tyramide signal amplification system. The primary antibody (1' Ab) binds to the antigen (Ag) and is recognized by the secondary antibody conjugated with HRP. A tyramide phenol complex conjugated to the fluorescent dye, fluorescein (F), is added. The tyramide is oxidized by HRP and binds to tyrosine residues near the antigen-antibody complex. Sequential addition of anti-fluorescein conjugated with HRP and the chromogen DAB results in a brown-colored precipitate in the area around the antigen which can be visualized in a conventional microscope.

the peroxidase detection system and involves HRP-catalyzed deposition of the phenol compound tyramide on and near a target protein/nucleic acid sequence *in situ*. In the presence of low concentrations of hydrogen peroxide, HRP is able to convert a labeled tyramide substrate into a highly reactive form that can covalently bind to tyrosine residues on proteins at or near the HRP. This generates high-density tyramide labeling of the target and improves the detection sensitivity up to 100-fold compared to conventional methods. Tyramide can be labeled with a fluorophore or a hapten such as biotin. The antigen-antibody complex can then be visualized in a brightfield microscope by sequential addition of a substrate conjugated with HRP and the chromogen [577, 578]. The concept of different chromogen detection systems is presented in **Figure 16**.

Fluorescent detection

Immunofluorescence is based on the same principles as described above. However, the primary or secondary antibody is conjugated with a fluorescent dye/fluorophore which emits upon photoexcitation via light of a shorter wavelength. The signal is observed through a conventional epifluorescence microscope or further enhanced with advanced confocal microscopy. The antibodies can be tagged to fluorescent dyes in different colors, and commonly used fluorophores are fluorescein isothiocyanate (FITC), 6-carboxyfluorescein (FAM), Texas Red, tetramethylrhodamine (TRITC), cyanine 5 (Cy5), and Alexa/Dylight Fluor dyes. As mentioned previously, amplification systems are also available in immunofluorescence stainings including TSA. It is important to choose the appropriate fluorophores and paired excitation/emission filter sets to optimize signal detection and minimize spectral overlap when applying multiple fluorophores. Also, fluorophores are susceptible to photobleaching by excess exposure to high-energy light sources, high temperatures or by long-term storage. The risk of photobleaching can be minimized by selecting photostable fluorophores, applying antifade mounting reagents and/or reducing excitation duration and intensity. While chromogenic immunohistochemistry is suitable for analyzing the distribution of proteins of interest in tissue samples, immunofluorescence is more suitable when investigating the subcellular localization and co-localization levels of specific targets [52, 581, 583]. Thus, in this thesis immunofluorescence was applied to explore co-expression/localization patterns of different proteins, and the combination of fluorophores FITC/FAM, Cy5, and 4',6-diamidino-2-phenylindole (DAPI) for nuclear counterstaining was used resulting in minimal spectral overlap (**Figure 17**).

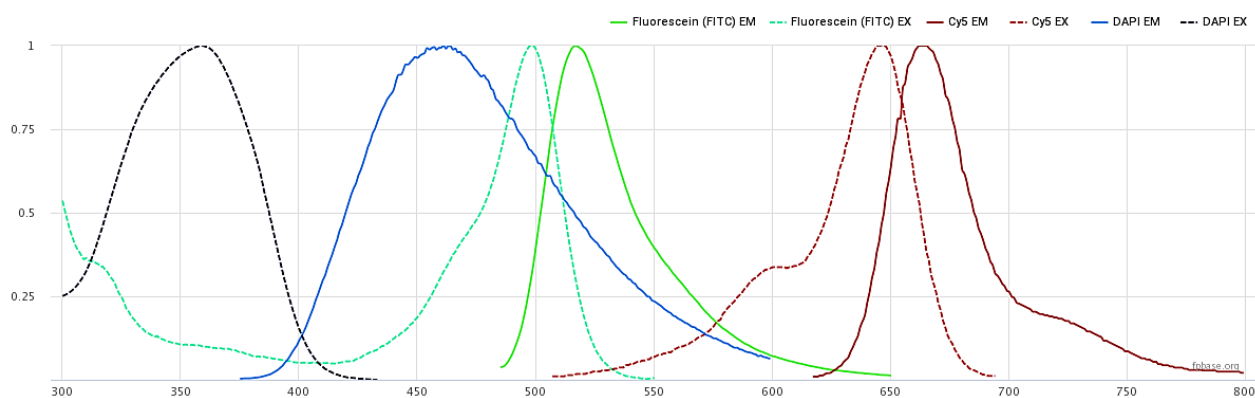


Figure 17 | Absorption and emission spectra for the used fluorophores DAPI, FITC/FAM and Cy5. Created through the online resource, <https://help.fpbase.org/tools/spectra-viewer> [584].

7.6.2 Multiplex immunohistochemistry and immunofluorescence

Nearly all clinical immunohistochemistry is performed to detect a single marker/target per slide-mounted specimen. Detecting more than one marker per slide, termed multiplexing, has important advantages compared to singleplex stains including preservation of patient tissue. Multiplexing also allows characterization of cellular phenotypes and spatial relationships among cells *in situ*. Several multiplexing technologies exist, and depending on the approach between two and up to more than 60 targets can be multiplexed with high precision and accuracy [52, 583, 585]. Chromogenic multiplex immunohistochemistry can be done by adding multiple

labels to the section simultaneously, sequentially or by using a stain-and-strip approach allowing 3-10-plex assays [586-589]. Numerous platforms are available for multiplex immunofluorescence techniques, including standard epifluorescence microscopes which can accommodate up to 4-5-plex assays and multispectral technologies which can support 6-60-plex assays by re-probing and re-staining cycles [182, 585, 590, 591]. Higher-order multiplex technologies include multiplex ion beam imaging, by time of flight (MIBI-TOF), imaging mass cytometry (IMC) and digital spatial profiling (DSP) [52, 583, 592]. All multiplex technologies requires meticulous optimization and validation, and it is often best to use singleplex stains for each marker of interest as the starting point and reference for method development as switching from a singleplex to a multiplex format can result in an increase or decrease of the individual marker signal [52]. A disadvantage of multiplexing methods is that they typically require the use of digital image software which is not always available/affordable [592].

When implementing a multiplex assay it is important to consider the following: the distribution and (co)localization of markers of interest, the host species of the antibodies, the choice of antigen retrieval, the antibody concentration and incubation time, and the choice of detection system(s). All these aspects contribute to assay optimization and achieve the best signal-to-noise ratio. In this thesis, sequential chromogenic multiplex immunohistochemistry and 2-plex immunofluorescence assays were developed as previously described [216, 588-591, 593].

Chromogenic multiplex immunohistochemistry has the advantages of being affordable, and automated platforms are available in most laboratories. Further, the stains can be reviewed using a conventional brightfield microscope. Multiplexing is performed by using different chromogen/enzyme pairs. Over the last decade, multiple new chromogens have been developed that are substrates of either HRP or AP. Among the colored precipitates are purple, red, teal, yellow, green, blue, and silver. The chromogenic multiplex technique is especially useful when distinguishing different cell types, but challenging when attempting to co-localize targets within cells due to the broad absorbance spectra of chromogens. This aspect overall limits the ability to multiplex beyond three targets [52, 583]. However, unique combinations of the newer, semi-transparent chromogens facilitate identification of co-expression of markers in a single cell due to color shifts when the chromogens overlay (e.g. yellow and purple produce an orange-red color) [52]. Also, several studies have attempted to circumvent the issue by developing covalently deposited dyes that e.g. rely on enzymatic activation of dyes conjugated with tyramide to produce stains covalently bound to cellular and tissue components surrounding the sites of targeted proteins; these dyes have narrower and more well-separated absorbance bands compared to traditional chromogens thereby increasing the dynamic range of chromogenic multiplexing [586, 594].

The principle behind multiplex immunofluorescence relies on the ability of individual fluorophores to be uniquely excited by one wavelength and emit at a characteristic wavelength. Availability of secondary antibodies in multiple wavelengths and from various species adds flexibility and specificity to the technique, facilitating detection of multiple markers in the same tissue and subcellular compartments. The antibodies can be labeled using semiconducting nanoparticles/quantum dots [595, 596], DNA barcodes [597, 598], and more frequently reactive fluorophores [52, 590, 592]. The most common method used for multiplex

immunofluorescence is the TSA approach [590]. As described previously, activated tyramide covalently binds to tyrosine residues on and surrounding the target of interest and importantly remains bound when exposed to heat, while heat removes non-covalently bound primary antibody and polymer/multimer-HRP. Thus, sequential staining detecting other targets is possible using different tyramide-linked fluorophores. Using this approach, it is possible to create a protocol that allow use of antibodies raised in the same species and create panels that can accommodate simultaneous detection of six to eight individual targets. The number of targets that can be visualized is limited by the number of wavelength band passes and paired excitation/emission filter sets coupled to the microscope/fluorescence scanner. As mentioned, there is a risk of bleedthrough/overlap of the signals if the spectral profiles are too close in wavelength causing false-positive reading in an adjacent channel. Normally four to five different colors can be imaged with a standard fluorescence microscope equipped with appropriate filters aligned with the peak absorption wavelengths. If more than four targets are to be imaged simultaneously, a more expensive multispectral imaging system can be used. Multispectral imaging software conduct linear unmixing to separate the signals and often subtract spectral overlap(s) as well as the intrinsic autofluorescence of the FFPE tissue [52, 583].

7.6.3 Digital image analysis

Immunohistochemical stains can be analyzed using different approaches. In routine diagnostic pathology most biomarkers are assessed by semi-quantitative scoring systems using conventional microscopy (e.g. mitotic index, the proliferation marker Ki67 labeling index, and human epidermal growth factor receptor 2 (HER2) score). However, these approaches are often flawed by significant measurement bias, intra- and interobserver as well as interlaboratory variation resulting in low reproducibility [599-603]. In the last decade digital pathology and the adoption of digital image analysis have evolved rapidly, partly motivated by the need for optimization and standardization of clinical pathology and partly due to the increasing importance of tissue-based research for biomarker discovery and personalized/targeted medicine. The development in digital pathology is mainly attributed to the use of whole-slide scanners as well as advances in software and computer processing capacity. Digital image analysis is a term used to describe the computer-assisted quantitative analysis of digital images to extract numerical data on the underlying structures e.g. area fraction and intensity [603]. Digital image analysis facilitates measurements of biological characteristics and processes which are visually accessible, but often also allows detection of features not readily definable to the naked eye. It also enables the measurements of protein expression within different tissue and subcellular compartments taking spatial heterogeneity into account [600, 601]. For image acquisition, several scanning systems and programs have been developed e.g. Nanozoomer (Hamamatsu), iScan (Ventana/Roche), Vectra/Polaris (Akoya Bioscience), and ScanScope (Leica Biosystems), and similarly different software programs are available for image analysis e.g. Visiopharm TissueMorph (Visiopharm), Image J (NIH), and Aperio image analysis (Leica Biosystems) [592].

Automated Quantitative Analysis (AQUA) was one of the first methods used to objectively and accurately measure protein expression based on fluorescent signals within tumor and subcellular compartments of FFPE specimens, and the AQUA score was found to match or even exceed pathologist-based scoring in regards to

identifying patients with a specific prognosis [51]. As Ki67 labeling index is used in diagnostic pathology in various cancer types, numerous studies have compared digital image analysis to semi-quantitative scoring, and most studies have shown good agreement between the two methods [604-606]. Similar results were reported for HER2 which is used as a predictive biomarker in breast cancer [607-609].

The strength of digital image analysis is that, if performed correctly, it provides more reliable and reproducible quantitative estimates than pathologist-based scoring. The methodology, however, has some basic requirements in order to obtain valid and robust results. These include standardization of: 1) tissue fixation, sampling and staining as well as image capturing, 2) selection of regions of interest (ROIs), 3) algorithm design and output [600, 601]. As the algorithms are developed by human beings, digital image analysis is also prone to both intra- and inter-algorithm variation especially in inexperienced hands. The algorithm design is somewhat complex, and the principle steps include: pre-processing of the image to enhance structures of interest and to suppress noise/background, segmentation of the image into its relevant components, postprocessing steps to refine the segmentation, and generation of output [600]. Digital image analysis can thus be a laborious process, and in many cases digital image analysis cannot compete with manual scoring in terms of time spent. However, it depends on the complexity of the image acquisition process and algorithm, and digital image analysis has been shown to reduce workload [610].

The most commonly used technique to obtain quantitative information from histologic tissue sections is two-dimensional morphometry, e.g. number of cells, linear measurements or total area of positive staining. A more accurate and precise technique is design-based stereology which is a mathematical science based in statistics and stochastic geometry [611-613]. Stereology provides efficient tools for estimation of three-dimensional structures contained within an organ (e.g. volume, surface area, length, and number of objects) using serial two-dimensional tissue sections, stringent sampling methods, and unbiased counting frames. The sampling method is a process known as systemic uniform random sampling (SURS). SURS ensures that every structure of interest within the tissue has an equal chance of being sampled thereby eliminating the risk of sampling bias. An advantage of stereology compared to two-dimensional histomorphometry is that it is unbiased seeing that it does not make assumptions about the tissue. A caveat of stereology is that it cannot be performed retrospectively as the entire tissue (or ROI) needs to be available for sampling [611-613]. Also, stereology is a more time-consuming process than morphometry, and these aspects overall limit the use of stereology in clinical pathology.

In this thesis, the immunohistochemical stains were analyzed as observer-independent as possible. Accordingly, computer-assisted and semi-quantitative techniques were used dependent on the staining. Concepts from the design-based stereological approach, including the unbiased counting frame and SURS, were incorporated as much as possible when performing two-dimensional cell counting.

7.6.4 NanoString

The NanoString nCounter technology has gained increasing impact in clinical pathology and research in the past decade due to its high sensitivity, robustness, and user-friendliness. The technique is hybridization-based and allows direct multiplexed measurements of hundreds of targets in a single reaction with a limited input

amount, without amplification or other enzymatic processing and without the need for cDNA or library production [63, 614, 615]. Using a novel molecular fluorescent barcode technology, RNA is directly tagged with a capture probe and a reporter probe that is specific to the target of interest creating a unique target-probe complex. For every target of interest, two adjacent 50 base pair sequences are designed which are complementary to a 100 base pair target region; one of the target-specific oligonucleotides is covalently linked to a biotin moiety at the 3'-end to create the capture probe, while the other target-specific oligonucleotide is covalently linked to a fluorescent labeled color-coded molecular barcode at the 5'-end to create the reporter probe. The barcode comprises six positions which are occupied by red, green, yellow, or blue fluorescent molecules (**Figure 18**). This barcode system allows generation of a large variety of fluorescent barcodes, each targeting specific gene transcripts, and each color-coded barcode represents a single target molecule [63, 615]. The nCounter assay includes three main steps: 1) hybridization, 2) purification and immobilization, and 3) counting and analysis. The hybridization process is solution-based and performed in the presence of excess probe to drive the reaction to completion. Up to 800 targets can be hybridized in a single reaction tube. The hybridized complexes are purified removing excess probe via an automated liquid handling robot called the prep station and bound to the streptavidin-coated surface of the cartridge. The purified hybridized molecules are elongated and immobilized by an electric field to facilitate subsequent imaging. Finally, an automated fluorescence digital analyzer scanner digitally counts the number of barcodes hybridized to a single RNA (or DNA) molecule for each target, and as no amplification is performed a single molecule equals to one counted barcode [615]. These counts are then normalized to reference genes and system controls for comparison within and across samples to accurately determine the expression of each target. The technology is particularly designed for gene expression analysis, but CNV, genomic mutations, chimeric RNAs and microRNA expression can also be analyzed using this technology. The barcoding technology offers several advantages, including highly reproducible data, robust performance (including FFPE samples), a simple protocol with minimal hands-on-time, flexible sample input (e.g. FFPE tissue, frozen tissue, serum/plasma, cell lysates) and flexible analyte type (RNA, microRNA, protein, and DNA) [63, 616, 617].

In the field of molecular diagnostics processing of FFPE specimens has always been challenging. As described previously, formalin fixation creates irreversible crosslinks between the proteins and nuclei acids which cause technical problems in DNA and RNA extraction thereby limiting the possibilities of subsequent downstream analyses including PCR, microarrays, and high-throughput sequencing which has frequently been used in RNA expression studies. Several studies have tested the performance of the nCounter platform on FPPE tissue by comparing mRNA expression levels between matching fresh/frozen and FFPE sample types. The NanoString technology was found favorable over other techniques including reverse transcription quantitative real-time PCR (RT-qPCR) based on sensitivity, accuracy, and technical reproducibility [614, 616-618]. NanoString also offers easy data analysis compared to other molecular techniques such as RNA sequencing, and since absolute transcript abundance is determined and normalized against the expression of housekeeping genes for each single sample, NanoString assays do not require use of control samples [63, 618].

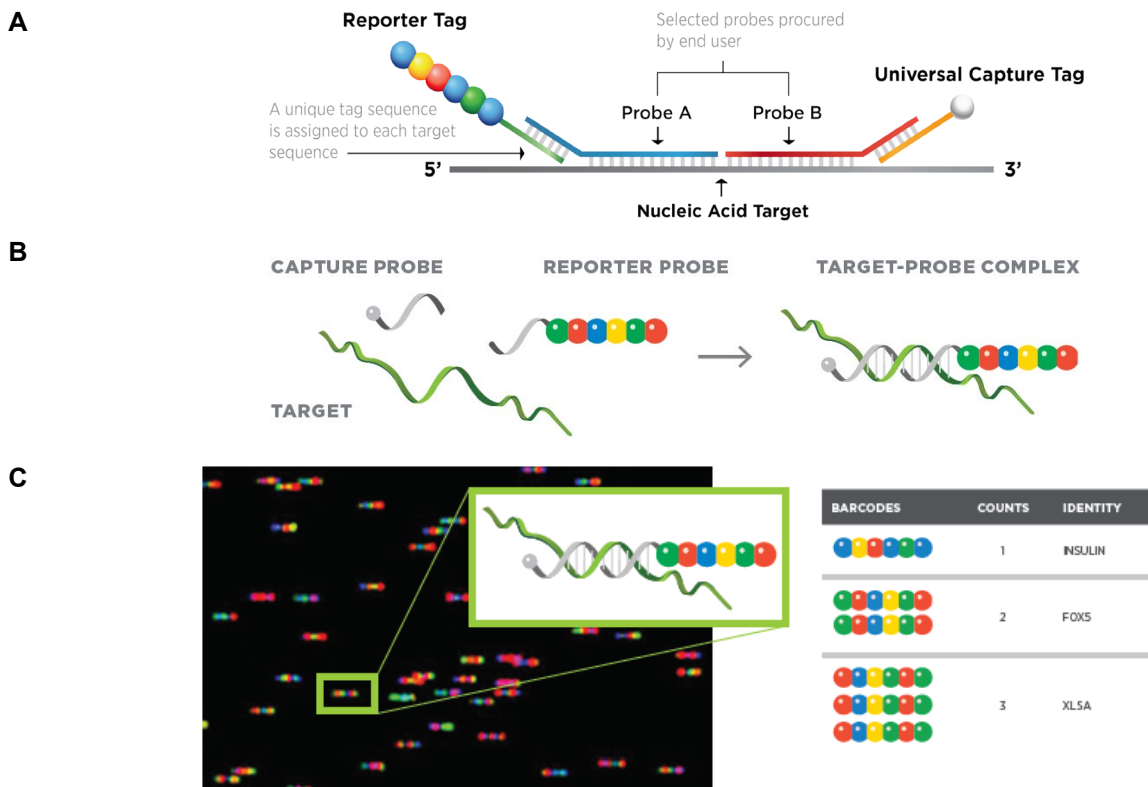


Figure 18 | NanoString technology. (A) Oligonucleotide probes hybridize with Reporter and Capture Tags and the target nucleic acid to create a Tag Complex. (B) Capture and Reporter Probes (left) hybridize with a single-stranded target to form a double-stranded probe-target complex (right). The reporter probe consists of the target-specific oligo covalently linked to a fluorescent labeled color-coded molecular barcode which can be occupied by one of four colors allowing a large diversity of codes. Barcodes are synthesized with a single target specific probe, so they bind to target in a 1:1 ratio. Capture probes work together with reporter probes to increase sensitivity and specificity. (C) Following hybridization, the probe-target complexes are immobilized and aligned on a sample cartridge by exposure to an electric current. Data is collected using a microscope and CCD camera by taking images of the surface where hundreds of thousands of barcodes are bound. Barcodes are sorted by code, individually counted, and cross-referenced to a target identity, yielding a digital count of target molecules present in a sample. Reprinted with permission from NanoString.

Although the NanoString technologies are popular for its obvious advantages, some challenges exist especially in regards to using it in a large-scale manner. The output from the NanoString nCounter requires additional processing, normalization, and analysis to account for sample variation, creating more workload. Also, the performance of reference genes was found to be platform specific possibly due to probe placement or specificity, leading to detection of distinct splice variants and other transcript isoforms. Moreover, the design of the probe set has to be accurate to avoid binding at any highly variable-untranslated regions or pseudogenes in order to minimize the number of false positives. In terms of large-scale gene expression studies and discovery studies, especially RNA sequencing is advantageous because the entire population of genes in the genome can be targeted, and the technology does not rely on sequence information and alignment. In contrast, NanoString assays require prior knowledge of genes of interest, is limited by its barcode counting system, and

can only measure up to 800 genes in a single reaction [615, 618]. **Table 6** compares the NanoString technology with other technologies used for gene expression profiling.

A Nanostring nCounter assay can be designed around a panel of genes, a signaling pathway, or a biological response e.g. immune infiltration, and the assays can be used for validation studies and discovery of gene expression profiles using either pre-defined and/or custom-made gene panels. The technology has been used previously in several glioma studies [39, 212, 268, 619] and has also been translated to clinically relevant molecular diagnostic assays e.g. breast cancer profiling/PAM50 [620, 621], lung cancer gene fusions [622], leukemia [623], and lymphoma [624]. E.g. the Prosigna breast cancer profiling assay is based on the PAM50 gene signature consisting of 50 genes that stratify breast cancer samples into risk groups to predict likelihood of relapse within a 10-year time frame [625, 626]. In this thesis a modified myeloid innate immune response mRNA panel was used to investigate the myeloid gene expression profile of CD204-enriched glioblastomas.

Table 6 | Comparison of different technologies used for gene expression profiling[§]

	NanoString	qPCR	Microarrays	RNA sequencing
Working principle	The expression level of a target gene is measured by counting the number of times the color-coded barcode is detected.	RNA is reverse-transcribed to cDNA and put into real-time PCR. DNA products are detected by fluorescent dyes	RNA is hybridized with the probes immobilized on the chip. The expression pattern is recorded.	RNA is converted to a cDNA library, which is then sequenced by high-throughput DNA sequencing.
Data collection and analysis	By visualization, color-coded images are taken by CCD camera and output as code counts; normalization required.	By absolute and relative quantification	By visualization; normalization and statistical tests required	Output as sequenced reads with quality scores or read alignments; normalization and statistical tests required
Turnaround time	Fast	Relatively slow	Fast	Medium
Resolution	High	High	High	High
Throughput	Medium	Low	High	High
Number of genes/transcripts detected	800	1-100	50,000	Whole transcriptome
Amount of sample required	Small, degraded samples possible	Relatively large	Small	Small
Background noise	Low	Low	High	Low
Dynamic range	High	High	Low	High
Sensitivity	< 1 copy /cell	10-200 copies /cell	1-10 copies /cell	< 1 copy /cell
Specificity	Depends on the design of capture and reporter probes	Depends on the design of forward and reverse primers	Depends on the design of probes and density of probes annealed	Depends on data analysis
Cost	Low	Low	High	High

[§] Based on [615, 618]

8. Methods

This chapter provides a brief overview of the methods used in the thesis. More detailed protocols are described in the individual manuscripts.

8.1 Patient tissue (manuscripts I-IV)

The Region of Southern Denmark glioma cohort is a population-based cohort. The cohort originally included tissue from 433 adult patients diagnosed with primary glioma, WHO grade I-IV, between 01.01.2005 and 31.12.2009. The cohort is well-described and has been used in several studies [216, 217, 261, 627-632]. Up to 240 patients had sufficient available tumor tissue for immunohistochemical analysis, and this cohort was used in manuscript I. Based on the results from manuscript I, tissue samples from 46 of the 240 patients were included for molecular and immunophenotypic analysis in manuscript II using the NanoString technology.

A patient cohort for comparison of IDH-mutant and IDH-wildtype primary astrocytomas (WHO grade III-IV) was established and used in manuscript III and manuscript IV. The cohort comprised 72 adult patients diagnosed between 1997-2017. Tumor grades were selected and sequenced to provide homologous tumor grades with or without IDH mutation, as such WHO grade II with high and WHO grade IV with low IDH mutational penetrance are under- and overrepresented, respectively. Of the 72 patients included in the cohort, 52 underwent initial surgery at the Department of Neurosurgery, Odense University Hospital, Denmark, and 20 had initial surgery at the Department of Neurosurgery, Heinrich Heine University, Düsseldorf, Germany. IDH mutation status was identified by immunohistochemistry or by NGS. Of the 72 tumors, 23 were IDH-mutant anaplastic astrocytomas, 16 were IDH-wildtype anaplastic astrocytomas, 14 were IDH-mutant glioblastomas, and 19 were IDH-wildtype glioblastomas.

Tissue arrays containing eight to 25 glioblastoma specimens were used for immunohistochemical or immunofluorescence analyses in manuscript I and manuscript IV. A cohort consisting of glioblastoma tissue from eight patients was included for double immunohistochemical analyses in manuscript II. All included tissue samples were from patients diagnosed with primary glioblastoma between 2004-2018.

All glioma samples were derived from initial surgical resection, and none of the patients had received treatment (radiation or chemotherapy) prior to surgery, apart from possibly corticosteroids. Further, all tumor samples were classified or reclassified according to the 2016 WHO classification of diffuse gliomas [91].

Two post-mortem adult normal brain tissue samples were included for double immunofluorescence analysis in manuscript I. Brain tumor tissue was obtained from 10 patients with primary diffuse large B cell lymphoma (DLBCL) in the CNS, 10 patients with first-time CNS metastasis from melanoma, and 10 patients with first-time CNS metastasis from NSCLC. Patients with DLBCL were diagnosed between 1999-2015, while patients with melanoma and NSCLC were diagnosed between 2012-2015 and 2013-2014, respectively.

All tissue specimens were fixed in 10% neutral-buffered formalin and embedded in paraffin.

8.2 Glioma reclassification (manuscripts I-IV)

An integrated diagnostic algorithm was used to reclassify the gliomas included the patient cohorts according to the 2016 WHO classification of tumors of the CNS if the tumors were originally classified according to the 2007 WHO classification. The algorithm included the following techniques: immunohistochemistry, FISH, NGS, and DNA methylation profiling. The work process of the reclassification is illustrated in **Figure 19**.

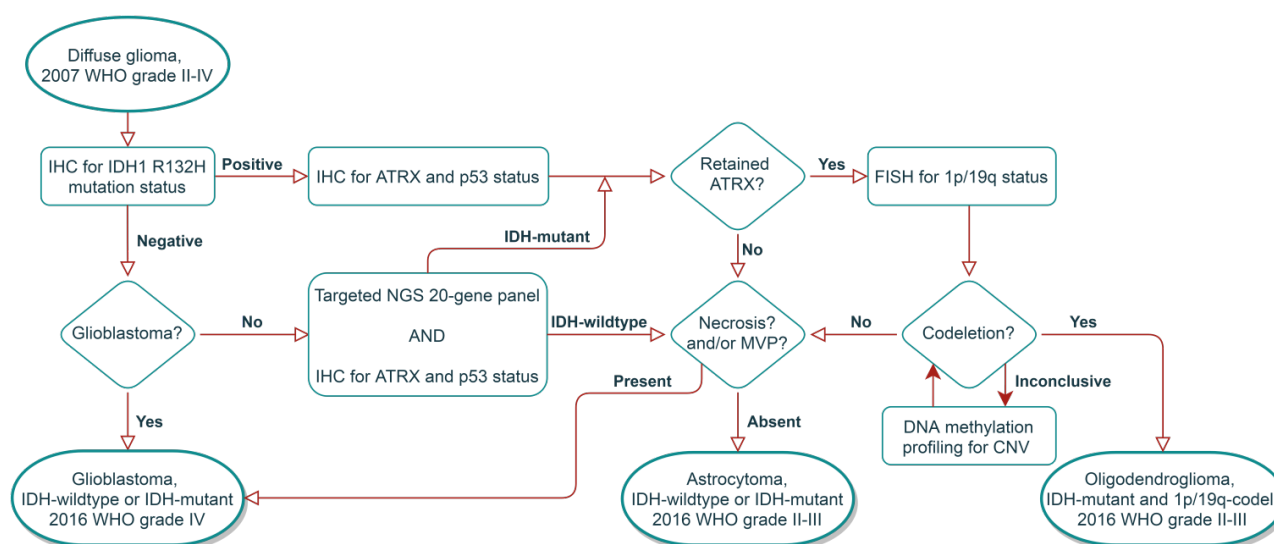


Figure 19 | Flowchart of the glioma reclassification process. All 2007 WHO grade II-IV gliomas were initially immunohistochemically stained with an antibody against IDH1 R132H. All grade II-III gliomas and IDH1 R132H-mutant glioblastomas were stained with antibodies against ATRX and p53. To identify less common variants of *IDH1* and *IDH2* mutations, targeted NGS analysis was performed on grade II-III gliomas when the IDH1 R132H stain was negative. For glioblastomas, IDH status was only investigated using immunohistochemistry (IHC). All IDH-mutant gliomas with retained nuclear ATRX expression were subdivided into IDH-mutant astrocytomas and IDH-mutant, 1p/19q-codeleted oligodendrogliomas by testing for chromosomal deletions of 1p/19q using FISH (or DNA methylation profiling). The integrated diagnostic distinction between tumors of oligodendroglial and astrocytic origin was aided by p53 status, as astrocytic tumors may have a mutation in the *TP53* gene that result in p53 overexpression. Histologic grading was performed according to the 2007 WHO criteria, which remained unchanged in the 2016 version, and consisted of an evaluation of cytological atypia and anaplasia, mitotic activity as well as presence of MVP and necrosis [91].

8.2.1 Next-generation sequencing (manuscripts I, III, and IV)

For 2007 WHO grade II-III gliomas with absent IDH1 R132H mutation immunohistochemically, NGS was performed to detect other mutations in the *IDH1/2* genes using the Ion AmpliSeq glioma-tailored 20-gene panel (Life Technologies, Carlsbad, CA, USA) which was designed and described by Zacher *et al.* [189]. A summary of the gene panel is provided in **Table 7**. DNA was extracted from FFPE tissue samples using the GeneRead DNA FFPE Kit (Qiagen, Hilden, Germany). NGS libraries were generated according to the manufacturer's protocol and as previously outlined [189]. Data were analyzed for sequence variants using Ion Reporter, and Binary Alignment Map files were visualized using Golden Helix GenomeBrowse 2.1.0 (Golden Helix, Bozeman, MT, USA).

Table 7 | Summary of the 20 glioma-associated candidate genes including the *IDH* genes analyzed by NGS

No.	Gene	Chromosome	Type	Exons (n)	Amplicons (n)	Total nucleotides	Covered nucleotides	Missed nucleotides	Overall coverage
1	<i>NRAS</i>	1	cds	4	9	614	614	0	1.000
2	<i>FUBP1</i>	1	cds	20	38	2155	2043	112	0.9480
3	<i>CDKN2C</i>	1	cds	2	6	529	529	0	1.000
4	<i>H3F3A</i>	1	hot spot	n/a	3	222	219	3	0.986
5	<i>IDH1</i>	2	hot spot	n/a	3	297	297	0	1.000
6	<i>PIK3CA</i>	3	cds	20	51	3427	3158	269	0.9215
7	<i>TERT</i>	5	hot spot	n/a	3	362	278	84	0.768
8	<i>PIK3R1</i>	5	cds	18	35	2524	2486	38	0.9849
9	<i>EGFR</i>	7	cds	31	59	4304	4304	0	1.0000
10	<i>BRAF</i>	7	hot spot	n/a	4	220	216	4	0.982
10	<i>BRAF</i>	7	hot spot	n/a	2	201	201	0	1.000
11	<i>CDKN2A</i>	9	cds	7	11	1345	1325	20	0.9851
12	<i>CDKN2B</i>	9	cds	3	9	1047	1038	9	0.9914
13	<i>PTEN</i>	10	cds	9	19	1311	1268	43	0.9672
14	<i>RB1</i>	13	cds	27	49	3084	2706	378	0.8774
15	<i>IDH2</i>	15	hot spot	n/a	2	201	201	0	1.000
16	<i>TP53</i>	17	cds	13	19	1569	1532	37	0.9764
17	<i>NF1</i>	17	cds	59	143	9310	9264	46	0.9951
18	<i>CIC</i>	19	cds	20	56	5047	4967	80	0.9841
19	<i>NF2</i>	22	cds	17	29	2011	2011	0	1.0000
20	<i>ATRX</i>	X	cds	35	110	7864	7482	382	0.9514

The table provides information on the chromosomal location of each gene, the numbers of exons analyzed from each gene, the number of amplicons analyzed per gene, the number of covered or missed nucleotides per gene, and the overall coverage rate. Type indicates whether the entire coding sequence (cds) or mutational hot spot regions were investigated. n/a, not applicable. Primarily results for the *IDH1* and *IDH2* genes (highlighted in blue) were used in the reclassification. Reprinted from Zacher *et al.* [189] after minor reformatting under the terms and conditions provided by John Wiley and Sons and the Copyright Clearance Center.

8.2.2 Fluorescent in situ hybridization analysis (manuscripts I, III, and IV)

Interphase FISH analysis was carried out for selected diffuse gliomas as part of the glioma reclassification process to detect possible chromosomal deletions in chromosomes 1 and 19. This method utilizes fluorophore-labeled DNA probes that are locus-specific with target probes hybridizing to subtelomeric 1p36 and 19q13 in conjunction with control probes on chromosomal control regions 1q25 and 19p13, respectively. The hybridization protocol was conducted according to the Dako Histology FISH Accessory Kit K5799 (Agilent Technologies, Santa Clara, CA, USA). Briefly, three- μ m-thick FFPE tissue sections were dewaxed in xylene, rehydrated in ethanol, and then placed in pre-treatment solution for 20 min which had been preheated to 95-99°C in a water bath. Next, sections were washed twice for 3 min in Wash Buffer, pepsin-digested for 10 min at RT, washed again twice for 3 min in Wash Buffer, and dehydrated in ethanol. Slides were air-dried for 15 min, and 10 μ l Vysis LSI Dual-Color Probe was applied targeting either 1p36/1q25 or 19q13/19p13 (Abbott Molecular, Des Plaines, IL, USA). Sections were then coverslipped, and slides were denatured at 85°C for 5 min and hybridized at 37°C for 20h in a humidified HYBrite (Vysis, Abbott Molecular). After hybridization,

slides were washed in 65°C diluted Stringency Buffer for 10 min, dehydrated in ethanol, air-dried, coverslipped and nuclear counterstained using VECTASHIELD® Mounting Media containing DAPI (VWR International, Radnor, PA, USA). Specimens were examined using a Leica DM5000B fluorescent microscope with filters appropriate for SpectrumOrange/SpectrumGreen and DAPI. Signals ratios were assessed as described by Woehrer *et al.* [633]. A total of 100-200 adjacent non-overlapping nuclei were evaluated at 100x magnification objective using immersion oil. The number of nuclei exhibiting a balance, imbalance or deletion (**Figure 20**) were summed and expressed as percentages. Tumors were considered to show a deletion if the percentage of nuclei with deletion exceeded 30%.

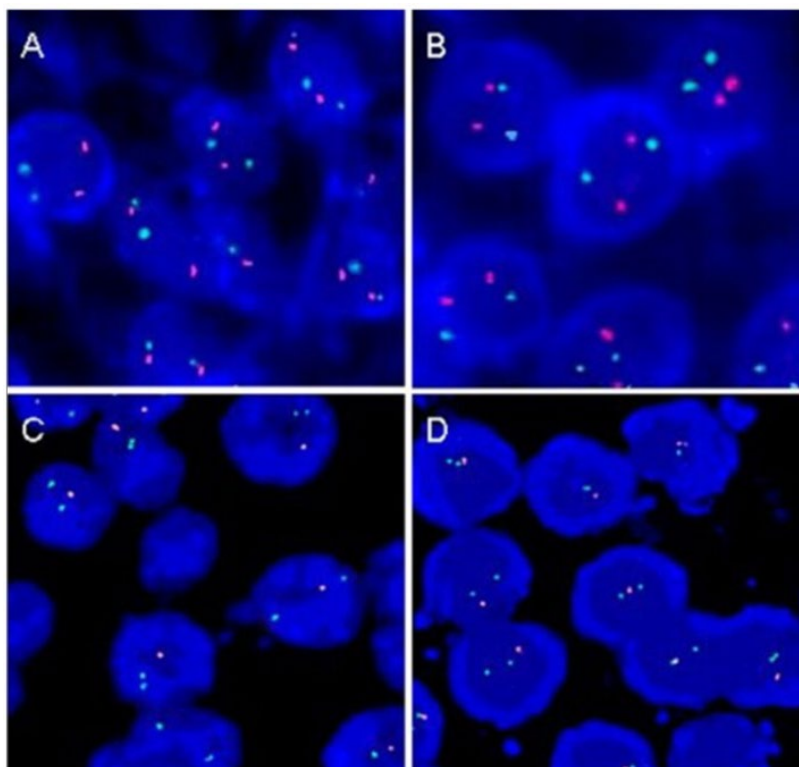


Figure 20 | Example of FISH analysis for 1p/19q status. (A, B) Diploid balanced ('non-deleted') nuclei for 1p36 (A) and 19q13 (B). (C, D) Diploid imbalanced and 'deleted' nuclei for both 1p36 (C) and 19q13 (D). Reprinted from Zhang GB *et al.* 2013 [634] under the terms and conditions provided by Springer Nature and the Copyright Clearance Center.

8.2.3 DNA methylation profiling (manuscripts I, III, and IV)

For tumors with inconclusive FISH analysis, 1p/19q status was determined by assessing CNV of chromosomes 1 and 19 using the Infinium Methylation 850K EPIC BeadChip array (Illumina, San Diego, CA, USA) according to manufacturer's description and analyzed as described by Capper *et al.* [200]. In short, DNA was isolated from FFPE tissue samples using the GeneRead DNA FFPE Kit (Qiagen). The quality of the purified DNA was evaluated by PCR using the Illumina FFPE QC kit. After bisulfite conversion using the EZ DNA Methylation Kit (Zymo Research, Irvine, CA, USA), DNA was restored with the ZR-96 DNA Clean & Concentrator-5 Kit (Zymo Research), and the restored DNA samples were amplified, fragmented, precipitated, and resuspended according to the Infinium HD FFPE Methylation Assay protocol followed by overnight hybridization onto EPIC BeadChips. After washing the BeadChips to remove unhybridized and non-

specifically hybridized DNA, labeled nucleotides were added to extend the primers, and the BeadChips were stained, coated, and scanned using the iScan Control Software (Illumina). The array data was viewed in the GenomeStudio Software (Illumina) to determine possible CNV (**Figure 21**).

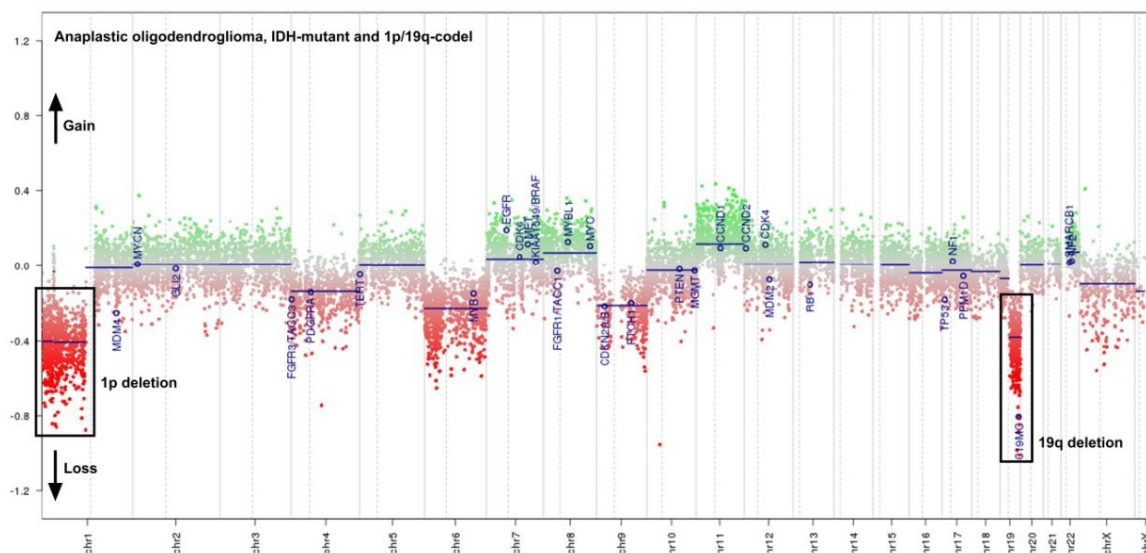


Figure 21 | Methylation profiling and CNV plot. The CNV plot shows a clear loss of both chromosome 1 and chromosome 19 indicating 1p/19q-codeletion.

8.3 Immunohistochemistry and immunofluorescence (manuscripts I-IV)

Immunohistochemical techniques were used in manuscripts I-IV. FFPE tissue was cut into three- μ m-thick sections on a RM2255 microtome (Leica Biosystems, Wetzlar, Germany) which were mounted on FLEX IHC slides (Dako, Glostrup, Denmark). All tumor specimens were stained routinely with H&E to define representative tumor regions. Immunostaining protocols were carried out on fully- or semi-automated immunostainers manufactured by Ventana Medical Systems (Tucson, AZ, USA) or Dako (Agilent Technologies, Santa Clara, CA, USA). Staining protocols were optimized for each antigen to achieve the highest signal-to-noise ratio. All antibodies used for immunofluorescence were initially implemented as chromogenic stains. Appropriate staining controls including omission of primary antibody and/or parts of the detection system were performed to check for possible cross-reactivity and non-specific staining related to the detection systems. Tissue arrays containing positive control tissue were included for each staining run to ensure inter-run staining consistency. Information regarding primary antibody, epitope retrieval procedure, dilution, incubation, detection systems, and chromogen/fluorophore for each antigen is presented in **Tables 8-11**. Overviews of the immunohistochemical methods used in this thesis are provided in the next four subsections.

8.3.1 Conventional immunohistochemistry (manuscripts I-IV)

Fully-automated protocols, including deparaffinization, epitope retrieval and quenching of endogenous peroxidase, were performed using the BenchMark ULTRA Immunostainer or the Ventana DISCOVERY ULTRA instrument with OptiView DAB IHC, ultraView Universal DAB, or DISCOVERY HQ-HRP-DAB

detection kits (Ventana Medical Systems). Semi-automated protocols were conducted on the Dako Autostainer Link 48 instrument with the EnVision FLEX+ detection system (Agilent) or the Dako Autostainer Plus instrument using the Dako EnVision+ (Agilent), Dako ADVANCE (Agilent), or Novocastra PowerVision Poly-HRP (Leica) detection systems. For the semi-automated protocols, deparaffinization, epitope retrieval, and endogen peroxidase inactivation were done manually. Briefly, tissue sections mounted on IHC slides were dewaxed in xylene and rehydrated in an ethanol gradient. Heat-induced epitope retrieval (HIER) was performed by submerging the tissue slides in a buffer solution consisting of TEG (10 mmol/L Trisbase and 0.5 mmol/L EGTA, pH 9) or EDTA and subjecting the tissue to three successive heating steps using a microwave oven: 1) preheating for 9 min at 900 W; 2) boiling for 15 min at 440 W; and 3) cooling for 15 min at room temperature (RT). Endogenous peroxidase activity was blocked by incubation in 1.5% hydrogen peroxide solution (Merck, Darmstadt, Germany) for 10 min. Following application of primary antibodies and incubation for 60 min at RT, detection of the antigen-antibody complexes was conducted on the Dako Autostainers. The tissue sections were counterstained using hematoxylin II and bluing reagent (Ventana protocols) or Mayer's hematoxylin (Autostainer protocols) followed by dehydration and clearing. Coverslips were mounted with a Tissue-Tek® Film® Coverslipper (Sakura, Alpen aan den Rijn, the Netherlands) or manually with Pertex or Aquatex mounting medium. Information on the antibodies and staining protocols used is found in **Table 8**.

8.3.2 Double immunohistochemistry (manuscripts II and III)

Double immunohistochemical stains were performed on the 1) BenchMark Ultra IHC/ISH staining system using the ultraView Universal DAB detection kit and the ultraView Universal AP Red Detection Kit plus amplification (Ventana) or on the 2) DISCOVERY ULTRA instrument using the DISCOVERY HQ-HRP-DAB, DISCOVERY HQ-HRP-Purple, or DISCOVERY NP-AP-Yellow detection kits (Ventana). The protocols were designed as sequential application of unconjugated primary antibodies with heat deactivation steps in between each sequence for elution purposes. For the CD133 and musashi-1 (MSI1) double stains, deparaffinization, HIER, and endogen peroxidase inactivation steps were performed manually, while the antigen-antibody complexes were detected and visualized on the Autostainer Plus with the Catalyzed Signal Amplification or EnVision+ HRP-systems using DAB as chromogen. The tissue slides were then loaded onto the BenchMark machine and stained with antibodies against CD204 and IBA1 using the ultraView Universal AP Red Detection Kit plus amplification. Tissue sections were counterstained with hematoxylin II and bluing reagent and coverslipped as described above. Information on antibodies and protocols is outlined in **Table 9**.

8.3.3 Chromogenic multiplex immunohistochemistry (manuscript IV)

A chromogenic multiplex immunohistochemistry panel was implemented on the Ventana DISCOVERY ULTRA instrument by sequential application of unconjugated primary antibodies with heat deactivation steps in between each sequence for elution purposes. The antigen-antibody complexes were detected by the DISCOVERY-HQ-HRP and DISCOVERY-NP-AP detection systems and three different chromogens. Prior to the development of the multiplex panel, antibodies were established as conventional immunohistochemistry

DAB stains using OptiView (Ventana) as detection system and then tested with the Discovery HQ-HRP detection system using DAB-chromogen. The multiplex protocol is outlined in **Table 10**.

8.3.4 Double immunofluorescence (manuscripts I, III, and IV)

Double immunofluorescence stainings were carried out semi- or fully-automatically on the Dako Autostainer Plus or DISCOVERY ULTRA platform. After deparaffinization, HIER was performed in TEG buffer or cell conditioning 1. The first primary antibody was applied and detected with the Dako CSA II detection system (Agilent) or Omnimap-Cy5 detection kit (Ventana). After a heat deactivation step in TEG buffer or cell conditioning 2, the second primary antibody was applied which was visualized with the TSA-Cy5 system (Perkin Elmer, Waltham, MA, USA) or Omnimap-FAM detection kit (Ventana). Sections were coverslipped and nuclear counterstained with VECTASHIELD® Mounting Media containing DAPI (VWR International). To minimize photobleaching, the stainings were stored at 5 °C until digital imaging acquisition. See **Table 11** for additional information.

Table 8 | List of antibodies used for conventional immunohistochemistry and their respective protocol

Antigen	Vendor and clone / catalog no.	Species/ clonality	Retrieval (min/°C)	Dilution, incubation (min/°C)	Detection and instrument / platform	Positive control tissue
ATRX	Atlas Antibodies, HPA001906	Rb, pAb	CC1, 32/100	1:100, 24/36	OV-HRP-DAB BenchMark ULTRA	Tonsil
BIRC3	Sigma-Aldrich, HPA002317	Rb, pAb	CC1, 32/100	1:200, 32/36	OV-HRP-DAB DISCOVERY ULTRA	Tonsil
CD3	Ventana Medical Systems2GV6	Rb, mAb	CC1, 32/100	RTU, 8/36	OV-HRP-DAB DISCOVERY ULTRA	Tonsil
CD4	Ventana Medical Systems, SP35	Rb, mAb	CC1, 32/100	RTU, 24/36	OV-HRP-DAB BenchMark ULTRA	Tonsil
CD8	Dako, C8/144B	Ms, mAb	CC1, 32/100	1:100, 32/36	OV-HRP-DAB BenchMark ULTRA	Tonsil
CD44	Dako, DF1485	Ms, mAb	CC1std, 64/99	1:25, 20/36	UV-HRP-DAB BenchMark ULTRA	Tonsil, skin
CD44	Dako, DF1485	Ms, mAb	CC1, 32/100	1:200, 32/36	OV-HRP-DAB DISCOVERY ULTRA	Tonsil, skin
CD204	Cosmo Bio Co. LTD, SRA-E5	Ms, mAb	TEG, 15/MWO	1+200, 60/RT	EnV+-HRP-DAB Autostainer Plus	Placenta, lung
CD204	Cosmo Bio Co. LTD, SRA-E5	Ms, mAb	CC1, 32/100	1:600, 32/36	OV-HRP-DAB DISCOVERY ULTRA	Placenta, lung
C3/C3b	Abcam, 755	Ms, mAb	CC1, 32/95 + protease-3, 4 min	1:1000, 32/36	OV-HRP-DAB BenchMark ULTRA	Spleen, tonsil
DLL3	Sigma-Aldrich, HPA056533	Rb, pAb	EDTA, 15/MWO	1+100, 60/RT	EnV+ -HRP-DAB Autostainer Plus	Testes
EGFR	Novocastra, Leica Bio-systems, EGFR.113	Ms, mAb	TEG, 15/MWO	1+50, 60/RT	PV+-HRP-DAB Autostainer Plus	Epidermis
FOXP3	Thermo Fisher Scientific236A/E7	Ms mAb	CC1, 64/100	1:40, 16/36	OV-HRP-DAB BenchMark ULTRA	Tonsil
GAL3	Santa Cruz Biotechnology, Inc, B2C10	Ms, mAb	CC1, 32/100	1:100, 32/36	OV-HRP-DAB DISCOVERY ULTRA	Duodenum

Methods

GAL9	Cell signaling technology, D9R4A	Rb, mAb	CC1, 32/100	1:100, 32/36	OV-HRP- or DISCO-HQ-HRP-DAB DISCOVERY ULTRA	Tonsil, colon,
GFAP	Dako, Z0334	Rb, pAb	TEG, 15/MWO	1+2000, 60/RT	EnV+-HRP-DAB Autostainer Plus	Cerebellum
IBA1	Wako Pure Chemical Ind., Ltd., 019-19741	Rb, pAb	TEG, 15/MWO	1+1000, 60/RT	EnV+-HRP-DAB Autostainer Plus	Brain tissue
IBA1	Wako Pure Chemical Ind., Ltd., 019-19741	Rb, pAb	CC1, 32/100	1:2000, 16/36	OV-HRP-DAB DISCOVERY ULTRA	Brain tissue
ICAM1	Abcam, EP1442Y	Rb, mAb	CC1, 48/100	1:100, 32/36	OV-HRP-DAB DISCOVERY ULTRA	Tonsil
IDH1 R132H	Dianova, H09	Ms, mAb	CC1std, 64/99	1:100, 32/36	UV-HRP-DAB + AMP BenchMark ULTRA	Oligodendro-glioma
IDH1 R132H	Dianova, H09	Ms, mAb	CC1, 64/100	1:100, 32/36	OV-HRP-DAB BenchMark ULTRA	Oligodendro-glioma
IL6	Abcam, ab9324	Ms, mAb	TEG, 15/MWO	1:1600, 60/RT	EnV FLEX+-HRP-DAB Autostainer Link 48	Spleen
IL10	Abcam, EPR1114	Rb, mAb	TEG, 15/MWO	1+100, 60/RT	EnV+-HRP-DAB Autostainer Plus	Pancreas, melanoma
MAP2	Sigma Aldrich, HM-2	Ms, mAb	TEG, 15/MWO	1+2000, 60/RT	EnV+-HRP-DAB Autostainer Plus	Cerebellum
NeuN	Chemicon, A60	Ms, mAb	CC1, 48/100	1:500, 32/36	OV-HRP-DAB BenchMark ULTRA	Cerebellum
NOD2	Sigma-Aldrich HPA041965	Rb, pAb	TEG, 15/MWO	1:100, 60/RT	EnV FLEX+-HRP-DAB Autostainer Link 48	Duodenum
OLIG2	Immuno-Biological Laboratories, 18953	Rb, pAb	CC1, 32/100	1:200, 32/36	OV-HRP-DAB BenchMark/DISCOVERY ULTRA	Glioma
PD-L1	Abcam, EPR19759	Rb, mAb	TEG, 15/MWO	1:500, 60/RT	EnV FLEX+-HRP-DAB Autostainer Link 48	Placenta, tonsil
p53	Ventana Medical Systems, DO7	Ms, mAb	CC1, 32/100	RTU, 8/36	OV-HRP-DAB BenchMark ULTRA	Serous ovarian carcinoma
TIM3	Cell signaling technology D5D5R	Rb, mAb	CC1, 32/100	1:25, 60/36	OV-HRP- or DISCO-HQ-HRP-DAB DISCOVERY ULTRA	Tonsil, lymphoma
TGFβ1	Sigma Aldrich, SAB4502954	Rb, pAb	TEG, 15/MWO	1+100, 60/RT	EnV+-HRP-DAB Autostainer Plus	Stomach, Intestine
TNF	Pierce Antibodies, R4-6A2	Rb, pAb	TEG, 15/MWO	1+100, 60/RT	ADVANCE-HRP-DAB Autostainer Plus	Gallbladder, intestine
TNFAIP3	Abcam, EPR2663	Rb, mAb	Protease-3, 4 min + CC1, 32/100	1:100, 24/36	OV-HRP-DAB DISCOVERY ULTRA	Kidney
VEGF	R&D Systems, 26503	Ms, mAb	TEG, 15/MWO	1+1000, 60/RT	PV+-HRP-DAB Autostainer Plus	Kidney
CHI3L1	Quidel Corporation, 4815	Rb, pAb	TEG, 15/MWO	1+100, 60/RT	ADVANCE-HRP-DAB Autostainer Plus	U87 cell line

Methods

Abbreviations for Tables 8-11: *AP*, alkaline phosphatase; *ASMA*, α -smooth muscle actin; *ATRX*, a-thalassemia/mental retardation X-linked syndrome; *BIRC3*, Baculoviral IAP Repeat Containing 3; *BM11*, BMI1 proto-oncogene, polycomb ring finger; *CC1*, cell conditioning solution 1 (tris-based buffer, pH 8-8.5); *CC2*, cell conditioning solution 2 (citrate-based buffer, pH 6.0); *CD*, cluster of differentiation; *CSA*, catalyzed signal amplification; *C3*, complement component 3; *Cy5*, cyanine 5; *DAB*, 3,3'-diaminobenzidin; *DLL3*, delta-like 3; *DISCO*, DISCOVERY, *EGFR*, epidermal growth factor receptor; *EDTA*, ethylene-diamine-tetraacetic acid; *EnV*, EnVision; *FAM*, 6-carboxyfluorescein; *FITC*, fluorescein-5,6-isothiocyanate; *FOXP3*, forkhead box P3; *GAL*, galectin; *GFAP*, glial fibrillary acidic protein; *HIF1 α* , hypoxia inducible factor 1alpha; *HLA-DR*, human leukocyte antigen class II; *HRP*, horseradish peroxidase, *IBA1*, ionized calcium-binding adaptor molecule 1; *ICAM1*, intercellular adhesion molecule 1; *IDH1* isocitrate dehydrogenase 1; *IL*, interleukin; *mAb*, monoclonal antibody; *MAP2*, microtubule-associated protein 2; *MMP14*, matrix metalloproteinase 14; *Ms*, mouse; *MS11*, musashi-1; *MWO*, microwave oven; *NeuN*, neuronal nuclei; *NOD2*, nucleotide-binding oligomerization domain-containing protein 2; *NP*, nitroprazole; *OLIG2*, oligodendrocyte transcription factor 2; *OV*, OptiView; *pAb*, polyclonal antibody; *PD-L1*, programmed death-ligand 1; *PDPN*, podoplanin; *PV*, PowerVision; *p53*, tumor protein 53; *Rb*, rabbit; *RTU*, ready-to-use; *SOX2*, sex determining region Y-box 2; *TEG*, Tris 10 mM, EGTA, 0.5 mM, pH9; *TGF β 1*, transforming growth factor beta 1; *TIM3*, T-cell immunoglobulin mucin-3; *TNF*, tumor necrosis factor; *TNFAIP3*, TNF, alpha-induced protein 3; *TSA*, tyramide signal amplification; *UV*, ultraView; *VEGF* vascular endothelial growth factor; *CHI3L1*, chitinase 3-like 1

Table 9 | List of antibodies used for double immunohistochemistry and their respective protocol

Antigen	Vendor and clone / catalog no.	Species/ clonality	Retrieval (min/ $^{\circ}$ C)	Dilution, incubation (min/ $^{\circ}$ C)	Detection and instrument / platform	Positive control tissue
BMI1	Merck Millipore, F6	Ms, mAb	CC1std, 64/99	1+100, 32/36	UV-HRP-DAB +AMP BenchMark ULTRA	Testes
CD44	Dako, DF1485	Ms, mAb	CC1std, 64/99	1:25, 20/36	UV-HRP-DAB BenchMark ULTRA	Tonsil, skin
CD133	Miltenyi Biotec, W6B3C1	Ms, mAb	TEG, 15/MWO	1+40, 60/RT	CSA II-HRP-DAB Autostainer Plus	Kidney, placenta
CD204	Cosmo Bio Co. LTD, SRA-E5	Ms, mAb	CC1std, 64/99	1+400, 32/36	UV-AP-RED +AMP BenchMark ULTRA	Placenta, lung
C3/C3b	Abcam, 755	Ms, mAb	CC1, 32/100	1:600, 32/36	DISCO-HQ-HRP-DAB DISCOVERY ULTRA	Spleen, tonsil
GAL9	Cell signaling technology, D9R4A	Rb, mAb	CC1, 32/100	1:100, 32/36	DISCO-NP-AP-Yellow DISCOVERY ULTRA	Tonsil, colon
IBA1	Wako Pure Chemical Ind., Ltd., 019-19741	Rb, pAb	CC1std, 64/99	1+2000, 32/36	UV-AP-RED +AMP BenchMark ULTRA	Brain tissue
MS11	MBL International Corporation, 14H1	Ms, mAb	TEG, 15/MWO	1+400, 60/RT	EnV+-HRP-DAB Autostainer Plus	Brain tissue
Nestin	R&D systems, 196908	Ms, mAb	CC1std, 64/99	1+1000, 32/36	UV-HRP-DAB BenchMark ULTRA	Brain tissue, melanoma
OLIG2	Immuno-Biological Laboratories, 18953	Rb, pAb	CC1, 32/100	1:200, 32/36	DISCO-HQ-HRP-Purple DISCOVERY ULTRA	Glioma
PDPN	Ventana Medical Systems, D2-40	Ms, mAb	CC1std, 64/99	RTU, 32/36	UV-HRP-DAB BenchMark ULTRA	Seminoma, lymphatic endothelium
SOX2	R&D systems, 245610	Ms, mAb	CC1std, 64/99	1+200, 32/36	UV-HRP-DAB +AMP BenchMark ULTRA	Brain tissue
TIM3	Cell signaling technology, D5D5R	Rb, mAb	CC1, 32/100	1:25, 60/36	DISCO-HQ-HRP-Purple DISCOVERY ULTRA	Tonsil, lymphoma

Methods

Table 10 | Overview of protocol used for the multiplex immunohistochemistry panel

OLIG2 / TIM3 / GAL9 multiplex panel	
Pretreatment	Cell Conditioning 1 (CC1, #950-500) 32 min 100°C
Inhibitor	Inhibitor CM (#760-4307) 8 min
Primary Ab#1	Anti-OLIG2 rabbit polyclonal Ab (Immuno-Biological Laboratories, #18953) 1:200, 32 min 36°C
Detection	Anti-Rabbit-HQ (#760-4815) 20 min + anti-HQ-HRP (#760-4820) 20 min
Amplification	No
Chromogen	ChromoMap DAB kit (#760-159) 4 min + 8 min
Elution	Cell Conditioning 2 (CC2, #950-123) 8 min 100°C
Primary Ab #2	Anti-TIM3 rabbit monoclonal Ab (Cell Signaling Technology, clone D5D5R) 1:25, 60 min 36°C
Detection	Anti-Rabbit-HQ (#760-4815) 16 min + anti-HQ-HRP (#760-4820) 16 min
Amplification	No
Chromogen	Purple kit (#760-229) 32 min
Elution	CC2 8 min 100 °C
Primary Ab #3	Anti-galectin-9 rabbit monoclonal Ab (Cell Signaling Technology, clone D9R4A) 1:100, 48 min 36°C
Detection	Anti-Rabbit-NP (#760-4817) 12 min + anti-NP-AP (#760-4827) 12 min
Amplification	No
Chromogen	Yellow kit (#760-239) 44 min

Chromogen colors are shown in the corresponding cells. Apart from the antibodies, slides were colored using #Ventana reagents.

Table 11 | List of antibodies used for double immunofluorescence and their respective protocol

Antigen	Vendor and clone / catalog no.	Species/ clonality	Retrieval (min/°C)	Dilution, incubation (min/°C)	Detection and instrument / platform	Positive control tissue
ASMA	Spring Bioscience, SP171	Rb, mAb	TEG, 15/MWO	1+200, 60/RT	TSA-Cy5 Autostainer Plus	Intestine
CD3	Ventana Medical Systems, 2GV6	Rb, mAb	CC1, 32/100	RTU, 8/36	OmniMap-FAM DISCOVERY ULTRA	Tonsil
CD204	Cosmo Bio Co. LTD, SRA-E5	Rb, mAb	TEG, 15/MWO	1+12000, 60/RT	CSA II-FITC Autostainer Plus	Placenta, lung
EGFR	Novocastra, Leica Bio-systems, EGFR.113	Ms, mAb	TEG, 15/MWO	1+100, 60/RT	TSA-Cy5 Autostainer Plus	Epidermis
GAL9	Cell signaling technology, D9R4A	Rb, mAb	CC1, 32/100	1:100, 32/36	OmniMap-Cy5 DISCOVERY ULTRA	Tonsil, colon
GAL9	Cell signaling technology, D9R4A	Rb, mAb	CC1, 48/100	1:100, 32/36	OmniMap-FAM DISCOVERY ULTRA	Tonsil, colon
GFAP	Dako, Z0334	Rb, pAb	TEG, 15/MWO	1+8000, 60/RT	TSA-Cy5 Autostainer Plus	Cerebellum
HIF1α	BD Transduction Laboratories, 54	Ms, mAb	TEG, 15/MWO	1+50, 60/RT	TSA-Cy5 Autostainer Plus	U87 cell line, seminoma
IBA1	Wako Pure Chemical Ind., Ltd., 019-19741	Rb, pAb	TEG, 15/MWO	1+12000, 60/RT	TSA-Cy5 Autostainer Plus	Brain tissue
IBA1	Wako Pure Chemical Ind., Ltd., 019-19741	Rb, pAb	CC1, 32/100	1:2000, 16/36	OmniMap-FAM DISCOVERY ULTRA	Brain tissue
IDH1 R132H	Dianova, H09	Ms, mAb	CC1, 48/100	1:100, 32/36	OmniMap-Cy5 DISCOVERY ULTRA	Oligodendro glioma

Methods

IL10	Abcam, EPR1114	Rb, mAb	TEG, 15/MWO	1+100, 60/RT	TSA-Cy5 Autostainer Plus	Pancreas, melanoma
MAP2	Sigma Aldrich, HM-2	Ms, mAb	TEG, 15/MWO	1+200, 60/RT	TSA-Cy5 Autostainer Plus	Cerebellum
MMP14	Novus Biologicals, EP1264Y	Rb, mAb	TEG, 15/MWO	1+8000, 60/RT	TSA-Cy5 Autostainer Plus	Intestine, Kidney
OLIG2	Immuno-Biological Laboratories, 18953	Rb, pAb	TEG, 15/MWO	1+100, 60/RT	TSA-Cy5 Autostainer Plus	Glioma
OLIG2	Immuno-Biological Laboratories, 18953	Rb, pAb	CC1, 32/100	1:200, 32/36	OmniMap-FAM DISCOVERY ULTRA	Glioma
TGFβ1	Sigma Aldrich, SAB4502954	Rb, pAb	TEG, 15/MWO	1+100, 60/RT	TSA-Cy5 Autostainer Plus	Stomach, Intestine
TIM3	Cell signaling technology, D5D5R	Rb, mAb	CC1, 32/100	1:25, 60/36	OmniMap-Cy5 DISCOVERY ULTRA	Tonsil, lymphoma
TIM3	Cell signaling technology, D5D5R	Rb, mAb	CC1, 32/100 or 48/100	1:25, 60/36	OmniMap-FAM DISCOVERY ULTRA	Tonsil, lymphoma
TNFα	Pierce Antibodies, R4-6A2	Rb, pAb	TEG, 15/MWO	1+50, 60/RT	TSA-Cy5 Autostainer Plus	Gallbladder, intestine
VEGF	R&D Systems, 26503	Ms, mAb	TEG, 15/MWO	1+200, 60/RT	TSA-Cy5 Autostainer Plus	Kidney

8.4 Digital image acquisition and analysis (manuscripts I-IV)

H&E and immunohistochemical stains were digitized using a NanoZoomer 2.0-HT whole-slide scanner (Hamamatsu Photonics, Hamamatsu, Japan) and a 20x or 40x objective. Image analyses were done in the NanoZoomer Digital Pathology (NDP) program or by importing the scanned files into the Visiopharm software (Visiopharm, Hørsholm, Denmark).

The immunofluorescence stainings were digitized using a Visiopharm integrated microscope and software module. The setup consisted of a Leica DM 6000B microscope equipped with an eight-slide Bioprecision2 stage (Ludl Electronic Products, Ltd, Hawthorne, NY, USA), an Olympus DP72 1.4 megapixel CCD camera (Olympus, Ballerup, Denmark) as well as a DAPI (Omega XF06), FITC (Leica), and Cy5 (Omega XF110-2) optical filter set. Super images were acquired with 1.25x objective using bright field settings resulting in an overview of whole tissue slide which enabled manual delineation of ROIs (**Figure 22**). Areas with large blood vessels, necrosis, and normal brain tissue were excluded from the ROI. Acquisition of sample images was performed at a 20x objective by SURS, and sample images were reviewed to ensure at least five clear, non-blurry images per tissue specimen. Images were then analyzed in the Visiopharm software.

Different approaches were used to analyze the digitized immunostainings including 1) automated digital analysis, 2) manual semi-quantitative scoring, and 3) cell counting. The methods utilized are outlined in the next three subsections.

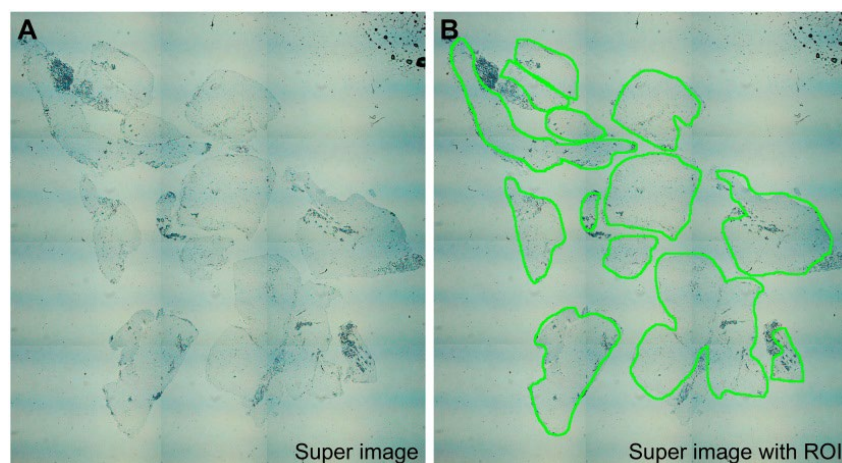


Figure 22 | Example of a brightfield super image and outlining of the ROI. **(A)** To digitize immunofluorescence stainings, a brightfield super image was acquired at a 1.25x objective. **(B)** Vital tumor tissue was outlined on the super image to define ROI/ROIs. Sample images were then obtained within the ROI using the optical filter set.

8.4.1 Digital automated image analysis (manuscripts I, II, and IV)

Automated digital image analysis and quantification were performed in the Visiopharm software module *Image analysis*. The expression of each antigen was quantified by developing pixel-based algorithms to detect the positive staining signal. For the double immunofluorescence stainings performed in manuscripts I and IV, the algorithms were designed as threshold-based classifications using the RGB (red-green-blue) three-color model (**Figure 23**). For the H&E and immunohistochemical stainings used in manuscript II, sample images were first acquired in the Visiopharm *Acquisition* software module by outlining the ROI manually and performing systematic uniform random sampling at 20x magnification (**Figure 24A, B**). The sample images were reviewed to check for blurring and to exclude areas with blood vessels, necrosis, and normal brain tissue from the ROI. The algorithms were developed as threshold-based or membrane classifications. The H&E-hematoxylin feature was used as input to detect blue/purple-stained nuclei in the H&E stains to obtain an estimate for cell density (cellularity). The hematoxylin-DAB-DAB (HDAB-DAB) and hematoxylin-DAB color deconvolution bands was used to detect and adjust the immunopositive signals (**Figure 24C-F**). The classified images were then used to obtain quantitative estimates of the respective marker of interest. For each staining, the output variable was area fraction which was defined as the positive area divided by the area of the respective ROI. In manuscript IV and in parts of the manuscript I, the fractions were converted to percent by multiplying by 100. In manuscript I, the mean intensity of the marker of interest was also measured. Area quantification of necrosis was performed in manuscript II as follows: H&E stained slides of the tumor specimens were imported into the Visiopharm software. Areas of vital tumor tissue and necrosis were manually outlined as ROIs. Normal brain tissue, tumor-infiltrating area, and large blood vessels/hemorrhages were marked as exclusion areas. The tissue slides were processed in the *Image analysis* module to calculate the areas of the ROIs in mm² and the necrotic component, which was defined as the area of necrosis divided by the area of total tumor tissue (i.e. necrosis + vital tumor tissue).

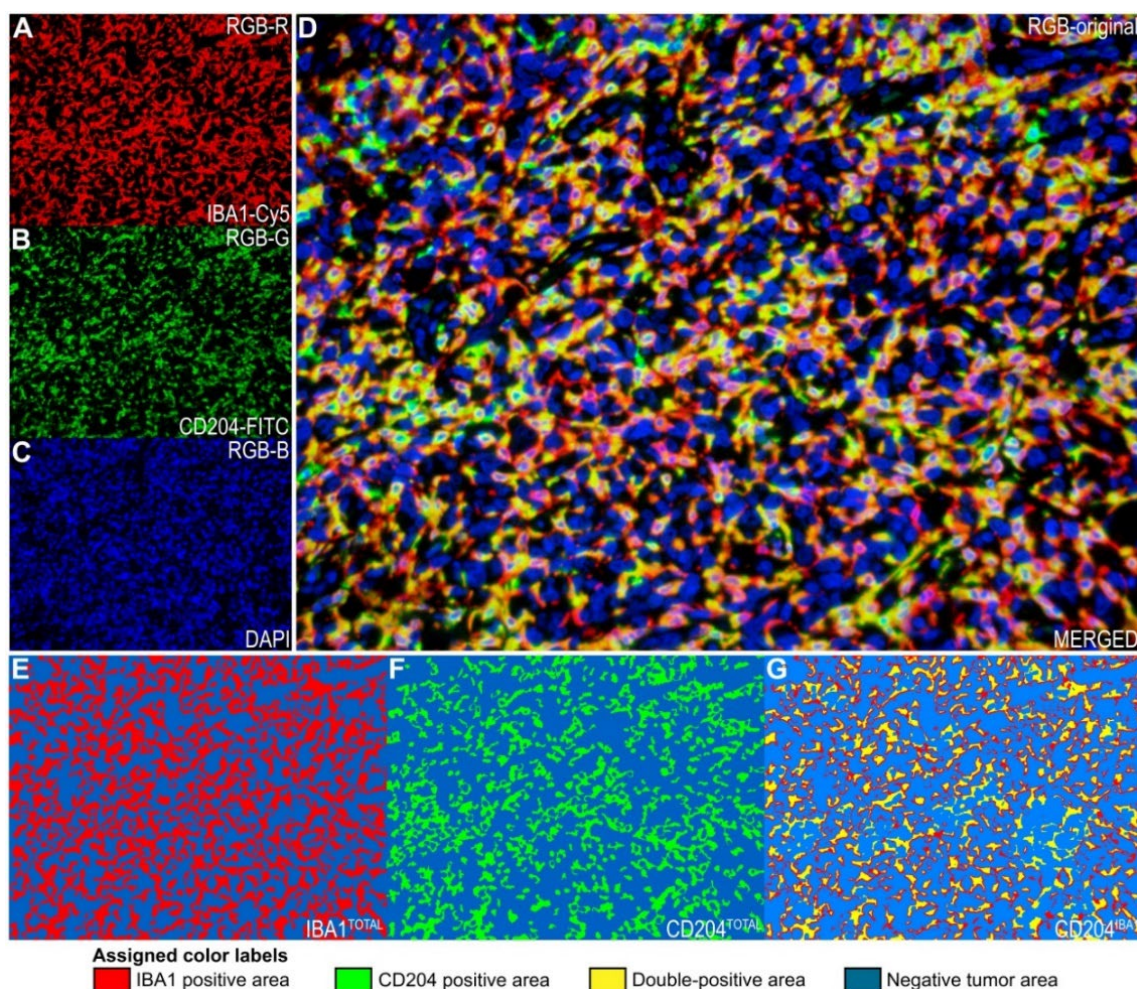


Figure 23 | An example of immunofluorescent image recording and classification. (A–D) Each image was recorded as three separate greyscale images for (A) Cy5 (IBA1), (B) FITC (CD204), and (C) DAPI (nuclei) and subsequently assigned pseudocolors and superimposed to form the (D) complete image. Images were quantified by performing signal segmentations based on pixel intensities of the red RGB (RGB-R), green RGB (RGB-G), and blue RGB (RGB-B) color bands. (E, F) To quantify the total expression of IBA1 (IBA1^{TOTAL}) and CD204 (CD204^{TOTAL}), the tumor area within each picture frame was defined as ROI with digital image analysis. (G) For the quantification of double-positive expression (i.e. IBA1⁺ CD204⁺), IBA1 was used as an inclusion marker and defined as a ROI, and then the expression of CD204 was evaluated within this ROI enabling measurements of double-labeled protein expression (CD204^{IBA1}).

8.4.2 Pathological scoring (manuscripts I and III)

In manuscript I, semi-quantitative pathological scoring was performed blinded in the NDP software at 40x magnification. The gemistocytic cell component was estimated in the H&E stainings of astrocytic tumors. Five positions per slide were assessed. Each position was scored from 0 to 4 based on the percentage of gemistocytes (0: no gemistocytes; 1: <10%; 2: 10–49%; 3: 50–90%; 4: >90% gemistocytes), and a mean score was calculated for each tumor. Immunohistochemical subtyping of 20 glioblastoma samples was done by evaluating the expression of three markers related to the proneural (DLL3, NeuN, OLIG2) and mesenchymal (CD44, VEGF, CHI3L1) subtypes. Scores were assigned based on the percentage of positive cells using the scoring system

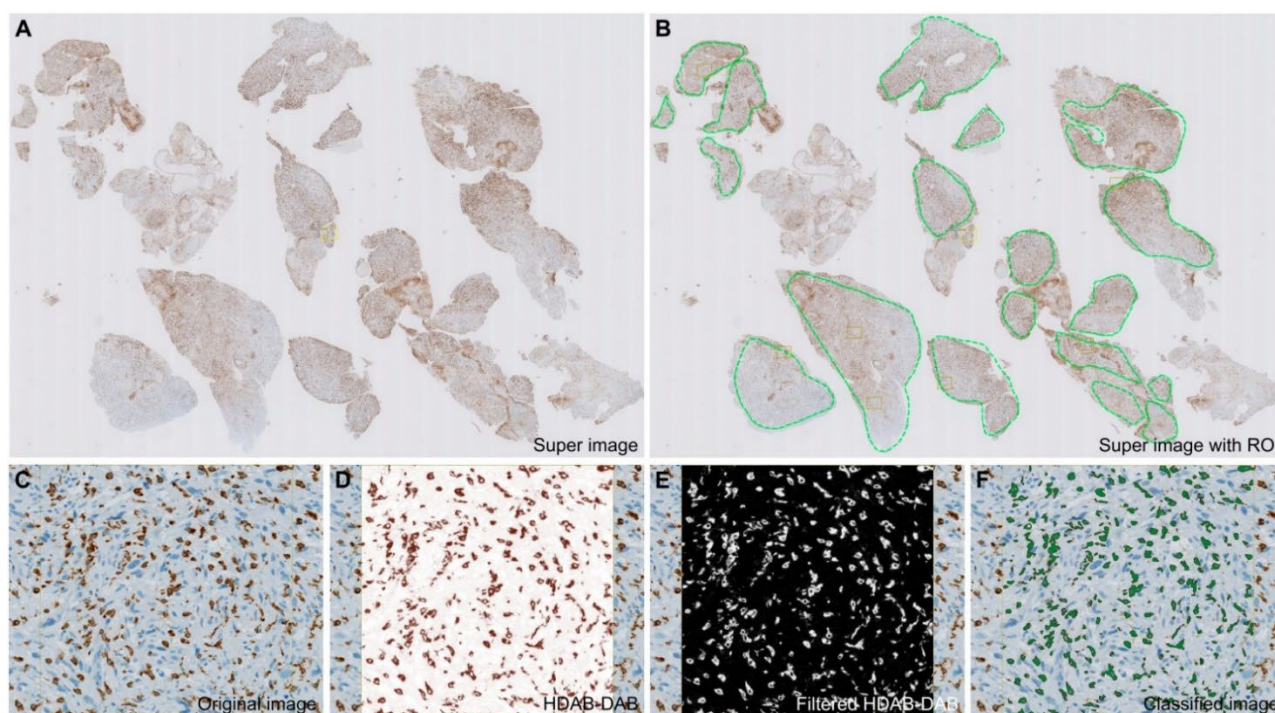


Figure 24 | An example of chromogenic image acquisition and classification. **(A)** Overview of a CD204 stained tissue slide (the super image). **(B)** The tissue slide was prepared for sampling by delineating the ROI on the super image. **(C)** The recorded image was reviewed and prepared for image processing. **(D)** The image was preprocessed by selecting the input feature that allowed the best pixel segmentation of positive and negative signals. **(E)** The input feature was modified to enhance the signal-to-noise ratio. A threshold was set based on the pixel intensity to differentiate between positive and negative pixels, and as a post-processing step, immunopositive areas that were too small were removed. **(F)** The image obtained after post-processing was used to produce the output variables. For the CD204 immunostaining, the threshold was set at 150. The area fraction and mean intensity in (F) was 0.087 and 203.7.

described above. The tumors were indexed as proneural or mesenchymal as described in [635] using the following equation: $\text{Index} = \sum (\mu_{\text{DLL3}} + \mu_{\text{NeuN}} + \mu_{\text{OLIG2}}) - \sum (\mu_{\text{CD44}} + \mu_{\text{YKL40}} + \mu_{\text{VEGF}})$. Tumors with an index above zero were classified as proneural, while tumors with an index below zero were classified as mesenchymal.

In manuscript III, the C3/C3b stains were scored semi-quantitatively using the Visiopharm *Acquisition* and *Stereology* modules. Sample images were obtained by SURS at 20x magnification ensuring at least five images with vital central tumor tissue per tumor. Each image was assessed for two parameters: 1) a fraction score, which was based on the percentage of C3/C3b expression (0: no expression; 1: <10% expression; 2: 10%–25% expression, 3: >25%–75%, 4: >75%), and 2) an intensity score based on the staining intensity of C3/C3b (0: faint, 1: moderate, 2: intense). The mean fraction and intensity scores were calculated for each tumor.

8.4.3 Stereology (manuscripts II, III, and IV)

Semi-stereological approaches were used to conduct cell counting in the Visiopharm software module *Stereology*. Sample images were first obtained in the *Acquisition* module at 20x or 40x magnification.

In manuscripts II and IV, cell counting was performed using a 1x1 or 2x2 counting frame that covered 30% or 10% of the sampled image area, respectively, and a count tool (**Figure 25**). The sampling algorithm and

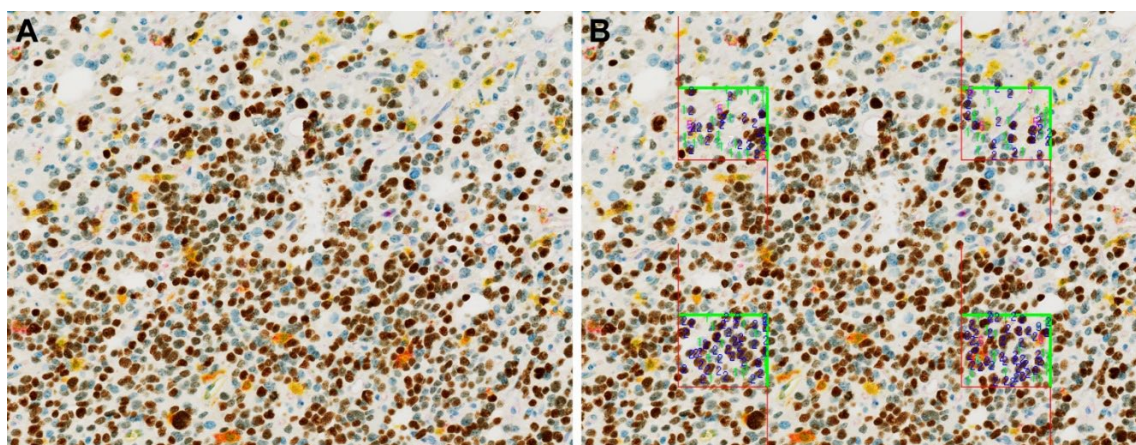


Figure 25 | An example of the stereological-based setup used for the OLIG2/TIM3/galectin-9 multiplex panel. **(A)** A sample image acquired at 20x magnification. **(B)** A sample image with a 2x2 counting frame covering 10% of the image area. A combination of cellular morphology as well as the expression of TIM3 (*purple*), galectin-9 (*yellow*), and/or OLIG2 (*brown*) was used to separate and count the different cell populations. The green line indicates the acceptance line of the counting frame, while the red line indicates the rejection line.

counting frame size were optimized to achieve accurate cell counting. The count tool was used to classify the specific cell populations, and cell fractions and percentages were calculated for the specific cell population based on the total cell count, the total number of tumor cells, and/or the total number of microglia/macrophages.

In manuscript III, the number of positive cells ($CD4^+$, $CD8^+$, and $FOXP3^+$ T cells) was counted in each sample images based on the staining intensity and cell morphology. No counting frame was used as the sample images were counted in their entirety. A mean cell count was calculated for each tumor by dividing the total positive cell count by the number of sample images for the respective tumor. The $FOXP3^+/CD4^+$ ratio was calculated by dividing the mean $FOXP3^+$ cell count with the mean $CD4^+$ cell count.

8.5 NanoString gene expression panel (manuscript II)

FFPE tissue samples were cut into 10- μ m-thick slices on a microtome which were then mounted on glass slides. Guided by a representative H&E stain, some of the freshly cut sections were macrodissected to exclude normal brain tissue and/or tumor-infiltrating areas thereby enriching the amount of central tumor RNA in the gene expression analyses. Next, sections were detached from glass slides and deparaffinized by subsequent submersion in a 3% glycerol solution and R-(+)-limonene followed by a washing step in absolute ethanol and rehydration in 3% glycerol. The tissue was then transferred to 1.5 mL Eppendorf tubes. Total RNA was extracted using the High Pure FFPE RNA Isolation Kit (Roche, Basel, Switzerland) as per the manufacturer's instructions. RNA quantity and quality was assessed using NanoDrop (Thermo Scientific, Waltham, MA, USA). mRNA gene expression analysis was done with the NanoString barcode technology (NanoString Technologies, Seattle, WA, USA) with the NanoString nCounter® Human Myeloid Innate Immunity Panel v2 consisting of 770 genes (**Table 12**), including 40 housekeeping genes, and a customized CodeSet of 30 genes (**Table 13**) which was spiked into the myeloid panel. The 30-gene panel included the genes for $CD204$ (*MSR1*), galectin-9 (*LGALS9*), two housekeeping genes [636, 637] as well as 26 genes related to cancer stemness [327,

328, 400, 401], glioma [10, 91], or the IFN pathway [638]. Total RNA input was 150–250 ng with an A260/280 optical density of 1.61-1.99. Standard nCounter XT protocols were followed. Briefly, reporter probes, hybridization buffer, RNA sample, and capture probes were added to hybridization tubes which were then placed at 65°C for overnight incubation. Next, the target-probe complexes were purified by magnetic beads and immobilized in cartridges on the nCounter Prep Station followed by data collection and barcode counting in the nCounter Digital Analyzer (FLEX Analysis System, NanoString). Data were imported into the nSolver Analysis Software v4.0 with the Advanced Analysis Module 2.0 plugin for quality control, normalization, and advanced analysis according to manufacturer’s guidelines.

Table 12 | Gene annotation summary

Annotation	# Genes	Examples
Angiogenesis	61	<i>ANGPT1, EGF, FYN</i>
Antigen Presentation	64	<i>CD74, HLA-DRA, TNF</i>
Cell Cycle and Apoptosis	21	<i>BID, BTG2, MCM5</i>
Cell Migration and Adhesion	101	<i>AIF1, CD274, ICAM1</i>
Chemokine signaling	75	<i>CCL2, CCL20, JAK3</i>
Complement Activation	18	<i>C3, C5, ITGAM</i>
Cytokine Signaling	157	<i>BIRC3, IL6, TNFAIP3</i>
Differentiation and Maintenance of Myeloid Cells	54	<i>CD163, CD38, MAFF</i>
ECM remodeling	73	<i>CD44, CTSG, MMP1</i>
Fc Receptor Signaling	67	<i>CDKN1A, CD28, CSF2</i>
Growth Factor Signaling	186	<i>CSF1R, FAS, IFNB1</i>
Interferon Signaling	35	<i>IRF4, MX1, STAT1</i>
Lymphocyte activation	131	<i>CD209, CD40, CD80</i>
Metabolism	92	<i>CD68, FABP4, NAMPT</i>
Pathogen Response	91	<i>CXCL8, LGALS3, PTX3</i>
T-cell Activation and Checkpoint Signaling	37	<i>CTLA4, ICOS, LAG3</i>
T _H 1 Activation	19	<i>HAVCR2, IL10, IL18</i>
T _H 2 Activation	20	<i>CXCR4, GATA3, IL4</i>
TLR signaling	68	<i>SOCS1, TLR1, TLR2</i>

Table 13 | Customized 30-gene panel

Gene group	Genes
Immune system	<i>MSR1 (CD204), LGALS9 (GAL9)</i>
Cancer stemness	<i>ALDH1A1, BMI1, ITGA6, MS11, NANOG, PDPN, POU5F1 (OCT4), PROM1 (CD133), SOX2</i>
Glioma	<i>CHI3L1, EGFR, GFAP, MGMT, MKI67, OLIG2, TP53</i>
Interferon signaling	<i>BST2, IFI27, IFI44, IFI44L, IFI6, PARP1, PARP9, PARP12, PARP14, RSAD2</i>
Housekeeping genes	<i>GAPDH, RPL13A</i>

8.6 *In silico* analyses (manuscripts I, II, and IV)

Bioinformatics databases were used to support and validate the results in the studies. mRNA datasets were exported directly from GlioVis portal (<http://gliovis.bioinfo.cnio.es/>) [639]. Three different datasets were explored including gene expression data from a study by Gravendeel et al. [640] and two studies associated with the Cancer Genome Atlas (TCGA) Research Network [147, 174]. The datasets were used to investigate

mRNA expression levels of various genes and to perform survival and correlation analyses. Differential expression analyses were also carried out as well as Kyoto Encyclopedia of Genes and Genomes (KEGG) and Gene ontology (GO) enrichment and pathway analyses of differentially expressed genes. The STRING online resource v11 (<https://string-db.org/>) [641] was assessed to visualize possible interaction networks and to perform connectivity and network as well as enrichment and pathway analyses.

8.7 Statistics (manuscripts I-IV)

Student's unpaired t-test or Mann-Whitney U-test was used when comparing two groups. One-way ANOVA with Bonferroni's Multiple Comparison Test or Kruskal-Wallis test with Dunn's Multiple Comparison Test was used when comparing more than two groups. Correlation analyses were done using Spearman's correlation test. These statistical analyses were performed in Prism (Version 5, GraphPad Software Inc., San Diego, CA, USA). Survival functions were estimated and plotted by the Kaplan-Meier approach. Difference in survival between groups was compared using the log rank test. Multivariate analyses were conducted using the Cox proportional-hazards regression model to obtain hazard ratios (HR) and confidence intervals (CI). All Cox models were tested for the proportional hazards assumption, interaction effects, and time-dependency of explanatory factors. Biomarkers were investigated as binary variables with the median pre-specified cut-off value. Exploratory cut-point analyses were performed in manuscript I. The optimal cut-off value was confirmed by receiver operating characteristic (ROC) analysis, and survival analyses were repeated using the optimal cut-off value. Survival and ROC analyses were done in STATA (StataCorp LP/LLC, College Station, TX, USA). For the NanoString mRNA expression data, the nCounter data files were imported into the nSolver software. The software uses open-source R programs for quality control, normalization, generation of heatmaps, differential expression analysis and fold change estimation as well as pathway scoring, and gene set analysis. Multiple comparison correction was performed using the Benjamini-Yekutieli False Discovery Rate (FDR) procedure [642] resulting in FDR adjusted P values. $P < 0.05$ was considered statistically significant.

8.8 Ethics (manuscripts I-IV)

Study approval was obtained from the Regional Committee on Health Research Ethics for Southern Denmark (Project ID: S-20150148), the Danish Data Protection Agency (file number: 16/11065), and the Institutional Review Board of the Medical Faculty, Heinrich Heine University, Düsseldorf, Germany (Study No.5848R). Written and/or verbal consents were not required as the study was done retrospectively using archival brain tumor tissue; however, the use of tissue was not prohibited by any patient according to the Danish Tissue Application Register. The study was carried out in accordance with the Declaration of Helsinki.

9. Results

This chapter contains brief summaries of all manuscripts included in this thesis. The full-length manuscripts are available in the *Appendix*.

9.1 Manuscript I

Title: Tumor-associated microglia/macrophages predict poor prognosis in high-grade gliomas and correlate with an aggressive tumor subtype

Aims:

- To investigate the prognostic value of TAMs in a population-based glioma patient cohort using an automated quantitative double immunofluorescence approach and antibodies against IBA1, a general TAM marker, and CD204, a marker for alternatively activated M2-like TAMs.
- To examine the correlation between TAMs, gemistocytic tumor cells and glioblastoma subtype.
- To characterize the phenotype of CD204⁺ TAMs using double immunofluorescence and a panel of eight markers (HLA-DR, MMP14, HIF1 α , TNF, TGF β 1, IL10, VEGF, and EGFR) related to immune activation and tumor aggressiveness as well as a panel of four markers related to tumor cells (GFAP, OLIG2) and vascular smooth muscle cells (MAP2, ASMA).

Main findings:

- The amount of TAMs, especially CD204⁺ TAMs, increased with malignancy grade ($P < 0.001$). In grade IV tumors, the IBA1⁺ area and the CD204⁺ area comprised up to 30% and 24% of the total tumor area, respectively, and up to 90% of the IBA1⁺ area co-expressed CD204.
- Gliomas had significantly higher expression levels of IBA1 compared to normal brain tissue, DLBCL, and brain metastases from malignant melanoma and NSCLC ($P < 0.001$ or $P < 0.01$). CD204 staining intensity was highest in gliomas ($P < 0.05$), and CD204 area fraction was higher in gliomas compared to normal brain tissue ($P < 0.001$) and DLBCL ($P < 0.05$).
- In WHO grade II, neither IBA1 nor CD204 showed prognostic value in univariate analyses ($P > 0.05$). When adjusting for performance status, IDH status, and histology in the multivariate analysis, a high IBA1 area fraction significantly correlated with improved survival (HR 0.10; 95% CI 0.01-0.94; $P = 0.044$).
- In WHO grade III, IBA1 did not correlate with survival ($P > 0.05$), while high area fraction and intensity level of CD204 had a negative prognostic value in both the univariate (HR 3.75, $P = 0.008$ and HR 4.14, $P = 0.004$) and multivariate analyses when adjusting for performance status, IDH status, and histology (HR 3.76, $P = 0.025$ and HR 7.83, $P = 0.001$).
- In WHO grade IV, IBA1 area fraction did not significantly impact prognosis ($P > 0.05$). High IBA1 intensity was independently associated with improved survival when dichotomized at the optimal cutoff value (HR = 0.66, $P = 0.026$), while high area fraction and intensity levels of CD204 independently correlated with poor prognosis (HR = 1.67, $P = 0.001$ and HR = 2.27, $P < 0.001$). Subdividing the patients

into four groups based on the area fractions of IBA1 and CD204 showed that patients with high CD204 and low IBA1 levels had the worst prognosis ($P < 0.01$).

- In the group of glioblastoma patients receiving postsurgical treatment, high IBA1 intensity correlated with longer survival (HR 0.78, $P = 0.013$), while high CD204 area fraction and intensity predicted shorter survival (HR 1.20, $P = 0.019$ and HR 1.52, $P < 0.001$).
- In patients with unmethylated MGMT promoter, high IBA1 area fraction and intensity were associated with improved outcome (HR 0.80, $P = 0.036$ and HR 0.72, $P = 0.020$). In patients with methylated MGMT promoter, high area fraction and intensity levels of CD204 correlated with shorter survival (HR 1.38, $P = 0.009$ and HR 1.67, $P = 0.005$). When MGMT status was included in the multivariate analysis, IBA1 was prognostically insignificant, whereas high area fraction and intensity of CD204 predicted worse outcome (HR 1.66, $P = 0.005$ and HR 2.11, $P = 0.002$).
- The tumor periphery had lower IBA1 ($P < 0.05$) and CD204 ($P < 0.01$) expression levels relative to the tumor core.
- The presence of gemistocytic tumor cells correlated with high IBA1 ($P = 0.005$) and CD204 ($P = 0.029$) area fractions.
- The mesenchymal subtype of glioblastomas had higher CD204 levels ($P < 0.001$) and IBA1 area fraction ($P = 0.022$) compared to the proneural subtype, but lower IBA1 intensity ($P = 0.012$).
- CD204⁺ TAMs showed conjunctionally expression of proteins related to M1 and M2 activation. On average, 44% (range: 3-85%) and 8% (range: 0-36%) of the CD204⁺ area co-expressed HLA-DR and TNF, while 10% (range: 0-39%) and 3% (range: 0-22%) co-localization was observed for IL10 and TGFβ1. Most CD204⁺ TAM co-expressed MMP14 (mean: 73%, range: 11-97%), and average co-expression with HIF1α was 13% (range: 0-54%). VEGF and CD204 rarely overlapped (mean: 1%, range: 0-11%), whereas 9% of the CD204⁺ area co-localized with EGFR (range: 0-72%). No co-expression was observed between CD204 and GFAP, OLIG2, MAP2, or ASMA suggesting that tumor cells and vascular smooth muscle cells are not part of the CD204⁺ cell population.
- The negative prognostic value of CD204 was confirmed in two bioinformatics mRNA databases ($P < 0.05$)

The results from manuscript is graphically summarized in **Figure 26**.

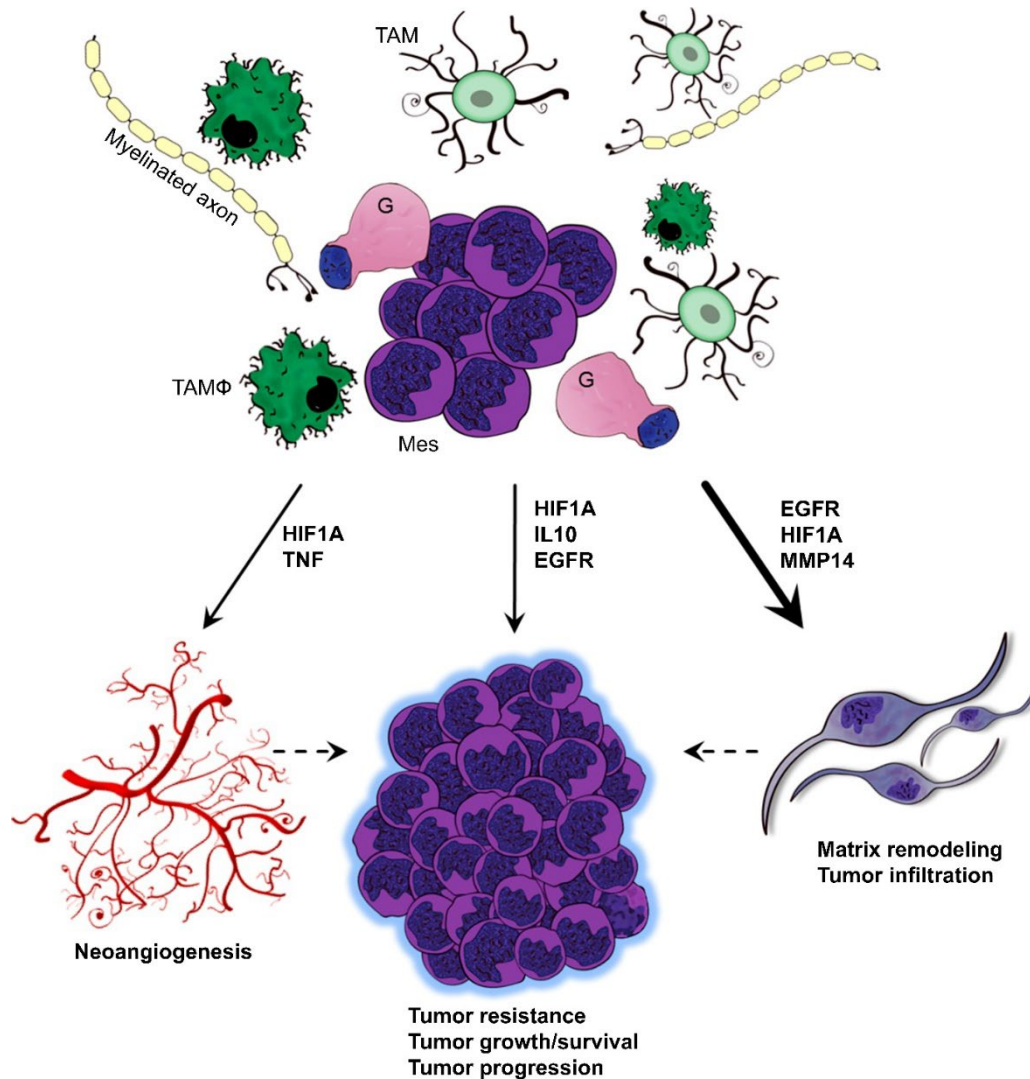


Figure 26 | Schematic illustration of the supposed crosstalk between glioblastoma cells and CD204⁺ TAMs. In the TME, CD204⁺ TAMs (tumor-associated microglia) and TAMΦs (tumor-associated macrophages) expressing high levels of CD204 with lower levels of IBA1 and HLA-DR interact with the glioblastoma cells supporting a mesenchymal shift in the tumor cells (Mes) with increased presence of gemistocytes (G). The CD204⁺ TAMs and TAMΦs express and secrete MMP14, HIF1 α , IL10, EGFR, and TNF possibly stimulating angiogenesis and matrix remodeling. With the scavenger functions of CD204 clearing e.g. apoptotic cells, myelin and extracellular matrix components, CD204⁺ TAMs could ultimately facilitate tumor invasion/infiltration and progression. Reprinted from [643] under the terms and conditions provided by John Wiley and Sons and the Copyright Clearance Center.

9.2 Manuscript II

Title: Tumor-associated CD204⁺ microglia/macrophages accumulate in perivascular and perinecrotic niches and correlate with an interleukin-6 enriched inflammatory profile in glioblastoma

Aims:

- To investigate the association between TAMs and glioblastoma cells expressing markers related to cancer stemness using double immunohistochemistry with antibodies directed against IBA1, CD204 and markers of the CSC phenotype (BMI1, CD44, CD133, MSI1, nestin, podoplanin, and SOX2) and by stereologically estimating the expression and interaction levels in three different tumor regions: 1) the perivascular area, 2) the perinecrotic area, and 3) the vital tumor area.
- To perform mRNA transcriptome profiling of CD204-enriched glioblastomas using the NanoString barcode technology.
- To validate the mRNA transcriptome profile of CD204-enriched glioblastomas by immunohistochemistry and bioinformatics databases.

Main findings:

- Both IBA1⁺ and CD204⁺ TAMs accumulated in areas around necrosis and vascular structures ($P < 0.05$).
- The densities of cells expressing BMI1 ($P = 0.44$), CD44 ($P = 0.31$), MSI1 ($P = 0.27$), nestin ($P = 0.78$), and SOX2 ($P = 0.39$) did not show any significant differences among the three tumor subregions.
- Tumor cells expressing CD133 ($P < 0.01$) and podoplanin ($P < 0.01$) were significantly higher in especially in the perivascular area and perinecrotic area, respectively, relative to the vital tumor area.
- Tumor cells expressing BMI1 ($P = 0.21$), CD44 ($P = 0.71$), CD133 ($P = 0.54$), and MSI1 ($P = 0.36$) did not significantly interact with IBA1⁺ TAMs in any of the three tumor subregions.
- Tumor cells expressing SOX2 ($P < 0.05$) and nestin ($P < 0.05$), podoplanin ($P < 0.05$) were often in direct interaction with IBA1⁺ TAMs in the perivascular region, and similar tendency was observed for tumor cells expressing podoplanin ($P = 0.15$).
- Most CD204⁺ TAMs co-localized with CD133⁺ tumor cells in the perivascular area ($P < 0.001$), whereas the interaction between CD204⁺ TAMs and with PDPN⁺ tumor cells was especially evident in the perinecrotic area ($P < 0.001$).
- mRNA transcriptome profiling revealed that glioblastomas with high levels of CD204 formed one major cluster which was associated with a poor survival outcome and displayed an unique gene expression profile. Pathway scoring, gene set and KEGG analyses of the gene expression profile showed enrichment in pathways related to the immune system including complement, antigen processing and presentation as well as TNF, nucleotide-binding oligomerization domain-like (NOD-like) receptor, IFN, and nuclear factor kappa-light-chain-enhancer of activated B cells (NFκB) signaling,
- CD204-enriched glioblastomas exhibited higher levels of necrosis ($P < 0.01$) and lower overall cell density ($P < 0.05$) compared to CD204-sparse glioblastomas.

- A total of 119 genes were uniquely differentially upregulated in CD204-enriched glioblastomas including *CCL20*, *IL6*, *ICAM1*, *PD-L1*, *IL8*, and *CXCL14*, and STRING connectivity analysis of the 119 genes identified three major and three minor clusters that were interconnected. The biggest cluster centralized around particularly *IL6* which interacted either directly or indirectly via e.g. *ICAM1*, *caspase-1*, or *CD86* with the other subnetworks including the second biggest cluster which among others comprised *HLA* genes, *CD44*, and *PD-L1*. Both *CD44* and *PD-L1* connected to a small cluster consisting of the immune checkpoint markers *TIM3* and *galectin-9* as well as *galectin-3*. KEGG and Reactome Pathway analyses demonstrated an enrichment in pathways related to activation and regulation of the immune system as well as cellular communication by cytokines or chemokines. Analyses of two bioinformatics databases validated the functional profile of the CD204-enriched glioblastomas, and cluster analyses confirmed that *IL6* may play a central role in CD204-enriched tumors, while CD204 itself especially cluster with genes related to extracellular matrix organization.
- Immunohistochemical analyses validated that CD204-enriched glioblastomas had increased expression of *IL6* ($P < 0.001$), *ICAM1* ($P < 0.01$), *CD44* ($P < 0.01$), *TNFAIP3* ($P < 0.01$), *galectin-3* ($P < 0.05$), *PD-L1* ($P < 0.05$), *galectin-9* ($P < 0.001$), and *TIM3* ($P < 0.001$) relative to CD204-sparse glioblastomas.
- The prognostic value of CD204 in glioblastoma was not significantly potentiated when accounting for the inflammatory profile identified by transcriptome analysis, and this finding was confirmed in the bioinformatics databases.

The results from manuscript is graphically summarized in **Figure 27**.

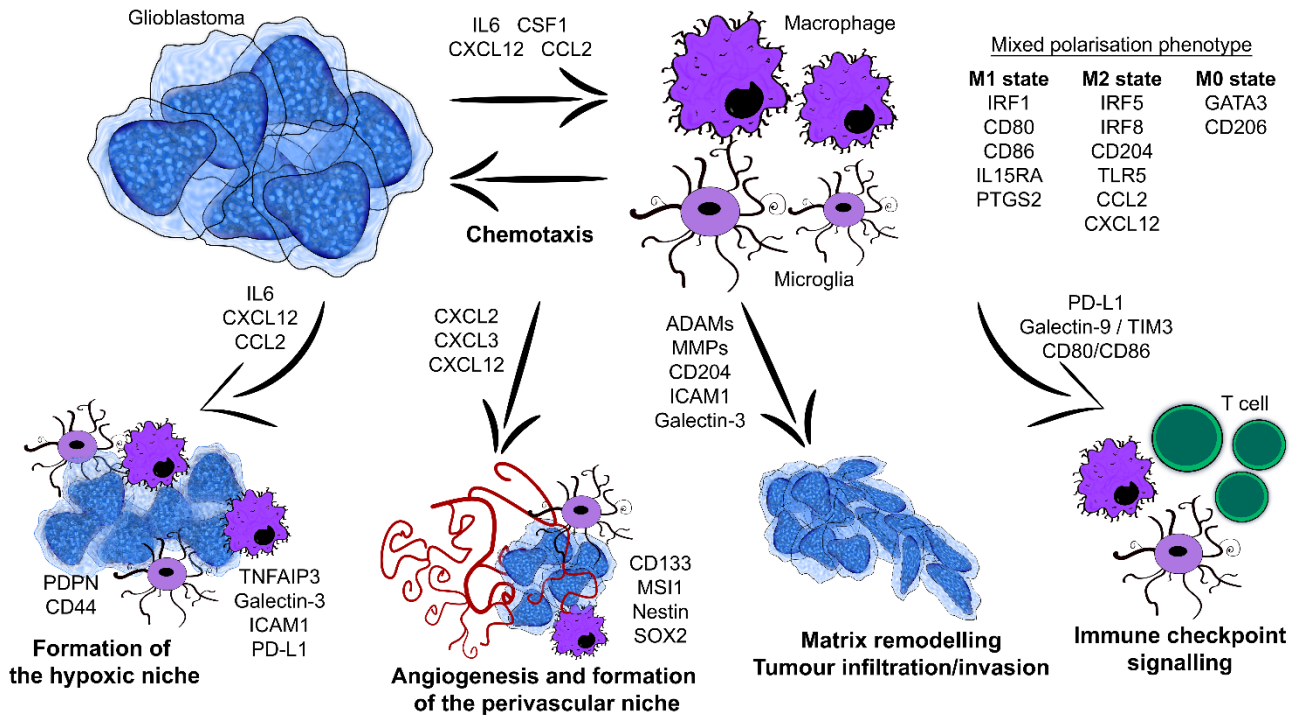


Figure 27 | Schematic depiction of the possible crosstalk between glioblastoma cells and TAMs in CD204-enriched glioblastomas. Tumor-derived factors e.g. IL6, CXCL12, CSF1, and CCL2 recruit brain-resident microglia and peripheral macrophages to the site of the tumor, while simultaneously activating and polarizing the TAMs. The crosstalk between the glioblastoma cells and TAMs leads to expression and secretion of different cytokines/chemokines or/and receptors which stimulate tumor hypoxia, angiogenesis, as well as matrix remodeling and impact immune checkpoint signaling. The TME in CD204-enriched glioblastoma may thus support tumor growth, resistance, and progression. Reprinted from [644] under the terms and conditions provided by John Wiley and Sons and of the Creative Commons Attribution License.

9.3 Manuscript III

Title: D-2-hydroxyglutarate is an intercellular mediator in IDH-mutant gliomas inhibiting complement and T cells

Aims:

- To investigate the association between IDH mutation status and complement activation as well as infiltration levels of CD4⁺ Th cell, CD8⁺ cytotoxic T cell, and FOXP3⁺ Tregs in astrocytic gliomas, WHO III-IV, using immunohistochemistry.
- To examine the impact of D-2-hydroxyglutarate on 1) activation of complement pathways, 2) dendritic cell differentiation and function, and 3) T cell migration, proliferation and cytokine secretion using *ex vivo* experiments.

Main findings:

- IDH mutation correlated with decreased levels of complement activation as the deposition of C3/C3b complement fragments was reduced in IDH-mutant astrocytomas compared to IDH-wildtype astrocytomas ($P < 0.001$). IDH-mutant astrocytomas also tended to have less complement deposition on the luminal surfaces of small blood vessels and capillaries ($P = 0.085$), and the intensity of deposited C3/C3b in necrotic areas was lower in IDH-mutant glioblastomas compared to IDH-wildtype glioblastomas ($P < 0.05$).
- The numbers of tumor-infiltrating CD4⁺ Th cells ($P < 0.01$), CD8⁺ cytotoxic T cells ($P < 0.001$), and FOXP3⁺ Treg cells ($P < 0.01$) were reduced in IDH-mutant astrocytomas compared to their IDH-wildtype counterparts. However, FOXP3/CD4 ratio was not significantly influenced by IDH status ($P = 0.13$).
- D-2-hydroxyglutarate inhibited the classical pathway of complement activation by 1) suppressing MAC-induced hemolysis in a dose-dependent manner, 2) inhibiting assembly of the C5 convertase, but not the C3 convertase, and 3) inhibiting the activity of assembled C3 and C5 convertases.
- D-2-hydroxyglutarate impaired the alternative pathway of complement activation by 1) reducing complement-mediated hemolysis in a dose-dependent manner and 2) inhibiting the assembly of C3/C5 convertases. D-2-hydroxyglutarate did not affect the activity of preassembled C3/C5 convertases.
- D-2-hydroxyglutarate significantly attenuated complement-mediated cell damage in the T98 glioblastoma cell line in a dose-dependent manner.
- D-2-hydroxyglutarate lowered C3b(iC3b) opsonization on the surface of erythrocytes and reduced the complement-mediated phagocytosis of the erythrocytes by macrophages.
- Proliferation of activated Th1 and Th17 cells was inhibited by D-2-hydroxyglutarate, as was the case for secretion of IFN γ by activated T cells. Interestingly, a high level of D-2-hydroxyglutarate augmented the differentiation of Tregs, but simultaneously inhibited their proliferation and IL10 production. In a transwell migration assay, D-2-hydroxyglutarate reduced migration of both CD4⁺ and CD8⁺ T cells.
- D-2-hydroxyglutarate neither influenced the differentiation nor antigen processing of dendritic cells.

The results from manuscript III is graphically summarized in **Figure 28**.

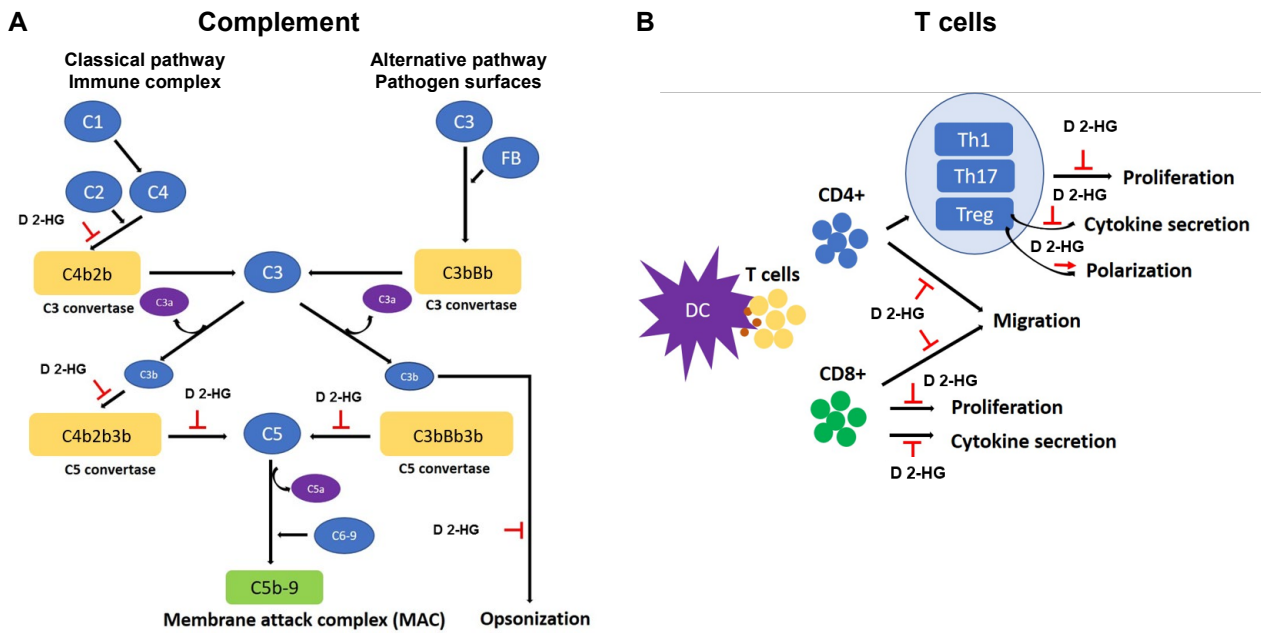


Figure 28 | D-2-hydroxyglutarate (D 2-HG) inhibits both complement and T cells. **(A)** D 2-HG inhibits complement at different steps of the complement activation cascade. **(B)** D 2-HG inhibits T cell migration, proliferation, and cytokine production, but enhances polarization of Tregs. Reprinted from [645] with permission from Clinical Cancer Research as agreed upon by the American Association for Cancer Research.

9.4 Manuscript IV

Title: The presence of TIM-3 positive cells in WHO grade III and IV astrocytic gliomas correlates with isocitrate dehydrogenase mutation status

Aim:

- To establish a chromogenic multiplex immunohistochemistry panel in order to better characterize the TIME in glioma.
- To investigate the association between IDH mutation status and presence of cells expressing the immune checkpoint proteins galectin-9 and/or TIM3 in malignant astrocytomas, WHO III-IV, using a chromogenic multiplex immunohistochemistry technique.

Main findings:

- A chromogenic multiplex immunohistochemistry panel was successfully established by sequential application of unconjugated primary antibodies with heat deactivation steps in between each sequence for elution purposes. The three antibodies used in the panel targeted OLIG2, TIM3, and galectin-9. OLIG2 was included as tumor cell marker to identify the potential expression of galectin-9 and/or TIM3 on tumor cells.
- Most TIM3⁺ and/or galectin-9⁺ cells resembled microglia/macrophages. This was confirmed using double immunofluorescence as ~80% of the galectin-9 and TIM3 positive area co-expressed IBA1, whereas only ~30% and ~20% of the IBA1⁺ cells expressed galectin-9 and TIM3, respectively. TIM3 was often co-expressed with galectin-9, while only of about a third of the galectin-9⁺ area co-localized TIM3. Very few galectin-9⁻ TIM3⁺ cells were seen, and these cells resembled either T cells or microglia/macrophages. Expression of TIM3 by T cells was verified using double immunofluorescence demonstrating that ~10% of the T cell population expressed TIM3.
- The overall percentage of galectin-9⁺ cells tended to be lower in IDH-mutant compared to IDH-wildtype tumors comprising ~15% and ~20% of all cells, respectively ($P = 0.10$).
- The overall percentage of TIM3⁺ cells was significantly lower in IDH-mutant than in IDH-wildtype tumors ($P = 0.024$) contributing with ~6% and ~10% of the total cell count, respectively.
- The presence of galectin-9⁺ cells positively correlated with the presence of TIM3⁺ cells ($r_s = 0.73$, $P < 0.0001$), but negatively correlated with the amount of OLIG2⁺ cells ($r_s = -0.54$, $P < 0.01$). Similarly, a negative correlation was found between OLIG2 and TIM3 ($r_s = -0.45$, $P < 0.05$).
- No IDH-dependent difference was observed for OLIG2 protein expression ($P = 0.58$) as OLIG2⁺ tumor cells accounted for ~45-50% of the cells in both IDH-mutant and IDH-wildtype tumors. Galectin-9 was only expressed by ~1% of the OLIG2⁺ cells, and this was irrespective of IDH mutation status. TIM3 was rarely expressed by OLIG2⁺ tumor cells and only in conjunction with galectin-9. Chromogenic co-expression patterns were confirmed by double immunofluorescence.
- Galectin-9⁺ TIM3⁻ microglia/macrophages comprised ~10% of the cells in both IDH-mutant and IDH-wildtype tumors ($P = 0.99$), whereas the percentage of galectin-9⁺ TIM3⁺ microglia/macrophages was significantly lower in IDH-mutant tumors compared to IDH-wildtype tumors (~5% vs. ~9%, respectively, $P = 0.044$). The presence of galectin-9⁻ TIM3⁺ microglia/macrophages was generally low irrespective of

the IDH mutation status, however, the percentage was significantly lower in IDH-mutant tumors (~0.15% vs. ~0.30%, $P = 0.004$).

- Fewer TIM-3⁺ T cells were observed in IDH-mutant tumors compared to their IDH-wildtype counterparts (0.00% vs. 0.26%, $P = 0.002$). Irrespective of IDH status, almost none of the TIM-3⁺ T cells interacted with galectin-9⁺ tumor cells. In contrast, ~85-100% of TIM-3⁺ T cells interacted with galectin-9⁺ TAMs in IDH-wildtype tumors which was significantly higher than the 50% interaction rate found in IDH-mutant tumors ($P = 0.025$).
- Galectin-9 and TIM-3 levels positively correlated with the presence of CD4⁺ Th cells ($r_s = 0.51$ and $r_s = 0.53$, $P < 0.001$), CD8⁺ cytotoxic T cells ($r_s = 0.58$ and $r_s = 0.52$, $P < 0.001$), and FOXP3⁺ Tregs ($r_s = 0.42$ and $r_s = 0.49$, $P < 0.001$).
- The immunohistochemical results were mostly confirmed at the transcriptional level using the TCGA data base. However, in contrast to the protein data, *OLIG2* mRNA expression was significantly higher in IDH-mutant compared to IDH-wildtype WHO grade III-IV astrocytic gliomas ($P < 0.001$).
- Using the TCGA dataset, glioblastomas with highest and lowest *TIM3* mRNA expression level were screened for possible changes in mRNA levels of 17,811 genes. A total of 75 genes were differentially upregulated ($\log_2 \text{FC} \geq 2.00$) in glioblastomas with the highest *TIM3* mRNA level; among these genes were e.g. *IBA1*, *IL6*, and *CD204*. No genes were differentially downregulated below a two-fold change. GO and KEGG enrichment and pathway analyses revealed that the upregulated genes were involved in biological processes such as leukocyte migration, regulation, aggregation, and chemotaxis as well as regulation of cell activation and production of chemokines and cytokines including the TNF superfamily. Additionally, the upregulated genes were enriched in signaling pathways of TLR, IL17, complement, NOD-like receptor, TNF and NF κ B as well as in the phagosome pathway and various inflammatory/infectious diseases.
- Many of the upregulated genes were associated with microglia/macrophage migration, chemotaxis, and/or polarization. Exploratory analyses revealed that the mRNA expression of the microglial/macrophage-associated genes, was significantly reduced in IDH-mutant astrocytic gliomas compared to the IDH-wildtype counterparts, apart from *IBA1* which did not show an IDH-related differential change. The mRNA results were confirmed at a protein level for IBA1 and CD204.

The results from manuscript is graphically summarized in **Figure 29**.

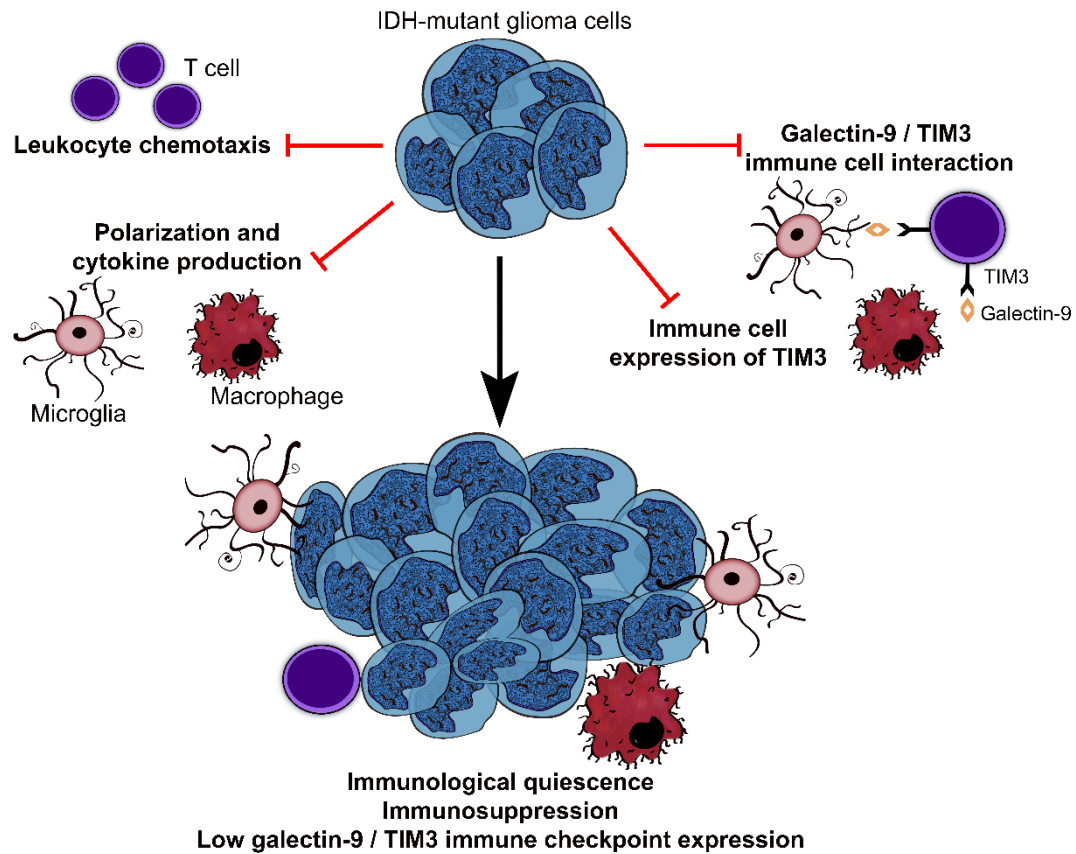


Figure 29 | Schematic illustration of the possible immunomodulatory of IDH mutation in glioma. IDH mutation and its oncometabolite D-2-hydroxyglutarate may cause suppression of leukocyte chemotaxis and microglia/macrophage polarization as well as cytokine production thereby reducing the expression and activity of the galectin-9/TIM3 immune checkpoint pathway. Reprinted from [646] under the terms and conditions provided by John Wiley and Sons and the Copyright Clearance Center.

10. General discussion

The overall aim of this thesis was to investigate the immune landscape in gliomas focusing on the possible clinical impact of CD204⁺ TAMs in glioblastoma and on the influence of IDH mutation on the immune microenvironment in diffuse glioma. We used different techniques and tools to accomplish our objective, including conventional immunohistochemistry, multiplex immunohistochemistry/immunofluorescence, transcriptome profiling with the NanoString digital barcode technology, digital image analysis, and bioinformatics databases. We found that high levels of CD204⁺ TAMs correlate with glioma malignancy and have an unfavorable impact on overall survival in patients with WHO grade III-IV gliomas. In contrast, TAM density in general showed little prognostic value. CD204⁺ TAMs accumulated in perivascular and perinecrotic regions/tumors closely interacting with podoplanin⁺ glioblastoma cells. Characterization of CD204⁺ TAMs and CD204-enriched glioblastoma revealed an association between CD204 and features of tumor aggressiveness, including hypoxia, angiogenesis, invasion, and treatment resistance. Transcriptome profiling of 46 glioblastomas with high or low CD204 and IBA1 protein expression followed by unsupervised clustering analysis identified two clusters. Cluster 1 was mainly composed of tumors with low levels of CD204 and high or low levels of IBA1, while cluster 2 primarily comprised tumors with high CD204 expression. The CD204-enriched cluster 2 conferred a poor prognosis and was characterized by enrichment in several pathways including the TNF, NFκB, and NOD-like receptor signaling pathways, which are involved in regulation of immune response, apoptosis and extracellular matrix [647-649]. We furthermore found that D-2-hydroxyglutarate significantly impaired complement activation and T cell effector functions *ex vivo*, and these findings translated to results obtained from immunohistochemical stainings. These results revealed that IDH-mutant astrocytic gliomas relative to their IDH-wildtype counterparts had decreased levels of complement deposition, fewer tumor-infiltrating T cells, fewer CD204⁺ TAMs, TIM3⁺ immune cells, and lower interaction rate between TIM3⁺ T cells and galectin-9⁺ TAMs, overall suggesting that the innate and adaptive immune system is suppressed or kept dormant in IDH-mutant tumors.

The following sections emphasize and discuss the most important results of the thesis. The full-length manuscripts contain more comprehensive discussion paragraphs and are accessible in the *Appendix*.

10.1 The prognostic value of M2-like TAMs in diffuse gliomas

In manuscript I, we examined the prognostic value of microglial/macrophage markers IBA1 and CD204 in a population-based glioma cohort with 240 patients using an automated quantitative double immunofluorescence assay. We found that both CD204 and IBA1 area fractions increased with WHO II-IV malignancy, contributing with up to 25-30% of the vital tumor area in glioblastoma. The positive correlation with malignancy grade is in agreement with other studies on primary gliomas that used general TAM markers CD68 [43, 45, 47, 492, 493] and IBA1 [37, 44, 45] as well as M2-related markers CD163 [32, 37, 43, 47, 49], CD204 [43, 47, 48], and CD206 [47, 650]. In regards to patient outcome, we demonstrated that the acquired phenotype of TAMs was the critical factor rather than the total amount TAMs. The area fraction of IBA1 did not correlate with overall survival in patients with WHO grade III-IV, but high levels may correlate with improved survival in

patients with WHO grade II gliomas. High amounts of CD204 were associated with shorter survival in patients with WHO grade III-IV gliomas, but not in patients with grade II gliomas possibly due the limited of number of patients included in the analysis and the paucity of CD204⁺ TAMs. Both previous and more recent studies reported similar results for CD163 showing that high CD163 expression holds a negative prognostic value in patients with glioblastoma and/or anaplastic astrocytoma at both a protein [43, 46, 47, 50, 498] and mRNA level [49, 651]. Similar prognostic impact was reported for CD206 protein in patients with glioblastoma [650]. Further, a recent smaller study including 18 IDH-wildtype glioblastomas found that high CD204 expression was associated with early recurrence [652]. Transcriptome profiling of glioblastomas demonstrated that TAMs had an M2-like phenotype in short-term survivors, while the transcriptional profile of TAMs in long-term survivors showed a predominance towards the M1-like phenotype [162]. In contrast, Zeiner *et al.* found that high CD163 and CD206 correlated with better outcome in glioblastoma patients, and similar beneficial impact was found for IBA1 when dichotomized at its optimal cut-off level. This discrepancy could be explained by the use of tissue microarrays (TMA) instead of whole tissue sections. Zeiner *et al.* only used one core per tumor for statistical analysis. Depending on the expressional heterogeneity of the biomarker of interest, the use of TMA increases the risk of a false-negative result if the number of TMA cores is not adjusted accordingly [653, 654]. In our study, we used whole tissue sections and observed a high level of both intra- and intertumoral heterogeneity. This finding suggests that whole tissue sections may be superior to TMAs when investigating the immune landscape in gliomas. Martinez-Lage *et al.* [498] also used TMAs in their study, however, they included up to six TMA cores accounting of the tumor heterogeneity. We selected CD204 to identify M2-like TAMs, as it may be a more reliable and microglial/macrophage-specific marker compared to CD163 [655] and CD206 [656-658]. In our multivariate analyses, CD204 was an independent predictor of poor prognosis in both grade III and IV gliomas when adjusting for clinico-pathological parameters. Further, in patients with glioblastoma, high CD204 levels were associated with shorter overall survival in the group of patients receiving post-surgical treatment, while no significant prognostic impact was observed in the group who only underwent surgery. Looking at the subgroup of patients with MGMT-methylated glioblastoma, high CD204 expression correlated with shorter survival, while the survival detriment was less pronounced in patients with MGMT-unmethylated tumors. These findings indicate that CD204 and M2-like TAMs may contribute to progression and treatment resistance in glioblastoma. Using online available microarray and RNA sequencing data, Yuan *et al.* also identified CD204 as an independent prognosticator in patients with diffuse gliomas, including malignancy grade, IDH status, age, and sex in their multivariate analysis [48]. CD204 and M2-like TAMs were reported to be negative determinants of tumor progression and patient outcome in several other cancer types [439, 659], including head and neck squamous cell carcinoma [660], hepatocellular carcinoma [661], and lung cancer [662], while no independent prognostic value was demonstrated in esophageal cancer [663] or in primary CNS lymphoma [664].

Interestingly, we found that high IBA1 intensity correlated with prolonged survival in patients with glioblastoma, and dichotomizing patients based on IBA1 and CD204 area fractions revealed that patients with CD204^{high}/IBA1^{low} levels had the worst prognosis. The finding was reproduced in manuscript II using a set of glioblastomas selected from the patient cohort in manuscript I and validated using bioinformatics databases.

Kaffes *et al.* also found that high *IBA1* mRNA levels conferred a survival benefit, but only in the mesenchymal subtype of glioblastoma. In contrast, high *IBA1* correlated with shorter survival in the proneural subtype [268]. *IBA1* is considered a general microglial/macrophage marker [53, 490], however, increasing evidence shows that its expression may be up- or downregulated in a disease-dependent manner [665], and *IBA1* upregulation is reportedly associated with a pro-inflammatory phenotype in macrophages [665, 666]. These findings suggest that TAMs with an *IBA-1*^{high} phenotype may represent a population of activated TAMs in glioma that has not (yet) been polarized into an M2 pro-tumorigenic state. Collectively, our results show that high CD204 expression is an unfavorable prognostic biomarker in especially glioblastoma and that the prognostic impact of TAMs in gliomas does not rely on the total amount of TAMs, but on their acquired phenotype.

10.2 The heterogeneity of TAMs in diffuse glioma

In manuscript I, we observed that TAMs were heterogeneously dispersed in gliomas at an inter- and intratumoral level. We found that *IBA1* and CD204 composed 0-30% and 0-25% of the tumor area, respectively, and we detected 0-90% co-expression between the two markers. In agreement with previous reports [37, 41, 45, 375, 470, 494], we demonstrated that the density of both *IBA1*⁺ cells and CD204⁺ cells was elevated in perivascular and perinecrotic areas compared to the vital tumor area. This spatial heterogeneity of TAM could be associated with the predominant transcriptional phenotype(s) or cellular state(s) of the individual glioma [9, 11, 408, 409]. We found that TAMs and especially CD204⁺ TAMs were more abundant in the mesenchymal subtype of glioblastoma. This finding is consistent with previous and later reports showing that TAM-related markers including CD204 [48] are enriched in mesenchymal glioblastomas [17, 174, 255, 258, 267, 268, 498]. Similar correlation was reported for tumor-infiltrating T cells [256, 268, 498]. The mesenchymal phenotype exhibits features associated with tumor aggressiveness, including high degrees of necrosis [17], poor prognosis [17, 258, 266], and treatment resistance [17, 20, 265]. Numerous studies have also shown that recurrent glioblastomas are characterized by a shift toward a mesenchymal phenotype [10, 258, 267, 270, 434], possibly due to a transition in the mesenchymal-like glioblastoma cells from a quiescent to a cycling state mediated by the transcription factor activator protein 1 [434] or through deactivation of the *NF1* gene [11, 258]. The mesenchymal subtype in recurrent tumors is accompanied by an increased frequency of M2-like or the more undifferentiated M0-polarized TAMs possibly related to prior radiotherapy [258, 434]. *NF1* loss was shown to drive infiltration of microglia/macrophages into the TME [258], and in turn, TAMs may induce transition to the mesenchymal phenotype [502] e.g. through IFN γ exposure [667], NF κ B activation [17, 668], or via the IL6-JAK-STAT3 pathway [669]. Overall, these results suggest that TAMs participate in tumor progression by favoring a more aggressive tumor phenotype. Strategies to reverse the mesenchymal state by targeting TAMs could thus be therapeutically relevant.

In manuscript I and II, we characterized CD204⁺ TAMs and CD204-enriched glioblastomas using double immunofluorescence and mRNA transcriptome profiling, respectively. We showed conjunctional expression of proteins related to the M1 (HLA-DR, TNF α) and M2 (IL10, TGF β 1) polarization as well as upregulation of genes associated with all macrophage/microglia polarization states: M1 (*CD86*, *CD80*, *IRF1*, *IL15RA*, and *PTGS2*), M2/M2c (e.g., *TLR5*, *CXCL12*, *CD204*, *CCL2*, and *HLA*-genes), and M0 (GATA binding protein 3

(*GATA3*), *CD206*). Our results underline the diversity among TAMs and are consistent with previous studies that interrogated the immune landscape of glioma using *in vitro* experiments/qPCR [36, 670], microarray analysis [38, 39], lineage tracing [42], fluorescence-activated cell sorting plus RNA sequencing [33], and single-cell RNA sequencing and mass cytometry/cytometry by time of flight (CyTOF) analyses [41, 500]. Collectively, increasing data indicates that TAMs cannot be delimited into a fixed activation state as their polarization might depend on the location of the specific TAM within the tumor tissue, its cellular origin (i.e. monocyte-derived macrophage vs. microglia) and on the stage of disease. In fact, a series of recent studies employing single cell sequencing on glioma tissue derived from patients and orthotopic mouse models demonstrate that the heterogeneity of TAMs is disease-, ontogenetic-, and spatiotemporal-dependent [13, 32, 41, 408, 434, 461, 500, 671].

In the past, CD11b and CD45 were usually used to separate microglia (CD11b⁺/CD45^{low}) from macrophages (CD11b⁺/CD45^{high}) [460, 672], however, microglia upregulate CD45 expression in a tumor context making them indistinguishable from monocyte-derived macrophages [673]. Instead a combination of markers are often employed, most importantly CD49d, purinergic receptor P2Y12 (P2RY12), transmembrane protein 119 (TREM119), spalt like transcription factor 1 (SALL1) as well as CD11b and CXCR3 [32, 33, 41, 42, 490]. These markers enable accurate discrimination between microglia and macrophage as well as delineation of TAM heterogeneity in lineage tracing experiments and at a single-cell resolution. Chimeric and cell lineage models in mice have revealed that TAMs in glioma can originate from either microglia or monocyte-derived macrophages accounting for ~85% and ~15% of all TAMs, respectively [41, 42, 459]. These models also demonstrated that the ontogenetic composition of TAMs changes over time [35, 41, 42]. As such, pro-inflammatory, M1-like microglial-derived TAMs dominate in the early phases of glioblastoma growth, while late-stage tumors contain a higher number of anti-inflammatory M2-like monocyte-derived TAMs, indicating an evolution that parallels the disruption of the BBB. The findings from these mouse studies were translational to patient-derived gliomas. Analyses of the immune cell composition in lower-grade glioma and glioblastoma using flow cytometry [35] and RNA sequencing [41] demonstrated that the relative proportion of monocyte-derived TAMs was higher in glioblastoma compared to grade II-III glioma; and interestingly, there was a significant increase in monocyte-derived TAMs, but not in microglial-derived TAMs, in glioblastoma compared to lower-grade glioma [41]. Similarly, TAMs showed a grade-dependent increase in the macrophage state relative to microglial state in patient-derived IDH-mutant gliomas [408]. Moreover, the percent of TAMs classified as monocyte-derived lineage cells was found to increase in recurrent glioblastoma at the expense of microglial-derived TAMs [267, 434, 437], possibly due to therapy-induced inflammation [502, 507].

As mentioned, we demonstrated that IBA1⁺ and CD204⁺ TAMs accumulated in perivascular and necrotic regions, while their abundance decreased from the tumor core to the tumor periphery. Interestingly, TAMs in the periphery morphologically resembled ramified microglia, whereas TAMs in the tumor core had an amoebic morphology. Further, IBA1 intensity was similar in two areas, indicating that the peritumoral TAMs were at least partially activated. This is consistent with results by Kaffes *et al.*, who showed that the number of microglial processes was lowest and the IBA1 area highest within the tumor core [268]. Spatial single-cell

profiling has also revealed a geographic variation in the TAM composition. Monocyte-derived TAMs invade the tumor core, especially in hypoxic [41, 461] and perivascular [32, 41, 459] areas, and exhibit an immunosuppressive and pro-angiogenic/hypoxic phenotype, while microglial-derived TAMs primarily occupy the peritumoral space which is characterized by high expression of especially immunomodulating markers, such as PD1, PD-L1/PD-L2, CD86, and CD276 [13, 41, 671, 674]. In aggregate, these findings imply that CD204 is expressed mostly on monocyte-derived macrophages upon extravasation into the brain TME. Preventing recruitment of monocytes combined with re-education of macrophages could thus be a beneficial therapeutic strategy in glioblastoma.

10.3 The possible biological role(s) of CD204 in glioblastoma

Due the negative prognostic value of CD204, our aim in manuscript II was to investigate the possible biological role of CD204 in glioblastoma. Seeing that TAMs accumulated in areas surrounding vasculature and necrosis, we explored using double immunohistochemistry whether there was a crosstalk between TAMs and glioblastoma cells expressing stem cell-associated markers. Apart from CD133 and podoplanin, we found that the stem cell-associated markers were widely expressed in glioblastoma, supporting the notions that most glioblastoma cells can exhibit stem cell-like properties dependent on the environmental cues and that multiple cellular and transitory states exist within most glioblastomas [9, 264, 369]. We further demonstrated that especially CD204⁺ TAMs and podoplanin⁺ glioblastoma cells co-resided and interacted in the perivascular and perinecrotic/hypoxic niches. Of the stem cell-related markers included in our NanoString panel, only *podoplanin*, *CD44*, and *ALDH1A1* were differentially upregulated in CD204-enriched glioblastoma. These genes are involved in promotion of hypoxia [366, 675], radio-chemo-resistance [17, 676, 677], and invasiveness through the actions of MMPs and metalloprotease-disintegrins [391, 677, 678]. Recent studies have also linked the three genes to an M2-like, immunosuppressive phenotype of TAMs [679-681]. Tumor hypoxia itself promotes angiogenesis [361], treatment resistance, tumor migration [360], invasion, and mesenchymal shift [62, 359, 364], ultimately resulting in an aggressive tumor phenotype [325, 359, 363, 682]. Hypoxia reportedly fine-tunes the M2-like polarization of TAMs [373] leading to upregulation of HIFs and HIF target genes including MMPs and pro-angiogenic factors [375]. Notably, immunofluorescent phenotyping of CD204⁺ TAMs in manuscript I showed an up to 50% co-expression with HIF1 α . We also examined if the presence of necrosis correlated with the amount of TAMs and observed that CD204-enriched glioblastomas contained the highest amount of necrosis. This finding is in line with the nature of CD204 as CD204 is a member of the scavenger receptor family capable of binding and internalizing a range of ligands, including apoptotic cells, low-density lipoproteins, collagen, and myelin [658, 683]. Our differential expression analysis revealed that 119 genes were uniquely upregulated in CD204-enriched glioblastomas, including *CCL20*, *IL6*, *CXCL8*, *CXCL14*, *galectin-3*, *CD44*, *ICAM1*, and *TNFAIP3*. By binding to their cognate receptors, CCL20, IL6, CXCL8, and CXCL14 have been reported to facilitate myeloid infiltration, immune evasion, hypoxia, angiogenesis, proliferation, migration/invasion, mesenchymal transition, and poor prognosis in glioblastoma [339, 466, 684-689]. ICAM1 and CD44 have both been linked to promotion of tumor hypoxia, migration/invasion, treatment resistance [690], matrix remodeling [691, 692] and mesenchymal shift [17, 693].

Further, TNFAIP3 and galectin-3 were reported to be hypoxia-induced and NF κ B-dependent genes involved in regulation of apoptosis [694-696] favoring cell survival [697, 698], cancer stemness and tumor growth [697], and possibly chemo-resistance [699]. Although we found few CD204⁺ TAMs in the tumor periphery, some CD204⁺ TAMs were present in the invasion zone adjacent to the tumor core, and CD204⁺ TAMs showed a pronounced co-expression of MMP14 which functions as a co-factor in extracellular matrix remodeling and tumor expansion [31, 480]. These findings are in line with a study on glioblastoma showing that TAMs reside at the invasive edge [395]. Additionally, high levels of CD204 in the marginal zone were associated with shorter disease-free survival in sarcoma [700], while high CD204 cell count in the seminal vesicle invasion area correlated with a greater risk of biochemical recurrence in prostate cancer [701], overall supporting the notion that CD204 may play a part in tumor invasion and progression/recurrence. Summarized, our results suggest that CD204⁺ TAMs flourish in hypoxic niches and may mediate formation of a pro-invasive, resistant and stem cell-like phenotype of glioblastoma.

Profiling of CD204-enriched glioblastoma revealed a differential upregulation of immune checkpoint markers, *PD-L1*, *TIM3*, and *galectin-9*, indicating a possible relation between CD204 and development of dysfunctional/exhausted T cells [77, 532, 537]. Yuan *et al.* reported a similar transcriptional correlation between CD204 and these immune checkpoints [48]. Interestingly, in oral squamous cell carcinoma, CD204⁺ TAMs significantly reduced the number of activated CD3⁺ T cells [702]. Further, CD204 was found to suppress CD4⁺ and CD8⁺ T cell activation by limiting the immunostimulatory ability of dendritic cells, and silencing of CD204 improved the capability of dendritic cells to prime antigen-specific T cells [703, 704]. Similarly, inhibition of CD204 in dendritic cells improved the efficacy of a dendritic cell vaccine in a melanoma model by restoring the T cell response and anti-tumor immunity [705], and in an ovarian cancer model, administration of CD204-targeted immunotoxin substantially reduced tumor burden and the amount of suppressive vascular leukocytes [706]. In syngeneic hypermutated experimental glioma, *CD204* along *PD-L1* and *TGF β 1* expression levels were significantly upregulated in CD45^{high}CD11b⁺ cells from tumors that were non-responsive to checkpoint inhibition, suggesting a significant correlation between PD-L1 and CD204 as well as a possible involvement of CD204 in resistance to checkpoint blockade [485]. In manuscript IV, we found that most TIM3⁺ cells in glioma were TAMs and not infiltrating T cells, and TIM3⁺ TAMs almost consistently co-expressed its ligand galectin-9. TIM3 is a type I transmembrane glycoprotein with an extracellular variable immunoglobulin domain connected to mucin-like domain. TIM3 was first recognized on T cells, but later found to be expressed on monocytes/macrophages, dendritic cells and some types of cancer cells. In T cells, TIM3 is upregulated upon antigen recognition through the TCR and in response to pro-inflammatory cytokines. TIM3 functions as a co-inhibitory receptor that promotes development of Tregs and inhibit CD4⁺ and CD8⁺ T cell activation upon ligation to its cognate ligands, e.g. galectin-9 [707]. TIM3 also plays a part in T cell exhaustion along with PD1 [77, 532, 549], and combined targeting of TIM3 and PD1 was able to restore the anti-tumorigenic functions of T cells and inhibit tumor growth in an *in vivo* colon carcinoma model [571] and in a glioma model [566]. In the clinic, we are awaiting the results of an ongoing phase I trial (NCT03961971) in recurrent glioblastoma that is exploring the safety and preliminary anti-tumor activity of combining the anti-TIM3 inhibitor MBG453 with the PD1 inhibitor spartalizumab and stereotactic radiosurgery [117]. In

macrophages, TIM3 is involved with cell activation and capture of apoptotic bodies and reportedly increase secretion of the immunosuppressive IL10 and IL6 [708]. Further, TIM3 was shown to mediate M2-like polarization of macrophages in colon cancer [709] and was expressed by ~15% of CD204⁺ TAMs in clear cell renal cell carcinoma [710]. Further Komohara *et al.* demonstrated that TIM3 expression was induced in CD14⁺ monocytes *in vitro* following long-term stimulation with renal carcinoma cells and in turn, the TIM3⁺ monocytes promoted resistance to the tyrosine kinase inhibitor sunitinib and mTOR inhibitor rapamycin [710]. We employed the TCGA dataset to screen for differential changes in gene expression levels between the glioblastomas with the highest and lowest *TIM3* mRNA levels. This revealed that several macrophage/immune-related genes, including *CD204* and *IL6*, were upregulated in TIM3-enriched glioblastomas, and pathway analysis showed that the upregulated genes were involved in many of the same pathways as CD204, including TNF and NFκB signaling. Collectively, these findings point to an immunoinhibitory function of CD204 and support the hypothesis that CD204⁺ TAMs exist in an immunosuppressive and pro-tumorigenic TME that favors immune evasion of tumor cells and resistance to checkpoint blockade in glioblastoma.

We identified IL6 as the essential player in the inflammatory milieu of CD204-enriched glioblastomas by performing connectivity and cluster analyses of the differentially upregulated genes. IL6 is an important regulator of the innate and adaptive immune system and has previously been viewed as a typical pro-inflammatory cytokine. However, in cancer, including glioblastoma, it is regarded as one of the major tumor-promoting cytokines secreted by both neoplastic and non-neoplastic cells [711, 712]. IL6 stimulates expression of adhesion molecules and chemokines e.g. ICAM1 and CCL2 [713], which in turn facilitate tumorigenesis and tumor-driven inflammation through multiple signaling pathways, including IFN, JAK-STAT and NFκB [684, 711, 712, 714-716]. In glioblastoma, IL6 is mainly produced by TAMs and endothelial cells, while its receptor IL6R is expressed mostly on glioma cells [31, 717-720]. Glioblastoma-derived IL6 was shown, nevertheless, to induce PD-L1 expression on myeloid cells leading to apoptosis of CD8⁺ T cells [473], and inhibiting PD-L1 during hypoxia facilitated MDSC-mediated T cell activation and reduced MDSC-derived IL6 and IL10 *in vitro* [721]. Further, IL6 induced an M2-like and immunosuppressive phenotype of TAMs characterized by expression of CD206, IL10, TGFβ2, and arginase-1/2. Interestingly, IL6 also promoted expression of the co-stimulatory receptor CD40 through HIF1α and STAT3 [688], suggesting a dual role of IL6 in regards to tumor immunity. In orthotopic murine glioblastoma models, inhibition of IL6 or its receptor diminished tumor growth and prolonged survival [473, 688, 717, 719, 720, 722], and combined treatment with anti-IL6 and anti-PD1 antibodies revealed an additive survival benefit [473]. IL6 knockout was also demonstrated to reduce recruitment of TAMs into the TME and enhance infiltration of CD8⁺ T cells, possibly due to decreased intratumoral expression of IL10 and TGFβ [688]. However, IL6 neutralization did not activate these infiltrating T cells, likely due to a concomitant downregulation of the co-stimulatory CD40 on TAMs. Combination therapy with CD40 agonist and IL6 neutralizing antibodies abrogated the TAM-mediated immunosuppression promoting T cell activation and sensitized the glioblastoma cells to CTLA4/PD1 inhibition. Moreover, triple targeting of IL6, CD40, and CTLA4/PD1 completely eradicated tumor growth *in vivo* in the murine GL261 glioma model [688]. In aggregate, these data suggest that IL6 is a central player in

CD204-enriched glioblastomas correlating with an aggressive and immunosuppressive tumor phenotype. Targeting CD204 and/or IL6, using e.g. neutralizing antibodies, could constitute a future therapeutic strategy to re-educate TAMs into an anti-tumorigenic phenotype, revoke the immunosuppressive TME, and enhance the effect of standard treatment as well as other immunotherapies such as checkpoint inhibition. Several anti-IL6 therapeutics are already used or in the pipeline for treatment of connective tissue disorders and myeloproliferative neoplasms [712] as well as COVID-19 [723].

10.4 The impact of IDH mutation on the immune microenvironment in diffuse glioma

In manuscript III and IV, we found that IDH mutation conferred an immunological quiet TIME in WHO grade III-IV astrocytomas. We chose to explore the influence of IDH mutation in high-grade astrocytomas, as we expected the immune infiltrate would be too low in grade II gliomas, especially in oligodendrogliomas, to reach a statistical significance. This assumption was made based on previous studies [72, 408, 514, 517] and our findings in manuscript I.

In manuscript III, we demonstrated that the levels of complement deposition as well as tumor-infiltrating CD4⁺, CD8⁺ and FOXP3⁺ T cells were significantly lower in IDH-mutant tumors than their IDH-wildtype counterparts. Similar results on tumor-infiltrating T cells have been reported by others [32, 64, 69, 70, 72, 73, 724]. Interestingly, the FOXP3/CD4 ratio tended to be lower in IDH-mutant tumors, but this was not statistically significant, suggesting that the influx of CD4⁺ T cells and Tregs into astrocytomas is relatively balanced. Our *ex vivo* experiments demonstrated that D-2-hydroxyglutarate compromised efficient activation of complement and impaired activation and cytokine production of effector T cells while stimulating proliferation of Tregs. In contrast, D-2-hydroxyglutarate did not significantly impact the function of dendritic cells. These findings indicate that D-2-hydroxyglutarate functions as a selective immune modulator rather than a general cytotoxin. There are some caveats of our study. The concentrations of D-2-hydroxyglutarate used in our *ex vivo* experiment were based on studies that modeled that approximate D-2-hydroxyglutarate levels in the tumor vicinity [69, 170]. However, we do not know the actual extracellular concentration of D-2-hydroxyglutarate that tumor-infiltrating T cells are exposed to *in vivo* in patients. Further, we did not investigate the effect of IDH inhibition on complement, dendritic cells, and T cells *in vivo* using e.g. a murine xenograft model. Even so, our results are supported by the findings in a preclinical study [70]. Using a murine glioma model Kohanbash *et al.* demonstrated that introduction of D-2-hydroxyglutarate, either transgenically or through therapeutic delivery, resulted in diminished STAT1-dependent production of the chemoattractants and IFN γ -inducible genes CXCL9 and CXCL10 leading to reduced CD8⁺ T cell trafficking into the TME. Notably, the reductions in CXCL10 and T cell accumulation were reversed by a specific mutant IDH inhibitor, and this inhibitor augmented the efficacy of vaccine immunotherapy in IDH-mutant gliomas [70]. D-2-hydroxyglutarate is believed to exert its immunosuppressive effect in T cells through paracrine modulation where D-2-hydroxyglutarate is endocytosed by T cells resulting in a HIF1 α -mediated metabolic shift towards oxidative phosphorylation [725] and/or disrupted nuclear factor of activated T cells (NFAT) transcription [73], overall leading to suppressed T cell proliferation and activity.

Reportedly, IDH-mutant glioma cells also resist NK cell-mediated lysis by silencing expression of NK group 2D ligands through D-2-hydroxyglutarate-induced hypermethylation [726]. The resistance could be reversed by hypomethylating therapy with decitabine *in vitro* [726] and *in vivo* inhibiting tumor growth in IDH-mutant xenografts accompanied by an altered immune landscape with increased infiltration of NK cells, dendritic cells, and M1-like macrophages [727]. In manuscript IV, we explored whether IDH status influenced the presence of TAMs. We found that CD204, but not IBA1, expression was reduced in IDH-mutant astrocytomas compared to their IDH-wildtype counterparts, possibly due to a lower frequency of monocyte-derived macrophages relative to microglia [32, 33, 71, 408, 495] and a repressed TIME in mutant tumors [64, 69, 71, 184].

In manuscript IV, we investigated if the checkpoint pathway TIM3/galectin-9 was affected by IDH mutation status, and we observed a decreased expression of TIM3, but not galectin-9, in IDH-mutant tumors. We further detected significantly fewer interactions between TIM3⁺ T cells and galectin-9⁺ TAMs, suggesting that the checkpoint pathway is suppressed in IDH-mutant tumors. However, consistent with other studies [517, 538, 540, 544, 728, 729] very few TIM3⁺ T cells were present in the glioma tissue irrespective of IDH status. Instead, most TIM3⁺ cells were identified as TAMs, as discussed previously. These results indicate that TIM3 checkpoint inhibition might not generate an efficient anti-tumor cytotoxic T cell response in diffuse glioma and especially not in IDH-mutant tumors, even though promising results of dual targeting of PD1 and TIM3 were demonstrated in murine tumor models [566, 571]. Nonetheless, targeting TIM3 may be able to repolarize TAMs into an anti-tumorigenic phenotype as seen with anti-PD1 antibodies [730]. PD1⁺ TAMs are frequently observed during disease progression [731] including in colorectal cancer [732] and recurrent glioblastoma [440] making them a possible amenable target, and PD1 inhibition was shown to induce an M1-like and phagocytic phenotype of TAMs [479, 730, 732]. Cumulatively, these data imply that response to checkpoint inhibition might not only reflect the function or activity of cytotoxic CD8⁺ T cells, and combination treatment involving innate immune cell modulation may need to be prioritized.

Studies have also demonstrated that PD-L1 expression is reduced in IDH-mutant relative to IDH-wildtype gliomas, possibly due to D-2-hydroxyglutarate-mediated epigenetic regulation and suppression [72, 84]. Additionally, in a study by Gao *et al.* immunophenotyping showed that grade II gliomas, which mainly harbored an IDH mutation, had an immunophenogram that was different from glioblastomas and correlated with poorer response to checkpoint blockade [184]. However, oral administration of a mutant IDH inhibitor in combination with R132H peptide vaccination, adoptive T cell transfer, or PD1 blockade had synergistic effects leading to increased overall survival in a syngeneic orthotopic IDH-mutant mouse model [73, 74]. The mutant IDH inhibitor also resulted in IFN γ -related gene expression and increased the frequency of CD4⁺ tumor-infiltrating cells [74]. Overall these results indicate that combining immunotherapy with mutant IDH inhibition could be clinically relevant. Interestingly, a phase 1 clinical trial (NCT03893903) is currently assessing the safety, tolerability, and immunogenicity of an IDH1 R132H vaccine in combination with a PD-L1 inhibitor in patients with resectable IDH1 R132H-mutant recurrent astrocytoma or oligodendrogliomas after standard-of-care treatment [733].

Gliomas and glioblastomas are usually regarded as immunological ‘cold’ tumors based on characterization of the immune landscape and their expected response to checkpoint inhibition [25, 27, 28, 64]. Biomarkers of response to checkpoint blockade include tumor mutational burden, PD-L1 expression, CD8⁺ T cell infiltration, deficient mismatch repair, and microsatellite instability [27]. These biomarkers are often associated with better prognosis [27], but not commonly detected in glioma/glioblastoma except for PD-L1 expression [26, 64, 266, 564, 734, 735]. Further, high mutational/neoantigen burden does not translate to better response to checkpoint inhibition [736] or prognosis [559, 737, 738] in glioblastoma, instead neoantigen quality rather than quantity may be more important [737]. The resistance to immunotherapy in glioma may thus be more complex and result from a combination of a low (or loss of) neoantigen expression [65], a lymphocyte-depleted and immunosuppressive TME, and intratumoral heterogeneity and cellular plasticity [6, 9, 369, 408, 409]. Treatment of brain metastases showcases that targeted therapies [739] and immunotherapies [553, 554] have the potential to reach tumors within the brain, suggesting that the lack of response to checkpoint inhibition in glioblastoma is not solely a result of a tumor residing within the CNS, but also reflects a difference in the immunobiology among the cancer types. Friebel *et al.* [32] and Klemm *et al.* [33] conducted an extensive and comprehensive analysis of the immune landscapes in gliomas and brain metastases using multiparameter fluorescence-activated cell sorting following by CyTOF analyses or RNA sequencing. They showed that microglia dominated the TIME in IDH-mutant gliomas, while monocyte-derived macrophages were enriched in IDH-wildtype glioblastoma and brain metastases. Brain metastases furthermore displayed a substantial infiltration of dysfunctional T cells and neutrophils, while especially IDH-mutant gliomas contained few T cells. Using orthogonal approaches both studies demonstrated that the plasticity of TAMs mostly depended on the adaptability of monocyte-derived macrophages that express various factors involved with immune modulation, inflammation, and extracellular matrix remodeling [32, 33]. Interestingly, TAMs and T cells were closely interacting in brain metastases, but not in glioma [33]. These differences are thus in line with the response to checkpoint inhibition observed in brain metastases from especially melanoma where T cells are plentiful, interact with antigen-presenting cells, and can be reinvigorated by checkpoint inhibitors. These studies highlight that thorough characterization of the TIME is warranted in order to design rational and optimized combination therapies, where scientists and clinicians account for the complexity and plasticity of the TME during tumor evolution. The studies also indicate that the presence of T cells may be vital for efficient response to checkpoint inhibition and that combined treatment with e.g. macrophage-therapy [503, 504, 509, 688] and tumor-specific vaccines [740, 741] is necessary in IDH-wildtype and IDH-mutant gliomas, respectively, to achieve a profound anti-glioma immune response in the clinic.

Overall, our findings in manuscript III and IV suggest that IDH mutation and its oncometabolite D-2-hydroxyglutarate may have immunomodulatory functions and promote an immunoquiescent [64] or even immunological ignorant/tolerant [27] TME in glioma. This seems rather counterintuitive, as IDH mutation confers a survival benefit in patients with glioma. However, the immunoquiescence could be explained by an IDH mutation-induced hypermethylation [172] which silences multiple biological processes involved in tumor aggressiveness, including tissue development, immune response, angiogenesis, and cell proliferation [172,

321, 742]. Taken together, accumulating evidence indicates that IDH mutation may convey a resistance to checkpoint inhibition; yet, thus far no clinical data support this hypothesis.

10.5 Profiling the immune landscape in diffuse glioma

Tumor heterogeneity and the interplay between tumor cells and the TME are important for the prognosis and treatment of cancer. Various approaches are available to profile tumor specimens. However, studies of tissue specimens are associated with hurdles of their own, including limited tissue availability, variation in tissue handling prior to paraffin embedding, spatial heterogeneity of protein/gene expression, and *in situ* detection of complex or rare cellular phenotypes. Methods such as flow cytometry and multiomics including single-cell RNA sequencing allow characterization of expression profiles also of individual cells, but information about the spatial context is lost. In contrast, immunohistochemistry is able to distinguish between different cell types expressing the same protein and can characterize the density, spatial distribution and crosstalk of specific cells within the TME [52, 583]. Typically, an immunohistochemical assay is designed to identify a single protein in a tissue section which is then reviewed by a pathologist using brightfield microscopy. However, newer technologies allow for simultaneous detection of multiple markers/targets in a single tissue section, referred to as multiplex immunohistochemistry or multiplex immunofluorescence. Depending on the approach, between two and up to more than 60 targets can be multiplexed with high precision and accuracy [52, 583, 585]. Chromogenic multiplex immunohistochemistry can be performed by adding multiple labels to the slide simultaneously, sequentially or by using a stain-and-strip approach [52, 583, 586, 587]. In manuscript IV, we analyzed an immune checkpoint pathway using a sequential chromogenic multiplex immunohistochemical approach. We mainly chose this approach based on the equipment and software available at our facility, and we were able to discriminate between three antigens/dyes while preserving tissue integrity. Chromogenic multiplexing holds several advantages over other multiplex technologies; it is easy to use and interpret as well as affordable and accessible at most facilities. Furthermore, the whole slide is imaged without the need for tiling/cropping of ROIs. However, chromogenic multiplexing also poses several drawbacks [52], which existed in our study as well. Digital automated quantification is often not feasible due to the overlap of the chromogenic spectra making assessment of cell-cell interaction almost impossible. Instead, we used a stereological-based approach that was relatively time-consuming, overall limiting the usability of chromogenic multiplexing in clinical pathology. Moreover, co-expression studies using simultaneous or sequential chromogenic stains require careful selection and combination of both antigens of interest and chromogen pairs; thus, the ability to multiplex sequentially beyond three antigens is limited in practice [52, 583]. Instead multiplexed immunohistochemical consecutive staining on single slide (MICSSS) [587] can be used as an alternative method that allows detection of up to 10 markers on a single section by iterative cycles of immunostaining, scanning, removal of enzyme substrate, and blocking previous primary antibody; however, this is laborious process with a risk of tissue damage [52]. Most studies performing multiplexed imaging of the immune landscape in cancer use multiplex immunofluorescence techniques, including standard epifluorescence microscopes and multispectral technologies, which support 4-60-plex assays depending on the approach [52]. In fluorescent multiplexing there is a risk of bleedthrough, and the cellular morphology and tissue context are

often more difficult to evaluate, presenting a disadvantage in fluorescent multiplexing. However, most multispectral imaging software can resolve these issues through conduction of linear unmixing of spectral signals, subtraction of spectral overlap(s) and intrinsic autofluorescence, and alignment of the multispectral images to their corresponding H&E images thereby providing a spatial context [52, 583, 743]. Higher-plex technologies include MIBI-TOF and IMC that entail mass spectrometry imaging of primary antibodies tagged with heavy metal isotopes, which are not found in biological samples. This enables high-resolution imaging at a single-cell level without spectral overlap issues facilitating assessment of cellular interactions as well as spatial composition and heterogeneity [744]. However, these technologies are expensive, limited by the number of available metal isotopes, and require extensive training as well as long imaging times [52]. DSP is a relatively novel technology developed by NanoString. Using DSP, up to 40-50 RNA or protein targets can be quantified in one section of FFPE or fresh frozen tissue specimen by counting targets linked to unique indexing oligonucleotides within fluorescent-labeled and manual or molecular selected ROIs. This method facilitates a high-throughput and affordable spatial protein or transcriptome profiling, but at a lower resolution compared to the mass spectrometry techniques [52, 744].

In manuscript II, we aimed to characterize the myeloid immune landscape of CD204-enriched glioblastoma using the NanoString nCounter technology, which generated a bulk transcriptional profile. The glioblastoma specimens were selected based on their protein expression of IBA1 and CD204, which had been obtained in manuscript I. We validated our findings with immunohistochemistry and also measured the necrotic area in each tumor. Collectively, these aspects provided us cellular and spatial context of the investigated tumors. As discussed previously in the *Background* chapter, the nCounter technology provides highly reproducible data and robust performance at a relatively low cost and with minimal hands-on-time [63, 616, 617], but can only measure up to 800 genes in a single reaction [615, 618]. This technology is therefore advantageous when investigating a specific research/diagnostic question, but is inferior to especially RNA sequencing for biomarker discovery studies. However, neither RNA sequencing nor the nCounter assay provides information on a single-cell level. Numerous single-cell RNA sequencing studies have been published over the last decade often combining single-cell sequencing with spatial transcriptomics or mass spectrometry (e.g. CyTOF) to obtain spatiotemporal and disease-related insights into the regulation and function of the individual cells within diffuse gliomas [6, 9, 13, 32, 35, 41, 264, 408, 409, 434, 461, 500, 671]. These reports have to some extent disentangled the intratumoral heterogeneity and cellular plasticity in glioma as well as the diversity, versatility, and ontogeny of the immune cell within these tumors, but further research is necessary to uncover the progressive and dynamic changes undergone by the TME under tumor evolution.

11. Conclusions and perspectives

A multitude of hypotheses may explain the poor prognosis and treatment resistance observed in patients with glioblastoma. Among these are a failure of drugs to penetrate the BBB, extensive tumor cell invasion into the brain parenchyma, a hypoxic microenvironment, CSCs, intratumoral heterogeneity and cellular plasticity as well as an immunosuppressive and lymphocyte-depleted milieu. Increasing data suggest that both TAMs and mutations in IDH play essential roles in glioma-associated immunosuppression and that TAMs are involved in tumor aggressiveness. The objective of this thesis was to characterize the immune landscape in glioma focusing on TAMs and the impact of IDH mutations on the immune composition.

The results of the thesis suggest that the prognostic and biological values of TAMs in gliomas do not depend on the total amount of TAMs, but rather on their acquired phenotype. High levels of the M2-related marker CD204 conferred shorter survival in patients with WHO grade III and IV gliomas independently of clinico-pathological parameters. CD204⁺ TAMs correlated with a more resilient tumor phenotype and expressed proteins associated with tumor aggressiveness. TAMs and especially CD204⁺ TAMs accumulated in perivascular and hypoxic niches interacting with especially podoplanin⁺ glioblastoma stem-like cells. Immunofluorescent and transcriptome profiling demonstrated that CD204⁺ TAMs and CD204-enriched glioblastoma expressed markers related to the entire M0-M2 spectrum of macrophage/microglial polarization underlining that TAMs are a diverse cell population within glioblastomas. Pathway and connectivity analyses revealed that CD204-enriched glioblastomas had an inflamed and tumor-promoting phenotype expressing high levels of especially IL6. Interrogating the influence of IDH mutation on the TME showed that mutant IDH and its oncometabolite D-2-hydroxyglutarate may have an immunomodulatory function. Compared to their IDH-wildtype counterparts, IDH-mutant tumors had reduced complement deposition and activity, lower frequency of tumor-infiltrating T cells and CD204⁺ TAMs as well as diminished TIM3 expression and fewer receptor-ligand interactions between TIM3⁺ T cells and galectin-9⁺ TAMs, overall supporting the notion that IDH-mutant tumors are immunological dormant and poor responders to checkpoint inhibition. Collectively, the findings of the thesis indicate that a novel therapeutic approach in glioblastoma could be reprogramming of TAMs into a tumoricidal phenotype by inhibiting CD204 and/or IL6 using e.g. neutralizing antibodies. Further, combining immunotherapy with inhibition of mutant IDH or an IDH1 R123H vaccine could have beneficial therapeutic value in patients with IDH-mutant tumors as a means to revoke the immunosuppressive TME. However, additional experimental analyses are necessary to strengthen these results.

Uncovering the complexity of the microenvironment that exists and evolves in gliomas is vital to identify potential vulnerabilities that might treat and cure these diseases. Single-cell technologies, spatial multiomics, and integrative analyses of gene and protein expression in combination with functional studies provide the opportunity to profile the nature, plasticity, and evolution of the cells within the TME. Studying the many ways immune cells, especially TAMs, interact with tumor cells is an active area of research. Understanding this crosstalk and the immune landscape can inform development of therapeutic strategies that generate durable anti-tumor immune responses and guide clinical decision making to treat gliomas as well as other cancer types with possibly different immune-targeting approaches.

“Cells are residents of a vast ‘landscape’ of possible states
over which they travel during development and in disease.”

A metaphor for cellular plasticity, described by Conrad H. Waddington, *The Strategy of the Genes*, 1957.

12. References

- 1 Ostrom QT, Price M, Neff C, et al. CBTRUS Statistical Report: Primary Brain and Other Central Nervous System Tumors Diagnosed in the United States in 2015-2019. *Neuro Oncol* 2022; 24: v1-v95
- 2 WHO Classification of Tumours Editorial Board. Central nervous system tumours. Fifth edition. International Agency for Research on Cancer (IARC), Lyon (France). 2021.
- 3 Cioffi G, Waite KA, Edelson JL, et al. Changes in survival over time for primary brain and other CNS tumors in the United States, 2004-2017. *J Neurooncol* 2022; 160: 209-19
- 4 Marenco-Hillebrand L, Wijesekera O, Suarez-Meade P, et al. Trends in glioblastoma: outcomes over time and type of intervention: a systematic evidence based analysis. *Journal of Neuro-Oncology* 2020; 147: 297-307
- 5 Stupp R, Mason WP, van den Bent MJ, et al. Radiotherapy plus concomitant and adjuvant temozolomide for glioblastoma. *The New England journal of medicine* 2005; 352: 987-96
- 6 Patel AP, Tirosh I, Trombetta JJ, et al. Single-cell RNA-seq highlights intratumoral heterogeneity in primary glioblastoma. *Science (New York, NY)* 2014; 344: 1396-401
- 7 Sottoriva A, Spiteri I, Piccirillo SGM, et al. Intratumor heterogeneity in human glioblastoma reflects cancer evolutionary dynamics. *Proceedings of the National Academy of Sciences* 2013; 110: 4009-14
- 8 Gill BJ, Pisapia DJ, Malone HR, et al. MRI-localized biopsies reveal subtype-specific differences in molecular and cellular composition at the margins of glioblastoma. *Proceedings of the National Academy of Sciences of the United States of America* 2014; 111: 12550-5
- 9 Neftel C, Laffy J, Filbin MG, et al. An Integrative Model of Cellular States, Plasticity, and Genetics for Glioblastoma. *Cell* 2019; 178: 835-49 e21
- 10 Phillips HS, Kharbanda S, Chen R, et al. Molecular subclasses of high-grade glioma predict prognosis, delineate a pattern of disease progression, and resemble stages in neurogenesis. *Cancer cell* 2006; 9: 157-73
- 11 Verhaak RGW, Hoadley KA, Purdom E, et al. An integrated genomic analysis identifies clinically relevant subtypes of glioblastoma characterized by abnormalities in PDGFRA, IDH1, EGFR and NF1. *Cancer cell* 2010; 17: 98
- 12 Brennan CW, Verhaak RG, McKenna A, et al. The somatic genomic landscape of glioblastoma. *Cell* 2013; 155: 462-77
- 13 Darmanis S, Sloan SA, Croote D, et al. Single-Cell RNA-Seq Analysis of Infiltrating Neoplastic Cells at the Migrating Front of Human Glioblastoma. *Cell Reports* 2017; 21: 1399-410
- 14 Broekman ML, Maas SLN, Abels ER, et al. Multidimensional communication in the microenvirons of glioblastoma. *Nat Rev Neurol* 2018; 14: 482-95
- 15 Alexandru O, Horescu C, Sevastre A-S, et al. Receptor tyrosine kinase targeting in glioblastoma: performance, limitations and future approaches. *Contemp Oncol (Pozn)* 2020; 24: 55-66
- 16 Lombardi G, Pambuku A, Bellu L, et al. Effectiveness of antiangiogenic drugs in glioblastoma patients: A systematic review and meta-analysis of randomized clinical trials. *Critical reviews in oncology/hematology* 2017; 111: 94-102
- 17 Bhat KP, Balasubramaniyan V, Vaillant B, et al. Mesenchymal differentiation mediated by NF-kappaB promotes radiation resistance in glioblastoma. *Cancer cell* 2013; 24: 331-46
- 18 Hunter C, Smith R, Cahill DP, et al. A hypermutation phenotype and somatic MSH6 mutations in recurrent human malignant gliomas after alkylator chemotherapy. *Cancer research* 2006; 66: 3987-91
- 19 Sarkaria JN, Kitange GJ, James CD, et al. Mechanisms of chemoresistance to alkylating agents in malignant glioma. *Clinical cancer research : an official journal of the American Association for Cancer Research* 2008; 14: 2900-8
- 20 Piao Y, Liang J, Holmes L, et al. Glioblastoma resistance to anti-VEGF therapy is associated with myeloid cell infiltration, stem cell accumulation, and a mesenchymal phenotype. *Neuro-oncology* 2012; 14: 1379-92
- 21 Galon J, Bruni D. Tumor Immunology and Tumor Evolution: Intertwined Histories. *Immunity* 2020; 52: 55-81
- 22 Lim M, Xia Y, Bettgeowda C, et al. Current state of immunotherapy for glioblastoma. *Nat Rev Clin Oncol* 2018; 15: 422-42
- 23 Andersen BM, Reardon DA. Immunotherapy approaches for adult glioma: knowledge gained from recent clinical trials. *Current Opinion in Neurology* 2022; 35: 803-13
- 24 Welty NE, Gill SI. Cancer Immunotherapy Beyond Checkpoint Blockade: JACC: CardioOncology State-of-the-Art Review. *JACC CardioOncol* 2022; 4: 563-78
- 25 Binnewies M, Roberts EW, Kersten K, et al. Understanding the tumor immune microenvironment (TIME) for effective therapy. *Nature Medicine* 2018; 24: 541-50
- 26 Hodges TR, Ott M, Xiu J, et al. Mutational burden, immune checkpoint expression, and mismatch repair in glioma: implications for immune checkpoint immunotherapy. *Neuro Oncol* 2017; 19: 1047-57
- 27 Smyth MJ, Ngiew SF, Ribas A, et al. Combination cancer immunotherapies tailored to the tumour microenvironment. *Nat Rev Clin Oncol* 2016; 13: 143-58

References

- 28 Jackson CM, Choi J, Lim M. Mechanisms of immunotherapy resistance: lessons from glioblastoma. *Nature Immunology* 2019; 20: 1100-9
- 29 Morimura T, Neuchrist C, Kitz K, et al. Monocyte subpopulations in human gliomas: expression of Fc and complement receptors and correlation with tumor proliferation. *Acta Neuropathol* 1990; 80: 287-94
- 30 Hambardzumyan D, Gutmann DH, Kettenmann H. The role of microglia and macrophages in glioma maintenance and progression. *Nat Neurosci* 2016; 19: 20-7
- 31 Li W, Graeber MB. The molecular profile of microglia under the influence of glioma. *Neuro Oncol* 2012; 14: 958-78
- 32 Friebel E, Kapolou K, Unger S, et al. Single-Cell Mapping of Human Brain Cancer Reveals Tumor-Specific Instruction of Tissue-Invasive Leukocytes. *Cell* 2020; 181: 1626-42.e20
- 33 Klemm F, Maas RR, Bowman RL, et al. Interrogation of the Microenvironmental Landscape in Brain Tumors Reveals Disease-Specific Alterations of Immune Cells. *Cell* 2020; 181: 1643-60 e17
- 34 González-Tablas Pimenta M, Otero Á, Arandia Guzman DA, et al. Tumor cell and immune cell profiles in primary human glioblastoma: Impact on patient outcome. *Brain Pathol* 2021; 31: 365-80
- 35 Yeo AT, Rawal S, Delcuze B, et al. Single-cell RNA sequencing reveals evolution of immune landscape during glioblastoma progression. *Nat Immunol* 2022; 23: 971-84
- 36 Hattermann K, Sebens S, Helm O, et al. Chemokine expression profile of freshly isolated human glioblastoma-associated macrophages/microglia. *Oncol Rep* 2014; 32: 270-6
- 37 Zeiner PS, Preusse C, Golebiewska A, et al. Distribution and prognostic impact of microglia/macrophage subpopulations in gliomas. *Brain Pathol* 2019; 29: 513-29
- 38 Szulzewsky F, Pelz A, Feng X, et al. Glioma-associated microglia/macrophages display an expression profile different from M1 and M2 polarization and highly express Gpnmb and Spp1. *PLoS One* 2015; 10: e0116644
- 39 Gabrusiewicz K, Rodriguez B, Wei J, et al. Glioblastoma-infiltrated innate immune cells resemble M0 macrophage phenotype. *JCI Insight* 2016; 1:
- 40 Mantovani A, Sica A, Sozzani S, et al. The chemokine system in diverse forms of macrophage activation and polarization. *Trends Immunol* 2004; 25: 677-86
- 41 Muller S, Kohanbash G, Liu SJ, et al. Single-cell profiling of human gliomas reveals macrophage ontogeny as a basis for regional differences in macrophage activation in the tumor microenvironment. *Genome Biol* 2017; 18: 234
- 42 Bowman RL, Klemm F, Akkari L, et al. Macrophage Ontogeny Underlies Differences in Tumor-Specific Education in Brain Malignancies. *Cell Rep* 2016; 17: 2445-59
- 43 Komohara Y, Ohnishi K, Kuratsu J, et al. Possible involvement of the M2 anti-inflammatory macrophage phenotype in growth of human gliomas. *J Pathol* 2008; 216: 15-24
- 44 Deininger MH, Seid K, Engel S, et al. Allograft inflammatory factor-1 defines a distinct subset of infiltrating macrophages/microglial cells in rat and human gliomas. *Acta Neuropathol* 2000; 100: 673-80
- 45 Yi L, Xiao H, Xu M, et al. Glioma-initiating cells: a predominant role in microglia/macrophages tropism to glioma. *J Neuroimmunol* 2011; 232: 75-82
- 46 Komohara Y, Horlad H, Ohnishi K, et al. Importance of direct macrophage-tumor cell interaction on progression of human glioma. *Cancer Sci* 2012; 103: 2165-72
- 47 Prośniak M, Harshyne LA, Andrews DW, et al. Glioma grade is associated with the accumulation and activity of cells bearing m2 monocyte markers. *Clin Cancer Res* 2013; 19: 3776-86
- 48 Yuan Y, Zhao Q, Zhao S, et al. Characterization of transcriptome profile and clinical features of a novel immunotherapy target CD204 in diffuse glioma. *Cancer Med* 2019; 8: 3811-21
- 49 Liu S, Zhang C, Maimela NR, et al. Molecular and clinical characterization of CD163 expression via large-scale analysis in glioma. *Oncoimmunology* 2019; 8: 1601478
- 50 Idoate Gastearena MA, Lopez-Janeiro A, Lecumberri Aznarez A, et al. A Quantitative Digital Analysis of Tissue Immune Components Reveals an Immunosuppressive and Anergic Immune Response with Relevant Prognostic Significance in Glioblastoma. *Biomedicines* 2022; 10:
- 51 Camp RL, Chung GG, Rimm DL. Automated subcellular localization and quantification of protein expression in tissue microarrays. *Nat Med* 2002; 8: 1323-7
- 52 Taube JM, Akturk G, Angelo M, et al. The Society for Immunotherapy of Cancer statement on best practices for multiplex immunohistochemistry (IHC) and immunofluorescence (IF) staining and validation. *J Immunother Cancer* 2020; 8:
- 53 Ito D, Imai Y, Ohsawa K, et al. Microglia-specific localisation of a novel calcium binding protein, Iba1. *Brain Res Mol Brain Res* 1998; 57: 1-9
- 54 Imai Y, Ibata I, Ito D, et al. A novel gene iba1 in the major histocompatibility complex class III region encoding an EF hand protein expressed in a monocytic lineage. *Biochem Biophys Res Commun* 1996; 224: 855-62
- 55 Karsy M, Gelbman M, Shah P, et al. Established and emerging variants of glioblastoma multiforme: review of morphological and molecular features. *Folia Neuropathol* 2012; 50: 301-21

References

- 56 Jung TY, Jung S, Moon JH, et al. Early prognostic factors related to progression and malignant transformation of low-grade gliomas. *Clin Neurol Neurosurg* 2011; 113: 752-7
- 57 Babu R, Bagley JH, Park JG, et al. Low-grade astrocytomas: the prognostic value of fibrillary, gemistocytic, and protoplasmic tumor histology. *J Neurosurg* 2013; 119: 434-41
- 58 Watanabe K, Tachibana O, Yonekawa Y, et al. Role of gemistocytes in astrocytoma progression. *Lab Invest* 1997; 76: 277-84
- 59 Aderetti DA, Hira VVV, Molenaar RJ, et al. The hypoxic peri-arteriolar glioma stem cell niche, an integrated concept of five types of niches in human glioblastoma. *Biochim Biophys Acta Rev Cancer* 2018; 1869: 346-54
- 60 Calabrese C, Poppleton H, Kocak M, et al. A Perivascular Niche for Brain Tumor Stem Cells. *Cancer Cell* 2007; 11: 69-82
- 61 Hira VV, Ploegmakers KJ, Grevers F, et al. CD133+ and Nestin+ Glioma Stem-Like Cells Reside Around CD31+ Arterioles in Niches that Express SDF-1alpha, CXCR4, Osteopontin and Cathepsin K. *J Histochem Cytochem* 2015; 63: 481-93
- 62 Heddleston JM, Li Z, McLendon RE, et al. The hypoxic microenvironment maintains glioblastoma stem cells and promotes reprogramming towards a cancer stem cell phenotype. *Cell Cycle* 2009; 8: 3274-84
- 63 Geiss GK, Bumgarner RE, Birditt B, et al. Direct multiplexed measurement of gene expression with color-coded probe pairs. *Nat Biotechnol* 2008; 26: 317-25
- 64 Thorsson V, Gibbs DL, Brown SD, et al. The Immune Landscape of Cancer. *Immunity* 2018; 48: 812-30.e14
- 65 Nejo T, Matsushita H, Karasaki T, et al. Reduced Neoantigen Expression Revealed by Longitudinal Multiomics as a Possible Immune Evasion Mechanism in Glioma. *Cancer Immunol Res* 2019; 7: 1148-61
- 66 Sampson JH, Gunn MD, Fecci PE, et al. Brain immunology and immunotherapy in brain tumours. *Nat Rev Cancer* 2020; 20: 12-25
- 67 Cairns RA, Mak TW. Oncogenic isocitrate dehydrogenase mutations: mechanisms, models, and clinical opportunities. *Cancer Discov* 2013; 3: 730-41
- 68 Waitkus MS, Diplas BH, Yan H. Isocitrate dehydrogenase mutations in gliomas. *Neuro-oncology* 2016; 18: 16-26
- 69 Amankulor NM, Kim Y, Arora S, et al. Mutant IDH1 regulates the tumor-associated immune system in gliomas. *Genes Dev* 2017; 31: 774-86
- 70 Kohanbash G, Carrera DA, Shrivastav S, et al. Isocitrate dehydrogenase mutations suppress STAT1 and CD8+ T cell accumulation in gliomas. *The Journal of clinical investigation* 2017; 127: 1425-37
- 71 Poon CC, Gordon PMK, Liu K, et al. Differential microglia and macrophage profiles in human IDH-mutant and -wild type glioblastoma. *Oncotarget* 2019; 10: 3129-43
- 72 Berghoff AS, Kiesel B, Widhalm G, et al. Correlation of immune phenotype with IDH mutation in diffuse glioma. *Neuro Oncol* 2017; 19: 1460-8
- 73 Bunse L, Pusch S, Bunse T, et al. Suppression of antitumor T cell immunity by the oncometabolite (R)-2-hydroxyglutarate. *Nat Med* 2018; 24: 1192-203
- 74 Chuntova P, Yamamichi A, Chen T, et al. Inhibition of D-2HG leads to upregulation of a proinflammatory gene signature in a novel HLA-A2/HLA-DR1 transgenic mouse model of IDH1R132H-expressing glioma. *J Immunother Cancer* 2022; 10:
- 75 Ricklin D, Hajishengallis G, Yang K, et al. Complement: a key system for immune surveillance and homeostasis. *Nat Immunol* 2010; 11: 785-97
- 76 Chaplin DD. Overview of the immune response. *J Allergy Clin Immunol* 2010; 125: S3-23
- 77 Chen L, Flies DB. Molecular mechanisms of T cell co-stimulation and co-inhibition. *Nat Rev Immunol* 2013; 13: 227-42
- 78 Baumeister SH, Freeman GJ, Dranoff G, et al. Coinhibitory Pathways in Immunotherapy for Cancer. *Annu Rev Immunol* 2016; 34: 539-73
- 79 Lim M, Weller M, Idbaih A, et al. Phase III trial of chemoradiotherapy with temozolomide plus nivolumab or placebo for newly diagnosed glioblastoma with methylated MGMT promoter. *Neuro Oncol* 2022; 24: 1935-49
- 80 Omuro A, Brandes AA, Carpentier AF, et al. Radiotherapy combined with nivolumab or temozolomide for newly diagnosed glioblastoma with unmethylated MGMT promoter: An international randomized phase III trial. *Neuro Oncol* 2023; 25: 123-34
- 81 Du W, Yang M, Turner A, et al. TIM-3 as a Target for Cancer Immunotherapy and Mechanisms of Action. *Int J Mol Sci* 2017; 18: 645
- 82 Li X, Wang B, Gu L, et al. Tim-3 expression predicts the abnormal innate immune status and poor prognosis of glioma patients. *Clin Chim Acta* 2018; 476: 178-84
- 83 Li G, Wang Z, Zhang C, et al. Molecular and clinical characterization of TIM-3 in glioma through 1,024 samples. *Oncoimmunology* 2017; 6: e1328339

References

- 84 Mu L, Long Y, Yang C, et al. The IDH1 Mutation-Induced Oncometabolite, 2-Hydroxyglutarate, May Affect DNA Methylation and Expression of PD-L1 in Gliomas. *Front Mol Neurosci* 2018; 11: 82
- 85 Wang H, Xiao Y, Ren X, et al. Prognostic value of programmed death ligand 1 (PD-L1) in glioblastoma: a systematic review, meta-analysis and validation based on dataset. *Bioengineered* 2021; 12: 10366-78
- 86 Wang Z, Zhang C, Liu X, et al. Molecular and clinical characterization of PD-L1 expression at transcriptional level via 976 samples of brain glioma. *Oncoimmunology* 2016; 5: e1196310
- 87 Liu C, Zhang Z, Ping Y, et al. Comprehensive Analysis of PD-1 Gene Expression, Immune Characteristics and Prognostic Significance in 1396 Glioma Patients. *Cancer Manag Res* 2020; 12: 4399-410
- 88 Liu F, Huang J, Liu X, et al. CTLA-4 correlates with immune and clinical characteristics of glioma. *Cancer Cell Int* 2020; 20: 7
- 89 Dansk Neuro-Onkologisk Gruppe. Kliniske retningslinjer: Gliomer hos voksne, version 3. DNOG 2022:
- 90 Ostrom QT, Cioffi G, Gittleman H, et al. CBTRUS Statistical Report: Primary Brain and Other Central Nervous System Tumors Diagnosed in the United States in 2012-2016. *Neuro-oncology* 2019; 21: v1-v100
- 91 Louis DN, Ohgaki H, Wiestler OD, et al. WHO classification of tumours of the central nervous system, Revised, 4th edition. International Agency for Research on Cancer (IARC), Lyon. 2016:
- 92 Gavrilovic IT, Posner JB. Brain metastases: epidemiology and pathophysiology. *Journal of neuro-oncology* 2005; 75: 5-14
- 93 Eichler AF, Loeffler JS. Multidisciplinary management of brain metastases. *Oncologist* 2007; 12: 884-98
- 94 Valiente M, Ahluwalia MS, Boire A, et al. The Evolving Landscape of Brain Metastasis. *Trends Cancer* 2018; 4: 176-96
- 95 Ostrom QT, Wright CH, Barnholtz-Sloan JS. Chapter 2 - Brain metastases: epidemiology. In *Handbook of clinical neurology* Eds. D Schiff, MJ van den Bent: Elsevier. 2018: 27-42
- 96 Stupp R, Hegi ME, Mason WP, et al. Effects of radiotherapy with concomitant and adjuvant temozolomide versus radiotherapy alone on survival in glioblastoma in a randomised phase III study: 5-year analysis of the EORTC-NCIC trial. *The lancet oncology* 2009; 10: 459-66
- 97 Walsh KM, Ohgaki H, Wrensch MR. Epidemiology. *Handbook of clinical neurology* 2016; 134: 3-18
- 98 Bondy ML, Scheurer ME, Malmer B, et al. Brain tumor epidemiology: consensus from the Brain Tumor Epidemiology Consortium. *Cancer* 2008; 113: 1953-68
- 99 Dong M, Cioffi G, Wang J, et al. Sex Differences in Cancer Incidence and Survival: A Pan-Cancer Analysis. *Cancer epidemiology, biomarkers & prevention : a publication of the American Association for Cancer Research, cosponsored by the American Society of Preventive Oncology* 2020; 29: 1389-97
- 100 Ostrom QT, Rubin JB, Lathia JD, et al. Females have the survival advantage in glioblastoma. *Neuro-oncology* 2018; 20: 576-7
- 101 Gittleman H, Ostrom QT, Stetson LC, et al. Sex is an important prognostic factor for glioblastoma but not for nonglioblastoma. *Neuro-oncology practice* 2019; 6: 451-62
- 102 Orrego E, Castaneda CA, Castillo M, et al. Distribution of tumor-infiltrating immune cells in glioblastoma. *CNS Oncol* 2018; 7: CNS21
- 103 Bayik D, Zhou Y, Park C, et al. Myeloid-Derived Suppressor Cell Subsets Drive Glioblastoma Growth in a Sex-Specific Manner. *Cancer Discov* 2020; 10: 1210-25
- 104 Shireman JM, Ammanuel S, Eickhoff JC, et al. Sexual dimorphism of the immune system predicts clinical outcomes in glioblastoma immunotherapy: A systematic review and meta-analysis. *Neurooncol Adv* 2022; 4: vda082
- 105 Molinaro AM, Taylor JW, Wiencke JK, et al. Genetic and molecular epidemiology of adult diffuse glioma. *Nature reviews Neurology* 2019; 15: 405-17
- 106 Bainbridge MN, Armstrong GN, Gramatges MM, et al. Germline mutations in shelterin complex genes are associated with familial glioma. *Journal of the National Cancer Institute* 2015; 107: 384
- 107 Bell DW, Varley JM, Szydlo TE, et al. Heterozygous germ line hCHK2 mutations in Li-Fraumeni syndrome. *Science (New York, NY)* 1999; 286: 2528-31
- 108 Andrade RC, Dos Santos AC, de Aguirre Neto JC, et al. TP53 and CDKN1A mutation analysis in families with Li-Fraumeni and Li-Fraumeni like syndromes. *Fam Cancer* 2017; 16: 243-8
- 109 Bruce-Brand C, Govender D. Gene of the month: IDH1. *J Clin Pathol* 2020; 73: 611-5
- 110 Bongaarts A, van Scheppingen J, Korotkov A, et al. The coding and non-coding transcriptional landscape of subependymal giant cell astrocytomas. *Brain : a journal of neurology* 2020; 143: 131-49
- 111 Lobbous M, Bernstock JD, Coffee E, et al. An Update on Neurofibromatosis Type 1-Associated Gliomas. *Cancers (Basel)* 2020; 12: 114
- 112 Reuss D, von Deimling A. Hereditary tumor syndromes and gliomas. Recent results in cancer research *Fortschritte der Krebsforschung Progres dans les recherches sur le cancer* 2009; 171: 83-102
- 113 Rice T, Lachance DH, Molinaro AM, et al. Understanding inherited genetic risk of adult glioma - a review. *Neuro-oncology practice* 2016; 3: 10-6

References

- 114 Ostrom QT, Adel Fahmideh M, Cote DJ, et al. Risk factors for childhood and adult primary brain tumors. *Neuro-oncology* 2019; 21: 1357-75
- 115 Ostrom QT, Gittleman H, Stetson L, et al. Epidemiology of Intracranial Gliomas. *Prog Neurol Surg* 2018; 30: 1-11
- 116 Shete S, Hosking FJ, Robertson LB, et al. Genome-wide association study identifies five susceptibility loci for glioma. *Nat Genet* 2009; 41: 899-904
- 117 Atkins I, Kinnersley B, Ostrom QT, et al. Transcriptome-Wide Association Study Identifies New Candidate Susceptibility Genes for Glioma. *Cancer research* 2019; 79: 2065-71
- 118 Labreche K, Kinnersley B, Berzero G, et al. Diffuse gliomas classified by 1p/19q co-deletion, TERT promoter and IDH mutation status are associated with specific genetic risk loci. *Acta neuropathologica* 2018; 135: 743-55
- 119 Melin BS, Barnholtz-Sloan JS, Wrensch MR, et al. Genome-wide association study of glioma subtypes identifies specific differences in genetic susceptibility to glioblastoma and non-glioblastoma tumors. *Nature genetics* 2017; 49: 789-94
- 120 Eckel-Passow JE, Drucker KL, Kollmeyer TM, et al. Adult diffuse glioma GWAS by molecular subtype identifies variants in D2HGDH and FAM20C. *Neuro Oncol* 2020; 22: 1602-13
- 121 Disney-Hogg L, Cornish AJ, Sud A, et al. Impact of atopy on risk of glioma: a Mendelian randomisation study. *BMC Med* 2018; 16: 42
- 122 Amirian ES, Ostrom QT, Armstrong GN, et al. Aspirin, NSAIDs, and Glioma Risk: Original Data from the Glioma International Case-Control Study and a Meta-analysis. *Cancer epidemiology, biomarkers & prevention : a publication of the American Association for Cancer Research, cosponsored by the American Society of Preventive Oncology* 2019; 28: 555-62
- 123 Cote DJ, Rosner BA, Smith-Warner SA, et al. Statin use, hyperlipidemia, and risk of glioma. *Eur J Epidemiol* 2019; 34: 997-1011
- 124 Gaist D, Hallas J, Friis S, et al. Statin use and survival following glioblastoma multiforme. *Cancer Epidemiol* 2014; 38: 722-7
- 125 Andersen L, Friis S, Hallas J, et al. Hormonal contraceptive use and risk of glioma among younger women: a nationwide case-control study. *British journal of clinical pharmacology* 2015; 79: 677-84
- 126 Zong H, Xu H, Geng Z, et al. Reproductive factors in relation to risk of brain tumors in women: an updated meta-analysis of 27 independent studies. *Tumour biology : the journal of the International Society for Oncodevelopmental Biology and Medicine* 2014; 35: 11579-86
- 127 Wrensch M, Fisher JL, Schwartzbaum JA, et al. The molecular epidemiology of gliomas in adults. *Neurosurg Focus* 2005; 19: E5
- 128 Schwartzbaum JA, Fisher JL, Aldape KD, et al. Epidemiology and molecular pathology of glioma. *Nat Clin Pract Neurol* 2006; 2: 494-503; quiz 1 p following 16
- 129 Louis DN, Ohgaki H, Wiestler OD, et al. WHO classification of tumours of the central nervous system 2007, 4th edition. International Agency for Research on Cancer (IARC), Lyon. 2007
- 130 Masui K, Mischel PS, Reifenberger G. Molecular classification of gliomas. *Handbook of clinical neurology* 2016; 134: 97-120
- 131 Ellison DW, Kocak M, Figarella-Branger D, et al. Histopathological grading of pediatric ependymoma: reproducibility and clinical relevance in European trial cohorts. *Journal of Negative Results in BioMedicine* 2011; 10: 7
- 132 Kristensen BW, Priesterbach-Ackley LP, Petersen JK, et al. Molecular pathology of tumors of the central nervous system. *Ann Oncol* 2019; 30: 1265-78
- 133 Bailey P. Further remarks concerning tumors of the glioma group. *Bull Johns Hopkins Hosp* 1927; 40: 354-89
- 134 Ringertz N. Grading of gliomas. *Acta Pathol Microbiol Scand* 1950; 27: 51-64
- 135 Daumas-Duport C, Scheithauer B, O'Fallon J, et al. Grading of astrocytomas. A simple and reproducible method. *Cancer* 1988; 62: 2152-65
- 136 Gonzales MF. Grading of gliomas. *Journal of clinical neuroscience : official journal of the Neurosurgical Society of Australasia* 1997; 4: 16-8
- 137 van den Bent MJ. Interobserver variation of the histopathological diagnosis in clinical trials on glioma: a clinician's perspective. *Acta Neuropathol* 2010; 120: 297-304
- 138 Jenkins RB, Blair H, Ballman KV, et al. A t(1;19)(q10;p10) mediates the combined deletions of 1p and 19q and predicts a better prognosis of patients with oligodendroglioma. *Cancer research* 2006; 66: 9852-61
- 139 Wiestler B, Capper D, Holland-Letz T, et al. ATRX loss refines the classification of anaplastic gliomas and identifies a subgroup of IDH mutant astrocytic tumors with better prognosis. *Acta neuropathologica* 2013; 126: 443-51
- 140 Reuss DE, Sahn F, Schrimpf D, et al. ATRX and IDH1-R132H immunohistochemistry with subsequent copy number analysis and IDH sequencing as a basis for an "integrated" diagnostic approach for adult astrocytoma, oligodendroglioma and glioblastoma. *Acta neuropathologica* 2015; 129: 133-46

References

- 141 Parsons DW, Jones S, Zhang X, et al. An integrated genomic analysis of human glioblastoma multiforme. *Science* (New York, NY) 2008; 321: 1807-12
- 142 Brat DJ, Verhaak RG, Aldape KD, et al. Comprehensive, Integrative Genomic Analysis of Diffuse Lower-Grade Gliomas. *The New England journal of medicine* 2015; 372: 2481-98
- 143 Eckel-Passow JE, Lachance DH, Molinaro AM, et al. Glioma Groups Based on 1p/19q, IDH, and TERT Promoter Mutations in Tumors. *The New England journal of medicine* 2015; 372: 2499-508
- 144 Hartmann C, Meyer J, Balss J, et al. Type and frequency of IDH1 and IDH2 mutations are related to astrocytic and oligodendroglial differentiation and age: a study of 1,010 diffuse gliomas. *Acta neuropathologica* 2009; 118: 469-74
- 145 Hartmann C, Hentschel B, Wick W, et al. Patients with IDH1 wild type anaplastic astrocytomas exhibit worse prognosis than IDH1-mutated glioblastomas, and IDH1 mutation status accounts for the unfavorable prognostic effect of higher age: implications for classification of gliomas. *Acta neuropathologica* 2010; 120: 707-18
- 146 Watanabe T, Nobusawa S, Kleihues P, et al. IDH1 mutations are early events in the development of astrocytomas and oligodendrogliomas. *The American journal of pathology* 2009; 174: 1149-53
- 147 The Cancer Genome Atlas Research Network. Comprehensive genomic characterization defines human glioblastoma genes and core pathways. *Nature* 2008; 455: 1061-8
- 148 Reifenberger J, Reifenberger G, Liu L, et al. Molecular genetic analysis of oligodendroglial tumors shows preferential allelic deletions on 19q and 1p. *Am J Pathol* 1994; 145: 1175-90
- 149 Sahm F, Reuss D, Koelsche C, et al. Farewell to oligoastrocytoma: in situ molecular genetics favor classification as either oligodendroglioma or astrocytoma. *Acta neuropathologica* 2014; 128: 551-9
- 150 Liu XY, Gerges N, Korshunov A, et al. Frequent ATRX mutations and loss of expression in adult diffuse astrocytic tumors carrying IDH1/IDH2 and TP53 mutations. *Acta neuropathologica* 2012; 124: 615-25
- 151 Killela PJ, Reitman ZJ, Jiao Y, et al. TERT promoter mutations occur frequently in gliomas and a subset of tumors derived from cells with low rates of self-renewal. *Proceedings of the National Academy of Sciences of the United States of America* 2013; 110: 6021-6
- 152 Jiao Y, Killela PJ, Reitman ZJ, et al. Frequent ATRX, CIC, FUBP1 and IDH1 mutations refine the classification of malignant gliomas. *Oncotarget* 2012; 3: 709-22
- 153 Yip S, Butterfield YS, Morozova O, et al. Concurrent CIC mutations, IDH mutations, and 1p/19q loss distinguish oligodendrogliomas from other cancers. *The Journal of pathology* 2012; 226: 7-16
- 154 Cahill DP, Louis DN, Cairncross JG. Molecular background of oligodendroglioma: 1p/19q, IDH, TERT, CIC and FUBP1. *CNS oncology* 2015; 4: 287-94
- 155 Ichimura K, Pearson DM, Kocialkowski S, et al. IDH1 mutations are present in the majority of common adult gliomas but rare in primary glioblastomas. *Neuro-oncology* 2009; 11: 341-7
- 156 Balss J, Meyer J, Mueller W, et al. Analysis of the IDH1 codon 132 mutation in brain tumors. *Acta neuropathologica* 2008; 116: 597-602
- 157 Yan H, Parsons DW, Jin G, et al. IDH1 and IDH2 mutations in gliomas. *The New England journal of medicine* 2009; 360: 765-73
- 158 Schwartzenuber J, Korshunov A, Liu XY, et al. Driver mutations in histone H3.3 and chromatin remodelling genes in paediatric glioblastoma. *Nature* 2012; 482: 226-31
- 159 Heaphy CM, de Wilde RF, Jiao Y, et al. Altered telomeres in tumors with ATRX and DAXX mutations. *Science* (New York, NY) 2011; 333: 425
- 160 Hegi ME, Diserens AC, Godard S, et al. Clinical trial substantiates the predictive value of O-6-methylguanine-DNA methyltransferase promoter methylation in glioblastoma patients treated with temozolomide. *Clinical cancer research : an official journal of the American Association for Cancer Research* 2004; 10: 1871-4
- 161 Korshunov A, Casalini B, Chavez L, et al. Integrated molecular characterization of IDH-mutant glioblastomas. *Neuropathology and applied neurobiology* 2019; 45: 108-18
- 162 Geisenberger C, Mock A, Warta R, et al. Molecular profiling of long-term survivors identifies a subgroup of glioblastoma characterized by chromosome 19/20 co-gain. *Acta Neuropathol* 2015; 130: 419-34
- 163 Stichel D, Ebrahimi A, Reuss D, et al. Distribution of EGFR amplification, combined chromosome 7 gain and chromosome 10 loss, and TERT promoter mutation in brain tumors and their potential for the reclassification of IDHwt astrocytoma to glioblastoma. *Acta neuropathologica* 2018; 136: 793-803
- 164 Arita H, Yamasaki K, Matsushita Y, et al. A combination of TERT promoter mutation and MGMT methylation status predicts clinically relevant subgroups of newly diagnosed glioblastomas. *Acta Neuropathol Commun* 2016; 4: 79
- 165 Biomarkers and surrogate endpoints: preferred definitions and conceptual framework. *Clin Pharmacol Ther* 2001; 69: 89-95
- 166 Oldenhuis CN, Oosting SF, Gietema JA, et al. Prognostic versus predictive value of biomarkers in oncology. *European journal of cancer* (Oxford, England : 1990) 2008; 44: 946-53
- 167 Louis DN, Perry A, Reifenberger G, et al. The 2016 World Health Organization Classification of Tumors of the Central Nervous System: a summary. *Acta neuropathologica* 2016; 131: 803-20

References

- 168 Louis DN, Perry A, Wesseling P, et al. The 2021 WHO Classification of Tumors of the Central Nervous System: a summary. *Neuro Oncol* 2021; 23: 1231-51
- 169 Horbinski C. What do we know about IDH1/2 mutations so far, and how do we use it? *Acta neuropathologica* 2013; 125: 621-36
- 170 Dang L, White DW, Gross S, et al. Cancer-associated IDH1 mutations produce 2-hydroxyglutarate. *Nature* 2009; 462: 739-44
- 171 Jin G, Reitman ZJ, Spasojevic I, et al. 2-hydroxyglutarate production, but not dominant negative function, is conferred by glioma-derived NADP-dependent isocitrate dehydrogenase mutations. *PloS one* 2011; 6: e16812
- 172 Unruh D, Zewde M, Buss A, et al. Methylation and transcription patterns are distinct in IDH mutant gliomas compared to other IDH mutant cancers. *Sci Rep* 2019; 9: 8946
- 173 Noushmehr H, Weisenberger DJ, Diefes K, et al. Identification of a CpG island methylator phenotype that defines a distinct subgroup of glioma. *Cancer Cell* 2010; 17: 510-22
- 174 Ceccarelli M, Barthel FP, Malta TM, et al. Molecular Profiling Reveals Biologically Discrete Subsets and Pathways of Progression in Diffuse Glioma. *Cell* 2016; 164: 550-63
- 175 Prensner JR, Chinnaiyan AM. Metabolism unhinged: IDH mutations in cancer. *Nature medicine* 2011; 17: 291-3
- 176 Zhang C, Moore LM, Li X, et al. IDH1/2 mutations target a key hallmark of cancer by deregulating cellular metabolism in glioma. *Neuro Oncol* 2013; 15: 1114-26
- 177 Ohgaki H, Kleihues P. The definition of primary and secondary glioblastoma. *Clin Cancer Res* 2013; 19: 764-72
- 178 Cai J, Zhu P, Zhang C, et al. Detection of ATRX and IDH1-R132H immunohistochemistry in the progression of 211 paired gliomas. *Oncotarget* 2016; 7: 16384-95
- 179 Sasaki M, Knobbe CB, Itsumi M, et al. D-2-hydroxyglutarate produced by mutant IDH1 perturbs collagen maturation and basement membrane function. *Genes Dev* 2012; 26: 2038-49
- 180 Suzuki H, Aoki K, Chiba K, et al. Mutational landscape and clonal architecture in grade II and III gliomas. *Nature genetics* 2015; 47: 458-68
- 181 Reifenberger J, Ring GU, Gies U, et al. Analysis of p53 mutation and epidermal growth factor receptor amplification in recurrent gliomas with malignant progression. *J Neuropathol Exp Neurol* 1996; 55: 822-31
- 182 Berens ME, Sood A, Barnholtz-Sloan JS, et al. Multiscale, multimodal analysis of tumor heterogeneity in IDH1 mutant vs wild-type diffuse gliomas. *PLoS One* 2019; 14: e0219724
- 183 Unruh D, Schwarze SR, Khoury L, et al. Mutant IDH1 and thrombosis in gliomas. *Acta Neuropathol* 2016; 132: 917-30
- 184 Gao Y, Weenink B, van den Bent MJ, et al. Expression-based intrinsic glioma subtypes are prognostic in low-grade gliomas of the EORTC22033-26033 clinical trial. *Eur J Cancer* 2018; 94: 168-78
- 185 Schumacher T, Bunse L, Pusch S, et al. A vaccine targeting mutant IDH1 induces antitumour immunity. *Nature* 2014; 512: 324-7
- 186 Waitkus MS, Diplas BH, Yan H. Biological Role and Therapeutic Potential of IDH Mutations in Cancer. *Cancer cell* 2018; 34: 186-95
- 187 Capper D, Weissert S, Balss J, et al. Characterization of R132H mutation-specific IDH1 antibody binding in brain tumors. *Brain pathology (Zurich, Switzerland)* 2010; 20: 245-54
- 188 Cykowski MD, Allen RA, Fung KM, et al. Pyrosequencing of IDH1 and IDH2 mutations in brain tumors and non-neoplastic conditions. *Diagn Mol Pathol* 2012; 21: 214-20
- 189 Zacher A, Kaulich K, Stepanow S, et al. Molecular Diagnostics of Gliomas Using Next Generation Sequencing of a Glioma-Tailored Gene Panel. *Brain pathology (Zurich, Switzerland)* 2017; 27: 146-59
- 190 Cairncross JG, Ueki K, Zlatescu MC, et al. Specific genetic predictors of chemotherapeutic response and survival in patients with anaplastic oligodendrogliomas. *Journal of the National Cancer Institute* 1998; 90: 1473-9
- 191 van den Bent MJ, Carpentier AF, Brandes AA, et al. Adjuvant procarbazine, lomustine, and vincristine improves progression-free survival but not overall survival in newly diagnosed anaplastic oligodendrogliomas and oligoastrocytomas: a randomized European Organisation for Research and Treatment of Cancer phase III trial. *Journal of clinical oncology : official journal of the American Society of Clinical Oncology* 2006; 24: 2715-22
- 192 Kouwenhoven MC, Gorlia T, Kros JM, et al. Molecular analysis of anaplastic oligodendroglial tumors in a prospective randomized study: A report from EORTC study 26951. *Neuro-oncology* 2009; 11: 737-46
- 193 van den Bent MJ, Brandes AA, Taphoorn MJ, et al. Adjuvant procarbazine, lomustine, and vincristine chemotherapy in newly diagnosed anaplastic oligodendroglioma: long-term follow-up of EORTC brain tumor group study 26951. *Journal of clinical oncology : official journal of the American Society of Clinical Oncology* 2013; 31: 344-50

References

- 194 Cairncross G, Wang M, Shaw E, et al. Phase III trial of chemoradiotherapy for anaplastic oligodendroglioma: long-term results of RTOG 9402. *Journal of clinical oncology : official journal of the American Society of Clinical Oncology* 2013; 31: 337-43
- 195 Vogazianou AP, Chan R, Bäcklund LM, et al. Distinct patterns of 1p and 19q alterations identify subtypes of human gliomas that have different prognoses†. *Neuro-oncology* 2010; 12: 664-78
- 196 Riemenschneider MJ, Jeuken JWM, Wesseling P, et al. Molecular diagnostics of gliomas: state of the art. *Acta neuropathologica* 2010; 120: 567-84
- 197 Wiestler B, Capper D, Hovestadt V, et al. Assessing CpG island methylator phenotype, 1p/19q codeletion, and MGMT promoter methylation from epigenome-wide data in the biomarker cohort of the NOA-04 trial. *Neuro-oncology* 2014; 16: 1630-8
- 198 Wiestler B, Capper D, Sill M, et al. Integrated DNA methylation and copy-number profiling identify three clinically and biologically relevant groups of anaplastic glioma. *Acta neuropathologica* 2014; 128: 561-71
- 199 Capper D, Stichel D, Sahm F, et al. Practical implementation of DNA methylation and copy-number-based CNS tumor diagnostics: the Heidelberg experience. *Acta neuropathologica* 2018; 136: 181-210
- 200 Capper D, Jones DTW, Sill M, et al. DNA methylation-based classification of central nervous system tumours. *Nature* 2018; 555: 469-74
- 201 Jiao Y, Shi C, Edil BH, et al. DAXX/ATRX, MEN1, and mTOR pathway genes are frequently altered in pancreatic neuroendocrine tumors. *Science (New York, NY)* 2011; 331: 1199-203
- 202 Ferreira MSV, Sørensen MD, Pusch S, et al. Alternative lengthening of telomeres is the major telomere maintenance mechanism in astrocytoma with isocitrate dehydrogenase 1 mutation. *Journal of neuro-oncology* 2020; 147: 1-14
- 203 Haase S, Garcia-Fabiani MB, Carney S, et al. Mutant ATRX: uncovering a new therapeutic target for glioma. *Expert opinion on therapeutic targets* 2018; 22: 599-613
- 204 Kannan K, Inagaki A, Silber J, et al. Whole-exome sequencing identifies ATRX mutation as a key molecular determinant in lower-grade glioma. *Oncotarget* 2012; 3: 1194-203
- 205 Xie Y, Tan Y, Yang C, et al. Omics-based integrated analysis identified ATRX as a biomarker associated with glioma diagnosis and prognosis. *Cancer Biol Med* 2019; 16: 784-96
- 206 Wick W, Weller M, van den Bent M, et al. MGMT testing-the challenges for biomarker-based glioma treatment. *Nature reviews Neurology* 2014; 10: 372-85
- 207 Hegi ME, Liu L, Herman JG, et al. Correlation of O6-methylguanine methyltransferase (MGMT) promoter methylation with clinical outcomes in glioblastoma and clinical strategies to modulate MGMT activity. *Journal of clinical oncology : official journal of the American Society of Clinical Oncology* 2008; 26: 4189-99
- 208 Hegi ME, Diserens AC, Gorlia T, et al. MGMT gene silencing and benefit from temozolomide in glioblastoma. *The New England journal of medicine* 2005; 352: 997-1003
- 209 Weller M, Felsberg J, Hartmann C, et al. Molecular predictors of progression-free and overall survival in patients with newly diagnosed glioblastoma: a prospective translational study of the German Glioma Network. *Journal of clinical oncology : official journal of the American Society of Clinical Oncology* 2009; 27: 5743-50
- 210 Esteller M, Garcia-Foncillas J, Andion E, et al. Inactivation of the DNA-Repair Gene MGMT and the Clinical Response of Gliomas to Alkylating Agents. *New England Journal of Medicine* 2000; 343: 1350-4
- 211 Wick W, Meisner C, Hentschel B, et al. Prognostic or predictive value of MGMT promoter methylation in gliomas depends on IDH1 mutation. *Neurology* 2013; 81: 1515-22
- 212 Gomes I, Moreno DA, Dos Reis MB, et al. Low MGMT digital expression is associated with a better outcome of IDH1 wildtype glioblastomas treated with temozolomide. *J Neurooncol* 2021; 151: 135-44
- 213 Gilbert MR, Wang M, Aldape KD, et al. Dose-dense temozolomide for newly diagnosed glioblastoma: a randomized phase III clinical trial. *Journal of clinical oncology : official journal of the American Society of Clinical Oncology* 2013; 31: 4085-91
- 214 Olson RA, Brastianos PK, Palma DA. Prognostic and predictive value of epigenetic silencing of MGMT in patients with high grade gliomas: a systematic review and meta-analysis. *Journal of neuro-oncology* 2011; 105: 325-35
- 215 Wick W, Platten M, Meisner C, et al. Temozolomide chemotherapy alone versus radiotherapy alone for malignant astrocytoma in the elderly: the NOA-08 randomised, phase 3 trial. *The lancet oncology* 2012; 13: 707-15
- 216 Dahlrot RH, Dowsett J, Fosmark S, et al. Prognostic value of O-6-methylguanine-DNA methyltransferase (MGMT) protein expression in glioblastoma excluding nontumour cells from the analysis. *Neuropathology and applied neurobiology* 2018; 44: 172-84
- 217 Dahlrot RH, Larsen P, Boldt HB, et al. Posttreatment Effect of MGMT Methylation Level on Glioblastoma Survival. *Journal of neuropathology and experimental neurology* 2019; 78: 633-40
- 218 Binabaj MM, Bahrami A, ShahidSales S, et al. The prognostic value of MGMT promoter methylation in glioblastoma: A meta-analysis of clinical trials. *J Cell Physiol* 2018; 233: 378-86

References

- 219 Malmstrom A, Gronberg BH, Marosi C, et al. Temozolomide versus standard 6-week radiotherapy versus hypofractionated radiotherapy in patients older than 60 years with glioblastoma: the Nordic randomised, phase 3 trial. *The lancet oncology* 2012; 13: 916-26
- 220 Reifenberger G, Hentschel B, Felsberg J, et al. Predictive impact of MGMT promoter methylation in glioblastoma of the elderly. *International journal of cancer Journal international du cancer* 2012; 131: 1342-50
- 221 Weller M, van den Bent M, Tonn JC, et al. European Association for Neuro-Oncology (EANO) guideline on the diagnosis and treatment of adult astrocytic and oligodendroglial gliomas. *The lancet oncology* 2017; 18: e315-e29
- 222 Vuong HG, Altibi AMA, Duong UNP, et al. TERT promoter mutation and its interaction with IDH mutations in glioma: Combined TERT promoter and IDH mutations stratifies lower-grade glioma into distinct survival subgroups-A meta-analysis of aggregate data. *Crit Rev Oncol Hematol* 2017; 120: 1-9
- 223 Brito C, Azevedo A, Esteves S, et al. Clinical insights gained by refining the 2016 WHO classification of diffuse gliomas with: EGFR amplification, TERT mutations, PTEN deletion and MGMT methylation. *BMC cancer* 2019; 19: 968
- 224 Pardo FS, Hsu DW, Zeheb R, et al. Mutant, wild type, or overall p53 expression: freedom from clinical progression in tumours of astrocytic lineage. *British journal of cancer* 2004; 91: 1678-86
- 225 Amatya VJ, Naumann U, Weller M, et al. TP53 promoter methylation in human gliomas. *Acta neuropathologica* 2005; 110: 178-84
- 226 Ekstrand AJ, Sugawa N, James CD, et al. Amplified and rearranged epidermal growth factor receptor genes in human glioblastomas reveal deletions of sequences encoding portions of the N- and/or C-terminal tails. *Proceedings of the National Academy of Sciences of the United States of America* 1992; 89: 4309-13
- 227 Hatanpaa KJ, Burma S, Zhao D, et al. Epidermal growth factor receptor in glioma: signal transduction, neuropathology, imaging, and radioresistance. *Neoplasia* 2010; 12: 675-84
- 228 Kleinschmidt-DeMasters BK, Aisner DL, Birks DK, et al. Epithelioid GBMs show a high percentage of BRAF V600E mutation. *The American journal of surgical pathology* 2013; 37: 685-98
- 229 Knobbe CB, Reifenberger J, Reifenberger G. Mutation analysis of the Ras pathway genes NRAS, HRAS, KRAS and BRAF in glioblastomas. *Acta neuropathologica* 2004; 108: 467-70
- 230 Louis DN, Wesseling P, Paulus W, et al. cIMPACT-NOW update 1: Not Otherwise Specified (NOS) and Not Elsewhere Classified (NEC). *Acta neuropathologica* 2018; 135: 481-4
- 231 van den Bent MJ, Weller M, Wen PY, et al. A clinical perspective on the 2016 WHO brain tumor classification and routine molecular diagnostics. *Neuro-oncology* 2017; 19: 614-24
- 232 Reuss DE, Mamatzjan Y, Schrimpf D, et al. IDH mutant diffuse and anaplastic astrocytomas have similar age at presentation and little difference in survival: a grading problem for WHO. *Acta neuropathologica* 2015; 129: 867-73
- 233 Louis DN, Wesseling P, Aldape K, et al. cIMPACT-NOW update 6: new entity and diagnostic principle recommendations of the cIMPACT-Utrecht meeting on future CNS tumor classification and grading. *Brain Pathology* 2020; 30: 844-56
- 234 Brat DJ, Aldape K, Colman H, et al. cIMPACT-NOW update 3: recommended diagnostic criteria for “Diffuse astrocytic glioma, IDH-wildtype, with molecular features of glioblastoma, WHO grade IV”. *Acta neuropathologica* 2018; 136: 805-10
- 235 Reifenberger G, Wirsching HG, Knobbe-Thomsen CB, et al. Advances in the molecular genetics of gliomas - implications for classification and therapy. *Nature reviews Clinical oncology* 2017; 14: 434-52
- 236 Petersen JK, Boldt HB, Sorensen MD, et al. Targeted next-generation sequencing of adult gliomas for retrospective prognostic evaluation and up-front diagnostics. *Neuropathology and applied neurobiology* 2020:
- 237 Paul Y, Mondal B, Patil V, et al. DNA methylation signatures for 2016 WHO classification subtypes of diffuse gliomas. *Clin Epigenetics* 2017; 9: 32
- 238 Priesterbach-Ackley LP, Boldt HB, Petersen JK, et al. Brain tumour diagnostics using a DNA methylation-based classifier as a diagnostic support tool. *Neuropathol Appl Neurobiol* 2020:
- 239 Jaunmuktane Z, Capper D, Jones DTW, et al. Methylation array profiling of adult brain tumours: diagnostic outcomes in a large, single centre. *Acta Neuropathol Commun* 2019; 7: 24
- 240 Iuchi T, Sugiyama T, Ohira M, et al. Clinical significance of the 2016 WHO classification in Japanese patients with gliomas. *Brain tumor pathology* 2018; 35: 71-80
- 241 Tabouret E, Nguyen AT, Dehais C, et al. Prognostic impact of the 2016 WHO classification of diffuse gliomas in the French POLA cohort. *Acta neuropathologica* 2016; 132: 625-34
- 242 Cimino PJ, Zager M, McFerrin L, et al. Multidimensional scaling of diffuse gliomas: application to the 2016 World Health Organization classification system with prognostically relevant molecular subtype discovery. *Acta neuropathologica communications* 2017; 5: 39
- 243 Louis DN, Ohgaki H, Wiestler OD, et al. WHO classification of tumours of the central nervous system, Revised, 4th edition. International Agency for Research on Cancer (IARC), Lyon. 2016

References

- 244 Arita H, Matsushita Y, Machida R, et al. TERT promoter mutation confers favorable prognosis regardless of 1p/19q status in adult diffuse gliomas with IDH1/2 mutations. *Acta Neuropathologica Communications* 2020; 8: 201
- 245 Arita H, Narita Y, Fukushima S, et al. Upregulating mutations in the TERT promoter commonly occur in adult malignant gliomas and are strongly associated with total 1p19q loss. *Acta Neuropathologica* 2013; 126: 267-76
- 246 Aihara K, Mukasa A, Nagae G, et al. Genetic and epigenetic stability of oligodendrogliomas at recurrence. *Acta Neuropathol Commun* 2017; 5: 18
- 247 Reuss DE, Kratz A, Sahm F, et al. Adult IDH wild type astrocytomas biologically and clinically resolve into other tumor entities. *Acta Neuropathol* 2015; 130: 407-17
- 248 Hasselblatt M, Jaber M, Reuss D, et al. Diffuse Astrocytoma, IDH-Wildtype: A Dissolving Diagnosis. *Journal of neuropathology and experimental neurology* 2018; 77: 422-5
- 249 Tesileanu CMS, Dirven L, Wijnenga MMJ, et al. Survival of diffuse astrocytic glioma, IDH1/2 wildtype, with molecular features of glioblastoma, WHO grade IV: a confirmation of the cIMPACT-NOW criteria. *Neuro-oncology* 2020; 22: 515-23
- 250 Fujimoto K, Arita H, Satomi K, et al. TERT promoter mutation status is necessary and sufficient to diagnose IDH-wildtype diffuse astrocytic glioma with molecular features of glioblastoma. *Acta Neuropathol* 2021; 142: 323-38
- 251 Richardson TE, Hatanpaa KJ, Walker JM. Molecular Characterization of “True” Low-Grade IDH-Wildtype Astrocytomas. *Journal of Neuropathology & Experimental Neurology* 2021; 80: 431-5
- 252 Berzero G, Di Stefano AL, Ronchi S, et al. IDH-wildtype lower-grade diffuse gliomas: the importance of histological grade and molecular assessment for prognostic stratification. *Neuro Oncol* 2021; 23: 955-66
- 253 Sturm D, Witt H, Hovestadt V, et al. Hotspot Mutations in H3F3A and IDH1 Define Distinct Epigenetic and Biological Subgroups of Glioblastoma. *Cancer cell* 2012; 22: 425-37
- 254 Aldape K, Zadeh G, Mansouri S, et al. Glioblastoma: pathology, molecular mechanisms and markers. *Acta neuropathologica* 2015; 129: 829-48
- 255 Doucette T, Rao G, Rao A, et al. Immune heterogeneity of glioblastoma subtypes: extrapolation from the cancer genome atlas. *Cancer immunology research* 2013; 1: 112-22
- 256 Rutledge WC, Kong J, Gao J, et al. Tumor-infiltrating lymphocytes in glioblastoma are associated with specific genomic alterations and related to transcriptional class. *Clinical cancer research : an official journal of the American Association for Cancer Research* 2013; 19: 4951-60
- 257 Brennan C, Momota H, Hambardzumyan D, et al. Glioblastoma Subclasses Can Be Defined by Activity among Signal Transduction Pathways and Associated Genomic Alterations. *PloS one* 2009; 4: e7752
- 258 Wang Q, Hu B, Hu X, et al. Tumor Evolution of Glioma-Intrinsic Gene Expression Subtypes Associates with Immunological Changes in the Microenvironment. *Cancer Cell* 2017; 32: 42-56.e6
- 259 Lai A, Kharbanda S, Pope WB, et al. Evidence for sequenced molecular evolution of IDH1 mutant glioblastoma from a distinct cell of origin. *J Clin Oncol* 2011; 29: 4482-90
- 260 Nobusawa S, Watanabe T, Kleihues P, et al. IDH1 mutations as molecular signature and predictive factor of secondary glioblastomas. *Clinical cancer research : an official journal of the American Association for Cancer Research* 2009; 15: 6002-7
- 261 Dahlrot RH, Kristensen BW, Hjelmborg J, et al. A population-based study of high-grade gliomas and mutated isocitrate dehydrogenase 1. *International journal of clinical and experimental pathology* 2013; 6: 31-40
- 262 Parker NR, Hudson AL, Khong P, et al. Intratumoral heterogeneity identified at the epigenetic, genetic and transcriptional level in glioblastoma. *Scientific reports* 2016; 6: 22477
- 263 Wenger A, Ferreyra Vega S, Kling T, et al. Intratumor DNA methylation heterogeneity in glioblastoma: implications for DNA methylation-based classification. *Neuro-oncology* 2019; 21: 616-27
- 264 Johnson KC, Anderson KJ, Courtois ET, et al. Single-cell multimodal glioma analyses identify epigenetic regulators of cellular plasticity and environmental stress response. *Nat Genet* 2021; 53: 1456-68
- 265 Mao P, Joshi K, Li J, et al. Mesenchymal glioma stem cells are maintained by activated glycolytic metabolism involving aldehyde dehydrogenase 1A3. *Proc Natl Acad Sci U S A* 2013; 110: 8644-9
- 266 Wang J, Cazzato E, Ladewig E, et al. Clonal evolution of glioblastoma under therapy. *Nat Genet* 2016; 48: 768-76
- 267 Varn FS, Johnson KC, Martinek J, et al. Glioma progression is shaped by genetic evolution and microenvironment interactions. *Cell* 2022; 185: 2184-99.e16
- 268 Kaffes I, Szulzewsky F, Chen Z, et al. Human Mesenchymal glioblastomas are characterized by an increased immune cell presence compared to Proneural and Classical tumors. *Oncoimmunology* 2019; 8: e1655360
- 269 Sandmann T, Bourgon R, Garcia J, et al. Patients With Proneural Glioblastoma May Derive Overall Survival Benefit From the Addition of Bevacizumab to First-Line Radiotherapy and Temozolomide: Retrospective Analysis of the AVAglio Trial. *Journal of clinical oncology : official journal of the American Society of Clinical Oncology* 2015; 33: 2735-44

References

- 270 van den Bent MJ, Gao Y, Kerkhof M, et al. Changes in the EGFR amplification and EGFRvIII expression between paired primary and recurrent glioblastomas. *Neuro Oncol* 2015; 17: 935-41
- 271 Lacroix M, Abi-Said D, Fourney DR, et al. A multivariate analysis of 416 patients with glioblastoma multiforme: prognosis, extent of resection, and survival. 2001; 95: 190
- 272 Jeremic B, Milicic B, Grujicic D, et al. Multivariate analysis of clinical prognostic factors in patients with glioblastoma multiforme treated with a combined modality approach. *Journal of cancer research and clinical oncology* 2003; 129: 477-84
- 273 Lutterbach J, Sauerbrei W, Guttenberger R. Multivariate Analysis of Prognostic Factors in Patients with Glioblastoma. *Strahlentherapie und Onkologie* 2003; 179: 8-15
- 274 Casartelli G, Dorcaratto A, Ravetti JL, et al. Survival of high grade glioma patients depends on their age at diagnosis. *Cancer biology & therapy* 2009; 8: 1719-21
- 275 Kim KJ, Lee KH, Kim HS, et al. The presence of stem cell marker-expressing cells is not prognostically significant in glioblastomas. *Neuropathology : official journal of the Japanese Society of Neuropathology* 2011; 31: 494-502
- 276 Weller M, van den Bent M, Preusser M, et al. EANO guidelines on the diagnosis and treatment of diffuse gliomas of adulthood. *Nat Rev Clin Oncol* 2021; 18: 170-86
- 277 Wick W, Hartmann C, Engel C, et al. NOA-04 randomized phase III trial of sequential radiochemotherapy of anaplastic glioma with procarbazine, lomustine, and vincristine or temozolomide. *Journal of clinical oncology : official journal of the American Society of Clinical Oncology* 2009; 27: 5874-80
- 278 Brat DJ, Aldape K, Colman H, et al. cIMPACT-NOW update 5: recommended grading criteria and terminologies for IDH-mutant astrocytomas. *Acta Neuropathol* 2020; 139: 603-8
- 279 Louis DN, Wesseling P, Aldape K, et al. cIMPACT-NOW update 6: new entity and diagnostic principle recommendations of the cIMPACT-Utrecht meeting on future CNS tumor classification and grading. *Brain Pathol* 2020; 30: 844-56
- 280 Roth P, Hottinger AF, Hundsberger T, et al. A contemporary perspective on the diagnosis and treatment of diffuse gliomas in adults. *Swiss Med Wkly* 2020; 150: w20256
- 281 Wen PY, Weller M, Lee EQ, et al. Glioblastoma in adults: a Society for Neuro-Oncology (SNO) and European Society of Neuro-Oncology (EANO) consensus review on current management and future directions. *Neuro Oncol* 2020; 22: 1073-113
- 282 Weller M, Le Rhun E, Preusser M, et al. How we treat glioblastoma. *ESMO Open* 2019; 4: e000520-e
- 283 Giese A, Bjerkvig R, Berens ME, et al. Cost of migration: invasion of malignant gliomas and implications for treatment. *J Clin Oncol* 2003; 21: 1624-36
- 284 van den Bent MJ, Afra D, de Witte O, et al. Long-term efficacy of early versus delayed radiotherapy for low-grade astrocytoma and oligodendroglioma in adults: the EORTC 22845 randomised trial. *Lancet* 2005; 366: 985-90
- 285 Recht L, van den Bent M, Shih H. Treatment and prognosis of diffuse (grade II) and anaplastic (grade III) astrocytomas in adults. In: *UpToDate*, Post, TW (Ed), *UpToDate*, Waltham, MA. 2020
- 286 Buckner JC, Shaw EG, Pugh SL, et al. Radiation plus Procarbazine, CCNU, and Vincristine in Low-Grade Glioma. *New England Journal of Medicine* 2016; 374: 1344-55
- 287 van den Bent MJ, Baumert B, Erridge SC, et al. Interim results from the CATNON trial (EORTC study 26053-22054) of treatment with concurrent and adjuvant temozolomide for 1p/19q non-co-deleted anaplastic glioma: a phase 3, randomised, open-label intergroup study. *Lancet* 2017; 390: 1645-53
- 288 Sorensen MD, Fosmark S, Hellwege S, et al. Chemoresistance and chemotherapy targeting stem-like cells in malignant glioma. *Adv Exp Med Biol* 2015; 853: 111-38
- 289 Blumenthal DT, Gorlia T, Gilbert MR, et al. Is more better? The impact of extended adjuvant temozolomide in newly diagnosed glioblastoma: a secondary analysis of EORTC and NRG Oncology/RTOG. *Neuro-oncology* 2017; 19: 1119-26
- 290 Gilbert MR, Dignam JJ, Armstrong TS, et al. A randomized trial of bevacizumab for newly diagnosed glioblastoma. *N Engl J Med* 2014; 370: 699-708
- 291 Wirsching HG, Tabatabai G, Roelcke U, et al. Bevacizumab plus hypofractionated radiotherapy versus radiotherapy alone in elderly patients with glioblastoma: the randomized, open-label, phase II ARTE trial. *Ann Oncol* 2018; 29: 1423-30
- 292 Chinot OL, Wick W, Mason W, et al. Bevacizumab plus radiotherapy-temozolomide for newly diagnosed glioblastoma. *The New England journal of medicine* 2014; 370: 709-22
- 293 Raizer JJ, Giglio P, Hu J, et al. A phase II study of bevacizumab and erlotinib after radiation and temozolomide in MGMT unmethylated GBM patients. *Journal of neuro-oncology* 2016; 126: 185-92
- 294 Ly KI, Wen PY. Clinical Relevance of Steroid Use in Neuro-Oncology. *Current neurology and neuroscience reports* 2017; 17: 5

References

- 295 Pitter KL, Tamagno I, Alikhanyan K, et al. Corticosteroids compromise survival in glioblastoma. *Brain : a journal of neurology* 2016; 139: 1458-71
- 296 Reardon DA, Brandes AA, Omuro A, et al. Effect of Nivolumab vs Bevacizumab in Patients With Recurrent Glioblastoma: The CheckMate 143 Phase 3 Randomized Clinical Trial. *JAMA Oncol* 2020; 6: 1003-10
- 297 Gustafson MP, Lin Y, New KC, et al. Systemic immune suppression in glioblastoma: the interplay between CD14+HLA-DRlo/neg monocytes, tumor factors, and dexamethasone. *Neuro Oncol* 2010; 12: 631-44
- 298 Swildens KX, Sillevs Smitt PAE, van den Bent MJ, et al. The effect of dexamethasone on the microenvironment and efficacy of checkpoint inhibitors in glioblastoma: a systematic review. *Neurooncol Adv* 2022; 4: vdc087
- 299 Kelly WJ, Gilbert MR. Glucocorticoids and immune checkpoint inhibitors in glioblastoma. *J Neurooncol* 2021; 151: 13-20
- 300 Korber V, Yang J, Barah P, et al. Evolutionary Trajectories of IDH(WT) Glioblastomas Reveal a Common Path of Early Tumorigenesis Instigated Years ahead of Initial Diagnosis. *Cancer Cell* 2019; 35: 692-704.e12
- 301 Baker GJ, Yadav VN, Motsch S, et al. Mechanisms of glioma formation: iterative perivascular glioma growth and invasion leads to tumor progression, VEGF-independent vascularization, and resistance to antiangiogenic therapy. *Neoplasia* 2014; 16: 543-61
- 302 Wick W, Gorlia T, Bendszus M, et al. Lomustine and Bevacizumab in Progressive Glioblastoma. *The New England journal of medicine* 2017; 377: 1954-63
- 303 Seystahl K, Hentschel B, Loew S, et al. Bevacizumab versus alkylating chemotherapy in recurrent glioblastoma. *Journal of cancer research and clinical oncology* 2020; 146: 659-70
- 304 Friedman HS, Prados MD, Wen PY, et al. Bevacizumab alone and in combination with irinotecan in recurrent glioblastoma. *Journal of clinical oncology : official journal of the American Society of Clinical Oncology* 2009; 27: 4733-40
- 305 Vredenburgh JJ, Desjardins A, Reardon DA, et al. Experience with irinotecan for the treatment of malignant glioma. *Neuro-oncology* 2009; 11: 80-91
- 306 Weller M, Cloughesy T, Perry JR, et al. Standards of care for treatment of recurrent glioblastoma--are we there yet? *Neuro-oncology* 2013; 15: 4-27
- 307 Kaka N, Hafazalla K, Samawi H, et al. Progression-Free but No Overall Survival Benefit for Adult Patients with Bevacizumab Therapy for the Treatment of Newly Diagnosed Glioblastoma: A Systematic Review and Meta-Analysis. *Cancers (Basel)* 2019; 11:
- 308 Stupp R, Wong ET, Kanner AA, et al. NovoTTF-100A versus physician's choice chemotherapy in recurrent glioblastoma: a randomised phase III trial of a novel treatment modality. *European journal of cancer (Oxford, England : 1990)* 2012; 48: 2192-202
- 309 Stupp R, Taillibert S, Kanner A, et al. Effect of Tumor-Treating Fields Plus Maintenance Temozolomide vs Maintenance Temozolomide Alone on Survival in Patients With Glioblastoma: A Randomized Clinical Trial. *Jama* 2017; 318: 2306-16
- 310 Weller M, Butowski N, Tran DD, et al. Rindopepimut with temozolomide for patients with newly diagnosed, EGFRvIII-expressing glioblastoma (ACT IV): a randomised, double-blind, international phase 3 trial. *Lancet Oncol* 2017; 18: 1373-85
- 311 Szerlip NJ, Pedraza A, Chakravarty D, et al. Intratumoral heterogeneity of receptor tyrosine kinases EGFR and PDGFRA amplification in glioblastoma defines subpopulations with distinct growth factor response. *Proceedings of the National Academy of Sciences of the United States of America* 2012; 109: 3041-6
- 312 Omuro A, Vlahovic G, Lim M, et al. Nivolumab with or without ipilimumab in patients with recurrent glioblastoma: results from exploratory phase I cohorts of CheckMate 143. *Neuro-oncology* 2018; 20: 674-86
- 313 Carter T, Shaw H, Cohn-Brown D, et al. Ipilimumab and Bevacizumab in Glioblastoma. *Clinical oncology (Royal College of Radiologists (Great Britain))* 2016; 28: 622-6
- 314 Butowski N, Colman H, De Groot JF, et al. Orally administered colony stimulating factor 1 receptor inhibitor PLX3397 in recurrent glioblastoma: an Ivy Foundation Early Phase Clinical Trials Consortium phase II study. *Neuro Oncol* 2016; 18: 557-64
- 315 Schalper KA, Rodriguez-Ruiz ME, Diez-Valle R, et al. Neoadjuvant nivolumab modifies the tumor immune microenvironment in resectable glioblastoma. *Nature medicine* 2019; 25: 470-6
- 316 Lara-Velazquez M, Shireman JM, Lehrer EJ, et al. A Comparison Between Chemo-Radiotherapy Combined With Immunotherapy and Chemo-Radiotherapy Alone for the Treatment of Newly Diagnosed Glioblastoma: A Systematic Review and Meta-Analysis. *Front Oncol* 2021; 11: 662302
- 317 Cloughesy TF, Mochizuki AY, Orpilla JR, et al. Neoadjuvant anti-PD-1 immunotherapy promotes a survival benefit with intratumoral and systemic immune responses in recurrent glioblastoma. *Nature medicine* 2019; 25: 477-86
- 318 Zhao J, Chen AX, Gartrell RD, et al. Immune and genomic correlates of response to anti-PD-1 immunotherapy in glioblastoma. *Nat Med* 2019; 25: 462-9
- 319 Loriger M. Tumor microenvironment in the brain. *Cancers (Basel)* 2012; 4: 218-43

References

- 320 Joyce JA, Pollard JW. Microenvironmental regulation of metastasis. *Nat Rev Cancer* 2009; 9: 239-52
- 321 Hanahan D, Weinberg RA. Hallmarks of cancer: the next generation. *Cell* 2011; 144: 646-74
- 322 Hanahan D, Coussens LM. Accessories to the crime: functions of cells recruited to the tumor microenvironment. *Cancer Cell* 2012; 21: 309-22
- 323 Mantovani A, Allavena P, Sica A, et al. Cancer-related inflammation. *Nature* 2008; 454: 436-44
- 324 Bader JE, Voss K, Rathmell JC. Targeting Metabolism to Improve the Tumor Microenvironment for Cancer Immunotherapy. *Mol Cell* 2020; 78: 1019-33
- 325 Liao C, Liu X, Zhang C, et al. Tumor hypoxia: From basic knowledge to therapeutic implications. *Semin Cancer Biol* 2023; 88: 172-86
- 326 Carmeliet P, Jain RK. Molecular mechanisms and clinical applications of angiogenesis. *Nature* 2011; 473: 298-307
- 327 Lathia JD, Mack SC, Mulkearns-Hubert EE, et al. Cancer stem cells in glioblastoma. *Genes Dev* 2015; 29: 1203-17
- 328 Gisina A, Kholodenko I, Kim Y, et al. Glioma Stem Cells: Novel Data Obtained by Single-Cell Sequencing. *International Journal of Molecular Sciences* 2022; 23: 14224
- 329 Sena IFG, Paiva AE, Prazeres P, et al. Glioblastoma-activated pericytes support tumor growth via immunosuppression. *Cancer Med* 2018; 7: 1232-9
- 330 Caspani EM, Crossley PH, Redondo-Garcia C, et al. Glioblastoma: a pathogenic crosstalk between tumor cells and pericytes. *PLoS One* 2014; 9: e101402
- 331 Venkatesh HS, Johung TB, Caretti V, et al. Neuronal Activity Promotes Glioma Growth through Neuroligin-3 Secretion. *Cell* 2015; 161: 803-16
- 332 Johung T, Monje M. Neuronal activity in the glioma microenvironment. *Curr Opin Neurobiol* 2017; 47: 156-61
- 333 Geha S, Pallud J, Junier MP, et al. NG2+/Olig2+ cells are the major cycle-related cell population of the adult human normal brain. *Brain Pathol* 2010; 20: 399-411
- 334 Philips T, Rothstein JD. Oligodendroglia: metabolic supporters of neurons. *The Journal of Clinical Investigation* 2017; 127: 3271-80
- 335 Hide T, Komohara Y, Miyasato Y, et al. Oligodendrocyte Progenitor Cells and Macrophages/Microglia Produce Glioma Stem Cell Niches at the Tumor Border. *EBioMedicine* 2018; 30: 94-104
- 336 Kawashima T, Yashiro M, Kasashima H, et al. Oligodendrocytes Up-regulate the Invasive Activity of Glioblastoma Cells via the Angiopoietin-2 Signaling Pathway. *Anticancer Res* 2019; 39: 577-84
- 337 Zhang H, Zhou Y, Cui B, et al. Novel insights into astrocyte-mediated signaling of proliferation, invasion and tumor immune microenvironment in glioblastoma. *Biomed Pharmacother* 2020; 126: 110086
- 338 Brandao M, Simon T, Critchley G, et al. Astrocytes, the rising stars of the glioblastoma microenvironment. *Glia* 2019; 67: 779-90
- 339 Chen W, Xia T, Wang D, et al. Human astrocytes secrete IL-6 to promote glioma migration and invasion through upregulation of cytomembrane MMP14. *Oncotarget* 2016; 7: 62425-38
- 340 Rath BH, Wahba A, Camphausen K, et al. Coculture with astrocytes reduces the radiosensitivity of glioblastoma stem-like cells and identifies additional targets for radiosensitization. *Cancer Med* 2015; 4: 1705-16
- 341 Lin Q, Liu Z, Ling F, et al. Astrocytes protect glioma cells from chemotherapy and upregulate survival genes via gap junctional communication. *Mol Med Rep* 2016; 13: 1329-35
- 342 Henrik Heiland D, Ravi VM, Behringer SP, et al. Tumor-associated reactive astrocytes aid the evolution of immunosuppressive environment in glioblastoma. *Nat Commun* 2019; 10: 2541
- 343 Marvel D, Gabilovich DI. Myeloid-derived suppressor cells in the tumor microenvironment: expect the unexpected. *J Clin Invest* 2015; 125: 3356-64
- 344 Cordell EC, Alghamri MS, Castro MG, et al. T lymphocytes as dynamic regulators of glioma pathobiology. *Neuro Oncol* 2022; 24: 1647-57
- 345 Lauko A, Lo A, Ahluwalia MS, et al. Cancer cell heterogeneity & plasticity in glioblastoma and brain tumors. *Semin Cancer Biol* 2022; 82: 162-75
- 346 Baker S, Ali I, Silins I, et al. Cancer Hallmarks Analytics Tool (CHAT): a text mining approach to organize and evaluate scientific literature on cancer. *Bioinformatics* 2017; 33: 3973-81
- 347 Harris AL. Hypoxia--a key regulatory factor in tumour growth. *Nat Rev Cancer* 2002; 2: 38-47
- 348 Jain RK, di Tomaso E, Duda DG, et al. Angiogenesis in brain tumours. *Nat Rev Neurosci* 2007; 8: 610-22
- 349 Arvanitis CD, Ferraro GB, Jain RK. The blood-brain barrier and blood-tumour barrier in brain tumours and metastases. *Nat Rev Cancer* 2020; 20: 26-41
- 350 Seano G, Jain RK. Vessel co-option in glioblastoma: emerging insights and opportunities. *Angiogenesis* 2020; 23: 9-16
- 351 Chiao MT, Yang YC, Cheng WY, et al. CD133+ glioblastoma stem-like cells induce vascular mimicry in vivo. *Curr Neurovasc Res* 2011; 8: 210-9

References

- 352 Liu XM, Zhang QP, Mu YG, et al. Clinical significance of vasculogenic mimicry in human gliomas. *J Neurooncol* 2011; 105: 173-9
- 353 Wang R, Chadalavada K, Wilshire J, et al. Glioblastoma stem-like cells give rise to tumour endothelium. *Nature* 2010; 468: 829-33
- 354 He H, Niu CS, Li MW. Correlation between glioblastoma stem-like cells and tumor vascularization. *Oncol Rep* 2012; 27: 45-50
- 355 Cheng L, Huang Z, Zhou W, et al. Glioblastoma stem cells generate vascular pericytes to support vessel function and tumor growth. *Cell* 2013; 153: 139-52
- 356 Liu Q, Cao P. Clinical and prognostic significance of HIF-1 α in glioma patients: a meta-analysis. *Int J Clin Exp Med* 2015; 8: 22073-83
- 357 Xiong Z, Liu H, He C, et al. Hypoxia Contributes to Poor Prognosis in Primary IDH-wt GBM by Inducing Tumor Cells MES-Like Transformation Trend and Inhibiting Immune Cells Activity. *Front Oncol* 2021; 11: 782043
- 358 Fallah J, Rini BI. HIF Inhibitors: Status of Current Clinical Development. *Curr Oncol Rep* 2019; 21: 6
- 359 Xu H, Rahimpour S, Nesvick CL, et al. Activation of hypoxia signaling induces phenotypic transformation of glioma cells: implications for bevacizumab antiangiogenic therapy. *Oncotarget* 2015; 6: 11882-93
- 360 Li P, Zhou C, Xu L, et al. Hypoxia enhances stemness of cancer stem cells in glioblastoma: an in vitro study. *Int J Med Sci* 2013; 10: 399-407
- 361 Kucharzewska P, Christianson HC, Welch JE, et al. Exosomes reflect the hypoxic status of glioma cells and mediate hypoxia-dependent activation of vascular cells during tumor development. *Proc Natl Acad Sci U S A* 2013; 110: 7312-7
- 362 Wang Y, Liu T, Yang N, et al. Hypoxia and macrophages promote glioblastoma invasion by the CCL4-CCR5 axis. *Oncol Rep* 2016; 36: 3522-8
- 363 Brat DJ, Castellano-Sanchez AA, Hunter SB, et al. Pseudopalisades in glioblastoma are hypoxic, express extracellular matrix proteases, and are formed by an actively migrating cell population. *Cancer Res* 2004; 64: 920-7
- 364 Joseph JV, Conroy S, Pavlov K, et al. Hypoxia enhances migration and invasion in glioblastoma by promoting a mesenchymal shift mediated by the HIF1 α -ZEB1 axis. *Cancer Lett* 2015; 359: 107-16
- 365 Hjelmeland AB, Wu Q, Heddleston JM, et al. Acidic stress promotes a glioma stem cell phenotype. *Cell Death Differ* 2011; 18: 829-40
- 366 Soehngen E, Schaefer A, Koeritzer J, et al. Hypoxia upregulates aldehyde dehydrogenase isoform 1 (ALDH1) expression and induces functional stem cell characteristics in human glioblastoma cells. *Brain Tumor Pathol* 2014; 31: 247-56
- 367 Soeda A, Park M, Lee D, et al. Hypoxia promotes expansion of the CD133-positive glioma stem cells through activation of HIF-1 α . *Oncogene* 2009; 28: 3949-59
- 368 Colwell N, Larion M, Giles AJ, et al. Hypoxia in the glioblastoma microenvironment: shaping the phenotype of cancer stem-like cells. *Neuro Oncol* 2017; 19: 887-96
- 369 Dirkse A, Golebiewska A, Buder T, et al. Stem cell-associated heterogeneity in Glioblastoma results from intrinsic tumor plasticity shaped by the microenvironment. *Nat Commun* 2019; 10: 1787
- 370 Wei J, Wu A, Kong LY, et al. Hypoxia potentiates glioma-mediated immunosuppression. *PLoS One* 2011; 6: e16195
- 371 Liu S, Liu X, Zhang C, et al. T-Cell Exhaustion Status Under High and Low Levels of Hypoxia-Inducible Factor 1 α Expression in Glioma. *Front Pharmacol* 2021; 12: 711772
- 372 Xu J, Zhang J, Zhang Z, et al. Hypoxic glioma-derived exosomes promote M2-like macrophage polarization by enhancing autophagy induction. *Cell Death Dis* 2021; 12: 373
- 373 Laoui D, Van Overmeire E, Di Conza G, et al. Tumor hypoxia does not drive differentiation of tumor-associated macrophages but rather fine-tunes the M2-like macrophage population. *Cancer Res* 2014; 74: 24-30
- 374 Colegio OR, Chu NQ, Szabo AL, et al. Functional polarization of tumour-associated macrophages by tumour-derived lactic acid. *Nature* 2014; 513: 559-63
- 375 Henze AT, Mazzone M. The impact of hypoxia on tumor-associated macrophages. *J Clin Invest* 2016; 126: 3672-9
- 376 Mahase S, Rattenni RN, Wesseling P, et al. Hypoxia-Mediated Mechanisms Associated with Antiangiogenic Treatment Resistance in Glioblastomas. *Am J Pathol* 2017; 187: 940-53
- 377 Ohno M, Miyakita Y, Takahashi M, et al. Survival benefits of hypofractionated radiotherapy combined with temozolomide or temozolomide plus bevacizumab in elderly patients with glioblastoma aged \geq 75 years. *Radiat Oncol* 2019; 14: 200
- 378 Nagpal S, Harsh G, Recht L. Bevacizumab improves quality of life in patients with recurrent glioblastoma. *Chemother Res Pract* 2011; 2011: 602812
- 379 Rich JN. Cancer stem cells: understanding tumor hierarchy and heterogeneity. *Medicine* 2016; 95: S2-S7

References

- 380 Gerlinger M, Swanton C. How Darwinian models inform therapeutic failure initiated by clonal heterogeneity in cancer medicine. *British Journal of Cancer* 2010; 103: 1139-43
- 381 Davis A, Gao R, Navin N. Tumor evolution: Linear, branching, neutral or punctuated? *Biochim Biophys Acta Rev Cancer* 2017; 1867: 151-61
- 382 Bonnet D, Dick JE. Human acute myeloid leukemia is organized as a hierarchy that originates from a primitive hematopoietic cell. *Nat Med* 1997; 3: 730-7
- 383 Ignatova TN, Kukekov VG, Laywell ED, et al. Human cortical glial tumors contain neural stem-like cells expressing astroglial and neuronal markers in vitro. *Glia* 2002; 39: 193-206
- 384 Singh SK, Clarke ID, Terasaki M, et al. Identification of a cancer stem cell in human brain tumors. *Cancer Res* 2003; 63: 5821-8
- 385 Singh SK, Hawkins C, Clarke ID, et al. Identification of human brain tumour initiating cells. *Nature* 2004; 432: 396-401
- 386 Beier D, Hau P, Proescholdt M, et al. CD133(+) and CD133(-) glioblastoma-derived cancer stem cells show differential growth characteristics and molecular profiles. *Cancer Res* 2007; 67: 4010-5
- 387 Gimple RC, Bhargava S, Dixit D, et al. Glioblastoma stem cells: lessons from the tumor hierarchy in a lethal cancer. *Genes Dev* 2019; 33: 591-609
- 388 Bao S, Wu Q, McLendon RE, et al. Glioma stem cells promote radioresistance by preferential activation of the DNA damage response. *Nature* 2006; 444: 756-60
- 389 Chen HY, Lin LT, Wang ML, et al. Musashi-1 regulates AKT-derived IL-6 autocrinal/paracrine malignancy and chemoresistance in glioblastoma. *Oncotarget* 2016; 7: 42485-501
- 390 Auffinger B, Tobias AL, Han Y, et al. Conversion of differentiated cancer cells into cancer stem-like cells in a glioblastoma model after primary chemotherapy. *Cell Death Differ* 2014; 21: 1119-31
- 391 Nishikawa M, Inoue A, Ohnishi T, et al. Significance of Glioma Stem-Like Cells in the Tumor Periphery That Express High Levels of CD44 in Tumor Invasion, Early Progression, and Poor Prognosis in Glioblastoma. *Stem Cells Int* 2018; 2018: 5387041
- 392 Munthe S, Petterson SA, Dahlrot RH, et al. Glioma Cells in the Tumor Periphery Have a Stem Cell Phenotype. *PLoS One* 2016; 11: e0155106
- 393 Munthe S, Sorensen MD, Thomassen M, et al. Migrating glioma cells express stem cell markers and give rise to new tumors upon xenografting. *J Neurooncol* 2016; 130: 53-62
- 394 Hambardzumyan D, Bergers G. Glioblastoma: Defining Tumor Niches. *Trends Cancer* 2015; 1: 252-65
- 395 Ye XZ, Xu SL, Xin YH, et al. Tumor-associated microglia/macrophages enhance the invasion of glioma stem-like cells via TGF-beta1 signaling pathway. *J Immunol* 2012; 189: 444-53
- 396 Li Y, Dong X, Cai J, et al. SERPINA3 induced by astroglia/microglia co-culture facilitates glioblastoma stem-like cell invasion. *Oncol Lett* 2018; 15: 285-91
- 397 Wu A, Wei J, Kong LY, et al. Glioma cancer stem cells induce immunosuppressive macrophages/microglia. *Neuro Oncol* 2010; 12: 1113-25
- 398 Gabrusiewicz K, Li X, Wei J, et al. Glioblastoma stem cell-derived exosomes induce M2 macrophages and PD-L1 expression on human monocytes. *Oncoimmunology* 2018; 7: e1412909
- 399 Otvos B, Silver DJ, Mulkearns-Hubert EE, et al. Cancer Stem Cell-Secreted Macrophage Migration Inhibitory Factor Stimulates Myeloid Derived Suppressor Cell Function and Facilitates Glioblastoma Immune Evasion. *Stem Cells* 2016; 34: 2026-39
- 400 Rasper M, Schafer A, Piontek G, et al. Aldehyde dehydrogenase 1 positive glioblastoma cells show brain tumor stem cell capacity. *Neuro Oncol* 2010; 12: 1024-33
- 401 Sulman E, Goodman L, Le T, et al. A novel marker of glioma stem cells that is prognostic for treatment response and patient outcome. *Cancer Research* 2008; 68: 3777-
- 402 Chen R, Nishimura MC, Bumbaca SM, et al. A hierarchy of self-renewing tumor-initiating cell types in glioblastoma. *Cancer Cell* 2010; 17: 362-75
- 403 Kolenda J, Jensen SS, Aaberg-Jessen C, et al. Effects of hypoxia on expression of a panel of stem cell and chemoresistance markers in glioblastoma-derived spheroids. *J Neurooncol* 2011; 103: 43-58
- 404 Brown DV, Filiz G, Daniel PM, et al. Expression of CD133 and CD44 in glioblastoma stem cells correlates with cell proliferation, phenotype stability and intra-tumor heterogeneity. *PLoS One* 2017; 12: e0172791-e
- 405 Flavahan WA, Wu Q, Hitomi M, et al. Brain tumor initiating cells adapt to restricted nutrition through preferential glucose uptake. *Nat Neurosci* 2013; 16: 1373-82
- 406 Richards LM, Whitley OKN, MacLeod G, et al. Gradient of Developmental and Injury Response transcriptional states defines functional vulnerabilities underpinning glioblastoma heterogeneity. *Nat Cancer* 2021; 2: 157-73
- 407 Flavahan WA, Gaskell E, Bernstein BE. Epigenetic plasticity and the hallmarks of cancer. *Science* 2017; 357: 408
- 408 Venteicher AS, Tirosch I, Hebert C, et al. Decoupling genetics, lineages, and microenvironment in IDH-mutant gliomas by single-cell RNA-seq. *Science* 2017; 355:

References

- 409 Tirosh I, Venteicher AS, Hebert C, et al. Single-cell RNA-seq supports a developmental hierarchy in human oligodendroglioma. *Nature* 2016; 539: 309-13
- 410 Suvà ML, Tirosh I. The Glioma Stem Cell Model in the Era of Single-Cell Genomics. *Cancer Cell* 2020; 37: 630-6
- 411 Louveau A, Harris TH, Kipnis J. Revisiting the Mechanisms of CNS Immune Privilege. *Trends Immunol* 2015; 36: 569-77
- 412 Yoshida TM, Wang A, Hafler DA. Basic principles of neuroimmunology. *Semin Immunopathol* 2022; 44: 685-95
- 413 Aspelund A, Antila S, Proulx ST, et al. A dural lymphatic vascular system that drains brain interstitial fluid and macromolecules. *J Exp Med* 2015; 212: 991-9
- 414 Louveau A, Smirnov I, Keyes TJ, et al. Structural and functional features of central nervous system lymphatic vessels. *Nature* 2015; 523: 337-41
- 415 Louveau A, Herz J, Alme MN, et al. CNS lymphatic drainage and neuroinflammation are regulated by meningeal lymphatic vasculature. *Nat Neurosci* 2018; 21: 1380-91
- 416 Absinta M, Ha SK, Nair G, et al. Human and nonhuman primate meninges harbor lymphatic vessels that can be visualized noninvasively by MRI. *Elife* 2017; 6:
- 417 Møllgård K, Beinlich FRM, Kusk P, et al. A mesothelium divides the subarachnoid space into functional compartments. *Science* 2023; 379: 84-8
- 418 Korin B, Ben-Shaanan TL, Schiller M, et al. High-dimensional, single-cell characterization of the brain's immune compartment. *Nature Neuroscience* 2017; 20: 1300-9
- 419 Mrdjen D, Pavlovic A, Hartmann FJ, et al. High-Dimensional Single-Cell Mapping of Central Nervous System Immune Cells Reveals Distinct Myeloid Subsets in Health, Aging, and Disease. *Immunity* 2018; 48: 380-95.e6
- 420 Van Hove H, Martens L, Scheyltjens I, et al. A single-cell atlas of mouse brain macrophages reveals unique transcriptional identities shaped by ontogeny and tissue environment. *Nat Neurosci* 2019; 22: 1021-35
- 421 Ginhoux F, Greter M, Leboeuf M, et al. Fate mapping analysis reveals that adult microglia derive from primitive macrophages. *Science* 2010; 330: 841-5
- 422 Goldmann T, Wieghofer P, Jordão MJC, et al. Origin, fate and dynamics of macrophages at central nervous system interfaces. *Nature immunology* 2016; 17: 797-805
- 423 Kettenmann H, Hanisch UK, Noda M, et al. Physiology of microglia. *Physiol Rev* 2011; 91: 461-553
- 424 Ransohoff RM, Cardona AE. The myeloid cells of the central nervous system parenchyma. *Nature* 2010; 468: 253-62
- 425 Ajami B, Bennett JL, Krieger C, et al. Local self-renewal can sustain CNS microglia maintenance and function throughout adult life. *Nat Neurosci* 2007; 10: 1538-43
- 426 Stifter SA, Greter M. BAM! Pathogen control at the brain border. *Immunity* 2022; 55: 1969-71
- 427 von Bartheld CS, Bahney J,erculano-Houzel S. The search for true numbers of neurons and glial cells in the human brain: A review of 150 years of cell counting. *J Comp Neurol* 2016; 524: 3865-95
- 428 Nimmerjahn A, Kirchhoff F, Helmchen F. Resting microglial cells are highly dynamic surveillants of brain parenchyma in vivo. *Science* 2005; 308: 1314-8
- 429 Yenyuwadee S, Sanchez-Trincado Lopez JL, Shah R, et al. The evolving role of tissue-resident memory T cells in infections and cancer. *Sci Adv* 2022; 8: eabo5871
- 430 Kierdorf K, Prinz M. Factors regulating microglia activation. *Front Cell Neurosci* 2013; 7: 44
- 431 Engelhardt B, Sorokin L. The blood-brain and the blood-cerebrospinal fluid barriers: function and dysfunction. *Semin Immunopathol* 2009; 31: 497-511
- 432 Schreiber RD, Old LJ, Smyth MJ. Cancer immunoediting: integrating immunity's roles in cancer suppression and promotion. *Science* 2011; 331: 1565-70
- 433 O'Rourke DM, Nasrallah MP, Desai A, et al. A single dose of peripherally infused EGFRvIII-directed CAR T cells mediates antigen loss and induces adaptive resistance in patients with recurrent glioblastoma. *Sci Transl Med* 2017; 9:
- 434 Wang L, Jung J, Babikir H, et al. A single-cell atlas of glioblastoma evolution under therapy reveals cell-intrinsic and cell-extrinsic therapeutic targets. *Nat Cancer* 2022; 3: 1534-52
- 435 Alanio C, Binder ZA, Chang RB, et al. Immunologic Features in De Novo and Recurrent Glioblastoma Are Associated with Survival Outcomes. *Cancer Immunol Res* 2022; 10: 800-10
- 436 D'Angelo A, Kilili H, Chapman R, et al. Immune-related pan-cancer gene expression signatures of patient survival revealed by NanoString-based analyses. *PLoS One* 2023; 18: e0280364
- 437 Pombo Antunes AR, Scheyltjens I, Duerinck J, et al. Understanding the glioblastoma immune microenvironment as basis for the development of new immunotherapeutic strategies. *eLife* 2020; 9: e52176

References

- 438 Lee AH, Sun L, Mochizuki AY, et al. Neoadjuvant PD-1 blockade induces T cell and cDC1 activation but fails to overcome the immunosuppressive tumor associated macrophages in recurrent glioblastoma. *Nat Commun* 2021; 12: 6938
- 439 Gentles AJ, Newman AM, Liu CL, et al. The prognostic landscape of genes and infiltrating immune cells across human cancers. *Nat Med* 2015; 21: 938-45
- 440 de Groot J, Penas-Prado M, Alfaro-Munoz K, et al. Window-of-opportunity clinical trial of pembrolizumab in patients with recurrent glioblastoma reveals predominance of immune-suppressive macrophages. *Neuro Oncol* 2020; 22: 539-49
- 441 Alban TJ, Alvarado AG, Sorensen MD, et al. Global immune fingerprinting in glioblastoma patient peripheral blood reveals immune-suppression signatures associated with prognosis. *JCI Insight* 2018; 3:
- 442 Raychaudhuri B, Rayman P, Huang P, et al. Myeloid derived suppressor cell infiltration of murine and human gliomas is associated with reduction of tumor infiltrating lymphocytes. *J Neurooncol* 2015; 122: 293-301
- 443 Friedmann-Morvinski D, Hambardzumyan D. Monocyte-neutrophil entanglement in glioblastoma. *J Clin Invest* 2023; 133:
- 444 Magod P, Mastandrea I, Rousso-Noori L, et al. Exploring the longitudinal glioma microenvironment landscape uncovers reprogrammed pro-tumorigenic neutrophils in the bone marrow. *Cell Rep* 2021; 36: 109480
- 445 Friedrich M, Hahn M, Michel J, et al. Dysfunctional dendritic cells limit antigen-specific T cell response in glioma. *Neuro Oncol* 2022:
- 446 Close HJ, Stead LF, Nsengimana J, et al. Expression profiling of single cells and patient cohorts identifies multiple immunosuppressive pathways and an altered NK cell phenotype in glioblastoma. *Clin Exp Immunol* 2020; 200: 33-44
- 447 Kemper C, Atkinson JP. T-cell regulation: with complements from innate immunity. *Nat Rev Immunol* 2007; 7: 9-18
- 448 Nesargikar PN, Spiller B, Chavez R. The complement system: history, pathways, cascade and inhibitors. *Eur J Microbiol Immunol (Bp)* 2012; 2: 103-11
- 449 Huber-Lang M, Sarma JV, Zetoune FS, et al. Generation of C5a in the absence of C3: a new complement activation pathway. *Nat Med* 2006; 12: 682-7
- 450 Veerhuis R, Nielsen HM, Tenner AJ. Complement in the brain. *Mol Immunol* 2011; 48: 1592-603
- 451 Zhang R, Liu Q, Li T, et al. Role of the complement system in the tumor microenvironment. *Cancer Cell Int* 2019; 19: 300
- 452 Zhu H, Yu X, Zhang S, et al. Targeting the Complement Pathway in Malignant Glioma Microenvironments. *Front Cell Dev Biol* 2021; 9: 657472
- 453 Mangogna A, Belmonte B, Agostinis C, et al. Prognostic Implications of the Complement Protein C1q in Gliomas. *Front Immunol* 2019; 10: 2366
- 454 Pio R, Ajona D, Ortiz-Espinosa S, et al. Complementing the Cancer-Immunity Cycle. *Front Immunol* 2019; 10: 774
- 455 Mäenpää A, Kovanen PE, Paetau A, et al. Lymphocyte adhesion molecule ligands and extracellular matrix proteins in gliomas and normal brain: expression of VCAM-1 in gliomas. *Acta Neuropathol* 1997; 94: 216-25
- 456 Junnikkala S, Jokiranta TS, Friese MA, et al. Exceptional resistance of human H2 glioblastoma cells to complement-mediated killing by expression and utilization of factor H and factor H-like protein 1. *J Immunol* 2000; 164: 6075-81
- 457 Geller A, Yan J. The Role of Membrane Bound Complement Regulatory Proteins in Tumor Development and Cancer Immunotherapy. *Front Immunol* 2019; 10: 1074
- 458 Wang Y, Zhang H, He YW. The Complement Receptors C3aR and C5aR Are a New Class of Immune Checkpoint Receptor in Cancer Immunotherapy. *Front Immunol* 2019; 10: 1574
- 459 Chen Z, Feng X, Herting CJ, et al. Cellular and Molecular Identity of Tumor-Associated Macrophages in Glioblastoma. *Cancer Res* 2017; 77: 2266-78
- 460 Parney IF, Waldron JS, Parsa AT. Flow cytometry and in vitro analysis of human glioma-associated macrophages. Laboratory investigation. *J Neurosurg* 2009; 110: 572-82
- 461 Pombo Antunes AR, Scheyltjens I, Lodi F, et al. Single-cell profiling of myeloid cells in glioblastoma across species and disease stage reveals macrophage competition and specialization. *Nat Neurosci* 2021; 24: 595-610
- 462 Shinjyo N, Kagaya W, Pekna M. Interaction Between the Complement System and Infectious Agents - A Potential Mechanistic Link to Neurodegeneration and Dementia. *Front Cell Neurosci* 2021; 15: 710390
- 463 Coniglio SJ, Eugenin E, Dobrenis K, et al. Microglial stimulation of glioblastoma invasion involves epidermal growth factor receptor (EGFR) and colony stimulating factor 1 receptor (CSF-1R) signaling. *Mol Med* 2012; 18: 519-27
- 464 Sielska M, Przanowski P, Wylot B, et al. Distinct roles of CSF family cytokines in macrophage infiltration and activation in glioma progression and injury response. *J Pathol* 2013:

References

- 465 Platten M, Kretz A, Naumann U, et al. Monocyte chemoattractant protein-1 increases microglial infiltration and aggressiveness of gliomas. *Annals of Neurology* 2003; 54: 388-92
- 466 Jung Y, Ahn SH, Park H, et al. MCP-1 and MIP-3 α Secreted from Necrotic Cell-Treated Glioblastoma Cells Promote Migration/Infiltration of Microglia. *Cell Physiol Biochem* 2018; 48: 1332-46
- 467 Okada M, Saio M, Kito Y, et al. Tumor-associated macrophage/microglia infiltration in human gliomas is correlated with MCP-3, but not MCP-1. *Int J Oncol* 2009; 34: 1621-7
- 468 Gabrusiewicz K, Ellert-Miklaszewska A, Lipko M, et al. Characteristics of the alternative phenotype of microglia/macrophages and its modulation in experimental gliomas. *PLoS One* 2011; 6: e23902
- 469 Held-Feindt J, Hattermann K, Muerkoster SS, et al. CX3CR1 promotes recruitment of human glioma-infiltrating microglia/macrophages (GIMs). *Exp Cell Res* 2010; 316: 1553-66
- 470 Wang SC, Hong JH, Hsueh C, et al. Tumor-secreted SDF-1 promotes glioma invasiveness and TAM tropism toward hypoxia in a murine astrocytoma model. *Lab Invest* 2012; 92: 151-62
- 471 Wang X, Li C, Chen Y, et al. Hypoxia enhances CXCR4 expression favoring microglia migration via HIF-1 α activation. *Biochem Biophys Res Commun* 2008; 371: 283-8
- 472 Liu H, Sun Y, Zhang Q, et al. Pro-inflammatory and proliferative microglia drive progression of glioblastoma. *Cell Rep* 2021; 36: 109718
- 473 Lamano JB, Lamano JB, Li YD, et al. Glioblastoma-Derived IL6 Induces Immunosuppressive Peripheral Myeloid Cell PD-L1 and Promotes Tumor Growth. *Clinical cancer research : an official journal of the American Association for Cancer Research* 2019; 25: 3643-57
- 474 Voisin P, Bouchaud V, Merle M, et al. Microglia in close vicinity of glioma cells: correlation between phenotype and metabolic alterations. *Front Neuroenergetics* 2010; 2: 131
- 475 Wagner S, Czub S, Greif M, et al. Microglial/macrophage expression of interleukin 10 in human glioblastomas. *Int J Cancer* 1999; 82: 12-6
- 476 Zhang J, Sarkar S, Cua R, et al. A dialog between glioma and microglia that promotes tumor invasiveness through the CCL2/CCR2/interleukin-6 axis. *Carcinogenesis* 2012; 33: 312-9
- 477 Li J, Kaneda MM, Ma J, et al. PI3K γ inhibition suppresses microglia/TAM accumulation in glioblastoma microenvironment to promote exceptional temozolomide response. *Proc Natl Acad Sci U S A* 2021; 118:
- 478 Ellert-Miklaszewska A, Dabrowski M, Lipko M, et al. Molecular definition of the pro-tumorigenic phenotype of glioma-activated microglia. *Glia* 2013; 61: 1178-90
- 479 Wang C, Chen Q, Chen M, et al. Interaction of glioma-associated microglia/macrophages and anti-PD1 immunotherapy. *Cancer Immunol Immunother* 2023:
- 480 Markovic DS, Vinnakota K, Chirasani S, et al. Gliomas induce and exploit microglial MT1-MMP expression for tumor expansion. *Proc Natl Acad Sci U S A* 2009; 106: 12530-5
- 481 Hu F, Ku MC, Markovic D, et al. Glioma-associated microglial MMP9 expression is upregulated by TLR2 signaling and sensitive to minocycline. *Int J Cancer* 2014; 135: 2569-78
- 482 Bettinger I, Thanos S, Paulus W. Microglia promote glioma migration. *Acta Neuropathol* 2002; 103: 351-5
- 483 Zhang L, Xu Y, Sun J, et al. M2-like tumor-associated macrophages drive vasculogenic mimicry through amplification of IL-6 expression in glioma cells. *Oncotarget* 2017; 8: 819-32
- 484 Antonios JP, Soto H, Everson RG, et al. Immunosuppressive tumor-infiltrating myeloid cells mediate adaptive immune resistance via a PD-1/PD-L1 mechanism in glioblastoma. *Neuro Oncol* 2017; 19: 796-807
- 485 Aslan K, Turco V, Blobner J, et al. Heterogeneity of response to immune checkpoint blockade in hypermutated experimental gliomas. *Nat Commun* 2020; 11: 931
- 486 Leblond MM, Pères EA, Helaine C, et al. M2 macrophages are more resistant than M1 macrophages following radiation therapy in the context of glioblastoma. *Oncotarget* 2017; 8: 72597-612
- 487 Kioi M, Vogel H, Schultz G, et al. Inhibition of vasculogenesis, but not angiogenesis, prevents the recurrence of glioblastoma after irradiation in mice. *J Clin Invest* 2010; 120: 694-705
- 488 Engblom C, Pfirschke C, Pittet MJ. The role of myeloid cells in cancer therapies. *Nat Rev Cancer* 2016; 16: 447-62
- 489 Wei Q, Singh O, Ekinici C, et al. TNF α secreted by glioma associated macrophages promotes endothelial activation and resistance against anti-angiogenic therapy. *Acta Neuropathol Commun* 2021; 9: 67
- 490 Paolicelli RC, Sierra A, Stevens B, et al. Microglia states and nomenclature: A field at its crossroads. *Neuron* 2022; 110: 3458-83
- 491 Holness CL, Simmons DL. Molecular Cloning of CD68, a Human Macrophage Marker Related to Lysosomal Glycoproteins. *Blood* 1993; 81: 1607-13
- 492 Paulus W, Roggendorf W, Kirchner T. Ki-M1P as a marker for microglia and brain macrophages in routinely processed human tissues. *Acta Neuropathol* 1992; 84: 538-44
- 493 Nishie A, Ono M, Shono T, et al. Macrophage infiltration and heme oxygenase-1 expression correlate with angiogenesis in human gliomas. *Clin Cancer Res* 1999; 5: 1107-13

References

- 494 Brandenburg S, Müller A, Turkowski K, et al. Resident microglia rather than peripheral macrophages promote vascularization in brain tumors and are source of alternative pro-angiogenic factors. *Acta Neuropathol* 2016; 131: 365-78
- 495 Yin W, Ping YF, Li F, et al. A map of the spatial distribution and tumour-associated macrophage states in glioblastoma and grade 4 IDH-mutant astrocytoma. *J Pathol* 2022; 258: 121-35
- 496 Kiss M, Van Gassen S, Movahedi K, et al. Myeloid cell heterogeneity in cancer: not a single cell alike. *Cell Immunol* 2018; 330: 188-201
- 497 Mantovani A, Sozzani S, Locati M, et al. Macrophage polarization: tumor-associated macrophages as a paradigm for polarized M2 mononuclear phagocytes. *Trends Immunol* 2002; 23: 549-55
- 498 Martinez-Lage M, Lynch TM, Bi Y, et al. Immune landscapes associated with different glioblastoma molecular subtypes. *Acta Neuropathologica Communications* 2019; 7: 203
- 499 PrabhuDas MR, Baldwin CL, Bollyky PL, et al. A Consensus Definitive Classification of Scavenger Receptors and Their Roles in Health and Disease. *J Immunol* 2017; 198: 3775-89
- 500 Sankowski R, Böttcher C, Masuda T, et al. Mapping microglia states in the human brain through the integration of high-dimensional techniques. *Nat Neurosci* 2019; 22: 2098-110
- 501 Muñoz-Rojas AR, Kelsey I, Pappalardo JL, et al. Co-stimulation with opposing macrophage polarization cues leads to orthogonal secretion programs in individual cells. *Nat Commun* 2021; 12: 301
- 502 Erbani J, Boon M, Akkari L. Therapy-induced shaping of the glioblastoma microenvironment: Macrophages at play. *Semin Cancer Biol* 2022; 86: 41-56
- 503 Khan F, Pang L, Dunterman M, et al. Macrophages and microglia in glioblastoma: heterogeneity, plasticity, and therapy. *J Clin Invest* 2023; 133:
- 504 Flores-Toro JA, Luo D, Gopinath A, et al. CCR2 inhibition reduces tumor myeloid cells and unmasks a checkpoint inhibitor effect to slow progression of resistant murine gliomas. *Proc Natl Acad Sci U S A* 2020; 117: 1129-38
- 505 Pyonteck SM, Akkari L, Schuhmacher AJ, et al. CSF-1R inhibition alters macrophage polarization and blocks glioma progression. *Nat Med* 2013; 19: 1264-72
- 506 Yan D, Kowal J, Akkari L, et al. Inhibition of colony stimulating factor-1 receptor abrogates microenvironment-mediated therapeutic resistance in gliomas. *Oncogene* 2017; 36: 6049-58
- 507 Akkari L, Bowman RL, Tessier J, et al. Dynamic changes in glioma macrophage populations after radiotherapy reveal CSF-1R inhibition as a strategy to overcome resistance. *Sci Transl Med* 2020; 12:
- 508 Quail DF, Bowman RL, Akkari L, et al. The tumor microenvironment underlies acquired resistance to CSF-1R inhibition in gliomas. *Science* 2016; 352: aad3018
- 509 Stafford JH, Hirai T, Deng L, et al. Colony stimulating factor 1 receptor inhibition delays recurrence of glioblastoma after radiation by altering myeloid cell recruitment and polarization. *Neuro Oncol* 2016; 18: 797-806
- 510 Przystal JM, Becker H, Canjuga D, et al. Targeting CSF1R Alone or in Combination with PD1 in Experimental Glioma. *Cancers (Basel)* 2021; 13:
- 511 Hutter G, Theruvath J, Graef CM, et al. Microglia are effector cells of CD47-SIRP α antiphagocytic axis disruption against glioblastoma. *Proc Natl Acad Sci U S A* 2019; 116: 997-1006
- 512 Colman H, Raizer JJ, Walbert T, et al. Phase 1b/2 study of pexidartinib (PEX) in combination with radiation therapy (XRT) and temozolomide (TMZ) in newly diagnosed glioblastoma. *Journal of Clinical Oncology* 2018; 36: 2015-
- 513 Lohr J, Ratliff T, Huppertz A, et al. Effector T-cell infiltration positively impacts survival of glioblastoma patients and is impaired by tumor-derived TGF- β . *Clin Cancer Res* 2011; 17: 4296-308
- 514 Heimberger AB, Abou-Ghazal M, Reina-Ortiz C, et al. Incidence and prognostic impact of FoxP3⁺ regulatory T cells in human gliomas. *Clin Cancer Res* 2008; 14: 5166-72
- 515 Weenink B, Draaisma K, Ooi HZ, et al. Low-grade glioma harbors few CD8 T cells, which is accompanied by decreased expression of chemo-attractants, not immunogenic antigens. *Sci Rep* 2019; 9: 14643
- 516 Zhang W, Wu S, Guo K, et al. Correlation and clinical significance of LC3, CD68⁺ microglia, CD4⁺ T lymphocytes, and CD8⁺ T lymphocytes in gliomas. *Clin Neurol Neurosurg* 2018; 168: 167-74
- 517 Han S, Ma E, Wang X, et al. Rescuing defective tumor-infiltrating T-cell proliferation in glioblastoma patients. *Oncol Lett* 2016; 12: 2924-9
- 518 Raphael I, Nalawade S, Eagar TN, et al. T cell subsets and their signature cytokines in autoimmune and inflammatory diseases. *Cytokine* 2015; 74: 5-17
- 519 Yamaguchi T, Wing JB, Sakaguchi S. Two modes of immune suppression by Foxp3(+) regulatory T cells under inflammatory or non-inflammatory conditions. *Semin Immunol* 2011; 23: 424-30
- 520 Rosenblum MD, Way SS, Abbas AK. Regulatory T cell memory. *Nat Rev Immunol* 2016; 16: 90-101
- 521 Kaech SM, Cui W. Transcriptional control of effector and memory CD8⁺ T cell differentiation. *Nat Rev Immunol* 2012; 12: 749-61

References

- 522 Mu L, Yang C, Gao Q, et al. CD4⁺ and Perivascular Foxp3⁺ T Cells in Glioma Correlate with Angiogenesis and Tumor Progression. *Front Immunol* 2017; 8: 1451
- 523 Jacobs JF, Idema AJ, Bol KF, et al. Regulatory T cells and the PD-L1/PD-1 pathway mediate immune suppression in malignant human brain tumors. *Neuro Oncol* 2009; 11: 394-402
- 524 Yang I, Tihan T, Han SJ, et al. CD8⁺ T-cell infiltrate in newly diagnosed glioblastoma is associated with long-term survival. *J Clin Neurosci* 2010; 17: 1381-5
- 525 Madkouri R, Kaderbhai CG, Bertaut A, et al. Immune classifications with cytotoxic CD8(+) and Th17 infiltrates are predictors of clinical prognosis in glioblastoma. *Oncoimmunology* 2017; 6: e1321186
- 526 Sayour EJ, McLendon P, McLendon R, et al. Increased proportion of FoxP3⁺ regulatory T cells in tumor infiltrating lymphocytes is associated with tumor recurrence and reduced survival in patients with glioblastoma. *Cancer Immunol Immunother* 2015; 64: 419-27
- 527 Jacobs JF, Idema AJ, Bol KF, et al. Prognostic significance and mechanism of Treg infiltration in human brain tumors. *J Neuroimmunol* 2010; 225: 195-9
- 528 Yue Q, Zhang X, Ye HX, et al. The prognostic value of Foxp3⁺ tumor-infiltrating lymphocytes in patients with glioblastoma. *J Neurooncol* 2014; 116: 251-9
- 529 Chang AL, Miska J, Wainwright DA, et al. CCL2 Produced by the Glioma Microenvironment Is Essential for the Recruitment of Regulatory T Cells and Myeloid-Derived Suppressor Cells. *Cancer Res* 2016; 76: 5671-82
- 530 Wainwright DA, Balyasnikova IV, Chang AL, et al. IDO expression in brain tumors increases the recruitment of regulatory T cells and negatively impacts survival. *Clin Cancer Res* 2012; 18: 6110-21
- 531 Fecci PE, Mitchell DA, Whitesides JF, et al. Increased regulatory T-cell fraction amidst a diminished CD4 compartment explains cellular immune defects in patients with malignant glioma. *Cancer Res* 2006; 66: 3294-302
- 532 Wherry EJ, Kurachi M. Molecular and cellular insights into T cell exhaustion. *Nat Rev Immunol* 2015; 15: 486-99
- 533 Bloch O, Crane CA, Kaur R, et al. Gliomas promote immunosuppression through induction of B7-H1 expression in tumor-associated macrophages. *Clin Cancer Res* 2013; 19: 3165-75
- 534 Berghoff AS, Kiesel B, Widhalm G, et al. Programmed death ligand 1 expression and tumor-infiltrating lymphocytes in glioblastoma. *Neuro Oncol* 2015; 17: 1064-75
- 535 Alexandrov LB, Nik-Zainal S, Wedge DC, et al. Signatures of mutational processes in human cancer. *Nature* 2013; 500: 415-21
- 536 Chongsathidkiet P, Jackson C, Koyama S, et al. Sequestration of T cells in bone marrow in the setting of glioblastoma and other intracranial tumors. *Nat Med* 2018; 24: 1459-68
- 537 Watowich MB, Gilbert MR, Larion M. T cell exhaustion in malignant gliomas. *Trends Cancer* 2023:
- 538 Ott M, Tomaszowski KH, Marisetty A, et al. Profiling of patients with glioma reveals the dominant immunosuppressive axis is refractory to immune function restoration. *JCI Insight* 2020; 5:
- 539 Davidson TB, Lee A, Hsu M, et al. Expression of PD-1 by T Cells in Malignant Glioma Patients Reflects Exhaustion and Activation. *Clin Cancer Res* 2019; 25: 1913-22
- 540 Goods BA, Hernandez AL, Lowther DE, et al. Functional differences between PD-1⁺ and PD-1⁻ CD4⁺ effector T cells in healthy donors and patients with glioblastoma multiforme. *PLoS One* 2017; 12: e0181538
- 541 Lowther DE, Goods BA, Lucca LE, et al. PD-1 marks dysfunctional regulatory T cells in malignant gliomas. *JCI Insight* 2016; 1:
- 542 Woroniecka K, Chongsathidkiet P, Rhodin K, et al. T-Cell Exhaustion Signatures Vary with Tumor Type and Are Severe in Glioblastoma. *Clin Cancer Res* 2018; 24: 4175-86
- 543 Park J, Kwon M, Kim KH, et al. Immune Checkpoint Inhibitor-induced Reinvigoration of Tumor-infiltrating CD8(+) T Cells is Determined by Their Differentiation Status in Glioblastoma. *Clin Cancer Res* 2019; 25: 2549-59
- 544 Mohme M, Schliffke S, Maire CL, et al. Immunophenotyping of Newly Diagnosed and Recurrent Glioblastoma Defines Distinct Immune Exhaustion Profiles in Peripheral and Tumor-infiltrating Lymphocytes. *Clin Cancer Res* 2018:
- 545 Alegre M-L, Frauwirth KA, Thompson CB. T-cell regulation by CD28 and CTLA-4. *Nature Reviews Immunology* 2001; 1: 220-8
- 546 Buzzatti G, Dellepiane C, Del Mastro L. New emerging targets in cancer immunotherapy: the role of GITR. *ESMO Open* 2020; 4: e000738
- 547 Chiang EY, Mellman I. TIGIT-CD226-PVR axis: advancing immune checkpoint blockade for cancer immunotherapy. *J Immunother Cancer* 2022; 10:
- 548 Francisco LM, Sage PT, Sharpe AH. The PD-1 pathway in tolerance and autoimmunity. *Immunol Rev* 2010; 236: 219-42
- 549 Kandel S, Adhikary P, Li G, et al. The TIM3/Gal9 signaling pathway: An emerging target for cancer immunotherapy. *Cancer Lett* 2021; 510: 67-78
- 550 Gaikwad S, Agrawal MY, Kaushik I, et al. Immune checkpoint proteins: Signaling mechanisms and molecular interactions in cancer immunotherapy. *Semin Cancer Biol* 2022; 86: 137-50

References

- 551 Chocarro L, Blanco E, Zuazo M, et al. Understanding LAG-3 Signaling. *Int J Mol Sci* 2021; 22:
- 552 Larkin J, Chiarion-Sileni V, Gonzalez R, et al. Combined Nivolumab and Ipilimumab or Monotherapy in Untreated Melanoma. *N Engl J Med* 2015; 373: 23-34
- 553 Long GV, Atkinson V, Lo S, et al. Combination nivolumab and ipilimumab or nivolumab alone in melanoma brain metastases: a multicentre randomised phase 2 study. *Lancet Oncol* 2018; 19: 672-81
- 554 Goldberg SB, Schalper KA, Gettinger SN, et al. Pembrolizumab for management of patients with NSCLC and brain metastases: long-term results and biomarker analysis from a non-randomised, open-label, phase 2 trial. *Lancet Oncol* 2020; 21: 655-63
- 555 Brahmer J, Reckamp KL, Baas P, et al. Nivolumab versus Docetaxel in Advanced Squamous-Cell Non-Small-Cell Lung Cancer. *N Engl J Med* 2015; 373: 123-35
- 556 de Castro G, Jr., Kudaba I, Wu YL, et al. Five-Year Outcomes With Pembrolizumab Versus Chemotherapy as First-Line Therapy in Patients With Non-Small-Cell Lung Cancer and Programmed Death Ligand-1 Tumor Proportion Score $\geq 1\%$ in the KEYNOTE-042 Study. *J Clin Oncol* 2022; Jco2102885
- 557 Motzer RJ, Escudier B, McDermott DF, et al. Survival outcomes and independent response assessment with nivolumab plus ipilimumab versus sunitinib in patients with advanced renal cell carcinoma: 42-month follow-up of a randomized phase 3 clinical trial. *J Immunother Cancer* 2020; 8:
- 558 McGranahan N, Furness AJ, Rosenthal R, et al. Clonal neoantigens elicit T cell immunoreactivity and sensitivity to immune checkpoint blockade. *Science* 2016; 351: 1463-9
- 559 Samstein RM, Lee CH, Shoushtari AN, et al. Tumor mutational load predicts survival after immunotherapy across multiple cancer types. *Nat Genet* 2019; 51: 202-6
- 560 Goodman AM, Kato S, Bazhenova L, et al. Tumor Mutational Burden as an Independent Predictor of Response to Immunotherapy in Diverse Cancers. *Mol Cancer Ther* 2017; 16: 2598-608
- 561 Nduom EK, Wei J, Yaghi NK, et al. PD-L1 expression and prognostic impact in glioblastoma. *Neuro-Oncology* 2015; 18: 195-205
- 562 Knudsen AM, Rudkjøbing SJ, Sørensen MD, et al. Expression and Prognostic Value of the Immune Checkpoints Galectin-9 and PD-L1 in Glioblastomas. *J Neuropathol Exp Neurol* 2021; 80: 541-51
- 563 Chen RQ, Liu F, Qiu XY, et al. The Prognostic and Therapeutic Value of PD-L1 in Glioma. *Front Pharmacol* 2018; 9: 1503
- 564 Nduom EK, Wei J, Yaghi NK, et al. PD-L1 expression and prognostic impact in glioblastoma. *Neuro Oncol* 2016; 18: 195-205
- 565 Reardon DA, Gokhale PC, Klein SR, et al. Glioblastoma Eradication Following Immune Checkpoint Blockade in an Orthotopic, Immunocompetent Model. *Cancer Immunol Res* 2016; 4: 124-35
- 566 Kim JE, Patel MA, Mangraviti A, et al. Combination Therapy with Anti-PD-1, Anti-TIM-3, and Focal Radiation Results in Regression of Murine Gliomas. *Clin Cancer Res* 2017; 23: 124-36
- 567 Zeng J, See AP, Phallen J, et al. Anti-PD-1 blockade and stereotactic radiation produce long-term survival in mice with intracranial gliomas. *Int J Radiat Oncol Biol Phys* 2013; 86: 343-9
- 568 Belcaid Z, Phallen JA, Zeng J, et al. Focal radiation therapy combined with 4-1BB activation and CTLA-4 blockade yields long-term survival and a protective antigen-specific memory response in a murine glioma model. *PLoS One* 2014; 9: e101764
- 569 Park J, Kim CG, Shim JK, et al. Effect of combined anti-PD-1 and temozolomide therapy in glioblastoma. *Oncoimmunology* 2019; 8: e1525243
- 570 Wainwright DA, Chang AL, Dey M, et al. Durable therapeutic efficacy utilizing combinatorial blockade against IDO, CTLA-4, and PD-L1 in mice with brain tumors. *Clin Cancer Res* 2014; 20: 5290-301
- 571 Sakuishi K, Apetoh L, Sullivan JM, et al. Targeting Tim-3 and PD-1 pathways to reverse T cell exhaustion and restore anti-tumor immunity. *J Exp Med* 2010; 207: 2187-94
- 572 Koyama S, Akbay EA, Li YY, et al. Adaptive resistance to therapeutic PD-1 blockade is associated with upregulation of alternative immune checkpoints. *Nat Commun* 2016; 7: 10501
- 573 Benci JL, Xu B, Qiu Y, et al. Tumor Interferon Signaling Regulates a Multigenic Resistance Program to Immune Checkpoint Blockade. *Cell* 2016; 167: 1540-54.e12
- 574 Qian J, Wang C, Wang B, et al. The IFN-gamma/PD-L1 axis between T cells and tumor microenvironment: hints for glioma anti-PD-1/PD-L1 therapy. *J Neuroinflammation* 2018; 15: 290
- 575 Cao TQ, Wainwright DA, Lee-Chang C, et al. Next Steps for Immunotherapy in Glioblastoma. *Cancers (Basel)* 2022; 14:
- 576 Prichard JW. Overview of automated immunohistochemistry. *Archives of pathology & laboratory medicine* 2014; 138: 1578-82
- 577 Ramos-Vara JA. Technical aspects of immunohistochemistry. *Vet Pathol* 2005; 42: 405-26
- 578 Vyberg M. Anvendt immunhistokemi. 7th ed: Academic Books. 2008

References

- 579 Werner M, Chott A, Fabiano A, et al. Effect of formalin tissue fixation and processing on immunohistochemistry. *The American journal of surgical pathology* 2000; 24: 1016-9
- 580 Shi SR, Key ME, Kalra KL. Antigen retrieval in formalin-fixed, paraffin-embedded tissues: an enhancement method for immunohistochemical staining based on microwave oven heating of tissue sections. *The journal of histochemistry and cytochemistry : official journal of the Histochemistry Society* 1991; 39: 741-8
- 581 Im K, Mareninov S, Diaz MFP, et al. An Introduction to Performing Immunofluorescence Staining. *Methods in molecular biology (Clifton, NJ)* 2019; 1897: 299-311
- 582 Ramos-Vara JA. Principles and Methods of Immunohistochemistry. In *Drug Safety Evaluation: Methods and Protocols* Ed. J-C Gautier. New York, NY: Springer New York. 2017: 115-28
- 583 Stack EC, Wang C, Roman KA, et al. Multiplexed immunohistochemistry, imaging, and quantitation: A review, with an assessment of Tyramide signal amplification, multispectral imaging and multiplex analysis. *Methods* 2014; 70: 46-58
- 584 Lambert TJ. FPbase: a community-editable fluorescent protein database. *Nature Methods* 2019; 16: 277-8
- 585 Gerdes MJ, Sevinsky CJ, Sood A, et al. Highly multiplexed single-cell analysis of formalin-fixed, paraffin-embedded cancer tissue. *Proc Natl Acad Sci U S A* 2013; 110: 11982-7
- 586 Morrison LE, Lefever MR, Behman LJ, et al. Brightfield multiplex immunohistochemistry with multispectral imaging. *Lab Invest* 2020; 100: 1124-36
- 587 Akturk G, Sweeney R, Remark R, et al. Multiplexed Immunohistochemical Consecutive Staining on Single Slide (MICSSS): Multiplexed Chromogenic IHC Assay for High-Dimensional Tissue Analysis. In *Biomarkers for Immunotherapy of Cancer: Methods and Protocols* Eds. M Thurin, A Cesano, FM Marincola. New York, NY: Springer New York. 2020: 497-519
- 588 Rakaee M, Busund L-TR, Jamaly S, et al. Prognostic Value of Macrophage Phenotypes in Resectable Non-Small Cell Lung Cancer Assessed by Multiplex Immunohistochemistry. *Neoplasia* 2019; 21: 282-93
- 589 Ilie M, Beaulande M, Ben Hadj S, et al. Chromogenic Multiplex Immunohistochemistry Reveals Modulation of the Immune Microenvironment Associated with Survival in Elderly Patients with Lung Adenocarcinoma. *Cancers (Basel)* 2018; 10:
- 590 Zhang W, Hubbard A, Jones T, et al. Fully automated 5-plex fluorescent immunohistochemistry with tyramide signal amplification and same species antibodies. *Lab Invest* 2017; 97: 873-85
- 591 Saylor J, Ma Z, Goodridge HS, et al. Spatial Mapping of Myeloid Cells and Macrophages by Multiplexed Tissue Staining. *Front Immunol* 2018; 9: 2925
- 592 Yaghoobi V, Martinez-Morilla S, Liu Y, et al. Advances in quantitative immunohistochemistry and their contribution to breast cancer. *Expert Rev Mol Diagn* 2020; 20: 509-22
- 593 Ilie M, Beaulande M, Hamila M, et al. Automated chromogenic multiplexed immunohistochemistry assay for diagnosis and predictive biomarker testing in non-small cell lung cancer. *Lung Cancer* 2018; 124: 90-4
- 594 Day WA, Lefever MR, Ochs RL, et al. Covalently deposited dyes: a new chromogen paradigm that facilitates analysis of multiple biomarkers in situ. *Lab Invest* 2017; 97: 104-13
- 595 Pandey S, Bodas D. High-quality quantum dots for multiplexed bioimaging: A critical review. *Adv Colloid Interface Sci* 2020; 278: 102137
- 596 Fountaine TJ, Wincovitch SM, Geho DH, et al. Multispectral imaging of clinically relevant cellular targets in tonsil and lymphoid tissue using semiconductor quantum dots. *Modern Pathology* 2006; 19: 1181-91
- 597 Goltsev Y, Samusik N, Kennedy-Darling J, et al. Deep Profiling of Mouse Splenic Architecture with CODEX Multiplexed Imaging. *Cell* 2018; 174: 968-81.e15
- 598 Kennedy-Darling J, Bhate SS, Hickey JW, et al. Highly multiplexed tissue imaging using repeated oligonucleotide exchange reaction. *Eur J Immunol* 2021; 51: 1262-77
- 599 Dowsett M, Nielsen TO, A'Hern R, et al. Assessment of Ki67 in breast cancer: recommendations from the International Ki67 in Breast Cancer working group. *J Natl Cancer Inst* 2011; 103: 1656-64
- 600 Riber-Hansen R, Vainer B, Steiniche T. Digital image analysis: a review of reproducibility, stability and basic requirements for optimal results. *Apmis* 2012; 120: 276-89
- 601 Hamilton PW, Bankhead P, Wang Y, et al. Digital pathology and image analysis in tissue biomarker research. *Methods* 2014; 70: 59-73
- 602 Nielsen LAG, Bangsø JA, Lindahl KH, et al. Evaluation of the proliferation marker Ki-67 in gliomas: Interobserver variability and digital quantification. *Diagn Pathol* 2018; 13: 38
- 603 Dahlrot RH, Sorensen MD, Rosager AM, et al. Novel approaches for quantifying protein biomarkers in gliomas: benefits and pitfalls. *CNS Oncol* 2014; 3: 287-98
- 604 Nielsen PS, Bentzer NK, Jensen V, et al. Immunohistochemical Ki-67/KL1 double stains increase accuracy of Ki-67 indices in breast cancer and simplify automated image analysis. *Appl Immunohistochem Mol Morphol* 2014; 22: 568-76

References

- 605 Coleman KE, Brat DJ, Cotsonis GA, et al. Proliferation (MIB-1 expression) in oligodendrogliomas: assessment of quantitative methods and prognostic significance. *Appl Immunohistochem Mol Morphol* 2006; 14: 109-14
- 606 Lejeune M, Jaén J, Pons L, et al. Quantification of diverse subcellular immunohistochemical markers with clinicobiological relevancies: validation of a new computer-assisted image analysis procedure. *J Anat* 2008; 212: 868-78
- 607 Brüggmann A, Eld M, Lelkaitis G, et al. Digital image analysis of membrane connectivity is a robust measure of HER2 immunostains. *Breast Cancer Research and Treatment* 2012; 132: 41-9
- 608 Laurinaviciene A, Dasevicius D, Ostapenko V, et al. Membrane connectivity estimated by digital image analysis of HER2 immunohistochemistry is concordant with visual scoring and fluorescence in situ hybridization results: algorithm evaluation on breast cancer tissue microarrays. *Diagn Pathol* 2011; 6: 87
- 609 Camp RL, Dolled-Filhart M, King BL, et al. Quantitative analysis of breast cancer tissue microarrays shows that both high and normal levels of HER2 expression are associated with poor outcome. *Cancer Res* 2003; 63: 1445-8
- 610 Holten-Rossing H, Talman MM, Jylling AMB, et al. Application of automated image analysis reduces the workload of manual screening of sentinel lymph node biopsies in breast cancer. *Histopathology* 2017; 71: 866-73
- 611 Brown DL. Practical Stereology Applications for the Pathologist. *Vet Pathol* 2017; 54: 358-68
- 612 Boyce RW, Dorph-Petersen KA, Lyck L, et al. Design-based stereology: introduction to basic concepts and practical approaches for estimation of cell number. *Toxicol Pathol* 2010; 38: 1011-25
- 613 Brown DL. Bias in image analysis and its solution: unbiased stereology. *J Toxicol Pathol* 2017; 30: 183-91
- 614 Reis PP, Waldron L, Goswami RS, et al. mRNA transcript quantification in archival samples using multiplexed, color-coded probes. *BMC Biotechnology* 2011; 11: 46
- 615 Eastel JM, Lam KW, Lee NL, et al. Application of NanoString technologies in companion diagnostic development. *Expert Rev Mol Diagn* 2019; 19: 591-8
- 616 Veldman-Jones MH, Brant R, Rooney C, et al. Evaluating Robustness and Sensitivity of the NanoString Technologies nCounter Platform to Enable Multiplexed Gene Expression Analysis of Clinical Samples. *Cancer Research* 2015; 75: 2587-93
- 617 Veldman-Jones MH, Lai Z, Wappett M, et al. Reproducible, Quantitative, and Flexible Molecular Subtyping of Clinical DLBCL Samples Using the NanoString nCounter System. *Clin Cancer Res* 2015; 21: 2367-78
- 618 Tsang HF, Xue VW, Koh SP, et al. NanoString, a novel digital color-coded barcode technology: current and future applications in molecular diagnostics. *Expert Rev Mol Diagn* 2017; 17: 95-103
- 619 Moyes KW, Davis A, Høglund V, et al. Effects of tumor grade and dexamethasone on myeloid cells in patients with glioma. *Oncoimmunology* 2018; 7: e1507668-e
- 620 Nielsen T, Wallden B, Schaper C, et al. Analytical validation of the PAM50-based Prosigna Breast Cancer Prognostic Gene Signature Assay and nCounter Analysis System using formalin-fixed paraffin-embedded breast tumor specimens. *BMC Cancer* 2014; 14: 177
- 621 Wallden B, Storhoff J, Nielsen T, et al. Development and verification of the PAM50-based Prosigna breast cancer gene signature assay. *BMC Med Genomics* 2015; 8: 54
- 622 Lira ME, Kim TM, Huang D, et al. Multiplexed gene expression and fusion transcript analysis to detect ALK fusions in lung cancer. *J Mol Diagn* 2013; 15: 51-61
- 623 Hu D, Zhou W, Wang F, et al. Development of a NanoString assay to detect leukemogenic fusion transcripts in acute myeloid leukemia. *Int J Lab Hematol* 2016; 38: 663-73
- 624 Scott DW, Abrisqueta P, Wright GW, et al. New Molecular Assay for the Proliferation Signature in Mantle Cell Lymphoma Applicable to Formalin-Fixed Paraffin-Embedded Biopsies. *J Clin Oncol* 2017; 35: 1668-77
- 625 Parker JS, Mullins M, Cheang MC, et al. Supervised risk predictor of breast cancer based on intrinsic subtypes. *J Clin Oncol* 2009; 27: 1160-7
- 626 Jensen MB, Lænkholm AV, Balslev E, et al. The Prosigna 50-gene profile and responsiveness to adjuvant anthracycline-based chemotherapy in high-risk breast cancer patients. *NPJ Breast Cancer* 2020; 6: 7
- 627 Beier CP, Rasmussen T, Dahlrot RH, et al. Aberrant neuronal differentiation is common in glioma but is associated neither with epileptic seizures nor with better survival. *Scientific reports* 2018; 8: 14965
- 628 Dahlrot RH, Hansen S, Herrstedt J, et al. Prognostic value of Musashi-1 in gliomas. *Journal of neuro-oncology* 2013; 115: 453-61
- 629 Dahlrot RH, Hansen S, Jensen SS, et al. Clinical value of CD133 and nestin in patients with glioma: a population-based study. *International journal of clinical and experimental pathology* 2014; 7: 3739-51
- 630 Dahlrot RH, Kristensen BW, Hjelmborg J, et al. A population-based study of low-grade gliomas and mutated isocitrate dehydrogenase 1 (IDH1). *Journal of neuro-oncology* 2013; 114: 309-17
- 631 Fosmark S, Hellwege S, Dahlrot RH, et al. APNG as a prognostic marker in patients with glioblastoma. *PloS one* 2017; 12: e0178693
- 632 Rosager AM, Sorensen MD, Dahlrot RH, et al. Expression and prognostic value of JAM-A in gliomas. *Journal of neuro-oncology* 2017; 135: 107-17

References

- 633 Woehrer A, Sander P, Haberler C, et al. FISH-based detection of 1p 19q codeletion in oligodendroglial tumors: procedures and protocols for neuropathological practice - a publication under the auspices of the Research Committee of the European Confederation of Neuropathological Societies (Euro-CNS). *Clinical neuropathology* 2011; 30: 47-55
- 634 Zhang GB, Cui XL, Sui DL, et al. Differential molecular genetic analysis in glioblastoma multiforme of long- and short-term survivors: a clinical study in Chinese patients. *Journal of neuro-oncology* 2013; 113: 251-8
- 635 Beier CP, Kumar P, Meyer K, et al. The cancer stem cell subtype determines immune infiltration of glioblastoma. *Stem cells and development* 2012; 21: 2753-61
- 636 Kreth S, Heyn J, Grau S, et al. Identification of valid endogenous control genes for determining gene expression in human glioma. *Neuro-oncology* 2010; 12: 570-9
- 637 Grube S, Göttig T, Freitag D, et al. Selection of suitable reference genes for expression analysis in human glioma using RT-qPCR. *Journal of neuro-oncology* 2015; 123: 35-42
- 638 Li MMH, MacDonald MR, Rice CM. To translate, or not to translate: viral and host mRNA regulation by interferon-stimulated genes. *Trends in cell biology* 2015; 25: 320-9
- 639 Bowman RL, Wang Q, Carro A, et al. GlioVis data portal for visualization and analysis of brain tumor expression datasets. *Neuro-oncology* 2017; 19: 139-41
- 640 Gravendeel LA, Kouwenhoven MC, Gevaert O, et al. Intrinsic gene expression profiles of gliomas are a better predictor of survival than histology. *Cancer research* 2009; 69: 9065-72
- 641 Szklarczyk D, Gable AL, Lyon D, et al. STRING v11: protein-protein association networks with increased coverage, supporting functional discovery in genome-wide experimental datasets. *Nucleic acids research* 2019; 47: D607-D13
- 642 Benjamini Y, Yekutieli D. The control of the false discovery rate in multiple testing under dependency. *Ann Statist* 2001; 29: 1165-88
- 643 Sorensen MD, Dahlrot RH, Boldt HB, et al. Tumour-associated microglia/macrophages predict poor prognosis in high-grade gliomas and correlate with an aggressive tumour subtype. *Neuropathol Appl Neurobiol* 2018; 44: 185-206
- 644 Sorensen MD, Kristensen BW. Tumour-associated CD204(+) microglia/macrophages accumulate in perivascular and perinecrotic niches and correlate with an interleukin-6-enriched inflammatory profile in glioblastoma. *Neuropathol Appl Neurobiol* 2022; 48: e12772
- 645 Zhang L, Sorensen MD, Kristensen BW, et al. D-2-Hydroxyglutarate Is an Intercellular Mediator in IDH-Mutant Gliomas Inhibiting Complement and T Cells. *Clinical Cancer Research* 2018; 24: 5381-91
- 646 Sorensen MD, Nielsen O, Reifemberger G, et al. The presence of TIM-3 positive cells in WHO grade III and IV astrocytic gliomas correlates with isocitrate dehydrogenase mutation status. *Brain Pathol* 2021; 31: e12921
- 647 Balkwill F. Tumour necrosis factor and cancer. *Nature reviews Cancer* 2009; 9: 361-71
- 648 Velloso FJ, Trombetta-Lima M, Anschau V, et al. NOD-like receptors: major players (and targets) in the interface between innate immunity and cancer. *Bioscience reports* 2019; 39: BSR20181709
- 649 Velasquez C, Mansouri S, Mora C, et al. Molecular and Clinical Insights into the Invasive Capacity of Glioblastoma Cells. *J Oncol* 2019; 2019: 1740763
- 650 Ding P, Wang W, Wang J, et al. Expression of tumor-associated macrophage in progression of human glioma. *Cell Biochem Biophys* 2014; 70: 1625-31
- 651 Miyazaki T, Ishikawa E, Matsuda M, et al. Infiltration of CD163-positive macrophages in glioma tissues after treatment with anti-PD-L1 antibody and role of PI3K γ inhibitor as a combination therapy with anti-PD-L1 antibody in in vivo model using temozolomide-resistant murine glioma-initiating cells. *Brain Tumor Pathol* 2020; 37: 41-9
- 652 Kurdi M, Mulla N, Katib Y, et al. The Cancer Driver Genes IDH1 and IDH2 and CD204 in WHO-Grade 4 Astrocytoma: Crosstalk Between Cancer Metabolism and Tumour Associated Macrophage Recruitment in Tumour Microenvironment. *Biologies* 2023; 17: 15-22
- 653 Eckel-Passow JE, Lohse CM, Sheinin Y, et al. Tissue microarrays: one size does not fit all. *Diagnostic Pathology* 2010; 5: 48
- 654 Lee ATJ, Chew W, Wilding CP, et al. The adequacy of tissue microarrays in the assessment of inter- and intra-tumoural heterogeneity of infiltrating lymphocyte burden in leiomyosarcoma. *Scientific Reports* 2019; 9: 14602
- 655 Barros MH, Hauck F, Dreyer JH, et al. Macrophage polarisation: an immunohistochemical approach for identifying M1 and M2 macrophages. *PLoS One* 2013; 8: e80908
- 656 Régnier-Vigouroux A. The mannose receptor in the brain. *Int Rev Cytol* 2003; 226: 321-42
- 657 van der Zande HJP, Nitsche D, Schlautmann L, et al. The Mannose Receptor: From Endocytic Receptor and Biomarker to Regulator of (Meta)Inflammation. *Front Immunol* 2021; 12: 765034
- 658 Husemann J, Loike JD, Anankov R, et al. Scavenger receptors in neurobiology and neuropathology: their role on microglia and other cells of the nervous system. *Glia* 2002; 40: 195-205
- 659 López-Janeiro Á, Padilla-Ansala C, de Andrea CE, et al. Prognostic value of macrophage polarization markers in epithelial neoplasms and melanoma. A systematic review and meta-analysis. *Mod Pathol* 2020; 33: 1458-65

References

- 660 Bisheskar SK, van der Kamp MF, de Ruiter EJ, et al. The prognostic role of tumor associated macrophages in squamous cell carcinoma of the head and neck: A systematic review and meta-analysis. *Oral Oncol* 2022; 135: 106227
- 661 Ding W, Tan Y, Qian Y, et al. Clinicopathologic and prognostic significance of tumor-associated macrophages in patients with hepatocellular carcinoma: A meta-analysis. *PLoS One* 2019; 14: e0223971
- 662 Yi B, Cheng Y, Chang R, et al. Prognostic significance of tumor-associated macrophages polarization markers in lung cancer: a pooled analysis of 5105 patients. *Bioscience Reports* 2023; 43:
- 663 Shigeoka M, Urakawa N, Nakamura T, et al. Tumor associated macrophage expressing CD204 is associated with tumor aggressiveness of esophageal squamous cell carcinoma. *Cancer Sci* 2013; 104: 1112-9
- 664 Komohara Y, Horlad H, Ohnishi K, et al. M2 macrophage/microglial cells induce activation of Stat3 in primary central nervous system lymphoma. *J Clin Exp Hematop* 2011; 51: 93-9
- 665 Lier J, Streit WJ, Bechmann I. Beyond Activation: Characterizing Microglial Functional Phenotypes. *Cells* 2021; 10: 2236
- 666 Yang ZF, Ho DW, Lau CK, et al. Allograft inflammatory factor-1 (AIF-1) is crucial for the survival and pro-inflammatory activity of macrophages. *Int Immunol* 2005; 17: 1391-7
- 667 Gangoso E, Southgate B, Bradley L, et al. Glioblastomas acquire myeloid-affiliated transcriptional programs via epigenetic immunoediting to elicit immune evasion. *Cell* 2021; 184: 2454-70.e26
- 668 Schmitt MJ, Company C, Dramaretska Y, et al. Phenotypic Mapping of Pathologic Cross-Talk between Glioblastoma and Innate Immune Cells by Synthetic Genetic Tracing. *Cancer Discov* 2021; 11: 754-77
- 669 Zhang G, Tanaka S, Jiapaer S, et al. RBPJ contributes to the malignancy of glioblastoma and induction of proneural-mesenchymal transition via IL-6-STAT3 pathway. *Cancer Sci* 2020; 111: 4166-76
- 670 Lisi L, Stigliano E, Lauriola L, et al. Proinflammatory-activated glioma cells induce a switch in microglial polarization and activation status, from a predominant M2b phenotype to a mixture of M1 and M2a/B polarized cells. *ASN Neuro* 2014; 6: 171-83
- 671 Yu K, Hu Y, Wu F, et al. Surveying brain tumor heterogeneity by single-cell RNA-sequencing of multi-sector biopsies. *National Science Review* 2020; 7: 1306-18
- 672 Badie B, Schartner JM. Flow cytometric characterization of tumor-associated macrophages in experimental gliomas. *Neurosurgery* 2000; 46: 957-61; discussion 61-2
- 673 Muller A, Brandenburg S, Turkowski K, et al. Resident microglia, and not peripheral macrophages, are the main source of brain tumor mononuclear cells. *Int J Cancer* 2015; 137: 278-88
- 674 Landry AP, Balas M, Alli S, et al. Distinct regional ontogeny and activation of tumor associated macrophages in human glioblastoma. *Sci Rep* 2020; 10: 19542
- 675 Mishima K, Kato Y, Kaneko MK, et al. Increased expression of podoplanin in malignant astrocytic tumors as a novel molecular marker of malignant progression. *Acta Neuropathol* 2006; 111: 483-8
- 676 Schafer A, Teufel J, Ringel F, et al. Aldehyde dehydrogenase 1A1--a new mediator of resistance to temozolomide in glioblastoma. *Neuro Oncol* 2012; 14: 1452-64
- 677 Dong F, Eibach M, Bartsch JW, et al. The metalloprotease-disintegrin ADAM8 contributes to temozolomide chemoresistance and enhanced invasiveness of human glioblastoma cells. *Neuro Oncol* 2015; 17: 1474-85
- 678 Wicki A, Christofori G. The potential role of podoplanin in tumour invasion. *Br J Cancer* 2007; 96: 1-5
- 679 Sanders S, Herpai DM, Rodriguez A, et al. The Presence and Potential Role of ALDH1A2 in the Glioblastoma Microenvironment. *Cells* 2021; 10:
- 680 Xiao Y, Yang K, Wang Z, et al. CD44-Mediated Poor Prognosis in Glioma Is Associated With M2-Polarization of Tumor-Associated Macrophages and Immunosuppression. *Front Surg* 2021; 8: 775194
- 681 Wang X, Wang X, Li J, et al. PDPN contributes to constructing immunosuppressive microenvironment in IDH wildtype glioma. *Cancer Gene Ther* 2023; 30: 345-57
- 682 Beier D, Schulz JB, Beier CP. Chemoresistance of glioblastoma cancer stem cells--much more complex than expected. *Molecular cancer* 2011; 10: 128
- 683 Kelley JL, Ozment TR, Li C, et al. Scavenger receptor-A (CD204): a two-edged sword in health and disease. *Crit Rev Immunol* 2014; 34: 241-61
- 684 Groblewska M, Litman-Zawadzka A, Mroczko B. The Role of Selected Chemokines and Their Receptors in the Development of Gliomas. *International journal of molecular sciences* 2020; 21:
- 685 Mantovani A, Allavena P, Sozzani S, et al. Chemokines in the recruitment and shaping of the leukocyte infiltrate of tumors. *Semin Cancer Biol* 2004; 14: 155-60
- 686 Wang L, Qin H, Li L, et al. Overexpression of CCL20 and its receptor CCR6 predicts poor clinical prognosis in human gliomas. *Med Oncol* 2012; 29: 3491-7
- 687 Chen Z, Mou L, Pan Y, et al. CXCL8 Promotes Glioma Progression By Activating The JAK/STAT1/HIF-1 α /Snail Signaling Axis. *Onco Targets Ther* 2019; 12: 8125-38
- 688 Yang F, He Z, Duan H, et al. Synergistic immunotherapy of glioblastoma by dual targeting of IL-6 and CD40. *Nat Commun* 2021; 12: 3424

References

- 689 Brat DJ, Bellail AC, Van Meir EG. The role of interleukin-8 and its receptors in gliomagenesis and tumoral angiogenesis. *Neuro Oncol* 2005; 7: 122-33
- 690 Piao Y, Henry V, Tiao N, et al. Targeting intercellular adhesion molecule-1 prolongs survival in mice bearing bevacizumab-resistant glioblastoma. *Oncotarget* 2017; 8: 96970-83
- 691 Lin JC, Tsai JT, Chao TY, et al. Musashi-1 Enhances Glioblastoma Migration by Promoting ICAM1 Translation. *Neoplasia* 2019; 21: 459-68
- 692 Bui TM, Wiesolek HL, Sumagin R. ICAM-1: A master regulator of cellular responses in inflammation, injury resolution, and tumorigenesis. *J Leukoc Biol* 2020:
- 693 Yoo KC, Kang JH, Choi MY, et al. Soluble ICAM-1 a Pivotal Communicator between Tumors and Macrophages, Promotes Mesenchymal Shift of Glioblastoma. *Adv Sci (Weinh)* 2022; 9: e2102768
- 694 Beyaert R, Heyninck K, Van Huffel S. A20 and A20-binding proteins as cellular inhibitors of nuclear factor-kappa B-dependent gene expression and apoptosis. *Biochemical pharmacology* 2000; 60: 1143-51
- 695 Murat A, Migliavacca E, Hussain SF, et al. Modulation of angiogenic and inflammatory response in glioblastoma by hypoxia. *PloS one* 2009; 4: e5947
- 696 Nakahara S, Oka N, Raz A. On the role of galectin-3 in cancer apoptosis. *Apoptosis* 2005; 10: 267-75
- 697 Hjelmeland AB, Wu Q, Wickman S, et al. Targeting A20 decreases glioma stem cell survival and tumor growth. *PLoS biology* 2010; 8: e1000319
- 698 Ikemori RY, Machado CM, Furuzawa KM, et al. Galectin-3 up-regulation in hypoxic and nutrient deprived microenvironments promotes cell survival. *PloS one* 2014; 9: e111592
- 699 Wang H, Song X, Huang Q, et al. LGALS3 Promotes Treatment Resistance in Glioblastoma and Is Associated with Tumor Risk and Prognosis. *Cancer epidemiology, biomarkers & prevention : a publication of the American Association for Cancer Research, cosponsored by the American Society of Preventive Oncology* 2019; 28: 760-9
- 700 Umakoshi M, Nakamura A, Tsuchie H, et al. Macrophage numbers in the marginal area of sarcomas predict clinical prognosis. *Sci Rep* 2023; 13: 1290
- 701 Yanai Y, Kosaka T, Mikami S, et al. CD8-positive T cells and CD204-positive M2-like macrophages predict postoperative prognosis of very high-risk prostate cancer. *Sci Rep* 2021; 11: 22495
- 702 Kubota K, Moriyama M, Furukawa S, et al. CD163(+)/CD204(+) tumor-associated macrophages contribute to T cell regulation via interleukin-10 and PD-L1 production in oral squamous cell carcinoma. *Sci Rep* 2017; 7: 1755
- 703 Yi H, Zuo D, Yu X, et al. Suppression of antigen-specific CD4+ T cell activation by SRA/CD204 through reducing the immunostimulatory capability of antigen-presenting cell. *J Mol Med (Berl)* 2012; 90: 413-26
- 704 Yi H, Yu X, Gao P, et al. Pattern recognition scavenger receptor SRA/CD204 down-regulates Toll-like receptor 4 signaling-dependent CD8 T-cell activation. *Blood* 2009; 113: 5819-28
- 705 Yi H, Guo C, Yu X, et al. Targeting the immunoregulator SRA/CD204 potentiates specific dendritic cell vaccine-induced T-cell response and antitumor immunity. *Cancer research* 2011; 71: 6611-20
- 706 Bak SP, Walters JJ, Takeya M, et al. Scavenger receptor-A-targeted leukocyte depletion inhibits peritoneal ovarian tumor progression. *Cancer research* 2007; 67: 4783-9
- 707 Lv Y, Ma X, Ma Y, et al. A new emerging target in cancer immunotherapy: Galectin-9 (LGALS9). *Genes & Diseases* 2022:
- 708 Ocana-Guzman R, Torre-Bouscoulet L, Sada-Ovalle I. TIM-3 Regulates Distinct Functions in Macrophages. *Front Immunol* 2016; 7: 229
- 709 Jiang X, Zhou T, Xiao Y, et al. Tim-3 promotes tumor-promoting M2 macrophage polarization by binding to STAT1 and suppressing the STAT1-miR-155 signaling axis. *Oncoimmunology* 2016; 5: e1211219
- 710 Komohara Y, Morita T, Annan DA, et al. The Coordinated Actions of TIM-3 on Cancer and Myeloid Cells in the Regulation of Tumorigenicity and Clinical Prognosis in Clear Cell Renal Cell Carcinomas. *Cancer Immunol Res* 2015; 3: 999-1007
- 711 Crusz SM, Balkwill FR. Inflammation and cancer: advances and new agents. *Nature reviews Clinical oncology* 2015; 12: 584-96
- 712 Garbers C, Heink S, Korn T, et al. Interleukin-6: designing specific therapeutics for a complex cytokine. *Nat Rev Drug Discov* 2018; 17: 395-412
- 713 Jones SA. Directing transition from innate to acquired immunity: defining a role for IL-6. *Journal of immunology (Baltimore, Md : 1950)* 2005; 175: 3463-8
- 714 Jin X, Kim SH, Jeon HM, et al. Interferon regulatory factor 7 regulates glioma stem cells via interleukin-6 and Notch signalling. *Brain : a journal of neurology* 2012; 135: 1055-69
- 715 McFarland BC, Hong SW, Rajbhandari R, et al. NF-kappaB-induced IL-6 ensures STAT3 activation and tumor aggressiveness in glioblastoma. *PloS one* 2013; 8: e78728
- 716 West AJ, Tsui V, Stylli SS, et al. The role of interleukin-6-STAT3 signalling in glioblastoma. *Oncology letters* 2018; 16: 4095-104

References

- 717 a Dzaye OD, Hu F, Derkow K, et al. Glioma Stem Cells but Not Bulk Glioma Cells Upregulate IL-6 Secretion in Microglia/Brain Macrophages via Toll-like Receptor 4 Signaling. *Journal of neuropathology and experimental neurology* 2016; 75: 429-40
- 718 Chang CY, Li MC, Liao SL, et al. Prognostic and clinical implication of IL-6 expression in glioblastoma multiforme. *Journal of clinical neuroscience : official journal of the Neurosurgical Society of Australasia* 2005; 12: 930-3
- 719 Wang Q, He Z, Huang M, et al. Vascular niche IL-6 induces alternative macrophage activation in glioblastoma through HIF-2 α . *Nature communications* 2018; 9: 559-
- 720 Wang H, Lathia JD, Wu Q, et al. Targeting interleukin 6 signaling suppresses glioma stem cell survival and tumor growth. *Stem cells (Dayton, Ohio)* 2009; 27: 2393-404
- 721 Noman MZ, Desantis G, Janji B, et al. PD-L1 is a novel direct target of HIF-1 α , and its blockade under hypoxia enhanced MDSC-mediated T cell activation. *The Journal of experimental medicine* 2014; 211: 781-90
- 722 Saidi A, Hagedorn M, Allain N, et al. Combined targeting of interleukin-6 and vascular endothelial growth factor potently inhibits glioma growth and invasiveness. *International Journal of Cancer* 2009; 125: 1054-64
- 723 The WHO Rapid Evidence Appraisal for COVID-19 Therapies Working Group. Association Between Administration of IL-6 Antagonists and Mortality Among Patients Hospitalized for COVID-19: A Meta-analysis. *JAMA* 2021; 326: 499-518
- 724 Richardson LG, Nieman LT, Stemmer-Rachamimov AO, et al. IDH-mutant gliomas harbor fewer regulatory T cells in humans and mice. *Oncoimmunology* 2020; 9: 1806662
- 725 Böttcher M, Renner K, Berger R, et al. D-2-hydroxyglutarate interferes with HIF-1 α stability skewing T-cell metabolism towards oxidative phosphorylation and impairing Th17 polarization. *Oncoimmunology* 2018; 7: e1445454
- 726 Zhang X, Rao A, Sette P, et al. IDH mutant gliomas escape natural killer cell immune surveillance by downregulation of NKG2D ligand expression. *Neuro-oncology* 2016; 18: 1402-12
- 727 Zhang X, Kim WJ, Rao AV, et al. In vivo efficacy of decitabine as a natural killer cell-mediated immunotherapy against isocitrate dehydrogenase mutant gliomas. *Neurosurg Focus* 2022; 52: E3
- 728 Han S, Feng S, Xu L, et al. Tim-3 on peripheral CD4(+) and CD8(+) T cells is involved in the development of glioma. *DNA Cell Biol* 2014; 33: 245-50
- 729 Liu Z, Han H, He X, et al. Expression of the galectin-9-Tim-3 pathway in glioma tissues is associated with the clinical manifestations of glioma. *Oncology letters* 2016; 11: 1829-34
- 730 Rao G, Latha K, Ott M, et al. Anti-PD-1 Induces M1 Polarization in the Glioma Microenvironment and Exerts Therapeutic Efficacy in the Absence of CD8 Cytotoxic T Cells. *Clin Cancer Res* 2020:
- 731 Lu D, Ni Z, Liu X, et al. Beyond T Cells: Understanding the Role of PD-1/PD-L1 in Tumor-Associated Macrophages. *Journal of Immunology Research* 2019; 2019: 1919082
- 732 Gordon SR, Maute RL, Dulken BW, et al. PD-1 expression by tumour-associated macrophages inhibits phagocytosis and tumour immunity. *Nature* 2017; 545: 495-9
- 733 Bunse L, Rupp AK, Poschke I, et al. AMPLIFY-NEOVAC: a randomized, 3-arm multicenter phase I trial to assess safety, tolerability and immunogenicity of IDH1-vac combined with an immune checkpoint inhibitor targeting programmed death-ligand 1 in isocitrate dehydrogenase 1 mutant gliomas. *Neurol Res Pract* 2022; 4: 20
- 734 Touat M, Li YY, Boynton AN, et al. Mechanisms and therapeutic implications of hypermutation in gliomas. *Nature* 2020; 580: 517-23
- 735 Eckert A, Kloor M, Giersch A, et al. Microsatellite instability in pediatric and adult high-grade gliomas. *Brain Pathol* 2007; 17: 146-50
- 736 Gatto L, Franceschi E, Tosoni A, et al. Hypermutation as a potential predictive biomarker of immunotherapy efficacy in high-grade gliomas: a broken dream? *Immunotherapy* 2022; 14: 799-813
- 737 Zhang J, Caruso FP, Sa JK, et al. The combination of neoantigen quality and T lymphocyte infiltrates identifies glioblastomas with the longest survival. *Commun Biol* 2019; 2: 135
- 738 Kang K, Xie F, Wu Y, et al. Comprehensive exploration of tumor mutational burden and immune infiltration in diffuse glioma. *Int Immunopharmacol* 2021; 96: 107610
- 739 Reungwetwattana T, Nakagawa K, Cho BC, et al. CNS Response to Osimertinib Versus Standard Epidermal Growth Factor Receptor Tyrosine Kinase Inhibitors in Patients With Untreated EGFR-Mutated Advanced Non-Small-Cell Lung Cancer. *J Clin Oncol* 2018; Jco2018783118
- 740 Wang J, Weiss T, Neidert MC, et al. Vaccination with Designed Neopeptides Induces Intratumoral, Cross-reactive CD4+ T-cell Responses in Glioblastoma. *Clin Cancer Res* 2022; 28: 5368-82
- 741 Keskin DB, Anandappa AJ, Sun J, et al. Neoantigen vaccine generates intratumoral T cell responses in phase Ib glioblastoma trial. *Nature* 2019; 565: 234-9
- 742 Unruh D, Mirkov S, Wray B, et al. Methylation-dependent Tissue Factor Suppression Contributes to the Reduced Malignancy of IDH1-mutant Gliomas. *Clin Cancer Res* 2019; 25: 747-59

References



- 743 Goossens P, Lu C, Cao J, et al. Integrating multiplex immunofluorescent and mass spectrometry imaging to map myeloid heterogeneity in its metabolic and cellular context. *Cell Metab* 2022; 34: 1214-25.e6
- 744 van Dam S, Baars MJD, Vercoulen Y. Multiplex Tissue Imaging: Spatial Revelations in the Tumor Microenvironment. *Cancers (Basel)* 2022; 14:

13. Appendix

13.1 Manuscript I

“Tumour-associated microglia/macrophages predict poor prognosis in high-grade gliomas and correlate with an aggressive tumour subtype”

Tumour-associated microglia/macrophages predict poor prognosis in high-grade gliomas and correlate with an aggressive tumour subtype

M. D. Sørensen*,† , R. H. Dahlrot‡ , H. B. Boldt*, S. Hansen†,‡ and B. W. Kristensen*,†

*Department of Pathology, Odense University Hospital, †Department of Clinical Research, University of Southern Denmark and ‡Department of Oncology, Odense University Hospital, Odense, Denmark

M. D. Sørensen, R. H. Dahlrot, H. B. Boldt, S. Hansen, B. W. Kristensen (2018) *Neuropathology and Applied Neurobiology* 44, 185–206

Tumour-associated microglia/macrophages predict poor prognosis in high-grade gliomas and correlate with an aggressive tumour subtype

Aims: Glioblastomas are highly aggressive and treatment resistant. Increasing evidence suggests that tumour-associated macrophages/microglia (TAMs) facilitate tumour progression by acquiring a M2-like phenotype. Our objective was to investigate the prognostic value of TAMs in gliomas using automated quantitative double immunofluorescence. **Methods:** Samples from 240 patients with primary glioma were stained with antibodies against ionized calcium-binding adaptor molecule-1 (IBA-1) and cluster of differentiation 204 (CD204) to detect TAMs and M2-like TAMs. The expression levels were quantified by software-based classifiers. The associations between TAMs, gemistocytic cells and glioblastoma subtype were examined with immuno- and haematoxylin–eosin stainings. Three tissue arrays containing glioblastoma specimens were included to study IBA-1/CD204 levels in central tumour and tumour periphery and to characterize CD204⁺ cells. **Results:** Our data revealed that the

amount of especially CD204⁺ TAMs increases with malignancy grade. In grade III–IV, high CD204 expression was associated with shorter survival, while high IBA-1 intensity correlated with a longer survival. In grade IV, CD204 showed independent prognostic value when adjusting for clinical data and the methylation status of O6-methylguanine–DNA methyltransferase. Our findings were confirmed in two bioinformatics databases. TAMs were more abundant in central tumour tissue, mesenchymal glioblastomas and gliomas with many gemistocytic cells. CD204⁺ TAMs co-expressed proteins related to tumour aggressiveness including matrix metalloproteinase-14 and hypoxia-inducible factor-1 α . **Conclusions:** This is the first study to use automated quantitative immunofluorescence to determine the prognostic impact of TAMs. Our results suggest that M2-like TAMs hold an unfavourable prognostic value in high-grade gliomas and may contribute to a pro-tumourigenic microenvironment.

Keywords: CD204, glioblastoma, glioma, macrophages, microglia, prognosis

Introduction

Gliomas are the most common primary brain tumours in adults. Patient prognosis differs considerably within

the different World Health Organization (WHO) grades being poorest for patients with the grade IV tumour – the glioblastoma multiforme (GBM). In 2005, temozolomide was introduced as supplement to standard treatment of GBM patients [1] resulting in improved survival, especially for patients with methylated O6-methylguanine–DNA methyltransferase (MGMT) promoter [2–4]. Additional therapeutic strategies have not

Correspondence: Mia D. Sørensen, Department of Pathology, Odense University Hospital, J. B. Winsloews Vej 15, Odense, Denmark. Tel: 0045 24222574; Fax: 0045 66122783; E-mail: mia.soerensen@rsyd.dk

© 2017 The Authors. *Neuropathology and Applied Neurobiology* published by John Wiley & Sons Ltd on behalf of British Neuropathological Society.

This is an open access article under the terms of the Creative Commons Attribution-NonCommercial License, which permits use, distribution and reproduction in any medium, provided the original work is properly cited and is not used for commercial purposes.

185

been able to further improve prognosis, and the 2- and 5-year survival remain below 25% and 10%, respectively [3,4]. The inefficacy may be explained by several mechanisms of resistance [4,5], and increasing evidence suggests that factors in the tumour microenvironment including hypoxia and nonneoplastic cells may constitute extrinsic resistance mechanisms [6]. The tumour microenvironment could, thus, be a target for anticancer therapy.

In removed GBM tissue, tumour-associated microglia/macrophages (TAMs) have been reported to constitute up to 30% [7–10]. TAMs are recruited from the brain and bone marrow to the site of the tumour through the action of signalling molecules released by glioma cells and other cells in the microenvironment [8,9,11,12]. Reportedly, glioma cells suppress the immune surveillance of TAMs by skewing them towards the pro-tumorigenic M2 phenotype while inhibiting development of the anti-tumorigenic M1 phenotype [8,9,13–16]. However, recent studies indicate that glioma cells induce a mixed population of TAMs expressing both M1- and M2-related molecules [11,17–20] possibly resembling a more undifferentiated M0 phenotype [21]. In return, TAMs support tumour growth and progression [8–10] by stimulating proliferation [22], migration [23,24], invasion [12,22–25] and angiogenesis [8,9,26], overall indicating a complex bidirectional communication between glioma cells and TAMs.

Using immunohistochemistry, the number of TAMs was shown to increase with malignancy grade in gliomas [15,27,28]. In addition, high amounts of TAMs expressing M2-related markers, e.g. cluster of differentiation 204 (CD204) and 163 (CD163), have been associated with increasing WHO grade and poorer prognosis [15,29,30]. However, these studies neither investigated the influence of M2 TAMs on survival in separate WHO grades nor performed multivariate analysis to examine the independent prognostic value. Based on these unresolved issues, our aim was to explore the prognostic impact of TAMs in a large population-based glioma cohort by quantifying the expression of the microglial/macrophage markers ionized calcium-binding adaptor molecule-1 (IBA-1) and CD204 using double immunofluorescence. IBA-1 is considered a specific TAM marker [31] and CD204 a marker of M2-like TAMs [9]. We used an automated quantitative fluorescence approach enabling continuous measurements of area and intensity reducing some of the inter- and intra-

observer variability seen in conventional semi-quantitative pathologist-based scoring [32,33]. Early on, we discovered that the distribution of TAMs in especially GBMs was highly heterogeneous. We, therefore, investigated the correlation between TAMs, gemistocytic tumour cells and GBM subtype as tumour aggressiveness may depend on both the specific molecular subtype and the level of gemistocytic tumour cells. In addition, we characterized the phenotype of CD204⁺ TAMs by double immunofluorescence using a panel of eight markers related to immune activation and tumour aggressiveness.

Materials and methods

Patient tissue

Samples were obtained from the Region of Southern Denmark (RSD) glioma cohort investigated and well-characterized previously [34–40]. Tissue from 240 patients was included for the IBA-1/CD204 analysis. All patients were diagnosed with a primary glioma between 2005 and 2009. Table S1 provides an overview of relevant patient characteristics including clinical and histological data. A tissue array containing eight GBM specimens was included to study the expression of IBA-1/CD204 in central tumour and tumour periphery. In addition, two tissue arrays with 34 GBM specimens were included to characterize CD204⁺ cells. All samples were evaluated by two pathologists and reclassified according to WHO guidelines 2016 [41]. See Data S1 for information on procedures used for reclassification.

Normal brain tissue was obtained from two adult patients at autopsy. Cause of death was unrelated to any disease in the central nervous system (CNS). Tissue was obtained from 10 patients with primary diffuse large B-cell lymphoma (DLBCL) in the CNS, 10 patients diagnosed with first-time CNS metastasis from malignant melanoma (MM), and 10 patients diagnosed with first-time CNS metastasis from non-small cell lung cancer (NSCLC).

Double immunofluorescence

Immunofluorescence stainings were performed as previously reported [34,35,42,43]. See Data S1 for information on the staining procedure and Table S2 for information on antibodies used.

Automated quantitative fluorescence analysis

Fluorescence image analysis and quantitation were done using the Visiopharm integrated microscope and software module (Visiopharm, Hørsholm, Denmark) consisting of a Leica DM 6000B microscope and Olympus DP72 camera (Olympus, Ballerup, Denmark). Super images were acquired at $1.25\times$ magnification using bright field settings, and sampling regions containing vital tumour tissue were manually outlined. Sample images were collected by systematic uniform random sampling at $20\times$ magnification. Images were reviewed ensuring at least five images per tumour, and only images with at least 20% viable tumour tissue within the picture frame were included for further processing. Images were classified using algorithms developed in the Visiomorph module. Individual pixels were assigned labels based on threshold intensities of the colour bands. To quantify the expressions of IBA-1 and CD204, the tumour area within each picture frame was defined manually as a region of interest (ROI). For the quantification of double-positive expression (i.e. IBA-1⁺ CD204⁺ pixels), IBA-1 was used as an inclusion marker and defined as a ROI, then the expression of CD204 was evaluated within this ROI enabling measurements of double-labelled protein expression (Figure 1). Output variables were area fractions (AF), defined as area of positive expression divided by the area of the respective ROI, and mean intensity (MI) of IBA-1 and CD204 in total tumour tissue as well as of CD204 within the IBA-1⁺ area (i.e. IBA-1^{TOTAL}, CD204^{TOTAL} and CD204^{IBA-1}). Prior to sampling, calibration was performed to adjust for run variation within the staining. This was accomplished using adjacent sections of a GBM tissue array (Figure S1).

Similar algorithms were generated to characterize the phenotype of the CD204⁺ cells. The area of double-stained area was quantified as a fraction of the total CD204⁺ area resulting in a quantitative estimate of double-positive cells. In addition, the intensity of the marker of interest was measured in the total CD204⁺ area.

MGMT status

O6-methylguanine–DNA methyltransferase promoter status was retrospectively obtained in 161 patients using pyrosequencing (QIAamp DNA FFPE Tissue kit; Qiagen, Hilden, Germany) as previously described [39].

Gemistocytic cell component

Presence of gemistocytic tumour cells (gemistocytes) was evaluated in 11 diffuse astrocytomas (DA), 17 anaplastic astrocytomas (AAs) and 20 GBMs from the RSD glioma cohort using haematoxylin–eosin stainings. The 20 GBMs represented 10 of the patients with the lowest and 10 of the patients with the highest AF CD204^{TOTAL}. All samples were scored blinded and semi-quantitatively. At $40\times$ magnification, five positions per slide were scored from 0 to 4 (0: no gemistocytes; 1: <10%; 2: 10–49%; 3: 50–90%; 4: >90% gemistocytes), and a mean score was calculated for each tumour.

Immunohistochemical subtyping

The association between TAMs and molecular subtype was investigated by staining the 20 GBM samples described above with three proneural markers: delta-like 3, NEURonal Nuclei and oligodendrocyte transcription factor 2 (OLIG-2), as well as three mesenchymal markers: CD44, vascular endothelial growth factor (VEGF) and chitinase 3-like 1 (YKL-40/CHI3L1) [44–47]. Immunohistochemistry was performed as previously described [36,37,39,40]. The tumours were scored and indexed as proneural or mesenchymal as previously reported [44]. See Data S1 for information on the staining procedure and Table S2 for information on antibodies used.

Patient dataset analysis

mRNA expressions of IBA-1 (AIF-1) and CD204 (MSR-1) in gliomas were explored using GlioVis (<https://gliovis.bioinfo.cnio.es>, data were exported July 2016). From the Cancer Genome Atlas (TCGA), mRNA data were available for 620 patients for analysing the association with malignancy grade [48] and for 460 GBM patients (the Agilent 4502SA dataset) for survival and subtype analyses [49]. From the Glavendel dataset, mRNA data were obtained for 276 patients including 159 GBM patients [50]. Datasets were exported directly from GlioVis. Survival analyses were carried out using the median as cut-off value.

Statistical analysis

Student's *t*-test or Mann–Whitney *U*-test was used when comparing two groups. One-way ANOVA with Bonferroni's

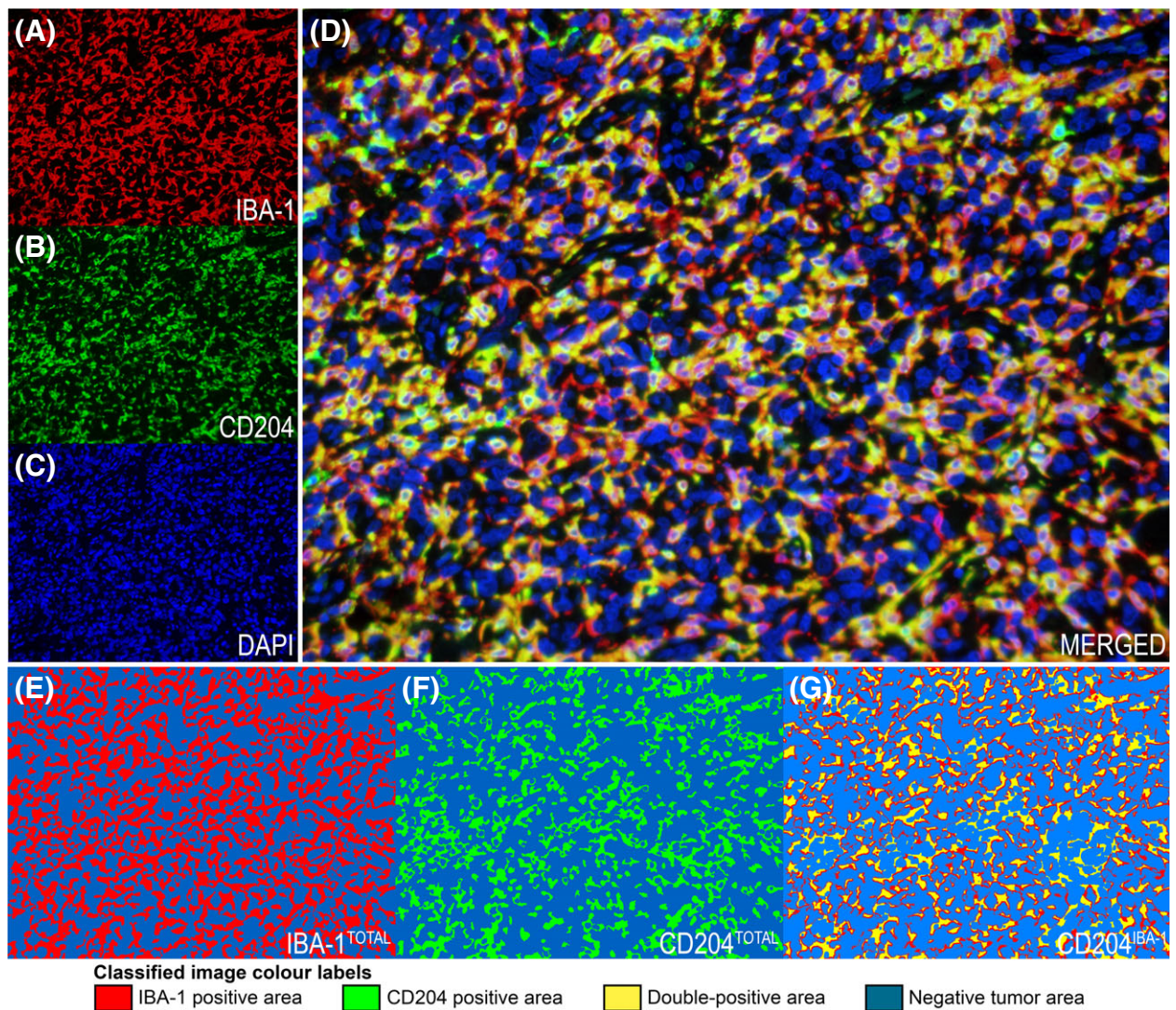


Figure 1. Image recording and classification. (A–D) Each image was recorded as three separate greyscale images for cyanine 5 [ionized calcium-binding adaptor molecule-1 (IBA-1)] (A), fluorescein (CD204) (B) and DAPI (nuclei) (C) and subsequently assigned colours and superimposed to form the complete image (D). Images were then classified by three classifiers based on threshold intensities of the colour bands. (E,F) To quantify the total expression of IBA-1 (IBA-1^{TOTAL}) and CD204 (CD204^{TOTAL}), the tumour area within each picture frame was defined as region of interest (ROI) with digital image analysis. (G) For the quantification of double-positive expression (i.e. IBA-1⁺ CD204⁺), IBA-1 was used as an inclusion marker and defined as a ROI, and then the expression of CD204 was evaluated within this ROI enabling measurements of double-labelled protein expression (CD204^{IBA-1}).

correction or Kruskal–Wallis test followed by Dunn’s multiple comparisons test was used for comparison of more than two groups. Correlation analyses were performed using Spearman’s correlation test. Overall survival (OS) was defined as time from primary surgery until death or date of censoring (May 2017). Survival functions were illustrated by Kaplan–Meier plots, and differences were compared by log-rank tests. WHO grade I was excluded in the statistical analysis due to limited

numbers ($n = 3$). CD204 and IBA-1 estimates were investigated as binary variables with the median as a prespecified cut-off value. Exploratory cut-point analyses were performed for grade IV as previously described [34,40], and only results using the optimal cut-points are shown. Multivariate analyses were performed using the Cox proportional hazard model.

All assumptions were tested. Statistical analyses were carried out in STATA (StataCorp LP) or Prism 5.0

(GraphPad Software Inc., San Diego, CA, USA). *P*-values <0.05 were considered significant.

Results

Expression of CD204 and IBA-1 in gliomas, normal brain, and other brain neoplasms

CD204 and IBA-1 were expressed in the membrane and cytoplasm of TAMs including their ramifications (Figure 2A–I). In pilocytic astrocytomas, the amount of IBA-1⁺ cells was moderate to high while few cells expressed CD204 (Figure 2A). Diffuse astrocytomas and oligodendrogliomas (OD) showed moderate IBA-1 and sparse CD204 expression (Figure 2B–D). AAs had moderate to high levels of IBA-1⁺ cells with some CD204⁺ cells, especially in isocitrate dehydrogenase (IDH) wild-type tumours, (Figure 2E,F), whereas anaplastic OD had lower IBA-1 levels compared with AAs with limited expression of CD204 (Figure 2G). GBM (Figure 2H) and especially gliosarcomas (Figure 2I) exhibited high expression of IBA-1 and/or CD204.

When applying the software-based classifiers, all quantitative estimates except MI IBA-1^{TOTAL} (*P* = 0.084) showed overall significant increases with malignancy grade (*P* < 0.001) being significantly highest in grade IV tumours (Figure 2J,K). In grade IV, the IBA-1⁺ area contributed with up to 0.30 of the total tumour area (median: 0.10), while the CD204⁺ area comprised up to 0.24 (median = 0.048). On average, 50% of the IBA-1⁺ area co-localized with CD204 (median = 0.45), but up to 90% co-expression was observed (Figure 2J).

To explore whether the vast existence of TAMs was specific to gliomas, expression levels of IBA-1 and CD204 were investigated in normal brain tissue, in tissue from primary brain DLBCL and metastases from NSCLC and MM (Figure S2A–H). AF IBA-1^{TOTAL} and MI IBA-1^{TOTAL} were highest in gliomas compared with normal brain, MM and DLBCL (*P* < 0.001), as well as NSCLC (*P* < 0.01 and <0.001). AF CD204^{TOTAL} was lower in normal brain (*P* < 0.001) and in DLBCL (*P* < 0.05) compared with gliomas, and gliomas had the highest MI CD204^{TOTAL} (*P* < 0.05). Similar was found for AF CD204^{IBA-1} and MI CD204^{IBA-1}, except for NSCLC which did not differ significantly from gliomas (Figure S2G,H).

TAMs and survival in WHO grade II–IV gliomas

Investigating the association between TAMs and prognosis in grade II–IV gliomas, high AF IBA-1^{TOTAL} was significantly associated with shorter OS when dichotomized at the median (HR = 1.50; 95% CI: 1.15–1.97; *P* = 0.003), while MI IBA-1^{TOTAL} did not correlate with survival (HR = 0.93; 95% CI: 0.71–1.20; *P* = 0.57). High levels of AF CD204^{TOTAL} and MI CD204^{TOTAL} correlated with poorer prognosis when divided at the median (HR = 2.02; 95% CI: 1.54–2.67; *P* < 0.001 and HR = 1.85; 95% CI: 1.41–2.42; *P* < 0.001). Similar was found for AF CD204^{IBA-1} and MI CD204^{IBA-1} (HR = 1.93; 95% CI: 1.48–2.53; *P* < 0.001 and HR = 1.92; 95% CI: 1.47–2.51; *P* < 0.001). In the multivariate analyses, high levels of AF CD204^{TOTAL} (HR = 1.81; 95% CI: 1.35–2.44; *P* < 0.001) and AF CD204^{IBA-1} (HR = 1.25; 95% CI: 1.01–1.81; *P* = 0.042) correlated with shorter OS (Table S3).

TAMs and survival in WHO grade II–III

In WHO grade II, neither IBA-1 nor CD204 expression levels were associated with prognosis when dichotomized at the median (Figure S3A–D). When adjusting for performance status, IDH status and histology in the multivariate analysis, high AF IBA-1^{TOTAL} correlated with better prognosis, while CD204 did not impact prognosis (Table S4).

In WHO grade III, no prognostic value was found for AF IBA-1^{TOTAL} when dichotomized at median (Figure S3E). High levels of MI IBA-1^{TOTAL} tended to associate with longer OS (Figure S3F), while high CD204 levels correlated significantly with shorter OS when divided at the median (Figure S3G,H). When accounting for performance status, IDH status and histology in the multivariate analysis, CD204 had a negative prognostic value (Table S5).

TAMs and survival in WHO grade IV

AF IBA-1^{TOTAL} was not associated with prognosis in univariate (HR = 0.99; 95% CI: 0.74–1.32; *P* = 0.95) (Figure 3A) or multivariate analyses (HR = 1.06; 95% CI: 0.79–1.43; *P* = 0.68) (Table 1) when dichotomized at the median, and no optimal cut-points were identified. High MI IBA-1^{TOTAL} tended to associate with

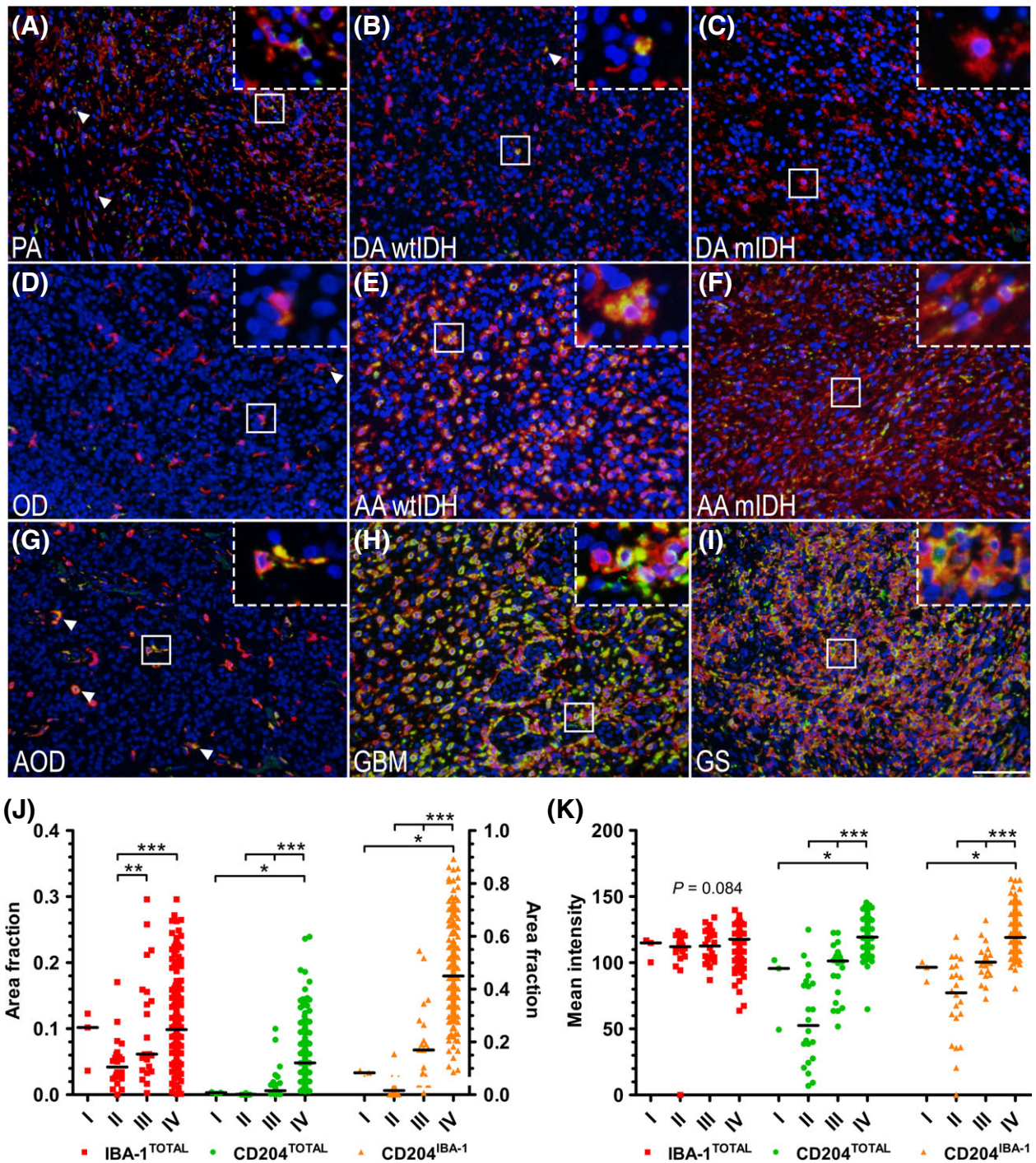


Figure 2. Expression of ionized calcium-binding adaptor molecule-1 (IBA-1) and CD204 in gliomas. (A–I) Examples of the double immunofluorescence staining in the different histological subtypes: PA (A), wtIDH DA (B), mIDH DA (C), OD (D), wtIDH AA (E), mIDH AA (F), AOD (G), GBM (H) and GS (I). Arrows and inserts show double-positive cells. (J) The area fraction of IBA-1^{TOTAL}, CD204^{TOTAL} and CD204^{IBA-1} increased with malignancy grade. (K) Mean intensities of CD204^{TOTAL} and CD204^{IBA-1} were higher in high-grade gliomas, while no difference was observed for MI IBA-1^{TOTAL}. Horizontal lines indicate the median. * $P < 0.05$; ** $P < 0.01$; *** $P < 0.001$. Scale bar 100 μm . AA, anaplastic astrocytoma; AOD anaplastic oligodendroglioma; DA, diffuse astrocytoma; GBM, glioblastoma multiforme; GS, gliosarcoma; mIDH, mutated isocitrate dehydrogenase; OD, oligodendroglioma; PA, pilocytic astrocytoma; wtIDH, wild-type IDH.

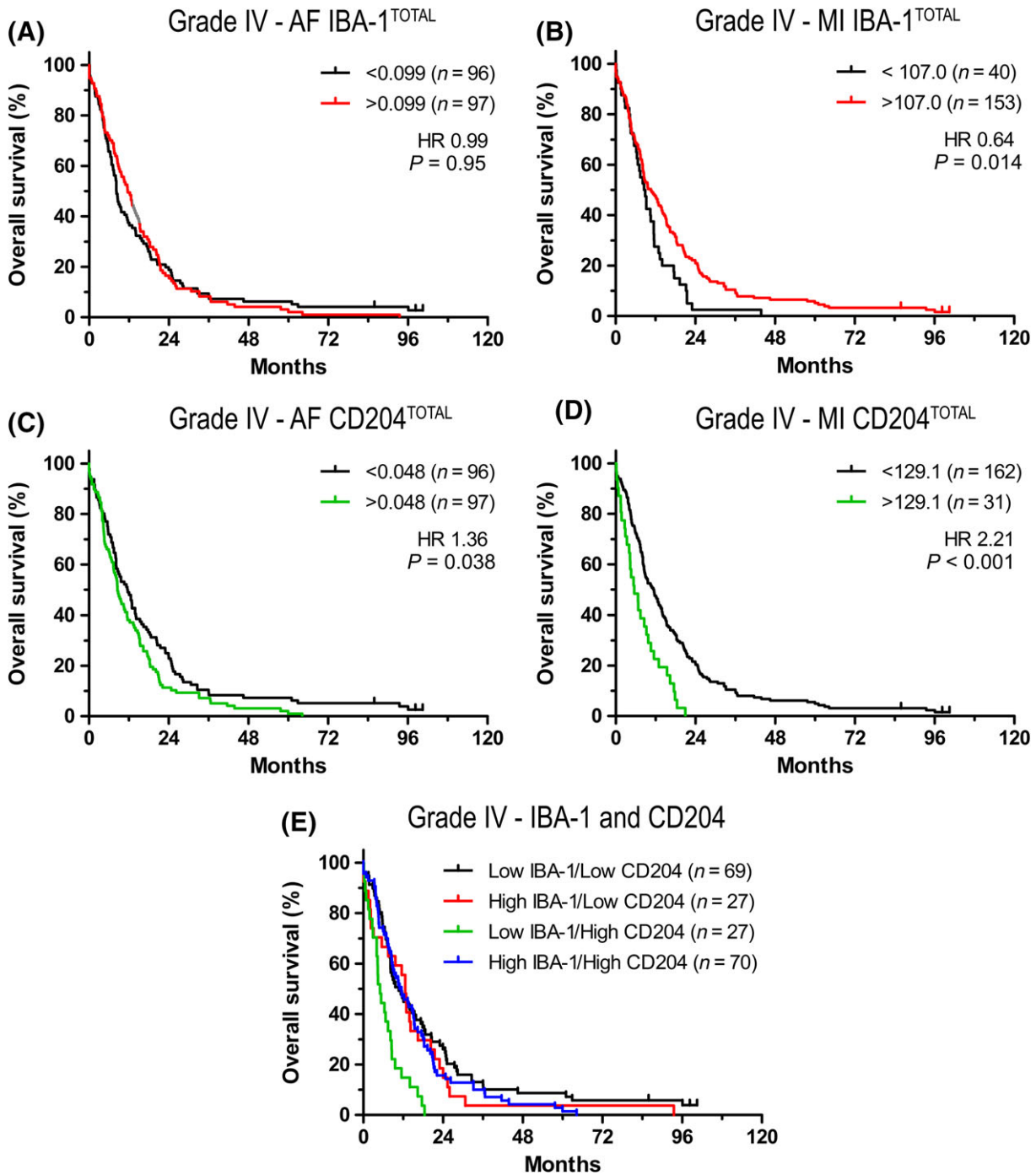


Figure 3. Tumour-associated microglia/macrophages and survival in grade IV gliomas. (A) The area fraction of ionized calcium-binding adaptor molecule-1^{TOTAL} (IBA-1^{TOTAL}) did not influence overall survival, while (B) high mean intensity of IBA-1^{TOTAL} correlated with better prognosis. (C–D) High area fraction and high mean intensity of CD204^{TOTAL} were associated with poorer prognosis. Patients with high area fraction of CD204^{TOTAL} and low area fraction of IBA-1^{TOTAL} had poorer outcome and shortest the median survival (E).

improved survival when divided at the median (data not shown). However, 40 patients (21%) had a MI above 107.0 which was the optimal cut-off, and these

patients survived significantly longer than patients with a lower intensity (HR = 0.64; 95% CI: 0.45–0.92; $P = 0.014$) (Figure 3B), and this was significant in the

that TAMs with intense expression of CD204 are the most important prognostic indicator.

TAMs, postsurgical treatment and survival

To further investigate the influence of TAMs, we stratified GBM patients based on postsurgical treatment and the level of total IBA-1 and CD204. AF IBA-1^{TOTAL} did not influence OS in the postsurgical-treated patients (HR = 1.00; 95% CI: 0.85–1.17; $P = 0.99$) or in patients only undergoing surgery (HR = 0.98; 95% CI: 0.70–1.38; $P = 0.91$) (Figure 4A). In the group who received postsurgical treatment, patients with high MI IBA-1^{TOTAL} had longer OS than patients with low MI (HR = 0.78; 95% CI: 0.64–0.95; $P = 0.013$), while this correlation was insignificant in patients who only received surgery (HR = 0.95; 95% CI: 0.63–1.42; $P = 0.79$) (Figure 4B). In the group receiving postsurgical treatment, high AF CD204^{TOTAL} predicted shorter OS (HR = 1.20; 95% CI: 1.03–1.42; $P = 0.019$), while no difference was found in the group who only underwent surgery (HR = 0.92; 95% CI: 0.66–1.31; $P = 0.66$) (Figure 4C). In the group receiving postsurgical treatment, patients with high MI CD204^{TOTAL} had poorer prognosis compared with patients with low MI CD204^{TOTAL} (HR = 1.52; 95% CI: 1.21–1.91; $P < 0.001$). No difference was found in the group undergoing surgery only (HR = 1.35; 95% CI: 0.88–2.07; $P = 0.17$) (Figure 4D).

TAMs, MGMT status and survival

The association between MGMT and TAMs was evaluated in 161 GBM patients, who were stratified based on MGMT methylation status and total IBA-1 or total CD204. High AF IBA-1^{TOTAL} levels tended to associate with shorter survival in patients with methylated MGMT promoter (m-MGMT) (HR = 1.26; 95% CI: 0.98–1.60; $P = 0.065$), while no association was found for MI IBA-1^{TOTAL} (HR = 0.83; 95% CI: 0.61–1.13; $P = 0.23$) (Figure 4E,F). In the patients with unmethylated MGMT promoter (u-MGMT), both high AF IBA-1^{TOTAL} and high MI IBA-1^{TOTAL} levels were associated with better outcome (HR = 0.80; 95% CI: 0.64–0.99; $P = 0.036$ and HR = 0.72; 95% CI: 0.54–0.95; $P = 0.020$) (Figure 4E,F). In the m-MGMT group, patients with high AF CD204^{TOTAL} had poorer prognosis than patients with low AF CD204^{TOTAL} (HR = 1.38;

95% CI: 1.07–1.77; $P = 0.009$), while this was not the case in the u-MGMT group (HR = 1.06; 95% CI: 0.85–1.31; $P = 0.61$) (Figure 4G). In patients with m-MGMT, high MI CD204^{TOTAL} was associated with shorter survival (HR = 1.67; 95% CI: 1.12–2.51; $P = 0.009$), whereas the prognostic value was less evident in patients with u-MGMT (HR = 1.34; 95% CI: 1.00–1.78; $P = 0.043$) (Figure 4H).

When MGMT status was included in the multivariate analysis, AF IBA-1^{TOTAL} and MI IBA-1^{TOTAL} were insignificant regarding prognosis, whereas high levels of both AF CD204^{TOTAL} (HR = 1.66; 95% CI: 1.16–2.37; $P = 0.005$) and MI CD204^{TOTAL} (HR = 2.11; 95% CI: 1.31–3.40; $P = 0.002$) predicted poorer OS (Table 2). Similar was found for both high AF CD204^{IBA-1} and MI CD204^{IBA-1} (data not shown).

TAMs and tumour heterogeneity

GBMs displayed intertumoural (Figure 5A–C) and intratumoural (Figure 5D) heterogeneity in terms of the expression of IBA-1 and CD204. IBA-1⁺ and/or CD204⁺ TAMs tended to accumulate in perivascular areas (Figure 5E,F), pseudopalisading necroses (Figure 5G) and perinecrotic areas (Figure 5H). In the tumour periphery, TAMs primarily expressed IBA-1 and appeared more ramified compared with the central tumour where they often had an amoeboid morphology. Interestingly, some double-positive TAMs were seen at the edge between central tumour and tumour periphery (Figure 5I). Quantified, the amount of TAMs was lower in the periphery compared with the central zone ($P < 0.01$ or $P < 0.05$) (Figure 5J and Table S6). The IBA-1 intensity was similar in the two areas, while the CD204 intensity decreased from the central to the peripheral tumour area ($P < 0.05$) (Figure 5K and Table S6).

The relation between TAMs and the presence of gemistocytes was examined by assessing the gemistocytic cell component in 48 astrocytomas (11 DAs, 17 AAs and 20 GBMs). High amounts of CD204 and high AF IBA-1^{TOTAL} positively correlated with gemistocytic score. Contrarily, in GBMs, high MI IBA-1^{TOTAL} inversely correlated with gemistocytic score (Table S7).

To estimate the associations between tumour subtype and TAMs, 20 GBMs were immunohistochemically subtyped using three proneural and three mesenchymal

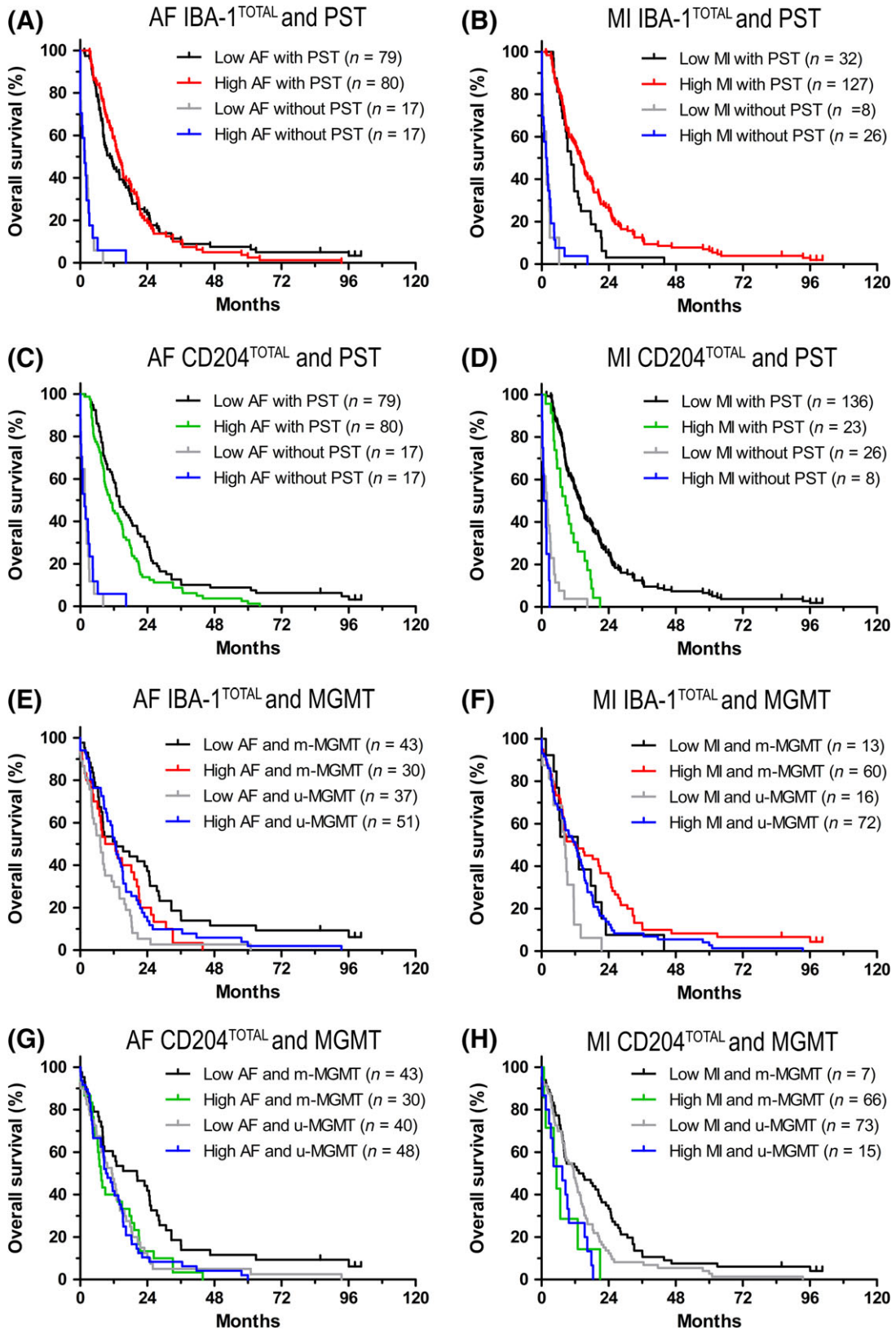


Figure 4. The association between tumour-associated microglia/macrophages and postsurgical treatment or MGMT methylation status. (A–D) Patients with glioblastoma ($n = 193$) were stratified based on whether they had received postsurgical treatment and on (A) AF IBA-1^{TOTAL}, (B) MI of IBA-1^{TOTAL}, (C) AF CD204^{TOTAL} or (D) MI of CD204^{TOTAL}. (E–F) Patients with glioblastoma ($n = 161$) were stratified based on MGMT methylation status and on the (E) AF IBA-1^{TOTAL}, (F) MI of IBA-1^{TOTAL}, (G) AF CD204^{TOTAL} or (H) MI of CD204^{TOTAL}. AF, area fraction; IBA-1, ionized calcium-binding adaptor molecule-1; MGMT, O6-methylguanine–DNA methyltransferase; m-MGMT, methylated MGMT promoter; MI, mean intensity; u-MGMT, unmethylated MGMT promoter; PST, postsurgical treatment.

markers (Figure 5L). The mesenchymal tumours generally had higher levels of AF IBA-1^{TOTAL} ($P = 0.022$) and CD204 ($P < 0.001$) (Figure 5M,N) and a higher gemistocytic score ($P = 0.020$) (Table S6), whereas the proneural tumours showed higher levels of MI IBA-1^{TOTAL} ($P = 0.012$) (Figure 5N and Table S6). In addition, high AF CD204^{TOTAL} (HR = 2.91; 95% CI: 1.03–8.18; $P = 0.035$) and the mesenchymal subtype (HR = 2.97; 95% CI: 1.01–8.76; $P = 0.040$) showed similar survival curves, and both correlated with decreased OS (Figure 5O).

TAMs and CD204 phenotype

To explore the phenotype of CD204⁺ TAMs in patient tissue, we performed double immunofluorescence with CD204 and markers related to inflammation and immune activation, as well as to infiltration, proliferation, angiogenesis and necrosis (Figure 6A–H) [8,9,11,21,51]. On average, 44% and 8% of the CD204⁺ area co-expressed the marker major histocompatibility complex class II (HLA-DR) and tumour necrosis factor alpha (TNF- α), respectively (Figure 6A,B,I), while 10% and 3% co-localization was seen with the anti-inflammatory markers interleukin 10 (IL10) and transforming growth factor beta1 (TGF- β 1) (Figure 6C, D,I). Most of the CD204⁺ area co-expressed matrix metalloproteinase 14 (MMP14). Average co-expression of hypoxia-inducible factor-1alpha (HIF-1 α) was 13%. VEGF and CD204 rarely overlapped, whereas 9% of the CD204⁺ area co-localized with epidermal growth factor receptor (EGFR) (Figure 6E–I). A comparable scatter plot was found when measuring the intensity of the marker of interest within the CD204⁺ area (Figure S4).

CD204⁺ cells did not express glial fibrillary acidic protein, OLIG-2, microtubule-associated protein 2, or smooth muscle actin indicating that tumour cells and vascular smooth muscle cells do not contribute to the CD204⁺ cell population (Figure S4).

Patient databases

We evaluated two bioinformatics databases, validating that both IBA-1 and CD204 increased with malignancy grade (Figure S5A,B). In the Glavendeel and TCGA datasets, high CD204 mRNA levels correlated with poorer prognosis in GBM (HR = 1.41; 95% CI: 1.01–1.95; $P = 0.039$ and HR = 1.29; 95% CI: 1.05–1.57; $P = 0.013$) (Figure S5C,D). As expected, the mesenchymal subtype had the highest level of CD204 compared with the proneural and classical subtypes ($P < 0.001$) (Figure S5E,F).

Discussion

This study shows that M2-like TAMs predict poorer prognosis in high-grade glioma and are associated with more aggressive tumours as these cells are more frequent in tumours with high gemistocytic cell count and in GBMs of the mesenchymal subtype. Characterizing the M2-like TAMs in patient-derived GBM tissue revealed that M2-like TAMs may contribute to a tumour microenvironment favouring especially tumour infiltration and expansion, but also angiogenesis and tumour resistance (Figure 7).

We found that CD204 and IBA-1 levels increased with malignancy. This is in accordance with other studies on primary gliomas using general TAM markers CD68 [15,26,28] and IBA-1 [27,28], as well as M2 markers CD163 and CD204 [15]. Prosnik *et al.* [30], too, showed malignancy to correlate with high expression of M2-related molecules including IL-10, TGF- β , CD163 and CD204 at mRNA levels and/or immunohistochemically using human glioma specimens. However, these studies primarily used semi-quantitative scoring, and fewer patients (between 32 and 107 patients) were included.

The acquired phenotype of TAMs was found to affect prognosis, while the general amount of TAMs was less important as the fraction of IBA-1⁺ in the total tumour

Table 2. Multivariate Cox regression analyses of IBA-1 and CD204 levels in patients with WHO grade IV tumours including clinical parameters and MGMT status

		HR (95% CI)		P-value	HR (95% CI)		P-value
No. of patients		Baseline model			AF IBA-1 ^{TOTAL}		MI IBA-1 ^{TOTAL}
Age	161	1.01 (1.00–1.03)		0.13	1.01 (1.00–1.03)		0.15
Performance status							
0–1	100	1.00			1.00		
2–4	61	1.43 (1.25–1.64)		<0.001	1.43 (1.25–1.64)		<0.001
Tumour crossing midline							
No	148	1.00			1.00		
Yes	13	1.78 (0.97–3.27)		0.064	1.79 (0.97–3.31)		0.064
Postsurgical treatment							
Stupp*	92	1.00			1.00		
PC†	40	1.45 (0.95–2.21)		0.084	1.45 (0.95–2.22)		0.084
None‡	29	9.50 (5.35–16.9)		<0.001	9.55 (5.36–17.0)		<0.001
MGMT methylation status							
Unmet	88	1.00			1.00		
Met	73	0.85 (0.59–1.23)		0.40	0.85 (0.58–1.24)		0.40
AF/MI							
Low	–	–			1.00		
High	–	–			0.98 (0.69–1.38)		0.89
		AF CD204 ^{TOTAL}			MI CD204 ^{TOTAL}		
Age	161	–	–	1.02 (1.00–1.03)	0.086	1.01 (1.00–1.03)	
Performance status							
0–1	100	–	–	1.00		1.00	
2–4	61	–	–	1.47 (1.28–1.69)	<0.001	1.40 (1.22–1.61)	
Tumour crossing midline							
No	148	–	–	1.00		1.00	
Yes	13	–	–	1.74 (0.94–3.22)	0.076	1.85 (1.00–3.41)	
Postsurgical treatment							
Stupp*	92	–	–	1.00		1.00	
PC†	40	–	–	1.67 (1.08–2.58)	0.022	1.47 (0.96–2.25)	
None‡	29	–	–	8.63 (4.88–15.3)	<0.001	10.4 (5.81–18.8)	
MGMT methylation status							
Unmet	88	1.00	–	1.00		1.00	
Met	73	–	–	0.96 (0.66–1.39)	0.82	0.89 (0.61–1.28)	
AF/MI							
Low	–	–	–	1.00		1.00	
High	–	–	–	1.66 (1.16–2.37)	0.005	2.11 (1.31–3.40)	

IBA-1, ionized calcium-binding adaptor molecule-1; WHO, World Health Organization; AF, area fraction; MI, mean intensity; PC, palliative care; MGMT, O6-methylguanine–DNA methyltransferase.

*Treatment according to the publication by Stupp *et al.* [1].

†Palliative treatment is radiotherapy alone (60 Gy/30–33 fractions), hypofractionated radiotherapy alone (30–34 Gy/10 fractions), hypofractionated radiotherapy with chemotherapy, or chemotherapy alone.

‡No postsurgical treatment.

Bold values represent the significant P values (P < 0.05)

area (AF IBA-1^{TOTAL}) did not influence OS. The IBA-1 intensity, however, seemed to correlate with better outcome in patients grade II, III and IV gliomas. In contrast, high amounts of CD204 predicted poorer survival in WHO grade III–IV gliomas, but not in grade II tumours. This was confirmed in two bioinformatics

databases. Previous studies have shown that high CD163/CD68 [15] and CD163/IBA-1 ratios [29] as well as high CD163 content [30] predict shorter survival in high-grade gliomas. We used CD204 to identify M2 TAMs as CD163 is only reliable as a M2 marker when in combination with the transcription factor

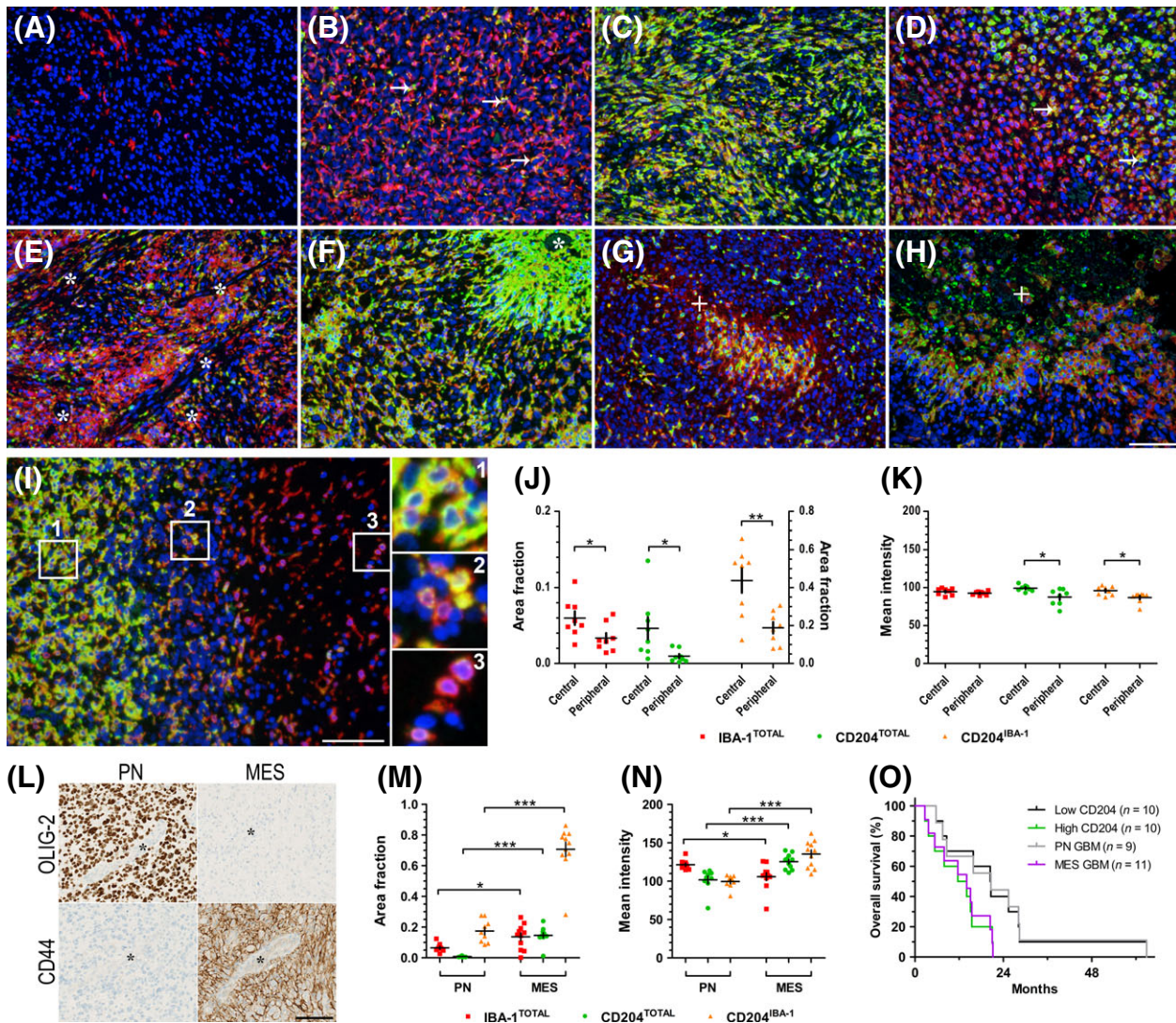


Figure 5. Tumour-associated microglia/macrophages (TAMs) heterogeneity in glioblastomas. (A–D) Phenotypic differences in ionized calcium-binding adaptor molecule-1 (IBA-1) (red) and CD204 (green) expression were seen between tumours (A–C) and within the individual tumour (D). Arrows indicate double-positive cells. (E–H) Besides expression in viable tumour tissue, TAMs were also present around blood vessels (Asterisk) (E,F) and in perinecrotic areas including pseudopalisading necroses (Plus) (G,H) often in clusters. (I) The density of TAMs, especially CD204⁺ TAMs, was higher in the central tumour (insert 1) compared with the border zone (insert 2) and the tumour periphery (insert 3). (J,K) The amount of CD204 was significantly lower in the tumour periphery compared with central tumour. (L) Tissue from 20 patients with glioblastoma was immunohistochemically subtyped using three proneural markers [PN, shown for oligodendrocyte transcription factor 2 (OLIG-2)] and three mesenchymal markers (MES, shown for CD44). (M,N) Especially CD204 expression was higher in the mesenchymal than in the proneural subtype. (O) Survival curve for the 20 patients with glioblastoma based on the area of CD204 in total tumour area (area fraction CD204^{TOTAL}) and subtype. Horizontal and vertical lines indicate mean \pm SEM. * $P < 0.05$; ** $P < 0.01$; *** $P < 0.001$. Scale bar 100 μ m.

V-maf avian musculoaponeurotic fibrosarcoma oncogene homologue (c-MAF) [51,52]. Further, assessing the general population of TAMs with CD68 may be problematic. Reportedly, M1 macrophages express high levels of CD68 [51], and recently, CD68 expression was found in many cases to be lower compared with

CD163 in GBMs [52,53]. In addition, CD68 was shown to be expressed by some human glioma cells [54,55]. Overall, these findings question its suitability as a general marker of TAMs.

In our study, we included more patients compared to previous prognostic studies on TAMs in gliomas [15,

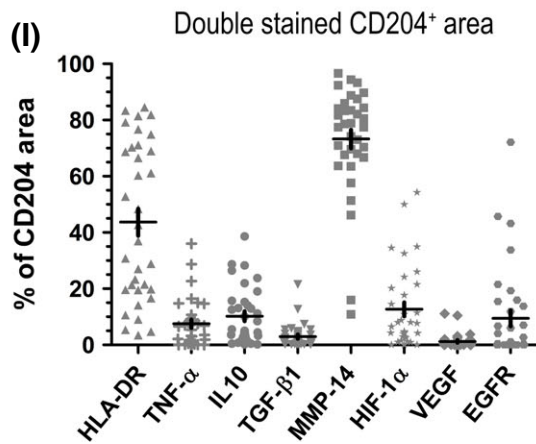
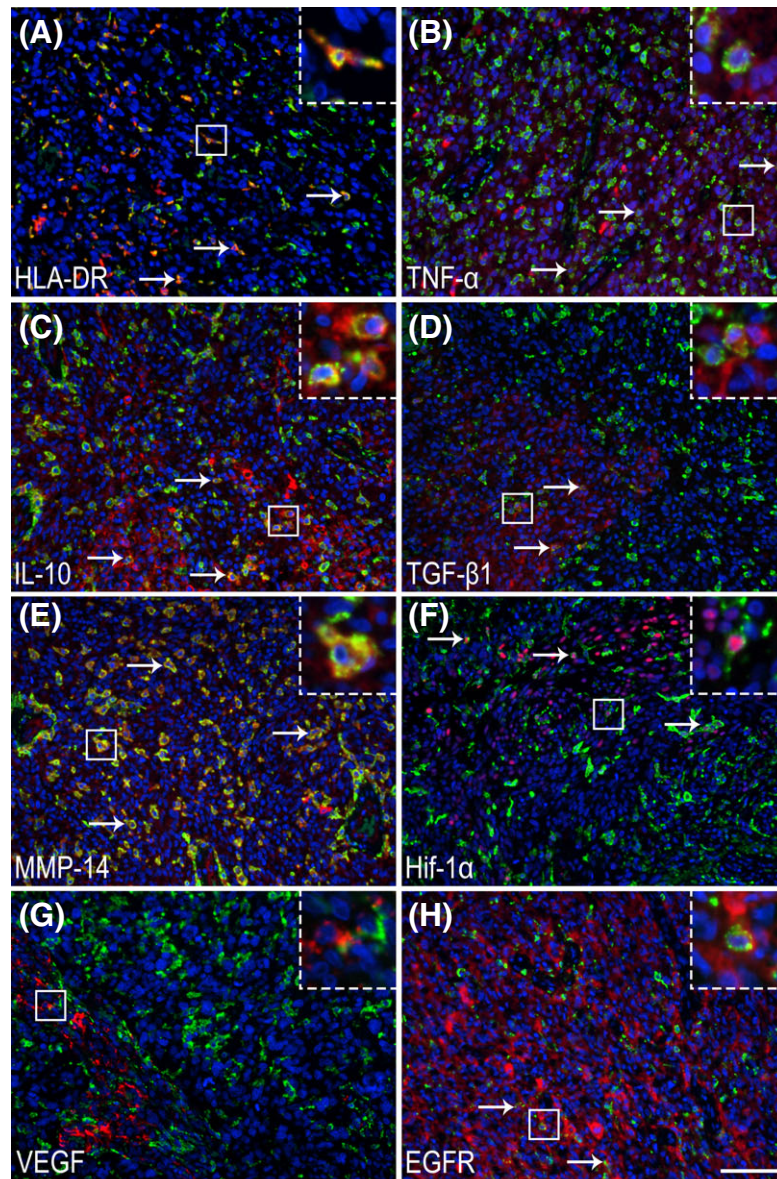


Figure 6. Characterization of CD204⁺ tumour-associated microglia/macrophages. (A–H) The phenotype of the CD204⁺ cells (green) was investigated using markers related to M1 polarization: HLA-DR (red) and TNF- α (red) (A, B), M2 polarization: IL10 (red) and TGF- β 1 (red) (C, D) as well as to tumour aggressiveness: MMP-14 (red), HIF-1 α (red), VEGF (red) and EGFR (red) (E–H). (I) For the marker of interest, the double-positive area was quantified as a percentage of the total CD204⁺ area. Arrows and inserts show double-positive cells. Horizontal and vertical lines indicate mean \pm SEM. Scale bar 100 μ M. HLA-DR, human leucocyte antigen DR/major histocompatibility complex class II DR; TNF- α , tumour necrosis factor alpha; IL10, interleukin 10; TGF- β 1, transforming growth factor beta1; MMP-14, matrix metalloproteinase 14; HIF-1 α , hypoxia-inducible factor-1alpha; VEGF, vascular endothelial growth factor; EGFR, epidermal growth factor receptor.

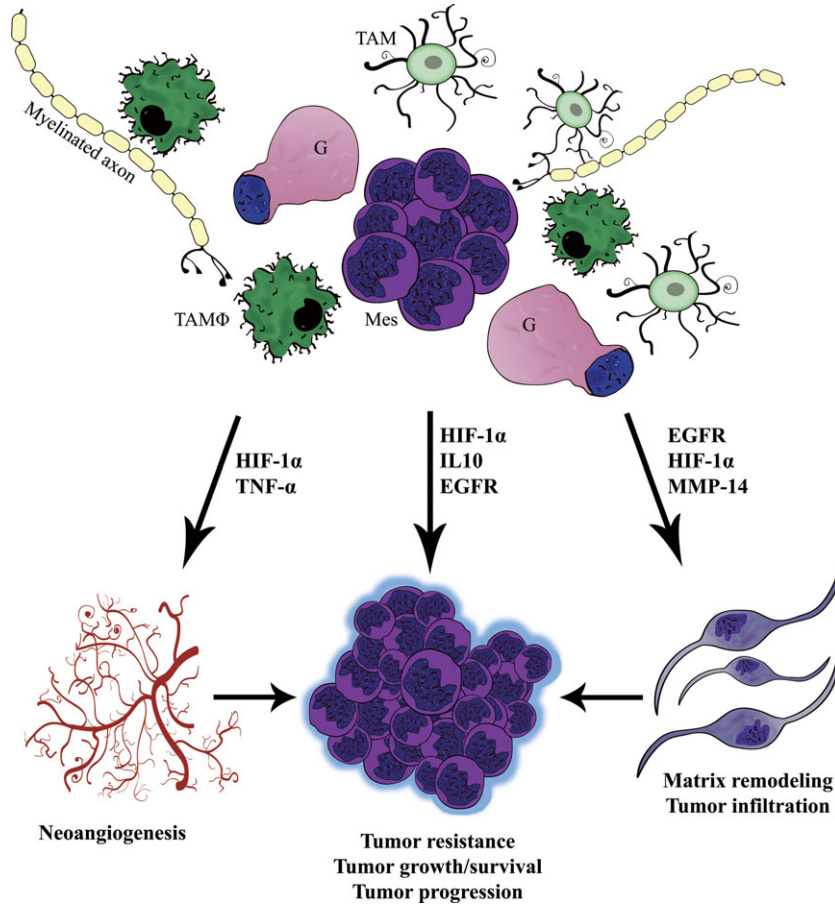


Figure 7. Schematic illustration of the presumed cross-talk between glioblastoma cells and M2-like TAMs. In the tumour microenvironment, M2-like tumour-associated microglia/macrophages expressing high amounts of CD204 with lower levels of ionized calcium-binding adaptor molecule-1 and HLA-DR interact with the glioblastoma cells favouring a mesenchymal shift in the tumour cells. The M2-like TAMs produce MMP14, HIF-1 α , IL10, EGFR and TNF- α possibly stimulating angiogenesis and especially matrix remodelling. With scavenger functions of CD204, e.g. clearance of myelin, extracellular matrix components and apoptotic cells, M2-like TAMs may ultimately enable tumour infiltration and progression. G, gemistocytes; TAM, tumour-associated microglia; TAM Φ , tumour-associated macrophage; MES, mesenchymal glioblastoma cells; IL10, interleukin 10; TNF- α , tumour necrosis factor alpha; EGFR, epidermal growth factor receptor; MMP14, matrix metalloproteinase 14; HLA-DR, human leucocyte antigen DR/major histocompatibility complex class II DR; HIF-1 α , hypoxia-inducible factor-1alpha.

26–28,30]. However, our study also had a limited number of patients with grade II–III gliomas and may not be representative for the entire population. The statistical analyses should, thus, be interpreted with caution.

In our multivariate analyses, CD204 was an independent predictor of poor OS in grade III–IV tumours. Similar has been reported in carcinomas including pancreatic [56,57], bladder [58] and lung cancers [59],

while no independent prognostic value was found of CD204⁺ TAMs in oesophageal cancer [60] or in primary CNS lymphoma [61]. Contradictory results have been reported in colorectal cancer [62–64], but in gastric [65] and ovarian cancer [66] high density of M1 TAMs and high M1/M2 ratio were associated with longer survival, whereas M2 TAMs themselves (identified with a CD163 antibody) showed no influence on prognosis. Zhang *et al.* [64] conducted a meta-analysis on solid tumours analysing primarily the impact of CD68⁺ TAMs and found that a high density of TAMs in most cancers appears to associate with poorer OS. Summarized, the prognostic value of TAMs may differ among and within the different cancers dependent on the tumour microenvironment, but also on the specific marker used to identify them. Most research including our results indicates that M2 TAMs favour tumour progression.

TAMs were heterogeneously distributed in gliomas at the inter- and intratumoral level. This is possibly explained by the predominant cellular component in the tumours and the molecular subclass of the glioma. For the first time, we report that CD204⁺ TAMs at a protein level are more abundant in astrocytomas with large fractions of gemistocytes and in GBMs of the mesenchymal subtype. This is comparable to previous results reporting a positive correlation between microglial and gemistocytic index in grade II–IV gemistocytic astrocytomas [67]. Further, at the mRNA level, TAM-related markers were enriched in GBMs with a mesenchymal molecular signature [45,68], and similar correlations were reported for tumour-infiltrating lymphocytes [69]. High frequency of gemistocytes has been linked to higher probability of tumour protein 53 mutations, B-cell lymphoma 2 expression and tumour progression/recurrence [70,71], while the mesenchymal subtype is associated with high degrees of necrosis, poorer patient prognosis, treatment resistance and is the most frequent subtype in recurrent GBMs [45,46,72]. Overall, this suggests that TAMs and especially M2 TAMs may contribute to tumour progression by stimulating the development of more aggressive tumours.

The M2-related marker CD204 belongs to the scavenger receptor family and is capable of binding and internalizing a range of ligands including apoptotic cells and chemically modified or altered molecules, for example, low-density lipoproteins, collagen and myelin [73,74]. Consistent with its function and with previous

observations [73], normal brain tissue had low levels of CD204. In GBMs, the amount and intensity of CD204 varied with some tumours expressing predominantly CD204 compared with IBA-1. IBA-1 is a general microglia/macrophage marker [75], but the expression level is upregulated upon cellular activation, and high levels of IBA-1 are associated with increased cell motility [31,76] and pro-inflammatory activity in macrophages [77,78]. Further, in Alzheimer's pathology, IBA-1 expression correlated with absence of dementia and better cognitive function possibly explained by a higher level of microglial active surveillance, while the opposite correlations were found for CD204 [79]. Analysing the relation between IBA-1 and CD204, we found an inverse correlation between the intensity levels (data not shown), and survival analysis showed that TAMs with IBA-1^{LOW}/CD204^{HIGH} phenotype correlated with worse patient outcome, overall indicating that TAMs with IBA-1^{HIGH} phenotype may represent a population of activated TAMs which have not been polarized in the M2 direction and that the extent of M2 polarization is important. Most research indicates that M2 macrophages are a heterogeneous population that can be divided into M2a, M2b and M2c subsets [80]. Gabrusiewicz *et al.* [21] showed that CD204 is mainly augmented in M2a and M2c macrophages in vitro. When we investigated the functional properties of the CD204⁺ TAMs, we found conjunctionally expression of proteins related to M1 (HLA-DR, TNF- α) and M2 (IL-10, TGF- β 1) activation. Our data contradict in vitro findings performed on rodent microglia arguing that M2 TAMs produce more TGF- β 1 and IL10 compared with TNF- α [16,81,82], as we found little to moderate overlap between CD204 and all three cytokines. Our data indicate that TAMs cannot be delimited into a classical M1 or M2 activation state, but represent a unique phenotype. This is supported by recent microarray and RNA sequencing data on TAMs isolated from murine and human gliomas [17–21] and by results found in pancreatic cancer [83]. Reportedly, M2 TAMs show reduced expression of HLA-DR resulting in poorer antigen presentation [9,51], although the downregulation of the co-stimulatory molecules CD80 and CD86 may be of greater importance [13,14]. We only found 50% co-expression between CD204 and HLA-DR indicating an overall impaired ability to present antigens. However, the range of HLA-DR co-expression was between 3% and

85% suggesting that a subset of M2 TAMs resembled the HLA-DR⁻ myeloid-derived suppressor cells (MDSCs), while another subset resembled a more classical HLA-DR^{HIGH} M1 phenotype. This reflects the heterogeneity also among M2 TAMs and indicates that their polarization might depend on the location of the specific TAM within the tumour tissue as well as its specific cellular origin (macrophages vs. microglia vs. MDSCs) and on the stage of disease.

M2 TAMs may contribute to treatment resistance

In GBM patients, CD204⁺ TAMs correlated with poorer survival in patients receiving postsurgical treatment. When we included MGMT methylation, high amounts of CD204 also predicted poorer survival in patients with MGMT methylated promoters, while the survival detriment was less evident in patients with unmethylated MGMT promoters. This suggests that M2 TAMs contribute to treatment resistance in GBMs. The importance of myeloid cells including TAMs in the therapeutic response in cancer has recently been reviewed [84]. In GBMs, tumour resistance has also been linked to tumour hypoxia [6,85]. Supported by previous reports [86–88], we observed that TAMs accumulated in areas of hypoxia, and when investigating the phenotype of CD204⁺ cells, we found up to 50% co-expression with HIF-1 α . Reportedly, hypoxic conditions induce a mesenchymal shift in GBMs [85,89] and fine-tune the M2 polarization of TAMs [90], leading to an upregulation of HIFs and HIF target genes by TAMs including MMPs and proangiogenic factors, for example, TNF- α [86,87]. In a breast carcinoma model, the tumour volume was reduced, and docetaxel proved more effective when the tumour environment contained HIF-1 α knockout macrophages as compared with a microenvironment with wild-type macrophages [91]. In summary, this suggests that TAMs and hypoxia co-ordinate a microenvironment favouring tumour resistance and progression.

Primarily, IBA-1⁺ TAMs were present in the tumour periphery, whereas CD204⁺ TAMs were restricted to the central tumour and the area adjacent to the tumour periphery, suggesting that M2 TAMs may contribute to tumour invasiveness. This is in agreement with a study in which TAMs were found to reside at the invasive front [82]. Our immunofluorescence characterization of the CD204⁺ TAMs revealed a substantial

co-expression of MMP-14, which reportedly acts as a co-factor for extracellular matrix breakdown and tumour expansion [8,9,22,24] as well as of EGFR which has been linked to increased tumour invasiveness and proliferation/survival [24,25]. Together with the scavenger function of CD204, this indicates that TAMs co-expressing CD204 and MMP14 may be effective mediators of matrix remodelling facilitating tumour infiltration.

Conclusions

Recent genetic profiling of TAMs in human GBM indicates that TAMs can take on several phenotypes along the M1-M2 spectrum including the more undifferentiated M0 state [21]. Our results demonstrate that the prognostic impact of TAMs in gliomas does not depend on the total amount of TAMs, but on their acquired functional phenotype. High levels of the M2-related marker CD204 correlated with increasing malignancy grade and poor patient survival in WHO grade III and IV independently of clinical-pathological parameters. CD204⁺ TAMs were associated with a more aggressive tumour subtype and expressed proteins that could enable tumour progression. These results highlight the significant existence of TAMs in the tumour microenvironment and demonstrate that quantitative assessment of CD204 is feasible and potentially a clinically valuable prognostic biomarker in high-grade gliomas. Deeper insight into the impact of TAMs in gliomas may open new possibilities and expand the field of treatment strategies using TAMs as novel targets.

Ethics approval and consent to participate

The study was approved by the Regional Committee on Health Research Ethics for Southern Denmark (Project-ID: S2D09Oo80) as well as the Danish Data Protection Agency (file number: 2009-41-3070). The use of tissue was not prohibited by any patient according to the Danish Tissue Application Register.

Acknowledgements

We thankfully acknowledge the excellent laboratory work performed by technicians Helle Wohlleben and Tanja Dreehsen Højgaard as well as the technical assistance performed by the Chromosome and PCR

laboratories at the Department of Pathology, Odense University Hospital. We thank Guido Reifenberger and his research group at the Department of Neuropathology, Heinrich Heine University, Düsseldorf, Germany, for sharing their design for the 20 glioma-associated gene panel used for next-generation sequencing.

Author contributions

MDS and BWK conceived and designed the experiments. MDS and RDH collected and assembled the data. MDS, RHD and HBH analysed and interpreted the results. SH and BWK contributed with reagents/materials/analysis tools. MDS drafted and edited the manuscript. All authors have read and approved the final manuscript.

Funding

This work was supported by The Danish Council for Independent Research (4183-00183), Odense University Hospital Research Funds, University of Southern Denmark, Danish Cancer Research Foundation, Oda and Hans Svenningsen's Foundation, Krista and Viggo Petersen's Foundation, Brødrene Hartmann's Foundation, Knud and Edith Eriksen's Memorial Foundation, Eva and Henry Frænkel's Memorial Foundation and Aase and Ejner Danielsen's Foundation.

Conflict of interests

The authors declare that they have no conflicts of interest.

References

- 1 Stupp R, Mason WP, van den Bent MJ, Weller M, Fisher B, Taphoorn MJ, Belanger K, Brandes AA, Marosi C, Bogdahn U, Curschmann J, Janzer RC, Ludwin SK, Gorlia T, Allgeier A, Lacombe D, Cairncross JG, Eisenhauer E, Mirimanoff RO. Radiotherapy plus concomitant and adjuvant temozolomide for glioblastoma. *N Engl J Med* 2005; **352**: 987–96
- 2 Gilbert MR, Wang M, Aldape KD, Stupp R, Hegi ME, Jaeckle KA, Armstrong TS, Wefel JS, Won M, Blumenthal DT, Mahajan A, Schultz CJ, Erridge S, Baumert B, Hopkins KI, Tzuk-Shina T, Brown PD, Chakravarti A, Curran WJ Jr, Mehta MP. Dose-dense temozolomide for newly diagnosed glioblastoma: a randomized phase III clinical trial. *J Clin Oncol* 2013; **31**: 4085–91
- 3 Stupp R, Hegi ME, Mason WP, van den Bent MJ, Taphoorn MJ, Janzer RC, Ludwin SK, Allgeier A, Fisher B, Belanger K, Hau P, Brandes AA, Gijtenbeek J, Marosi C, Vecht CJ, Mokhtari K, Wesseling P, Villa S, Eisenhauer E, Gorlia T, Weller M, Lacombe D, Cairncross JG, Mirimanoff RO. Effects of radiotherapy with concomitant and adjuvant temozolomide versus radiotherapy alone on survival in glioblastoma in a randomised phase III study: 5-year analysis of the EORTC-NCIC trial. *Lancet Oncol* 2009; **10**: 459–66
- 4 Wick W, Weller M, van den Bent M, Sanson M, Weiler M, von Deimling A, Plass C, Hegi M, Platten M, Reifenberger G. MGMT testing—the challenges for biomarker-based glioma treatment. *Nat Rev Neurol* 2014; **10**: 372–85
- 5 Sarkaria JN, Kitange GJ, James CD, Plummer R, Calvert H, Weller M, Wick W. Mechanisms of chemoresistance to alkylating agents in malignant glioma. *Clin Cancer Res* 2008; **14**: 2900–8
- 6 Beier D, Schulz JB, Beier CP. Chemoresistance of glioblastoma cancer stem cells—much more complex than expected. *Mol Cancer* 2011; **10**: 128
- 7 Badie B, Schartner JM. Flow cytometric characterization of tumor-associated macrophages in experimental gliomas. *Neurosurgery* 2000; **46**: 957–61; discussion 61–2
- 8 Charles NA, Holland EC, Gilbertson R, Glass R, Kettenmann H. The brain tumor microenvironment. *Glia* 2011; **59**: 1169–80
- 9 Li W, Graeber MB. The molecular profile of microglia under the influence of glioma. *Neuro Oncol* 2012; **14**: 958–78
- 10 Lima FR, Kahn SA, Soletti RC, Biasoli D, Alves T, da Fonseca AC, Garcia C, Romao L, Brito J, Holanda-Afonso R, Faria J, Borges H, Moura-Neto V. Glioblastoma: therapeutic challenges, what lies ahead. *Biochem Biophys Acta* 2012; **1826**: 338–49
- 11 Sica A, Schioppa T, Mantovani A, Allavena P. Tumour-associated macrophages are a distinct M2 polarised population promoting tumour progression: potential targets of anti-cancer therapy. *Eur J Cancer* 2006; **42**: 717–27
- 12 Zhang J, Sarkar S, Cua R, Zhou Y, Hader W, Yong VW. A dialog between glioma and microglia that promotes tumor invasiveness through the CCL2/CCR2/interleukin-6 axis. *Carcinogenesis* 2012; **33**: 312–19
- 13 Hussain SF, Yang D, Suki D, Aldape K, Grimm E, Heimberger AB. The role of human glioma-infiltrating microglia/macrophages in mediating antitumor immune responses. *Neuro Oncol* 2006; **8**: 261–79
- 14 Hussain SF, Yang D, Suki D, Grimm E, Heimberger AB. Innate immune functions of microglia isolated from human glioma patients. *J Transl Med* 2006; **4**: 15
- 15 Komohara Y, Ohnishi K, Kuratsu J, Takeya M. Possible involvement of the M2 anti-inflammatory macrophage

- phenotype in growth of human gliomas. *J Pathol* 2008; **216**: 15–24
- 16 Wu A, Wei J, Kong LY, Wang Y, Priebe W, Qiao W, Sawaya R, Heimberger AB. Glioma cancer stem cells induce immunosuppressive macrophages/microglia. *Neuro Oncol* 2010; **12**: 1113–25
 - 17 Hattermann K, Sebens S, Helm O, Schmitt AD, Mentlein R, Mehdorn HM, Held-Feindt J. Chemokine expression profile of freshly isolated human glioblastoma-associated macrophages/microglia. *Oncol Rep* 2014; **32**: 270–6
 - 18 Lisi L, Stigliano E, Lauriola L, Navarra P, Dello Russo C. Proinflammatory-activated glioma cells induce a switch in microglial polarization and activation status, from a predominant M2b phenotype to a mixture of M1 and M2a/B polarized cells. *ASN Neuro* 2014; **6**: 171–83
 - 19 Szulzewsky F, Pelz A, Feng X, Synowitz M, Markovic D, Langmann T, Holtman IR, Wang X, Eggen BJ, Bodecke HW, Hambarzumyan D, Wolf SA, Kettenmann H. Glioma-associated microglia/macrophages display an expression profile different from m1 and m2 polarization and highly express gpnmb and spp1. *PLoS ONE* 2015; **10**: e0116644
 - 20 Szulzewsky F, Arora S, de Witte L, Ulas T, Markovic D, Schultze JL, Holland EC, Synowitz M, Wolf SA, Kettenmann H. Human glioblastoma-associated microglia/monocytes express a distinct RNA profile compared to human control and murine samples. *Glia* 2016; **64**: 1416–36
 - 21 Gabrusiewicz K, Rodriguez B, Wei J, Hashimoto Y, Healy LM, Maiti SN, Thomas G, Zhou S, Wang Q, Elakkad A, Liebelt BD, Yaghi NK, Ezhilarasan R, Huang N, Weinberg JS, Prabhu SS, Rao G, Sawaya R, Langford LA, Bruner JM, Fuller GN, Bar-Or A, Li W, Colen RR, Curran MA, Bhat KP, Antel JP, Cooper LJ, Sulman EP, Heimberger AB. Glioblastoma-infiltrated innate immune cells resemble M0 macrophage phenotype. *JCI Insight* 2016; **1**: 1–19. DOI: 10.1172/jci.insight.85841
 - 22 Markovic DS, Vinnakota K, Chirasani S, Synowitz M, Raguette H, Stock K, Sliwa M, Lehmann S, Kalin R, van Rooijen N, Holmbeck K, Heppner FL, Kiwit J, Matyash V, Lehnardt S, Kaminska B, Glass R, Kettenmann H. Gliomas induce and exploit microglial MT1-MMP expression for tumor expansion. *Proc Natl Acad Sci U S A* 2009; **106**: 12530–5
 - 23 Bettinger I, Thanos S, Paulus W. Microglia promote glioma migration. *Acta Neuropathol* 2002; **103**: 351–5
 - 24 Coniglio SJ, Segall JE. Review: molecular mechanism of microglia stimulated glioblastoma invasion. *Matrix Biol* 2013; **32**: 372–80
 - 25 Coniglio SJ, Eugenin E, Dobrenis K, Stanley ER, West BL, Symons MH, Segall JE. Microglial stimulation of glioblastoma invasion involves epidermal growth factor receptor (EGFR) and colony stimulating factor 1 receptor (CSF-1R) signaling. *Mol Med* 2012; **18**: 519–27
 - 26 Nishie A, Ono M, Shono T, Fukushi J, Otsubo M, Onoue H, Ito Y, Inamura T, Ikezaki K, Fukui M, Iwaki T, Kuwano M. Macrophage infiltration and heme oxygenase-1 expression correlate with angiogenesis in human gliomas. *Clin Cancer Res* 1999; **5**: 1107–13
 - 27 Deininger MH, Seid K, Engel S, Meyermann R, Schluesener HJ. Allograft inflammatory factor-1 defines a distinct subset of infiltrating macrophages/microglial cells in rat and human gliomas. *Acta Neuropathol* 2000; **100**: 673–80
 - 28 Yi L, Xiao H, Xu M, Ye X, Hu J, Li F, Li M, Luo C, Yu S, Bian X, Feng H. Glioma-initiating cells: a predominant role in microglia/macrophages tropism to glioma. *J Neuroimmunol* 2011; **232**: 75–82
 - 29 Komohara Y, Horlad H, Ohnishi K, Fujiwara Y, Bai B, Nakagawa T, Suzu S, Nakamura H, Kuratsu J, Takeya M. Importance of direct macrophage-tumor cell interaction on progression of human glioma. *Cancer Sci* 2012; **103**: 2165–72
 - 30 Prosniak M, Harshyne LA, Andrews DW, Kenyon LC, Bedelbaeva K, Apanasovich TV, Heber-Katz E, Curtis MT, Cotzia P, Hooper DC. Glioma grade is associated with the accumulation and activity of cells bearing m2 monocyte markers. *Clin Cancer Res* 2013; **19**: 3776–86
 - 31 Ito D, Imai Y, Ohsawa K, Nakajima K, Fukuuchi Y, Kohsaka S. Microglia-specific localisation of a novel calcium binding protein, Iba1. *Brain Res Mol Brain Res* 1998; **57**: 1–9
 - 32 Dahlrot RH, Sorensen MD, Rosager AM, Hellwege S, Bangso JA, Rosenberg T, Petterson SA, Klitkou J, Fosmark S, Hansen S, Kristensen BW. Novel approaches for quantifying protein biomarkers in gliomas: benefits and pitfalls. *CNS Oncol* 2014; **3**: 287–98
 - 33 Taylor CR, Levenson RM. Quantification of immunohistochemistry—issues concerning methods, utility and semiquantitative assessment II. *Histopathology* 2006; **49**: 411–24
 - 34 Dahlrot RH, Hansen S, Herrstedt J, Schroder HD, Hjelmberg J, Kristensen BW. Prognostic value of Musashi-1 in gliomas. *J Neurooncol* 2013; **115**: 453–61
 - 35 Dahlrot RH, Hansen S, Jensen SS, Schroder HD, Hjelmberg J, Kristensen BW. Clinical value of CD133 and nestin in patients with glioma: a population-based study. *Int J Clin Exp Pathol* 2014; **7**: 3739–51
 - 36 Dahlrot RH, Kristensen BW, Hjelmberg J, Herrstedt J, Hansen S. A population-based study of high-grade gliomas and mutated isocitrate dehydrogenase 1. *Int J Clin Exp Pathol* 2013; **6**: 31–40
 - 37 Dahlrot RH, Kristensen BW, Hjelmberg J, Herrstedt J, Hansen S. A population-based study of low-grade gliomas and mutated isocitrate dehydrogenase 1 (IDH1). *J Neurooncol* 2013; **114**: 309–17
 - 38 Hermansen SK, Dahlrot RH, Nielsen BS, Hansen S, Kristensen BW. MiR-21 expression in the tumor cell compartment holds unfavorable prognostic value in gliomas. *J Neurooncol* 2013; **111**: 71–81

- 39 Music D, Dahlrot RH, Hermansen SK, Hjelmberg J, de Stricker K, Hansen S, Kristensen BW. Expression and prognostic value of the WEE1 kinase in gliomas. *J Neurooncol* 2016; **127**: 381–9
- 40 Petterson SA, Dahlrot RH, Hermansen SK, Munthe SK, Gundesen MT, Wohlleben H, Rasmussen T, Beier CP, Hansen S, Kristensen BW. High levels of c-Met is associated with poor prognosis in glioblastoma. *J Neurooncol* 2015; **122**: 517–27
- 41 Louis DN, Ohgaki H, Wiestler OD, Cavenee WK, Ellison DW, Figarella-Branger D, Perry A, Reifenberger G, Von Deimling A. *WHO Classification of Tumours of the Central Nervous System, Revised 4th edn*. Lyon: International Agency for Research on Cancer (IARC), 2016
- 42 Halle B, Thomassen M, Venkatesan R, Kaimal V, Marcussen EG, Munthe S, Sorensen MD, Aaberg-Jessen C, Jensen SS, Meyer M, Kruse TA, Christiansen H, Schmidt S, Mollenhauer J, Schulz MK, Andersen C, Kristensen BW. Shift of microRNA profile upon orthotopic xenografting of glioblastoma spheroid cultures. *J Neurooncol* 2016; **128**: 395–404
- 43 Munthe S, Petterson SA, Dahlrot RH, Poulsen FR, Hansen S, Kristensen BW. Glioma cells in the tumor periphery have a stem cell phenotype. *PLoS ONE* 2016; **11**: e0155106
- 44 Beier CP, Kumar P, Meyer K, Leukel P, Bruttel V, Aschenbrenner I, Riemenschneider MJ, Fragoulis A, Rummele P, Lamszus K, Schulz JB, Weis J, Bogdahn U, Wischhusen J, Hau P, Spang R, Beier D. The cancer stem cell subtype determines immune infiltration of glioblastoma. *Stem Cells Dev* 2012; **21**: 2753–61
- 45 Bhat KP, Balasubramanian V, Vaillant B, Ezhilarasan R, Hummelink K, Hollingsworth F, Wani K, Heathcock L, James JD, Goodman LD, Conroy S, Long L, Lelic N, Wang S, Gumin J, Raj D, Kodama Y, Raghunathan A, Olar A, Joshi K, Pelloski CE, Heimberger A, Kim SH, Cahill DP, Rao G, Den Dunnen WF, Boddeke HW, Phillips HS, Nakano I, Lang FF, Colman H, Sulman EP, Aldape K. Mesenchymal differentiation mediated by NF-kappaB promotes radiation resistance in glioblastoma. *Cancer Cell* 2013; **24**: 331–46
- 46 Phillips HS, Kharbanda S, Chen R, Forrest WF, Soriano RH, Wu TD, Misra A, Nigro JM, Colman H, Soroceanu L, Williams PM, Modrusan Z, Feuerstein BG, Aldape K. Molecular subclasses of high-grade glioma predict prognosis, delineate a pattern of disease progression, and resemble stages in neurogenesis. *Cancer Cell* 2006; **9**: 157–73
- 47 Wang Q, Hu X, Muller F, Kim H, Squatrito M, Millesen T, Scarpace L, Barthel F, Lin Y-H, Satani N, Martinez-Ledesma E, Chang E, Olar A, Hu B, deCarvalho AC, Eskilsson E, Zheng S, Heimberger AB, Sulman EP, Nam D-H, Verhaak RGW. Tumor evolution of glioma intrinsic gene expression subtype associates with immunological changes in the microenvironment. *Cancer Cell* 2016; **32**: 42–56.e6 DOI: 10.1016/j.ccell.2017.06.003
- 48 Ceccarelli M, Barthel FP, Malta TM, Sabedot TS, Salama SR, Murray BA, Morozova O, Newton Y, Radenbaugh A, Pagnotta SM, Anjum S, Wang J, Manyam G, Zoppoli P, Ling S, Rao AA, Grifford M, Cherniack AD, Zhang H, Poisson L, Carlotti CG Jr, Tirapelli DP, Rao A, Mikkelsen T, Lau CC, Yung WK, Rabadan R, Huse J, Brat DJ, Lehman NL, Barnholtz-Sloan JS, Zheng S, Hess K, Rao G, Meyerson M, Beroukhir R, Cooper L, Akbani R, Wensch M, Haussler D, Aldape KD, Laird PW, Gutmann DH, Nounshmehr H, Iavarone A, Verhaak RG. Molecular profiling reveals biologically discrete subsets and pathways of progression in diffuse glioma. *Cell* 2016; **164**: 550–63
- 49 Cancer Genome Atlas Research N. Comprehensive genomic characterization defines human glioblastoma genes and core pathways. *Nature* 2008; **455**: 1061–8
- 50 Gravendeel LA, Kouwenhoven MC, Gevaert O, de Rooij JJ, Stubbs AP, Duijm JE, Daemen A, Bleeker FE, Bralten LB, Kloosterhof NK, De Moor B, Eilers PH, van der Spek PJ, Kros JM, Sillevius Smitt PA, van den Bent MJ, French PJ. Intrinsic gene expression profiles of gliomas are a better predictor of survival than histology. *Can Res* 2009; **69**: 9065–72
- 51 Chavez-Galan L, Olleros M, Vesin D, Garcia I. Much more than M1 and M2 macrophages, there are also CD169⁺ and TCR⁺ macrophages. *Front Immunol* 2015; **6**: 263
- 52 Barros MH, Hauck F, Dreyer JH, Kempkes B, Niedobitek G. Macrophage polarisation: an immunohistochemical approach for identifying M1 and M2 macrophages. *PLoS ONE* 2013; **8**: e80908
- 53 Mignogna C, Signorelli F, Vismara MF, Zeppa P, Camastro C, Barni T, Donato G, Di Vito A. A reappraisal of macrophage polarization in glioblastoma: histopathological and immunohistochemical findings and review of the literature. *Pathol Res Pract* 2016; **212**: 491–9 DOI: 10.1016/j.prp.2016.02.020
- 54 Leenstra S, Das PK, Troost D, de Boer OJ, Bosch DA. Human malignant astrocytes express macrophage phenotype. *J Neuroimmunol* 1995; **56**: 17–25
- 55 Strojnik T, Kavalar R, Zajc I, Diamandis EP, Oikonomopoulou K, Lah TT. Prognostic impact of CD68 and kallikrein 6 in human glioma. *Anticancer Res* 2009; **29**: 3269–79
- 56 Sugimoto M, Mitsunaga S, Yoshikawa K, Kato Y, Gotohda N, Takahashi S, Konishi M, Ikeda M, Kojima M, Ochiai A, Kaneko H. Prognostic impact of M2 macrophages at neural invasion in patients with invasive ductal carcinoma of the pancreas. *Eur J Cancer* 2014; **50**: 1900–8
- 57 Yoshikawa K, Mitsunaga S, Kinoshita T, Konishi M, Takahashi S, Gotohda N, Kato Y, Aizawa M, Ochiai A. Impact of tumor-associated macrophages on invasive ductal carcinoma of the pancreas head. *Cancer Sci* 2012; **103**: 2012–20

- 58 Wang B, Liu H, Dong X, Wu S, Zeng H, Liu Z, Wan D, Dong W, He W, Chen X, Zheng L, Huang J, Lin T. High CD204⁺ tumor-infiltrating macrophage density predicts a poor prognosis in patients with urothelial cell carcinoma of the bladder. *Oncotarget* 2015; **6**: 20204–14
- 59 Hirayama S, Ishii G, Nagai K, Ono S, Kojima M, Yamauchi C, Aokage K, Hishida T, Yoshida J, Suzuki K, Ochiai A. Prognostic impact of CD204-positive macrophages in lung squamous cell carcinoma: possible contribution of CD204-positive macrophages to the tumor-promoting microenvironment. *J Thorac Oncol* 2012; **7**: 1790–7
- 60 Shigeoka M, Urakawa N, Nakamura T, Nishio M, Watajima T, Kuroda D, Komori T, Kakeji Y, Semba S, Yokozaki H. Tumor associated macrophage expressing CD204 is associated with tumor aggressiveness of esophageal squamous cell carcinoma. *Cancer Sci* 2013; **104**: 1112–19
- 61 Komohara Y, Horlad H, Ohnishi K, Ohta K, Makino K, Hondo H, Yamanaka R, Kajiwara K, Saito T, Kuratsu J, Takeya M. M2 macrophage/microglial cells induce activation of Stat3 in primary central nervous system lymphoma. *J Clin Exp Hematop* 2011; **51**: 93–9
- 62 Edin S, Wikberg ML, Dahlin AM, Rutegard J, Oberg A, Oldenborg PA, Palmqvist R. The distribution of macrophages with a M1 or M2 phenotype in relation to prognosis and the molecular characteristics of colorectal cancer. *PLoS ONE* 2012; **7**: e47045
- 63 Herrera M, Herrera A, Dominguez G, Silva J, Garcia V, Garcia JM, Gomez I, Soldevilla B, Munoz C, Provencio M, Campos-Martin Y, Garcia de Herreros A, Casal I, Bonilla F, Pena C. Cancer-associated fibroblast and M2 macrophage markers together predict outcome in colorectal cancer patients. *Cancer Sci* 2013; **104**: 437–44
- 64 Zhang QW, Liu L, Gong CY, Shi HS, Zeng YH, Wang XZ, Zhao YW, Wei YQ. Prognostic significance of tumor-associated macrophages in solid tumor: a meta-analysis of the literature. *PLoS ONE* 2012; **7**: e50946
- 65 Pantano F, Berti P, Guida FM, Perrone G, Vincenzi B, Amato MM, Righi D, Dell'aquila E, Graziano F, Catalano V, Caricato M, Rizzo S, Muda AO, Russo A, Tonini G, Santini D. The role of macrophages polarization in predicting prognosis of radically resected gastric cancer patients. *J Cell Mol Med* 2013; **17**: 1415–21
- 66 Zhang M, He Y, Sun X, Li Q, Wang W, Zhao A, Di W. A high M1/M2 ratio of tumor-associated macrophages is associated with extended survival in ovarian cancer patients. *J Ovarian Res* 2014; **7**: 19
- 67 Geranmayeh F, Scheithauer BW, Spitzer C, Meyer FB, Svensson-Engwall AC, Graeber MB. Microglia in gemistocytic astrocytomas. *Neurosurgery* 2007; **60**: 159–66; discussion 66.
- 68 Doucette T, Rao G, Rao A, Shen L, Aldape K, Wei J, Dziurzynski K, Gilbert M, Heimberger AB. Immune heterogeneity of glioblastoma subtypes: extrapolation from the cancer genome atlas. *Cancer Immunol Res* 2013; **1**: 112–22
- 69 Rutledge WC, Kong J, Gao J, Gutman DA, Cooper LA, Appin C, Park Y, Scarpace L, Mikkelsen T, Cohen ML, Aldape KD, McLendon RE, Lehman NL, Miller CR, Schniederjan MJ, Brennan CW, Saltz JH, Moreno CS, Brat DJ. Tumor-infiltrating lymphocytes in glioblastoma are associated with specific genomic alterations and related to transcriptional class. *Clin Cancer Res* 2013; **19**: 4951–60
- 70 Karsy M, Gelbman M, Shah P, Balumbu O, Moy F, Arslan E. Established and emerging variants of glioblastoma multiforme: review of morphological and molecular features. *Folia Neuropathol* 2012; **50**: 301–21
- 71 Okita Y, Narita Y, Miyakita Y, Ohno M, Fukushima S, Kayama T, Shibui S. Pathological findings and prognostic factors in recurrent glioblastomas. *Brain Tumor Pathol* 2012; **29**: 192–200
- 72 Piao Y, Liang J, Holmes L, Zurita AJ, Henry V, Heymach JV, de Groot JF. Glioblastoma resistance to anti-VEGF therapy is associated with myeloid cell infiltration, stem cell accumulation, and a mesenchymal phenotype. *Neuro Oncol* 2012; **14**: 1379–92
- 73 Husemann J, Loike JD, Anankov R, Febbraio M, Silverstein SC. Scavenger receptors in neurobiology and neuropathology: their role on microglia and other cells of the nervous system. *Glia* 2002; **40**: 195–205
- 74 Kelley JL, Ozment TR, Li C, Schweitzer JB, Williams DL. Scavenger receptor-A (CD204): a two-edged sword in health and disease. *Crit Rev Immunol* 2014; **34**: 241–61
- 75 Imai Y, Ibata I, Ito D, Ohsawa K, Kohsaka S. A novel gene *iba1* in the major histocompatibility complex class III region encoding an EF hand protein expressed in a monocytic lineage. *Biochem Biophys Res Comm* 1996; **224**: 855–62
- 76 Imai Y, Kohsaka S. Intracellular signaling in M-CSF-induced microglia activation: role of *Iba1*. *Glia* 2002; **40**: 164–74
- 77 Yang ZF, Ho DW, Lau CK, Lam CT, Lum CT, Poon RT, Fan ST. Allograft inflammatory factor-1 (AIF-1) is crucial for the survival and pro-inflammatory activity of macrophages. *Int Immunol* 2005; **17**: 1391–7
- 78 Yang ZF, Ho DW, Ngai P, Lau CK, Zhao Y, Poon RT, Fan ST. Antiinflammatory properties of IL-10 rescue small-for-size liver grafts. *Liver Transpl* 2007; **13**: 558–65
- 79 Minett T, Classey J, Matthews FE, Fahrenhold M, Taga M, Brayne C, Ince PG, Nicoll JA, Boche D. Microglial immunophenotype in dementia with Alzheimer's pathology. *J Neuroinflammation* 2016; **13**: 135
- 80 Mantovani A, Sica A, Sozzani S, Allavena P, Vecchi A, Locati M. The chemokine system in diverse forms of macrophage activation and polarization. *Trends Immunol* 2004; **25**: 677–86
- 81 Ellert-Miklaszewska A, Dabrowski M, Lipko M, Sliwa M, Maleszewska M, Kaminska B. Molecular definition of the pro-tumorigenic phenotype of glioma-activated microglia. *Glia* 2013; **61**: 1178–90

- 82 Ye XZ, Xu SL, Xin YH, Yu SC, Ping YF, Chen L, Xiao HL, Wang B, Yi L, Wang QL, Jiang XF, Yang L, Zhang P, Qian C, Cui YH, Zhang X, Bian XW. Tumor-associated microglia/macrophages enhance the invasion of glioma stem-like cells via TGF-beta1 signaling pathway. *J Immunol* 2012; **189**: 444–53
- 83 Helm O, Held-Feindt J, Grage-Griebenow E, Reiling N, Ungefroren H, Vogel I, Kruger U, Becker T, Ebsen M, Rocken C, Kabelitz D, Schafer H, Sebens S. Tumor-associated macrophages exhibit pro- and anti-inflammatory properties by which they impact on pancreatic tumorigenesis. *Int J Cancer* 2014; **135**: 843–61
- 84 Achyut BR, Arbab AS. Myeloid cell signatures in tumor microenvironment predicts therapeutic response in cancer. *Onco Targets Ther* 2016; **9**: 1047–55
- 85 Xu H, Rahimpour S, Nesvick CL, Zhang X, Ma J, Zhang M, Zhang G, Wang L, Yang C, Hong CS, Germanwala AV, Elder JB, Ray-Chaudhury A, Yao Y, Gilbert MR, Lonser RR, Heiss JD, Brady RO, Mao Y, Qin J, Zhuang Z. Activation of hypoxia signaling induces phenotypic transformation of glioma cells: implications for bevacizumab antiangiogenic therapy. *Oncotarget* 2015; **6**: 11882–93
- 86 Lewis C, Murdoch C. Macrophage responses to hypoxia: implications for tumor progression and anti-cancer therapies. *Am J Pathol* 2005; **167**: 627–35
- 87 Murdoch C, Muthana M, Lewis CE. Hypoxia regulates macrophage functions in inflammation. *J Immunol* 2005; **175**: 6257–63
- 88 Wang SC, Hong JH, Hsueh C, Chiang CS. Tumor-secreted SDF-1 promotes glioma invasiveness and TAM tropism toward hypoxia in a murine astrocytoma model. *Lab Invest* 2012; **92**: 151–62
- 89 Joseph JV, Conroy S, Pavlov K, Sontakke P, Tomar T, Eggens-Meijer E, Balasubramanian V, Wagemakers M, den Dunnen WF, Kruyt FA. Hypoxia enhances migration and invasion in glioblastoma by promoting a mesenchymal shift mediated by the HIF1alpha-ZEB1 axis. *Cancer Lett* 2015; **359**: 107–16
- 90 Laoui D, Van Overmeire E, Di Conza G, Aldeni C, Keirse J, Morias Y, Movahedi K, Houbracken I, Schoupe E, Elkrim Y, Karroum O, Jordan B, Carmeliet P, Gysemans C, De Baetselier P, Mazzone M, Van Ginderachter JA. Tumor hypoxia does not drive differentiation of tumor-associated macrophages but rather fine-tunes the M2-like macrophage population. *Can Res* 2014; **74**: 24–30
- 91 Chen D, Bobko AA, Gross AC, Evans R, Marsh CB, Khramtsov VV, Eubank TD, Friedman A. Involvement of tumor macrophage HIFs in chemotherapy effectiveness: mathematical modeling of oxygen, pH, and glutathione. *PLoS ONE* 2014; **9**: e107511

Supporting information

Additional Supporting Information may be found in the online version of this article at the publisher's web-site:

Figure S1. Run variation and calibration.

Figure S2. Expression of IBA-1 and CD204 in normal brain tissue and brain neoplasms.

Figure S3. Impact of TAMs on overall survival in WHO grade II and grade III gliomas.

Figure S4. Characterization of CD204⁺ TAMs.

Figure S5. Bioinformatics databases.

Table S1. Patient characteristics.

Table S2. List of applied antibodies and detection systems.

Table S3. Multivariate Cox regression analyses of IBA-1 and CD204 levels in patients with WHO grade II–IV gliomas.

Table S4. Multivariate Cox regression analyses of IBA-1 and CD204 levels in patients with WHO grade II tumours, including performance status, IDH status and histology ($n = 22$).

Table S5. Multivariate Cox regression analyses of IBA-1 and CD204 levels in patients with WHO grade III tumours, including performance status, IDH status and histology ($n = 22$).

Table S6. TAMs and tumour heterogeneity.

Table S7. Correlation between the gemistocytic cell score and the level of TAMs in astrocytomas.

Data S1. Materials and methods.

Received 6 September 2016

Accepted after revision 27 July 2017

Published online Article Accepted on 2 August 2017

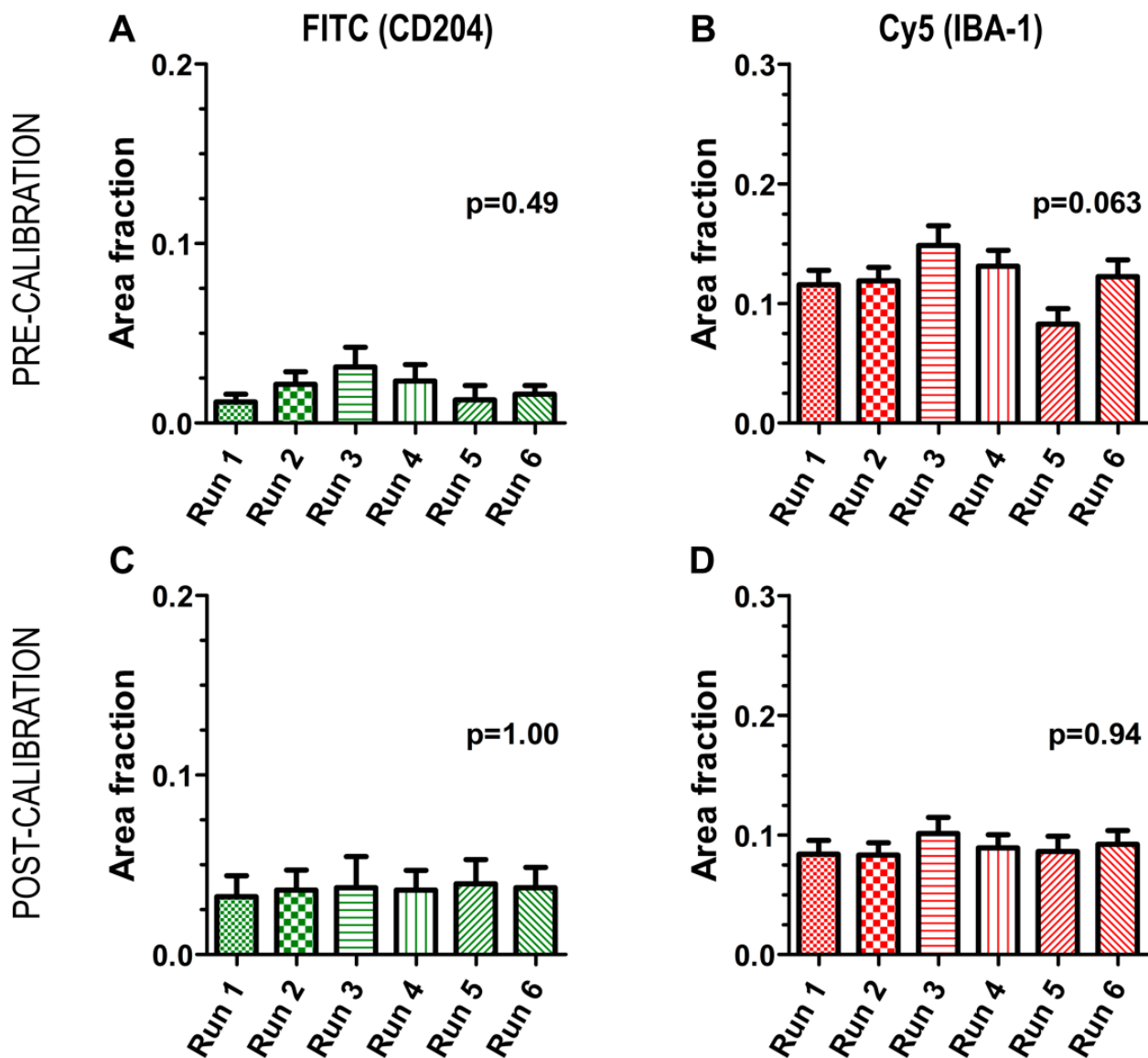


Figure S1 Run-variation and calibration. The staining of the patient cohort (n=240) was performed in six runs. To reduce the possible variation in the stainings between runs, calibration was performed using the positive controls of each run. The optimal target values for the area of IBA-1 in the total tumor area (AF IBA-1^{TOTAL}) and for the area of CD204 in the total tumor area (AF CD204^{TOTAL}) were determined in run 1 based on visual experience with the staining and the exposure time. The following runs (run 2-6) were then calibrated to match the optimal target values of run 1 by adjusting the exposure time for both fluorescein (FITC) and cyanine 5 (Cy5). (A) Before calibration, AF IBA-1^{TOTAL} tended to differ between runs. (B) Calibration successfully reduced this variation. (C, D) The same was true for AF CD204^{TOTAL}.

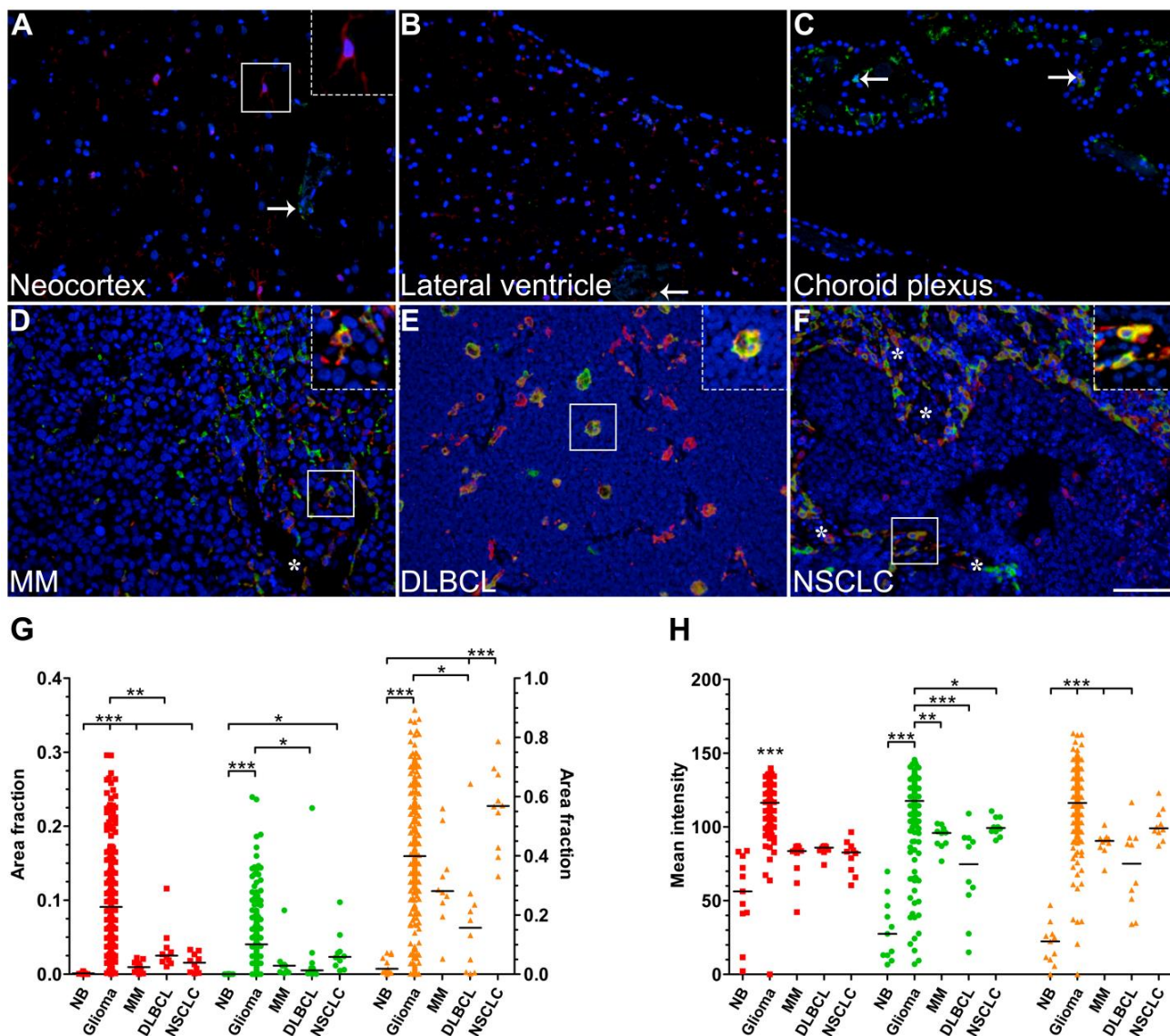


Figure S2 Expression of IBA-1 and CD204 in normal brain tissue and brain neoplasms. (A, B) In normal brain tissue IBA-1⁺ microglia (red) were present in limited numbers and exhibited a ramified morphology (*insert*). Very few CD204⁺ cells (green) was seen in the parenchyma, and they primarily surrounded small blood vessels (*arrows*). (C) A higher number was observed in choroid plexus (*arrows*). (D) A moderate number of IBA-1⁺ and CD204⁺ cells were found in malignant melanoma (MM) and tended to be located around blood vessels (*asterisk*). (E) Fewer positive cells were present in diffuse large B-cell lymphoma (DLBCL), but instead they exhibited a large amoeboid morphology. (F) A greater amount was found in non-small cell lung cancer (NSCLC) with perivascular accumulation (*asterisk*). (G-H) Quantifications of IBA-1^{TOTAL}, CD204^{TOTAL}, and CD204^{IBA-1} in normal brain tissue (NB), glioma (WHO grade I-IV), MM, DLBCL, and NSCLC.

Vertical lines indicate the median. * indicates p<0.05; ** p<0.01; *** p<0.001. Scale bar 100 μ m

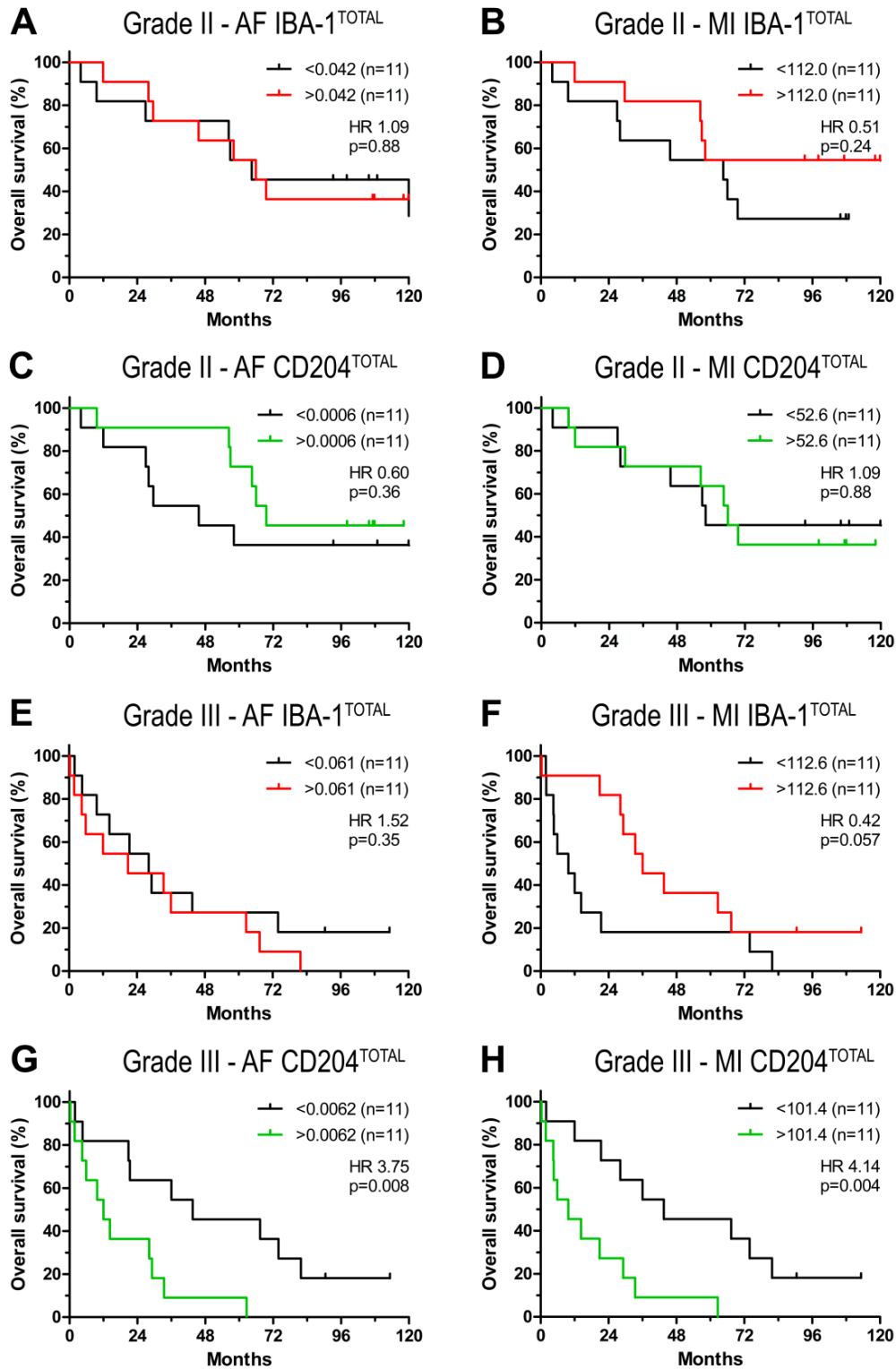


Figure S3 Impact of TAMs on overall survival in WHO grade II and grade III gliomas. Each variable was dichotomized at the median. In grade II gliomas neither (A, B) IBA-1 in total tumor tissue (IBA-1^{TOTAL}) nor (C, D) CD204 in total tumor tissue (CD204^{TOTAL}) influenced survival. In grade III gliomas, (E, F) IBA-1 in total tumor tissue (IBA-1^{TOTAL}) did not show significant prognostic value, while high values of CD204 in total tumor tissue (CD204^{TOTAL}) (G, H) were associated with poorer patient survival.

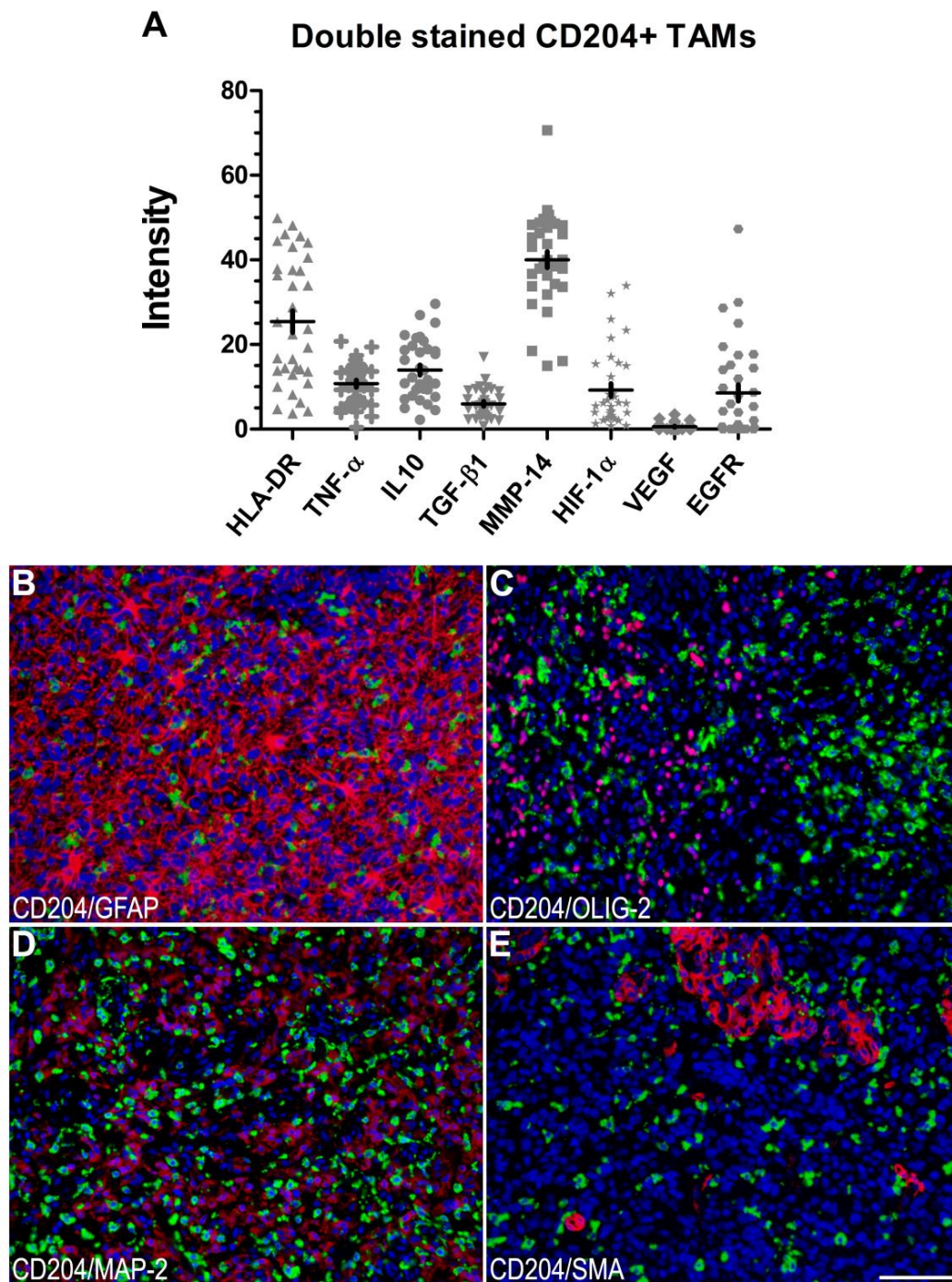


Figure S4 Characterization of CD204⁺ TAMs. (A) The phenotype of the CD204⁺ cells was examined using double immunofluorescence in two tissue arrays containing glioblastoma specimens (n=34). The investigated markers were related to M1 polarization: HLA-DR and TNF- α , M2 polarization: IL10 and TGF- β 1 as well as to tumor aggressiveness: MMP-14, HIF-1 α , VEGF, and EGFR. For the marker of interest, the mean intensity was measured in the total CD204⁺ area using a threshold-based software algorithm. (B-E) CD204⁺ cells (green) did not express GFAP (red) (B), OLIG-2 (red) (C), MAP-2 (red) (D), or SMA (red) (E). Vertical lines indicate mean \pm SEM. Scale bar 100 μ m

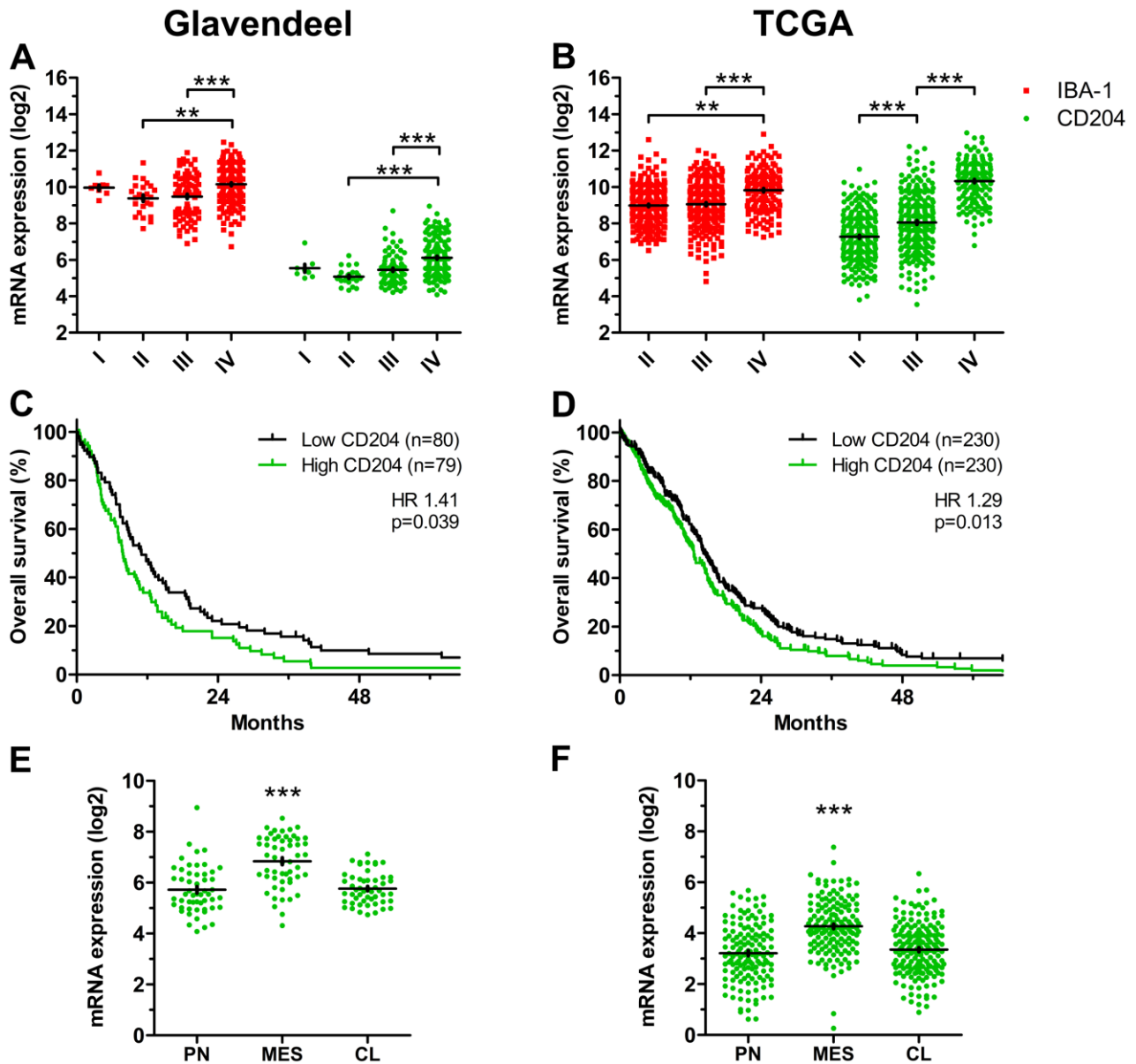


Figure S5 Bioinformatics databases. **(A, B)** mRNA expression of IBA-1 and CD204 increased significantly with malignancy in the Glavendeel dataset **(A)** and in the Cancer Research Atlas (TCGA) **(B)**. **(C)** In the Glavendeel dataset, high CD204 was significantly associated with shorter overall survival in patients with primary glioblastoma when dichotomized at the median. **(D)** Similar was observed in the TCGA dataset. **(E, F)** Mesenchymal glioblastomas showed the highest levels of CD204 in both the Glavendeel dataset **(E)** and in the TCGA **(F)**. Vertical lines indicate mean \pm SEM. ** indicates $p < 0.01$; *** $p < 0.001$.

Table S1 Patient characteristics

Parameter	Grade I	Grade II	Grade III	Grade IV	All grades
	No (%)	No (%)	No (%)	No (%)	No (%)
Patients (n)	3 (100)	22 (100)	22	193	240
Sex (n)					
Male	1 (33)	13 (59)	18 (82)	111	143
Female	2 (67)	9 (41)	4 (18)	82	97
Age					
Mean ± SD	43.1 ± 17.6	43.9 ± 14.2	52.1 ± 16.7	64.1 ± 10.3	60.9 ± 13.2
Performance status					
0-1	2 (67%)	16 (73)	18 (82)	121	157
2-4	1 (33%)	6 (27)	4 (18)	72	83
Crossing midline					
No	3 (100)	19 (86)	18 (82)	174	214
Yes	0 (0)	2 (9)	4 (18)	18	24
Unknown	-	1 (5)	-	1	2
Status (n)					
Alive	2 (67)	8 (36)	2 (9)	3	15
Dead	1 (33)	14 (64)	20 (91)	190	225
OS (months)					
Median	88.9	65.2	24.8	9.6	12.1
IDH status					
Wildtype	3 (100)	2 (9)	7 (32)	189	201
Mutated	0 (0)	20 (91)	15 (68)	4	39
MGMT status					
Unmethylated	-	-	-	88	88
Methylated	-	-	-	73	73
Not determined	3 (100)	22 (100)	22 (100)	32	79
Histology					
Astrocytic	3 (100)	11 (50)	17 (77)	193 ^a	224
Oligodendroglial	0 (0)	11 (50)	5 (23)	0	16
Mean intensity^b					
IBA-1 ^{TOTAL}	115.0	112.0	112.6	117.8	116.3
CD204 ^{TOTAL}	95.7	52.6	101.4	119.4	117.6
CD204 ^{IBA-1}	96.6	77.3	100.4	119.1	116.2
Area fraction^b					
IBA-1 ^{TOTAL}	0.102	0.042	0.061	0.099	0.091
CD204 ^{TOTAL}	0.003	0.0006	0.0062	0.048	0.040
CD204 ^{IBA-1}	0.083	0.016	0.170	0.449	0.398

^a of 193 patients with grade IV gliomas, 10 were diagnosed with gliosarcoma

^b indicates that data are provided in median

Abbreviations: *IBA-1* ionized calcium-binding adaptor molecule-1, *SD* standard deviation

Table S2 List of applied antibodies and detection systems

Antibody	Vendor	Species/type	Clone	Dilution	Detection	Control
Immunofluorescence						
CD204	Cosmo Bio Co. LTD	Mouse/mono	SRA-E5	1+12000	CSA II	Lung Intestine
EGFR	NovoCastra, Leica Biosystems	Mouse/mono	EGFR.113	1+100	TSACy5	GBM Epidermis
GFAP	Dako	Rabbit/poly	Z0334	1+8000	TSACy5	GBM Cerebellum
HIF-1 α	BD Transduction Laboratories	Mouse/mono	54	1+50	TSACy5	U87 MG Seminoma
HLA-DR	Dako	Mouse/mono	CR3/43	1+200	TSACy5	Tonsil Intestine
IBA-1	Wako Pure Chemical Industries	Rabbit/poly	019-19741	1+12000	TSACy5	GBM Cerebellum
IL10	Abcam	Rabbit/mono	EPR1114	1+100	TSACy5	GBM Cerebellum
MAP-2	Sigma Aldrich	Mouse/mono	HM-2	1+8000	TSACy5	Cerebellum
MMP-14	Novus Biologicals	Rabbit/mono	EP1264Y	1+200	TSACy5	Intestine Kidney
OLIG-2	Immuno-Biological Laboratories	Rabbit/poly	18953	1+100	TSACy5	Cerebellum
SMA	Spring Bioscience	Rabbit/mono	SP171	1+200	TSACy5	Small/large Intestine
TGF- β 1	Sigma Aldrich	Rabbit/poly	SAB45029 54	1+100	TSACy5	Stomach Intestine
TNF- α	Pierce Antibodies	Rabbit/poly	R4-6A2	1+50	TSACy5	Gallbladder Intestine
VEGF	R&D Systems	Mouse/mono	26503	1+200	TSACy5	GBM, kidney
Immunohistochemistry						
ATRX	Atlas Antibodies	Rabbit/poly	HPA00190 6	1:100	OV-DAB	Tonsil, cerebellum
CD44	Dako	Mouse/mono	DF1485	1:25	UV-DAB	Tonsil
DLL-3	Atlas Antibodies	Rabbit/poly	HPA05653 3	1+100	pEnV	Testis
IDH1 R132H	Dianova	Mouse/mono	H09	1:100	OV-DAB	
NeuN	Chemicon	Mouse/mono	A60	1:500	OV-DAB	Cerebellum
OLIG-2	Immuno-Biological Laboratories	Rabbit/poly	18953	1:200	OV-DAB	Cerebellum
P53	Ventana Medical Systems	Mouse/mono	DO7	RTU	OV-DAB	Serous ovarian carcinoma
VEGF	R&D Systems	Mouse/mono	26503	1+1000	PV	GBM, kidney
YKL-40/CHI3L1	Quidel Corporation	Rabbit/poly	4815	1+100	ADV	U87 MG, GBM

Abbreviations: *ADV* Advance; *CSA* Catalyzed Signal Amplification System; *ATRX* a-thalassemia/mental retardation X-linked syndrome; *DAB* 3,3'-diaminobenzidin; *DLL-3* delta-like 3; *EGFR* epidermal growth factor receptor; *EnV* EnVision; *GFAP* glial fibrillary acidic protein; *HIF-1 α* hypoxia inducible factor 1alpha; *HLA-DR* human leukocyte antigen class II; *IBA-1* ionized calcium-binding adaptor molecule 1; *IDH1* isocitrate dehydrogenase 1; *IL10* interleukin-10; *MAP-2* microtubule-associated protein 2; *MMP-14* matrix metalloproteinase 14; *NeuN* NEURonal Nuclei; *OLIG-2* oligodendrocyte transcription factor 2; *OV* OptiView; *P53* tumor protein 53; *SMA* smooth muscle actin; *TGF- β 1* transforming growth factor beta1; *TNF- α* tumor necrosis factor alpha; *TSACy5* Tyramide Signal Amplification cyanine 5; *UV* UltraView; *VEGF* vascular endothelial growth factor; *YKL-40/CHI3L1* chitinase 3-like 1

Table S3 Multivariate cox regression analyses of IBA-1 and CD204 levels in patients with WHO grade II-IV gliomas

	No. of patients	Baseline model		AF IBA-1 ^{TOTAL}		AF CD204 ^{TOTAL}		p-value	HR (95% CI)	p-value	HR (95% CI)	p-value	HR (95% CI)	p-value
		HR (95% CI)	p-value	HR (95% CI)	p-value	HR (95% CI)	p-value							
Age	235	1.02 (1.00-1.03)	0.007	1.02 (1.01-1.03)	0.006	1.02 (1.00-1.03)	0.010	1.02 (1.00-1.03)	0.008					
Performance status														
0-1	154	1.00		1.00		1.00		1.00						
2-4	81	1.55 (1.39-1.72)	<0.001	1.55 (1.39-1.72)	<0.001	1.64 (1.47-1.83)	<0.001	1.57 (1.40-1.74)	<0.001					
Tumor crossing midline														
No	211	1.00		1.00		1.00		1.00						
Yes	24	1.69 (1.07-2.67)	0.023	1.61 (1.01-2.56)	0.044	1.64 (1.04-2.58)	0.033	1.72 (1.09-2.72)	0.020					
IDH status														
WT	197	1.00		1.00		1.00		1.00						
Mut	38	0.41 (0.19-0.90)	0.026	0.39 (0.18-0.87)	0.021	0.36 (0.17-0.78)	0.010	0.43 (0.20-0.94)	0.035					
Histology														
OD	10	1.00		1.00		1.00		1.00						
DA	11	3.95 (1.19-13.1)	0.025	3.72 (1.12-12.4)	0.033	3.93 (1.18-13.0)	0.025	4.01 (1.21-13.3)	0.023					
AOD	5	3.72 (0.81-17.1)	0.092	3.65 (0.79-16.8)	0.096	4.13 (0.90-19.0)	0.069	3.84 (0.83-17.6)	0.084					
AA	17	8.59 (2.77-26.7)	<0.001	7.92 (2.52-24.9)	<0.001	8.53 (2.74-26.5)	<0.001	8.67 (2.79-30.0)	<0.001					
GBM	192	5.52 (1.56-19.5)	0.008	4.83 (1.33-17.6)	0.017	4.04 (1.14-14.3)	0.031	5.02 (1.42-17.8)	0.012					
AF/MI														
Low	-	-	-	1.00		1.00		1.00						
High	-	-	-	1.15 (0.87-1.53)	0.32	1.81 (1.35-2.44)	<0.001	1.35 (1.01-1.81)	0.042					
Age	235	-	-	1.02 (1.00-1.03)	0.008	1.02 (1.00-1.03)	0.010	1.02 (1.00-1.03)	0.008					
Performance status														
0-1	154	-	-	1.00		1.00		1.00						
2-4	81	-	-	1.54 (1.39-1.72)	<0.001	1.56 (1.40-1.74)	<0.001	1.56 (1.40-1.74)	<0.001					
Tumor crossing midline														
No	211	-	-	1.00		1.00		1.00						
Yes	24	-	-	1.70 (1.08-2.68)	0.022	1.67 (1.06-2.64)	0.026	1.68 (1.07-2.64)	0.026					
IDH status														
WT	197	-	-	1.00		1.00		1.00						
Mut	38	-	-	0.40 (0.18-0.88)	0.022	0.41 (0.19-0.89)	0.025	0.44 (0.20-0.97)	0.041					
Histology														
OD	10	-	-	1.00		1.00		1.00						
DA	11	-	-	3.65 (1.10-12.2)	0.035	3.90 (1.17-12.9)	0.026	3.95 (1.19-13.1)	0.025					
AOD	5	-	-	4.00 (0.87-18.5)	0.076	3.81 (0.83-17.5)	0.085	3.78 (0.82-17.4)	0.087					
AA	17	-	-	8.22 (2.64-25.6)	<0.001	8.63 (2.78-26.81)	<0.001	8.59 (2.76-26.7)	<0.001					
GBM	192	-	-	5.44 (1.54-19.2)	0.009	5.00 (1.42-17.6)	0.012	5.27 (1.50-18.5)	0.010					
AF/MI														
Low	-	-	-	1.00		1.00		1.00						
High	-	-	-	0.85 (0.64-1.11)	0.24	1.25 (0.94-1.68)	0.13	1.27 (0.95-1.69)	0.11					

Table S3 Multivariate cox regression analyses of IBA-1 and CD204 levels in patients with WHO grade II-IV gliomas

Abbreviations: *AF* area fraction; *AA* anaplastic astrocytoma; *AOD* anaplastic oligodendroglioma; *DA* diffuse astrocytoma; *GBM* glioblastoma multiforme; *IDH* isocitrate dehydrogenase; *MI* mean intensity; *Mut* mutated; *OD* oligodendroglioma

Table S4 Multivariate cox regression analyses of IBA-1 and CD204 levels in patients with WHO grade II tumors including performance status, IDH status, and histology (n=22)

	No. of patients	HR (95% CI)	p-value	HR (95% CI)	p-value	HR (95% CI)	p-value
		Baseline model		AF IBA-1 ^{TOTAL}		MI IBA-1 ^{TOTAL}	
Performance status							
0-1	16	1.00		1.00		1.00	
2-4	6	1.17 (0.79-1.75)	0.43	1.30 (0.86-1.97)	0.21	1.19 (0.80-1.77)	0.39
IDH status							
WT	2	1.00		1.00		1.00	
Mut	20	0.08 (0.007-0.97)	0.047	0.12 (0.009-1.54)	0.10	0.06 (0.005-0.79)	0.032
Histology							
Astro	11	1.00		1.00		1.00	
Oligo	11	0.33 (0.10-1.13)	0.079	0.05 (0.004-0.50)	0.012	0.42 (0.11-1.65)	0.22
AF/MI							
Low	-	-		1.00		1.00	
High	-	-	-	0.10 (0.01-0.94)	0.044	0.58 (0.16-2.11)	0.41
				AF CD204 ^{TOTAL}		MI CD204 ^{TOTAL}	
Performance status							
0-1	16	-		1.00		1.00	
2-4	6	-	-	1.17 (0.78-1.75)	0.46	1.18 (0.79-1.76)	0.42
IDH status							
WT	2	-		1.00		1.00	
Mut	20	-	-	0.08 (0.007-1.04)	0.054	0.07 (0.004-0.89)	0.041
Histology							
Astro	11	-		1.00		1.00	
Oligo	11	-	-	0.33 (0.10-1.15)	0.082	0.32 (0.09-1.10)	0.071
AF/MI							
Low	-	-		1.00		1.00	
High	-	-	-	0.71 (0.23-2.20)	0.55	0.72 (0.21-2.41)	0.59

* Similar results were found when analyzing the association between overall survival and the co-expression of IBA-1 and CD204 (AF CD204^{IBA-1} and MI CD204^{IBA-1}) (data not shown).

Abbreviations: *AF* area fraction; *Astro* astrocytic; *IDH* isocitrate dehydrogenase; *MI* mean intensity; *Mut* mutated; *Oligo* oligodendroglial; *WT* wildtype

Table S5 Multivariate cox regression analyses of IBA-1 and CD204 levels in patients with WHO grade III tumors including performance status, IDH status, and histology (n=22)

	No. of patients	HR (95% CI)	p-value	HR (95% CI)	p-value	HR (95% CI)	p-value
		Baseline model		AF IBA-1 ^{TOTAL}		MI IBA-1 ^{TOTAL}	
Performance status							
0-1	18	1.00		1.00		1.00	
2-4	4	2.28 (1.35-3.87)	0.002	2.21 (1.29-3.78)	0.004	2.18 (1.28-3.74)	0.004
IDH status							
WT	7	1.00		1.00		1.00	
Mut	15	0.26 (0.09-0.79)	0.018	0.14 (0.03-0.68)	0.015	0.24 (0.08-0.76)	0.016
Histology							
Astro	17	1.00		1.00		1.00	
Oligo	5	0.58 (0.15-2.24)	0.43	1.17 (0.18-7.56)	0.87	0.78 (0.17-3.58)	0.75
AF/MI							
Low	-	-		1.00		1.00	
High	-	-	-	2.36 (0.54-10.3)	0.25	0.61 (0.18-1.98)	0.41
				*AF CD204^{TOTAL}		*MI CD204^{TOTAL}	
Performance status							
0-1	18	-		1.00		1.00	
2-4	4	-	-	2.19 (1.28-3.75)	0.004	3.75 (1.82-7.77)	<0.001
IDH status							
WT	7	-		1.00		1.00	
Mut	15	-	-	0.20 (0.06-0.69)	0.011	0.21 (0.06-0.78)	0.020
Histology							
Astro	17	-		1.00		1.00	
Oligo	5	-	-	0.60 (0.15-2.36)	0.47	0.73 (0.18-2.95)	0.66
AF/MI							
Low	-	-		1.00		1.00	
High	-	-	-	3.76 (1.18-12.0)	0.025	7.83 (2.21-27.8)	0.001

* Similar results were found when analyzing the association between overall survival and the co-expression of IBA-1 and CD204 (AF CD204^{IBA-1} and MI CD204^{IBA-1}) (data not shown).

Abbreviations: *AF* area fraction; *Astro* astrocytic; *IDH* isocitrate dehydrogenase; *MI* mean intensity; *Mut* mutated; *Oligo* oligodendroglial; *WT* wildtype

Table S6 TAMs and tumor heterogeneity

Parameter	Tumor area			Tumor subtype		
	Central (n=8)	Periphery (n=8)	p-value	Proneural (n=9)	Mesenchymal (n=11)	p-value
	Mean ± SD	Mean ± SD		Mean ± SD	Mean ± SD	
Area fraction						
IBA-1 ^{TOTAL}	0.060 ± 0.026	0.033 ± 0.018	0.033	0.066 ± 0.027	0.14 ± 0.080	0.022
CD204 ^{TOTAL}	0.046 ± 0.041	0.010 ± 0.008	0.010	0.008 ± 0.003	0.15 ± 0.054	<0.001
CD204 ^{IBA-1}	0.44 ± 0.18	0.19 ± 0.085	0.004	0.17 ± 0.074	0.71 ± 0.16	<0.001
Mean intensity						
IBA-1 ^{TOTAL}	94.8 ± 4.4	92.7 ± 2.5	0.28	121.4 ± 6.5	105.9 ± 16.7	0.012
CD204 ^{TOTAL}	99.3 ± 4.0	87.6 ± 10.7	0.010	101.8 ± 14.9	125.4 ± 9.8	<0.001
CD204 ^{IBA-1}	96.0 ± 5.8	87.0 ± 6.9	0.013	99.5 ± 8.4	135.4 ± 17.4	<0.001
Gemistocytic score	-	-	-	0.67 ± 0.9	1.86 ± 1.1	0.020

Table S7 Correlation between the gemistocytic cell score and the level of TAMs in astrocytomas

Variable	Diffuse astrocytoma (n=11)			Anaplastic astrocytoma (n=17)			Glioblastoma (n=20)			All astrocytomas (n=48)		
	r_s	95% CI	p	r_s	95% CI	p	r_s	95% CI	p	r_s	95% CI	p
Area fraction												
IBA-1 ^{TOTAL}	0.90	0.63-0.97	< 0.001	0.28	-0.25-0.68	0.28	0.28	-0.19-0.65	0.22	0.40	0.12-0.62	0.005
CD204 ^{TOTAL}	0.38	-0.31-0.80	0.25	0.01	-0.48-0.50	0.97	0.62	0.23-0.84	0.004	0.32	0.03-0.56	0.029
CD204 ^{IBA-1}	0.06	-0.57-0.65	0.77	-0.07	-0.54-0.44	0.78	0.55	0.13-0.80	0.012	0.25	-0.04-0.50	0.082
Mean intensity												
IBA-1 ^{TOTAL}	0.04	-0.59-0.64	0.91	-0.11	-0.57-0.40	0.66	-0.49	-0.77- (-0.04)	0.029	-0.18	-0.45-0.11	0.21
CD204 ^{TOTAL}	0.23	-0.45-0.74	0.51	0.02	-0.48-0.51	0.94	0.46	0.00-0.75	0.043	0.20	-0.10-0.47	0.17
CD204 ^{IBA-1}	0.17	-0.50-0.71	0.63	0.07	-0.44-0.54	0.79	0.50	0.06-0.78	0.025	0.24	-0.05-0.50	0.098

Supplemental materials and methods

Double immunofluorescence

Formaldehyde-fixed, paraffin embedded tissues were cut into 3µm thin slices on a microtome and placed on glass slides. Sections were deparaffinized with xylene and rehydrated with ethanol. Heat-induced epitope retrieval (HIER) was performed in a buffer solution consisting of 10 mmol/L Tris-base and 0.5 mmol/L ethylene glycol tetraacetic acid (EGTA), pH 9. After quenching of endogen peroxidase with 1.5% hydrogen peroxide (H₂O₂), sections were incubated with anti-CD204 (**Table S2**) and detected using Catalyzed Signal Amplification II kit with fluorescein (FITC) as fluorochrome (CSA II kit, Dako). A second round of HIER and endogen peroxidase blocking was performed followed by incubation with the respective primary antibody (IBA-1, HLA-DR, TNF- α , IL10, TGF- β 1, MMP-14, HIF-1 α , VEGF, EGFR) (**Table S2**) and detection with Tyramide Amplification Signal Cyanine 5 (TSACy5, Perkin Elmer, USA). Nuclei were counterstained using VECTASHIELD Mounting Medium containing 4,6-diamidino-2-phenylindole (DAPI, VWR International, USA). Primary antibodies were expressed in positive controls and absent in negative controls.

Immunohistochemistry and molecular pathology

Isocitrate dehydrogenase 1 (IDH1) status was determined using a mIDH1R132H antibody (clone H13, 1:100, Dianova, Germany) as described previously (1, 2). For grade II and III tumors with absent IDH1-R132H mutation immunohistochemically, next generation sequencing was performed to detect other mutations in the IDH1/2 genes using a 20-gene panel as previously reported (3).

Nuclear expressions of α -thalassemia/mental retardation X-linked syndrome (ATRX) (HPA001906, 1:100, Atlas Antibodies, Sweden) and p53 (DO7, Ready-to-use, Ventana Medical Systems Inc, USA), were detected immunohistochemically using the BenchMark Ultra IHC/ISH staining system (Ventana Medical Systems Inc). ATRX and p53 status were determined for all WHO grade II-III gliomas as well as glioblastomas with the IDH1-R132H mutation.

For tumors with retained nuclear expression of ATRX, testing for chromosomal deletions of 1p/19q was carried out by FISH on formalin-fixed paraffin-embedded tissue using the Vysis LSI 1p36 / LSI 1q25 and LSI 19q13/19p13 Dual-Color Probe (Abbott Molecular, Vysis, USA) and the Dako Histology FISH Accessory Kit K5799. For tumors with inconclusive FISH analysis, 1p/19q status was determined by assessing copy number variation of chromosomes 1 and 19 using the Infinium Methylation 850K EPIC BeadChip array (Illumina, USA) according to manufacturer's description. Briefly, DNA was extracted from formaldehyde-fixed paraffin embedded tissue samples using the GeneRead DNA FFPE Kit (Qiagen, Germany), and the quality of the purified DNA was evaluated by real-time PCR using the Illumina FFPE QC kit. Following bisulfite conversion using the EZ DNA Methylation Kit (Zymo Research, USA), DNA was restored using the ZR-96 DNA Clean & Concentrator-5 Kit (Zymo Research, USA), and the restored DNA samples were amplified, fragmented, precipitated, and resuspended according to the Infinium HD FFPE Methylation Assay protocol. Next, the DNA samples were hybridized onto BeadChips. After washing the

BeadChips, labeled nucleotides were added to extend the primers, and the BeadChips were stained, coated, and scanned using the iScan Control Software (Illumina). The array data was analyzed using GenomeStudio Software (Illumina).

Immunohistochemistry and immunohistochemical subtyping

The relation between TAMs and molecular glioblastoma subtype was investigated by staining 20 glioblastomas with three proneural (OLIG-2, DLL-3 and NeuN) and three mesenchymal markers (CD44, VEGF, and YKL-40) (Table S2).

Briefly, formalin-fixed, paraffin-embedded human glioblastoma samples were mounted onto slides, deparaffinized, rehydrated, subjected to epitope retrieval, and incubated with the respective antibodies. Immunostainings were carried out on an automated immunostainer (BenchMark Ultra IHC/ISH staining system, Ventana Medical Systems, USA) or the AutostainerPlus (Dako, Denmark).

Staining with CD44, NeuN and OLIG-2 was performed on the BenchMark Ultra (Ventana). Sections were dried at 75° C for 4 minutes and deparaffinized at 72° C. The staining procedure included pre-treatment with cell conditioner 1 at 100° C for 32 minutes and quenching of endogenous peroxidase with H₂O₂. Slides were then incubated with the respective primary antibody at 36° C for 32 minutes (OLIG-2, NeuN) or 20 minutes (CD44) and visualized with OptiView-DAB or UltraView-DAB with amplification, respectively. Tissue slides were counterstained with Hematoxylin II (Ventana) and Bluing Reagent (Ventana) followed by rehydration, clearing and coverslipping with Tissue-Tek Film Coverslipper (Sakura).

Staining with DLL-3, VEGF and YKL-40 was done on the AutostainerPlus (Dako) as follows. Sections were deparaffinized and HIER performed by incubation in a buffer solution consisting of 10 mmol/L Tris-base and 0.5 mmol/L EGTA, pH 9 or EDTA. After blocking of endogenous peroxidase activity by incubation in 1.5% H₂O₂, sections were incubated with primary antibody for 60 minutes. The antigen-antibody complex was detected using Advance (Dako), pEnVision (Dako) or PowerVision (Novacastra) and visualized with DAB as chromogen. Sections were then counterstained with Mayers Haematoxylin, and coverslips were mounted using AquaTex.

Primary antibodies were expressed in positive controls and absent in negative controls. Omission of primary antibodies served as negative controls and controls for non-specific staining related to the detection systems.

All slides were scanned on a Hamamatsu Digital Slide Scanner (Hamamatsu, Japan).

References

1. Dahlrot RH, Kristensen BW, Hjelmberg J, Herrstedt J, Hansen S. A population-based study of high-grade gliomas and mutated isocitrate dehydrogenase 1. *International journal of clinical and experimental pathology*. 2013;6(1):31-40.
2. Dahlrot RH, Kristensen BW, Hjelmberg J, Herrstedt J, Hansen S. A population-based study of low-grade gliomas and mutated isocitrate dehydrogenase 1 (IDH1). *Journal of neuro-oncology*. 2013;114(3):309-17.
3. Zacher A, Kaulich K, Stepanow S, Wolter M, Kohrer K, Felsberg J, Malzkorn B, Reifenberger G. Molecular Diagnostics of Gliomas Using Next Generation Sequencing of a Glioma-Tailored Gene Panel. *Brain pathology (Zurich, Switzerland)*. 2017;27(2):146-59.

13.2 Manuscript II

“Tumour-associated CD204+ microglia/macrophages accumulate in perivascular and perinecrotic niches and correlate with an interleukin-6 enriched inflammatory profile in glioblastoma”

ORIGINAL ARTICLE

Tumour-associated CD204⁺ microglia/macrophages accumulate in perivascular and perinecrotic niches and correlate with an interleukin-6-enriched inflammatory profile in glioblastoma

Mia D. Sørensen^{1,2}  | Bjarne W. Kristensen^{1,2,3,4}¹Department of Pathology, Odense University Hospital, Odense, Denmark²Department of Clinical Research, University of Southern Denmark, Odense, Denmark³Department of Pathology, Rigshospitalet, Copenhagen University Hospital, Copenhagen, Denmark⁴Department of Clinical Medicine and Biotech Research and Innovation Center (BRIC), University of Copenhagen, Copenhagen, Denmark**Correspondence**Mia D. Sørensen, Department of Pathology, Odense University Hospital, J. B. Winsloews Vej 15, 5000. Odense C, Denmark.
Email: mia.soerensen@rsyd.dk**Funding information**

Harboefonden; Købmand M. Kristjan Kjær og Hustru Margrethe Kjær, Født la Cour-Holmes Fond; Sundhed og Sygdom, Det Frie Forskningsråd; Arkitekt Holger Hjortenberg og Hustru Dagmar Hjortenbergs Fond; Marie og Børge Kroghs Fond; Torben og Alice Frimodts Fond; A. J. Andersen og Hustrus Fond; Thora og Viggo Groves Mindelegat; Oda og Hans Svenningsens Fond; født de la Cour-Holmes Fond; Familien Erichsens Mindefond; Fabrikant Einar Willumsens Mindelegat; Odense University Hospital

Abstract

Aims: Glioblastomas are heterogeneous tumours with a rich tumour microenvironment particularly comprised of tumour-associated microglia/macrophages (TAMs), but also containing a population of dedifferentiated/stem-like glioblastoma cells. Both cell populations contribute to tumour aggressiveness and immune evasion through the actions of various signalling molecules. The scavenger and pattern recognition receptor CD204 is associated with a pro-tumourigenic phenotype of TAMs and has a negative prognostic value. Our objective was to investigate the possible interaction between TAMs and dedifferentiated glioblastoma cells and characterise the myeloid phenotype of CD204-enriched glioblastomas.

Methods: Double immunohistochemistry and cell counting was performed on eight glioblastoma samples to estimate the expression and interaction level between dedifferentiated/stem-like tumour cells and TAMs. Using the NanoString technology, myeloid transcriptome profiling was performed on 46 glioblastomas, which had been selected based on their protein expression levels of CD204 and ionised calcium-binding adaptor molecule-1 (IBA1). The results were validated by immunohistochemistry and *in silico* gene expression analyses.

Results: TAMs especially CD204⁺ TAMs accumulated in perivascular and perinecrotic niches in close proximity to podoplanin⁺ glioblastoma cells. Gene profiling revealed that CD204-enriched glioblastoma has a unique signature with upregulation of genes related to hypoxia, angiogenesis and invasion, including interleukin-6. The gene signature favoured a poor prognosis in patients with glioblastoma.

Conclusions: This is the first study to characterise the role of CD204 in the myeloid microenvironment of glioblastoma. Our results support the unfavourable prognostic impact of CD204 and suggest that CD204 and interleukin-6 could serve as targets for re-education of TAMs and potentiation of current anti-glioma therapy.

KEYWORDS

CD204, glioblastoma, immunotherapy, interleukin-6, macrophage, microglia, nanostring, tumour microenvironment

This is an open access article under the terms of the Creative Commons Attribution-NonCommercial License, which permits use, distribution and reproduction in any medium, provided the original work is properly cited and is not used for commercial purposes.

© 2021 The Authors. *Neuropathology and Applied Neurobiology* published by John Wiley & Sons Ltd on behalf of British Neuropathological Society.

INTRODUCTION

Glioblastoma, World Health Organization (WHO) Grade IV, is the most frequent and lethal primary brain tumour in adults accounting for almost 50% of all primary malignant brain neoplasms [1, 2]. Despite standard-of-care with surgery and adjuvant radio-chemotherapy [3], the prognosis is dismal with only 5% to 10% of patients alive at 5 years [2, 4]. Glioblastomas are highly invasive in nature and exhibit great intra- [5, 6] and inter-tumoural heterogeneity [7–9]. The heterogeneous tumour landscape is a result of both intrinsic [6, 8, 9] and extrinsic factors including the tumour microenvironment (TME) [10–13] and is believed to contribute to the inefficient treatment response, ultimately resulting in poor patient outcome [14–16]. Treatment resistance is partly due to tumour cell plasticity allowing glioblastoma cells to dedifferentiate to a stem cell-like state. Reportedly, cancer cells expressing markers related to a stem-like phenotype (e.g., CD133, CD44, and nestin) represent a population of cells which is highly proliferative, aggressive, and resistant towards radiation, as well as anti-angiogenic and chemotherapeutic agents [16–19]. These dedifferentiated cancer cells often reside and thrive in perivascular [20–22] and necrotic/hypoxic [20, 23] niches, closely interacting with several non-neoplastic cell types in the TME including endothelial cells and immune cells [11, 18, 24–27] that favour an immunosuppressive TME [28, 29].

In recent years, the interest in targeting the TME, especially the tumour immune microenvironment, has increased as a means to enhance the efficacy of anti-cancer therapies [9]. The immune cell landscape in cancer including brain tumours is highly diverse adding to the overall complexity of the tumour biology, and the composition of the immune infiltrate has been reported to predict response to immunotherapy including immune checkpoint inhibitors [13, 30]. Tumour-associated microglia and macrophages (TAMs) are the dominant immune cell population in gliomas [31], comprising up to 30% of the cellular content of glioblastomas [10, 32, 33]. Resident brain microglia and infiltrating peripheral macrophages are recruited and polarised towards a tumour-supportive phenotype by a variety of tumour-derived signalling molecules including colony-stimulating factor 1 (CSF1), (C-C motif) ligand 2 (CCL2), (C-X-C motif) ligand 3 (CXCL3), and interleukin-6 (IL6) [10, 33–35]. Increasing evidence suggests that TAMs are a mixed cell population taking on several phenotypes along the M1-M2 spectrum [32, 36–38], including the more undifferentiated M0 phenotype [39]. Single-cell RNA sequencing of TAMs has shown that pro-inflammatory M1 and anti-inflammatory M2 genes are co-expressed at a cellular level [40].

We previously reported that high levels of M2-like CD204⁺ TAMs correlated with tumour malignancy, had a detrimental effect on overall survival in patients with WHO Grades III–IV glioma, and possibly contributed to treatment resistance, while the TAM density in general showed little prognostic value [32]. Similar results have been published by others [35, 41]. Further, we found that CD204⁺ TAMs co-expressed markers of both M1 and M2 activation as well as markers related to tumour aggressiveness. Further, CD204⁺ TAMs tended to accumulate in areas surrounding blood vessels and necrosis

suggesting a possible interaction with dedifferentiated stem-like glioma cells [32]. In this study, our aim was to explore the possible biological relevance of CD204 in glioblastoma. We examined by double immunohistochemistry the association between TAMs and glioblastoma cells expressing markers related to the stem-like phenotype. We also aimed to characterise CD204-enriched glioblastoma more thoroughly using the validated NanoString nCounter mRNA multiplex technology [42–44]. Lastly, we used immunohistochemistry and bioinformatics databases to confirm the gene expression profile of CD204-enriched glioblastoma and its prognostic value.

MATERIALS AND METHODS

Patient tissue

Archival formalin-fixed paraffin-embedded (FFPE) tissue samples from eight patients diagnosed with primary glioblastoma in 2006 were randomly included for the double immunohistochemical part of the study. For the NanoString gene expression part of the study, samples were obtained from the well-characterised Region of Southern Denmark glioma cohort [32, 45]. FFPE tissue specimens from 46 patients were included, and all patients had been diagnosed with primary glioblastoma between 2005 and 2009. The glioblastoma samples were selected based on their expression levels of CD204 and ionised calcium-binding adapter molecule-1 (IBA1), which had been determined by an immunofluorescence approach in our previous study [32], subdividing the 46 glioblastoma into four groups: (1) low levels of both CD204 and IBA1 (CD204^{LOW}/IBA1^{LOW}, $n = 12$); (2) high levels of both CD204 and IBA1 (CD204^{HIGH}/IBA1^{HIGH}, $n = 12$); (3) high and low levels of CD204 and IBA1, respectively (CD204^{HIGH}/IBA1^{LOW}, $n = 11$); and (4) low and high levels of CD204 and IBA1, respectively (CD204^{LOW}/IBA1^{HIGH}, $n = 11$). Isocitrate dehydrogenase (IDH) mutation and O6-methylguanine–DNA methyltransferase (MGMT) promoter status were assessed as previously described [32, 45]. An overview of patient characteristics including clinical and histological data is provided in Table 1. Based on their protein expression level of CD204 and IBA1, 20 of the 46 glioblastomas were included for immunohistochemical validation of some of the differentially deregulated genes found in the NanoString gene expression analysis.

All tissue samples were stained routinely with haematoxylin–eosin (H&E) to define representative tumour areas and reclassified by two pathologists according to WHO guidelines 2016 [1]. All patients underwent initial surgery at the Department of Neurosurgery, Odense University Hospital, Odense, Denmark.

Sample acquisition and RNA preparation

A total of 46 FFPE tissue samples were cut into 10- μ m-thick sections on a microtome and mounted on glass slides. Guided by representative H&E stains, freshly cut sections were macrodissected to exclude areas with normal brain tissue and/or infiltrating tumour thereby

TABLE 1 Patient characteristics

		HR (95% CI)	p value
Patients (n)	46	—	—
Status (n)			
Alive/dead	0/46	—	—
Overall survival (months)			
Median (range)	8.70–30.7	—	—
Age			
Mean	65.6	1.03 (0.99–1.08)	0.10
Range	49.2–79.1	—	—
Sex (n)			
Male	22	1.00	0.38
Female	24	1.30 (0.72–2.34)	—
Performance status (n)			
0–1	22	1.00	—
2–4	24	1.44 (1.17–1.78)	<0.001
Tumour crossing midline (n)			
No	42	1.00	—
Yes	4	1.54 (0.54–4.44) ^d	0.42
Postsurgical treatment (n)			
Stupp ^a	24	1.00	—
Palliative treatment ^b	13	1.86 (0.91–3.81)	0.090
None ^c	9	117 (13.6–1011) ^d	<0.001
IDH status (n)			
Mutated	0	—	—
Wildtype	46	—	—
MGMT promoter status (n)			
Unmethylated	23	1.00	—
Methylated	22	0.53 (0.28–1.03)	0.058
Not determined	1	—	—
CD204/IBA1 levels (n)			
Low/low	12	1.00	—
High/high	12	1.51 (0.65–3.48)	0.34
High/low	11	2.44 (1.02–5.86)	0.045
Low/high	11	1.06 (0.45–2.45)	0.90

^aTreatment according to the publication by Stupp et al. [3].

^bPalliative treatment is radiotherapy alone (60 Gy/30–33 fractions), hypofractionated radiotherapy alone (30–34 Gy/10 fractions), hypofractionated radiotherapy with chemotherapy, or chemotherapy alone.

^cNo postsurgical treatment.

^dThis hazard ratio should be interpreted with caution as $n < 10$.

enriching the amount of central tumour RNA in the subsequent gene expression analysis. Next, sections were detached from the glass slides and deparaffinised by subsequent submersion in a 3% glycerol solution and R-(+)-limonene followed by a washing step in absolute ethanol and rehydration in 3% glycerol. The tissue was then transferred to 1.5-ml Eppendorf tubes. Total RNA was

extracted using the High Pure FFPE RNA Isolation Kit (Roche, Basel, Switzerland) according to the manufacturer's instructions. RNA quantity and quality was assessed using NanoDrop (Thermo Scientific, Waltham, MA, USA). Extracted RNA was stored at -80°C until further use.

NanoString gene expression analysis

mRNA gene expression analysis was performed using the NanoString barcode technology (NanoString Technologies, Seattle, WA, USA) with the NanoString nCounter[®] Human Myeloid Innate Immunity Panel v2 consisting of 770 genes and a customised CodeSet of 30 genes which was spiked into the standard myeloid panel. The customised 30-gene panel included the genes for CD204 (*MSR1*), the immune checkpoint marker galectin-9 (*GAL9*, *LGALS9*) [46], 26 genes related to cancer stemness [18, 19, 47, 48], glioma [1, 7], chemoresistance [15, 49] or the interferon pathway [50–52] as well as two additional housekeeping genes [53, 54] (File S1). Total RNA input was 150–250 ng with an A260/280 optical density between 1.61 and 1.99. Standard nCounter XT protocols were employed. Immediately after overnight hybridization, the target-probe complexes were purified and immobilised on the nCounter Prep Station followed by data collection and barcode counting in the nCounter Digital Analyser (nCounter[®] FLEX Analysis System, NanoString Technologies).

Conventional immunohistochemistry

Three μm sections from FFPE tissue blocks were mounted on FLEX IHC slides (Dako, Glostrup, Denmark). Immunohistochemical staining with unconjugated primary antibodies against baculoviral IAP repeat containing-3 (*BIRC3*), CD44, CD204, galectin-3 (*GAL3*), IBA1, intercellular adhesion molecule-1 (*ICAM1*) and tumour necrosis factor (*TNF*), alpha-induced protein-3 (*TNFAIP3*, also known as A20) were carried out on a fully-automated immunostainer (DISCOVERY ULTRA, Ventana Medical Systems, Inc., Tucson, AZ, USA). Standard protocols included deparaffinisation, epitope retrieval, and quenching of endogenous peroxidase followed by detection with the OptiView-HRP-DAB detection kit (Ventana). Immunostaining with primary antibodies against IL6, nucleotide-binding oligomerisation domain-containing protein 2 (*NOD2*) and programmed death-ligand 1 (*PD-L1*) were done semi-automatically using the Dako Autostainer Link 48 instrument and EnVision FLEX+ detection system (Agilent Technologies, Santa Clara, CA, USA). Tissue slides were counterstained using haematoxylin II and bluing reagent (Ventana protocols) or Mayer's haematoxylin (Autostainer protocols). Coverslips were mounted with Pertex[®] Mounting Medium (#00811, HistoLab Products AB, Gothenburg, Sweden). Information regarding primary antibodies, clone, epitope retrieval procedures, dilutions, incubation times and detection platforms is presented in Table S1.

Double immunohistochemistry

The protocols for the double immunohistochemical staining were designed as sequential application of unconjugated primary antibodies with heat deactivation steps in between each sequence for elution purposes. Adjacent sections of eight glioblastomas were stained with a panel of markers related to the stem-like phenotype (B lymphoma Mo-MLV insertion region 1 homologue [BMI1], CD44, CD133, musashi-1 [MSI1], nestin, podoplanin [PDPN] and [sex-determining region Y]-box 2 [SOX2]) [18, 19, 47] and the general microglial/macrophage marker IBA1 [55] or the M2-related marker CD204 [33]. Additionally, 20 glioblastomas were stained with antibodies against the immune checkpoint markers T-cell immunoglobulin and mucin-domain containing-3 (TIM3) and GAL9 [46]. See Data S1 and Table S2 for information regarding primary antibodies, clone, epitope retrieval procedures, dilutions, incubation times and detection platforms.

Quantitative digital image analysis

The stained slides were digitised using a NanoZoomer 2.0-HT whole slide scanner (Hamamatsu Photonics, Hamamatsu, Japan) equipped with a 40 \times objective. For the H&E, as well as the conventional single immunohistochemical staining, automated digital image analysis and quantification was performed using the Visiopharm Image Analysis Software, version 2018.4 (Hørsholm, Denmark) as previously reported [32, 56]. For each stain, the output variable was area fraction, which was defined as the positive area divided by the total tumour area. See Data S1 for additional information on the image analysis process. Estimates of necrosis were calculated in the Visiopharm software following manual delineation of areas containing vital tumour tissue and necrosis using digitised H&E stained slides. The necrotic component was defined as the area of necrosis divided by the area of total tumour tissue (i.e., necrosis + vital tumour tissue).

Quantification of the double immunostaining was done by stereological-based cell counting in the Visiopharm software. For the TIM3/GAL9 dual staining, sample images were acquired by systematic uniform random sampling at 20 \times magnification ensuring at least 10 images per tumour. Cell counting was performed using a 2 \times 2 counting frame that covered 10% of the sampled image area. Reproducibility was tested by independently performing random sampling and cell counting twice on a training set of five glioblastoma specimens ($r_s = 1.00$, $p < 0.001$). Four different cell populations were counted: (1) negative cells (i.e., GAL9⁻ TIM3⁻), (2) GAL9⁺ cells (i.e., GAL9⁺ TIM3⁻), (3) TIM3⁺ cells (i.e., GAL9⁻ TIM3⁺) and (4) double⁺ cells (i.e., GAL9⁺ TIM3⁺). Cell fractions were calculated based on the total cell count. For the stem-like cell marker and IBA1/CD204 double staining, cell counting was performed in three subregions for each tumour: (1) vital tumour area, (2) perivascular area and (3) perinecrotic area (Figure 1A1–A3). A maximum of five positions per subregion, when possible, were identified on a representative H&E for each tumour, and sample images were acquired for each double staining at 40 \times magnification. Cell counting was performed using a 1 \times 1

counting frame that covered 30% of the sampled image area. CD204 and IBA1 served as internal controls for the counting system and tests of reproducibility ($r_s = 0.85$ – 0.96 for IBA1 and $r_s = 0.85$ for CD204, $p < 0.0001$). Following cell populations were counted: (1) tumour cells with stem-like cell phenotype (i.e., cells positive for the respective stem cell-related marker and negative for IBA1/CD204), (2) TAMs (i.e., IBA1⁺ or CD204⁺ cells) and (3) negative cells (i.e., cells negative for IBA1/CD204 and the respective stem cell-related marker). For the tumour cells expressing the stem cell-related marker, it was assessed whether they interacted directly with microglia/macrophage or not. Cells were categorised as proximal/interacting when they were directly adjacent with no other nuclei in between, and cells were classified as distal/non-interacting when one or more nuclei were located between the two cell populations. Similar evaluation was performed for CD204⁺ cells with respect to CD133⁺ and PDPN⁺ tumour cells. Cell fractions were calculated based on the total cell count, the total number of tumour cells or the total number of CD204⁺ cells.

Patient dataset analyses

mRNA expression data were explored using the GlioVis portal (<http://gliovis.bioinfo.cnio.es/>) [57]. Datasets were exported for the following genes: *IBA1* (*AIF1*), *CD204* (*MSR1*), *IL6*, *TNFAIP3*, *ICAM1*, *CD44*, *PD-L1* (*CD274*), *GAL3* (*LGALS3*), *GAL9* (*LGALS9*) and *TIM3* (*HAVCR2*), and used for survival analyses. Two different glioblastoma datasets were employed. From the Cancer Genome Atlas (TCGA), mRNA data were available for 324 patients diagnosed with primary IDH-wildtype glioblastoma (the Agilent 4502SA dataset) [58]. From the Gravendeel dataset [59], mRNA data were obtained for 91 patients with primary IDH-wildtype glioblastomas. Differential expression analysis was performed on both datasets to explore quantitative changes in gene expression levels between the groups of glioblastomas with the highest ($n = 120$ and $n = 37$, respectively) and lowest ($n = 123$ and $n = 40$, respectively) mRNA expression level of CD204. The lists of differential deregulated genes with log₂ fold-change (FC) ≥ 1.5 or ≤ -1.5 and adjusted $p < 0.05$ were exported directly from GlioVis for further analysis in the online resource STRING.

Statistics

Data files from the NanoString gene expression analyses were imported into the nSolver Analysis Software v4.0 with the Advanced Analysis Module 2.0 plugin (NanoString) for quality control, data normalisation and advanced analysis, including differential gene expression analyses, according to manufacturer's guidelines. p values were adjusted for multiple comparison by the Benjamini–Yekutieli false discovery rate (FDR) procedure [60].

The STRING online resource v11 (<https://www.string-db.org/>) [61] was accessed to conduct connectivity network analyses. Using the STRING resource Kyoto Encyclopedia of Genes and Genomes (KEGG) and Reactome enrichment analyses were performed for

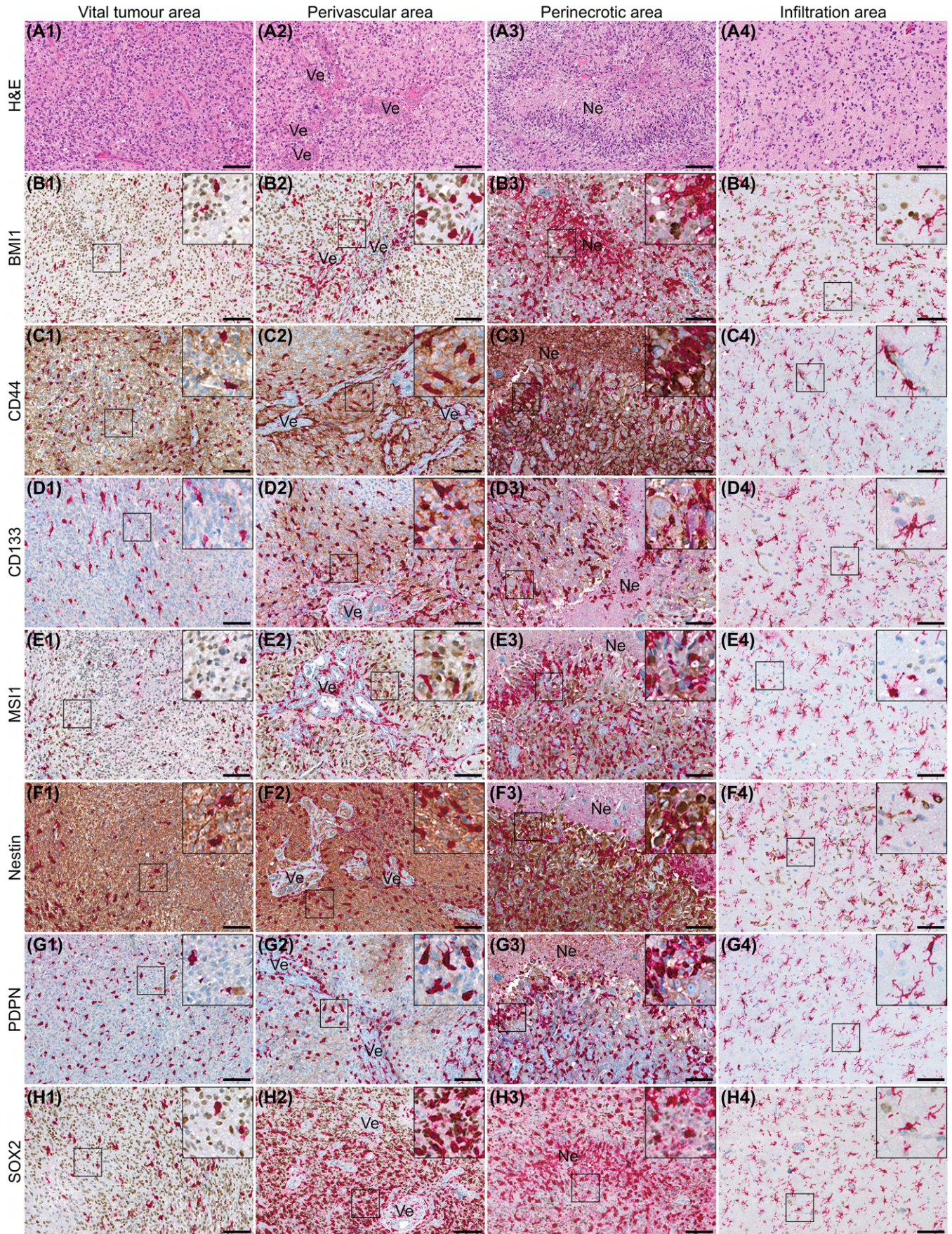


FIGURE 1 Legend on next page.

FIGURE 1 Expression of IBA1 and stem-like cell related markers in glioblastoma. Eight glioblastoma samples were stained using double immunohistochemistry with markers related to cancer stemness (brown) and IBA1 (red). IBA1⁺ cells generally accumulated in perivascular and perinecrotic areas often showing an amoeboid morphology. IBA1⁺ cells were morphologically ramified in the tumour infiltration area. (A1–A4) Representative haematoxylin–eosin (H&E) images of the different tumour subregions: Vital tumour area (A1), perivascular area (A2), perinecrotic area (A3), and tumour infiltration area (A4). (B1–B4) BMI1 expression appeared evenly distributed across the tumour and was also expressed in the infiltration area. (C1–C4) CD44 was widely expressed, but appeared more intense around necrotic areas and was rarely seen in the tumour infiltration area. (D1–D4) CD133 tumour cell density was higher in areas surrounding vasculature and necrosis. (E1–E4) MSI1⁺ tumour cells were present in all tumour subregions showing a higher staining intensity in perivascular and necrotic areas, but was rarely observed in the tumour infiltration area. (F1–F4) Nestin was highly expressed in all tumour areas. (G1–G4) PDPN expression was primarily observed in perivascular and perinecrotic regions, while expression was limited in vital tumour and in the infiltration zone. (H1–H4) SOX2 was frequently expressed in all tumour subregions, but staining intensity seemed highest in vital and perivascular tumour areas. Scale bar 50 µM. Abbreviations: BMI1, B lymphoma Mo-MLV insertion region 1 homologue; IBA1, ionised calcium-binding adaptor molecule-1; MSI1, musashi-1; Ne, necrosis; PDPN, podoplanin; SOX2, sex-determining region Y-box 2; Ve, blood vessel

differentially regulated genes which had a log₂ FC ≥ 1.50 and an FDR-adjusted $p < 0.05$. STRING network analyses were set to require a minimum interaction score of 0.70 or 0.40 (high and medium confidence, respectively), and network clustering was performed by applying the Markov cluster (MCL) algorithm with an inflation parameter of 1.8 [62].

An expression-based heatmap was generated using the web server Heatmapper (available at <http://www.heatmapper.ca/>) [63] to visualise and cluster the results of the quantitative staining analyses. Unsupervised hierarchical clustering was conducted based on the Euclidean distance and complete linkage methods.

Student's unpaired *t* test or its non-parametric equivalent Mann–Whitney *U*-test was used when comparing two groups. One-way ANOVA with Bonferroni's multiple comparison test or the non-parametric Kruskal–Wallis test with Dunn's multiple comparison test was used to compare more than two groups. Correlation analyses were conducted by Spearman's rank-order correlation coefficient. Survival functions were illustrated using the Kaplan–Meier estimator. Overall survival was defined as time from primary surgery until death or date of censoring. Survival distributions were compared using the log-rank test. Multivariate analyses were conducted using the Cox proportional-hazards model to obtain hazard ratios (HRs). All Cox models were tested for proportional hazard, time-dependency and interaction effects of the explanatory factors. The median value of the investigated biomarkers was used as pre-specified cut-off value. The statistical analyses were carried out in STATA v16 (StataCorp LLC, College Station, TX, USA) or Prism 5.0 (GraphPad Software Inc., San Diego, CA, USA). $p < 0.05$ were considered statistically significant.

RESULTS

Tumour-associated microglia/macrophages accumulate in perivascular and perinecrotic areas often in close proximity to dedifferentiated/stem-like glioblastoma cells

IBA1⁺ TAMs were present in all samples often in moderate numbers and often displayed an amoeboid morphology. Significantly higher densities were observed in perivascular and perinecrotic areas,

including areas of pseudo-palisading necrosis, compared with the vital tumour area ($p < 0.05$), comprising approximately 40% of the total cell count in these areas (Figures 1 and 2A). Morphologically more ramified IBA1⁺ cells were observed in the tumour infiltration area.

BMI1 was expressed in all tumours and appeared evenly distributed throughout the whole tumour; however, the staining intensity seemed to decrease in perinecrotic areas (Figure 1B1–B4). No significant difference in BMI1⁺ cell density was observed among in different tumour subregions ($p = 0.44$) (Figure 2A), and the interaction rate between BMI1⁺ and IBA1⁺ cells did not show any significant subregional differences ($p = 0.21$) (Figure 2B).

CD44 was widely expressed (Figure 1C1–C3) regardless of tumour area ($p = 0.31$) (Figure 2A), and no subregional difference in microglial interaction was observed ($p = 0.71$) (Figure 2B). The staining intensity appeared higher in perinecrotic areas, while CD44 lacked or was only weakly expressed by a few cells in the infiltration zone (Figure 1C4).

CD133 was mostly expressed in areas surrounding vascular structures and necroses displaying more intense staining in these areas compared to vital tumour areas and the tumour infiltration zone (Figure 1D1–D4). The CD133⁺ tumour cell density (Figure 2A) was higher in the perivascular ($p < 0.001$) and perinecrotic areas ($p < 0.01$) relative to the vital tumour area, but the ratio of CD133⁺ cells interacting with IBA1⁺ cells did not differ among the three subregions ($p = 0.54$) (Figure 2B).

MSI1 showed high inter-tumoural heterogeneity. The staining intensity seemed to increase in perivascular and perinecrotic areas compared to vital tumour tissue and the infiltration area (Figure 1E1–E4); however, no significant differences were found among the tumour subregions ($p = 0.27$) (Figure 2A). In tumours with high MSI1 levels in general, MSI1 was expressed in all areas regardless of the number of IBA1⁺ cells. In tumours with lower expression levels, MSI1⁺ cells tended to accumulate in IBA1-rich areas especially in the perivascular regions (data not shown); however, overall, no significant difference in the interaction rate was found ($p = 0.36$) (Figure 2B).

Nestin was widely expressed in most tumours independent of the tumour subregion ($p = 0.78$) (Figures 1F1–F4 and 2A). In the perivascular areas, the ratio of nestin⁺ tumour cells interacting with IBA1⁺ cells was significantly higher in the perivascular area compared to the vital tumour area ($p < 0.05$) (Figure 2B).

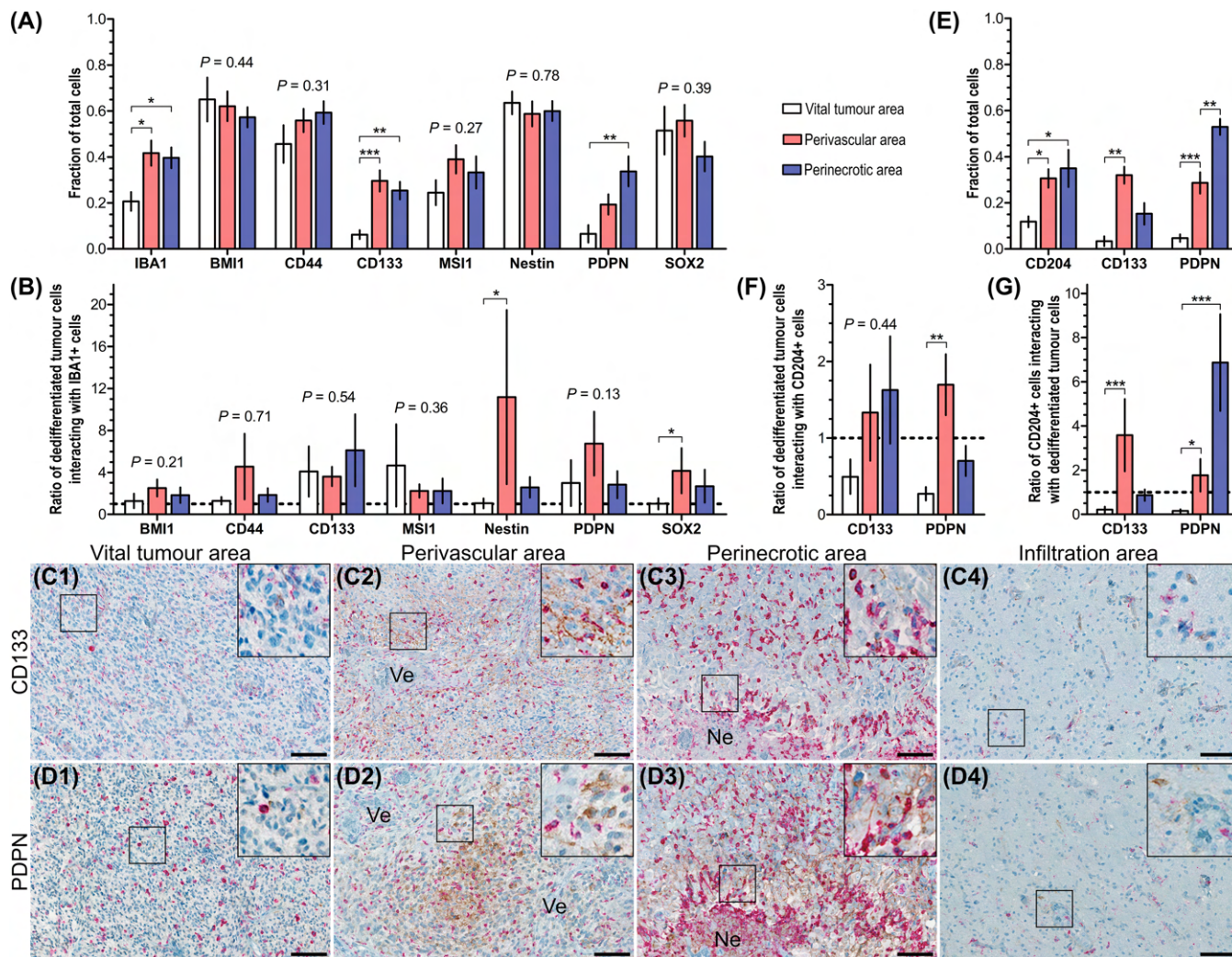


FIGURE 2 Quantitative estimates of the expression and interaction levels of IBA1, CD204 and stem-like cell related markers in glioblastoma. (A) Quantification of the IBA1 double immunohistochemistry stains showed that the fractions of IBA1⁺ TAMs as well as CD133⁺ tumour cells were significantly higher in perivascular and perinecrotic areas relative to vital tumour. The fraction of PDPN⁺ tumour cells was significantly higher in areas of necrosis compared with vital tumour regions and tended to be higher in perivascular regions. (B) BMI1⁺, CD44⁺, CD133⁺ and MSI1⁺ tumour cells did not interact significantly with IBA1⁺ TAMs in any of the tumour subregions. Nestin⁺ and SOX2⁺ tumour cells often interacted with IBA1⁺ TAMs in areas surrounding vasculature, and similar tendency was found for PDPN⁺ tumour cells. (C, D) CD204, CD133 and PDPN expression levels were elevated in perivascular and perinecrotic areas compared with vital tumour area and were rarely observed in the infiltration zone. (E) Quantification of the CD204 double immunohistochemistry stains showed that the fractions CD204⁺ TAMs and PDPN⁺ tumour cells were significantly higher in perivascular and perinecrotic areas relative to vital tumour area, while the fraction of CD133⁺ tumour cells was especially high in the perivascular region. (F) Looking at the CD133⁺ tumour population, the ratio of CD133⁺ tumour cells interacting with CD204⁺ TAMs did not differ among the three subregions. Looking at the PDPN⁺ tumour population, the ratio of PDPN⁺ tumour cells were in direct contact with CD204⁺ TAMs was significantly higher in the perivascular area relative to the vital tumour area. (G) CD204⁺ TAMs were rarely in contact with CD133⁺ and PDPN⁺ tumours cell in the vital tumour, but significantly interacted with CD133⁺ and PDPN⁺ tumour cells in the perivascular area and exhibited an especially high interaction rate with PDPN⁺ tumour cells in the perinecrotic area. Horizontal and vertical lines indicate mean \pm SEM. * $p < 0.05$; ** $p < 0.01$; *** $p < 0.001$. Scale bar 50 μ M. Abbreviations: BMI1, B lymphoma Mo-MLV insertion region 1 homologue; IBA1, ionised calcium-binding adaptor molecule-1; MSI1, musashi-1; Ne, necrosis; PDPN, podoplanin; SOX2, sex-determining region Y-box 2; Ve, blood vessel

PDPN⁺ tumour cells were only sporadically observed in vital tumour areas and absent in the tumour-infiltrating area. Instead, PDPN⁺ cells particularly accumulated in perinecrotic areas ($p < 0.01$) (Figure 1G1–G4 and Figure 2A) and tended to directly interact with IBA1⁺ cells in the perivascular region ($p = 0.13$) (Figure 2B).

SOX2 was expressed in all tumours. The staining intensity appeared higher in vital tumour tissue and around blood vessels compared to perinecrotic areas and the infiltration zone (Figure 1H1–H4), but the fraction of SOX2⁺ cells was similar across the different tumour subregions ($p = 0.39$) (Figure 2A). However, in the

perivascular area, the SOX2⁺ cells significantly co-localised with IBA1⁺ cells compared to the vital tumour area ($p < 0.05$) (Figure 2B).

As the presence of especially CD133⁺ and PDPN⁺ tumour cells was higher in the perivascular and perinecrotic niches, we chose to investigate the level of co-location with CD204⁺ TAMs for these two markers only. We found similar regional expression patterns when investigating the CD204/CD133 (Figure 2C1–C4) and CD204/PDPN double staining (Figure 2D1–D4) with increased expression levels around blood vessels and areas of necrosis (Figure 2E). In the perinecrotic areas, the fraction of CD204⁺ cells was almost the same to that of IBA1 constituting approximately 40% of cells, while the CD204⁺ cells were less frequent in the perivascular and vital tumour areas relative to the IBA1⁺ cells (Figure 2A,E). Looking at the tumour cell populations, limited interaction was observed between CD133⁺ tumour cells and CD204⁺ cells (Figure 2F), while the fraction of PDPN⁺ tumour cells in direct contact with CD204⁺ cells was significantly higher in the perivascular area relative to vital tumour area ($p < 0.01$) (Figure 2F). Looking specifically at the CD204⁺ TAMs, the ratio of CD204⁺ cells interacting directly with CD133⁺ cells was higher in the perivascular area than in the vital tumour area ($P < 0.001$), and a similar increase in interaction rate was found for CD204⁺ and PDPN⁺ cells in both the perivascular ($P < 0.05$) and perinecrotic area ($P < 0.001$) compared with the vital tumour area (Figure 2G).

Overall, IBA1⁺ and CD204⁺ cells (i.e., TAMs) seemed to accumulate in perivascular and perinecrotic areas showing close interaction with tumour cells expressing PDPN in perivascular and perinecrotic regions.

CD204-enriched glioblastomas display a unique gene expression profile and associate with necrosis

Myeloid mRNA profiling was performed on 46 glioblastomas using the NanoString barcode technology. The 46 glioblastomas were selected and subdivided into four groups based on their protein levels of CD204 and IBA1. A scatter plot illustrating the four groups and their expression levels is shown in Figure 3A. The level of IBA1 and CD204 protein co-expression was significantly highest in the CD204^{HIGH}/IBA1^{LOW} group (Figure 3B). Patients in the CD204^{HIGH}/IBA1^{LOW} group had the poorest survival outcome in both the univariate (HR 2.44, $p = 0.045$) (Figure 3C and Table 1) and multivariate analysis (HR 3.54, $p = 0.015$) (Figure 3D). A heatmap of the normalised mRNA data generated via unsupervised hierarchical clustering revealed that two major clusters existed within the glioblastomas (Figure 3E). Cluster 1 primarily comprised tumours of the CD204^{LOW}/IBA1^{LOW} and CD204^{LOW}/IBA1^{HIGH} groups, whereas Cluster 2 mainly consisted of tumours with high CD204 levels (i.e., the CD204^{HIGH}/IBA1^{HIGH} and CD204^{HIGH}/IBA1^{LOW} groups). Survival analysis showed that Cluster 2 was associated with poorer prognosis (HR 2.01, $p = 0.026$) (Figure 3F), also independent of performance status, postsurgical treatment, and MGMT status (HR 3.19, $p = 0.004$) (Figure 3G), but the cluster pattern was

not a stronger prognosticator of survival than the CD204/IBA1 signature.

Pathway scoring was used to condense the gene expression profile of each sample into a set of 47 pathway scores. Unsupervised cluster analyses re-identified the two clusters described above, and a high level of pathway activity was observed in Cluster 2 compared with Cluster 1, predominantly due to low pathway scores in the CD204^{LOW}/IBA1^{LOW} samples (Figures 4A and S1). Many of the pathways were related to the immune response. To better characterise the immune composition of the glioblastoma samples, raw cell type abundances were measured for macrophages, cytotoxic cells and neutrophils. As expected the CD204^{LOW}/IBA1^{LOW} group displayed the lowest measurements for all three immune cell populations, especially macrophages and neutrophils ($p < 0.001$) (Figure 4B). Because immune activation may be initiated by necrosis and depend on cellular density within the tumour, the presence of necrosis and cellularity/cell density were estimated in all 46 samples (Figure S2). These analyses showed that necrotic areas were more frequently observed in glioblastomas with high protein expression of primarily CD204 ($p < 0.01$) (Figure 4C). Inversely, CD204-enriched glioblastomas had significantly lower cellularity ($p < 0.05$) (Figure 4D).

CD204-enriched glioblastomas are immunologically inflamed tumours and have a mixed M1/M2 phenotype

Genes included in the NanoString panel were tested for differential expression in response to the CD204/IBA1 subgroups using the CD204^{LOW}/IBA1^{LOW} group as baseline. Gene set analyses (GSA) were performed by summarising the results of the differential expression analysis at gene set level identifying the most differentially expressed genes. The extent of differential expression in each gene set was then measured using a global significance score. GSA showed that expression levels of genes involved in complement coagulation cascades, NOD-like receptor and TNF signalling pathways, transport and catabolism, immune diseases, and infectious diseases were higher in CD204-rich tumours (Figure S3). Mapping the differentially expressed genes to KEGG pathways supported the observation that the differentially expressed genes were enriched for the TNF signalling pathway, but also for additional signalling pathways, for example, Toll-like receptor (TLR), chemokine, nuclear factor kappa B (NF-kappa B), and Janus kinases-signal transducer and activator of transcription protein (Jak-STAT) as well as in pathways related to phagosome, cytokine-cytokine receptor interaction, cell adhesion molecules (CAMs), proteoglycans and transcriptional misregulation in cancer (Table S3). Focusing on the differentially deregulated genes, 164 and 87 genes were significantly (adj. $p < 0.05$) ≥ 1.50 -fold upregulated in the CD204^{HIGH}/IBA1^{HIGH} and CD204^{HIGH}/IBA1^{LOW} groups, respectively, relative to the CD204^{LOW}/IBA1^{LOW} baseline group. Among the highest upregulated genes were *CCL20*, *IL6*, *CXCL14*, *CXCL8* [IL8], *ICAM1*, *OSM*, *S100A8*, *S100A9* and *PD-L1* (Figure 4E,F and Table 2). The CD204-enriched groups expressed genes related to both the M1

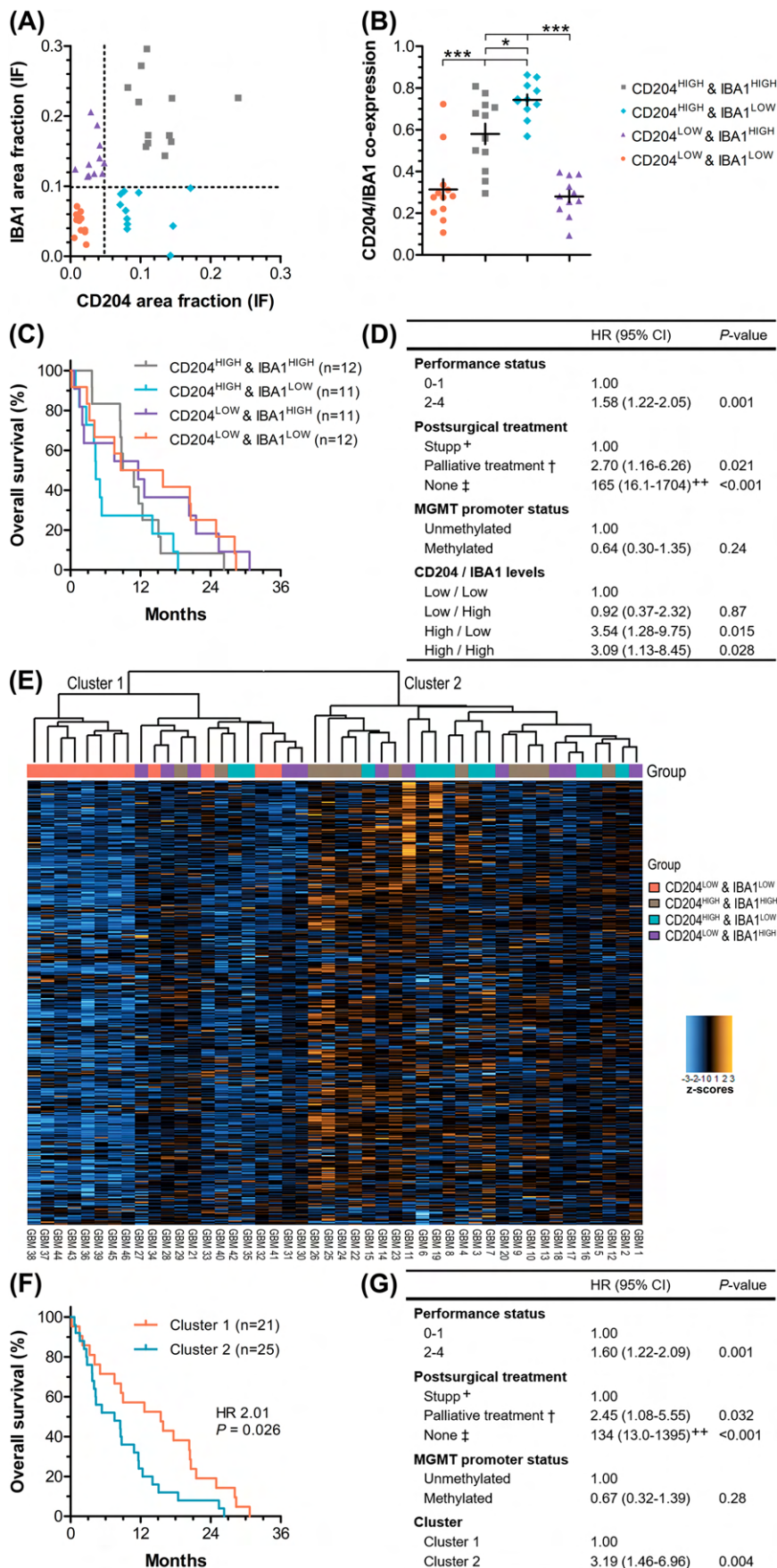


FIGURE 3 Legend on next page.

FIGURE 3 The prognostic value of the CD204/IBA1 signature and gene expression profiling of CD204-enriched glioblastomas. (A) A total of 46 glioblastomas were included for gene expression profiling using the NanoString barcode multiplex technology. The 46 samples were selected based on the CD204 and IBA1 expression levels, which had been determined previously using double immunofluorescence. This resulted in a subdivision of the samples into four groups: CD204^{LOW}/IBA1^{LOW} (n = 12), CD204^{HIGH}/IBA1^{HIGH} (n = 12), CD204^{HIGH}/IBA1^{LOW} (n = 11), and CD204^{LOW}/IBA1^{HIGH} (n = 11). (C) The CD204^{HIGH}/IBA1^{LOW} group also exhibited the highest level of CD204-IBA1 co-expression. (C,D) Kaplan-Meier plot illustrating that the patients in the CD204^{HIGH}/IBA1^{LOW} and CD204^{HIGH}/IBA1^{HIGH} groups had the worst survival in both the univariate and multivariate analyses. (E) Heatmap generation and unsupervised hierarchical clustering of the normalised data from the NanoString analysis identified two major clusters. Cluster 1 mostly comprised glioblastomas of the CD204^{LOW}/IBA1^{LOW} group, whereas Cluster 2 consisted of tumours with high CD204 levels. (F,G) Log-rank and cox regression analyses showed that Cluster 2 correlated with shorter overall survival. + Treatment according to the publication by Stupp et al. [3]. †Palliative treatment is radiotherapy alone (60 Gy/30–33 fractions), hypofractionated radiotherapy alone (30–34 Gy/10 fractions), hypofractionated radiotherapy with chemotherapy or chemotherapy alone. ‡No postsurgical treatment. ++This hazard ratio should be interpreted with caution as n < 10

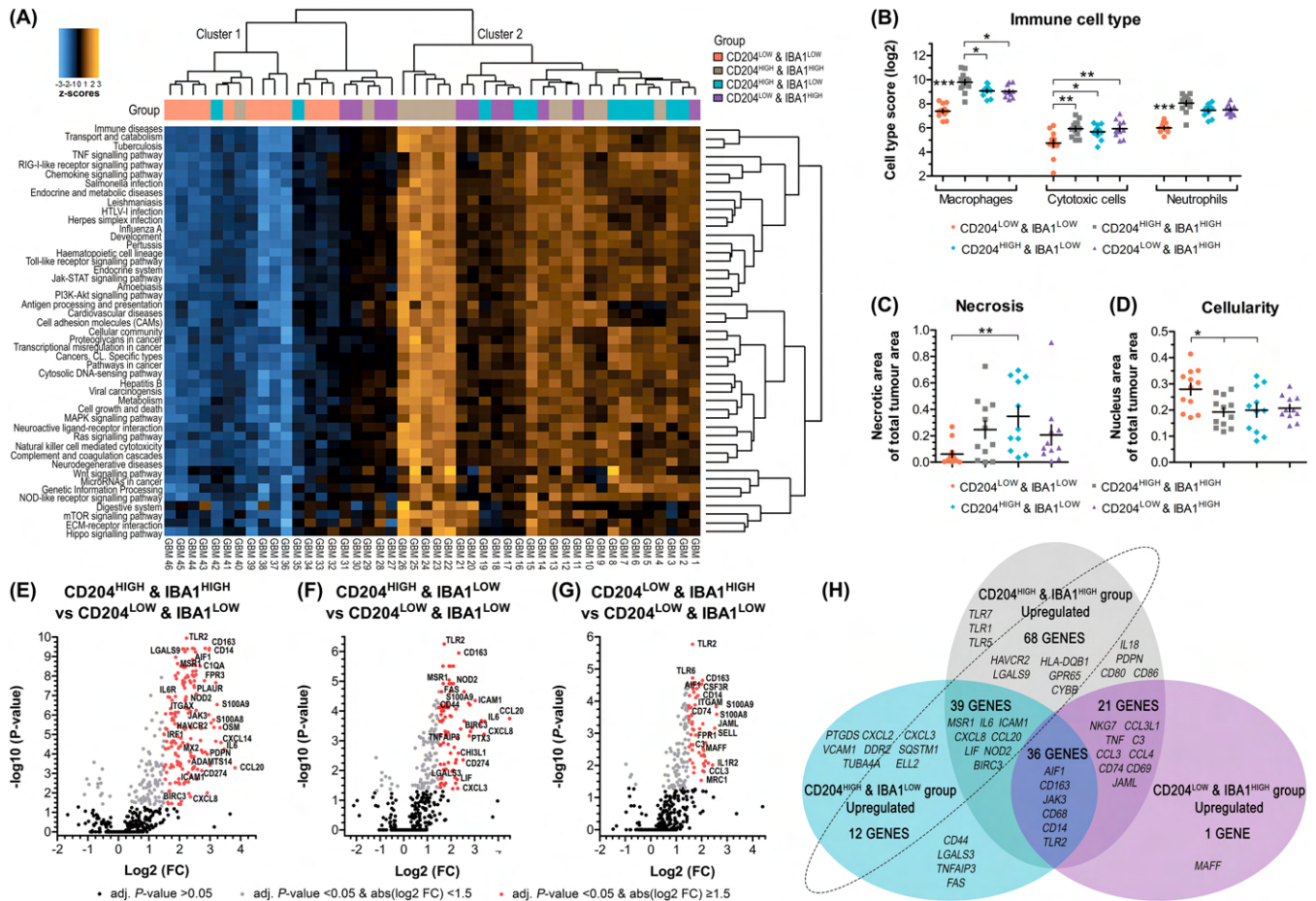


FIGURE 4 Altered gene expression pattern in CD204-enriched glioblastomas. (A) Condensing the gene expression profile of each sample provided a set of pathway scores and generated a heatmap. Unsupervised cluster analysis generated a cluster pattern similar to the one seen for the normalised gene expression data. Cluster 2 mainly comprised CD204-enriched glioblastomas and was associated with a higher level of pathway activity. (B) Cell type abundance measurements showed that glioblastomas with low levels of TAMs (i.e., the CD204^{LOW}/IBA1^{LOW} group) displayed in lowest levels of macrophages (based on the mRNA levels of CD163, CD68 and CD84), cytotoxic cells (based on the mRNA levels of NKG7 and KLRK1), and neutrophils (based on the mRNA levels of FPR1, SIGLEC5, CSF3R and FCGR3A). (C) Assessment of the necrotic component revealed that necrosis was more common in glioblastomas with high CD204 expression. (D) Estimation of cellularity showed that glioblastomas with high CD204 levels had lower cell density. (E) Differential gene expression analysis revealed that 164 of 585 genes were significantly upregulated above 1.50 log2 fold-change (FC) in the CD204^{HIGH}/IBA1^{HIGH} group relative to the CD204^{LOW}/IBA1^{LOW} group. (F) Differential gene expression analysis revealed that 87 of 585 genes were significantly upregulated above 1.50 log2 FC in the CD204^{HIGH}/IBA1^{LOW} group relative to the CD204^{LOW}/IBA1^{LOW} group. (G) Differential gene expression analysis revealed that 58 of 585 genes were significantly upregulated above 1.50 log2 FC in the CD204^{LOW}/IBA1^{HIGH} group relative to the CD204^{LOW}/IBA1^{LOW} group. (H) Graphical representation of the overlap of the differentially upregulated genes in the CD204^{HIGH}/IBA1^{HIGH}, CD204^{HIGH}/IBA1^{LOW} and CD204^{LOW}/IBA1^{HIGH} groups relative to the CD204^{LOW}/IBA1^{LOW} group showed that 119 genes were uniquely upregulated in CD204^{HIGH} (i.e., CD204-enriched) glioblastomas. Horizontal and vertical lines indicate mean ± SEM. *p < 0.05; **p < 0.01; ***p < 0.001

TABLE 2 List of differentially expressed genes ($n = 119$) in CD204^{HIGH} tumours

	CD204 ^{HIGH} & IBA1 ^{HIGH}		CD204 ^{HIGH} & IBA1 ^{LOW}	
	vs. CD204 ^{LOW} & IBA1 ^{LOW}		vs. CD204 ^{LOW} & IBA1 ^{LOW}	
	Log2 FC	Adj. p value	Log2 FC	Adj. p value
Genes only differentially upregulated in CD204 ^{HIGH} tumours ($n = 39$)				
ADAM8	2.84	8.10E-05	2.09	9.72E-03
ADAMTS14	2.32	2.39E-04	1.56	3.72E-02
ALDH1A1	1.87	2.93E-03	1.89	5.44E-03
ALOX5AP	2.34	1.79E-08	1.92	1.21E-05
BIRC3	1.75	3.56E-02	2.88	3.70E-04
C5AR1	2.22	1.17E-07	1.81	5.48E-05
CCL2	2.49	4.41E-04	2.22	4.38E-03
CCL20	3.82	5.18E-04	4.48	1.80E-04
CD274	2.73	7.15E-04	2.51	4.41E-03
CHI3L1	2.45	5.11E-04	2.31	2.62E-03
CSF1	1.77	1.46E-06	1.59	6.41E-05
CTSD	1.68	1.23E-07	1.66	3.09E-06
CXCL1	2.06	2.65E-02	2.07	4.11E-02
CXCL14	3.36	2.62E-05	2.17	1.74E-02
CXCL8	2.36	1.60E-02	3.40	6.06E-04
DPP4	2.43	6.02E-04	2.04	1.06E-02
FOSL1	2.04	3.26E-04	1.71	6.20E-03
ICAM1	1.97	3.00E-03	3.02	4.47E-05
IL1R1	2.38	1.25E-04	2.24	7.87E-04
IL4I1	2.17	5.38E-06	1.96	1.44E-04
IL6	3.46	5.75E-05	3.43	2.20E-04
LIF	3.00	3.74E-04	2.26	2.01E-02
MAFB	2.23	4.71E-07	1.75	1.59E-04
MAPK13	2.48	3.09E-08	2.10	1.21E-05
MMP19	2.15	3.15E-03	2.19	5.59E-03
MSR1	2.17	3.49E-09	1.67	1.20E-05
MX2	2.27	3.17E-05	1.88	1.31E-03
NAMPT	1.74	3.58E-04	2.01	1.52E-04
NCF2	2.17	4.15E-08	1.92	9.07E-06
NFKBIZ	1.87	9.23E-05	1.77	6.12E-04
NOD2	2.20	1.58E-07	2.02	1.20E-05
OSCAR	1.96	7.28E-07	1.66	7.70E-05
PLAUR	2.49	3.81E-08	1.84	7.70E-05
PTGS2	1.98	3.77E-02	2.20	2.69E-02
PTX3	2.59	6.24E-04	2.77	6.87E-04
SERPINE1	2.10	5.90E-04	1.59	2.69E-02
SIGLEC1	2.72	6.51E-05	1.77	2.69E-02
TGM2	1.96	1.30E-04	1.55	6.20E-03
TNFRSF14	1.54	5.31E-05	1.58	1.33E-04
Genes only differentially upregulated in CD204 ^{HIGH} & IBA1 ^{LOW} tumours ($n = 12$)				
CD44	—	—	1.73	7.70E-05
CXCL2	—	—	1.69	9.45E-03

(Continues)

TABLE 2 (Continued)

	CD204 ^{HIGH} & IBA1 ^{HIGH}		CD204 ^{HIGH} & IBA1 ^{LOW}	
	vs. CD204 ^{LOW} & IBA1 ^{LOW}		vs. CD204 ^{LOW} & IBA1 ^{LOW}	
	Log2 FC	Adj. p value	Log2 FC	Adj. p value
CXCL3	–	–	2.28	4.00E-02
DDR2	–	–	1.84	6.41E-05
ELL2	–	–	1.50	7.70E-05
FAS	–	–	1.60	2.24E-05
LGALS3	–	–	1.59	1.87E-02
PTGDS	–	–	3.29	2.11E-04
SQSTM1	–	–	1.80	6.41E-05
TNFAIP3	–	–	1.68	1.17E-03
TUBA4A	–	–	1.79	9.07E-03
VCAM1	–	–	1.98	2.62E-03
Genes only differentially upregulated in CD204 ^{HIGH} & IBA1 ^{HIGH} tumours (n = 68)				
ADORA3	2.05	1.55E-05	–	–
AOAH	1.93	2.39E-04	–	–
BTK	2.14	3.55E-09	–	–
CASP1	1.78	2.17E-05	–	–
CCRL2	1.71	8.46E-07	–	–
CD180	2.04	3.89E-05	–	–
CD80	2.03	4.14E-04	–	–
CD84	2.18	5.68E-10	–	–
CD86	1.98	4.09E-06	–	–
CEBPA	1.82	2.18E-05	–	–
CEBPB	1.50	1.02E-05	–	–
CLEC5A	1.88	2.83E-05	–	–
CSF1R	2.13	2.99E-08	–	–
CSF2RA	1.59	5.38E-06	–	–
CTSL	1.50	4.69E-04	–	–
CTSS	2.17	2.06E-08	–	–
CX3CR1	1.66	8.16E-03	–	–
CXCL12	2.19	2.69E-03	–	–
CYBB	2.42	2.76E-09	–	–
EGR2	1.69	3.34E-03	–	–
ENPP2	1.64	3.68E-02	–	–
GATA3	1.62	3.11E-02	–	–
GPR65	2.55	8.30E-08	–	–
HAVCR2	1.85	2.81E-06	–	–
HBEGF	1.70	5.11E-04	–	–
HLA-DMA	1.76	1.85E-06	–	–
HLA-DMB	1.87	1.12E-07	–	–
HLA-DPB1	1.64	5.19E-05	–	–
HLA-DQB1	2.91	1.01E-02	–	–
HLA-DRA	1.55	5.61E-05	–	–
HPGDS	2.02	2.92E-04	–	–
IER3	1.73	2.60E-05	–	–

(Continues)

TABLE 2 (Continued)

	CD204 ^{HIGH} & IBA1 ^{HIGH}		CD204 ^{HIGH} & IBA1 ^{LOW}	
	vs. CD204 ^{LOW} & IBA1 ^{LOW}		vs. CD204 ^{LOW} & IBA1 ^{LOW}	
	Log2 FC	Adj. p value	Log2 FC	Adj. p value
<i>IGF1</i>	2.04	3.83E-02	—	—
<i>IL15RA</i>	1.75	8.46E-07	—	—
<i>IL17RA</i>	1.55	8.80E-07	—	—
<i>IL18</i>	2.19	1.91E-07	—	—
<i>IL4R</i>	1.85	8.80E-07	—	—
<i>IL6R</i>	1.63	1.17E-07	—	—
<i>IRF1</i>	1.58	2.28E-05	—	—
<i>IRF5</i>	1.71	4.70E-07	—	—
<i>IRF8</i>	1.77	2.56E-05	—	—
<i>ITGAL</i>	1.96	2.64E-04	—	—
<i>ITGAX</i>	1.76	1.74E-07	—	—
<i>LAT2</i>	1.90	1.36E-08	—	—
<i>LGALS9</i>	1.88	1.07E-09	—	—
<i>LST1</i>	1.58	8.86E-04	—	—
<i>MPEG1</i>	1.94	3.58E-04	—	—
<i>NLRP3</i>	1.55	3.56E-04	—	—
<i>PDPN</i>	2.91	1.04E-04	—	—
<i>PIK3CG</i>	2.11	1.76E-08	—	—
<i>PLAU</i>	1.68	8.01E-03	—	—
<i>PTAFR</i>	1.94	2.30E-09	—	—
<i>PYCARD</i>	2.21	3.11E-09	—	—
<i>RUNX2</i>	2.31	1.08E-02	—	—
<i>S100A4</i>	1.99	4.49E-05	—	—
<i>SIGLEC5</i>	1.88	1.09E-04	—	—
<i>STAT6</i>	1.55	4.91E-06	—	—
<i>SYK</i>	2.26	4.08E-10	—	—
<i>TLR1</i>	1.95	6.96E-09	—	—
<i>TLR5</i>	1.80	4.63E-04	—	—
<i>TLR7</i>	2.45	5.53E-04	—	—
<i>TNFAIP8</i>	1.81	1.85E-06	—	—
<i>TNFRSF11A</i>	1.87	7.35E-07	—	—
<i>TNFRSF1B</i>	1.87	9.51E-09	—	—
<i>TNFSF10</i>	2.11	2.65E-05	—	—
<i>TREM2</i>	2.14	4.08E-10	—	—
<i>TYROBP</i>	2.11	2.30E-08	—	—
<i>WAS</i>	2.11	4.08E-10	—	—

(e.g., *CD80*, *CD86*, *IL18*, *IL1R1*, *CCL2*, *IL15*, *IL1B*, *CCL5* and *HLA*) and M2 (*TLR1*, *TGM2*, *CD204* [*MSR1*], *CD206* [*MRC1*], *IL1R2* and *CD163*) polarisation profiles [10, 33, 38, 64–66]. In the CD204^{LOW}/IBA1^{HIGH} group, 58 genes, including *S100A8*, *S100A9*, *JAML* [*AMICA1*] and *OSM*, were ≥ 1.50 -fold upregulated compared with baseline (Figure 4G and Table S4). The IBA1-enriched group differentially expressed, in particular, M1-related genes (*TLR2*, *TNF*, *CCL3*, *CCL4*, *IL15*, *IL1B* and

CCL5), but also some M2-related genes (*CD206*, *IL1R2* and *CD163*). No genes were differentially downregulated below a log2 FC of -1.50 in any of the three subgroups relative to the CD204^{LOW}/IBA1^{LOW} group. Among the genes related to cancer stemness, only *ALDH1A1* [aldehyde dehydrogenase 1 family, member A1], *CD44* and *PDPN* had significant log2 FC ≥ 1.50 and only in CD204^{HIGH} tumours (Table S5). None of the glioblastoma-related genes were differentially

expressed (Table S5). File S2 lists all genes identified with differential expression analysis in the corresponding groups.

IL6 plays a central role in the genetic interaction network in CD204-enriched glioblastomas

To identify genes that were exclusively upregulated in CD204^{HIGH} glioblastomas, the differentially upregulated genes from all three subgroups were investigated for potential overlap (Figure 4H), and 119 genes were found to be upregulated only in CD204^{HIGH} glioblastomas including *CD204*, *IL6*, *ICAM1*, *PD-L1*, *BIRC3* and *CCL20* (Table 2), while 22 upregulated genes were shared only between the IBA1^{HIGH} groups including *C3*, *C1QA*, *C1QB*, *CCL3*, *CD74* and *TNF* (Table S6), and 36 genes were shared among all three subgroups compared with the baseline group including *IBA1*, *S100A8* and *S100A9* (Table S7). The 119 genes that were uniquely upregulated in the CD204^{HIGH} glioblastoma showed a strong interaction enrichment when performing STRING connectivity analysis, and cluster analysis identified three major and three minor clusters that were interconnected (Figure 5A). The biggest cluster (red) appeared to centre on *IL6*, which was the gene with the highest number of gene–gene interactions (Figure 5B). *IL6* connected either directly or indirectly, for example, via *CCL2*, *ICAM1*, *CXCL8* and *IRF1* with the other subnetworks including the second biggest cluster (yellow) which comprised *HLA* genes, *IRF1*, *CD44* and *PD-L1* among others. Both *CD44* and *PD-L1* were connected to a smaller cluster (blue) consisting of the immune checkpoint markers *TIM3* and *GAL9* as well as *GAL3*. KEGG and Reactome Pathway analyses demonstrated an overrepresentation of terms related to activation and regulation of the immune system as well as cellular communication by cytokines or chemokines including ‘Cytokine–cytokine receptor interaction’, ‘TNF signalling pathway’, ‘NOD-like receptor signalling pathway’, ‘NF-kappa B signalling pathway’ and ‘Interferon signalling’. The upregulated genes were also involved in ‘Extracellular matrix organisation’, ‘haemostasis’, ‘transcriptional misregulation in cancer’ as well as various autoimmune and infectious diseases. Further, the signalling pathways related to promotion of the M2 polarisation phenotype (i.e., *IL10*, *IL4* and *IL13* [10, 33, 64–66]) were overrepresented (Figure 5C,D and Tables S8,S9). Connectivity and enrichment analyses of the 36 shared differentially expressed genes and the 22 differentially upregulated genes in the IBA1^{HIGH} group showed an association with phagocytic pathways and the complement cascade, respectively, as well as immune-related pathways (Figure S4 and Tables S10–S13). The TCGA and Gravendeel datasets were employed to screen for changes in mRNA levels of 17,811 and 19,944 genes between the glioblastomas with the highest and lowest *CD204* mRNA levels. Interaction network analyses of the differentially upregulated genes from these two datasets confirmed the central role of *IL6* in CD204-enriched tumours. *CD204* itself clustered with genes related to collagen and extracellular matrix modelling. Further, KEGG and Reactome enrichment and pathway analyses of the *in*

silico datasets verified the functional profile of the CD204-enriched glioblastomas identified by NanoString (Figures S5 and S6 and Tables S14–S17).

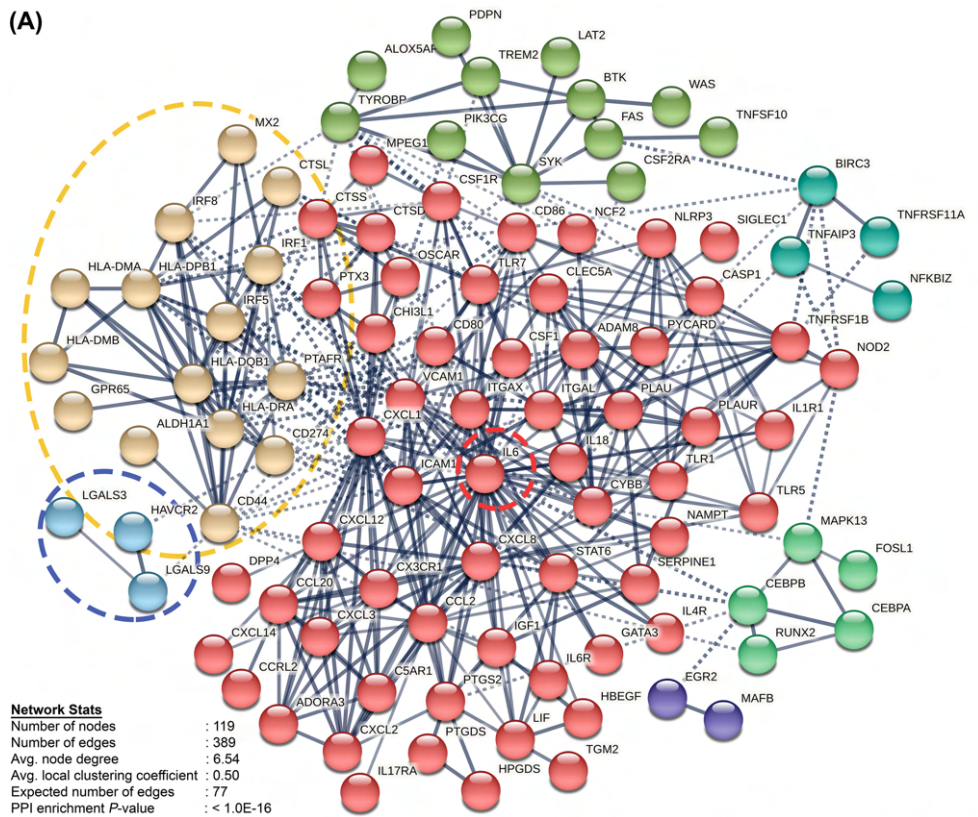
Validation of gene expression profile in CD204-enriched glioblastoma

The unique gene expression profile for CD204-enriched glioblastomas was corroborated by immunohistochemical analysis. Of the 46 glioblastoma samples, 10 were included from the CD204^{LOW}/IBA1^{LOW} group and 10 from the CD204^{HIGH} groups. A gene signature comprising 10 differentially upregulated genes was used for protein validation. The genes included in the signature were selected based on their fold-changes, connectivity levels in the interaction network analysis, level of gene matches in the pathway analyses, and antibody availability. Ultimately, protein expression was investigated for the following genes: *BIRC3*, *TNFAIP3*, *NOD2*, *IL6*, *ICAM1*, *CD44*, *PD-L1*, *GAL3*, *GAL9* and *TIM3*. STRING connectivity analysis was used to verify that the 10 genes as well as *CD204* were able to form an interacting network with *IL6* in the epicentre (Figure 5E). The subgrouping of the 20 samples was verified by chromogenic staining for IBA1 and CD204 (Figure 6A,B). Immunostaining showed that *BIRC3* was primarily localised in the nucleus (Figure 6C), but expression was also observed in the cytoplasm (not shown). *TNFAIP3*, *NOD2*, *IL6*, *ICAM1*, *CD44*, *PD-L1* and *GAL3* were expressed in the membrane and/or the cytoplasm, and expression levels seemed to depend on CD204 level being highest in CD204^{HIGH} glioblastomas (Figure 6D–J). When applying software-based algorithms, the area fractions were significantly higher in CD204^{HIGH} compared with CD204^{LOW}/IBA1^{LOW} tumours for IBA1 ($p < 0.01$), *CD204* ($p < 0.001$), *TNFAIP3* ($p < 0.01$), *IL6* ($p < 0.001$), *ICAM1* ($p < 0.01$), *CD44* ($p < 0.01$) and *GAL3* ($p < 0.05$) (Figure 6K). The same tendency was observed for *NOD2* ($p = 0.075$), while no significant difference was found for *BIRC3* ($p = 0.17$). *GAL9*⁺ and *TIM3*⁺ cells were also significantly more frequent in CD204^{HIGH} tumours ($p < 0.01$ or $p < 0.001$) (Figure 6L).

CD204 is an important prognostic factor and is associated with worse overall survival

A heatmap was generated for the 20 tumours based on the level of *CD204*, necrosis, cellularity and the eight significantly overexpressed proteins of 10-gene signature described above. Unsupervised hierarchical clustering revealed two major clusters (Figure 6M) similar to the pattern found in the NanoString transcriptome analysis. Cluster 1 was mostly characterised by CD204^{LOW} tumours, whereas Cluster 2 consisted solely of CD204^{HIGH} tumours. Kaplan–Meier estimator and log-rank testing showed a significant separation in overall survival between the two clusters (HR 2.92, $P = 0.044$) (Figure 6N). However, similar to the findings from the transcriptome analysis, the two clusters did not show greater prognostic impact compared with *CD204* alone (HR 3.93, $P = 0.016$, Kaplan–Meier plot not shown). To further

FIGURE 5 STRING connectivity network and enrichment analysis of CD204-enriched glioblastomas. (A,B) The interaction network analysis was performed on the 119 genes that were uniquely upregulated in CD204-enriched glioblastomas. Clustering identified three major clusters and three minor clusters. The biggest cluster (red) centralised around *IL6*, which had the most interactions of all the genes (B) and connected to the other subnetworks either directly or indirectly via, for example, *ICAM1* and *PD-L1* [CD274]. (C,D) KEGG and Reactome enrichment analyses revealed that the differentially upregulated genes were especially involved cytokine signalling pathways including TNF, IL10, IL4/13, interferon as well as the NOD-like receptor and NF-kappa B signalling pathways. (E) Some of the upregulated genes were selected for protein and *in silico* mRNA validation. The selected genes formed a connectivity network which also centralised around *IL6*. *Line annotations*: thick = highest edge confidence (0.90), thin = high edge confidence (0.70); dotted = intercluster connections

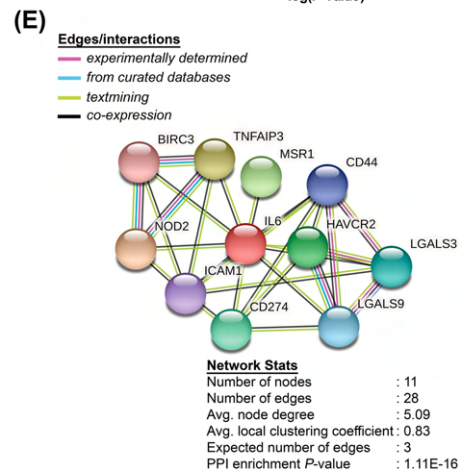
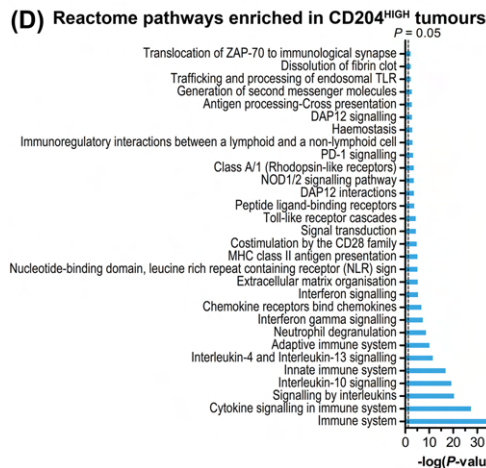
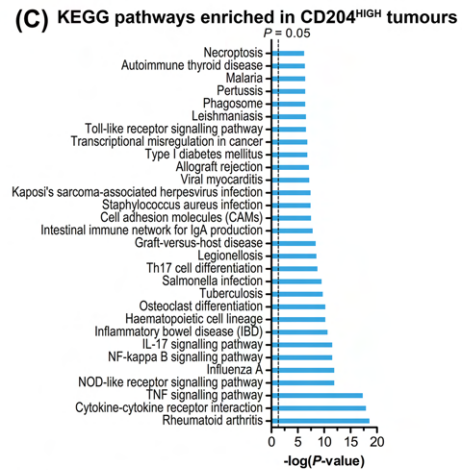


Network Stats

Number of nodes	: 119
Number of edges	: 389
Avg. node degree	: 6.54
Avg. local clustering coefficient	: 0.50
Expected number of edges	: 77
PPI enrichment P-value	: < 1.0E-16

(B)

Node 1	# interactions	Node 2	# interactions
<i>IL6</i>	34	<i>CCL2</i>	19
<i>ITGAX</i>	20	<i>ICAM1</i>	19
<i>CD44</i>	15	<i>CXCL8</i>	14
<i>HLA-DPB1</i>	15	<i>IRF1</i>	13
<i>HLA-DRA</i>	15	<i>CSF1R</i>	10
<i>CXCL1</i>	14	<i>IL18</i>	10
<i>CASP1</i>	13	<i>CD80</i>	9
<i>CXCL12</i>	13	<i>CD86</i>	9
<i>CXCL2</i>	11	<i>CTSD</i>	9
<i>CXCL8</i>	10	<i>CXCL3</i>	9
<i>HLA-DQB1</i>	10	<i>IRF8</i>	8
<i>TLR7</i>	10	<i>PTAFR</i>	8
<i>CYBB</i>	9	<i>STAT6</i>	8
<i>PTGS2</i>	9	<i>C5AR1</i>	7
<i>ADAM8</i>	8	<i>CX3CR1</i>	7
<i>CLEC5A</i>	7	<i>ITGAL</i>	7
<i>OSCAR</i>	7	<i>NLRP3</i>	7
<i>PTAFR</i>	7	<i>BIRC3</i>	6
<i>TLR5</i>	7	<i>CTSS</i>	6
<i>TNFRSF1B</i>	7	<i>IL6</i>	6



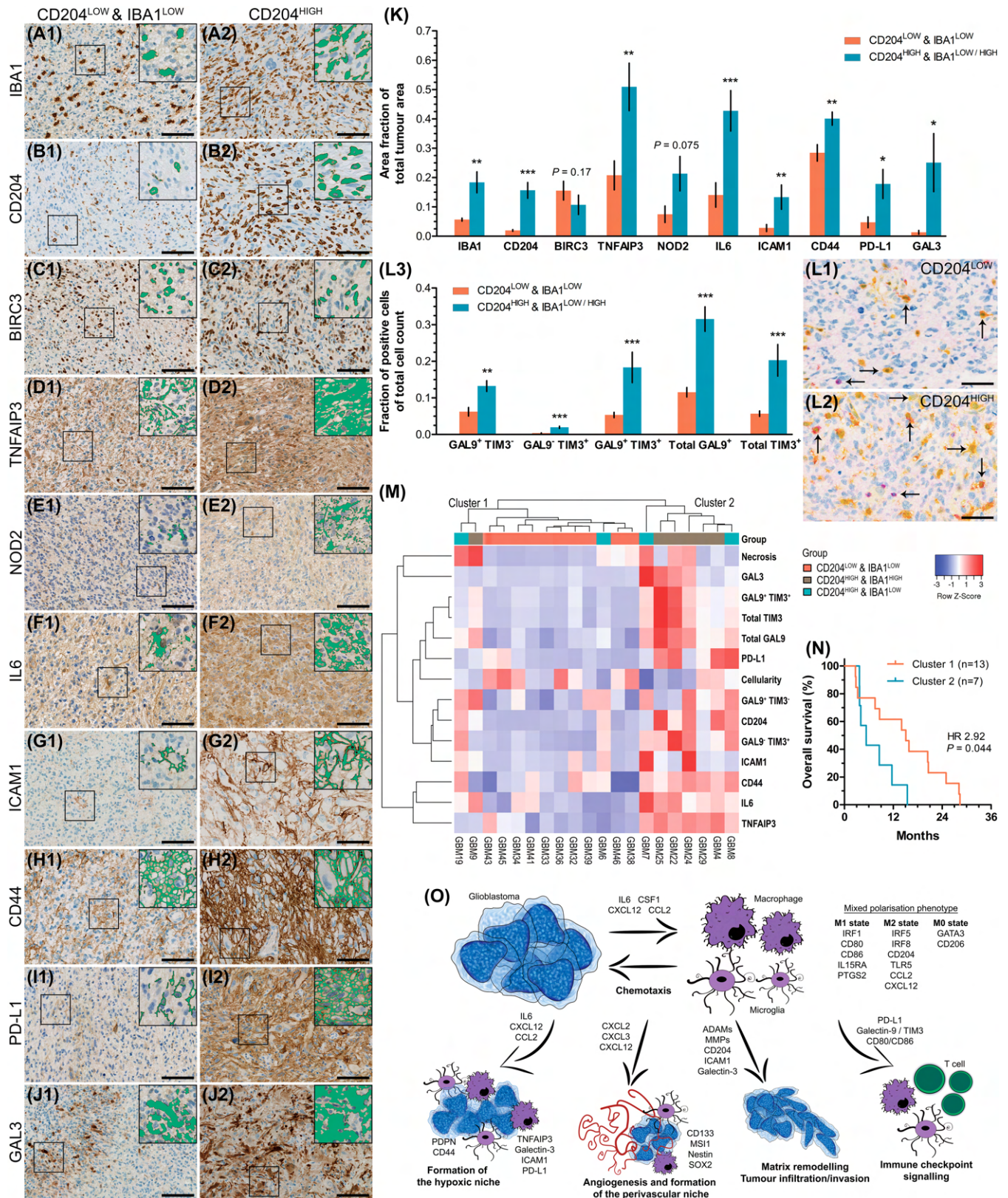


FIGURE 6 Legend on next page.

FIGURE 6 Validation of selected upregulated genes in the CD204-enriched glioblastoma profile. (A,B) High levels of IBA1 and CD204 was confirmed by immunohistochemistry in the validation cohort consisting of 20 glioblastomas. (C) BIRC3 was expressed primarily in the nuclei, and its protein expression did not appear to be influenced by CD204 levels. (D) TNFAIP3 showed a cytoplasmic expression pattern which appeared more intense and widespread in glioblastomas with high CD204 levels. (E) NOD2 exhibited a diffuse cytoplasmic expression pattern and seemed to be expressed to a higher extent in CD204-enriched glioblastomas. (F) IL6 also showed a diffuse staining pattern, which seemed more pronounced in CD204-enriched glioblastomas. (G) ICAM1 was expressed in membrane of some of the glioblastomas, especially CD204-enriched glioblastomas. (H) CD44 was widely expressed in all tumours, but exhibited a more dense and intense staining pattern in CD204-enriched tumours. (I) PD-L1 was detected in the cytoplasm and membrane at low-moderate level in most tumours, but expression appeared more pronounced in CD204-enriched tumours. (J) GAL3 had a cytoplasmic expression pattern, but was rarely expressed in CD204-sparse tumours. (K) Software-based algorithms was used to quantify the expression level of the investigated proteins, and their overexpression in the CD204-enriched glioblastomas was validated for all but NOD2 and BIRC3. (L) TIM3 (purple) and GAL9 (yellow) expression was evaluated by double immunohistochemistry and cell counting. Both TIM3⁺ and GAL9⁺ cells were more frequent in CD204-enriched glioblastomas. (M) Data from the validated proteins, CD204 as well as necrotic level and cellularity was used to generate a heatmap and cluster analysis grouped most of the CD204-enriched into more cluster (Cluster 2). (N) The CD204-enriched cluster was associated with shorter overall survival. (O) Schematic illustration of the presumed cross-talk between glioblastoma cells and tumour-associated microglia/macrophages (TAMs) in CD204-enriched glioblastomas. Tumour-derived factors, for example, IL6, CXCL12, CSF1 and CCL2 attract brain-resident microglia and peripheral macrophages to the site of the tumour, while simultaneously activating and polarising the TAMs. The cross-talk between the glioblastoma cells and TAMs results in expression and secretion of different cytokines/chemokines or/and receptors, which promote tumour hypoxia, angiogenesis and matrix remodelling and influence immune checkpoint signalling. The tumour microenvironment in CD204-enriched glioblastoma may thus ultimately enable tumour growth, resistance and progression. *Inserts* in A–J show examples of the software-based algorithms. In L upwards and downwards arrows indicate double-positive cells (i.e., TIM3⁺ GAL9⁺ cells), rightwards arrows indicate GAL9⁺ TIM3⁻ cells, and leftwards arrows indicate TIM3⁺ GAL9⁻ cells. Horizontal and vertical lines indicate mean \pm SEM. * $p < 0.05$; ** $p < 0.01$; *** $p < 0.001$. Scale bar 50 μ M. *Abbreviations*: BIRC3, baculoviral IAP repeat containing-3; GAL3, galectin-3; GAL9, galectin-9; IBA1, ionised calcium-binding adaptor molecule-1; ICAM1, intercellular adhesion molecule-1; IL6, interleukin-6; NOD2, nucleotide-binding oligomerisation domain-containing protein-2; PD-L1, programmed death-ligand 1; TIM3, T-cell immunoglobulin and mucin-domain containing-3; TNFAIP3, tumour necrosis factor, alpha-induced protein-3

examine the prognostic value of CD204-enriched glioblastomas, the TCGA and Gravendeel datasets were evaluated, and patients with glioblastoma were stratified based on the mRNA expression levels of CD204 and IBA1. Survival analyses confirmed that high CD204 had a detrimental impact on survival (Figure S7A,B); in particular, patients with high CD204 and low IBA1 levels had a poorer prognosis (TCGA: HR 1.91, $p = 0.001$, and Gravendeel: 2.50, $p = 0.022$). The survival detriment was not potentiated when adjusting for mRNA expression of the eight genes from the 10-gene signature (TCGA: HR 2.02, $p = 0.001$, and Gravendeel: 2.37, $p = 0.047$) (Figure S7C).

DISCUSSION

In the present study, we demonstrated that perivascular and perinecrotic areas were densely populated by IBA-1⁺ and CD204⁺ TAMs which co-localised with mainly PDPN⁺ tumour cells, but to a certain extent also with nestin⁺ and SOX2⁺ tumour cells in the perivascular niche, overall suggesting a possible crosstalk between TAMs and dedifferentiated tumour cells with a stem cell-like phenotype. We have previously reported that CD204 was a negative prognostic biomarker in high-grade glioma, including glioblastoma, favouring tumour progression [32]. Here, we performed mRNA transcriptome profiling of CD204-enriched glioblastomas using the NanoString digital barcode technology on FFPE tissue samples, which offers direct multiplexed detection of RNA targets without amplification and with a high level of reproducibility and robustness [42–44]. We identified genes (e.g., CCL2, CXCL12, IL6, ICAM1, TNFAIP3 and PD-L1) that were specifically upregulated in CD204-enriched tumours compared to

glioblastomas with low levels of TAMs, especially CD204⁺ TAMs. We selected some of these genes and validated their expression using immunohistochemistry and by performing *in silico* mRNA analyses.

We performed transcriptome profiling of 46 glioblastomas with either high or low CD204 protein expression levels, and unsupervised clustering grouped the glioblastomas into two clusters. One cluster (Cluster 2)— which contained most of the CD204-enriched glioblastomas—correlated with shorter overall survival and was characterised by enrichment of multiple pathways especially the TNF and NOD-like receptor signalling pathways, which regulate immune response, apoptosis and shaping of the extracellular matrix [67, 68]. Consistent with previous studies [38, 39], our profiling of CD204-enriched glioblastomas revealed upregulation of genes belonging to all macrophage/microglia polarisation states: M1 (CD86, CD80, IRF1, IL15RA and PTGS2), M2/M2c (e.g., TLR5, CXCL12, CD204, CCL2, IRF5, HLA-genes and IRF8), and M0 (GATA3 and CD206). Similar results have been found in recent studies using the single-cell RNA-sequencing and CyTOF techniques [40, 69]. This altogether suggests that the myeloid immune composition in brain tumours is highly heterogeneous, and single-cell profiling has shown that this heterogeneity is disease-, ontogenetic- and spatiotemporal-dependent [69–71].

In agreement with previous reports, we observed that both TAMs and dedifferentiated/stem-like glioblastoma cells accumulate [20–23, 37] and tend to co-reside [24, 26] in areas surrounding vasculature and necrosis/hypoxic niches. However, to our knowledge, we are the first to systemically perform a proximity study using a panel of seven markers related to cancer stemness and TAM markers. Our results showed that especially CD204⁺ TAMs and PDPN⁺ dedifferentiated tumour cells co-resided in these niches. Reportedly, the tumour cells

attract TAMs to the tumour sites by secreting, for example, CSF1, CCL2, CXCL12 and IL6 while simultaneously inducing an immunosuppressive TAM phenotype [24, 26, 28, 29] which in turn enhances tumour invasiveness in an autocrine and paracrine manner [24, 25]. Of the stem-like cell-related markers included in our NanoString panel, only *PDPN*, *CD44* and *ALDH1A1* were differentially upregulated in CD204-enriched glioblastoma. These genes have been linked to hypoxia [72, 73], radio-chemoresistance [14, 74, 75] and invasiveness through the actions of matrix metalloproteases (MMPs) and metalloprotease-disintegrins (ADAMs) [75–78]. Tumour hypoxia constitutes one of the cancer hallmarks and is associated with treatment resistance and angiogenesis [79], as well as an aggressive nature of glioblastoma [17, 80, 81] promoting migration [82], invasion and a mesenchymal shift [12, 23, 81]. To further investigate the possible relation between TAMs and tumour hypoxia, we investigated if the presence of necrosis correlated with the number of TAMs. We found that CD204-enriched glioblastomas had the highest level of necrosis. This finding is consistent with the nature of CD204 as CD204 belongs to the pattern recognition/scavenger receptor family and is known to phagocytise several ligands including apoptotic cells, collagen, low-density lipoproteins and myelin [73, 74]. In contrast, we observed that the overall tumour cellularity/cell density was lower in CD204-enriched glioblastoma relative to glioblastoma with low levels of TAMs. Interestingly, in cancer cell lines including the glioblastoma cell line U87-MG, cells grown at low cell density were reported to exhibit higher invasive capacity *in vitro* compared with cells grown at high density [83]. This effect was partly mediated through the Hippo and CXCR2 signalling pathways, and low-density cells showed an upregulation of several genes including the pro-angiogenic chemokines *CXCL1*, *CXCL2*, *CXCL3* and *CXCL8* [84, 85], as well as *IL6* and *CD44* [83]. Further, in oesophageal cancer, the response to neo-adjuvant chemotherapy was influenced by the tumour cell density found in the pre-chemo biopsy being poorest in patients with the lowest and highest density levels [86]. Collectively, these results suggest that CD204⁺ TAMs thrive in hypoxic niches and may facilitate the formation of a pro-invasive, resistant and dedifferentiated phenotype of glioblastoma.

Our differential expression analysis showed that several chemokines (*CCL2*, *CCL20*, *CXCL1*, *CXCL2*, *CXCL3*, *CXCL8*, *CXCL12*, *CXCL14* and *CCRL2*) and cytokines (*CSF1*, *IL6*, *LIF*, *IL411* and *IL18*) were uniquely upregulated in CD204-enriched glioblastomas, especially *CCL20*, *IL6*, *CXCL8* and *CXCL14*. By binding to their respective receptors, these molecules promote myeloid infiltration, immune evasion, hypoxia, angiogenesis, proliferation, migration/invasion, mesenchymal transition and progression in glioblastoma [11, 84, 87–91]. We identified *IL6* as an integral player in the inflammatory environment of CD204-enriched glioblastomas by performing connectivity analysis of the differentially upregulated genes, and we confirmed its upregulation at a protein level using immunohistochemistry. We also investigated the protein expression of genes that interacted either directly or indirectly with *IL6*, and we were able to validate the over-expression of TNFAIP3, ICAM1, CD44 and GAL3 as well as the co-inhibitory immune checkpoint molecules PD-L1, GAL9 and TIM3 in

glioblastomas with high CD204 levels. NOD2 expression tended to positively correlate with CD204 as well, while BIRC3 expression was CD204-independent possibly due to posttranscriptional down-regulation [92]. Similar to the transcriptome data, clustering of the overexpressed proteins identified two clusters. One cluster (Cluster 2)—which contained most of the CD204-enriched glioblastomas—predicted an unfavourable patient outcome, but the cluster was not a stronger prognosticator of survival than CD204 alone. As recently reported by Yuan et al. [41], we also found that high CD204 levels correlated with expression of the immune checkpoint markers PD-L1, TIM3 and GAL9, which suggests a possible synergy between CD204 and promotion of exhausted T cells [30, 46]. Interestingly, inhibition of CD204 in dendritic cells (DC) enhanced the efficacy of a DC vaccine in a melanoma model by restoring the T cell response and anti-tumour immunity [93]. Similarly, in an ovarian cancer model, administration of CD204-targeted immunotoxin substantially inhibited tumour burden and reduced the amount of suppressive vascular leukocytes [94]. Summarised, our findings suggest that CD204-enriched glioblastomas are associated with a highly inflamed TME, which produces several molecules such as *IL6* that can facilitate progression. Further, CD204 may have an immunoregulatory function that could mediate immune evasion (Figure 6O).

IL6 is an essential regulator of innate and acquired immunity. In cancer, it is considered one of the major tumour-promoting cytokines and is produced by both neoplastic and non-neoplastic cells [95, 96]. *IL6* stimulates expression of adhesion molecules and chemokines such as ICAM1, vascular cell adhesion protein-1 (VCAM1) and *CCL2* [97], which in turn promote tumourigenesis and tumour-driven inflammation through multiple signalling pathways including interferon, Jak-STAT and NF-kappa B [84, 95, 96, 98–100]. In glioblastoma, *IL6* is especially expressed by TAMs and endothelial cells, while its receptor *IL6R* is expressed to a higher extent by glioma cells [27, 33, 101–103]. Reportedly, TNFAIP3 and GAL3 are hypoxia-driven and NF-kappa B-dependent genes involved in regulation of apoptosis [104–106] promoting cell survival [107, 108], cancer stemness/dedifferentiation, tumour growth [107] and possibly chemoresistance [109]. Interestingly, GAL3 was reported to be expressed by microglia only in neoplastic brain tissue [110] and was associated with the myelination/remyelination process as activated GAL3⁺ microglia were able to engulf and internalise myelin-debris [111, 112] suggesting that GAL3 may act in concert with MMPs as well as CD204 in the matrix remodelling process. ICAM1 and CD44 are both associated with tumour hypoxia, treatment resistance [113], as well migration/invasion and matrix remodelling [114, 115] and were found to correlate with PD-L1 expression [116]. A previous study reported that PD-L1 is a direct target of hypoxia-inducible factor 1-alpha (HIF1A), and inhibition of PD-L1 during hypoxia augmented myeloid-derived suppressor cell (MDSC)-mediated T cell activation and reduced MDSC-derived *IL6* and *IL10* *in vitro* [117]. In turn, glioblastoma-derived *IL6* was reported to induce PD-L1 expression on myeloid cells and promote apoptosis of CD8⁺ T cells, overall promoting immunosuppression [118]. In glioblastoma xenografts, depletion or inhibition of *IL6*, its receptor *IL6R*, or endothelial-produced *IL6* by short hair RNA or an

IL6 antibody reduced glioma growth and prolonged overall survival in mice [27, 102, 103, 118, 119], and the anti-tumour activity was potentiated when combining with an immune checkpoint antibody against programmed death-1 (PD-1) [118] or the anti-angiogenic antibody bevacizumab [119]. Overall, these data suggest that IL6 is an important player in CD204-enriched glioblastoma, correlates with an aggressive tumour profile, and may be a candidate for targeted treatment in glioblastoma. Several anti-IL6 therapeutics (targeting either IL6/IL6R or downstream signalling molecules, e.g., Jak and STAT) are already used or in the pipeline for treatment of connective tissue disorders and myeloproliferative diseases [96].

In recent years, the interest in targeting myeloid cells (i.e., TAMs and MDSCs) has increased as a means of enhancing the anti-glioma response of standard treatment [95, 120–122]. One of the therapeutic strategies is re-education or elimination of TAMs by blockade of key chemokine/cytokine signalling pathways including the CCL2-CCR2 [123], CXCL2/8-CXCR2 [124, 125] and CSF1-CSF1R [126, 127] axes. This approach has shown great promise *in vivo*. However, administration of the anti-CSF1R antibody PLX3397 showed no efficacy in a phase II clinical trial with recurrent glioblastoma patients [128] possibly due to the innate self-renewing ability of microglia ensuring rapid recolonisation within the brain [129] and tumour-derived survival factors [130]. These findings underscore the importance of the bidirectional crosstalk between tumour cells and the microenvironment, in which the tumour grows and evolves. Deeper insight into the spatiotemporal dynamics of TAMs and the tumour immune microenvironment in general is necessary to achieve efficient immunotherapies including those directed against TAMs. The results of our study suggest that a future therapeutic strategy could be repolarisation of TAMs into an anti-tumourigenic phenotype by targeting CD204 and/or IL6 using, for example, neutralising antibodies. This strategy could especially be relevant in patients whose tumours express high levels of CD204 and/or IL6 at time of diagnosis, thus possibly serving as predictive and prognostic biomarkers.

In conclusion, our findings show that TAMs including CD204⁺ TAMs accumulate in perivascular and perinecrotic/hypoxic niches in close proximity to dedifferentiated/stem-like glioblastoma cells. Gene profiling revealed that CD204-enriched glioblastoma differentially expressed markers related to the entire M0–M2 spectrum. Pathway and connectivity analyses demonstrated that CD204-enriched glioblastomas were associated with an inflamed phenotype. This phenotype correlated with poor prognosis and expressed high levels of several pro-tumourigenic factors especially IL6. These results highlight the importance of CD204 in the glioblastoma microenvironment and suggest that CD204 is a possible immunoregulatory molecule which could serve as a valuable target in combined immunotherapy.

ACKNOWLEDGEMENTS

We thankfully acknowledge the outstanding laboratory work performed by histotechnicians Helle Wohlleben, Lisbet Mortensen, Lone Christiansen and senior histotechnician Ole Nielsen as well as the

technical assistance provided by the PCR laboratory at the Department of Pathology, Odense University Hospital. Parts of the study were based on data generated by the TCGA Research Network, and we gratefully acknowledge all tissue donors and workers involved in this project.

CONFLICT OF INTEREST

Both authors declare that they have no conflicts of interest.

AUTHOR CONTRIBUTIONS

M. D. S. and B. W. K. conceived the study and designed the experiments. M. D. S. collected, assembled, analysed the data, and interpreted the results. B. W. K. contributed with the reagents/materials/analysis tools. MDS drafted and edited the manuscript. Both authors have read and approved the final manuscript.

FUNDING INFORMATION

This work was supported by grants from The Danish Council for Independent Research (4183-00183), Fabrikant Einar Willumsens Mindelegat, Familien Erichsens Mindefond, Købmand M. Kristjan Kjær og Hustru Margrethe Kjær, født de la Cour-Holmes Fond, Oda og Hans Svenningsens Fond, Thora og Viggo Groves Mindelegat, Harboefonden, A. J. Andersen og Hustrus Fond, Torben og Alice Frimodts Fond, Marie og Børge Kroghs Fond, and Arkitekt Holger Hjortenberg og Hustru Dagmar Hjortenbergs Fond.

ETHICS STATEMENT

Study approval was obtained from by the Regional Scientific Ethical Committee of the Region of Southern Denmark (Project-ID: S-20150148) and the Danish Data Protection Authority (file number: 16/11065). The use of tissue was permitted by all patients in the Danish Tissue Application Register. The study was performed in agreement with the Declaration of Helsinki.

PEER REVIEW

The peer review history for this article is available at <https://publons.com/publon/10.1111/nan.12772>.

DATA AVAILABILITY STATEMENT

The data that supports the findings of this study are available either in the supplementary material of this article or from the corresponding author upon reasonable request.

ORCID

Mia D. Sørensen  <https://orcid.org/0000-0002-0105-2940>

REFERENCES

1. Louis DN, Ohgaki H, Wiestler OD, et al. *WHO Classification of Tumours of the Central Nervous System, Revised*. 4th ed. Lyon: International Agency for Research on Cancer (IARC); 2016.
2. Ostrom QT, Gittleman H, Xu J, et al. CBTRUS statistical report: primary brain and other central nervous system tumors diagnosed in the United States in 2009–2013. *Neuro-Oncol*. 2016;18(suppl_5):v1–v75.

3. Stupp R, Mason WP, van den Bent MJ, et al. Radiotherapy plus concomitant and adjuvant temozolomide for glioblastoma. *N Engl J Med*. 2005;352(10):987-996.
4. Stupp R, Hegi ME, Mason WP, et al. Effects of radiotherapy with concomitant and adjuvant temozolomide versus radiotherapy alone on survival in glioblastoma in a randomised phase III study: 5-year analysis of the EORTC-NCIC trial. *Lancet Oncol*. 2009;10:459-466.
5. Patel AP, Tirosh I, Trombetta JJ, et al. Single-cell RNA-seq highlights intratumoral heterogeneity in primary glioblastoma. *Science*. 2014;344:1396-1401.
6. Sottoriva A, Spiteri I, Piccirillo SGM, et al. Intratumor heterogeneity in human glioblastoma reflects cancer evolutionary dynamics. *Proc Natl Acad Sci*. 2013;110(10):4009-4014.
7. Phillips HS, Kharbanda S, Chen R, et al. Molecular subclasses of high-grade glioma predict prognosis, delineate a pattern of disease progression, and resemble stages in neurogenesis. *Cancer Cell*. 2006;9(3):157-173.
8. Brennan CW, Verhaak RG, McKenna A, et al. The somatic genomic landscape of glioblastoma. *Cell*. 2013;155:462-477.
9. Neftel C, Laffy J, Filbin MG, et al. An integrative model of cellular states, plasticity, and genetics for glioblastoma. *Cell*. 2019;178:835-849.
10. Charles NA, Holland EC, Gilbertson R, Glass R, Kettenmann H. The brain tumor microenvironment. *Glia*. 2011;59(8):1169-1180.
11. Chen W, Xia T, Wang D, et al. Human astrocytes secrete IL-6 to promote glioma migration and invasion through upregulation of cytomembrane MMP14. *Oncotarget*. 2016;7(38):62425-62438.
12. Joseph JV, Conroy S, Pavlov K, et al. Hypoxia enhances migration and invasion in glioblastoma by promoting a mesenchymal shift mediated by the HIF1alpha-ZEB1 axis. *Cancer Lett*. 2015;359(1):107-116.
13. Tomaszewski W, Sanchez-Perez L, Gajewski TF, Sampson JH. Brain tumor microenvironment and host state: implications for immunotherapy. *Clin Cancer Res: Off J Am Assoc Cancer Res*. 2019;25(14):4202-4210.
14. Bhat KP, Balasubramanian V, Vaillant B, et al. Mesenchymal differentiation mediated by NF-κB promotes radiation resistance in glioblastoma. *Cancer Cell*. 2013;24(3):331-346.
15. Sarkaria JN, Kitange GJ, James CD, et al. Mechanisms of chemoresistance to alkylating agents in malignant glioma. *Clin Cancer Res: Off J Am Assoc Cancer Res*. 2008;14(10):2900-2908.
16. Piao Y, Liang J, Holmes L, et al. Glioblastoma resistance to anti-VEGF therapy is associated with myeloid cell infiltration, stem cell accumulation, and a mesenchymal phenotype. *Neuro-Oncol*. 2012;14(11):1379-1392.
17. Beier D, Schulz JB, Beier CP. Chemoresistance of glioblastoma cancer stem cells—much more complex than expected. *Mol Cancer*. 2011;10(1):128.
18. Schonberg DL, Lubelski D, Miller TE, Rich JN. Brain tumor stem cells: molecular characteristics and their impact on therapy. *Mol Asp Med*. 2013;39:82-101.
19. Filatova A, Acker T, Garvalov BK. The cancer stem cell niche(s): the crosstalk between glioma stem cells and their microenvironment. *Biochim Biophys Acta*. 1830;2013(2):2496-2508.
20. Aderetti DA, Hira VVV, Molenaar RJ, van Noorden CJF. The hypoxic peri-arteriolar glioma stem cell niche, an integrated concept of five types of niches in human glioblastoma. *Biochim Biophys Acta Rev Cancer*. 1869;2018(2):346-354.
21. Calabrese C, Poppleton H, Kocak M, et al. A perivascular niche for brain tumor stem cells. *Cancer Cell*. 2007;11(1):69-82.
22. Hira VV, Ploegmakers KJ, Grevers F, et al. CD133⁺ and Nestin⁺ glioma stem-like cells reside around CD31⁺ arterioles in niches that express SDF-1alpha, CXCR4, osteopontin and cathepsin K. *J Histochem Cytochem*. 2015;63(7):481-493.
23. Heddleston JM, Li Z, McLendon RE, Hjelmeland AB, Rich JN. The hypoxic microenvironment maintains glioblastoma stem cells and promotes reprogramming towards a cancer stem cell phenotype. *Cell Cycle*. 2009;8:3274-3284.
24. Yi L, Xiao H, Xu M, et al. Glioma-initiating cells: a predominant role in microglia/macrophages tropism to glioma. *J Neuroimmunol*. 2011;232(1-2):75-82.
25. Ye XZ, Xu SL, Xin YH, et al. Tumor-associated microglia/macrophages enhance the invasion of glioma stem-like cells via TGF-beta1 signaling pathway. *J Immunol*. 2012;189:444-453.
26. Wang SC, Hong JH, Hsueh C, Chiang CS. Tumor-secreted SDF-1 promotes glioma invasiveness and TAM tropism toward hypoxia in a murine astrocytoma model. *Lab Invest: J Tech Methods Pathol*. 2012;92:151-162.
27. Dzaye OD, Hu F, Derkow K, et al. Glioma stem cells but not bulk glioma cells upregulate IL-6 secretion in microglia/brain macrophages via Toll-like receptor 4 signaling. *J Neuropathol Exp Neurol*. 2016;75(5):429-440.
28. Wu A, Wei J, Kong LY, et al. Glioma cancer stem cells induce immunosuppressive macrophages/microglia. *Neuro-Oncol*. 2010;12(11):1113-1125.
29. Gabrusiewicz K, Li X, Wei J, et al. Glioblastoma stem cell-derived exosomes induce M2 macrophages and PD-L1 expression on human monocytes. *Onco Targets Ther*. 2018;7(4):e1412909.
30. Binnewies M, Roberts EW, Kersten K, et al. Understanding the tumor immune microenvironment (TIME) for effective therapy. *Nat Med*. 2018;24(5):541-550.
31. Graeber MB, Scheithauer BW, Kreutzberg GW. Microglia in brain tumors. *Glia*. 2002;40(2):252-259.
32. Sorensen MD, Dahlrot RH, Boldt HB, Hansen S, Kristensen BW. Tumour-associated microglia/macrophages predict poor prognosis in high-grade gliomas and correlate with an aggressive tumour subtype. *Neuropathol Appl Neurobiol*. 2018;44(2):185-206.
33. Li W, Graeber MB. The molecular profile of microglia under the influence of glioma. *Neuro-Oncology*. 2012;14(8):958-978.
34. Sielska M, Przanowski P, Wylot B, et al. Distinct roles of CSF family cytokines in macrophage infiltration and activation in glioma progression and injury response. *J Pathol*. 2013;230(3):310-321.
35. Komohara Y, Ohnishi K, Kuratsu J, Takeya M. Possible involvement of the M2 anti-inflammatory macrophage phenotype in growth of human gliomas. *J Pathol*. 2008;216(1):15-24.
36. Lisi L, Stigliano E, Lauriola L, Navarra P, Dello RC. Proinflammatory-activated glioma cells induce a switch in microglial polarization and activation status, from a predominant M2b phenotype to a mixture of M1 and M2a/B polarized cells. *ASN Neuro*. 2014;6(3):171-183.
37. Zeiner PS, Preusse C, Golebiewska A, et al. Distribution and prognostic impact of microglia/macrophage subpopulations in gliomas. *Brain Pathol*. 2018;29(4):513-529.
38. Szulzewsky F, Pelz A, Feng X, et al. Glioma-associated microglia/macrophages display an expression profile different from M1 and M2 polarization and highly express Gpnmb and Spp1. *PLoS ONE*. 2015;10(2):e0116644.
39. Gabrusiewicz K, Rodriguez B, Wei J, et al. Glioblastoma-infiltrated innate immune cells resemble M0 macrophage phenotype. *JCI Insight*. 2016;1(2).
40. Muller S, Kohanbash G, Liu SJ, et al. Single-cell profiling of human gliomas reveals macrophage ontogeny as a basis for regional differences in macrophage activation in the tumor microenvironment. *Genome Biol*. 2017;18(1):234.
41. Yuan Y, Zhao Q, Zhao S, et al. Characterization of transcriptome profile and clinical features of a novel immunotherapy target CD204 in diffuse glioma. *Cancer Med*. 2019;8(8):3811-3821.
42. Veldman-Jones MH, Brant R, Rooney C, et al. Evaluating robustness and sensitivity of the NanoString technologies nCounter platform to

- enable multiplexed gene expression analysis of clinical samples. *Cancer Res.* 2015;75(13):2587-2593.
43. Reis PP, Waldron L, Goswami RS, et al. mRNA transcript quantification in archival samples using multiplexed, color-coded probes. *BMC Biotechnol.* 2011;11(1):46.
 44. Goytain A, Ng T. NanoString nCounter technology: high-throughput RNA validation. *Methods Mol Biol.* 2020;2079:125-139.
 45. Dahlrot RH, Kristensen BW, Hjelmberg J, Herrstedt J, Hansen S. A population-based study of high-grade gliomas and mutated isocitrate dehydrogenase 1. *Int J Clin Exp Pathol.* 2013;6(1):31-40.
 46. Baumeister SH, Freeman GJ, Dranoff G, Sharpe AH. Coinhibitory pathways in immunotherapy for cancer. *Annu Rev Immunol.* 2016;34(1):539-573.
 47. Ravindran S, Rasool S, Maccalli C. The cross talk between cancer stem cells/cancer initiating cells and tumor microenvironment: the missing piece of the puzzle for the efficient targeting of these cells with immunotherapy. *Cancer Microenviron.* 2019;12(2-3):133-148.
 48. Rasper M, Schafer A, Piontek G, et al. Aldehyde dehydrogenase 1 positive glioblastoma cells show brain tumor stem cell capacity. *Neuro-Oncology.* 2010;12(10):1024-1033.
 49. Leonetti C, Biroccio A, Graziani G, Tentori L. Targeted therapy for brain tumours: role of PARP inhibitors. *Curr Cancer Drug Targets.* 2012;12(3):218-236.
 50. Zhu C, Chen X, Guan G, et al. IFI30 is a novel immune-related target with predicting value of prognosis and treatment response in glioblastoma. *Onco Targets Ther.* 2020;13:1129-1143.
 51. Metz P, Reuter A, Bender S, Bartenschlager R. Interferon-stimulated genes and their role in controlling hepatitis C virus. *J Hepatol.* 2013;59(6):1331-1341.
 52. Tiwari R, de la Torre JC, McGavern DB, Nayak D. Beyond tethering the viral particles: immunomodulatory functions of tetherin (BST-2). *DNA Cell Biol.* 2019;38(11):1170-1177.
 53. Kreth S, Heyn J, Grau S, Kretschmar HA, Egensperger R, Kreth FW. Identification of valid endogenous control genes for determining gene expression in human glioma. *Neuro-Oncology.* 2010;12(6):570-579.
 54. Grube S, Göttig T, Freitag D, Ewald C, Kalf R, Walter J. Selection of suitable reference genes for expression analysis in human glioma using RT-qPCR. *J Neuro-Oncol.* 2015;123(1):35-42.
 55. Ito D, Imai Y, Ohsawa K, Nakajima K, Fukuuchi Y, Kohsaka S. Microglia-specific localisation of a novel calcium binding protein, Iba1. *Brain Res Mol Brain Res.* 1998;57(1):1-9.
 56. Ramachandran RK, Sorensen MD, Aaberg-Jessen C, Hermansen SK, Kristensen BW. Expression and prognostic impact of matrix metalloproteinase-2 (MMP-2) in astrocytomas. *PLoS ONE.* 2017;12(2):e0172234.
 57. Bowman RL, Wang Q, Carro A, Verhaak RG, Squatrito M. GlioVis data portal for visualization and analysis of brain tumor expression datasets. *Neuro-Oncology.* 2017;19(1):139-141.
 58. The Cancer Genome Atlas Research Network. Comprehensive genomic characterization defines human glioblastoma genes and core pathways. *Nature.* 2008;455(7216):1061-1068.
 59. Gravendeel LA, Kouwenhoven MC, Gevaert O, et al. Intrinsic gene expression profiles of gliomas are a better predictor of survival than histology. *Cancer Res.* 2009;69(23):9065-9072.
 60. Benjamini Y, Yekutieli D. The control of the false discovery rate in multiple testing under dependency. *Ann Stat.* 2001;29(4):1165-1188.
 61. Szklarczyk D, Gable AL, Lyon D, et al. STRING v11: protein-protein association networks with increased coverage, supporting functional discovery in genome-wide experimental datasets. *Nucleic Acids Res.* 2019;47(D1):D607-D613.
 62. Brohée S, van Helden J. Evaluation of clustering algorithms for protein-protein interaction networks. *BMC Bioinformatics.* 2006;7(1):1-9.
 63. Babicki S, Arndt D, Marcu A, et al. Heatmapper: web-enabled heat mapping for all. *Nucleic Acids Res.* 2016;44(W1):W147-W153.
 64. Sica A, Schioppa T, Mantovani A, Allavena P. Tumour-associated macrophages are a distinct M2 polarised population promoting tumour progression: potential targets of anti-cancer therapy. *Eur J Cancer.* 2006;42:717-727.
 65. Mantovani A, Sica A, Sozzani S, Allavena P, Vecchi A, Locati M. The chemokine system in diverse forms of macrophage activation and polarization. *Trends Immunol.* 2004;25(12):677-686.
 66. Hao N-B, Lü M-H, Fan Y-H, Cao Y-L, Zhang Z-R, Yang S-M. Macrophages in tumor microenvironments and the progression of tumors. *Clin Dev Immunol.* 2012;2012:948098.
 67. Balkwill F. Tumour necrosis factor and cancer. *Nat Rev Cancer.* 2009;9(5):361-371.
 68. Velloso FJ, Trombetta-Lima M, Anschau V, Sogayar MC, Correa RG. NOD-like receptors: major players (and targets) in the interface between innate immunity and cancer. *Biosci Rep.* 2019;39(4):BSR20181709.
 69. Sankowski R, Böttcher C, Masuda T, et al. Mapping microglia states in the human brain through the integration of high-dimensional techniques. *Nat Neurosci.* 2019;22(12):2098-2110.
 70. Masuda T, Sankowski R, Staszewski O, et al. Spatial and temporal heterogeneity of mouse and human microglia at single-cell resolution. *Nature.* 2019;566(7744):388-392.
 71. Friebel E, Kapolou K, Unger S, et al. Single-cell mapping of human brain cancer reveals tumor-specific instruction of tissue-invading leukocytes. *Cell.* 2020;181:1626-1642.
 72. Soehngen E, Schaefer A, Koeritzer J, et al. Hypoxia upregulates aldehyde dehydrogenase isoform 1 (ALDH1) expression and induces functional stem cell characteristics in human glioblastoma cells. *Brain Tumor Pathol.* 2014;31(4):247-256.
 73. Mishima K, Kato Y, Kaneko MK, Nishikawa R, Hirose T, Matsutani M. Increased expression of podoplanin in malignant astrocytic tumors as a novel molecular marker of malignant progression. *Acta Neuropathol.* 2006;111(5):483-488.
 74. Schafer A, Teufel J, Ringel F, et al. Aldehyde dehydrogenase 1A1—a new mediator of resistance to temozolomide in glioblastoma. *Neuro-Oncology.* 2012;14(12):1452-1464.
 75. Dong F, Eibach M, Bartsch JW, et al. The metalloprotease-disintegrin ADAM8 contributes to temozolomide chemoresistance and enhanced invasiveness of human glioblastoma cells. *Neuro-Oncology.* 2015;17(11):1474-1485.
 76. Xu SL, Liu S, Cui W, et al. Aldehyde dehydrogenase 1A1 circumscribes high invasive glioma cells and predicts poor prognosis. *Am J Cancer Res.* 2015;5(4):1471-1483.
 77. Wicki A, Christofori G. The potential role of podoplanin in tumour invasion. *Br J Cancer.* 2007;96(1):1-5.
 78. Nishikawa M, Inoue A, Ohnishi T, et al. Significance of glioma stem-like cells in the tumor periphery that express high levels of CD44 in tumor invasion, early progression, and poor prognosis in glioblastoma. *Stem Cells Int.* 2018;2018:5387041.
 79. Kucharzewska P, Christianson HC, Welch JE, et al. Exosomes reflect the hypoxic status of glioma cells and mediate hypoxia-dependent activation of vascular cells during tumor development. *Proc Natl Acad Sci U S A.* 2013;110(18):7312-7317.
 80. Brat DJ, Castellano-Sanchez AA, Hunter SB, et al. Pseudopalisades in glioblastoma are hypoxic, express extracellular matrix proteases, and are formed by an actively migrating cell population. *Cancer Res.* 2004;64(3):920-927.
 81. Xu H, Rahimpour S, Nesvick CL, et al. Activation of hypoxia signaling induces phenotypic transformation of glioma cells: implications for bevacizumab antiangiogenic therapy. *Oncotarget.* 2015;6(14):11882-11893.
 82. Li P, Zhou C, Xu L, Xiao H. Hypoxia enhances stemness of cancer stem cells in glioblastoma: an in vitro study. *Int J Med Sci.* 2013;10(4):399-407.

83. Sharif GM, Schmidt MO, Yi C, et al. Cell growth density modulates cancer cell vascular invasion via Hippo pathway activity and CXCR2 signaling. *Oncogene*. 2015;34(48):5879-5889.
84. Groblewska M, Litman-Zawadzka A, Mroczko B. The role of selected chemokines and their receptors in the development of gliomas. *Int J Mol Sci*. 2020;21(10).
85. Balkwill FR. The chemokine system and cancer. *J Pathol*. 2012;226(2):148-157.
86. Hale MD, Nankivell MG, Mueller W, et al. The relationship between tumor cell density in the pretreatment biopsy and survival after chemotherapy in OE02 trial esophageal cancer patients. *J Clin Oncol*. 2014;32:49-49.
87. Mantovani A, Allavena P, Sozzani S, Vecchi A, Locati M, Sica A. Chemokines in the recruitment and shaping of the leukocyte infiltrate of tumors. *Semin Cancer Biol*. 2004;14(3):155-160.
88. Wang L, Qin H, Li L, et al. Overexpression of CCL20 and its receptor CCR6 predicts poor clinical prognosis in human gliomas. *Med Oncol*. 2012;29(5):3491-3497.
89. Jung Y, Ahn SH, Park H, et al. MCP-1 and MIP-3 α secreted from necrotic cell-treated glioblastoma cells promote migration/infiltration of microglia. *Cell Physiol Biochem*. 2018;48(3):1332-1346.
90. Chen Z, Mou L, Pan Y, Feng C, Zhang J, Li J. CXCL8 promotes glioma progression by activating the JAK/STAT1/HIF-1 α /snail signaling axis. *Onco Targets Ther*. 2019;12:8125-8138.
91. Yin F, Xu Z, Wang Z, et al. Elevated chemokine CC-motif receptor-like 2 (CCRL2) promotes cell migration and invasion in glioblastoma. *Biochem Biophys Res Commun*. 2012;429(3-4):168-172.
92. Conze DB, Albert L, Ferrick DA, et al. Posttranscriptional down-regulation of c-IAP2 by the ubiquitin protein ligase c-IAP1 in vivo. *Mol Cell Biol*. 2005;25(8):3348-3356.
93. Yi H, Guo C, Yu X, et al. Targeting the immunoregulator SRA/CD204 potentiates specific dendritic cell vaccine-induced T-cell response and antitumor immunity. *Cancer Res*. 2011;71(21):6611-6620.
94. Bak SP, Walters JJ, Takeya M, Conejo-Garcia JR, Berwin BL. Scavenger receptor-A-targeted leukocyte depletion inhibits peritoneal ovarian tumor progression. *Cancer Res*. 2007;67(10):4783-4789.
95. Crusz SM, Balkwill FR. Inflammation and cancer: advances and new agents. *Nat Rev Clin Oncol*. 2015;12(10):584-596.
96. Garbers C, Heink S, Korn T, Rose-John S. Interleukin-6: designing specific therapeutics for a complex cytokine. *Nat Rev Drug Discov*. 2018;17(6):395-412.
97. Jones SA. Directing transition from innate to acquired immunity: defining a role for IL-6. *J Immunol*. 2005;175:3463-3468.
98. Jin X, Kim SH, Jeon HM, et al. Interferon regulatory factor 7 regulates glioma stem cells via interleukin-6 and Notch signalling. *Brain: J Neurol*. 2012;135(4):1055-1069.
99. McFarland BC, Hong SW, Rajbhandari R, et al. NF- κ B-induced IL-6 ensures STAT3 activation and tumor aggressiveness in glioblastoma. *PLoS ONE*. 2013;8(11):e78728.
100. West AJ, Tsui V, Stylli SS, et al. The role of interleukin-6-STAT3 signalling in glioblastoma. *Oncol Lett*. 2018;16(4):4095-4104.
101. Chang CY, Li MC, Liao SL, Huang YL, Shen CC, Pan HC. Prognostic and clinical implication of IL-6 expression in glioblastoma multiforme. *J Clin Neurosci: Off J Neurosurg Soc Australasia*. 2005;12(8):930-933.
102. Wang Q, He Z, Huang M, et al. Vascular niche IL-6 induces alternative macrophage activation in glioblastoma through HIF-2 α . *Nat Commun*. 2018;9(1):1-5.
103. Wang H, Lathia JD, Wu Q, et al. Targeting interleukin 6 signaling suppresses glioma stem cell survival and tumor growth. *Stem Cells*. 2009;27:2393-2404.
104. Beyaert R, Heyninck K, Van Huffel S. A20 and A20-binding proteins as cellular inhibitors of nuclear factor-kappa B-dependent gene expression and apoptosis. *Biochem Pharmacol*. 2000;60(8):1143-1151.
105. Murat A, Migliavacca E, Hussain SF, et al. Modulation of angiogenic and inflammatory response in glioblastoma by hypoxia. *PLoS ONE*. 2009;4(6):e5947.
106. Nakahara S, Oka N, Raz A. On the role of galectin-3 in cancer apoptosis. *Apoptosis*. 2005;10(2):267-275.
107. Hjelmeland AB, Wu Q, Wickman S, et al. Targeting A20 decreases glioma stem cell survival and tumor growth. *PLoS Biol*. 2010;8(2):e1000319.
108. Ikemori RY, Machado CM, Furuzawa KM, et al. Galectin-3 up-regulation in hypoxic and nutrient deprived microenvironments promotes cell survival. *PLoS ONE*. 2014;9(11):e111592.
109. Wang H, Song X, Huang Q, et al. LGALS3 promotes treatment resistance in glioblastoma and is associated with tumor risk and prognosis. *Cancer Epidemiol Biomarkers Prevent: Publ Am Assoc Cancer Res Cosponsored Am Soc Prevent Oncol*. 2019;28(4):760-769.
110. Binh NH, Satoh K, Kobayashi K, et al. Galectin-3 in preneoplastic lesions of glioma. *J Neuro-Oncol*. 2013;111(2):123-132.
111. Thomas L, Pasquini LA. Galectin-3-mediated glial crosstalk drives oligodendrocyte differentiation and (re)myelination. *Front Cell Neurosci*. 2018;12:297.
112. Reichert F, Rotshenker S. Galectin-3 (MAC-2) controls microglia phenotype whether amoeboid and phagocytic or branched and non-phagocytic by regulating the cytoskeleton. *Front Cell Neurosci*. 2019;13:90.
113. Piao Y, Henry V, Tiao N, et al. Targeting intercellular adhesion molecule-1 prolongs survival in mice bearing bevacizumab-resistant glioblastoma. *Oncotarget*. 2017;8(57):96970-96983.
114. Lin JC, Tsai JT, Chao TY, Ma HI, Liu WH. Musashi-1 enhances glioblastoma migration by promoting ICAM1 translation. *Neoplasia*. 2019;21(5):459-468.
115. Bui TM, Wiesolek HL, Sumagin R. ICAM-1: a master regulator of cellular responses in inflammation, injury resolution, and tumorigenesis. *J Leukoc Biol*. 2020;108(3):787-799.
116. Qian J, Wang C, Wang B, et al. The IFN-gamma/PD-L1 axis between T cells and tumor microenvironment: hints for glioma anti-PD-1/PD-L1 therapy. *J Neuroinflammation*. 2018;15(1):290.
117. Noman MZ, Desantis G, Janji B, et al. PD-L1 is a novel direct target of HIF-1 α , and its blockade under hypoxia enhanced MDSC-mediated T cell activation. *J Exp Med*. 2014;211(5):781-790.
118. Lamano JB, Lamano JB, Li YD, et al. Glioblastoma-derived IL6 induces immunosuppressive peripheral myeloid cell PD-L1 and promotes tumor growth. *Clin Cancer Res: Off J Am Assoc Cancer Res*. 2019;25(12):3643-3657.
119. Saidi A, Hagedorn M, Allain N, et al. Combined targeting of interleukin-6 and vascular endothelial growth factor potentially inhibits glioma growth and invasiveness. *Int J Cancer*. 2009;125(5):1054-1064.
120. Lim M, Xia Y, Bettgowda C, Weller M. Current state of immunotherapy for glioblastoma. *Nat Rev Clin Oncol*. 2018;15(7):422-442.
121. Wei J, Chen P, Gupta P, et al. Immune biology of glioma-associated macrophages and microglia: functional and therapeutic implications. *Neuro-Oncology*. 2020;22(2):180-194.
122. Grégoire H, Roncali L, Rousseau A, et al. Targeting tumor associated macrophages to overcome conventional treatment resistance in glioblastoma. *Front Pharmacol*. 2020;11:368.
123. Flores-Toro JA, Luo D, Gopinath A, et al. CCR2 inhibition reduces tumor myeloid cells and unmasks a checkpoint inhibitor effect to slow progression of resistant murine gliomas. *Proc Natl Acad Sci U S A*. 2020;117(2):1129-1138.
124. Brandenburg S, Muller A, Turkowski K, et al. Resident microglia rather than peripheral macrophages promote vascularization in brain tumors and are source of alternative pro-angiogenic factors. *Acta Neuropathol*. 2015;131(3):365-378.

125. Angara K, Borin TF, Rashid MH, et al. CXCR2-expressing tumor cells drive vascular mimicry in antiangiogenic therapy-resistant glioblastoma. *Neoplasia*. 2018;20(10):1070-1082.
126. Yan D, Kowal J, Akkari L, et al. Inhibition of colony stimulating factor-1 receptor abrogates microenvironment-mediated therapeutic resistance in gliomas. *Oncogene*. 2017;36(43):6049-6058.
127. Pyonteck SM, Akkari L, Schuhmacher AJ, et al. CSF-1R inhibition alters macrophage polarization and blocks glioma progression. *Nat Med*. 2013;19(10):1264-1272.
128. Butowski N, Colman H, De Groot JF, et al. Orally administered colony stimulating factor 1 receptor inhibitor PLX3397 in recurrent glioblastoma: an Ivy Foundation Early Phase Clinical Trials Consortium phase II study. *Neuro-Oncology*. 2015;18(4):557-564.
129. Zhan L, Krabbe G, Du F, et al. Proximal recolonization by self-renewing microglia re-establishes microglial homeostasis in the adult mouse brain. *PLoS Biol*. 2019;17(2):e3000134.
130. Quail DF, Bowman RL, Akkari L, et al. The tumor microenvironment underlies acquired resistance to CSF-1R inhibition in gliomas. *Science*. 2016;352:aad3018.

SUPPORTING INFORMATION

Additional supporting information may be found in the online version of the article at the publisher's website.

How to cite this article: Sørensen MD, Kristensen BW. Tumour-associated CD204⁺ microglia/macrophages accumulate in perivascular and perinecrotic niches and correlate with an interleukin-6-enriched inflammatory profile in glioblastoma. *Neuropathol Appl Neurobiol*. 2022;48(2):e12772. doi:10.1111/nan.12772

TUMOUR-ASSOCIATED CD204+ MICROGLIA/MACROPHAGES ACCUMULATE IN PERIVASCULAR AND PERINECROTIC NICHES AND CORRELATE WITH AN INTERLEUKIN-6 ENRICHED INFLAMMATORY PROFILE IN GLIOBLASTOMA

Mia D. Sørensen^{1,2}, Bjarne W. Kristensen¹⁻⁴

¹ Department of Pathology, Odense University Hospital, Odense, Denmark

² Department of Clinical Research, University of Southern Denmark, Odense, Denmark

³ Department of Pathology, Rigshospitalet, Copenhagen University Hospital, Copenhagen, Denmark

⁴ Department of Clinical Medicine and Biotech Research and Innovation Center (BRIC), University of Copenhagen, Copenhagen, Denmark.

Supplementary figures

Figures S1-S7

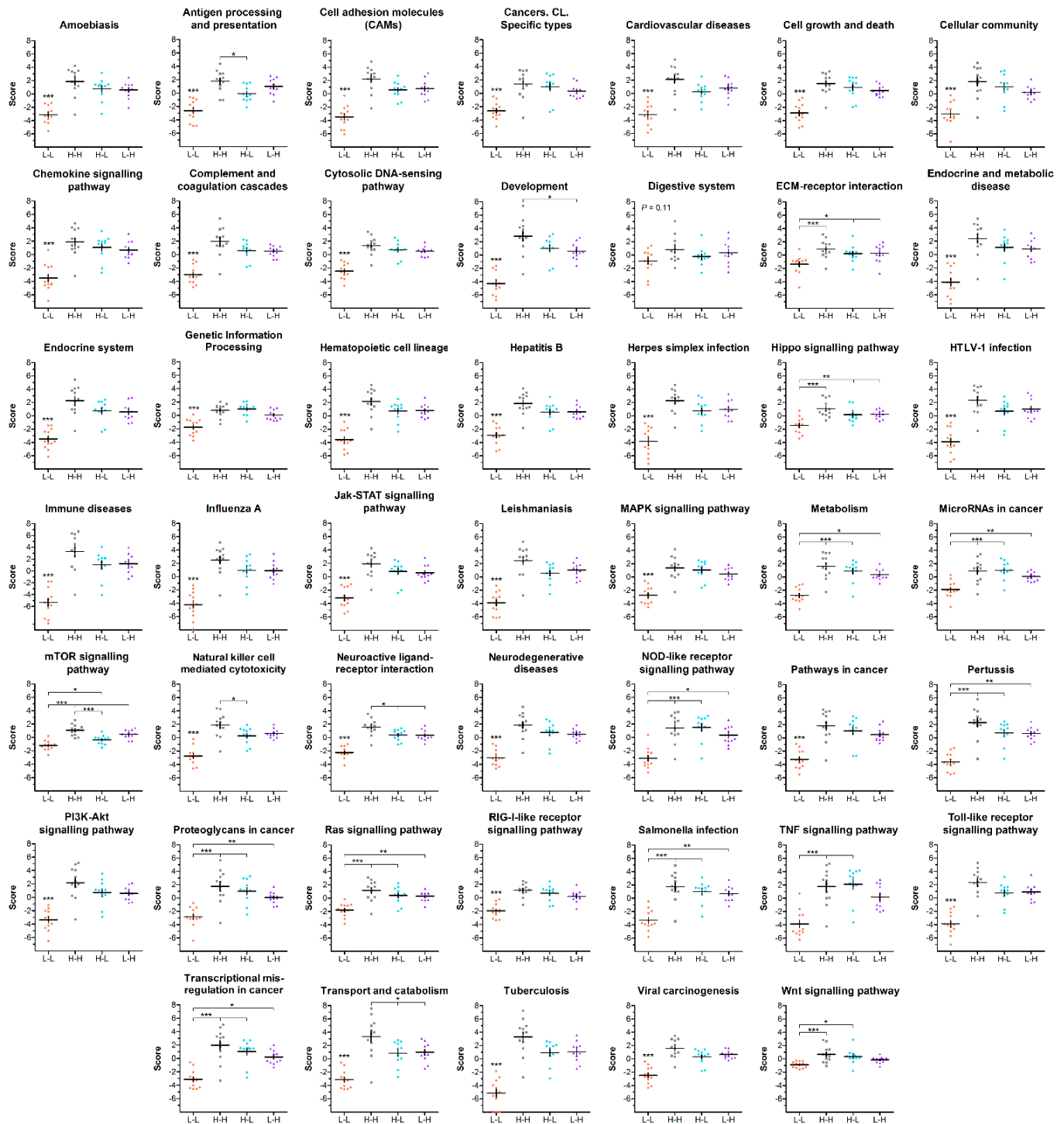


FIGURE S1. Pathway scores plotted against CD204/IBA1 subgroup. The gene expression profile of each sample was condensed into a set of 47 pathway scores. The pathway scores were fit using the first principle component of the data of each gene set. All 47 pathway scores are illustrated in scatter plots. * indicate $P < 0.05$, ** $P < 0.01$, and *** $P < 0.001$. Horizontal and vertical lines indicate mean \pm SEM. L-L: CD204^{LOW}/IBA1^{LOW} group; H-H: CD204^{HIGH}/IBA1^{HIGH} group; H-L: CD204^{HIGH}/IBA1^{LOW} group; L-H: CD204^{LOW}/IBA1^{HIGH} group

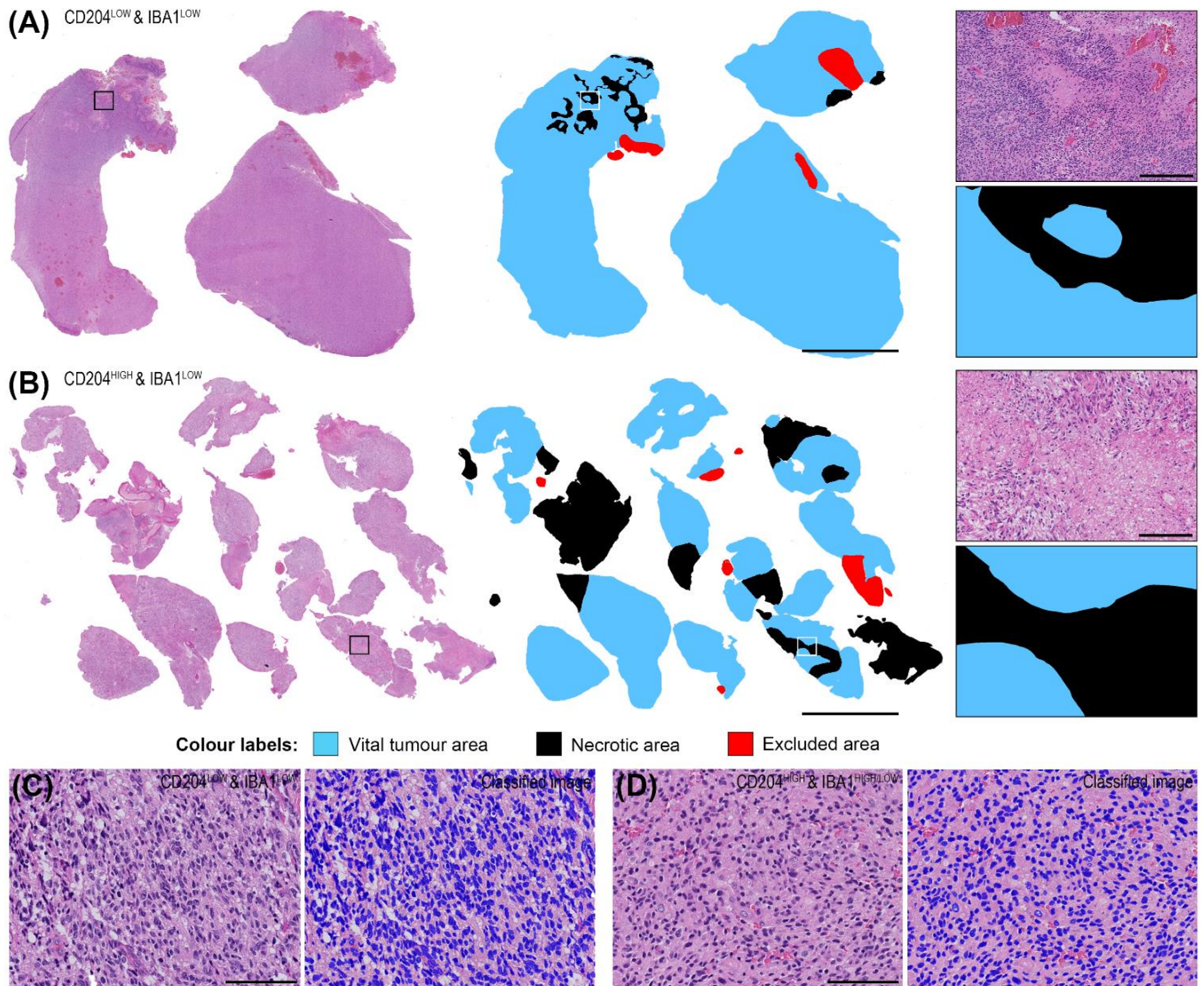


FIGURE S2. Quantification of tumour necrosis and cellularity. Automated image analyses were performed using digitised haematoxylin-eosin stainings to obtain estimates of the necrotic component and cell density (cellularity). (A, B) Areas containing vital tumour tissue (blue) and necrosis (black) were manually outlined as regions of interest (ROIs). Normal brain tissue, tumour-infiltrating area, and large blood vessels/haemorrhages were marked as exclusion areas (red). The tissue slides were processed automatically to calculate the areas of the ROIs in mm² and the necrotic component, which was defined as area of necrosis divided by the area of total tumour tissue (necrosis + vital tumour tissue). The necrotic areas constituted a higher proportion of the total tumour area in CD204^{HIGH} tumours in regards to CD204^{LOW} tumours. (C, D) Cellularity was estimated by designing a threshold-based algorithm that could identify the blue/purple nuclei based on pixel intensity. CD204^{HIGH} tumours had lower cellularity compared to CD204^{LOW} tumours. Scale bar 5 mm (overview images in A, B), 250 μm (inserts in A, B), 100 μm (C, D)

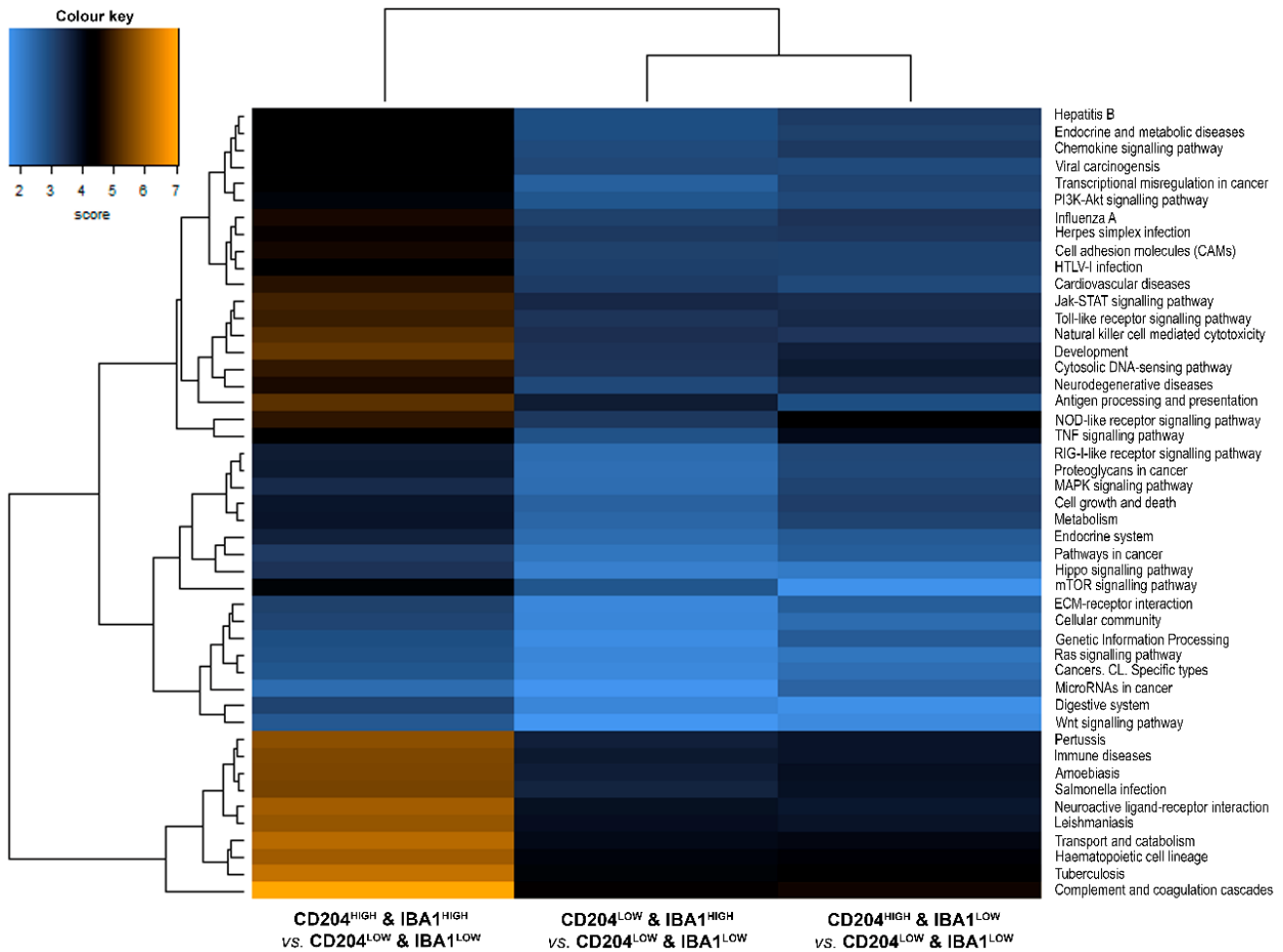


FIGURE S3. Gene set analysis. A heatmap was generated based on the global significance scores. Genes involved in e.g. immune and infectious diseases, the complement cascade, the NOD-like receptor and TNF signalling pathways were expressed to a higher extent in CD204^{HIGH} tumours. *Orange* denotes gene sets whose genes exhibit extensive differential expression with the subgrouping and *blue* denotes gene sets with less differential expression.

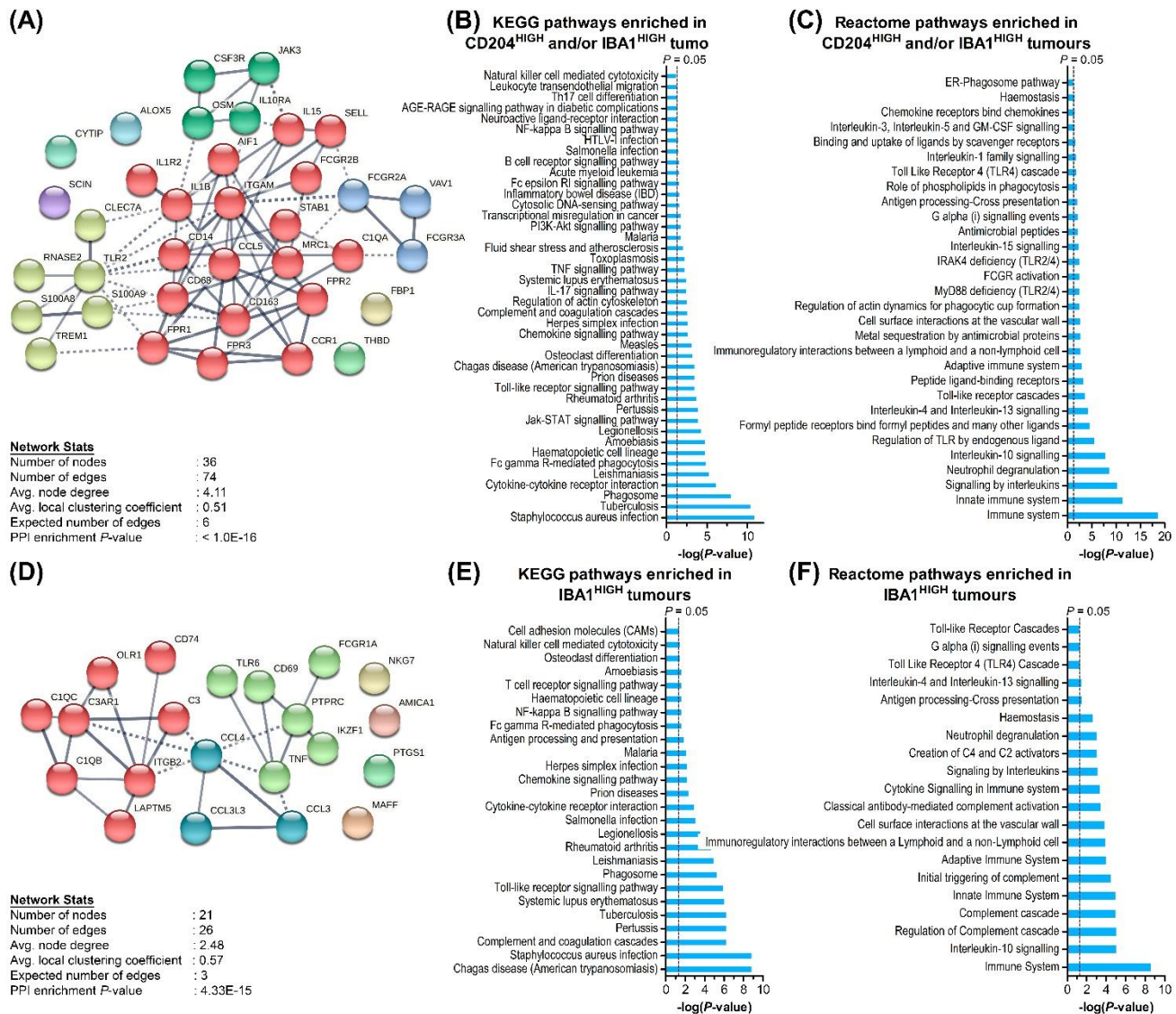


FIGURE S4. STRING connectivity network and enrichment analysis. **(A)** A total of 36 genes were differentially upregulated in CD204^{HIGH} and/or IBA1^{HIGH} glioblastomas (\log_2 fold-change ≥ 1.50 , adj. $P < 0.05$) relative to CD204^{LOW}/IBA1^{LOW} glioblastomas. These shared genes formed a network that clustered into one major cluster and three minor clusters. **(B, C)** KEGG and Reactome analyses of the 36 shared genes showed enrichment of pathways involved in e.g. the immune system, Jak-STAT signalling, TLR signalling, and cytokine signalling. **(D)** A total of 22 genes were differentially upregulated in IBA1^{HIGH} glioblastomas relative to CD204^{LOW} and/or IBA1^{LOW} glioblastomas. The upregulated genes (except for HLA-DRB3, which was not found in the STRING resource) were significantly interconnected in a network consisting of three clusters. **(E, F)** Enrichment analyses revealed that the differentially upregulated genes were especially involved in activation and regulation of complement as well as in the cytokine, chemokine and TLR signalling pathways.

Line annotations: thick = highest edge confidence (0.90), thin = high edge confidence (0.70); dotted = intercluster connections

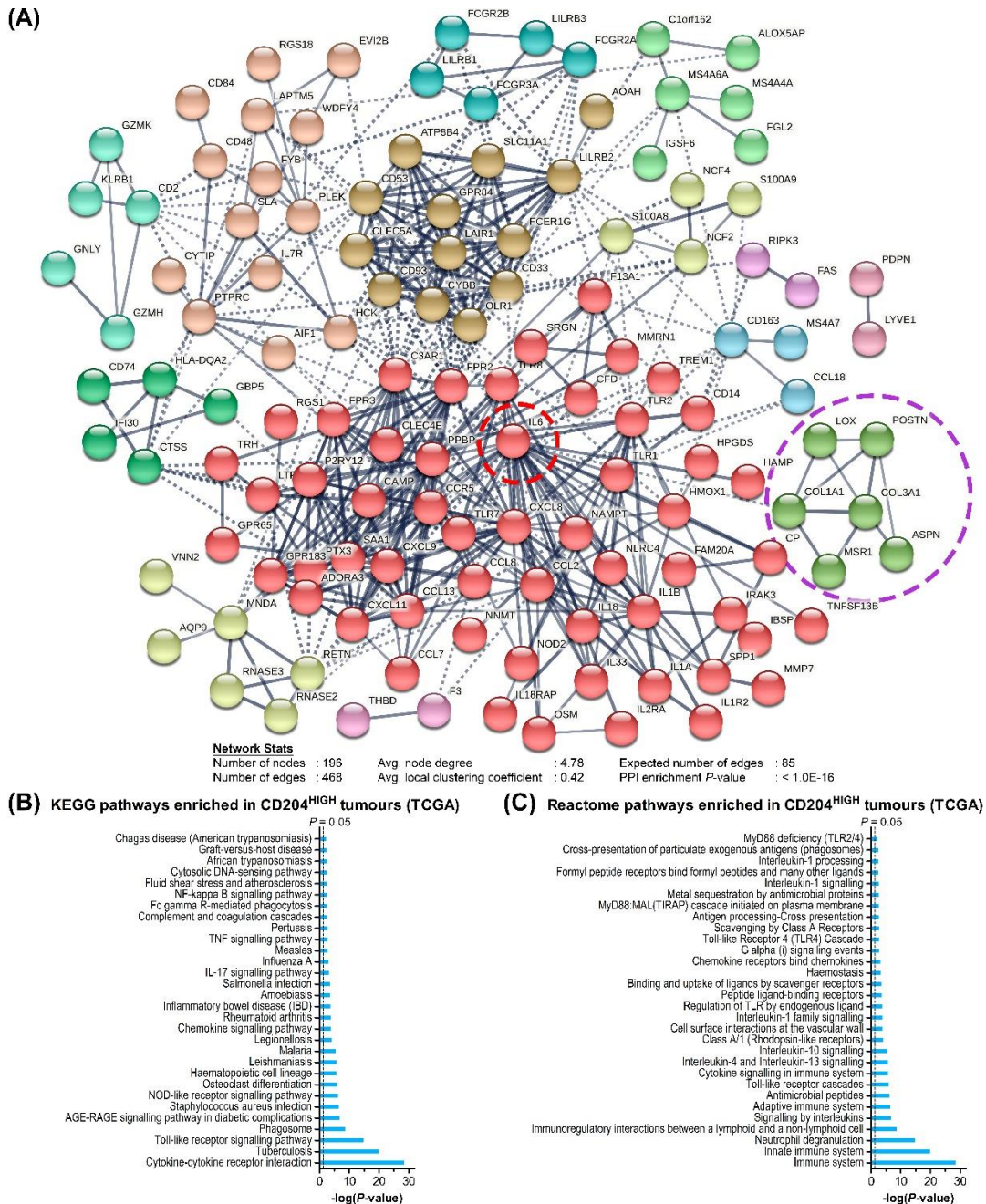


FIGURE S5. STRING connectivity network and enrichment analysis of the TCGA dataset. **(A)** Of the 17,811 genes, 200 were differentially upregulated in the group of glioblastomas with highest *CD204* mRNA level ($n=120$) relative to the group with the lowest level ($n=123$) (\log_2 fold-change ≥ 1.50 , adj. $P < 0.05$), and 196 of the 200 genes were available for analysis in STRING. The genes formed a network that clustered into one major cluster, with *IL6* in a central position in the network (red circle, # node connections: 35), and eight minor clusters; one of which included *CD204* [*MSR1*] (purple circle). **(B, C)** KEGG and Reactome analyses showed enrichment of pathways involved in e.g. the immune system and phagosome as well as TLR, NOD-like, TNF, IL17, IL4, IL13, and overall cytokine signalling. *Line annotations:* thick = highest edge confidence (0.90), thin = high edge confidence (0.70); dotted = intercluster connections

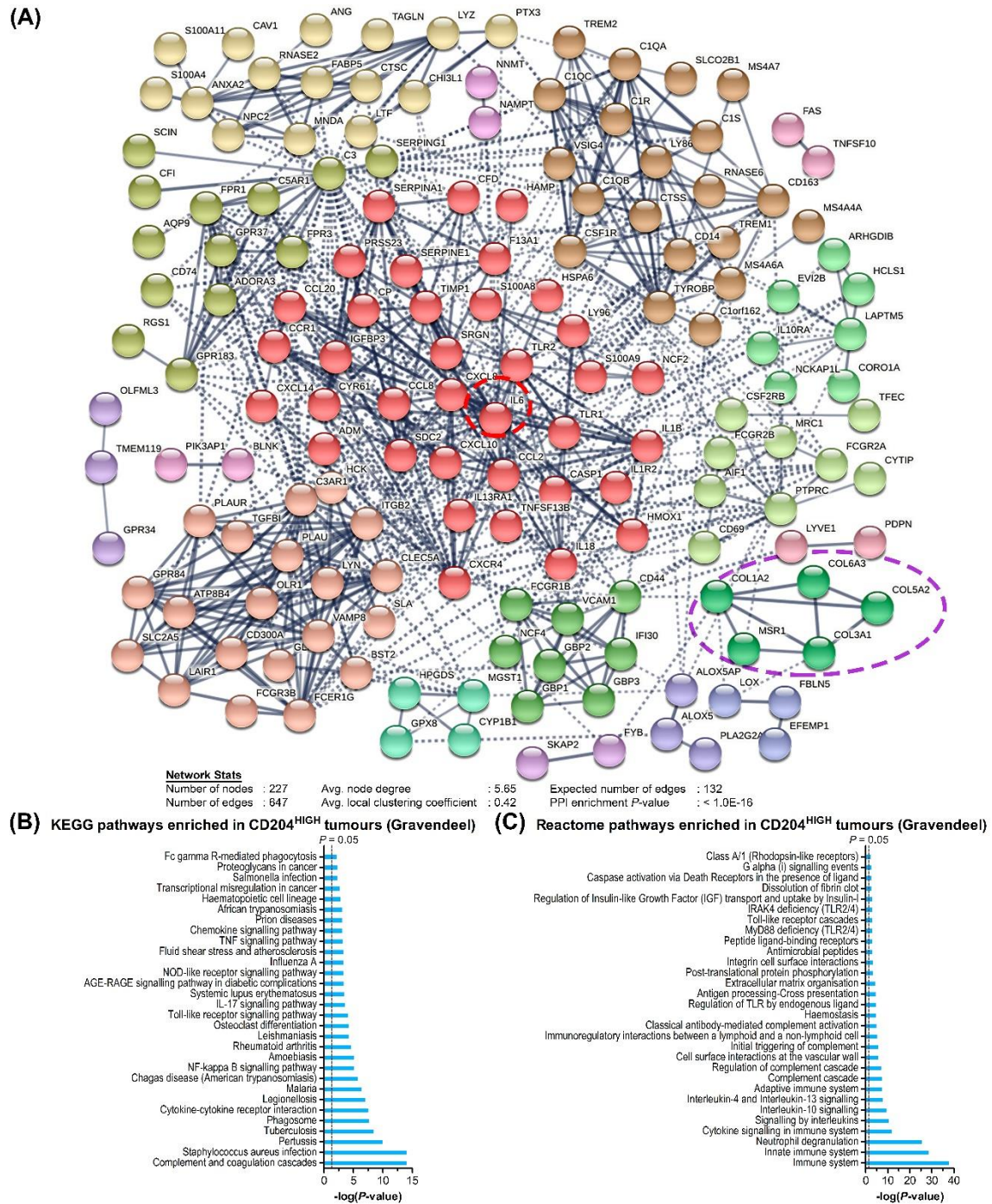


FIGURE S6. STRING connectivity network and enrichment analysis of the Gravendeel dataset. **(A)** Of the 19,944 genes, 236 were differentially upregulated in the group of glioblastomas with highest CD204 mRNA level ($n=37$) relative to the group with the lowest level ($n=40$) (\log_2 fold-change ≥ 1.50 , adj. $P < 0.05$), and 227 of the 236 genes were available for analysis in STRING. The genes formed a network that clustered into five major clusters, one of which had *IL6* in a central position (*red circle*, # node connections: 35), and four minor clusters; one of which included *CD204* [*MSR1*] (*purple circle*). **(B, C)** KEGG and Reactome analyses showed enrichment of pathways involved in e.g. the immune system and phagosome as well as TLR, NOD-like, TNF, IL17, IL4, IL13, and overall cytokine signalling. *Line annotations*: thick = highest edge confidence (0.90), thin = high edge confidence (0.70); dotted = intercluster connections

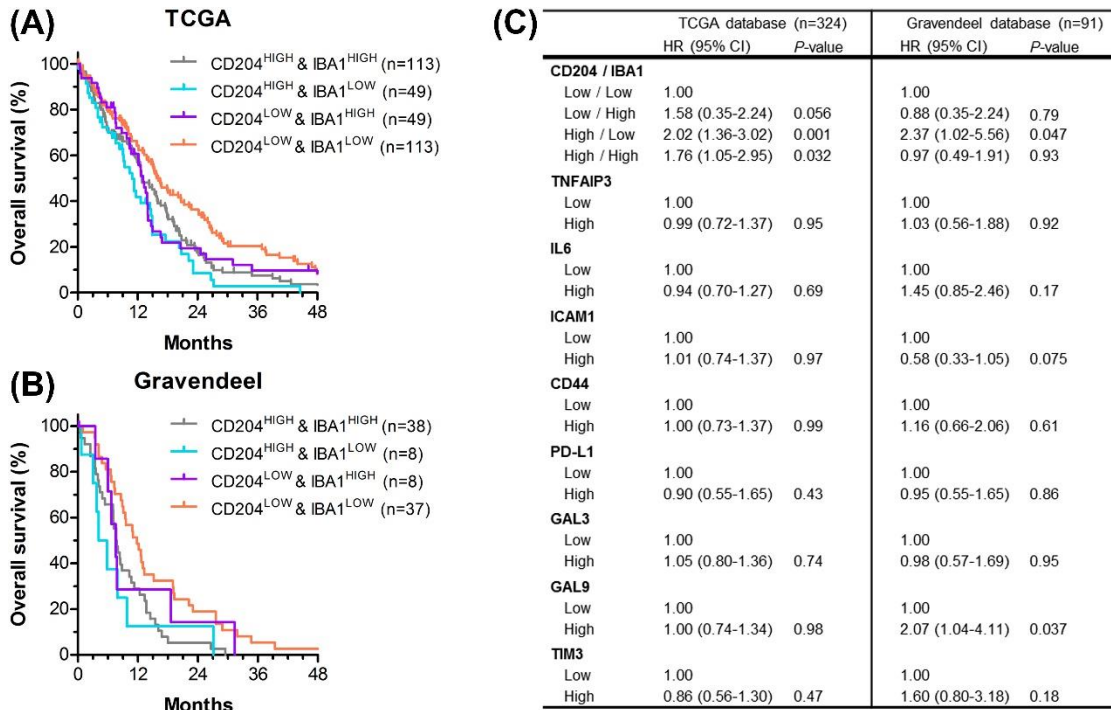


FIGURE S7. *In silico* databases. **(A, B)** Two bioinformatics databases were used to validate the prognostic impact of CD204. **(C)** CD204 remained the most important prognosticator in multivariate analysis when accounting for mRNA expressions of genes selected from the gene profile.

TUMOUR-ASSOCIATED CD204+ MICROGLIA/MACROPHAGES ACCUMULATE IN PERIVASCULAR AND PERINECROTIC NICHES AND CORRELATE WITH AN INTERLEUKIN-6 ENRICHED INFLAMMATORY PROFILE IN GLIOBLASTOMA

M. D. Sørensen^{1,2}, B. W. Kristensen¹⁻⁴

¹ Department of Pathology, Odense University Hospital, Odense, Denmark

² Department of Clinical Research, University of Southern Denmark, Odense, Denmark

³ Department of Pathology, Rigshospitalet, Copenhagen University Hospital, Copenhagen, Denmark

⁴ Department of Clinical Medicine and Biotech Research and Innovation Center (BRIC), University of Copenhagen, Copenhagen, Denmark.

Supplementary tables

Tables S1-S17

TABLE S1. Antibodies and protocols used for conventional immunohistochemistry

Antigen	Vendor	Clone / catalog no.	Species, clonality	Retrieval	Dilution and incubation	Detection system and platform
BIRC3	Sigma-Aldrich	HPA002317	Rb, pAb	CC1, 32 min 100 °C	1:200 32 min / 36 °C	OV-HRP-DAB DISCOVERY ULTRA
CD44	Dako	DF1485	Ms, mAb	CC1, 32 min 100 °C	1:200 32 min / 36 °C	OV-HRP-DAB DISCOVERY ULTRA
CD204	Cosmo Bio Co. LTD	SRA-E5	Ms, mAb	CC1, 32 min 100 °C	1:600 32 min / 36 °C	OV-HRP-DAB DISCOVERY ULTRA
GAL3	Santa Cruz Biotechnology, Inc	B2C10	Ms, mAb	CC1, 32 min 100 °C	1:100 32 min / 36 °C	OV-HRP-DAB DISCOVERY ULTRA
IBA1	Wako Pure Chemical Ind., Ltd.	019-19741	Rb, pAb	CC1, 32 min 100 °C	1:2000 16 min / 36 °C	OV-HRP-DAB DISCOVERY ULTRA
ICAM1	Abcam	EP1442Y	Rb, mAb	CC1, 48 min 100 °C	1:100 32 min / 36 °C	OV-HRP-DAB DISCOVERY ULTRA
IL6	Abcam	ab9324	Ms, mAb	TEG, 15 min MWO	1:1600 60 min / RT	EnV FLEX+-HRP-DAB Autostainer Link 48
NOD2	Sigma-Aldrich	HPA041965	Rb , pAb	TEG, 15 min MWO	1:100 60 min / RT	EnV FLEX+-HRP-DAB Autostainer Link 48
PD-L1	Abcam	EPR19759	Rb, mAb	TEG, 15 min MWO	1:500 60 min / RT	EnV FLEX+-HRP-DAB Autostainer Link 48
TNFAIP3	Abcam	EPR2663	Rb, mAb	Protease-3, 4 min + CC1, 32 min 100 °C	1:100 24 min / 36 °C	OV-HRP-DAB DISCOVERY ULTRA

Abbreviations: *BIRC3*, baculoviral IAP Repeat Containing 3; *CC1*, cell conditioning 1; *CD*, cluster of differentiation; *DAB*, 3,3' diaminobenzidine; *EnV*, EnVision; *GAL3*, galectin-3; *HRP*, horseradish peroxidase; *IBA1*, ionized calcium-binding adaptor molecule 1; *ICAM1*, intercellular adhesion molecule 1; *IL6*, interleukin-6; *mAb*, monoclonal antibody; *Ms*, mouse; *MWO*, microwave oven; *NOD2*, nucleotide-binding oligomerisation domain-containing protein 2; *OV*, OptiView; *pAb*, polyclonal antibody; *PD-L1*, programmed death-ligand 1; *Rb*, rabbit; *RT*, room temperature; *TEG*, 10 mmol/L Tris-base and 0.5 mmol/L ethylene glycol tetraacetic acid (EGTA), pH 9; *TNFAIP3*, tumour necrosis factor, alpha-induced protein 3

TABLE S2. Antibodies and protocols used for double immunohistochemistry

Antigen	Vendor	Clone / catalog no.	Species, clonality	Retrieval	Dilution and incubation	Detection system and platform
BMI1	Merck Millipore	F6	Ms, mAb	CC1std, 64 min 99 °C	1+100 32 min / 36 °C	UV-HRP-DAB +AMP BenchMark ULTRA
CD44	Dako	DF1485	Ms, mAb	CC1std, 64 min 99 °C	1:25 20 min / 36 °C	UV-HRP-DAB BenchMark ULTRA
CD133	Miltenyi Biotec	W6B3C1	Ms, mAb	TEG, 15 min MWO	1+40 60 min / RT	CSA II-HRP-DAB Autostainer Plus
CD204	Cosmo Bio Co. LTD	SRA-E5	Ms, mAb	CC1std, 64 min 99 °C	1+400 32 min / 36 °C	UV-AP-RED +AMP BenchMark ULTRA
GAL9	Cell signaling technology	D9R4A	Rb, mAb	CC1, 32 min 100 °C	1:100 32 min / 36 °C	DISCO-NP-AP-Yellow DISCOVERY ULTRA
IBA1	Wako Pure Chemical Ind., Ltd.	019-19741	Rb, pAb	CC1std, 64 min 99 °C	1+2000 32 min / 36 °C	UV-AP-RED +AMP BenchMark ULTRA
MSI1	MBL International Corporation	14H1	Ms, mAb	TEG, 15 min MWO	1+400 60 min / RT	EnV+-HRP-DAB Autostainer Plus
Nestin	R&D systems	196908	Ms, mAb	CC1std, 64 min 99 °C	1+1000 32 min / 36 °C	UV-HRP-DAB BenchMark ULTRA
PDPN	Ventana Medical Systems	D2-40	Ms, mAb	CC1std, 64 min 99 °C	RTU 32 min / 36 °C	UV-HRP-DAB BenchMark ULTRA
SOX2	R&D systems	245610	Ms, mAb	CC1std, 64 min 99 °C	1+200 32 min / 36 °C	UV-HRP-DAB +AMP BenchMark ULTRA
TIM3	Cell signaling technology	D5D5R	Rb, mAb	CC1, 32 min 100 °C	1:25 60 min / 36 °C	DISCO-HQ-HRP-Purple DISCOVERY ULTRA

Abbreviations: AMP, amplification; AP, alkaline phosphatase; BMI1, polycomb complex protein BMI1; CC1std, cell conditioning 1 standard; CD, cluster of differentiation; CSA, catalysed signal amplification; DAB, 3,3' diaminobenzidine; EnV, EnVision; GAL9, galectin-9; HRP, horseradish peroxidase; IBA1, ionized calcium-binding adaptor molecule 1; mAb, monoclonal antibody; Ms, mouse; MSI1, musashi-1; MWO, microwave oven; pAb, polyclonal antibody; PDPN, podoplanin; Rb, rabbit; RT, room temperature; SOX2, (sex determining region Y)-box 2; TEG, 10 mmol/L Tris-base and 0.5 mmol/L ethylene glycol tetraacetic acid (EGTA), pH 9; TIM3, T-cell immunoglobulin and mucin-domain containing-3; UV, UltraView

TABLE S3. KEGG pathway analysis of differentially expressed genes

ID	KEGG pathway description
hsa04060	Cytokine-cytokine receptor interaction
hsa05152	Tuberculosis
hsa05164	Influenza A
hsa05323	Rheumatoid arthritis
hsa04145	Phagosome
hsa04380	Osteoclast differentiation
hsa04668	TNF signalling pathway
hsa04620	Toll-like receptor signalling pathway
hsa05166	HTLV-I infection
hsa05168	Herpes simplex infection
hsa04062	Chemokine signalling pathway
hsa05140	Leishmaniasis
hsa05142	Chagas disease (American trypanosomiasis)
hsa04640	Hematopoietic cell lineage
hsa04514	Cell adhesion molecules (CAMs)
hsa05145	Toxoplasmosis
hsa05202	Transcriptional misregulation in cancer
hsa05321	Inflammatory bowel disease (IBD)
hsa05200	Pathways in cancer
hsa04151	PI3K-Akt signalling pathway
hsa05133	Pertussis
hsa04064	NF-kappa B signalling pathway
hsa04630	Jak-STAT signalling pathway
hsa05161	Hepatitis B
hsa05205	Proteoglycans in cancer
hsa05169	Epstein-Barr virus infection
hsa05162	Measles
hsa04933	AGE-RAGE signalling pathway in diabetic complications
hsa04015	Rap1 signalling pathway
hsa04010	MAPK signalling pathway

TABLE S4. Top-50 highest differentially upregulated genes compared to CD204^{LOW} & IBA1^{LOW} glioblastomas

CD204 ^{HIGH} & IBA1 ^{HIGH} vs. CD204 ^{LOW} & IBA1 ^{LOW}			CD204 ^{HIGH} & IBA1 ^{LOW} vs. CD204 ^{LOW} & IBA1 ^{LOW}			CD204 ^{LOW} & IBA1 ^{HIGH} vs. CD204 ^{LOW} & IBA1 ^{LOW}		
Gene	Log2 FC	Adj. P-value	Gene	Log2 FC	Adj. P-value	Gene	Log2 FC	Adj. P-value
<i>CCL20</i>	3.82	5.18E-04	<i>CCL20</i>	4.48	1.80E-04	<i>S100A8</i>	2.59	2.55E-04
<i>IL6</i>	3.46	5.75E-05	<i>IL6</i>	3.43	2.20E-04	<i>S100A9</i>	2.57	1.49E-04
<i>CXCL14</i>	3.36	2.62E-05	<i>CXCL8</i>	3.40	6.06E-04	<i>JAML</i>	2.51	6.95E-04
<i>OSM</i>	3.33	4.52E-06	<i>PTGDS</i>	3.29	2.11E-04	<i>IL1R2</i>	2.43	9.77E-03
<i>S100A9</i>	3.23	2.91E-07	<i>IL1R2</i>	3.22	2.86E-04	<i>SELL</i>	2.31	9.56E-04
<i>FCGR2B</i>	3.19	2.21E-08	<i>ICAM1</i>	3.02	4.47E-05	<i>CCL3L1</i>	2.26	8.41E-03
<i>MRC1</i>	3.19	2.25E-05	<i>BIRC3</i>	2.88	3.70E-04	<i>TREM1</i>	2.16	1.98E-03
<i>RNASE2</i>	3.13	4.37E-06	<i>MRC1</i>	2.82	4.91E-04	<i>NKG7</i>	2.15	7.32E-03
<i>S100A8</i>	3.12	1.79E-06	<i>TREM1</i>	2.80	6.24E-05	<i>OSM</i>	2.11	1.04E-02
<i>SELL</i>	3.04	2.55E-06	<i>PTX3</i>	2.77	6.87E-04	<i>RNASE2</i>	2.11	5.16E-03
<i>LIF</i>	3.00	3.74E-04	<i>S100A9</i>	2.74	5.48E-05	<i>CCL3</i>	2.09	1.57E-02
<i>CD163</i>	2.98	3.81E-10	<i>FCGR2B</i>	2.55	2.24E-05	<i>FPR2</i>	2.08	3.41E-03
<i>CD14</i>	2.97	4.65E-10	<i>S100A8</i>	2.55	2.19E-04	<i>TNF</i>	2.08	4.67E-03
<i>SCIN</i>	2.96	9.69E-07	<i>CD274</i>	2.51	4.41E-03	<i>CD69</i>	2.07	8.83E-03
<i>HLA-DQB1</i>	2.91	1.01E-02	<i>CCL5</i>	2.41	4.00E-04	<i>MAFF</i>	2.06	2.96E-03
<i>PDPN</i>	2.91	1.04E-04	<i>CD163</i>	2.33	1.12E-06	<i>CCL4</i>	2.04	1.47E-02
<i>ADAM8</i>	2.84	8.10E-05	<i>CHI3L1</i>	2.31	2.62E-03	<i>FCGR2B</i>	2.04	5.06E-04
<i>STAB1</i>	2.84	3.81E-10	<i>CXCL3</i>	2.28	4.00E-02	<i>CD163</i>	2.03	2.25E-05
<i>FPR3</i>	2.82	1.76E-08	<i>FPR2</i>	2.28	7.61E-04	<i>CSF3R</i>	2.00	2.97E-05
<i>NKG7</i>	2.76	8.45E-05	<i>LIF</i>	2.26	2.01E-02	<i>CCL5</i>	1.99	4.96E-03
<i>CD274</i>	2.73	7.15E-04	<i>IL1R1</i>	2.24	7.87E-04	<i>MRC1</i>	1.98	2.93E-02
<i>SIGLEC1</i>	2.72	6.51E-05	<i>CCL2</i>	2.22	4.38E-03	<i>IL1B</i>	1.92	7.33E-04
<i>VAV1</i>	2.71	4.91E-06	<i>IL1B</i>	2.21	8.60E-05	<i>SCIN</i>	1.90	4.03E-03
<i>TREM1</i>	2.69	2.05E-05	<i>PTGS2</i>	2.20	2.69E-02	<i>IL10RA</i>	1.87	2.97E-05
<i>CIQA</i>	2.68	3.11E-09	<i>MMP19</i>	2.19	5.59E-03	<i>CD14</i>	1.85	6.73E-05
<i>PTX3</i>	2.59	6.24E-04	<i>OSM</i>	2.19	5.48E-03	<i>STAB1</i>	1.81	4.04E-05
<i>IL1R2</i>	2.57	1.97E-03	<i>CXCL14</i>	2.17	1.74E-02	<i>FPR1</i>	1.77	1.14E-03
<i>FPR1</i>	2.55	5.76E-07	<i>SELL</i>	2.14	1.68E-03	<i>ITGAM</i>	1.77	7.80E-05
<i>GPR65</i>	2.55	8.30E-08	<i>MAPK13</i>	2.10	1.21E-05	<i>CIQA</i>	1.74	1.32E-04
<i>CIQB</i>	2.54	8.60E-09	<i>STAB1</i>	2.10	3.09E-06	<i>ALOX5</i>	1.73	2.97E-05
<i>FCGR1A</i>	2.54	5.45E-09	<i>ADAM8</i>	2.09	9.72E-03	<i>VAV1</i>	1.70	1.16E-02
<i>ALOX5</i>	2.53	5.86E-10	<i>CXCL1</i>	2.07	4.11E-02	<i>IKZF1</i>	1.69	5.20E-05
<i>IL10RA</i>	2.52	2.80E-09	<i>DPP4</i>	2.04	1.06E-02	<i>IL15</i>	1.69	1.70E-02
<i>CCL2</i>	2.49	4.41E-04	<i>NOD2</i>	2.02	1.20E-05	<i>JAK3</i>	1.69	7.82E-04
<i>CSF3R</i>	2.49	1.79E-08	<i>NAMPT</i>	2.01	1.52E-04	<i>CLEC7A</i>	1.67	4.11E-05
<i>LAPTM5</i>	2.49	4.08E-10	<i>CD14</i>	1.98	2.24E-05	<i>AIF1</i>	1.66	4.11E-05
<i>PLAUR</i>	2.49	3.81E-08	<i>VCAM1</i>	1.98	2.62E-03	<i>C3</i>	1.65	2.27E-03
<i>MAPK13</i>	2.48	3.09E-08	<i>FCGR2A</i>	1.97	3.09E-06	<i>HLA-DRB3</i>	1.64	7.38E-04
<i>TNF</i>	2.48	1.37E-04	<i>IL4I1</i>	1.96	1.44E-04	<i>PTPRC</i>	1.64	8.44E-03
<i>ITGAM</i>	2.47	1.05E-08	<i>ALOX5</i>	1.92	3.09E-06	<i>TLR2</i>	1.64	1.69E-06
<i>CHI3L1</i>	2.45	5.11E-04	<i>ALOX5AP</i>	1.92	1.21E-05	<i>TLR6</i>	1.64	1.91E-05
<i>TLR7</i>	2.45	5.53E-04	<i>NCF2</i>	1.92	9.07E-06	<i>CIQB</i>	1.63	2.54E-04
<i>CIQC</i>	2.44	5.79E-09	<i>ALDH1A1</i>	1.89	5.44E-03	<i>OLRI</i>	1.63	4.47E-04
<i>AIF1</i>	2.43	1.42E-09	<i>FBP1</i>	1.89	7.70E-05	<i>PTGS1</i>	1.63	3.31E-03
<i>DPP4</i>	2.43	6.02E-04	<i>MX2</i>	1.88	1.31E-03	<i>CYTIP</i>	1.62	5.24E-04
<i>ITGB2</i>	2.43	3.81E-10	<i>THBD</i>	1.87	5.20E-04	<i>FCGR3A</i>	1.60	2.72E-04
<i>CD68</i>	2.42	8.80E-09	<i>DDR2</i>	1.84	6.41E-05	<i>FCGR1A</i>	1.59	2.82E-04
<i>CYBB</i>	2.42	2.76E-09	<i>PLAUR</i>	1.84	7.70E-05	<i>ITGB2</i>	1.59	2.97E-05
<i>FPR2</i>	2.40	1.49E-04	<i>CSAR1</i>	1.81	5.48E-05	<i>CD74</i>	1.58	1.58E-04
<i>IL1B</i>	2.39	4.77E-06	<i>FPR1</i>	1.81	6.61E-04	<i>FBP1</i>	1.58	1.10E-03

TABLE S5. List of differentially expressed genes related to glioblastoma and cancer stemness

	CD204 ^{HIGH} & IBA1 ^{HIGH} vs. CD204 ^{LOW} & IBA1 ^{LOW}		CD204 ^{HIGH} & IBA1 ^{LOW} vs. CD204 ^{LOW} & IBA1 ^{LOW}		CD204 ^{LOW} & IBA1 ^{HIGH} vs. CD204 ^{LOW} & IBA1 ^{LOW}	
	Log2 FC	Adj. <i>P</i> -value	Log2 FC	Adj. <i>P</i> -value	Log2 FC	Adj. <i>P</i> -value
Glioblastoma-related genes						
<i>GFAP</i>	0.07	1.00E+00	0.53	1.00E+00	0.53	1.00E+00
<i>MGMT</i>	1.19	3.61E-02	0.49	1.00E+00	0.53	1.00E+00
<i>MKI67</i>	-0.39	5.80E-01	-0.76	1.60E-02	-0.76	1.94E-02
<i>OLIG2</i>	-1.31	5.33E-02	-1.19	1.51E-01	-0.41	1.00E+00
<i>TP53</i>	-0.51	3.73E-02	-0.51	6.02E-02	-0.26	1.00E+00
Cancer stemness-related genes						
<i>ALDH1A1</i>	1.87	2.93E-03	1.89	5.44E-03	1.11	3.39E-01
<i>BMI1</i>	-0.11	1.00E+00	-0.07	1.00E+00	0.09	1.00E+00
<i>CD36</i>	1.12	1.39E-01	0.72	1.00E+00	1.07	2.90E-01
<i>CD44</i>	1.42	3.75E-04	1.73	7.70E-05	1.10	1.92E-02
<i>MET</i>	-0.09	1.00E+00	0.97	1.00E+00	-1.48	9.67E-01
<i>EGFR</i>	-0.32	1.00E+00	-2.12	1.51E-01	-0.79	1.00E+00
<i>ID1</i>	1.03	2.03E-01	0.61	1.00E+00	0.49	1.00E+00
<i>ITGA6</i>	0.04	1.00E+00	-0.56	7.31E-01	-0.03	1.00E+00
<i>MSI1</i>	-0.04	1.00E+00	0.09	1.00E+00	-0.06	1.00E+00
<i>MYC</i>	0.36	1.00E+00	0.69	4.64E-01	0.00	1.00E+00
<i>NANOG</i>	0.01	1.00E+00	-0.01	1.00E+00	0.46	4.63E-01
<i>POU5F1 (OCT4)</i>	0.35	1.00E+00	0.31	1.00E+00	0.49	5.27E-01
<i>PDPN</i>	2.91	1.04E-04	0.88	1.00E+00	0.24	1.00E+00
<i>PROM1 (CD133)</i>	-1.08	3.72E-01	-0.34	1.00E+00	-0.22	1.00E+00
<i>SOX2</i>	-0.26	1.00E+00	0.04	1.00E+00	-0.14	1.00E+00

Significantly differentially expressed genes with a log2 fold-change ≥ 1.50 are indicated with **bold**.

TABLE S6. List of 22 genes differentially upregulated in only IBA1^{HIGH} tumours

Gene	CD204 ^{HIGH} & IBA1 ^{HIGH} vs. CD204 ^{LOW} & IBA1 ^{LOW}		CD204 ^{LOW} & IBA1 ^{HIGH} vs. CD204 ^{LOW} & IBA1 ^{LOW}	
	Log2 FC	Adj. <i>P</i> -value	Log2 FC	Adj. <i>P</i> -value
<i>CIQB</i>	2.54	8.60E-09	1.63	2.54E-04
<i>CIQC</i>	2.44	5.79E-09	1.51	2.99E-04
<i>C3</i>	1.97	5.18E-05	1.65	2.27E-03
<i>C3ARI</i>	2.12	1.79E-08	1.50	1.38E-04
<i>CCL3</i>	2.38	1.51E-03	2.09	1.57E-02
<i>CCL3L1</i>	2.29	2.80E-03	2.26	8.41E-03
<i>CCL4</i>	2.15	3.45E-03	2.04	1.47E-02
<i>CD69</i>	2.29	9.25E-04	2.07	8.83E-03
<i>CD74</i>	1.87	1.18E-06	1.58	1.58E-04
<i>FCGR1A</i>	2.54	5.45E-09	1.59	2.82E-04
<i>HLA-DRB3</i>	1.95	1.30E-05	1.64	7.38E-04
<i>IKZF1</i>	2.28	1.11E-08	1.69	5.20E-05
<i>ITGB2</i>	2.43	3.81E-10	1.59	2.97E-05
<i>JAML</i>	2.00	3.47E-03	2.51	6.95E-04
<i>LAPTM5</i>	2.49	4.08E-10	1.52	6.73E-05
<i>MAFF*</i>	-	-	2.06	2.96E-03
<i>NKG7</i>	2.76	8.45E-05	2.15	7.32E-03
<i>OLR1</i>	1.99	3.45E-06	1.63	4.47E-04
<i>PTGS1</i>	1.54	2.02E-03	1.63	3.31E-03
<i>PTPRC</i>	2.37	1.65E-05	1.64	8.44E-03
<i>TLR6</i>	2.05	3.11E-09	1.64	1.91E-05
<i>TNF</i>	2.48	1.37E-04	2.08	4.67E-03

* *MAFF* was only differentially expressed gene with ≥ 1.50 log2 fold-change in the CD204^{LOW} / IBA1^{HIGH} group

TABLE S7. List of the 36 genes differentially upregulated in CD204^{HIGH} and/or IBA1^{HIGH} tumours

	CD204 ^{HIGH} & IBA1 ^{HIGH} vs. CD204 ^{LOW} & IBA1 ^{LOW}		CD204 ^{HIGH} & IBA1 ^{LOW} vs. CD204 ^{LOW} & IBA1 ^{LOW}		CD204 ^{LOW} & IBA1 ^{HIGH} vs. CD204 ^{LOW} & IBA1 ^{LOW}	
	Log2 FC	Adj. <i>P</i> -value	Log2 FC	Adj. <i>P</i> -value	Log2 FC	Adj. <i>P</i> -value
<i>AIF1</i>	2.43	1.42E-09	1.53	7.70E-05	1.66	4.11E-05
<i>ALOX5</i>	2.53	5.86E-10	1.92	3.09E-06	1.73	2.97E-05
<i>CIQA</i>	2.68	3.11E-09	1.98	2.24E-05	1.74	1.32E-04
<i>CCL5</i>	1.98	1.92E-03	1.61	2.28E-04	1.99	4.96E-03
<i>CCR1</i>	2.29	8.07E-07	2.41	4.00E-04	1.51	2.66E-03
<i>CD14</i>	2.97	4.65E-10	1.54	1.42E-03	1.85	6.73E-05
<i>CD163</i>	2.98	3.81E-10	2.33	1.12E-06	2.03	2.25E-05
<i>CD68</i>	2.42	8.80E-09	1.53	2.20E-04	1.50	3.77E-04
<i>CLEC7A</i>	2.19	1.26E-08	1.56	7.60E-05	1.67	4.11E-05
<i>CSF3R</i>	2.49	1.79E-08	1.66	2.01E-04	2.00	2.97E-05
<i>CYTIP</i>	1.74	4.14E-05	1.56	6.24E-04	1.62	5.24E-04
<i>FBP1</i>	2.28	4.70E-07	1.89	7.70E-05	1.58	1.10E-03
<i>FCGR2A</i>	2.26	9.51E-09	1.97	3.09E-06	1.51	1.62E-04
<i>FCGR2B</i>	3.19	2.21E-08	2.55	2.24E-05	2.04	5.06E-04
<i>FCGR3A</i>	2.37	2.22E-08	1.68	9.93E-05	1.60	2.72E-04
<i>FPR1</i>	2.55	5.76E-07	1.81	6.61E-04	1.77	1.14E-03
<i>FPR2</i>	2.40	1.49E-04	2.28	7.61E-04	2.08	3.41E-03
<i>FPR3</i>	2.82	1.76E-08	1.75	4.91E-04	1.58	2.24E-03
<i>IL10RA</i>	2.52	2.80E-09	1.60	1.00E-04	1.87	2.97E-05
<i>IL15</i>	2.36	8.38E-05	1.55	2.88E-02	1.69	1.70E-02
<i>IL1B</i>	2.39	4.77E-06	2.21	8.60E-05	1.92	7.33E-04
<i>IL1R2</i>	2.57	1.97E-03	3.22	2.86E-04	2.43	9.77E-03
<i>ITGAM</i>	2.47	1.05E-08	1.77	6.24E-05	1.77	7.80E-05
<i>JAK3</i>	2.36	6.42E-07	1.57	1.36E-03	1.69	7.82E-04
<i>MRC1</i>	3.19	2.25E-05	2.82	4.91E-04	1.98	2.93E-02
<i>OSM</i>	3.33	4.52E-06	2.19	5.48E-03	2.11	1.04E-02
<i>RNASE2</i>	3.13	4.37E-06	1.71	3.14E-02	2.11	5.16E-03
<i>SI00A8</i>	3.12	1.79E-06	2.55	2.19E-04	2.59	2.55E-04
<i>SI00A9</i>	3.23	2.91E-07	2.74	5.48E-05	2.57	1.49E-04
<i>SCIN</i>	2.96	9.69E-07	1.62	1.60E-02	1.90	4.03E-03
<i>SELL</i>	3.04	2.55E-06	2.14	1.68E-03	2.31	9.56E-04
<i>STAB1</i>	2.84	3.81E-10	2.10	3.09E-06	1.81	4.04E-05
<i>THBD</i>	2.34	3.91E-06	1.87	5.20E-04	1.54	6.69E-03
<i>TLR2</i>	2.23	1.13E-10	1.71	5.60E-07	1.64	1.69E-06
<i>TREM1</i>	2.69	2.05E-05	2.80	6.24E-05	2.16	1.98E-03
<i>VAV1</i>	2.71	4.91E-06	1.59	1.84E-02	1.70	1.16E-02

TABLE S8. List of KEGG pathways significantly enriched in CD204^{HIGH} tumours relative to CD204^{LOW} & IBA1^{LOW} tumours

ID	KEGG Term description	Observed Gene count	Background gene count	FDR	Matching genes in the network
hsa05323	Rheumatoid arthritis	18	84	1.49E-19	CCL2, CCL20, CD80, CD86, CSF1, CTSL, CXCL1, CXCL2, CXCL8, HLA-DMA, HLA-DMB, HLA-DPBI, HLA-DRA, ICAMI, IL18, IL6, ITGAL, TNFRSF11A
hsa04060	Cytokine-cytokine receptor interaction	24	263	6.69E-19	CCL2, CCL20, CSF1, CSF1R, CSF2RA, CX3CR1, CXCL1, CXCL2, CXCL14, CXCL2, CXCL3, CXCL8, FAS, IL17RA, IL18, IL4R, IL6, IL6R, LIF, TNFRSF11A, TNFRSF14, TNFRSF1B, TNFSF10
hsa04668	TNF signalling pathway	18	108	2.73E-18	BIRC3, CCL2, CCL20, CEBPB, CSF1, CXCL1, CXCL2, CXCL3, FAS, ICAMI, IL6, LIF, MAPK13, NOD2, PTGS2, TNFAIP3, TNFRSF1B, VCAMI
hsa04621	NOD-like receptor signalling pathway	16	166	7.05E-13	BIRC3, CASP1, CCL2, CXCL1, CXCL2, CXCL3, CXCL8, CYBB, IL18, IL6, MAPK13, NAMPT, NLRP3, NOD2, PYCARD, TNFAIP3
hsa05164	Influenza A	16	168	7.05E-13	CASP1, CCL2, CXCL8, FAS, HLA-DMA, HLA-DMB, HLA-DPBI, HLA-DRA, ICAMI, IL18, IL6, MAPK13, NLRP3, PYCARD, TLR7, TNFSF10
hsa04064	NF-kappa B signalling pathway	13	93	1.76E-12	BIRC3, BTK, CXCL12, CXCL2, CXCL8, ICAMI, IL1R1, PLAU, PTGS2, SYK, TNFAIP3, TNFRSF11A, VCAMI
hsa04657	IL-17 signalling pathway	13	92	1.76E-12	CCL2, CCL20, CEBPB, CXCL1, CXCL2, CXCL3, CXCL8, FOSL1, IL17RA, IL6, MAPK13, PTGS2, TNFAIP3
hsa05321	Inflammatory bowel disease (IBD)	11	62	1.31E-11	GATA3, HLA-DMA, HLA-DMB, HLA-DPBI, HLA-DRA, IL18, IL4R, IL6, NOD2, STAT6, TLR5
hsa04640	Haematopoietic cell lineage	12	94	3.36E-11	CD44, CSF1, CSF1R, CSF2RA, HLA-DMA, HLA-DMB, HLA-DPBI, HLA-DRA, IL1R1, IL4R, IL6, IL6R
hsa04380	Osteoclast differentiation	13	124	3.45E-11	BTK, CSF1, CSF1R, FOSL1, IL1R1, MAPK13, NCF2, OSCAR, SQSTM1, SYK, TNFRSF11A, TREM2, TYROBP
hsa05152	Tuberculosis	14	172	1.03E-10	CEBPB, CTSD, CTSS, HLA-DMA, HLA-DMB, HLA-DPBI, HLA-DRA, IL18, IL6, ITGAX, MAPK13, NOD2, SYK, TLR1
hsa05132	Salmonella infection	11	84	1.71E-10	CASP1, CXCL1, CXCL2, CXCL3, CXCL8, IL18, IL6, MAPK13, PYCARD, TLR5, WAS
hsa04659	Th17 cell differentiation	11	102	1.08E-09	GATA3, HLA-DMA, HLA-DMB, HLA-DPBI, HLA-DRA, IL1R1, IL4R, IL6, IL6R, MAPK13, STAT6
hsa05134	Legionellosis	9	54	1.67E-09	CASP1, CXCL1, CXCL2, CXCL3, CXCL8, IL18, IL6, PYCARD, TLR5
hsa05332	Graft-versus-host disease	8	36	2.27E-09	CD80, CD86, FAS, HLA-DMA, HLA-DMB, HLA-DPBI, HLA-DRA, IL6
hsa04672	Intestinal immune network for IgA production	8	44	8.68E-09	CD80, CD86, CXCL12, HLA-DMA, HLA-DMB, HLA-DPBI, HLA-DRA, IL6
hsa04514	Cell adhesion molecules (CAMs)	11	139	1.75E-08	CD274, CD80, CD86, HLA-DMA, HLA-DMB, HLA-DPBI, HLA-DRA, ICAMI, ITGAL, SIGLEC1, VCAMI
hsa05150	Staphylococcus aureus infection	8	51	2.18E-08	C5AR1, HLA-DMA, HLA-DMB, HLA-DPBI, HLA-DRA, ICAMI, ITGAL, PTAFR
hsa05167	Kaposi's sarcoma-associated herpesvirus infection	12	183	2.18E-08	CD86, CXCL1, CXCL2, CXCL3, CXCL8, FAS, ICAMI, IL6, MAPK13, PIK3CG, PTGS2, SYK
hsa05416	Viral myocarditis	8	56	3.85E-08	CD80, CD86, HLA-DMA, HLA-DMB, HLA-DPBI, HLA-DRA, ICAMI, ITGAL
hsa05330	Allograft rejection	7	35	4.37E-08	CD80, CD86, FAS, HLA-DMA, HLA-DMB, HLA-DPBI, HLA-DRA
hsa04940	Type I diabetes mellitus	7	40	9.19E-08	CD80, CD86, FAS, HLA-DMA, HLA-DMB, HLA-DPBI, HLA-DRA
hsa05202	Transcriptional misregulation in cancer	11	169	9.19E-08	BIRC3, CD86, CEBPA, CEBPB, CSF1R, CXCL8, IGFI, IL6, NFKB1Z, PLAUI, RUNX2
hsa04620	Toll-like receptor signalling pathway	9	102	1.58E-07	CD80, CD86, CXCL8, IL6, IRF5, MAPK13, TLR1, TLR5, TLR7
hsa05140	Leishmaniasis	8	70	1.58E-07	CYBB, HLA-DMA, HLA-DMB, HLA-DPBI, HLA-DRA, MAPK13, NCF2, PTGS2
hsa04145	Phagosome	10	145	2.18E-07	CTSL, CTSS, CYBB, HLA-DMA, HLA-DMB, HLA-DPBI, HLA-DRA, MSRI, NCF2, TUBA4A
hsa05133	Pertussis	8	74	2.18E-07	CASP1, CXCL8, IL6, IRF1, IRF8, MAPK13, NLRP3, PYCARD
hsa05144	Malaria	7	47	2.18E-07	CCL2, CXCL8, ICAMI, IL18, IL6, ITGAL, VCAMI
hsa05320	Autoimmune thyroid disease	7	49	2.53E-07	CD80, CD86, FAS, HLA-DMA, HLA-DMB, HLA-DPBI, HLA-DRA
hsa04217	Necroptosis	10	155	3.45E-07	BIRC3, CASP1, CYBB, FAS, NLRP3, PYCARD, SQSTM1, STAT6, TNFAIP3, TNFSF10
hsa04658	Th1 and Th2 cell differentiation	8	88	6.33E-07	GATA3, HLA-DMA, HLA-DMB, HLA-DPBI, HLA-DRA, IL4R, MAPK13, STAT6
hsa04062	Chemokine signalling pathway	10	181	1.28E-06	CCL2, CCL20, CX3CR1, CXCL1, CXCL2, CXCL14, CXCL2, CXCL3, CXCL8, WAS
hsa04933	AGE-RAGE signalling pathway in diabetic complications	8	98	1.29E-06	CCL2, CXCL8, CYBB, ICAMI, IL6, MAPK13, SERPINE1, VCAMI
hsa05166	HTLV-I infection	11	250	2.59E-06	EGR2, FOSL1, HLA-DMA, HLA-DMB, HLA-DPBI, HLA-DRA, ICAMI, IL1R1, IL6, ITGAL, VCAMI
hsa05418	Fluid shear stress and atherosclerosis	8	133	1.07E-05	CCL2, CTSL, ICAMI, IL1R1, MAPK13, NCF2, SQSTM1, VCAMI
hsa05143	African trypanosomiasis	5	34	1.65E-05	FAS, ICAMI, IL18, IL6, VCAMI
hsa04612	Antigen processing and presentation	6	66	2.15E-05	CTSL, CTSS, HLA-DMA, HLA-DMB, HLA-DPBI, HLA-DRA

hsa05145	Toxoplasmosis	7	109	2.88E-05	<i>BIRC3, HLA-DMA, HLA-DMB, HLA-DPBI, HLA-DRA, MAPK13, PIK3CG</i>
hsa04670	Leukocyte transendothelial migration	7	112	3.33E-05	<i>CXCL12, CYBB, ICAMI, ITGAL, MAPK13, NCF2, VCAMI</i>
hsa05200	Pathways in cancer	13	515	7.69E-05	<i>BIRC3, CEBPA, CSF1R, CSF2RA, CXCL12, CXCL8, FAS, IGF1, IL4R, IL6, IL6R, PTGS2, STAT6</i>
hsa05168	Herpes simplex infection	8	181	7.87E-05	<i>CC12, FAS, HLA-DMA, HLA-DMB, HLA-DPBI, HLA-DRA, IL6, TNFRSF14</i>
hsa04210	Apoptosis	7	135	9.78E-05	<i>BIRC3, CTSD, CTSL, CTSS, FAS, TNFSF10, TUBA4A</i>
hsa05169	Epstein-Barr virus infection	8	194	1.20E-04	<i>CD44, HLA-DPBI, HLA-DRA, ICAMI, ITGAL, MAPK13, SYK, TNFAIP3</i>
hsa05205	Proteoglycans in cancer	8	195	1.20E-04	<i>CD44, CTSL, FAS, HBEGF, IGF1, MAPK13, PLAU, PLAUR</i>
hsa05322	Systemic lupus erythematosus	6	94	1.20E-04	<i>CD80, CD86, HLA-DMA, HLA-DMB, HLA-DPBI, HLA-DRA</i>
hsa05310	Asthma	4	28	1.40E-04	<i>HLA-DMA, HLA-DMB, HLA-DPBI, HLA-DRA</i>
hsa05142	Chagas disease (American trypanosomiasis)	6	101	1.60E-04	<i>CCL2, CXCL8, FAS, IL6, MAPK13, SERPINE1</i>
hsa05131	Shigellosis	5	63	1.90E-04	<i>CD44, CXCL8, MAPK13, NOD2, WAS</i>
hsa04650	Natural killer cell mediated cytotoxicity	6	124	4.70E-04	<i>FAS, ICAMI, ITGAL, SYK, TNFSF10, TYROBP</i>
hsa04610	Complement and coagulation cascades	5	78	4.90E-04	<i>C5ARI, ITGAX, PLAU, PLAUR, SERPINE1</i>
hsa04066	HIF-1 signalling pathway	5	98	1.30E-03	<i>CYBB, IGF1, IL6, IL6R, SERPINE1</i>
hsa04630	Jak-STAT signalling pathway	6	160	1.60E-03	<i>CSF2RA, IL4R, IL6, IL6R, LIF, STAT6</i>
hsa04623	Cytosolic DNA-sensing pathway	4	62	2.10E-03	<i>CASPI, IL18, IL6, PYCARD</i>
hsa05120	Epithelial cell signalling in <i>Helicobacter pylori</i> infection	4	66	2.60E-03	<i>CXCL1, CXCL8, HBEGF, MAPK13</i>
hsa04664	Fe epsilon RI signalling pathway	4	67	2.70E-03	<i>ALOX5AP, BTK, MAPK13, SYK</i>
hsa04151	PI3K-Akt signalling pathway	8	348	4.30E-03	<i>CSF1, CSF1R, IGF1, IL4R, IL6, IL6R, PIK3CG, SYK</i>
hsa05162	Measles	5	133	4.40E-03	<i>FAS, IL6, TLR7, TNFAIP3, TNFSF10</i>
hsa05161	Hepatitis B	5	142	5.70E-03	<i>CXCL8, EGR2, FAS, IL6, STAT6</i>
hsa04932	Non-alcoholic fatty liver disease (NAFLD)	5	149	6.80E-03	<i>CEBPA, CXCL8, FAS, IL6, IL6R</i>
hsa04218	Cellular senescence	5	156	8.10E-03	<i>CXCL8, IL6, MAPK13, SERPINE1, SQSTM1</i>
hsa05146	Amoebiasis	4	94	8.10E-03	<i>CXCL1, CXCL8, IL1R1, IL6</i>
hsa05014	Amyotrophic lateral sclerosis (ALS)	3	50	1.07E-02	<i>CASPI, MAPK13, TNFRSF1B</i>
hsa05130	Pathogenic <i>Escherichia coli</i> infection	3	53	1.23E-02	<i>TLR5, TUBA4A, WAS</i>
hsa00590	Arachidonic acid metabolism	3	61	1.76E-02	<i>HPGDS, PTGDS, PTGS2</i>
hsa04611	Platelet activation	4	123	1.87E-02	<i>BTK, MAPK13, PIK3CG, SYK</i>
hsa04015	Rap1 signalling pathway	5	203	2.16E-02	<i>CSF1, CSF1R, IGF1, ITGAL, MAPK13</i>
hsa04068	p53 signalling pathway	4	130	2.18E-02	<i>IGF1, IL6, MAPK13, TNFSF10</i>
hsa04917	Prolactin signalling pathway	3	68	2.20E-02	<i>FAS, IGF1, SERPINE1</i>
hsa04115	MAPK signalling pathway	3	69	2.26E-02	<i>IRF1, MAPK13, TNFRSF1A</i>
hsa04010	EGFR tyrosine kinase inhibitor resistance	6	293	2.27E-02	<i>CSF1, CSF1R, FAS, IGF1, IL1R1, MAPK13</i>
hsa01521	Inflammatory mediator regulation of TRP channels	3	78	3.02E-02	<i>IGF1, IL6, IL6R</i>
hsa04750	Endocrine resistance	3	92	4.54E-02	<i>IGF1, IL1R1, MAPK13</i>
hsa01522		3	95	4.86E-02	<i>HBEGF, IGF1, MAPK13</i>

TABLE S9. List of Reactome pathways significantly enriched in CD204^{HIGH} tumours relative to CD204^{LOW} & IBA1^{LOW} tumours

ID	Reactome Term description	Observed Gene count	Background gene count	FDR	Matching genes in the network
HSA-168256	Immune System	75	1925	3.43E-42	ADAM8, BIRC3, BTK, C5AR1, CASP1, CCL2, CCL20, CD180, CD274, CD44, CD80, CD86, CH13L1, CLEC5A, CSF1, CSF1R, CSF2RA, CTSD, CTSL, CTSS, CXCL1, CXCL2, CXCL8, CYBB, GATA3, HAVCR2, HLA-DMA, HLA-DMB, HLA-DPBI, HLA-DQBI, HLA-DRA, ICAMI, IL17RA, IL18, ILIR1, ILIRI, IL6, IL6R, IRF1, IRF5, IRF8, ITGAL, ITGAX, LAT2, LGALS3, LGALS9, LIF, MAPK13, MX2, NCF2, NLRP3, NOD2, OSCAR, PLAU, PLAUR, PTAFR, PTGS2, PTK3, PYCARD, SIGLECI, SQSTM1, STAT6, SYK, TLR1, TLR5, TLR7, TNFAIP3, TNFRSF11A, TNFRSF14, TNFRSF1B, TREM2, TUBA4A, TYROBP, VCAMI, WAS
HSA-1280215	Cytokine Signalling in Immune system	42	654	1.33E-28	BIRC3, CASP1, CCL2, CCL20, CD44, CD80, CD86, CSF1, CSF1R, CSF2RA, CXCL1, CXCL2, CXCL8, GATA3, HAVCR2, HLA-DPBI, HLA-DQBI, HLA-DRA, ICAMI, IL17RA, IL18, ILIR1, IL4R, IL6, IL6R, IRF1, IRF5, IRF8, ITGAX, LGALS9, LIF, MX2, NOD2, PTAFR, PTGS2, SQSTM1, STAT6, SYK, TNFRSF1B, VCAMI
HSA-449147	Signalling by Interleukins	31	439	1.33E-21	CASP1, CCL2, CCL20, CD80, CD86, CSF1, CSF1R, CSF2RA, CXCL1, CXCL2, CXCL8, GATA3, HAVCR2, ICAMI, IL17RA, IL18, ILIR1, IL4R, IL6, IL6R, ITGAX, LGALS9, LIF, NOD2, PTAFR, PTGS2, SQSTM1, STAT6, SYK, TNFRSF1B, VCAMI
HSA-6783783	Interleukin-10 signalling	16	45	1.75E-20	CCL2, CCL20, CD80, CD86, CSF1, CXCL1, CXCL2, CXCL8, ICAMI, IL18, ILIR1, IL6, LIF, PTAFR, PTGS2, TNFRSF1B
HSA-168249	Innate Immune System	38	1012	4.91E-18	ADAM8, BIRC3, BTK, C5AR1, CASP1, CD180, CD44, CH13L1, CLEC5A, CTSD, CTSL, CTSS, CXCL1, CYBB, ITGAL, ITGAX, LAT2, LGALS3, MAPK13, NCF2, NLRP3, NOD2, OSCAR, PLAU, PLAUR, PTAFR, PTK3, PYCARD, STAT6, SYK, TLR1, TLR5, TLR7, TNFAIP3, TNFRSF1B, TREM2, TYROBP, WAS
HSA-6785807	Interleukin-4 and Interleukin-13 signalling	14	106	1.01E-12	CCL2, CXCL8, GATA3, ICAMI, IL18, IL4R, IL6, IL6R, ITGAX, LIF, PTGS2, STAT6, TNFRSF1B, VCAMI
HSA-1280218	Adaptive Immune System	26	733	2.53E-11	BTK, CD274, CD80, CD86, CTSD, CTSL, CTSS, CYBB, HLA-DMA, HLA-DMB, HLA-DPBI, HLA-DQBI, HLA-DRA, ICAMI, ITGAL, NCF2, OSCAR, SIGLECI, SYK, TLR1, TNFRSF14, TREM2, TUBA4A, TYROBP, VCAMI, WAS
HSA-6798695	Neutrophil degranulation	20	471	7.19E-10	ADAM8, C5AR1, CD44, CH13L1, CLEC5A, CTSD, CTSS, CXCL1, CYBB, ITGAL, ITGAX, LGALS3, OSCAR, PLAU, PLAUR, PTAFR, PTK3, PYCARD, TNFRSF1B, TYROBP
HSA-877300	Interferon gamma signalling	10	86	1.40E-08	CD44, HLA-DPBI, HLA-DQBI, HLA-DRA, ICAMI, IRF1, IRF5, IRF8, PTAFR, VCAMI
HSA-380108	Chemokine receptors bind chemokines	8	48	6.08E-08	CCL20, CCRL2, CX3CRI, CXCL1, CXCL2, CXCL8, CXCL3, CXCL8
HSA-913531	Interferon Signalling	11	189	1.29E-06	CD44, HLA-DPBI, HLA-DQBI, HLA-DRA, ICAMI, IRF1, IRF5, IRF8, MX2, PTAFR, VCAMI
HSA-1474244	Extracellular matrix organisation	13	298	1.68E-06	ADAM8, ADAMTS14, CD44, CTSD, CTSL, CTSS, DDR2, ICAMI, ITGAL, ITGAX, MMP19, SERPINE1, VCAMI
HSA-168643	Nucleotide-binding domain, leucine rich repeat containing receptor (NLR) signalling pathways	7	54	2.45E-06	BIRC3, CASP1, MAPK13, NLRP3, NOD2, PYCARD, TNFAIP3
HSA-2132295	MHC class II antigen presentation	9	119	2.45E-06	CTSD, CTSL, CTSS, HLA-DMA, HLA-DMB, HLA-DPBI, HLA-DQBI, HLA-DRA, TUBA4A
HSA-388841	Costimulation by the CD28 family	7	61	4.56E-06	CD274, CD80, CD86, HLA-DPBI, HLA-DQBI, HLA-DRA, TNFRSF14
HSA-162582	Signal Transduction	37	2605	1.10E-05	ALDH1A1, BIRC3, BTK, C5AR1, CCL20, CCRL2, CD80, CD86, CSF2RA, CTSD, CX3CRI, CXCL1, CXCL2, CXCL3, CXCL8, CYBB, FAS, GATA3, GPR65, HBEGF, IER3, IGFI, IL6, IL6R, MAPK13, NCF2, PIK3CG, PTAFR, SERPINE1, SQSTM1, STAT6, SYK, TNFAIP3, TNFSF10, TUBA4A, WAS
HSA-168898	Toll-like Receptor Cascades	9	151	1.27E-05	BIRC3, BTK, CD180, CTSL, CTSS, NOD2, TLR1, TLR5, TLR7
HSA-375276	Peptide ligand-binding receptors	9	183	5.48E-05	C5AR1, CCL20, CCR1, CX3CRI, CXCL1, CXCL2, CXCL3, CXCL8
HSA-217127	DAPI2 interactions	5	34	7.40E-05	BTK, CLEC5A, SYK, TREM2, TYROBP
HSA-168638	NOD1/2 Signalling Pathway	5	35	8.00E-05	BIRC3, CASP1, MAPK13, NOD2, TNFAIP3
HSA-373076	Class A1 (Rhodopsin-like receptors)	11	311	8.00E-05	C5AR1, CCL20, CCR1, CX3CRI, CXCL1, CXCL2, CXCL3, CXCL8, GPR65, PTAFR
HSA-389948	PD-1 signalling	4	18	1.50E-04	CD274, HLA-DPBI, HLA-DQBI, HLA-DRA
HSA-198933	Immunoregulatory interactions between a Lymphoid and a non-Lymphoid cell	7	125	2.60E-04	ICAMI, ITGAL, OSCAR, SIGLECI, TREM2, TYROBP, VCAMI

HSA-109582	Haemostasis	14	601	3.40E-04	CD44, CD84, GATA3, IGF1, IRF1, ITGAL, ITGAX, PDPN, PIK3CG, PLAU, PLAUR, SERPINE1, SYK, TUBA4A
HSA-2424491	DAP12 signalling	4	26	4.80E-04	BTK, SYK, TREM2, TYROBP
HSA-1236975	Antigen processing-Cross presentation	6	96	5.30E-04	BTK, CTSL, CTSS, CYBB, NCF2, TLR1
HSA-202433	Generation of second messenger molecules	4	27	5.30E-04	HLA-DPB1, HLA-DQB1, HLA-DRA, WAS
HSA-1679131	Trafficking and processing of endosomal TLR	3	13	1.50E-03	CTSL, CTSS, TLR7
HSA-75205	Dissolution of Fibrin Clot	3	13	1.50E-03	PLAU, PLAUR, SERPINE1
HSA-202430	Translocation of ZAP-70 to Immunological synapse	3	14	1.70E-03	HLA-DPB1, HLA-DQB1, HLA-DRA
HSA-2162123	Synthesis of Prostaglandins and Thromboxanes	3	15	2.00E-03	HPGDS, PTGDS, PTGS2
HSA-844456	The NLRP3 inflammasome	3	15	2.00E-03	CASPI, NLRP3, PYCARD
HSA-451927	Interleukin-2 family signalling	4	43	2.10E-03	CSF2RA, HAVCR2, LGALS9, SYK
HSA-216083	Integrin cell surface interactions	5	83	2.20E-03	CD44, ICAM1, ITGAL, ITGAX, VCAM1
HSA-202427	Phosphorylation of CD3 and TCR zeta chains	3	17	2.50E-03	HLA-DPB1, HLA-DQB1, HLA-DRA
HSA-5675482	Regulation of necroptotic cell death	3	17	2.50E-03	BIRC3, FAS, TNFSF10
HSA-1474228	Degradation of the extracellular matrix	6	139	2.60E-03	ADAM8, CD44, CTSD, CTSL, CTSS, MMP19
HSA-844615	The AIM2 inflammasome	2	3	3.30E-03	CASPI, PYCARD
HSA-2142753	Arachidonic acid metabolism	4	59	5.10E-03	ALOX5AP, HPGDS, PTGDS, PTGS2
HSA-5602358	Diseases associated with the TLR signalling cascade	3	24	5.10E-03	BTK, TLR1, TLR5
HSA-6783589	Interleukin-6 family signalling	3	24	5.10E-03	IL6, IL6R, LIF
HSA-909733	Interferon alpha/beta signalling	4	66	7.10E-03	IRF1, IRF5, IRF8, MX2
HSA-166016	Toll Like Receptor 4 (TLR4) Cascade	5	126	9.70E-03	BIRC3, BTK, CD180, NOD2, TLR1
HSA-114604	Interleukin-1 processing	2	7	1.00E-02	CASPI, IL18
HSA-448706	GPVI-mediated activation cascade	3	34	1.12E-02	PDPN, PIK3CG, SYK
HSA-112411	MAPK1 (ERK2) activation	2	8	1.19E-02	IL6, IL6R
HSA-1236973	Cross-presentation of particulate exogenous antigens (phagosomes)	2	8	1.19E-02	CYBB, NCF2
HSA-446652	Interleukin-1 family signalling	5	134	1.19E-02	CASPI, IL18, IL1RI, NOD2, SQSTM1
HSA-73887	Death Receptor Signalling	5	139	1.31E-02	BIRC3, FAS, SQSTM1, TNFAIP3, TNFSF10
HSA-110056	MAPK3 (ERK1) activation	2	9	1.36E-02	IL6, IL6R
HSA-6811558	PI5P, PP2A and IER3 Regulate PI3K/AKT Signalling	4	85	1.45E-02	CD80, CD86, HBEGF, IER3
HSA-3371378	Regulation by c-FLIP	2	10	1.56E-02	FAS, TNFSF10
HSA-5218900	CASP8 activity is inhibited	2	10	1.56E-02	FAS, TNFSF10
HSA-5602498	MyD88 deficiency (TLR2/4)	2	10	1.56E-02	BTK, TLR1
HSA-69416	Dimerization of procaspase-8	2	10	1.56E-02	FAS, TNFSF10
HSA-1059683	Interleukin-6 signalling	2	11	1.72E-02	IL6, IL6R
HSA-1236977	Endosomal/Vacuolar pathway	2	11	1.72E-02	CTSL, CTSS
HSA-389359	CD28 dependent Vav1 pathway	2	11	1.72E-02	CD80, CD86
HSA-418594	G alpha (i) signalling events	8	387	1.72E-02	C5ARI, CCL20, CX3CRI, CXCL1, CXCL12, CXCL2, CXCL3, CXCL8
HSA-5603041	IRAK4 deficiency (TLR2/4)	2	11	1.72E-02	BTK, TLR1
HSA-5668541	TNFR2 non-canonical NF-kB pathway	4	96	1.84E-02	BIRC3, TNFRSF11A, TNFRSF14, TNFRSF1B
HSA-5668599	RHO GTPases Activate NADPH Oxidases	2	13	2.06E-02	CYBB, NCF2
HSA-2730905	Role of LAT2/NTAL/LAB on calcium mobilization	2	15	2.61E-02	LAT2, SYK
HSA-5676594	TNF receptor superfamily (TNFSF) members mediating non-canonical NF-kB pathway	2	16	2.80E-02	BIRC3, TNFRSF11A
HSA-76002	Platelet activation, signalling and aggregation	6	256	2.80E-02	IGF1, PDPN, PIK3CG, SERPINE1, SYK, TUBA4A
HSA-2219530	Constitutive Signalling by Aberrant PI3K in Cancer	3	58	3.15E-02	CD80, CD86, HBEGF
HSA-9018678	Biosynthesis of specialized proresolving mediators	2	18	3.32E-02	ALOX5AP, PTGS2
HSA-2029482	Regulation of actin dynamics for phagocytic cup formation	3	60	3.35E-02	BTK, SYK, WAS
HSA-197264	Nicotinamide salvaging	2	19	3.56E-02	NAMPT, PTGS2
HSA-416700	Other semaphorin interactions	2	19	3.56E-02	TREM2, TYROBP
HSA-1442490	Collagen degradation	3	64	3.80E-02	CTSD, CTSL, MMP19

HSA-389513	CTLA4 inhibitory signalling	2	20	3.80E-02	CD80, CD86
HSA-389357	CD28 dependent PI3K/Akt signalling	2	22	4.39E-02	CD80, CD86
HSA-202733	Cell surface interactions at the vascular wall	4	135	4.73E-02	CD44, CD84, ITGAL, ITGAX

TABLE S10. List of KEGG pathways significantly enriched in CD204^{HIGH} & IBA1^{HIGH} tumours, CD204^{HIGH} & IBA1^{LOW} tumours, and CD204^{LOW} & IBA1^{HIGH} tumours (shared genes) relative to CD204^{LOW} & IBA1^{LOW} tumours

ID	KEGG Term description	Observed Gene count	Background gene count	FDR	Matching genes in the network
hsa05150	Staphylococcus aureus infection	8	51	9.90E-12	<i>CIQA, FCGR2A, FCGR2B, FCGR3A, FPRI, FPR2, FPR3, ITGAM</i>
hsa05152	Tuberculosis	10	172	3.25E-11	<i>CD14, CLEC7A, FCGR2A, FCGR2B, FCGR3A, IL10RA, IL1B, ITGAM, MRC1, TLR2</i>
hsa04145	Phagosome	8	145	8.16E-09	<i>CD14, CLEC7A, FCGR2A, FCGR2B, FCGR3A, ITGAM, MRC1, TLR2</i>
hsa04060	Cytokine-cytokine receptor interaction	8	263	5.54E-07	<i>CCL5, CCRI, CSF3R, IL10RA, IL15, IL1B, IL1R2, OSM</i>
hsa05140	Leishmaniasis	5	70	4.18E-06	<i>FCGR2A, FCGR3A, IL1B, ITGAM, TLR2</i>
hsa04666	Fe gamma R-mediated phagocytosis	5	89	1.08E-05	<i>FCGR2A, FCGR2B, FCGR3A, SCIN, VAVI</i>
hsa04640	Hematopoietic cell lineage	5	94	1.20E-05	<i>CD14, CSF3R, IL1B, IL1R2, ITGAM</i>
hsa05146	Amoebiasis	5	94	1.20E-05	<i>CD14, IL1B, IL1R2, ITGAM, TLR2</i>
hsa05134	Legionellosis	4	54	3.58E-05	<i>CD14, IL1B, ITGAM, TLR2</i>
hsa04630	Jak-STAT signalling pathway	5	160	1.00E-04	<i>CSF3R, IL10RA, IL15, JAK3, OSM</i>
hsa05133	Pertussis	4	74	1.00E-04	<i>CIQA, CD14, IL1B, ITGAM</i>
hsa05323	Rheumatoid arthritis	4	84	1.40E-04	<i>CCL5, IL15, IL1B, TLR2</i>
hsa04620	Toll-like receptor signalling pathway	4	102	2.50E-04	<i>CCL5, CD14, IL1B, TLR2</i>
hsa05020	Prion diseases	3	33	2.50E-04	<i>CIQA, CCL5, IL1B</i>
hsa05142	Chagas disease (American trypanosomiasis)	4	101	2.50E-04	<i>CIQA, CCL5, IL1B, TLR2</i>
hsa04380	Osteoclast differentiation	4	124	4.60E-04	<i>FCGR2A, FCGR2B, FCGR3A, IL1B</i>
hsa05162	Measles	4	133	5.70E-04	<i>FCGR2B, IL1B, JAK3, TLR2</i>
hsa04062	Chemokine signalling pathway	4	181	1.70E-03	<i>CCL5, CCRI, JAK3, VAVI</i>
hsa05168	Herpes simplex infection	4	181	1.70E-03	<i>CCL5, IL15, IL1B, TLR2</i>
hsa04610	Complement and coagulation cascades	3	78	1.90E-03	<i>CIQA, ITGAM, THBD</i>
hsa04810	Regulation of actin cytoskeleton	4	205	2.30E-03	<i>CD14, ITGAM, SCIN, VAVI</i>
hsa04657	IL-17 signalling pathway	3	92	2.70E-03	<i>IL1B, ST00A8, ST00A9</i>
hsa05322	Systemic lupus erythematosus	3	94	2.80E-03	<i>CIQA, FCGR2A, FCGR3A</i>
hsa04668	TNF signalling pathway	3	108	3.90E-03	<i>CCL5, IL15, IL1B</i>
hsa05145	Toxoplasmosis	3	109	3.90E-03	<i>ALOX5, IL10RA, TLR2</i>
hsa05418	Fluid shear stress and atherosclerosis	3	133	6.40E-03	<i>IL1B, IL1R2, THBD</i>
hsa05144	Malaria	2	47	1.15E-02	<i>IL1B, TLR2</i>
hsa04151	PI3K-Akt signalling pathway	4	348	1.16E-02	<i>CSF3R, JAK3, OSM, TLR2</i>
hsa05202	Transcriptional misregulation in cancer	3	169	1.16E-02	<i>CD14, IL1R2, ITGAM</i>
hsa04623	Cytosolic DNA-sensing pathway	2	62	1.74E-02	<i>CCL5, IL1B</i>
hsa05321	Inflammatory bowel disease (IBD)	2	62	1.74E-02	<i>IL1B, TLR2</i>
hsa04664	Fe epsilon RI signalling pathway	2	67	1.84E-02	<i>ALOX5, VAVI</i>
hsa05221	Acute myeloid leukemia	2	66	1.84E-02	<i>CD14, ITGAM</i>
hsa04662	B cell receptor signalling pathway	2	71	1.99E-02	<i>FCGR2B, VAVI</i>
hsa05132	Salmonella infection	2	84	2.64E-02	<i>CD14, IL1B</i>
hsa05166	HTLV-I infection	3	250	2.64E-02	<i>IL15, IL1R2, JAK3</i>
hsa04064	NF-kappa B signalling pathway	2	93	3.02E-02	<i>CD14, IL1B</i>
hsa04080	Neuroactive ligand-receptor interaction	3	272	3.10E-02	<i>FPRI, FPR2, FPR3</i>
hsa04933	AGE-RAGE signalling pathway in diabetic complications	2	98	3.16E-02	<i>IL1B, THBD</i>
hsa04659	Th17 cell differentiation	2	102	3.32E-02	<i>IL1B, JAK3</i>
hsa04670	Leukocyte transendothelial migration	2	112	3.85E-02	<i>ITGAM, VAVI</i>
hsa04650	Natural killer cell mediated cytotoxicity	2	124	4.53E-02	<i>FCGR3A, VAVI</i>

TABLE S11. List of Reactome pathways significantly enriched in CD204^{HIGH} & IBA1^{HIGH} tumours, CD204^{LOW} & IBA1^{LOW} tumours, and CD204^{LOW} & IBA1^{HIGH} tumours (shared genes) relative to CD204^{LOW} & IBA1^{LOW} tumours

ID	KEGG Term description	Observed Gene count	Background gene count	FDR	Matching genes in the network
HSA-168256	Immune System	28	1925	1.59E-19	<i>ALOX5, C1QA, CCL5, CCRI, CD14, CD68, CLEC7A, CSF3R, FCGR2A, FCGR2B, FCGR3A, FPR1, FPR2, IL10RA, IL15, IL1B, IL1R2, ITGAM, JAK3, MRC1, OSM, RNASE2, S100A8, S100A9, SELL, TLR2, TREM1, VAV1</i>
HSA-168249	Innate Immune System	18	1012	2.29E-12	<i>ALOX5, C1QA, CD14, CD68, CLEC7A, FCGR2A, FCGR3A, FPR1, FPR2, IL1B, ITGAM, RNASE2, S100A8, S100A9, SELL, TLR2, TREM1, VAV1</i>
HSA-449147	Signalling by Interleukins	13	439	3.22E-11	<i>ALOX5, CCL5, CCRI, CSF3R, FPR1, IL10RA, IL15, IL1B, IL1R2, ITGAM, JAK3, OSM, VAV1</i>
HSA-6798695	Neutrophil degranulation	12	471	1.23E-09	<i>ALOX5, CD14, CD68, FCGR2A, FPR1, FPR2, ITGAM, RNASE2, S100A8, S100A9, SELL, TLR2</i>
HSA-6783783	Interleukin-10 signalling	6	45	1.08E-08	<i>CCL5, CCRI, FPR1, IL10RA, IL1B, IL1R2</i>
HSA-5686938	Regulation of TLR by endogenous ligand	4	19	1.82E-06	<i>CD14, S100A8, S100A9, TLR2</i>
HSA-444473	Formyl peptide receptors bind formyl peptides and many other ligands	3	7	1.30E-05	<i>FPR1, FPR2, FPR3</i>
HSA-6785807	Interleukin-4 and Interleukin-13 signalling	5	106	2.98E-05	<i>ALOX5, IL1B, ITGAM, JAK3, OSM</i>
HSA-168898	Toll-like Receptor Cascades	5	151	1.40E-04	<i>CD14, ITGAM, S100A8, S100A9, TLR2</i>
HSA-375276	Peptide ligand-binding receptors	5	183	3.20E-04	<i>CCL5, CCRI, FPR1, FPR2, FPR3</i>
HSA-1280218	Adaptive Immune System	8	733	6.10E-04	<i>CD14, FCGR2B, FCGR3A, MRC1, SELL, TLR2, TREM1, VAV1</i>
HSA-198933	Immunoregulatory interactions between a Lymphoid and a non-Lymphoid cell	4	125	1.10E-03	<i>FCGR2B, FCGR3A, SELL, TREM1</i>
HSA-6799990	Metal sequestration by antimicrobial proteins	2	6	1.10E-03	<i>S100A8, S100A9</i>
HSA-202733	Cell surface interactions at the vascular wall	4	135	1.20E-03	<i>ITGAM, SELL, THBD, TREM1</i>
HSA-2029482	Regulation of actin dynamics for phagocytic cup formation	3	60	2.00E-03	<i>FCGR2A, FCGR3A, VAV1</i>
HSA-5602498	MyD88 deficiency (TLR2/4)	2	10	2.00E-03	<i>CD14, TLR2</i>
HSA-2029481	FCGR activation	2	11	2.20E-03	<i>FCGR2A, FCGR3A</i>
HSA-5603041	IRAK4 deficiency (TLR2/4)	2	11	2.20E-03	<i>CD14, TLR2</i>
HSA-8983432	Interleukin-15 signalling	2	13	2.50E-03	<i>IL15, JAK3</i>
HSA-6803157	Antimicrobial peptides	3	87	4.00E-03	<i>S100A8, S100A9, TLR2</i>
HSA-418594	G alpha (i) signalling events	5	387	4.50E-03	<i>CCL5, CCRI, FPR1, FPR2, FPR3</i>
HSA-1236975	Antigen processing-Cross presentation	3	96	4.90E-03	<i>CD14, MRC1, TLR2</i>
HSA-2029485	Role of phospholipids in phagocytosis	2	25	6.20E-03	<i>FCGR2A, FCGR3A</i>
HSA-166016	Toll Like Receptor 4 (TLR4) Cascade	3	126	8.70E-03	<i>CD14, ITGAM, TLR2</i>
HSA-446652	Interleukin-1 family signalling	3	134	1.00E-02	<i>ALOX5, IL1B, IL1R2</i>
HSA-2173782	Binding and Uptake of Ligands by Scavenger Receptors	2	40	1.30E-02	<i>CD163, STAB1</i>
HSA-512988	Interleukin-3, Interleukin-5 and GM-CSF signalling	2	47	1.65E-02	<i>JAK3, VAV1</i>
HSA-380108	Chemokine receptors bind chemokines	2	48	1.67E-02	<i>CCL5, CCRI</i>
HSA-109582	Haemostasis	5	601	2.03E-02	<i>ITGAM, SELL, THBD, TREM1, VAV1</i>
HSA-1236974	ER-Phagosome pathway	2	80	4.13E-02	<i>CD14, TLR2</i>

TABLE S12. List of KEGG pathways significantly enriched in IBA1^{HIGH} tumours relative to CD204^{LOW} & IBA1^{LOW} tumours

ID	KEGG Term description	Observed Gene count	Background gene count	FDR	Matching genes in the network
hsa05142	Chagas disease (American trypanosomiasis)	7	101	1.11E-09	<i>CIQB, CIQC, C3, CCL3, CCL3L3, TLR6, TNF</i>
hsa05150	Staphylococcus aureus infection	6	51	1.11E-09	<i>CIQB, CIQC, C3, C3ARI, FCGRIA, ITGB2</i>
hsa04610	Complement and coagulation cascades	5	78	4.84E-07	<i>CIQB, CIQC, C3, C3ARI, ITGB2</i>
hsa05133	Pertussis	5	74	4.84E-07	<i>CIQB, CIQC, C3, ITGB2, TNF</i>
hsa05152	Tuberculosis	6	172	4.84E-07	<i>C3, CD74, FCGRIA, ITGB2, TLR6, TNF</i>
hsa05322	Systemic lupus erythematosus	5	94	7.58E-07	<i>CIQB, CIQC, C3, FCGRIA, TNF</i>
hsa04620	Toll-like receptor signalling pathway	5	102	9.60E-07	<i>CCL3, CCL3L3, CCL4, TLR6, TNF</i>
hsa04145	Phagosome	5	145	4.54E-06	<i>C3, FCGRIA, ITGB2, OLR1, TLR6</i>
hsa05140	Leishmaniasis	4	70	9.51E-06	<i>C3, FCGRIA, ITGB2, TNF</i>
hsa05323	Rheumatoid arthritis	4	84	1.72E-05	<i>CCL3, CCL3L3, ITGB2, TNF</i>
hsa05134	Legionellosis	3	54	2.20E-04	<i>C3, ITGB2, TNF</i>
hsa05132	Salmonella infection	3	84	7.10E-04	<i>CCL3, CCL3L3, CCL4</i>
hsa04060	Cytokine-cytokine receptor interaction	4	263	1.00E-03	<i>CCL3, CCL3L3, CCL4, TNF</i>
hsa05020	Prion diseases	2	33	3.60E-03	<i>CIQB, CIQC</i>
hsa04062	Chemokine signalling pathway	3	181	5.10E-03	<i>CCL3, CCL3L3, CCL4</i>
hsa05168	Herpes simplex infection	3	181	5.10E-03	<i>C3, CD74, TNF</i>
hsa05144	Malaria	2	47	5.90E-03	<i>ITGB2, TNF</i>
hsa04612	Antigen processing and presentation	2	66	1.06E-02	<i>CD74, TNF</i>
hsa04666	Fe gamma R-mediated phagocytosis	2	89	1.78E-02	<i>FCGRIA, PTPRC</i>
hsa04064	NF-kappa B signalling pathway	2	93	1.84E-02	<i>CCL4, TNF</i>
hsa04640	Hematopoietic cell lineage	2	94	1.84E-02	<i>FCGRIA, TNF</i>
hsa04660	T cell receptor signalling pathway	2	99	1.84E-02	<i>PTPRC, TNF</i>
hsa05146	Amoebiasis	2	94	1.84E-02	<i>ITGB2, TNF</i>
hsa04380	Osteoclast differentiation	2	124	2.65E-02	<i>FCGRIA, TNF</i>
hsa04650	Natural killer cell mediated cytotoxicity	2	124	2.65E-02	<i>ITGB2, TNF</i>
hsa04514	Cell adhesion molecules (CAMs)	2	139	3.04E-02	<i>ITGB2, PTPRC</i>

TABLE S13. List of Reactome pathways significantly enriched in IBA1^{HIGH} tumours relative to CD204^{LOW} & IBA1^{LOW} tumours

ID	KEGG Term description	Observed Gene count	Background gene count	FDR	Matching genes in the network
HSA-168256	Immune System	15	1925	1.90E-09	AMICAI, CIQB, CIQC, C3, C3ARI, CCL3, CCL3L3, CCL4, CD74, FCGRIA, ITGB2, OLR1, PTPRC, TLR6, TNF
HSA-6783783	Interleukin-10 signalling	4	45	7.62E-06	CCL3, CCL3L3, CCL4, TNF
HSA-977606	Regulation of Complement cascade	4	47	7.62E-06	CIQB, CIQC, C3, C3ARI
HSA-166658	Complement cascade	4	56	8.68E-06	CIQB, CIQC, C3, C3ARI
HSA-168249	Innate Immune System	9	1012	8.68E-06	CIQB, CIQC, C3, C3ARI, FCGRIA, ITGB2, OLR1, PTPRC, TLR6
HSA-166663	Initial triggering of complement	3	21	2.68E-05	CIQB, CIQC, C3
HSA-1280218	Adaptive Immune System	7	733	8.48E-05	AMICAI, C3, CD74, FCGRIA, ITGB2, PTPRC, TLR6
HSA-198933	Immunoregulatory interactions between a Lymphoid and a non-Lymphoid cell	4	125	9.36E-05	AMICAI, C3, FCGRIA, ITGB2
HSA-202733	Cell surface interactions at the vascular wall	4	135	1.10E-04	AMICAI, CD74, ITGB2, OLR1
HSA-173623	Classical antibody-mediated complement activation	2	7	3.00E-04	CIQB, CIQC
HSA-1280215	Cytokine Signalling in Immune system	6	654	3.50E-04	CCL3, CCL3L3, CCL4, FCGRIA, ITGB2, TNF
HSA-449147	Signalling by Interleukins	5	439	5.60E-04	CCL3, CCL3L3, CCL4, ITGB2, TNF
HSA-166786	Creation of C4 and C2 activators	2	13	6.70E-04	CIQB, CIQC
HSA-6798695	Neutrophil degranulation	5	471	6.70E-04	C3, C3ARI, ITGB2, OLR1, PTPRC
HSA-109582	Haemostasis	5	601	1.90E-03	AMICAI, CD74, ITGB2, MAFF, OLR1
HSA-1236975	Antigen processing-Cross presentation	2	96	2.32E-02	FCGRIA, TLR6
HSA-6785807	Interleukin-4 and Interleukin-13 signalling	2	106	2.64E-02	ITGB2, TNF
HSA-166016	Toll Like Receptor 4 (TLR4) Cascade	2	126	3.37E-02	ITGB2, TLR6
HSA-418594	G alpha (i) signalling events	3	387	3.37E-02	C3, C3ARI, CCL4
HSA-168898	Toll-like Receptor Cascades	2	151	4.39E-02	ITGB2, TLR6

TABLE S14. List of KEGG pathways significantly enriched in CD204^{HIGH} tumours relative to CD204^{LOW} tumours in the TCGA dataset

ID	KEGG Term description	Observed Gene count	Background gene count	FDR	Matching genes in the network
hsa04060	Cytokine-cytokine receptor interaction	21	263	1. 19E-10	CCL13, CCL18, CCL2, CCL7, CCL8, CCR5, CXCL11, CXCL8, CXCL9, FAS, IL18, IL18RAP, IL1A, IL1B, IL1R2, IL2RA, IL6, IL7R, OSM, PPBP, TNFSF13B
hsa05152	Tuberculosis	17	172	4. 40E-10	CAMP, CD14, CD74, CLEC4E, CTSS, FCER1G, FCGR2A, FCGR2B, FCGR3A, IL18, IL1A, IL1B, IL6, THBD, NOD2, TLR1, TLR2, VDR
hsa04620	Toll-like receptor signalling pathway	12	102	6. 78E-08	CD14, CXCL11, CXCL8, CXCL9, IL1B, IL6, MAP3K8, SPPI, TLR1, TLR2, TLR7, TLR8
hsa04145	Phagosome	12	145	1. 94E-06	CD14, CTSS, CYBB, FCGR2A, FCGR3A, MARCO, MSRI, NCF2, NCF4, OLRI, TLR2
hsa04933	AGE-RAGE signalling pathway in diabetic complications	10	98	3. 28E-06	CCL2, COL1A1, COL3A1, CXCL8, CYBB, F3, IL1A, IL1B, IL6, THBD
hsa05150	Staphylococcus aureus infection	8	51	3. 28E-06	C1S, C3ARI, CFD, FCGR2A, FCGR2B, FCGR3A, FPR2, FPR3
hsa04621	NOD-like receptor signalling pathway	12	166	4. 39E-06	CAMP, CCL2, CXCL8, CYBB, GBP5, IL18, IL1B, IL6, NAMPT, NLRCA, NOD2, RIPK3
hsa04380	Osteoclast differentiation	10	124	1. 52E-05	FCGR2A, FCGR2B, FCGR3A, IL1A, IL1B, LILRB1, LILRB2, LILRB3, NCF2, NCF4
hsa04640	Haematopoietic cell lineage	9	94	1. 52E-05	CD14, CD2, CD33, IL1A, IL1B, IL1R2, IL2RA, IL6, IL7R
hsa05140	Leishmaniasis	8	70	1. 52E-05	CYBB, FCGR2A, FCGR3A, IL1A, IL1B, NCF2, NCF4, TLR2
hsa05144	Malaria	7	47	1. 52E-05	CCL2, CXCL8, IL18, IL1B, IL6, KLRB1, TLR2
hsa05134	Legionellosis	7	54	2. 77E-05	CD14, CXCL8, IL18, IL1B, IL6, NLRCA, TLR2
hsa04062	Chemokine signalling pathway	11	181	3. 79E-05	CCL13, CCL18, CCL2, CCL7, CCL8, CCR5, CXCL11, CXCL8, CXCL9, HCK, PPBP
hsa05323	Rheumatoid arthritis	8	84	3. 79E-05	CCL2, CXCL8, IL18, IL1A, IL1B, IL6, TLR2, TNFSF13B
hsa05321	Inflammatory bowel disease (IBD)	7	62	5. 12E-05	IL18, IL18RAP, IL1A, IL1B, IL6, NOD2, TLR2
hsa05146	Amoebiasis	8	94	7. 06E-05	CD14, COL1A1, COL3A1, CXCL8, IL1B, IL1R2, IL6, TLR2
hsa05132	Salmonella infection	7	84	2. 80E-04	CD14, CXCL8, IL18, IL1A, IL1B, IL6, NLRCA
hsa04657	IL-17 signalling pathway	7	92	4. 60E-04	CCL2, CCL7, CXCL8, IL1B, IL6, S100A8, S100A9
hsa05164	Influenza A	9	168	5. 20E-04	CCL2, CXCL8, FAS, IL18, IL1A, IL1B, IL33, IL6, TLR7
hsa05162	Measles	8	133	5. 90E-04	FAS, FCGR2B, IL1A, IL1B, IL2RA, IL6, TLR2, TLR7
hsa04668	TNF signalling pathway	7	108	9. 70E-04	CCL2, FAS, IL1B, IL6, MAP3K8, NOD2, RIPK3
hsa05133	Pertussis	6	74	9. 70E-04	C1S, CD14, CXCL8, IL1A, IL1B, IL6
hsa04610	Complement and coagulation cascades	6	78	1. 20E-03	C1S, C3ARI, CFD, F13A1, F3, THBD
hsa04666	Fc gamma R-mediated phagocytosis	6	89	2. 20E-03	FCGR2A, FCGR2B, FCGR3A, HCK, PTPRC, SCIN
hsa04064	NF-kappa B signalling pathway	6	93	2. 60E-03	BCL2A1, CCL13, CD14, CXCL8, IL1B, TNFSF13B
hsa05418	Fluid shear stress and atherosclerosis	7	133	2. 70E-03	CCL2, HMOX1, IL1A, IL1B, IL1R2, NCF2, THBD
hsa04623	Cytosolic DNA-sensing pathway	5	62	2. 80E-03	IL18, IL1B, IL33, IL6, RIPK3
hsa05143	African trypanosomiasis	4	34	2. 80E-03	FAS, IL18, IL1B, IL6
hsa05332	Graft-versus-host disease	4	36	3. 20E-03	FAS, IL1A, IL1B, IL6
hsa05142	Chagas disease (American trypanosomiasis)	6	101	3. 30E-03	CCL2, CXCL8, FAS, IL1B, IL6, TLR2
hsa04151	PI3K-Akt signalling pathway	10	348	1. 43E-02	COL1A1, FGF20, IBSP, IL2RA, IL6, IL7R, OSM, PIK3AP1, SPPI, TLR2
hsa01523	Antifolate resistance	3	31	2. 06E-02	ABCC3, IL1B, IL6
hsa04217	Necroptosis	6	155	2. 35E-02	CYBB, FAS, IL1A, IL1B, IL33, RIPK3
hsa05020	Prion diseases	3	33	2. 35E-02	IL1A, IL1B, IL6
hsa04662	B cell receptor signalling pathway	4	71	2. 70E-02	CD72, FCGR2B, LILRB3, PIK3API
hsa05202	Transcriptional misregulation in cancer	6	169	3. 21E-02	BCL2A1, CD14, CXCL8, DEFA3, IL1R2, IL6
hsa04216	Ferroptosis	3	40	3. 45E-02	CP, CYBB, HMOX1
hsa04611	Platelet activation	5	123	3. 45E-02	COL1A1, COL3A1, FCER1G, FCGR2A, P2RY12
hsa04940	Type I diabetes mellitus	3	40	3. 45E-02	FAS, IL1A, IL1B
hsa05168	Herpes simplex infection	6	181	3. 93E-02	CCL2, CD74, FAS, IL1B, IL6, TLR2
hsa05167	Kaposi's sarcoma-associated herpesvirus infection	6	183	4. 02E-02	CCR5, CLEC2B, CXCL8, FAS, HCK, IL6
hsa04974	Protein digestion and absorption	4	90	4. 89E-02	COL1A1, COL3A1, KCNE3, SLC7A7

TABLE S15. List of Reactome pathways significantly enriched in CD204^{HIGH} tumours relative to CD204^{LOW} tumours in the TCGA dataset

ID	KEGG Term description	Observed Gene count	Background gene count	FDR	Matching genes in the network
HSA-168256	Immune System	83	1925	1.21E-29	ATP8B4, BAF7, C1S, C3AR1, CAMP, CCL2, CCR5, CD14, CD300LF, CD33, CD53, CD74, CD93, CFD, CLEC2B, CLEC4E, CLEC5A, COL1A1, COL3A1, CTSS, CXCL8, CYBB, DEFA3, F13A1, FCER1G, FCGR2A, FCGR2B, FCGR3A, FGL2, FPR2, FYB, GBP5, GNLY, GPR84, HAVCR2, HCK, HMOX1, IL130, IL18, IL18RAP, IL1A, IL1B, IL1R2, IL2RA, IL33, IL6, IL7R, IRAK3, KLRB1, LAIR1, LILRB1, LILRB2, LILRB3, LTF, MAP3K8, MNDA, NCF2, NCF4, NLR4, NOD2, OLR1, OSM, PIK3API, PLA2G2A, PPBP, PTPRC, PTX3, RETN, RIPK3, RNASE2, RNASE3, S100A8, S100A9, SAA1, SIGLEC10, SIGLEC9, SLC11A1, TLR1, TLR2, TLR7, TLR8, TNFSF13B, TREM1
HSA-168249	Innate Immune System	53	1012	4.96E-21	ATP8B4, C1S, C3AR1, CAMP, CD14, CD33, CD53, CD93, CFD, CLEC4E, CLEC5A, CTSS, CYBB, DEFA3, FCER1G, FCGR2A, FCGR3A, FGL2, FPR2, GNLY, GPR84, HCK, IL1B, IRAK3, LAIR1, LILRB2, LILRB3, LTF, MAP3K8, MNDA, NCF2, NCF4, NLR4, NOD2, OLR1, PLA2G2A, PPBP, PTPRC, PTX3, RETN, RIPK3, RNASE2, RNASE3, S100A8, S100A9, SAA1, SIGLEC9, SLC11A1, TLR1, TLR2, TLR7, TLR8, TREM1
HSA-6798695	Neutrophil degranulation	33	471	6.75E-16	ATP8B4, C3AR1, CAMP, CD14, CD33, CD53, CD93, CFD, CLEC5A, CTSS, CYBB, FCER1G, FCGR2A, FGL2, FPR2, GPR84, LAIR1, LILRB2, LILRB3, LTF, MNDA, OLR1, PPBP, PTPRC, PTX3, RETN, RNASE2, RNASE3, S100A8, S100A9, SIGLEC9, SLC11A1, TLR2
HSA-198933	Immunoregulatory interactions between a Lymphoid and a non-Lymphoid cell	15	125	9.01E-10	CD300LF, CD33, CLEC2B, COL1A1, COL3A1, FCGR2B, FCGR3A, KLRB1, LAIR1, LILRB1, LILRB2, LILRB3, SIGLEC10, SIGLEC9, TREM1
HSA-449147	Signalling by Interleukins	22	439	9.29E-08	BATF, CCL2, CCR5, CXCL8, F13A1, HAVCR2, HCK, HMOX1, IL18, IL18RAP, IL1A, IL1B, IL1R2, IL2RA, IL33, IL6, IL7R, IRAK3, MAP3K8, NOD2, OSM, SAA1
HSA-1280218	Adaptive Immune System	28	733	1.32E-07	CD14, CD300LF, CD33, CD74, CLEC2B, COL1A1, COL3A1, CTSS, CYBB, FCGR2B, FCGR3A, FYB, IFI30, KLRB1, LAIR1, LILRB1, LILRB2, LILRB3, MAP3K8, NCF2, NCF4, PIK3API, PTPRC, SIGLEC10, SIGLEC9, TLR1, TLR2, TREM1
HSA-6803157	Antimicrobial peptides	11	87	2.01E-07	CAMP, DEFA3, GNLY, LTF, PLA2G2A, RNASE3, S100A8, S100A9, SLC11A1, TLR1, TLR2
HSA-168898	Toll-like Receptor Cascades	13	151	4.77E-07	CD14, CTSS, IRAK3, MAP3K8, NOD2, RIPK3, S100A8, S100A9, SAA1, TLR1, TLR2, TLR7, TLR8
HSA-1280215	Cytokine Signalling in Immune system	25	654	6.95E-07	BATF, CCL2, CCR5, CXCL8, F13A1, GBP5, HAVCR2, HCK, HMOX1, IFI30, IL18, IL18RAP, IL1A, IL1B, IL1R2, IL2RA, IL33, IL6, IL7R, IRAK3, MAP3K8, NOD2, OSM, SAA1, TNFSF13B
HSA-6785807	Interleukin-4 and Interleukin-13 signalling	11	106	9.26E-07	BATF, CCL2, CXCL8, F13A1, HMOX1, IL18, IL1A, IL1B, IL1R2, IL6
HSA-6783783	Interleukin-10 signalling	8	45	1.75E-06	CCL2, CCR5, CXCL8, IL18, IL1A, IL1B, IL1R2, IL6
HSA-373076	Class A/1 (Rhodopsin-like receptors)	15	311	3.05E-05	C3AR1, CCL13, CCR5, CMKLR1, CXCL11, CXCL8, CXCL9, FPR2, FPR3, GPR183, GPR65, P2RY12, PPBP, SAA1, TRH
HSA-202733	Cell surface interactions at the vascular wall	10	135	5.31E-05	CD2, CD48, CD74, CD84, COL1A1, FCER1G, OLR1, SLC7A7, THBD, TREM1
HSA-446652	Interleukin-1 family signalling	10	134	5.31E-05	IL18, IL18RAP, IL1A, IL1B, IL1R2, IL33, IRAK3, MAP3K8, NOD2, SAA1
HSA-5686938	Regulation of TLR by endogenous ligand	5	19	8.80E-05	CD14, S100A8, S100A9, TLR1, TLR2
HSA-375276	Peptide ligand-binding receptors	11	183	9.49E-05	C3AR1, CCL13, CCR5, CXCL11, CXCL8, CXCL9, FPR2, FPR3, PPBP, SAA1, TRH
HSA-2173782	Binding and Uptake of Ligands by Scavenger Receptors	6	40	1.40E-04	CD163, COL1A1, COL3A1, MARCO, MSRI, SAA1
HSA-109582	Haemostasis	19	601	2.90E-04	CD2, CD48, CD74, CD84, CFD, COL1A1, F13A1, F3, FCER1G, MMRN1, OLR1, P2RY12, PDPN, PLEK, PPBP, SLC7A7, SRGN, THBD, TREM1
HSA-380108	Chemokine receptors bind chemokines	6	48	3.20E-04	CCL13, CCR5, CXCL11, CXCL8, CXCL9, PPBP
HSA-418594	G alpha (i) signalling events	14	387	9.60E-04	C3AR1, CCL13, CCR5, CXCL11, CXCL8, CXCL9, FPR2, FPR3, GPR183, P2RY12, PPBP, RGS1, RGS18, SAA1
HSA-166016	Toll Like Receptor 4 (TLR4) Cascade	8	126	1.00E-03	CD14, IRAK3, MAP3K8, NOD2, RIPK3, SAA1, TLR1, TLR2
HSA-3000480	Scavenging by Class A Receptors	4	18	1.00E-03	COL1A1, COL3A1, MARCO, MSRI
HSA-1236975	Antigen processing-Cross presentation	7	96	1.10E-03	CD14, CTSS, CYBB, NCF2, NCF4, TLR1, TLR2
HSA-166058	MyD88:MAL(TIRAP) cascade initiated on plasma membrane	7	94	1.10E-03	CD14, IRAK3, MAP3K8, NOD2, SAA1, TLR1, TLR2
HSA-6799990	Metal sequestration by antimicrobial proteins	3	6	1.10E-03	LTF, S100A8, S100A9
HSA-9020702	Interleukin-1 signalling	7	98	1.10E-03	IL1A, IL1B, IL1R2, IRAK3, MAP3K8, NOD2, SAA1

HSA-444473	Formyl peptide receptors bind formyl peptides and many other ligands	3	7	1.40E-03	<i>FPR2, FPR3, SAA1</i>
HSA-448706	Interleukin-1 processing	3	7	1.40E-03	<i>IL18, IL1A, IL1B</i>
HSA-1236973	Cross-presentation of particulate exogenous antigens (phagosomes)	3	8	1.80E-03	<i>CYBB, NCF2, NCF4</i>
HSA-5602498	MyD88 deficiency (TLR2/4)	3	10	3.00E-03	<i>CD14, TLR1, TLR2</i>
HSA-1222556	ROS, RNS production in phagocytes	4	30	3.70E-03	<i>CYBB, NCF2, NCF4, SLC11A1</i>
HSA-2029481	FCGR activation	3	11	3.70E-03	<i>FCGR2A, FCGR3A, HCK</i>
HSA-5603041	IRAK4 deficiency (TLR2/4)	3	11	3.70E-03	<i>CD14, TLR1, TLR2</i>
HSA-76002	Platelet activation, signalling and aggregation	10	256	3.70E-03	<i>CFD, COL1A1, F13A1, FCER1G, MMRN1, P2RY12, PDPN, PLEK, PPBP, SRGN</i>
HSA-975138	TRAF6 mediated induction of NFkB and MAP kinases upon TLR7/8 or 9 activation	6	91	4.20E-03	<i>CD14, MAP3K8, NOD2, SAA1, TLR7, TLR8</i>
HSA-2022090	Assembly of collagen fibrils and other multimeric structures	5	60	4.40E-03	<i>COL1A1, COL3A1, CTSS, LOX, MMP7</i>
HSA-1679131	Trafficking and processing of endosomal TLR	3	13	4.60E-03	<i>CTSS, TLR7, TLR8</i>
HSA-5668599	RHO GTPases Activate NADPH Oxidases	3	13	4.60E-03	<i>CYBB, NCF2, NCF4</i>
HSA-114608	Platelet degranulation	6	125	1.70E-02	<i>CFD, F13A1, MMRN1, PLEK, PPBP, SRGN</i>
HSA-168164	Toll Like Receptor 3 (TLR3) Cascade	5	95	2.51E-02	<i>CD14, MAP3K8, NOD2, RIPK3, SAA1</i>
HSA-937061	TRIF(TICAM1)-mediated TLR4 signalling	5	96	2.56E-02	<i>CD14, MAP3K8, NOD2, RIPK3, SAA1</i>
HSA-1474244	Extracellular matrix organisation	9	298	2.66E-02	<i>ASPN, COL1A1, COL3A1, CTSS, EFEMP1, IBSP, LOX, MMP7, SPP1</i>
HSA-9012546	Interleukin-18 signalling	2	8	3.06E-02	<i>IL18, IL18RAP</i>
HSA-2562578	TRIF-mediated programmed cell death	2	9	3.65E-02	<i>CD14, RIPK3</i>
HSA-114604	GPVI-mediated activation cascade	3	34	4.10E-02	<i>COL1A1, FCER1G, PDPN</i>
HSA-3299685	Detoxification of Reactive Oxygen Species	3	35	4.35E-02	<i>CYBB, NCF2, NCF4</i>

TABLE S16. List of KEGG pathways significantly enriched in CD204^{HIGH} tumours relative to CD204^{LOW} tumours in the Gravendeel dataset

ID	KEGG Term description	Observed Gene count	Background gene count	FDR	Matching genes in the network
hsa04610	Complement and coagulation cascades	18	78	5.74E-15	<i>C1QA, C1QB, C1QC, C1R, C1S, C3, C3ARI, C5ARI, CFD, CFI, F13A1, ITGB2, PLA1, PLAUR, SERPINA1, SERPINE1, SERPING1, VSI1G4</i>
hsa05150	Staphylococcus aureus infection	16	51	5.74E-15	<i>C1QA, C1QB, C1QC, C1R, C1S, C3, C3ARI, C5ARI, CFD, CFI, FCGR2A, FCGR2B, FCGR3B, FPR1, FPR3, ITGB2</i>
hsa05133	Pertussis	14	74	7.52E-11	<i>C1QA, C1QB, C1QC, C1R, C1S, C3, CASP1, CD14, CXCL8, IL1B, IL6, ITGB2, LY96, SERPING1</i>
hsa05152	Tuberculosis	17	172	2.70E-09	<i>C3, CD14, CD74, CORO1A, CTSS, FCER1G, FCGR2A, FCGR2B, FCGR3B, IL10RA, IL18, IL1B, IL6, ITGB2, MRC1, TLR1, TLR2</i>
hsa04145	Phagosome	15	145	1.65E-08	<i>C1R, C3, CD14, CORO1A, CTSS, FCGR2A, FCGR2B, FCGR3B, ITGB2, MRC1, MSRI, NCF2, NCF4, OLR1, TLR2</i>
hsa04060	Cytokine-cytokine receptor interaction	19	263	1.92E-08	<i>CCL2, CCL20, CCL8, CCRI, CSF1R, CSF2RB, CXCL10, CXCL14, CXCL8, CXCR4, FAS, IL10RA, IL13RA1, IL18, IL1B, IL1R2, IL6, TNFSF10, TNFSF13B</i>
hsa05134	Legionellosis	10	54	6.63E-08	<i>C3, CASP1, CD14, CXCL8, HSPA6, IL18, IL1B, IL6, ITGB2, TLR2</i>
hsa05144	Malaria	9	47	2.83E-07	<i>CCL2, CXCL8, IL18, IL1B, IL6, ITGB2, SDC2, TLR2, VCAMI</i>
hsa05142	Chagas disease (American trypanosomiasis)	11	101	1.22E-06	<i>C1QA, C1QB, C1QC, C3, CCL2, CXCL8, FAS, IL1B, IL6, SERPINE1, TLR2</i>
hsa04064	NF-kappa B signalling pathway	10	93	4.90E-06	<i>BCL2A1, BLNK, CD14, CXCL8, IL1B, LY96, LYN, PLAU, TNFSF13B, VCAMI</i>
hsa05146	Amoebiasis	10	94	4.90E-06	<i>CD14, COL1A2, COL3A1, CXCL8, IL1B, IL1R2, IL6, ITGB2, SERPINB1, TLR2</i>
hsa05323	Rheumatoid arthritis	9	84	1.66E-05	<i>CCL2, CCL20, CXCL8, IL18, IL1B, IL6, ITGB2, TLR2, TNFSF13B</i>
hsa05140	Leishmaniasis	8	70	3.90E-05	<i>C3, FCGR2A, FCGR3B, IL1B, ITGB2, NCF2, NCF4, TLR2</i>
hsa04380	Osteoclast differentiation	10	124	3.97E-05	<i>BLNK, CSF1R, FCGR2A, FCGR2B, FCGR3B, IL1B, NCF2, NCF4, TREM2, TYROBP</i>
hsa04620	Toll-like receptor signalling pathway	9	102	5.84E-05	<i>CD14, CXCL10, CXCL8, IL1B, IL6, LY96, MAP3K8, TLR1, TLR2</i>
hsa04657	IL-17 signalling pathway	8	92	2.00E-04	<i>CCL2, CCL20, CXCL10, CXCL8, IL1B, IL6, SI00A8, SI00A9</i>
hsa05322	Systemic lupus erythematosus	8	94	2.20E-04	<i>C1QA, C1QB, C1QC, C1R, C1S, C3, FCGR2A, FCGR3B</i>
hsa04933	AGE-RAGE signalling pathway in diabetic complications	8	98	2.80E-04	<i>CCL2, COL1A2, COL3A1, CXCL8, IL1B, IL6, SERPINE1, VCAMI</i>
hsa04621	NOD-like receptor signalling pathway	10	166	3.20E-04	<i>CASP1, CCL2, CXCL8, GBP1, GBP2, GBP3, IL18, IL1B, IL6, NAMPT</i>
hsa05164	Influenza A	10	168	3.20E-04	<i>CASP1, CCL2, CXCL10, CXCL8, FAS, HSPA6, IL18, IL1B, IL6, TNFSF10</i>
hsa05418	Fluid shear stress and atherosclerosis	9	133	3.20E-04	<i>CAV1, CCL2, HMOX1, IL1B, IL1R2, MGST1, NCF2, SDC2, VCAMI</i>
hsa04668	TNF signalling pathway	8	108	4.30E-04	<i>CCL2, CCL20, CXCL10, FAS, IL1B, IL6, MAP3K8, VCAMI</i>
hsa04062	Chemokine signalling pathway	10	181	5.00E-04	<i>CCL2, CCL20, CCL8, CCRI, CXCL10, CXCL14, CXCL8, CXCR4, HCK, LYN</i>
hsa05020	Prion diseases	5	33	5.00E-04	<i>C1QA, C1QB, C1QC, IL1B, IL6</i>
hsa05143	African trypanosomiasis	5	34	5.20E-04	<i>FAS, IL18, IL1B, IL6, VCAMI</i>
hsa04640	Hematopoietic cell lineage	7	94	1.00E-03	<i>CD14, CD37, CD44, CSF1R, IL1B, IL1R2, IL6</i>
hsa05202	Transcriptional misregulation in cancer	9	169	1.30E-03	<i>BCL2A1, CD14, CSF1R, CXCL8, IGFBP3, IL1R2, IL6, NFKB1Z, PLA1</i>
hsa05132	Salmonella infection	6	84	3.50E-03	<i>CASP1, CD14, CXCL8, IL18, IL1B, IL6</i>
hsa05205	Proteoglycans in cancer	9	195	3.50E-03	<i>CAV1, CD44, FAS, FZD7, HCLSI, PLA1, PLAUR, SDC2, TLR2</i>
hsa04666	Fc gamma R-mediated phagocytosis	6	89	4.30E-03	<i>FCGR2A, FCGR2B, HCK, LYN, PTPRC, SCIN</i>
hsa04974	Protein digestion and absorption	6	90	4.40E-03	<i>COL1A2, COL3A1, COL5A2, COL6A3, SLC16A10, SLC7A7</i>
hsa04623	Cytosolic DNA-sensing pathway	5	62	5.20E-03	<i>CASP1, CXCL10, IL18, IL1B, IL6</i>
hsa05162	Measles	7	133	5.80E-03	<i>FAS, FCGR2B, HSPA6, IL1B, IL6, TLR2, TNFSF10</i>
hsa05167	Kaposi's sarcoma-associated herpesvirus infection	8	183	8.00E-03	<i>C3, CCRI, CXCL8, FAS, HCK, IL6, LYN, RCAN1</i>
hsa04611	Platelet activation	6	123	1.75E-02	<i>COL1A2, COL3A1, FCER1G, FCGR2A, LYN, VAMP8</i>
hsa04650	Natural killer cell mediated cytotoxicity	6	124	1.77E-02	<i>FAS, FCER1G, FCGR3B, ITGB2, TNFSF10, TYROBP</i>

hsa04210	Apoptosis	6	135	2.55E-02	<i>BCL2A1, CSF2RB, CTSC, CTSS, FAS, TNFSF10</i>
hsa05168	Herpes simplex infection	7	181	2.61E-02	<i>C3, CCL2, CD74, FAS, IL1B, IL6, TLR2</i>
hsa00590	Arachidonic acid metabolism	4	61	2.76E-02	<i>ALOX5, GPX8, HPGDS, PLA2G2A</i>
hsa05321	Inflammatory bowel disease (IBD)	4	62	2.84E-02	<i>IL18, IL1B, IL6, TLR2</i>
hsa04612	Antigen processing and presentation	4	66	3.40E-02	<i>CD74, CTSS, HSPA6, IFI30</i>
hsa04664	Fc epsilon RI signalling pathway	4	67	3.49E-02	<i>ALOX5, ALOX5AP, FCER1G, LYN</i>
hsa05145	Toxoplasmosis	5	109	3.81E-02	<i>ALOX5, HSPA6, IL10RA, LY96, TLR2</i>
hsa05332	Graft-versus-host disease	3	36	3.81E-02	<i>FAS, IL1B, IL6</i>
hsa04662	B cell receptor signalling pathway	4	71	3.93E-02	<i>BLNK, FCGR2B, LYN, PIK3API</i>
hsa04670	Leukocyte transendothelial migration	5	112	4.00E-02	<i>CXCR4, ITGB2, NCF2, NCF4, VCAM1</i>

TABLE S17. List of Reactome pathways significantly enriched in CD204^{HIGH} tumours relative to CD204^{LOW} tumours in the Gravendeel dataset

ID	Reactome Term description	Observed Gene count	Background gene count	FDR	Matching genes in the network
HSA-168256	Immune System	102	1925	5.04E-39	<i>ALOX5, ANXA2, ATP8B4, BLNK, BST2, C1QA, C1QB, C1QC, C1R, C1S, C3, C3AR1, C5ARI, CASP1, CCL2, CCL20, CCRI, CD14, CD300A, CD44, CD58, CD74, CEBPD, CFD, CFI, CH3LI, CLEC5A, COL1A2, COL3A1, CSF1, CSF2RB, CTSC, CTSS, CXCL10, CXCL8, F13A1, FABP5, FBXO32, FCER1G, FCGR1B, FCGR2A, FCGR3B, FPR1, FYB, GBP2, GLIPR1, GPR84, HAVCR2, HCK, HMOX1, HSPA6, IFI30, IL10RA, IL13RA1, IL18, IL1B, IL1R2, IL6, ITGB2, LAIR1, LTF, LY86, LY96, LYN, LYZ, MAP3K8, MGST1, MND, MRC1, NCF2, NCF4, NCKAP1L, NPC2, OLR1, PIK3API, PLA2G2A, PLAU, PLAU, PTPRC, PTX3, RNASE2, RNASE6, S100A11, S100A8, S100A9, SERPINA1, SERPING1, SIGLEC10, SLC2A5, TIMP1, TLR1, TLR2, TNFSF13B, TREM1, TREM2, TYROBP, VAMP8, VCAM1</i>
HSA-168249	Innate Immune System	68	1012	8.36E-30	<i>ALOX5, ANXA2, ATP8B4, BST2, C1QA, C1QB, C1QC, C1R, C1S, C3, C3AR1, C5ARI, CASP1, CD14, CD300A, CD44, CD58, CFD, CFI, CH3LI, CLEC5A, CTSC, CTSS, FABP5, FCER1G, FCGR2A, FCGR3B, FPR1, GLIPR1, GPR84, HCK, HSPA6, IL1B, ITGB2, LAIR1, LTF, LY86, LY96, LYN, LYZ, MAP3K8, MGST1, MND, NCF2, NCF4, NCKAP1L, NPC2, OLR1, PLA2G2A, PLAU, PLAU, PTPRC, PTX3, RNASE2, RNASE6, S100A11, S100A8, S100A9, SERPINA1, SERPING1, SERPING1, SLC2A5, TIMP1, TLR2, TREM1, TREM2, TYROBP, VAMP8</i>
HSA-6798695	Neutrophil degranulation	47	471	1.37E-26	<i>ALOX5, ANXA2, ATP8B4, BST2, C3, C3AR1, C5ARI, CD14, CD300A, CD44, CD58, CFD, CH3LI, CLEC5A, CTSC, CTSS, FABP5, FCER1G, FCGR2A, FCGR3B, FPR1, GLIPR1, GPR84, HSPA6, ITGB2, LAIR1, LTF, LY86, LY96, LYN, LYZ, MGST1, MND, NCKAP1L, NPC2, OLR1, PLAU, PLAU, PTPRC, PTX3, RNASE2, S100A11, S100A8, S100A9, SERPINA1, SERPING1, SLC2A5, TLR2, TYROBP, VAMP8</i>
HSA-1280215	Cytokine Signalling in Immune system	37	654	5.00E-13	<i>ALOX5, ANXA2, BLNK, BST2, CASP1, CCL2, CCL20, CCRI, CD44, CEBPD, COL1A2, CSF1R, CSF2RB, CXCL10, CXCL8, F13A1, FCGR1B, FPR1, GBP1, GBP2, GBB3, HAVCR2, HCK, HMOX1, IFI30, IL10RA, IL13RA1, IL18, IL1B, IL1R2, IL6, ITGB2, LYN, MAP3K8, TIMP1, TNFSF13B, VCAM1</i>
HSA-449147	Signalling by Interleukins	29	439	1.28E-11	<i>ALOX5, ANXA2, BLNK, CASP1, CCL2, CCL20, CCRI, CEBPD, COL1A2, CSF1R, CSF2RB, CXCL10, CXCL8, F13A1, FPR1, HAVCR2, HCK, HMOX1, IL10RA, IL13RA1, IL18, IL1B, IL1R2, IL6, ITGB2, LYN, MAP3K8, TIMP1, VCAM1</i>
HSA-6783783	Interleukin-10 signalling	12	45	1.28E-10	<i>CCL2, CCL20, CCRI, CXCL10, CXCL8, FPR1, IL10RA, IL18, IL1B, IL1R2, IL6, TIMP1</i>
HSA-6785807	Interleukin-4 and Interleukin-13 signalling	14	106	6.60E-09	<i>ALOX5, CCL2, CEBPD, COL1A2, CXCL8, F13A1, HMOX1, IL13RA1, IL18, IL1B, IL6, ITGB2, TIMP1, VCAM1</i>
HSA-1280218	Adaptive Immune System	32	733	1.35E-08	<i>BLNK, C3, CD14, CD300A, CD74, COL1A2, COL3A1, CTSC, CTSS, FBXO32, FCGR1B, FCGR2B, FYB, IFI30, ITGB2, LAIR1, LY96, LYN, MAP3K8, MRC1, NCF2, NCF4, PIK3API, PTPRC, SIGLEC10, TLR1, TLR2, TREM1, TREM2, TYROBP, VAMP8, VCAM1</i>
HSA-166658	Complement cascade	11	56	1.35E-08	<i>C1QA, C1QB, C1QC, C1R, C1S, C3, C3AR1, C5ARI, CFD, CFI, SERPING1</i>
HSA-977606	Regulation of Complement cascade	10	47	3.86E-08	<i>C1QA, C1QB, C1QC, C1R, C1S, C3, C3AR1, C5ARI, CFI, SERPING1</i>
HSA-202733	Cell surface interactions at the vascular wall	13	135	6.61E-07	<i>CAV1, CD44, CD58, CD74, COL1A2, FCER1G, ITGB2, LYN, OLR1, SDC2, SLC16A3, SLC7A7, TREM1</i>
HSA-166663	Initial triggering of complement	7	21	8.47E-07	<i>C1QA, C1QB, C1QC, C1R, C1S, C3, CFD</i>
HSA-198933	Immunoregulatory interactions between a Lymphoid and a non-Lymphoid cell	12	125	2.08E-06	<i>C3, CD300A, COL1A2, COL3A1, FCGR2B, ITGB2, LAIR1, SIGLEC10, TREM1, TREM2, TYROBP, VCAM1</i>
HSA-173623	Classical antibody-mediated complement activation	5	7	4.46E-06	<i>C1QA, C1QB, C1QC, C1R, C1S</i>
HSA-109582	Haemostasis	24	601	7.29E-06	<i>ANXA2, CAV1, CD44, CD58, CD74, CFD, COL1A2, F13A1, FCER1G, ITGB2, LYN, OLR1, PDPN, PLAU, PLAU, SDC2, SERPINA1, SERPINE1, SERPING1, SLC16A3, SLC7A7, SRGN, TIMP1, TREM1, CD14, LY96, S100A8, S100A9, TLR1, TLR2</i>
HSA-5686938	Regulation of TLR by endogenous ligand	6	19	8.70E-06	<i>CD14, CTSS, FCGR1B, LY96, MRC1, NCF2, NCF4, TLR1, TLR2, VAMP8</i>
HSA-1236975	Antigen processing-Cross presentation	10	96	1.03E-05	<i>ADAM9, CD44, COL1A2, COL3A1, COL5A2, COL6A3, CTSS, EFEMP1, FBLN5, IBSP, ITGB2, LOX, SDC2, SERPINE1, TIMP1, VCAM1</i>
HSA-1474244	Extracellular matrix organisation	16	298	1.84E-05	<i>ADAM9, CD44, COL1A2, COL3A1, COL5A2, COL6A3, CTSS, EFEMP1, FBLN5, IBSP, ITGB2, LOX, SDC2, SERPINE1, TIMP1, VCAM1</i>
HSA-8957275	Post-translational protein phosphorylation	9	106	1.60E-04	<i>C3, CP, CYR61, IGF1R3, IL6, PRSS23, SDC2, SERPINA1, TIMP1</i>
HSA-216083	Integrin cell surface interactions	8	83	2.10E-04	<i>CD44, COL1A2, COL3A1, COL5A2, COL6A3, IBSP, ITGB2, VCAM1</i>
HSA-6803157	Antimicrobial peptides	8	87	2.70E-04	<i>LTF, LYZ, PLA2G2A, RNASE6, S100A8, S100A9, TLR1, TLR2</i>
HSA-375276	Peptide ligand-binding receptors	11	183	3.00E-04	<i>C3, C3AR1, C5ARI, CCL20, CCRI, CXCL10, CXCL8, CXCR4, FPR1, FPR3, GPR37</i>

HSA-5602498	MyD88 deficiency (TLR2/4)	4	10	3.00E-04	10	CD14, LY96, TLR1, TLR2
HSA-168898	Toll-like Receptor Cascades	10	151	3.10E-04	151	CD14, CTSS, ITGB2, LY86, LY96, MAP3K8, S100A8, S100A9, TLR1, TLR2
HSA-5603041	IRAK4 deficiency (TLR2/4)	4	11	3.50E-04	11	CD14, LY96, TLR1, TLR2
HSA-381426	Regulation of Insulin-like Growth Factor (IGF) transport and uptake by Insulin-like Growth Factor Binding Proteins (IGFBPs)	9	123	3.60E-04	123	C3, CP, CYR61, IGFBP3, IL6, PRSS23, SDC2, SERPINAI1, TIMP1
HSA-75205	Caspase activation via Death Receptors in the presence of ligand	4	13	5.60E-04	13	ANXA2, PLAU, PLAUR, SERPINE1
HSA-140534	G alpha (i) signalling events	4	15	8.70E-04	15	CD14, FAS, LY96, TNFSF10
HSA-418594	Class A/1 (Rhodopsin-like receptors)	15	387	9.80E-04	387	C3, C3ARI, C5ARI, CCL20, CCRI, CXCL10, CXCL8, CXCR4, FPRI, FPR3, GPR183, GPR37, RGS1, RGS18, SDC2
HSA-373076	Interferon gamma signalling	13	311	1.40E-03	311	C3, C3ARI, C5ARI, CCL20, CCRI, CXCL10, CXCL8, CXCR4, FPRI, FPR3, GPR183, GPR37, GPR65
HSA-877300	Assembly of collagen fibrils and other multimeric structures	7	86	1.40E-03	86	CD44, FCGR1B, GBP1, GBP2, GBP3, IFI50, VCAMI
HSA-2022090	Metal sequestration by antimicrobial proteins	6	60	1.50E-03	60	COL1A2, COL3A1, COL5A2, COL6A3, CTSS, LOX
HSA-6799990	Interleukin-1 processing	3	6	1.50E-03	6	LTF, S100A8, S100A9
HSA-448706	Degradation of the extracellular matrix	3	7	2.10E-03	7	CASPI, IL18, IL1B
HSA-1474228	GPCR ligand binding	8	139	3.40E-03	139	ADAM9, CD44, COL1A2, COL3A1, COL5A2, COL6A3, CTSS, TIMP1
HSA-500792	Platelet activation, signalling and aggregation	15	443	3.40E-03	443	ADAM, C3, C3ARI, C5ARI, CCL20, CCRI, CXCL10, CXCL8, CXCR4, FPRI, FPR3, FZD7, GPR183, GPR37, GPR65
HSA-76002	ECM proteoglycans	11	256	3.40E-03	256	CFD, COL1A2, F13A1, FCER1G, LYN, PDPN, SERPINA1, SERPINE1, SERPING1, SRGN, TIMP1
HSA-3000178	Chemokine receptors bind chemokines	6	75	3.60E-03	75	COL1A2, COL3A1, COL5A2, COL6A3, IBSP, SERPINE1
HSA-380108	Syndecan interactions	5	48	3.60E-03	48	CCL20, CCRI, CXCL10, CXCL8, CXCR4
HSA-3000170	FCGR activation	4	26	3.70E-03	26	COL1A2, COL3A1, COL5A2, SDC2
HSA-2029481	Platelet degranulation	3	11	4.90E-03	11	FCGR2A, HCK, LYN
HSA-114608	Toll Like Receptor 4 (TLR4) Cascade	7	125	7.90E-03	125	CFD, F13A1, SERPINA1, SERPINE1, SERPING1, SRGN, TIMP1
HSA-166016	GPVI-mediated activation cascade	7	126	8.00E-03	126	CD14, ITGB2, LY86, LY96, MAP3K8, TLR1, TLR2
HSA-2172127	DAP12 interactions	4	34	8.10E-03	34	COL1A2, FCER1G, LYN, PDPN
HSA-391160	Signal regulatory protein family interactions	4	34	8.10E-03	34	CLEC5A, TREM1, TREM2, TYROBP
HSA-75892	Platelet Adhesion to exposed collagen	3	14	8.10E-03	14	FYB, SKAP2, TYROBP
HSA-1442490	Collagen degradation	3	15	8.90E-03	15	COL1A2, FCER1G, LYN
HSA-2173782	Binding and Uptake of Ligands by Scavenger Receptors	5	64	9.60E-03	64	ADAM9, COL1A2, COL3A1, COL5A2, COL6A3
HSA-3000480	Scavenging by Class A Receptors	4	40	1.29E-02	40	CD163, COL1A2, COL3A1, MSRI
HSA-419037	NCAM1 interactions	3	18	1.34E-02	18	COL1A2, COL3A1, MSRI
HSA-416700	Other semaphorin interactions	4	42	1.47E-02	42	COL3A1, COL5A2, COL6A3, ST8SIA4
HSA-913531	Interferon Signalling	3	19	1.49E-02	19	PTPRC, TREM2, TYROBP
HSA-8948216	Collagen chain trimerization	8	189	1.52E-02	189	BST2, CD44, FCGR1B, GBP1, GBP2, GBP3, IFI30, VCAMI
HSA-912631	Regulation of signalling by CBL	4	44	1.63E-02	44	COL1A2, COL3A1, COL5A2, COL6A3
HSA-173736	Alternative complement activation	4	21	1.83E-02	21	BLNK, HCK, LYN
HSA-512988	Interleukin-3, Interleukin-5 and GM-CSF signalling	3	5	1.89E-02	5	C3, CFD
HSA-1236974	ER-Phagosome pathway	2	47	1.94E-02	47	BLNK, CSF2RB, HCK, LYN
HSA-1614517	Sulfide oxidation to sulfate	4	80	2.05E-02	80	CD14, LY96, TLR1, TLR2, VAMP8
HSA-2142700	Synthesis of Lipoxins (LX)	2	6	2.39E-02	6	SQDL, TSTD1
HSA-210991	Basigin interactions	2	6	2.39E-02	6	ALOX5, ALOX5AP
HSA-983169	Class I MHC mediated antigen processing & presentation	3	25	2.61E-02	25	CAVI, SLC16A3, SLC7A7
HSA-444473	Formyl peptide receptors bind formyl peptides and many other ligands	11	365	2.76E-02	365	CD14, CTSS, FBXO32, FCGR1B, LY96, MRC1, NCF2, NCF4, TLR1, TLR2, VAMP8
HSA-1236973	Cross-presentation of particulate exogenous antigens (phagosomes)	2	7	2.87E-02	7	FPRI, FPR3
		2	8	3.51E-02	8	NCF2, NCF4

HSA-166058	MyD88:MAL(TIRAP) cascade initiated on plasma membrane	5	94	3.51E-02	<i>CD14, LY96, MAP3K8, TLR1, TLR2</i>
HSA-2142753	Arachidonic acid metabolism	4	59	3.51E-02	<i>ALOX5, ALOX5AP, CYP11B1, HPGDS</i>
HSA-446652	Interleukin-1 family signalling	6	134	3.51E-02	<i>ALOX5, CASP1, IL18, IL1B, IL1R2, MAP3K8</i>
HSA-8874081	MET activates PTK2 signalling	3	29	3.51E-02	<i>COL1A2, COL3A1, COL5A2</i>
HSA-9012546	Interleukin-18 signalling	2	8	3.51E-02	<i>ALOX5, IL18</i>
HSA-983695	Antigen activates B Cell Receptor (BCR) leading to generation of second messengers	3	30	3.55E-02	<i>BLNK, LYN, PIK3AP1</i>
HSA-2142688	Synthesis of 5- <i>e</i> -icosatetraenoic acids	2	9	3.63E-02	<i>ALOX5, ALOX5AP</i>
HSA-2562578	TRIF-mediated programmed cell death	2	9	3.63E-02	<i>CD14, LY96</i>
HSA-3371378	Regulation by <i>e</i> -FLIP	2	10	4.23E-02	<i>FAS, TNFSF10</i>
HSA-5218900	CASP8 activity is inhibited	2	10	4.23E-02	<i>FAS, TNFSF10</i>
HSA-69416	Dimerisation of procaspase-8	2	10	4.23E-02	<i>FAS, TNFSF10</i>
HSA-3299685	Detoxification of Reactive Oxygen Species	3	35	4.70E-02	<i>GPX8, NCF2, NCF4</i>

TUMOUR-ASSOCIATED CD204+ MICROGLIA/MACROPHAGES ACCUMULATE IN PERIVASCULAR AND PERINECROTIC NICHES AND CORRELATE WITH AN INTERLEUKIN-6 ENRICHED INFLAMMATORY PROFILE IN GLIOBLASTOMA

Mia D. Sørensen^{1,2}, Bjarne W. Kristensen¹⁻⁴

¹ Department of Pathology, Odense University Hospital, Odense, Denmark

² Department of Clinical Research, University of Southern Denmark, Odense, Denmark

³ Department of Pathology, Rigshospitalet, Copenhagen University Hospital, Copenhagen, Denmark

⁴ Department of Clinical Medicine and Biotech Research and Innovation Center (BRIC), University of Copenhagen, Copenhagen, Denmark.

Data S1

Supplementary materials and methods

Double immunohistochemistry

Formalin-fixed, paraffin-embedded tissue was sliced by a microtome into three- μ M-thick sections which were then mounted on FLEX IHC slides (Dako, Glostrup, Denmark). The tissue sections were subjected to deparaffinisation, retrieval and antigen-antibody detection and visualisation as specified below.

Immunostainings with unconjugated primary antibodies against CD44, BMI1, SOX2, nestin, and PDPN were performed on the BenchMark IHC/ISH staining system (Ventana Medical Systems, Inc., Tucson, AZ, USA) using the ultraView Universal HRP-DAB detection kit (Ventana) containing 5 pre-diluted and ready-to-use dispensers (DAB Inhibitor, HRP Multimer, DAB Chromogen, DAB H₂O₂, Copper) plus amplification (SOX2, and BMI1) as follows: sections were dried at 75°C for 4 minutes and deparaffinised at 72°C. The staining procedure included pre-treatment with cell conditioning buffer 1 (CC1) at 99°C (CC1std99) for 64 minutes and blockade of endogenous peroxidase with H₂O₂. Slides were then incubated with the respective antibody for 32 min at 36°C. For staining with antibodies against MS1 and CD133, sections were deparaffinised with xylene and rehydrated in ethanol followed by heat-induced epitope retrieval in TEG buffer (10 mmol/L Tris-base and 0.5 mmol/L ethylene glycol tetraacetic acid (EGTA), pH 9), and quenching of endogenous peroxidase activity with H₂O₂. The staining procedure was done on the Dako Autostainer Plus system (Agilent Technologies, Santa Clara, CA, USA). For CD133 antigen catalysed signal amplification (CSA) detection, sections were incubated with protein block to suppress non-specific binding of subsequent reagents, followed by sequential incubation with mouse anti-human CD133 antibody, anti-mouse immunoglobulins-HRP, fluorescyl-tyramide H₂O₂, and anti-fluorescein-HRP (Agilent). For MS1, sections were incubated with primary antibody and the antibody-antigen complex was detected using EnVision+ HRP-polymer (Agilent). Next, a second round of heat deactivation and endogen peroxidase blocking was performed followed by incubation with an IBA1 or CD204 antibody on the BenchMark Ultra IHC/ISH staining system using the ultraView Universal Alkaline Phosphatase Red Detection Kit plus amplification (Ventana).

The double immunohistochemical staining with primary antibodies against GAL9 and TIM3 was conducted on the DISCOVERY ULTRA staining system (Ventana). In brief, after deparaffinisation, sections were subjected to epitope retrieval in CC1 for 32 min at 100 °C, inactivation of endogenous peroxidase and incubation with primary antibody against TIM3 for 60 min at 36 °C followed by detection with DISCOVERY anti-rabbit HQ and DISCOVERY anti-HQ HRP using DISCOVERY Purple kit as chromogen. Next, slides were denatured for 8 min in cell conditioning buffer 2 at 100 °C followed by incubation with the second primary antibody against GAL9 for 32 min at 36 °C which was detected using DISCOVERY anti-rabbit-NP and DISCOVERY anti-NP AP using DISCOVERY Yellow kit as chromogen.

The tissue sections were counterstained using hematoxylin II and bluing reagent (Ventana protocols), and coverslips were mounted with a Tissue-Tek® Film® Coverslipper (Sakura, Alpen aan den Rijn, the Netherlands) or manually using Pertex® mounting medium (#00811, HistoLab Products AB, Gothenburg, Sweden).

Information regarding primary antibodies, clone, epitope retrieval procedures, dilutions, incubation times, and detection platforms is outlined in **Table S2**.

Automated quantitative digital image analysis

The stained slides were digitised using a NanoZoomer 2.0-HT whole slide scanner (Hamamatsu Photonics, Hamamatsu, Japan) equipped with a 40x objective. For the H&E as well as the conventional, single immunohistochemistry stainings, automated digital image analysis and quantification was performed using the Visiopharm Image Analysis Software, version 2018.4 (Hoersholm, Denmark) as previously reported [1-3]. Tissue slides were prepared for image processing by manually outlining sampling regions containing viable tumour tissue (e.g. the regions of interest). Sample images were then collected by systematic uniform random sampling at 20x magnification ensuring at least five usable images per tumour as previously

described [1]. Sample images were reviewed, and areas with staining artefacts, normal brain tissue, peripheral tumour, necrosis, and larger blood vessels were manually excluded from the region of interest. Pixel-based algorithms were developed to detect, classify, and quantify the positive staining signal of interest. The algorithms were designed as threshold-based classifications (IBA1, CD204, BIRC3, GAL3, IL6, NOD2, and TNFAIP3), or membrane classifications (CD44, ICAM1, and PD-L1) using the haematoxylin-3,3'-Diaminobenzidine (HDAB)-DAB colour deconvolution band/feature. The haematoxylin-DAB was employed as a supplement feature to optimise the detection of BIRC3 signal. The H&E-haematoxylin colour band was used to detect the blue/purple-stained nuclei in the haematoxylin-eosin stains resulting in a quantitative estimate for cell density (cellularity). For each staining, the output variable was area fraction which was defined as the positive area divided by the total tumour area.

References

- 1 Sorensen MD, Dahlrot RH, Boldt HB, Hansen S, Kristensen BW. Tumour-associated microglia/macrophages predict poor prognosis in high-grade gliomas and correlate with an aggressive tumour subtype. *Neuropathology and applied neurobiology* 2018; 44: 185-206
- 2 Rosager AM, Sorensen MD, Dahlrot RH, Boldt HB, Hansen S, Lathia JD, Kristensen BW. Expression and prognostic value of JAM-A in gliomas. *Journal of neuro-oncology* 2017; 135: 107-17
- 3 Ramachandran RK, Sorensen MD, Aaberg-Jessen C, Hermansen SK, Kristensen BW. Expression and prognostic impact of matrix metalloproteinase-2 (MMP-2) in astrocytomas. *PloS one* 2017; 12: e0172234

13.3 Manuscript III

“D-2-Hydroxyglutarate Is an Intercellular Mediator in IDH-Mutant Gliomas Inhibiting Complement and T Cells”

D-2-Hydroxyglutarate Is an Intercellular Mediator in IDH-Mutant Gliomas Inhibiting Complement and T Cells



Lingjun Zhang¹, Mia D. Sorensen^{2,3}, Bjarne W. Kristensen^{2,3}, Guido Reifenberger⁴, Thomas M. McIntyre⁵, and Feng Lin¹

Abstract

Purpose: Somatic mutations in the isocitrate dehydrogenase (IDH)-1 and -2 genes are remarkably penetrant in diffuse gliomas. These highly effective gain-of-function mutations enable mutant IDH to efficiently metabolize isocitrate to D-2-hydroxyglutarate (D 2-HG) that accumulates to high concentrations within the tumor microenvironment. D 2-HG is an intracellular effector that promotes tumor growth through widespread epigenetic changes in IDH-mutant tumor cells, but its potential role as an intercellular immune regulator remains understudied.

Experimental Design: Complement activation and CD4⁺, CD8⁺, or FOXP3⁺ T-cell infiltration into primary tumor tissue were determined by immunohistochemistry using sections from 72 gliomas of World Health Organization (WHO) grade III and IV with or without IDH mutations.

Ex vivo experiments with D 2-HG identified immune inhibitory mechanisms.

Results: IDH mutation associated with significantly reduced complement activation and decreased numbers of tumor-infiltrating CD4⁺ and CD8⁺ T cells with comparable FOXP3⁺/CD4⁺ ratios. D 2-HG potently inhibited activation of complement by the classical and alternative pathways, attenuated complement-mediated glioma cell damage, decreased cellular C3b(iC3b) opsonization, and impaired complement-mediated phagocytosis. Although D 2-HG did not affect dendritic cell differentiation or function, it significantly inhibited activated T-cell migration, proliferation, and cytokine secretion.

Conclusions: D 2-HG suppresses the host immune system, potentially promoting immune escape of IDH-mutant tumors. *Clin Cancer Res*; 24(21); 5381–91. ©2018 AACR.

Introduction

Site-specific mutations of isocitrate dehydrogenase (IDH)-1 or -2 are present in 80% to 90% of patients with diffuse WHO grade II–III gliomas and a small subset of patients with WHO grade IV glioblastomas (1–4). IDH mutations are also present but less penetrant in acute myeloid leukemia (5), angioimmunoblastic T-cell lymphoma (6), and chondrosarcomas (7). However, precisely how IDH mutations might confer an advantage to tumorigenesis is not well understood.

Missense mutations of R132 in IDH-1 or R172 in IDH-2 that change this arginyl residue to any of several other residues confer a remarkable gain of function to IDH catalytic activity enabling mutant enzyme to stereospecifically reduce isocitrate to D-2-hydroxyglutarate (D 2-HG; refs. 2, 8, 9) rather than its normal product α -ketoglutarate. D 2-HG accumulates to 30 mmol/L

within (10) and 3 mmol/L surrounding (11) gliomas carrying a mutant IDH-1 or IDH-2 gene. D 2-HG alters tumor cell metabolism and epigenetic regulation (12–14), but the full significance of IDH mutations or more precisely the unique nature of excessive D 2-HG accumulation is undefined. For instance, we now know that tumor IDH mutation tightly correlates to the absence of microthrombi within the tumor vasculature of diffuse gliomas, and that D 2-HG directly suppresses *ex vivo* activation and thrombosis of purified platelets (15). Potentially, then, tumor-derived D 2-HG functions as an intercellular mediator that affects nonneoplastic cells of the tumor microenvironment. Tumor-infiltrating CD4⁺ helper and CD8⁺ cytotoxic T cells are present in the glioma microenvironment (16), and mutant IDH associates with fewer infiltrating immune cells, including macrophages, T cells, and B cells, in tumors (17–19), and IDH-mutant gliomas may escape from natural killer (NK) cell immune surveillance by downregulation of their NK group 2, member D (NKG2D) ligand expression (20).

Complement is a key component of the innate immune system that defends against pathogen invasion and clears apoptotic cells and immune complexes. When activated by either classical, alternative, or lectin pathways, activated complement forms membrane attack complex (MAC) pores that lyse targeted cells (21). Complement activation also leads the deposition of C3b (iC3b) fragments on target cells for "opsonization" that facilitates phagocytosis through interactions with C3b(iC3b) receptors (C3aR) expressed on phagocytes. Recent studies (22–24) also found that complement directly regulates T-cell function, in part through signaling of G-protein coupled C3aR and C5aR receptors on antigen-presenting cells and T cells.

¹Department of Immunology, Lerner Research Institute, Cleveland Clinic, Cleveland, Ohio. ²Department of Pathology, Odense University Hospital, Odense C, Denmark. ³Department of Clinical Research, University of Southern Denmark, Odense C, Denmark. ⁴Department of Neuropathology, Heinrich Heine University, Düsseldorf, Germany. ⁵Department of Cellular and Molecular Medicine, Lerner Research Institute, Cleveland Clinic, Cleveland, Ohio.

Note: Supplementary data for this article are available at Clinical Cancer Research Online (<http://clincancerres.aacrjournals.org/>).

Corresponding Author: Feng Lin, Cleveland Clinic, Cleveland, OH 44095. Phone: 2164456637; E-mail: linf2@ccf.org

doi: 10.1158/1078-0432.CCR-17-3855

©2018 American Association for Cancer Research.

Translational Relevance

D-2-Hydroxyglutarate produced by gliomas expressing mutant isocitrate dehydrogenase (IDH) is an intercellular modulator inhibiting innate and adaptive immune systems. These new insights could aid the development of better immunotherapy for tumors with mutant IDH.

Here, we determined whether the immunologic microenvironment of adult diffuse gliomas is affected by IDH mutational status. We find that IDH mutation associates with reduced complement activation, decreased CD4⁺, FOXP3⁺, and CD8⁺ T-cell infiltration in gliomas *in situ*, and that D 2-HG directly suppresses these essential elements of both innate and adaptive immunity.

Materials and Methods

Expanded Materials and Methods are presented in a supplement to this article.

Patient tissue

Tissues were obtained from patients diagnosed with primary high-grade astrocytoma between 1997 and 2017. All tumor samples were classified or reclassified according to the WHO Classification 2016 (25). Patients underwent initial surgery at the Department of Neurosurgery, Odense University Hospital, Denmark, or at the Department of Neurosurgery, Heinrich Heine University, Düsseldorf, Germany. None of the patients had received treatment prior to surgery. Of the 72 patients included in the current study, 23 were WHO grade III anaplastic astrocytomas and IDH-mutant (mIDH), 16 were WHO grade III anaplastic astrocytomas and IDH-wild-type (wtIDH), 14 were WHO grade IV glioblastomas with mIDH, and 19 were WHO grade IV glioblastomas with wtIDH. IDH status was determined by immunohistochemistry using an antibody against the most common IDH-1-R132H mutation (clone H14, Dianova) using the BenchMark Ultra IHC/ISH staining system (Ventana Medical Systems, Inc.; ref. 26), and/or by next-generation sequencing as previously described (27). Of the 37 detected IDH mutations, 31 were IDH-1-R132H, three were IDH-1-R132C, and one each corresponded to IDH-1-R132S, IDH-1-R132G, or IDH-2 R140W.

Additionally, double immunohistochemistry with antibodies against C3/C3b and the tumor marker oligodendrocyte transcription factor (OLIG2) was performed on six of the 72 astrocytomas included in the patient cohort (one mIDH and one wtIDH anaplastic astrocytoma, two mIDH and two wtIDH glioblastomas) to verify and localize deposition of C3 on tumor cells.

Complement activation pathway assays

The potential effects of D 2-HG in inhibiting the classical and alternative pathways of complement activation were analyzed using antibody-sensitized sheep erythrocytes (E^{shA}) or rabbit erythrocytes (E^{rabb}) following well-established protocols (28).

Complement convertase assays

Complement convertases of the classical and alternative pathways were analyzed following a published protocol using E^{shA} or E^{rabb} (29, 30).

Complement-mediated tumor cytotoxicity assay

Complement-mediated brain tumor cell damage assay was done based on the measurement of lactate dehydrogenase (LDH) leakage using a commercial kit (Sigma-Aldrich).

Complement C3b deposition assay

E^{shA} were incubated with 2% C5-depleted serum in gelatin veronal buffer with calcium and magnesium (GVB⁺⁺) containing defined concentrations of D 2-HG. For negative controls, 5 mmol/L EDTA was added to the buffer. After 10 minutes at 37°C, E^{shA} were washed and stained with an Alexa Fluor 488-conjugated anti-human C3 antibody (MP Biomedicals) for additional 30 minutes on ice, followed by flow cytometry analysis.

Complement opsonization-mediated phagocytosis assay

The myeloid cell line U937 was differentiated into macrophages for the complement opsonization-mediated phagocytosis assay based on a published protocol (31, 32).

T-cell inhibition and migration assays

Nylon wool-enriched T cells, or negative selection-purified CD4⁺ and CD8⁺ T cells from WT mice were activated by monoclonal antibodies against CD3 and CD28, then cultured in different polarization conditions in the presence of different concentrations of D 2-HG. The inhibitory effect of D 2-HG was assessed by measuring the proliferation of the activated T cells using carboxyfluorescein succinimidyl ester (CFSE) dilution and bromodeoxyuridine (BrdU) incorporation. In addition, cytokines produced by the activated T cells were quantitatively assessed in the culture supernatants by ELISA, and the generation of Tregs were assessed by analyzing CD4⁺ CD25⁺ FOXP3⁺ cells using flow cytometry.

Impact of D 2-HG on T-cell migration was assessed in a conventional transwell migration assay.

Bone marrow-derived dendritic cell differentiation and function assay

Dendritic cells (DC) were generated from bone marrow using a published protocol (33), and their function was assessed using antigen-specific T cells from ovalbumin peptide 323–339 (OVA₃₂₃₋₃₃₉)-specific TCR transgenic mice (OT II mice) and ovalbumin peptide 257–264 (OVA₂₅₇₋₂₆₄)-specific TCR transgenic mice (OT I mice).

Statistical analyses

Statistical analyses were performed in GraphPad Prism (Version 5). Mann–Whitney U test or Student unpaired *t* test, as appropriate, were used to investigate the difference in protein expression between mIDH and wtIDH tumors. One-way ANOVA with Bonferroni correction was used to analyze data of more than two groups and Student *t* test was used to analyze data of two sets. *P* < 0.05 was considered significant.

Results

IDH mutations associate with decreased levels of complement activation in astrocytic brain tumors

To examine whether IDH mutational status, and thus the presence of excessive D 2-HG, associates with complement activation in the tumor microenvironment, we performed immunohistochemistry on tissue samples from 72 patients

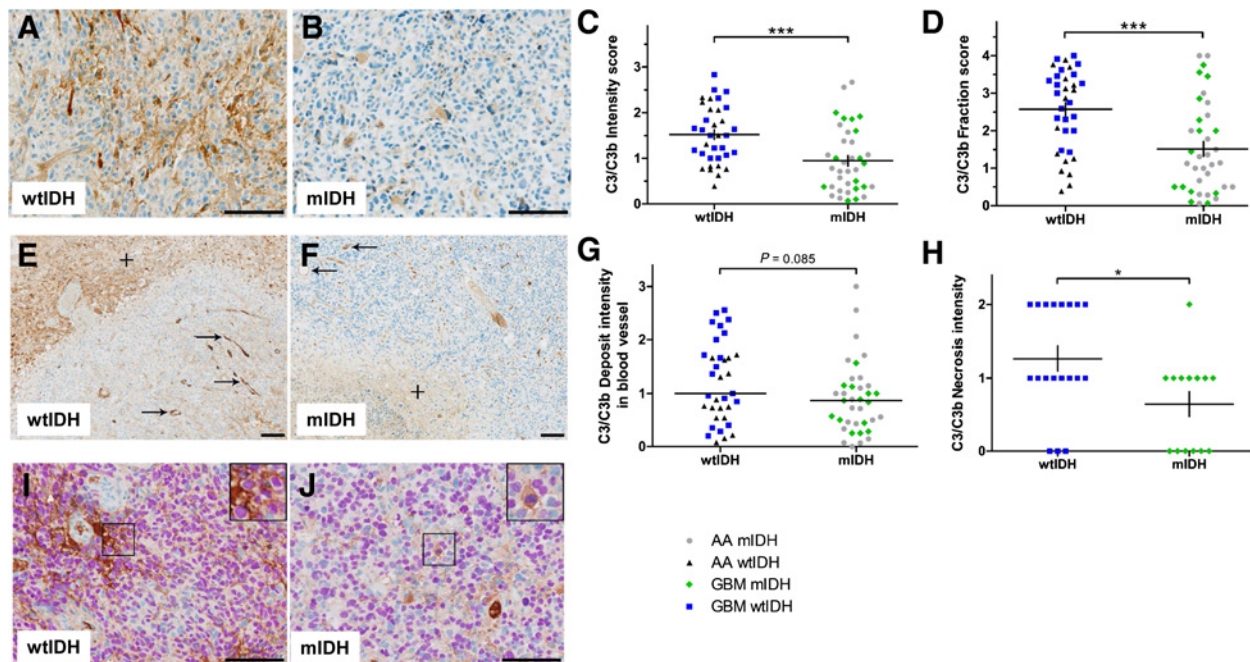


Figure 1.

IDH mutations associate with diminished complement activation in astrocytic brain tumors. Immunohistochemical staining for C3b(iC3b) deposition in tumor tissue sections from patients with anaplastic astrocytoma (AA) WHO grade III or glioblastoma (GBM) WHO grade IV. **A**, Representative C3b(iC3b) staining of a section from an IDH-wild-type tumor (wtIDH). **B**, C3b(iC3b) staining of a section from an IDH-mutant tumor (mIDH). **C**, Levels of complement activation semiquantitated by C3b (iC3b) deposition intensity scores in AA and glioblastomas (GBM). **D**, complement activation semiquantitated by C3b (iC3b) deposition fraction scores in AAs and glioblastomas. **E** and **F**, Representative C3b(iC3b) staining in small blood vessels (arrows) and necrotic areas (+) in sections of GBM samples. **G** and **H**, Complement activations in blood vessels and necrotic areas were semiquantitated by C3b (iC3b) deposition intensity scores. **I** and **J**, C3b(iC3b)/OLIG2 double staining of sections from glioblastomas with wtIDH and mIDH. Each dot in panels **C**, **D**, **G**, **H** represents a single patient. *, $P < 0.05$; **, $P < 0.01$; ***, $P < 0.001$. Scale bar, 100 μm .

using an antibody against C3(C3b) fragments deposited on cell surfaces after activation of the complement cascade. We found in representative sections (Fig. 1A and B) that deposition of these complement fragments, assessed by their staining density, was less in tumors from the 37 patients with mIDH than in samples from 35 patients with wtIDH. Accordingly, the overall intensity (Fig. 1C; $P < 0.001$) and fraction score (Fig. 1D; $P < 0.001$) of C3(C3b) were lower in WHO grade III and IV astrocytomas with mIDH as compared with WHO grade III and IV astrocytomas with wtIDH (Supplementary Table S1). Similar results were found when separately analyzing C3(C3b) immunopositivity in the groups of anaplastic astrocytomas and glioblastomas (Supplementary Table S1). Further, we found that mIDH astrocytomas tended to have less complement deposition on the luminal surfaces of small blood vessel and capillaries compared with wtIDH tumors ($P = 0.085$), and this was especially the case when looking separately at glioblastomas ($P < 0.01$; Fig. 1E–G; Supplementary Table S1). Additionally, the intensity of deposited C3(C3b) in necrotic zones was lower in mIDH glioblastomas than in wtIDH glioblastomas (Fig. 1E, F, H, and Supplementary Table S1). Double labeling with C3(C3b) and the tumor marker OLIG2 showed deposition of complement fragments in close proximity to OLIG2⁺ nuclei suggesting that C3(C3b) is also deposited on tumor cell surfaces. This was seen both in astrocytomas with wtIDH and mIDH (Fig. 1I and J).

D 2-HG inhibits the classical pathway of complement activation

To explore the mechanism underlying the reduced complement activation/deposition in gliomas with IDH mutation, we used a conventional complement-mediated hemolytic assay to test whether D 2-HG inhibits the classical pathway of complement activation and the cellular lysis it generates through MAC complex formation (28). This experiment showed D 2-HG suppressed MAC-induced hemolysis, that suppression was a function of the concentration of normal human serum (NHS) and hence MAC complex abundance, and that this inhibition became statistically significant by 5% NHS (Fig. 2A). We also tested the effects of different concentrations of D 2-HG in this assay, using a fixed amount of NHS, to find that D 2-HG inhibited the classical pathway of complement activation in a dose-dependent manner with a minimally effective concentration of 2 mmol/L (Fig. 2B).

D 2-HG inhibits assembly of C5, but not C3, convertase in the classical pathway of complement activation

D 2-HG could inhibit complement-mediated cell damage at multiple steps of the complement activation cascade. To explore underlying mechanisms, we determined whether D 2-HG affected assembly of C3 and C5 convertases leading to MAC complex-induced hemolysis (29). These assays showed that D 2-HG had no effect on C3 convertase assembly in the classical pathway of complement activation (Fig. 2C) but significantly inhibited the

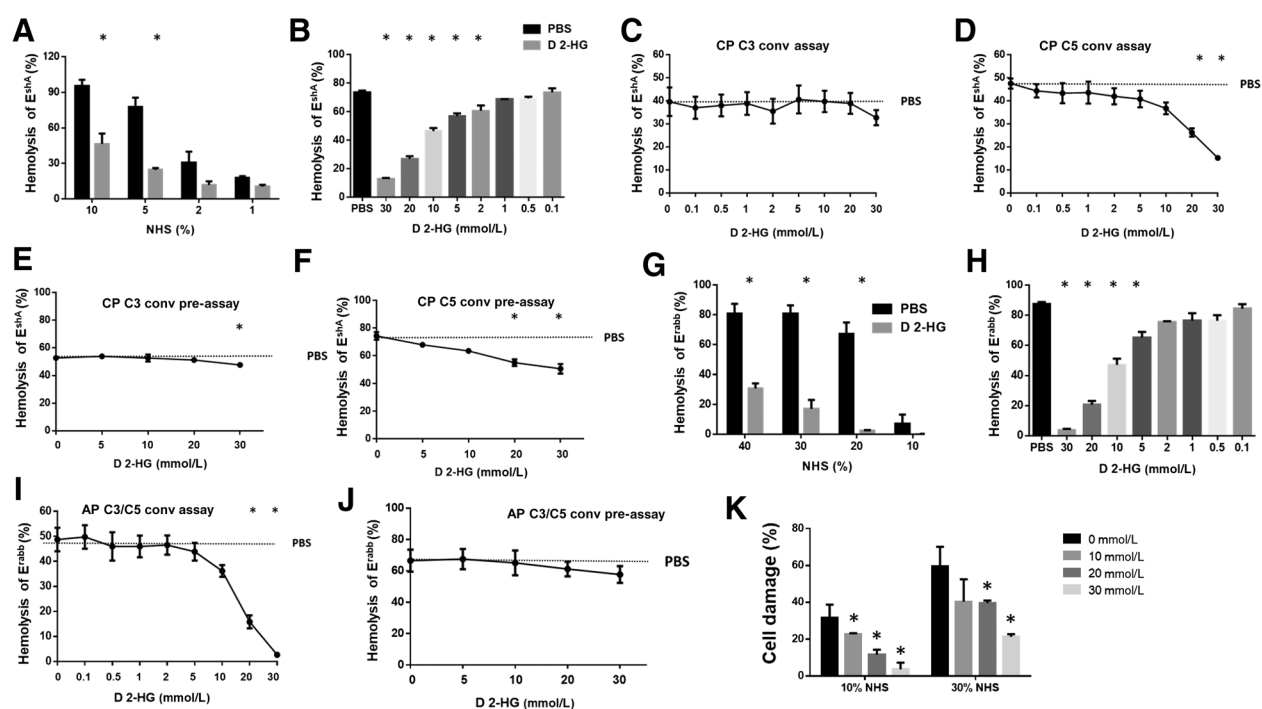


Figure 2.

D 2-HG inhibits both the classical and alternative pathways of complement activation through distinct mechanisms. **A**, D 2-HG reduces complement-dependent hemolysis as a function of complement concentration in NHS. Complement-mediated hemolysis by the classical pathway using E^{shA} in the presence of varied concentrations of NHS in the absence or presence of 30 mmol/L D 2-HG before hemolysis was quantitated. **B**, Complement-mediated hemolysis by the classical pathway as a function of D 2-HG concentration using E^{shA} in 5% NHS. **C**, Effect of D 2-HG on assembly of C3 convertases of the classical pathway using E^{shA} and C3-depleted serum. **D**, Effect of D 2-HG on assembly of C5 convertases of the classical pathway using E^{shA} and C5-depleted serum. **E**, Effect of varied D 2-HG concentrations on the activity of preassembled C3 convertases of the classical pathway using E^{shA} and C3-depleted serum. **F**, Effect of varied D 2-HG concentrations on the activity of preassembled C5 convertases of the classical pathway using E^{shA} and C5-depleted serum. **G**, Effect of 30 mmol/L D 2-HG on complement activation by the alternative pathway assessed by MAC-mediated E^{rabbb} hemolysis. **H**, Concentration-dependent effect of D 2-HG in 20% NHS on alternative complement activation assessed by MAC-mediated E^{rabbb} hemolysis. **I**, Effect of varied D 2-HG concentrations on assembly of C3/C5 convertases of the alternative pathway of complement activation using E^{rabbb} and C5-depleted serum. **J**, D 2-HG effect on the activity of preassembled C3/C5 convertases of the alternative pathway of complement activation using E^{rabbb} and C5-depleted serum as a function of D 2-HG concentration. **K**, Concentration-dependent effect of D 2-HG in inhibiting different concentrations of complement (10% and 30% NHS)-mediated damage of antibody-sensitized T98 glioma cells. For all panels, PBS was used in all assays and data are presented as mean \pm SD that has been analyzed by Student *t* test and one-way ANOVA. *, $P < 0.05$. CP, classical pathway; AP, alternative pathway, conv, convertase, assay, assembly.

assembly of C5 convertases of the classical pathway at concentrations of 20 mmol/L and 30 mmol/L (Fig. 2D).

D-2HG inhibits activity of assembled C3 and C5 convertases in the classical pathway of complement activation

To determine whether D 2-HG inhibits the activities of preassembled C3 and/or C5 convertases in the classical pathway of complement activation, we incubated E^{shA} with C3- or C5-depleted serum alone to allow the assembly of C3 or C5 convertases and, after washing, we incubated these cells with guinea pig serum in the presence of EDTA (to prevent new convertase assembly) and different concentrations of D 2-HG to measure complement-mediated hemolysis (29). These experiments showed that D 2-HG modestly decreased complement-mediated hemolysis in a dose-dependent manner (Fig. 2E and F), indicating that D 2-HG can inhibit the activity of both assembled C3 and C5 convertases in the classical pathway of complement activation, and that D 2-HG is not inhibiting complement activity through simple Ca^{++} ligation (15).

D 2-HG inhibits the alternative pathway of complement activation

The alternative complement pathway is a distinct, major route for complement activation that additionally amplifies complement activation initiated through other pathways. To evaluate the potential effects of D 2-HG on this route to complement activation, we used an E^{rabbb} -based complement-mediated hemolytic assay (28). The results of this assay showed that D 2-HG additionally inhibited the alternative pathway of complement activation (Fig. 2G). We then incubated E^{rabbb} with 20% NHS in the absence or presence of different concentrations of D 2-HG over the range from 0.1 to 30 mmol/L, and found that D 2-HG also significantly reduced the complement-mediated hemolysis in a dose-dependent manner with a minimally required concentration of 5 mmol/L (Fig. 2H).

D 2-HG inhibits the assembly of C3/C5 convertases in the alternative pathway of complement activation

To elucidate the mechanisms by which D 2-HG inhibits the alternative pathway of complement activation, we used

convertase assays similar to the above-described protocol for the classical pathway, but with the E^{rabbb} as the complement activator (28, 29). Because both C3 and C5 convertases in the alternative pathway require C3b, these two enzymes cannot be distinguished by using C3- or C5-depleted sera. These experiments showed that at concentrations of 20 mmol/L and 30 mmol/L, D 2-HG significantly inhibited the assembly of the C3/C5 convertases of the alternative pathway (Fig. 2I).

D 2-HG does not inhibit the activity of preassembled C3/C5 convertases in the alternative pathway of complement activation

We next tested the effects of D 2-HG on preassembled C3/C5 convertases in the alternative pathway of complement activation by incubating E^{rabbb} with C5-depleted serum, washing the cells, then incubating them again with guinea pig serum in the presence of EDTA and varied amounts of D 2-HG. These experiments showed that D 2-HG did not significantly inhibit the activity of preassembled C3/C5 convertases in the alternative pathway of complement activation (Fig. 2J), so there are enzymatic and functional differences between preassembled and assembled convertases.

D 2-HG protects brain tumor cells from complement-mediated injury

The above studies based on complement-mediated hemolysis assays suggest that D 2-HG could inhibit complement activation and thereby MAC-mediated brain tumor cell damage. To test this, we incubated antibody-sensitized T98 glioblastoma cells with different concentrations of complement in the presence of varied D 2-HG concentrations, then evaluated the complement-mediated cell injury by measuring levels of LDH that leaked from the cells. These experiments showed that D 2-HG significantly inhibited cell injury from complement-mediated cellular damage in a dose-dependent manner (Fig. 2K).

D 2-HG inhibits C3b(iC3b) opsonization and complement-mediated phagocytosis

In addition to the MAC formation, complement activation deposits C3b(iC3b) on target cells for opsonization that facilitates phagocytosis (34). To determine whether this complement function also was compromised by D 2-HG, we examined the effects of D 2-HG on both C3b(iC3b) opsonization and complement-mediated phagocytosis. We incubated E^{shA} with C5-depleted serum (to avoid MAC formation and cellular lysis) in the presence of different concentrations of D 2-HG, then quantitated the levels of C3b(iC3b) deposited on the cell surface by flow cytometry. We found that C3 deposition on the cells was significantly decreased by D 2-HG in a dose-dependent manner (Fig. 3A and B). In parallel experiments to assess phagocytosis, we first incubated E^{shA} with C5-depleted serum in the absence or presence of 30 mmol/L D 2-HG, then fluorescently labeled them before mixing these cells with macrophages labeled with a different fluorophore. After incubation for either 30 or 120 minutes, phagocytosis was quantitated by analyzing the double-positive cells by flow cytometry (Fig. 3C and D). This showed that D 2-HG markedly reduced the efficiency of complement-mediated phagocytosis.

IDH mutations associate with decreased number of infiltrating lymphocytes in astrocytic brain tumors

To elucidate a potential association between IDH mutations and the adaptive immune system in patients with WHO grade III

and IV astrocytomas, we quantitatively evaluated tumor-infiltrating lymphocytes by immunohistochemistry in the same 72 primary tumors we used to assess complement deposition (Fig. 1). We found fewer tumor-infiltrating $CD4^+$ T cells in the group of mIDH gliomas than in the group of wtIDH gliomas of WHO grade III and IV ($P < 0.01$; Fig. 4A–C). Similar outcomes were obtained when analyzing the subgroup of WHO grade III anaplastic astrocytomas ($P < 0.05$) stratified according to IDH mutational status, with a similar tendency in subgroup of WHO grade IV glioblastomas ($P = 0.14$; Supplementary Table S1). We then investigated the infiltration of glioma tissues by $CD8^+$ cytotoxic T cells and observed decreased numbers of these cells in mIDH compared with wtIDH WHO grade III or IV gliomas ($P < 0.001$; Fig. 4D–F). Again, this difference was also observed for the subgroup of anaplastic astrocytomas ($P < 0.01$), with a similar tendency in the subgroup of glioblastomas that was not, however, significant ($P = 0.33$). Interestingly, staining for the Treg cell marker FOXP3 showed that numbers of tumor-infiltrating FOXP3⁺ T cells were lower in mIDH grade III and IV gliomas compared with their wtIDH counterparts (Fig. 4G–I; $P < 0.01$). Although both FOXP3 positive and negative cells were decreased, the difference in the tumor-infiltrating FOXP3⁺/ $CD4^+$ ratio between the two groups was not statistically significant ($P = 0.13$; Fig. 4J).

D 2-HG inhibits proliferation and cytokine production of activated T cells

Although D 2-HG inhibits $CD8^+$ T-cell accumulation in tumors (17), whether it directly inhibits proliferation of activated T cells and/or stimulated cytokine production is unknown. We labeled purified T cells with fluorescent CFSE and activated them with anti-CD3 and anti-CD28 monoclonal antibodies in the absence or presence of D 2-HG at concentrations ranging from 5 to 30 mmol/L. We then assessed proliferation of these activated T cells by CFSE dilution (Fig. 5A) to find D 2-HG significantly inhibited the proliferation of activated T cells. We confirmed this by assessing BrdUrd incorporation into the total DNA content of dividing cells (Fig. 5B). We also found that D 2-HG suppressed IFN γ production from the activated T cells in a dose-dependent manner (Fig. 5C).

To test whether D 2-HG inhibits different subsets of effector $CD4^+$ T cells, we isolated $CD4^+$ T cells from naïve WT mice, activated them by monoclonal antibodies against CD3 and CD28, and cultured these cells in Th1, Th17, and Treg polarization conditions in the presence or absence of D 2-HG. We then assessed the proliferation of these various cells to find D 2-HG significantly inhibited proliferation of activated Th1, Th17, and Tregs (Fig. 5D). Surprisingly, when we analyzed the differentiation of $CD4^+CD25^+FOXP3^+$ Tregs in the presence of D 2-HG, we found that 30 mmol/L D 2-HG significantly augmented differentiation of these cells (Fig. 5E and F). However, levels of IL10 in the Treg culture supernatants were reduced in the presence of 30 mmol/L D 2-HG. Thus, while D 2-HG augments Treg differentiation, it concurrently inhibits proliferation of the differentiated Tregs (Fig. 5D). Accordingly, D 2-HG led to reduced numbers of tumor-infiltrating Tregs (Fig. 4G–I) *in vivo* and decreased production of IL10 *in vitro* (Fig. 5G).

D 2-HG directly inhibits T-cell migration

Inhibition of T-cell proliferation by D 2-HG would reduce the presence of both $CD4^+$ and $CD8^+$ T cells in tumors from patients with mutant IDH, as would suppressed T-cell migration. To

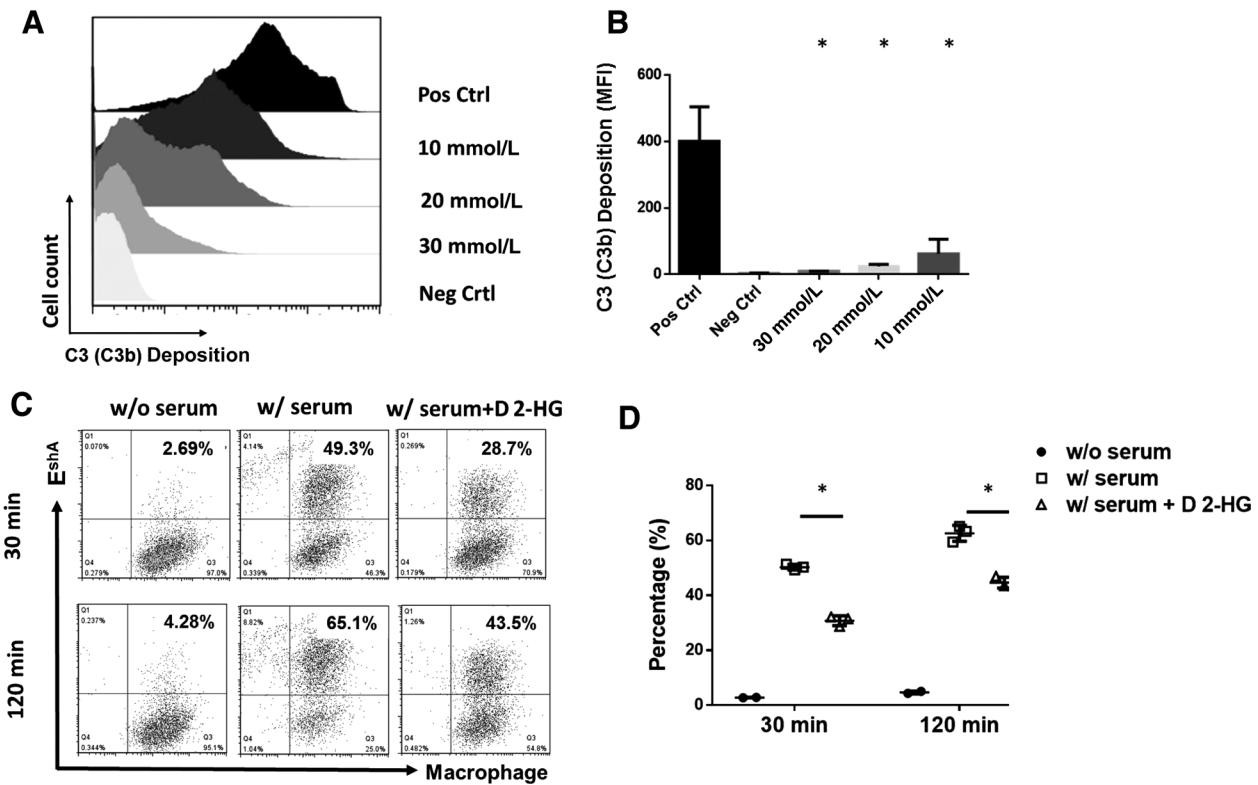


Figure 3. D 2-HG reduces complement opsonization-induced phagocytosis and complement-mediated glioma cell line damage. **A**, Representative flow cytometric histogram of C3b(i3Cb) deposition on the E^{shA} cell surface in the presence of different concentrations of D 2-HG. For complement opsonization assays, E^{shA} were incubated with 2% C5-depleted serum in the presence of the stated concentration of D 2-HG before C3b(i3Cb) deposited on the cell surface was quantitated by flow cytometry. **B**, Summarized results of the levels of C3b/i3Cb deposition on the cell surface in the presence of defined concentrations of D 2-HG as measured by mean fluorescence intensity (MFI). Pos Ctrl, positive control, cells were incubated with serum in the absence of D 2-HG; Neg Ctrl, negative control, cells were incubated with serum in the presence of EDTA (to completely inhibit complement activation), data are mean ± SD and analyzed by one-way ANOVA. *, *P* < 0.05. **C**, Representative results of D 2-HG on phagocytosis. For complement-mediated phagocytosis assays, macrophages were prepared and labeled with CellTrace far-red fluorophore, while E^{shA} were incubated with or without 2% C5-depleted serum in the absence or presence of 30 mmol/L D 2-HG (for complement opsonization) and labeled with fluorescent Dil. Then, the processed macrophages and E^{shA} were cocultured at a 1:10 ratio, and after either 30- or 120-minute incubation, the cells were analyzed by flow cytometry to measure the efficiency of phagocytosis (frequency of double-positive cells). w/o serum, E^{shA} were incubated without serum (no opsonization, negative control), w/serum, E^{shA} were incubated with serum in the absence of D 2-HG (maximum opsonization, positive control), w/serum+ D 2-HG, E^{shA} were incubated with serum in the presence of 30 mmol/L D 2-HG. **D**, Summarized results of phagocytosis assays. Data are mean ± SD and analyzed by Student *t* test. *, *P* < 0.05.

address this question, we set up a transwell T-cell migration assay following an established protocol using Chemokine (C-C motif) ligand 19 (CCL19) as a chemoattractant to evaluate the effect of D 2-HG on T-cell migration. These studies showed that 30 mmol/L D 2-HG significantly inhibited the migration of both CD4⁺ and CD8⁺ T cells (Fig. 5H).

D 2-HG does not inhibit differentiation of DCs or the function of differentiated DC

DCs are pivotal for T-cell activation, so DCs were differentiated from bone marrow cells in the presence of defined concentrations of D 2-HG and then compared 6 days later with the DCs differentiated in the absence of D 2-HG using cell surface markers CD11c, MHCII, CD11b, CD80, and CD86. We found that D 2-HG, even at 30 mmol/L, did not significantly affect the ratio of differentiated DCs (Fig. 6A and B), suggesting that D 2-HG does not indirectly suppress T-cell function through DC differentiation.

Even though D 2-HG did not have an appreciable effect on DC differentiation, it might still affect their function. We assessed this in the presence or absence of varied concentrations of D 2-HG by mixing the same numbers of these DCs with purified T cells from OT II transgenic mice that specifically recognize the ovalbumin 323-339 (OVA₃₂₃₋₃₃₉) peptide together with this peptide antigen. We then compared proliferation of the OT II T cells activated by the DCs presenting the OVA peptide, again by BrdUrd incorporation, and quantified their functional response by IFN γ ELISA. These assays showed that there was no appreciable difference between DCs differentiated in the absence or presence of D 2-HG in stimulating antigen-specific T-cell proliferation (Fig. 6C) or IFN γ production (Fig. 6D).

To determine whether D 2-HG affects DC antigen processing or presentation and to confirm that D 2-HG inhibits antigen-specific CD4⁺ and CD8⁺ T cells, we first incubated DCs with OVA protein in the presence or absence of 30 mmol/L D 2-HG for 4 hours, then washed the cells and incubated them with CD4⁺ T cells from OT II

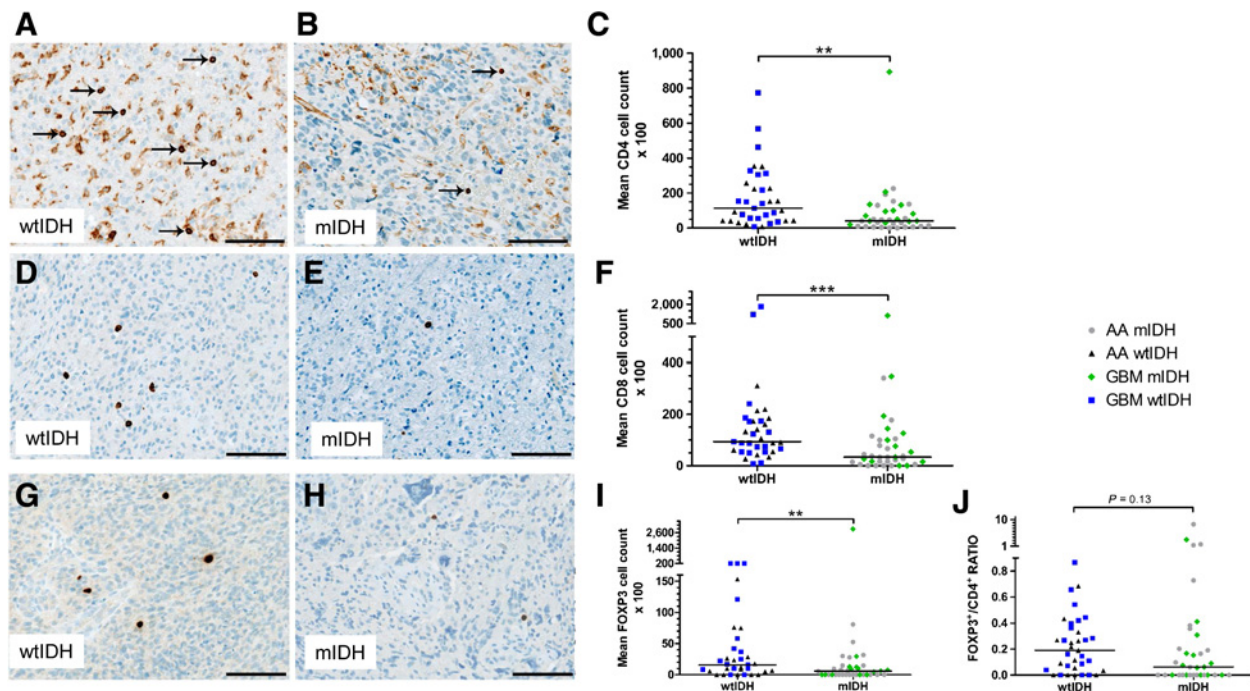


Figure 4.

IDH mutations associate with decreased numbers of infiltrating $CD4^+$, $CD8^+$, and $FOXP3^+$ T cells in astrocytic brain tumors. **A**, Representative $CD4^+$ immunohistochemistry in tumor sections from patients with WHO grade III anaplastic astrocytoma (AA) or WHO grade IV glioblastoma (GBM) wild-type IDH (wtIDH). Arrows indicate $CD4^+$ T cells. **B**, Representative $CD4^+$ immunohistochemistry in tumor sections from patients with WHO grade III AA or WHO grade IV glioblastoma with mutant IDH (mIDH). **C**, Statistical analysis of tumor-infiltrating $CD4^+$ T cells in AA and GBM with wtIDH and mIDH. **D**, Representative CD8 staining of tumor sections derived from a wtIDH tumor. **E**, Representative CD8 staining of tumor sections derived from a mIDH tumor. **F**, Statistical summary of tumor-infiltrating $CD8^+$ T cells in AA and GBM tumors. **G**, Representative FOXP3 immunostaining in sections obtained from a wtIDH astrocytoma. **H**, Representative FOXP3 staining of tumor sections derived from a mIDH astrocytoma. **I**, Statistical summary of tumor-infiltrating FOXP3⁺ T cells and (**J**) the ratio of FOXP3⁺ to total $CD4^+$ T cells in AA and GBM sections. Each dot in all statistical analyses represents data from a single patient. **, $P < 0.01$; ***, $P < 0.001$. Scale bar, 100 μ m.

mice or $CD8^+$ T cells from OT I mice for another 3 days. We then analyzed proliferation of the OVA-specific $CD4^+$ T cells and $CD8^+$ T cells by flow cytometry, and measured levels of $IFN\gamma$ produced from the activated $CD4^+$ T cells, and levels of granzyme B produced from the activated $CD8^+$ T cells in the culture supernatants by ELISA. These assays showed that both OVA-specific $CD4^+$ and $CD8^+$ T cells had comparable proliferation (Fig. 6E) and produced similar levels of $IFN\gamma$ ($CD4^+$; Fig. 6F) or granzyme B ($CD8^+$; Fig. 6G) after coculturing with DCs incubated with OVA protein in the presence or absence of D 2-HG. This indicates that D 2-HG even at 30 mmol/L has no effect on DC antigen processing or presentation. In contrast, when the same DCs with processed/presented OVA (in the absence of D 2-HG) were incubated with $CD4^+$ T cells from OT II mice or $CD8^+$ T cells from OT I mice with or without 30 mmol/L D 2-HG, proliferation of the OVA-specific $CD4^+$ and $CD8^+$ were significantly inhibited by D 2-HG (Fig. 6E), as was their production of $IFN\gamma$ ($CD4^+$; Fig. 6F) or granzyme B ($CD8^+$) (Fig. 6G). This shows that D 2-HG directly inhibits antigen-specific $CD4^+$ and $CD8^+$ T cells without interfering with DC antigen processing or presentation.

Discussion

We report that IDH mutation associates with significantly decreased levels of complement deposition within human glioma tissues. From a molecular perspective, we found that D 2-HG

inhibited both the classical and the alternative pathways of complement activation, reduced MAC-mediated cellular injury, and decreased complement-mediated opsonization and phagocytosis. We found that IDH mutation was also significantly associated with reduced numbers of tumor-infiltrating $CD4^+$, $CD8^+$, and $FOXP3^+$ T cells in tumor tissue samples from patients with either WHO grade III anaplastic astrocytomas or WHO grade IV glioblastomas. In mechanistic studies, we found that although D 2-HG did not inhibit the differentiation of DCs or their function after differentiation, D 2-HG directly suppressed proliferation of activated T cells and their production of key cytokines. These results elucidate a novel transcellular effect of tumor-derived D 2-HG on select cells and effector pathways of the immune system in a tumor microenvironment.

Complement forms a central part of the host immune surveillance mechanism against tumor cells, yet may have opposing roles in tumorigenesis because activated complement also promotes inflammation that favors tumor growth. Complement can be activated on tumor cells, either directly by the tumor cells themselves (35, 36) or by tumor-reactive antibodies that bind to neoantigens on the tumor cell surface, enabling MAC-mediated lysis and facilitated phagocytosis to dissolve the tumor (37). Conversely, tumors significantly upregulate expression of complement inhibitors including CD55 and CD59 on their surface that shield them from complement-driven attacks (38, 39). Our finding that D 2-HG significantly inhibited the activation of

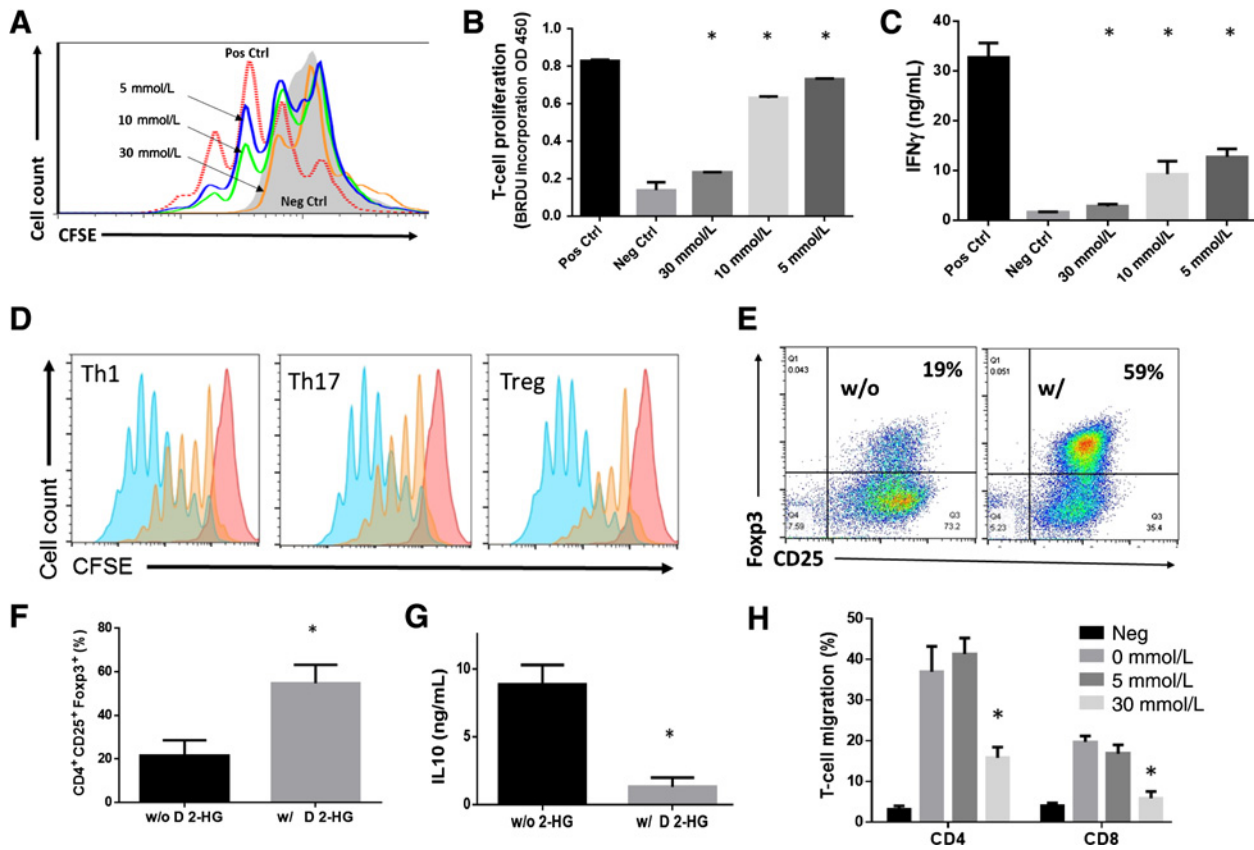


Figure 5.

D 2-HG inhibits proliferation of activated T cells and their cytokine production. **A**, Concentration-dependent inhibition of T-cell proliferation by D 2-HG. T cells enriched from WT mice were labeled with CFSE and activated with anti-CD3 and anti-CD28 monoclonal antibodies in the presence of the stated concentration of D 2-HG. After 3 days of culture, CFSE dilution from the proliferation of the activated T cells was assessed by flow cytometry. **B**, Statistical analysis of concentration-dependent inhibition of T-cell proliferation by D 2-HG assessed by bromodeoxyuridine (BrdUrd) incorporation. **C**, Statistical analysis of the concentration-dependent inhibition of IFN γ by D 2-HG assessed by ELISA. Pos Ctrl, positive control, T cells were activated in the absence of D 2-HG; Neg Ctrl, negative control, unactivated T cells; data were mean \pm SD and analyzed by one-way ANOVA. *, $P < 0.05$ compared with the positive controls. **D**, Histograms of concentration-dependent inhibition of proliferation of Th1 cells, Th17, cells and Tregs by D 2-HG. CD4⁺ T cells were purified from naïve WT mice, labeled with CFSE, activated with anti-CD3 and anti-CD28 monoclonal antibodies, and cultured under respective Th1, Th17, or Treg polarization conditions in the absence (blue peaks) or presence of 30 mmol/L D 2-HG (orange peaks). Proliferations of these T cells were analyzed in 3 days by measuring the dilution of intracellular CFSE by flow cytometry. **E**, D 2-HG enhances CD4⁺CD25⁺ FOXP3⁺ Treg differentiation. Percentages of CD4⁺CD25⁺ FOXP3⁺ Tregs in the absence or presence of 30 mmol/L D 2-HG were analyzed by flow cytometry. **F**, Statistical analysis of the fraction of differentiated CD4⁺CD25⁺ FOXP3⁺ Tregs determined by flow cytometry. *, $P < 0.05$. **G**, D 2-HG inhibits IL10 secretion by cultured CD4⁺CD25⁺ FOXP3⁺ Tregs determined by ELISA analysis of the cellular supernatants. **H**, D 2-HG inhibits T-cell migration. CD4⁺ or CD8⁺ T cells were isolated from naïve WT mice, and migration of these cells in the presence of the stated concentrations of D 2-HG in response to CCL19 was assessed in a standard transwell-based migration assay. *, $P < 0.05$.

complement from both the classical and the alternative pathways suggest a new mechanism that would facilitate mDHD glioma cell survival. The classical pathway of complement activation is primarily initiated by antibody-antigen complexes. During tumor development, the proteome of the transformed cell includes neoantigens that can provoke B-cell response to generate tumor-reactive antibodies against these neoepitopes. These anti-tumor antibodies, once bound to their antigens on tumor cell surface, initiate selective complement activation by binding circulating C1 molecules. This leads to MACs formation of transmembrane pores that permeabilize tumor cells, and additionally deposits C3b(iC3b) on the tumor cell surface to facilitate subsequent clearance by phagocytosis. The effect of the inhibition of the classical pathway activation of complement by D 2-HG would thus act to reduce the efficiency of antitumor antibodies in at least two ways.

In addition to direct attack by antitumor antibodies and their activation of complement through the classical pathway, altered expression patterns of surface molecules on tumor cells can trigger complement activation through the alternative pathway. This mechanism also forms MAC and deposits C3b(iC3b) on the target cells. Furthermore, the alternative pathway is a component of the amplification loop for complement activation initiated by other pathways, including the classical pathway (40). Complement is highly conserved among species, and we observed D 2-HG inhibited complement from normal mice, rats, and guinea pigs (not shown). Thus, a propensity of D 2-HG to enhance tumorigenesis, in part, proceeds through effects on different routes to complement activation.

Our studies suggest that D 2-HG does not have a significant effect on at least the C3 convertases from the classical pathway of complement activation (Fig. 2). However, detection of deposited

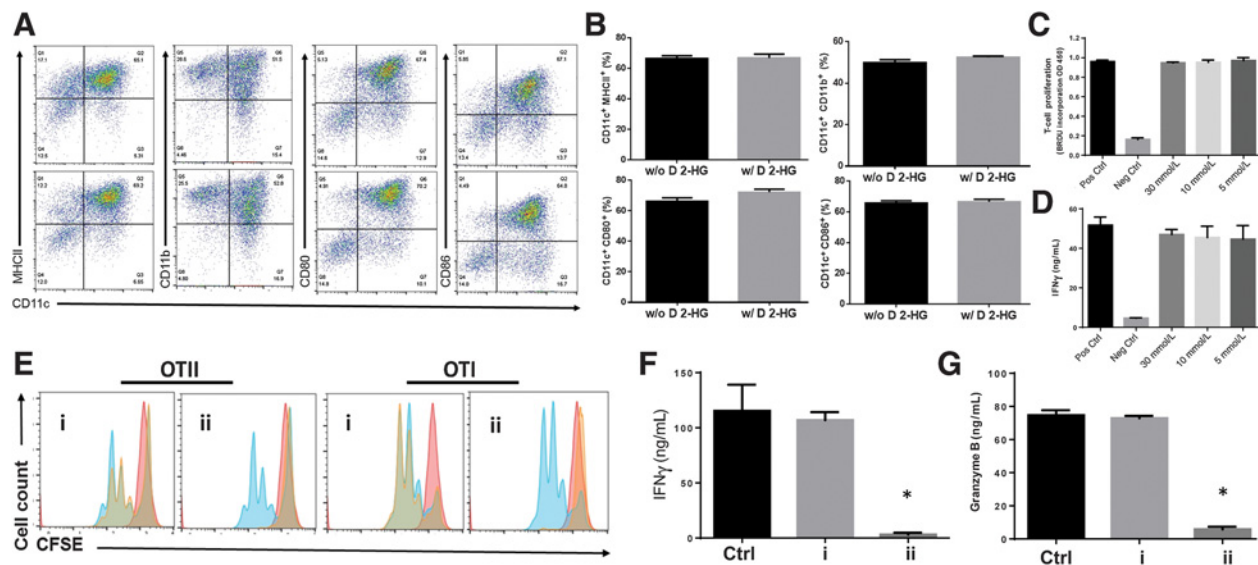


Figure 6.

D 2-HG has no significant effect on DC differentiation or the function of differentiated DCs. **A**, D 2-HG does not affect DC differentiation. DCs were differentiated from bone marrow cells in the absence or presence of 30 mmol/L D 2-HG before surface markers on the surface of differentiated DCs were analyzed by flow cytometry. The top panel are untreated, and the bottom panel exposed to D 2-HG during differentiation. **B**, Statistical analysis of D 2-HG effect on the fraction of cells expressing the stated surface antigen. **C**, D 2-HG fails to affect DC proliferation. DCs differentiated in the presence of the defined concentrations of D 2-HG were cultured with CD4⁺ T cells from OT II mice together with OVA protein before the DC-activated T cells were assessed by measuring proliferation through BrdUrd incorporation. **D**, D 2-HG fails to affect DC function. IFN γ release in the foregoing panel was quantified by ELISA. **E**, D 2-HG has no effect on DC antigen processing/presentation but inhibits antigen-specific CD4⁺ and CD8⁺ T cells. Differentiated bone marrow-derived DCs were incubated with OVA protein in the absence or presence of 30 mmol/L of D 2-HG, then washed and cultured with CD4⁺ T cells from OTII mice, or CD8⁺ T cells from OT I mice without further additional D 2-HG (i). As control, marrow-derived DCs incubated with OVA protein in the absence of D 2-HG were washed and cultured with CD4⁺ T cells from OTII mice, or CD8⁺ T cells from OTI mice together with 30 mmol/L D 2-HG (ii). Proliferation of the DC-activated antigen-specific T cells was analyzed by CFSE dilution using flow cytometry. **F**, D 2-HG inhibits OT II CD4⁺ T-cell release of IFN γ . Statistical analysis of IFN γ quantified by ELISA after DC-activated antigen-induced release. *, $P < 0.05$. **G**, D 2-HG inhibits OT I CD8⁺ T-cell release of granzyme B. Statistical analysis of released granzyme B defined by ELISA in the supernatants from cultures including OT I CD8⁺ T cells. *, $P < 0.05$.

C3 antigens (C3b/iC3b) is robust. This suggests that alternative pathway might play a major role in activating complement in these tumors. In addition, our C3b uptake assays (Fig. 3) also suggest that even though D 2-HG might not have a drastic effect on the C3 convertases, it significantly inhibits the binding (deposition) of activated C3 onto the cell surface.

Inhibition of complement convertases by D 2-HG will be independent of Ca⁺⁺ sequestration (15), because extracellular Ca⁺⁺ significantly exceeds D 2-HG, although suppression of T-cell function might reflect effective Ca⁺⁺/D 2-HG ligation at the far lower intracellular Ca⁺⁺ levels (15). These new data also suggest that D 2-HG from the altered catalytic activity of mutant IDH in tumor cells has a profound role in suppressing both the innate and the adaptive immune systems that may underlie reduction of tumor-infiltrating T cells in human astrocytoma.

The adaptive immune system plays a vital role in tumor immune surveillance (41, 42) through tumor-reactive T cells, activated by tumor antigen-presenting cells such as DCs, to proliferate, release cytotoxins such as granzymes, and produce inflammatory cytokines including IFN γ . T cells also facilitate the humoral response to produce tumor-directed antibodies that activate complement on tumor cells leading to the assembly of MAC pores, lysis, and recognition and engulfment by macrocytic cells. Contravening this, tumor cells stimulate induction of myeloid-derived suppressor cells, upregulate programmed death-

ligand 1 (PD-L1; ref. 43) on their cell surface (44), and as we show here interfere with complement activation, and directly suppress T-cell function.

We found that astrocytic gliomas expressing either mutant IDH-1 or IDH-2 contained significantly fewer tumor-infiltrating T cells relative to histologically similar tumors with WT IDH. Importantly, we show that the abundance of CD4⁺ helper cells, cytotoxic CD8⁺ T cells, and total FOXP3⁺ Tregs was lower in gliomas with mutant as compared with tumors with WT IDH. Previously, the abundance of CD8⁺ cells in a smaller cohort glioblastoma patients was found to be reduced in tumors with mutant enzyme relative to tumors with WT enzyme (17), and we confirmed a reduction of these cells, but we also found fewer CD4⁺ and FOXP3⁺ T cells in a larger number of both WHO grade III and grade IV tumors. These data indicate that tumors expressing mutant IDH and synthesizing D 2-HG would be subject to lower levels of immune surveillance and immune-mediated elimination that includes reduced NK cell-mediated immunosurveillance (20).

The fact that any of the several mutations of IDH that induce the gain-of-function production of D 2-HG were associated with fewer tumor-infiltrating T cells suggests that the D 2-HG product itself is the likely functional effector limiting immunosurveillance. In a recent study (17), D 2-HG was found to suppress STAT1 activation and CD8⁺ T-cell trafficking into gliomas correlating to loss of NK cell ligand expression (20). Additionally, we

found that D 2-HG inhibited the proliferation of activated T cells and their cytokine production, which are central components of acquired immunity. However, in contrast to suppression of the proliferation of activated T cells and their production of cytokines, D 2-HG did not have an appreciable effect on DC differentiation or function, while it actually stimulated FOXP3⁺ CD4 T-cell proliferation, although this occurred with sharp reduction of their stimulated function. This finding indicates that D 2-HG is selective in the cells and processes it inhibits and is not a general cytotoxin or cell-cycle inhibitor.

The limitations of this study include that we postulate, but do not test, whether glioblastomas expressing IDH mutations abundantly release D 2-HG to their environment, similar to their extensive release of glutamate. The immune-inhibition we explore here occurs at the high D 2-HG levels found within or within centimeters of gliomas, but because the extracellular D 2-HG concentration in these locations is only modeled, we do not know the actual concentrations of D 2-HG experienced by tumor-infiltrating lymphocytes. Additionally, this study correlates IDH mutational status in human glial tumors with reduced immune cell infiltration but did not directly test the role of the IDH mutation in isolation using murine xenograft models.

Overall, our studies found that the overproduction of D 2-HG in tumors expressing mutant IDH-1 and IDH-2 influences the tumor microenvironment by intervention in immunosurveillance at two key points, extracellular suppression of both classical and alternative complement deposition, as well as direct suppression of the T-cell response. These results provide new insights into the mechanism by which the oncometabolite D 2-HG facilitates tumorigenesis of glioma cells carrying the IDH mutations.

References

- Parsons DW, Jones S, Zhang X, Lin JC, Leary RJ, Angenendt P, et al. An integrated genomic analysis of human glioblastoma multiforme. *Science* 2008;321:1807–12.
- Yan H, Parsons DW, Jin G, McLendon R, Rasheed BA, Yuan W, et al. IDH1 and IDH2 mutations in gliomas. *N Engl J Med* 2009;360:765–73.
- Hartmann C, Hentschel B, Wick W, Capper D, Felsberg J, Simon M, et al. Patients with IDH1 wild type anaplastic astrocytomas exhibit worse prognosis than IDH1-mutated glioblastomas, and IDH1 mutation status accounts for the unfavorable prognostic effect of higher age: implications for classification of gliomas. *Acta Neuropathol* 2010;120:707–18.
- Hartmann C, Meyer J, Balss J, Capper D, Mueller W, Christians A, et al. Type and frequency of IDH1 and IDH2 mutations are related to astrocytic and oligodendroglial differentiation and age: a study of 1,010 diffuse gliomas. *Acta Neuropathol* 2009;118:469–74.
- Mardis ER, Ding L, Dooling DJ, Larson DE, McLellan MD, Chen K, et al. Recurring mutations found by sequencing an acute myeloid leukemia genome. *N Engl J Med* 2009;361:1058–66.
- Cairns RA, Iqbal J, Lemonnier F, Kucuk C, de Leval L, Jais JP, et al. IDH2 mutations are frequent in angioimmunoblastic T-cell lymphoma. *Blood* 2012;119:1901–3.
- Amary MF, Bacsi K, Maggiani F, Damato S, Halai D, Berisha F, et al. IDH1 and IDH2 mutations are frequent events in central chondrosarcoma and central and periosteal chondromas but not in other mesenchymal tumours. *J Pathol* 2011;224:334–43.
- Dang L, White DW, Gross S, Bennett BD, Bittinger MA, Driggers EM, et al. Cancer-associated IDH1 mutations produce 2-hydroxyglutarate. *Nature* 2009;462:739–44.
- Ward PS, Patel J, Wise DR, Abdel-Wahab O, Bennett BD, Collier HA, et al. The common feature of leukemia-associated IDH1 and IDH2 mutations is a neomorphic enzyme activity converting alpha-ketoglutarate to 2-hydroxyglutarate. *Cancer Cell* 2010;17:225–34.
- Horbinski C. What do we know about IDH1/2 mutations so far, and how do we use it? *Acta Neuropathol* 2013;125:621–36.
- Linninger A, Hartung GA, Liu BP, Mirkov S, Tangen K, Lukas RV, et al. Modeling the diffusion of D-2-hydroxyglutarate from IDH1 mutant gliomas in the central nervous system. *Neuro Oncol* 2018.
- Xu W, Yang H, Liu Y, Yang Y, Wang P, Kim SH, et al. Oncometabolite 2-hydroxyglutarate is a competitive inhibitor of alpha-ketoglutarate-dependent dioxygenases. *Cancer Cell* 2011;19:17–30.
- Lu C, Ward PS, Kapoor GS, Rohle D, Turcan S, Abdel-Wahab O, et al. IDH mutation impairs histone demethylation and results in a block to cell differentiation. *Nature* 2012;483:474–8.
- Koivunen P, Lee S, Duncan CG, Lopez G, Lu G, Ramkissoon S, et al. Transformation by the (R)-enantiomer of 2-hydroxyglutarate linked to EGLN activation. *Nature* 2012;483:484–8.
- Unruh D, Schwarze SR, Khoury L, Thomas C, Wu M, Chen L, et al. Mutant IDH1 and thrombosis in gliomas. *Acta Neuropathol* 2016;132:917–30.
- Domingues P, Gonzalez-Tablas M, Otero A, Pascual D, Miranda D, Ruiz L, et al. Tumor infiltrating immune cells in gliomas and meningiomas. *Brain Behav Immun* 2016;53:1–15.
- Kohanbash G, Carrera DA, Shrivastav S, Ahn BJ, Jahan N, Mazor T, et al. Isocitrate dehydrogenase mutations suppress STAT1 and CD8⁺ T cell accumulation in gliomas. *J Clin Invest* 2017;127:1425–37.
- Amankulor NM, Kim Y, Arora S, Kargl J, Szulzewsky F, Hanke M, et al. Mutant IDH1 regulates the tumor-associated immune system in gliomas. *Genes Dev* 2017;31:774–86.
- Berghoff AS, Kiesel B, Widhalm G, Wilhelm D, Rajky O, Kurscheid S, et al. Correlation of immune phenotype with IDH mutation in diffuse glioma. *Neuro Oncol* 2017;19:1460–8.
- Zhang X, Rao A, Sette P, Deibert C, Pomerantz A, Kim WJ, et al. IDH mutant gliomas escape natural killer cell immune surveillance by downregulation of NKG2D ligand expression. *Neuro Oncol* 2016;18:1402–12.

Disclosure of Potential Conflicts of Interest

No potential conflicts of interest were disclosed.

Authors' Contributions

Conception and design: B.W. Kristensen, T.M. McIntyre, F. Lin
Development of methodology: L. Zhang, M. Sorensen, B.W. Kristensen, T.M. McIntyre
Acquisition of data (provided animals, acquired and managed patients, provided facilities, etc.): L. Zhang, M. Sorensen, B.W. Kristensen, G. Reifenberger
Analysis and interpretation of data (e.g., statistical analysis, biostatistics, computational analysis): L. Zhang, M. Sorensen, B.W. Kristensen, F. Lin
Writing, review, and/or revision of the manuscript: L. Zhang, M. Sorensen, B.W. Kristensen, G. Reifenberger, T.M. McIntyre, F. Lin
Administrative, technical, or material support (i.e., reporting or organizing data, constructing databases): L. Zhang, B.W. Kristensen
Study supervision: B.W. Kristensen, F. Lin

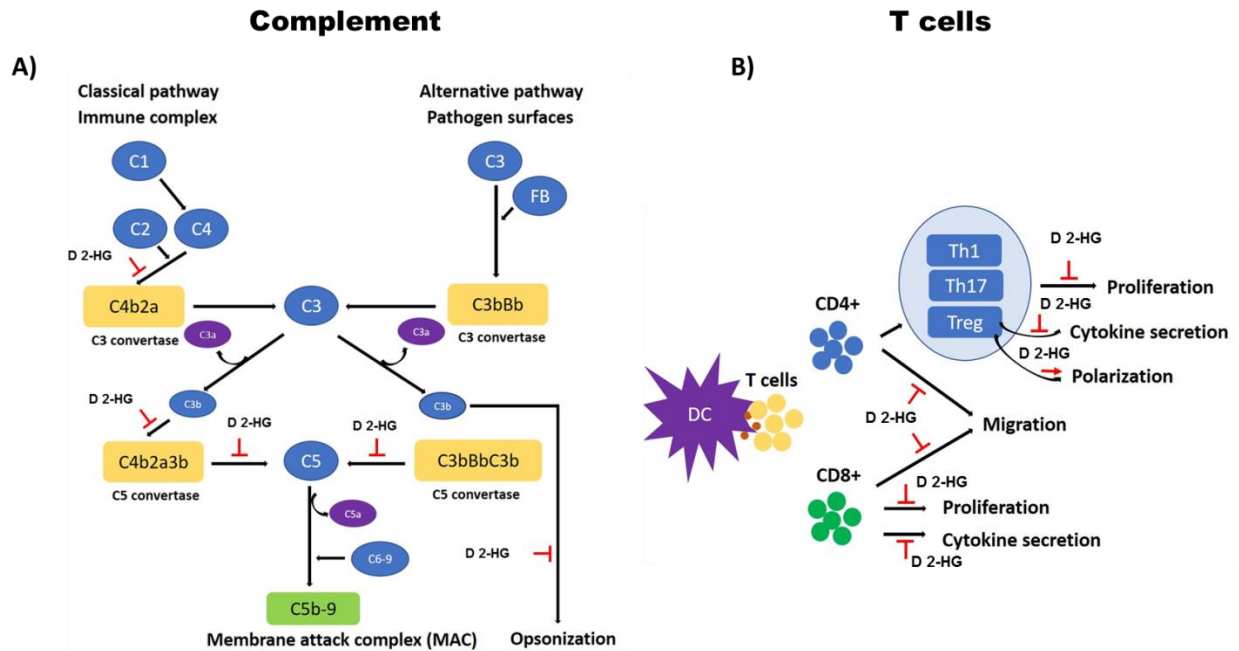
Acknowledgments

This work is supported in part by grants NIH R01 DK 10358 (F. Lin), Cleveland Clinic Center of Excellence in Cancer-Associated Thrombosis Award (F. Lin and T.M. McIntyre), and VeloSano Pilot Project Award (T.M. McIntyre and F. Lin). We thank Justin D. Lathia for his helpful insights and discussions in creating and formulating this article. We also thank technician Helle Wohlleben and senior histotechnician, project coordinator Ole Nielsen for assistance with immunohistochemical staining.

The costs of publication of this article were defrayed in part by the payment of page charges. This article must therefore be hereby marked *advertisement* in accordance with 18 U.S.C. Section 1734 solely to indicate this fact.

Received December 28, 2017; revised May 16, 2018; accepted July 9, 2018; published first July 13, 2018.

21. Ricklin D, Hajishengallis G, Yang K, Lambris JD. Complement: a key system for immune surveillance and homeostasis. *Nat Immunol* 2010;11:785–97.
22. Cravedi P, van der Touw W, Heeger PS. Complement regulation of T-cell alloimmunity. *Semin Nephrol* 2013;33:565–74.
23. Arbore G, West EE, Spolski R, Robertson AAB, Klos A, Rheinheimer C, et al. T helper 1 immunity requires complement-driven NLRP3 inflammasome activity in CD4(+) T cells. *Science* 2016;352:aad1210.
24. Kolev M, Le Friec G, Kemper C. Complement-tapping into new sites and effector systems. *Nat Rev Immunol* 2014;14:811–20.
25. Louis DN, Perry A, Reifenberger G, von Deimling A, Figarella-Branger D, Cavenee WK, et al. The 2016 World Health Organization classification of tumors of the central nervous system: a summary. *Acta Neuropathol* 2016;131:803–20.
26. Dahlrot RH, Kristensen BW, Hjelmberg J, Herrstedt J, Hansen S. A population-based study of low-grade gliomas and mutated isocitrate dehydrogenase 1 (IDH1). *J Neurooncol* 2013;114:309–17.
27. Zacher A, Kaulich K, Stepanow S, Wolter M, Kohrer K, Felsberg J, et al. Molecular diagnostics of gliomas using next generation sequencing of a glioma-tailored gene panel. *Brain Pathol* 2017;27:146–59.
28. Morgan BP. Complement methods and protocols. Totowa, NJ: Humana Press; 2000.
29. Blom AM, Volokhina EB, Fransson V, Stromberg P, Berghard L, Viktorelius M, et al. A novel method for direct measurement of complement convertases activity in human serum. *Clin Exp Immunol* 2014;178:142–53.
30. Okroj M, Holmquist E, King BC, Blom AM. Functional analyses of complement convertases using C3 and C5-depleted sera. *PLoS One* 2012;7:e47245.
31. Passmore JS, Lukey PT, Ress SR. The human macrophage cell line U937 as an in vitro model for selective evaluation of mycobacterial antigen-specific cytotoxic T-cell function. *Immunology* 2001;102:146–56.
32. Nagata Y, Diamond B, Bloom BR. The generation of human monocyte/macrophage cell lines. *Nature* 1983;306:597–9.
33. Huang AY, Golumbek P, Ahmadzadeh M, Jaffee E, Pardoll D, Levitsky H. Role of bone marrow-derived cells in presenting MHC class I-restricted tumor antigens. *Science* 1994;264:961–5.
34. Ehlenberger AG, Nussenzweig V. The role of membrane receptors for C3b and C3d in phagocytosis. *J Exp Med* 1977;145:357–71.
35. Praz F, Lesavre P. Alternative pathway of complement activation by human lymphoblastoid B and T cell lines. *J Immunol* 1983;131:1396–9.
36. Kurita M, Matsumoto M, Tsuji S, Kawakami M, Suzuki Y, Hayashi H, et al. Antibody-independent classical complement pathway activation and homologous C3 deposition in xeroderma pigmentosum cell lines. *Clin Exp Immunol* 1999;116:547–53.
37. Rogers LM, Veeramani S, Weiner GJ. Complement in monoclonal antibody therapy of cancer. *Immunol Res* 2014;59:203–10.
38. Gorter A, Meri S. Immune evasion of tumor cells using membrane-bound complement regulatory proteins. *Immunol Today* 1999;20:576–82.
39. Fishelson Z, Donin N, Zell S, Schultz S, Kirschfink M. Obstacles to cancer immunotherapy: expression of membrane complement regulatory proteins (mCRPs) in tumors. *Mol Immunol* 2003;40:109–23.
40. Thurman JM, Holers VM. The central role of the alternative complement pathway in human disease. *J Immunol* 2006;176:1305–10.
41. Swann JB, Smyth MJ. Immune surveillance of tumors. *J Clin Invest* 2007;117:1137–46.
42. Ho PC, Kaech SM. Reenergizing T cell anti-tumor immunity by harnessing immunometabolic checkpoints and machineries. *Curr Opin Immunol* 2017;46:38–44.
43. Yao S, Chen L. Adaptive resistance: a tumor strategy to evade immune attack. *Eur J Immunol* 2013;43:576–9.
44. Alsaab HO, Sau S, Alzhrani R, Tatiparti K, Bhise K, Kashaw SK, et al. PD-1 and PD-L1 checkpoint signaling inhibition for cancer immunotherapy: mechanism, combinations, and clinical outcome. *Front Pharmacol* 2017;8:561.



Suppl. Fig. 1. D 2-HG inhibits both complement and T cells. **A.** D 2-HG inhibits complement at different steps of the complement activation cascade. **B.** D 2-HG inhibits T cell migration, proliferation and cytokine production but enhances Treg cell polarization.

Table S1. Summary of the immunohistochemical staining results

	Grade III astrocytomas		Grade IV astrocytomas		Grade III-IV astrocytomas	
	wtIDH	mIDH	wtIDH	mIDH	wtIDH	mIDH
	N=16	N=23	N=19	N=14	N=35	N=37
C3/C3b						
Intensity score						
Mean ± SEM	1.39 ± 0.17	0.91 ± 0.15	1.63 ± 0.13	0.99 ± 0.19	1.52 ± 0.11	0.94 ± 0.12
Median	1.40	0.75	1.50	0.94	1.50	0.78
P value		0.031*		0.0085#		0.0005#
Fraction score						
Mean ± SEM	2.23 ± 0.32	1.43 ± 0.24	2.86 ± 0.18	1.66 ± 0.37	2.57 ± 0.18	1.52 ± 0.20
Median	2.47	1.13	3.00	1.72	2.87	1.14
P value		0.058*		0.003#		0.0002#
Necrosis intensity						
Mean ± SEM	-	-	1.26 ± 0.17	0.64 ± 0.17	-	-
Median	-	-	1.00	1.00	-	-
P value				0.016#		
Blood vessel intensity						
Mean ± SEM	0.92 ± 0.14	0.99 ± 0.17	1.44 ± 0.19	0.77 ± 0.11	1.20 ± 0.13	0.90 ± 0.11
Median	0.76	0.89	1.50	0.85	1.00	0.87
P value		0.78#		0.0076#		0.085*
CD4						
Mean ± SEM	1.34 ± 0.29	0.54 ± 0.14	2.08 ± 0.47	1.38 ± 0.60	1.74 ± 0.29	0.86 ± 0.25
Median	0.97	0.31	1.40	0.76	1.14	0.41
P value		0.011*		0.14*		0.0013*
CD8						
Mean ± SEM	1.28 ± 0.20	0.56 ± 0.16	2.49 ± 1.06	1.60 ± 0.77	1.94 ± 0.59	0.95 ± 0.31
Median	1.20	0.33	0.89	0.65	0.94	0.33
P value		0.0013*		0.33*		0.0010*
FOXP3						
Mean ± SEM	0.28 ± 0.10	0.12 ± 0.04	0.53 ± 0.17	2.12 ± 2.05	0.41 ± 0.10	0.88 ± 0.77
Median	0.12	0.00	0.17	0.070	0.16	0.059
P value		0.12*		0.042*		0.0064*
FOXP3/CD4 ratio						
Mean ± SEM	0.18 ± 0.05	0.65 ± 0.40	0.27 ± 0.06	0.32 ± 0.22	0.23 ± 0.037	0.52 ± 0.26
Median	0.15	0.06	0.27	0.069	0.19	0.063
P value		0.59*		0.11*		0.13*

* Mann Whitney U test.; # Student's t-test

Supplementary Material and Methods

Patient tissue

The use of human tissue was approved by the Institutional Review Board of the Medical Faculty, Heinrich Heine University, Düsseldorf, Germany (Study No.5848R), the official Danish ethical review board named the Regional Scientific Ethical Committee of the Region of Southern Denmark (Project-ID: S-20150148) and the official Danish data registration authority named the Data Protection Authority (file number: 16/11065), and was performed in accordance with the Declaration of Helsinki. As this study was retrospective using archival brain tumor tissue, no written or verbal consent need be obtained, and none of the patients had prohibited the use of their tissue according to the Danish Tissue Application Register. Tumor grades were selected and sequenced to provide homologous tumor grades expressing, or not, mutant IDH-1, so grade II with high and grade IV with low IDH mutational penetrance are under and over represented, respectively.

Mice, D 2-HG, and complement reagents

Wild-type C57BL/6 mice, ovalbumin peptide 323-339 (OVA₃₂₃₋₃₃₉)-specific TCR transgenic mice (OT II mice), OVA₂₅₇₋₂₆₄ specific TCR transgenic mice (OT I mice) on a C57BL/6 background were purchased from Jackson Laboratory and maintained in the animal facility of the Cleveland Clinic, OH, USA. All animal care and procedures were approved by the Institutional Animal Care and Use Committee of the Cleveland Clinic.

D 2-HG was purchased from Cayman Chemical Company (Ann Arbor, MI, USA) and diluted in PBS. Sheep erythrocytes (E^{shA}) and rabbit erythrocytes (E^{rabb}) were purchased from Hemostat Laboratories (Dixon, CA, USA). Rabbit anti-sheep erythrocyte antibody for the preparation of antibody-sensitized E^{shA} was purchased from Sigma-Aldrich (St. Louis, MO, USA). Veronal Buffer with Mg⁺⁺ & Ca⁺⁺ (GVB⁺⁺) (10 mM Barbitol, 145 mM NaCl, 0.5 mM MgCl₂, 0.15 mM CaCl₂, gelatin 0.1%, pH 7.2 ± 0.15) and Gelatin Veronal Buffer with Mg⁺⁺ & EGTA (GVB-Mg-EGTA) (5 mM Barbitol, 145 mM NaCl, 0.5 mM MgCl₂, 10 mM EGTA and 0.1% gelatin, pH 7.2 ± 0.15) were obtained from Boston BioProducts (Ashland, MA, USA).

Pooled normal human serum (NHS), C3, or C5-depleted sera were purchased from Innovative Research (Novi, MI, USA) and Complement Technology (Tyler, TX, USA), respectively. Guinea pig serum was purchased from MP Biomedicals (Solon, OH, USA).

Immunohistochemistry and image analysis

Formaldehyde-fixed and paraffin-embedded (FFPE) tissue was sliced by microtome into three μm thick sections. Immunohistochemical staining with primary antibodies against C3/C3b (clone 755, 1:1000, Abcam, Cambridge, United Kingdom), CD4 (clone SP35, Ready-to-use, Ventana, Tucson, AZ, USA), CD8 (clone C8/144B, 1:100, Dako, Glostrup, Denmark), and FOXP3 (clone 236A/E7, 1:40 ThermoFisher Scientific, Waltham, MA, USA) were carried out with an automated immunostainer (BenchMark Ultra, Ventana Medical Systems, Inc., Tucson, AZ, USA). Standard protocols included epitope retrieval in cell conditioning 1 buffer (Ventana Medical Systems) for 32 min (CD4, CD8) or 64 min (FOXP3) at 100°C or in mild cell conditioning 1 x buffer for 32 min at 95°C for 32 min followed by protease-3 for 4 min (C3/C3b). Endogenous peroxidase activity was quenched using OptiView peroxidase inhibitor (Ventana Medical Systems). Following incubation with primary antibodies for 16 min (FOXP3), 24 min (CD4) or 32 min (CD8, C3/C3b) at 36°C, the bound antigen-antibody complexes were visualized with OptiView-DAB according to the manufacturer's recommendations. Tissue slides were then counterstained with Hematoxylin II and Bluing Reagent, dehydrated and cleared before coverslipping with a Tissue-Tek® Film® Coverslipper (Sakura, Alphen aan den Rijn, the Netherlands). All slides were scanned with a Hamamatsu Digital Slide Scanner (Hamamatsu, Japan). Image analysis was performed using the Visiopharm software module Stereology (Visiopharm, Hørsholm, Denmark). Sample images were acquired using systematic uniform random sampling (meander fraction based) at 400x magnification (CD4, CD8, FOXP3) or 200x magnification (C3/C3b) ensuring at least 10 images (CD4, CD8, FOXP3) or 5 images (C3/C3b) with vital central tumor tissue per tumor. C3/C3b expression was scored semi-quantitatively assessing both fraction score and intensity score. The fraction score was based on the percentage of C3/C3b expression (0: no expression; 1: <10% expression; 2: 10%–25% expression, 3: >25%–75%, 4: >75%), while the intensity score was based on the staining intensity of C3/C3b (0: faint, 1: moderate, 2: intense). For the CD4, CD8, and FOXP3 staining, the number of CD4⁺, CD8⁺, and FOXP3⁺ T cells was counted in each image based

on the staining and their lymphocyte-like morphology, and a mean cell count was calculated for each tumor. A mean fraction and intensity score was calculated for each tumor. The FOXP3⁺/CD4⁺ ratio was calculated by dividing the mean FOXP3 cell count with the mean CD cell count for each tumor.

A double immunohistochemical staining with primary antibodies against C3/C3b (clone 755, 1:600, Abcam, Cambridge, United Kingdom) and Oligodendrocyte transcription factor (OLIG2, product code 18953, Immuno-Biological Laboratories, Fujioka, Japan), was carried out on the automated DISCOVERY ULTRA staining system (Ventana Medical Systems). Standard protocol included deparaffinization, epitope retrieval in cell conditioning 1 buffer for 32 min and blocking of endogen peroxidase. Sections were then incubated with primary antibody against C3/C3b for 32 min at 36°C followed by detection with DISCOVERY anti-mouse HQ and DISCOVERY anti-HQ HRP using DISCOVERY DAB as chromogen. Next, slides were denatured for 8 min in cell conditioner 2 at 100°C followed by incubation with the second primary antibody against OLIG2 for 32 min at 36°C which was detected using DISCOVERY anti-rabbit HQ and DISCOVERY anti-HQ HRP using DISCOVERY Purple as chromogen. Tissue slides were then counterstained, coverslipped, and digitalized as described above.

Complement classical pathway assay

E^{shA} used in the complement classical pathway assay were first prepared following the manufacturer's protocol. To test the complement inhibitory activity of D 2-HG, approximately 5×10^6 E^{shA} were incubated with 100 μ L of GVB⁺⁺ containing the stated concentrations (10%, 5%, 2%, and 1%) of NHS with 30 mM D 2-HG at 37°C for 10 min. In the D 2-HG titration assay, the same amount of E^{shA} were incubated in 5% of NHS in GVB⁺⁺, in the absence or presence of 0.1 to 30 mM D 2-HG. Spontaneous hemolysis, as the negative control, was detected from E^{shA} that were incubated with 5 mM EDTA in GVB⁺⁺. After incubation, samples were centrifuged at 1000 x g for 1 min. Supernatants (80 μ L) containing released hemoglobin were transferred to a 96-well flat bottom plate to quantitate absorbance at 414 nm. The following equation was used to calculate the percentage of hemolysis: hemolysis (%) = $[(A - B)/(C - B)] \times 100\%$. A = optical density (OD) reading of sample in GVB⁺⁺ with NHS, B = OD reading of sample in GVB⁺⁺ with EDTA, and C = OD reading of maximum hemolysis induced by H₂O.

Complement alternative pathway assay

Approximately 5×10^6 of E^{rabb} were incubated in a total volume of 100 μ L GVB-Mg-EGTA with different amounts of NHS and 30 mM D 2-HG at 37°C for 30 min. Then 20% NHS was chosen for the titration assay, in which E^{rabb} were incubated with or without defined concentrations of the D 2-HG at 37°C for 30 min. For the negative control, 5 mM EDTA was added in GVB Mg-EGTA to inhibit complement activation.

After incubation, cells were recovered by centrifugation, and 80 μ L of the supernatants were collected to measure the optical density at 414 nm. To calculate the percentage of hemolysis, the following equation was used: hemolysis (%) = $[(A - B)/(C - B)] \times 100\%$. A = OD reading of sample in GVB-Mg-EGTA with NHS, B = OD reading of sample in GVB-Mg-EGTA with EDTA, and C = OD reading of maximum hemolysis caused by H₂O.

Complement convertase assays

Erythrocytes (E^{shA} or E^{rabb}) were first incubated with C3- or C5-depleted serum. The lack of C3 or C5 allows the complement cascade to progress only to the stage of C3 (C4b2a, C3bBb) or C5 convertase (C4b2a3b, C3bBbC3b). Then, the addition of guinea pig serum with EDTA initiates lysis only from existing convertase without additional convertase formation.

To test the effects of D 2-HG on the assembly of classical C3 and C5 convertases, E^{shA} were incubated with 5% C3- or C5-depleted serum in GVB⁺⁺ respectively, with or without defined amounts of D 2-HG at 37°C for 5 min. E^{shA} incubated with depleted serum together with 5 mM EDTA were used as negative controls. Afterwards, E^{shA} were washed twice with 500 μ L of GVB⁺⁺. To initiate complement-mediated lysis from pre-assembled convertases, 100 μ L of 20 mM EDTA-GVB⁺⁺ containing 3% guinea pig serum was added to each tube, and samples were incubated for another 20 min at 37°C. Then E^{shA} were centrifuged, and 80 μ L supernatants were collected to measure OD reading at 414 nm. Hemolysis rates were calculated according to the same equation used in the classical pathway functional assay.

The effects of D 2-HG on the assembly of alternative pathway convertase formation were assessed according to the same protocols as for the classical pathway. Here, however, 20% C5-depleted serum in GVB-Mg-EGTA was used to incubate E^{rabb} for 20 min to allow convertase formation.

The role of D 2-HG on the pre-assembled convertases in both classical and alternative pathway was also tested; instead of adding D 2-HG in the first step of convertase formation, D 2-HG at defined concentrations were added after convertase formation, which in the second step with guinea pig serum and EDTA. All the other conditions are the same as described above.

Complement opsonization-mediated phagocytosis assay

The myeloid cell line U937 was cultured with 10 ng/mL phorbol-12-myristate-13-acetate (PMA) (Sigma-Aldrich, St. Louis, MO, USA) for 5 days to differentiate and mature these cells (37, 38). Detached macrophages were labeled by CellTrace™ far red-fluorescent dye (Thermo Fisher Scientific, Waltham, MA, USA) according to manufacturer's instruction and re-suspended to a concentration of 1×10^6 cells/mL. Meanwhile, E^{shA} were labeled by Dil cell-labeling solutions (Thermo Fisher Scientific, Waltham, MA, USA) and re-suspended to 1×10^7 cells/ml. 100 μ L of each cell suspension was added together into glass tubes with or without 30 mM D 2-HG in the presence of 2% C5-depleted serum in HBSS. Mixed cells without C5-depleted serum incubation constituted the negative controls. After 30 min and 120 min incubation at 37°C, double-positive fluorescent cells were quantified by flow cytometry.

Complement-mediated glioma cell damage assay

Complement-mediated glioma cell damage was assessed by a cell cytotoxicity detection kit (Sigma), based on the measurement of lactate dehydrogenase (LDH) activity released from the damaged cells into the culture supernatant. In brief, after sensitization with 5 μ g/ml of each anti-human HLA, anti-human CD55 and anti-human CD46 IgG, 2×10^5 of glioma T98 cells were incubated with 10% or 30% NHS in the presence or absence of various concentrations of D 2-HG (10-30mM), in 100 μ L GVB++ for 30 min or 3 hours. After incubation, supernatants were collected, and the released LDH was detected by reaction mixture and measured by a microtiter plate reader with 490 nm. To calculate the cell damage, the following equation was used: cell damage (percentage of LDH released) = $[(A-B)/(C-B)] \times 100\%$. A represents experimental LDH release, B represents the spontaneous LHD release, and C represents the maximum LDH released that was induced by lysis buffer.

T cell inhibition assays

T cells from the spleens of C57BL/6 mice were enriched by nylon wool and labeled with carboxyfluorescein succinimidyl ester (CFSE) according to manufacturer's instructions (Thermo Fisher Scientific, Waltham, MA USA). T cells (4×10^5) were stimulated with 1 $\mu\text{g}/\text{mL}$ of anti-mouse CD3 and anti-CD28 monoclonal antibodies (BD Biosciences, San Jose, CA, USA) and cultured in RPMI 1640 media with or without defined concentrations of D 2-HG for 3 days. CFSE dilution among T cells was analyzed by flow cytometry. For the bromodeoxyuridine (BrdU) incorporation assays, 10 nM BrdU was added 16h before collection of cells and their supernatants. Then, levels of the incorporated BrdU was measured by BrdU ELISA according to the manufacturer's instructions (Sigma-Aldrich, St. Louis, MO, USA). The culture supernatants were collected for measurements of IFN- γ concentration using an ELISA kit (BioLegend, San Diego, CA, USA).

In another set of experiments, CD4⁺ T cells were isolated from naïve WT C57BL/6 mice, labeled with CFSE, activated by monoclonal antibodies against CD3 and CD28, then cultured under respective Th1, Th17 and Treg polarization conditions following an established protocol in the absence or presence of 30 mM D 2-HG. Proliferation of the CD4⁺ T cells was assessed by CFSE dilution and BrdU incorporation assays on day 3. On day 5, differentiation of Tregs was assessed by staining for CD4, CD25 and FOXP3 followed by flow cytometric analyses, and by measuring levels of IL-10 in the culture supernatants using ELISA (Biolegend)

Bone marrow-derived dendritic cell (DC) differentiation

Total bone marrow cells were flushed from the femurs and tibia of C57BL/6 mice. Erythrocytes were cleared using lysis buffer (155 mM NH₄Cl, 12 mM NaHCO₃, 0.1 mM EDTA). The resultant cells were re-suspended at 2×10^6 /mL in RPMI 1640 with 10% fetal bovine serum, 2 mM glutamine, 100 U/mL penicillin, and 100 mg/mL streptomycin and then cultured in 12-well plates. Additional GM-CSF (10 ng/mL) and IL-4 (100 U/mL) were added into this culture media. Two days later, media with non-adherent cells was gently removed and a half volume of fresh media with the same amount of cytokines was added to the adherent cells. Recovered media was centrifuged and a half volume of the supernatant was added back into the original culture. Simultaneously, final concentrations of D 2-HG (0, 5, 10, and 30 mM) were added. After

another two days, 500 U/mL IFN- γ was added to the media for 24h. Then the expression profile of MHC II, CD11b, CD11c, CD80 and CD86 on the resultant cells were assessed by flow cytometric analyses using respective mAbs (Biolegend,CA).

T cell migration assay

CD4⁺ and CD8⁺ T cells were isolated from splenocytes of C57BL/6 mice using respective isolation kits (Biolegend). 1×10^6 of CFSE-labeled CD4⁺ or CD8⁺ T cells were cultured in the upper chambers a transwell insert cell culture system (Corning, NY, USA) , with or without 5 mM or 30 mM of D 2-HG. 50 ng/mL of Chemokine (C-C motif) ligand 19 (CCL19) were added into the lower chamber to facilitate the cell migration. Transwell inserts without CCL19 were set up as negative controls to measure the spontaneous leakage of cells. After 4h, cells that remained in the inserts and those that migrated into the bottom chambers were quantitated by flow cytometry, and T cell migration was calculated using the following formula: T cell migration (%)= number of T cells in the bottom chamber/ (number of T cells in the bottom chamber + number of T cells in the upper chamber) X 100%.

Differentiated DC function assay

The function of differentiated DCs in the absence or presence of D 2-HG was assessed by their ability to activate antigen-specific T cells isolated from the spleens of OT II mice. In these experiments, 4×10^5 OT II T cells were co-cultured with DCs in the ratio of 10:1 in the absence or presence of 2 μ g/mL OVA₃₂₃₋₃₃₉ peptide (Genscript, NJ). For BrdU-based T cell proliferation assays, 10 nM BrdU was added 16h before the collection of cells and supernatants after a 3-day incubation. The levels of incorporated BrdU was detected by ELISA following the manufacturer's protocol. IFN- γ concentration in culture supernatants was measured by ELISA as before.

DC antigen processing/presentation assay

To assess the potential effect of D 2-HG on DC antigen processing and presentation, bone marrow derived dendritic cells (BM-DCs) were first prepared as before, then incubated with 20 μ g/m OVA protein for 4h in the presence or absence of 30 mM D 2-HG. After this, DCs were washed three times to remove

the D 2-HG in the media, then incubated with 2×10^5 CFSE-labeled CD4⁺ T cells isolated from OT II mice, or CD8⁺ T cells isolated from OT I mice in the ratio of 1:10 in RPMI 1640 media. After 3 days, T cells were stained with either APC-anti-mouse CD4 or CD8 IgGs, and CFSE dilution of the activated OVA-specific T cells were assessed by flow cytometry. Concentrations of IFN- γ and granzyme B in the respective CD4⁺ and CD8⁺ T cells culture supernatants were measured using conventional ELISA (BioLlegend). For BrdU-based T cell proliferation assays, 10 nM BrdU was added 16h before the collection of cells in the third day. The BrdU incorporation was detected by ELISA according to the manufacturer's protocol (Sigma).

13.4 Manuscript IV

“The presence of TIM-3 positive cells in WHO grade III and IV astrocytic gliomas correlates with isocitrate dehydrogenase mutation status”

RESEARCH ARTICLE

The presence of TIM-3 positive cells in WHO grade III and IV astrocytic gliomas correlates with isocitrate dehydrogenase mutation status

Mia D. Sørensen^{1,2} | Ole Nielsen¹ | Guido Reifenberger^{2,3,4} | Bjarne W. Kristensen^{1,2,5,6}

¹Department of Pathology, Odense University Hospital, Odense, Denmark

²Department of Clinical Research, University of Southern Denmark, Odense, Denmark

³Institute of Neuropathology, Heinrich Heine University, Düsseldorf, Germany

⁴German Cancer Consortium (DKT), partner site Essen/Düsseldorf, Essen, Germany

⁵Department of Pathology, Rigshospitalet, Copenhagen University Hospital, Copenhagen, Denmark

⁶Department of Clinical Medicine and Biotech Research and Innovation Center (BRIC), University of Copenhagen, Copenhagen, Denmark

Correspondence

Mia D. Sørensen, Department of Pathology, Odense University Hospital, J. B. Winsløvs Vej 15, 5000, Odense C, Denmark.

Funding information

Danish Council for Independent Research, Grant/Award Number: 4183-00183

Abstract

Diffuse gliomas are aggressive brain tumors that respond poorly to immunotherapy including immune checkpoint inhibition. This resistance may arise from an immunocompromised microenvironment and deficient immune recognition of tumor cells because of low mutational burden. The most prominent genetic alterations in diffuse glioma are mutations in the isocitrate dehydrogenase (IDH) genes that generate the immunosuppressive oncometabolite D-2-hydroxyglutarate. Our objective was to explore the association between IDH mutation and presence of cells expressing the immune checkpoint proteins galectin-9 and/or T cell immunoglobulin and mucin-domain containing-3 (TIM-3). Astrocytic gliomas of World Health Organization (WHO) grades III or IV (36 IDH-mutant and 36 IDH-wild-type) from 72 patients were included in this study. A novel multiplex chromogenic immunohistochemistry panel was applied using antibodies against galectin-9, TIM-3, and the oligodendrocyte transcription factor 2 (OLIG2). Validation studies were performed using data from The Cancer Genome Atlas (TCGA) project. IDH mutation was associated with decreased levels of TIM-3⁺ cells ($p < 0.05$). No significant association was found between galectin-9 and IDH status ($p = 0.10$). Most TIM-3⁺ and galectin-9⁺ cells resembled microglia/macrophages, and very few TIM-3⁺ and/or galectin-9⁺ cells co-expressed OLIG2. The percentage of TIM-3⁺ T cells was generally low, however, IDH-mutant tumors contained significantly fewer TIM-3⁺ T cells ($p < 0.01$) and had a lower interaction rate between TIM-3⁺ T cells and galectin-9⁺ microglia/macrophages ($p < 0.05$). TCGA data confirmed lower *TIM-3* mRNA expression in IDH-mutant compared to IDH-wild-type astrocytic gliomas ($p = 0.013$). Our results show that IDH mutation is associated with diminished levels of TIM-3⁺ cells and fewer interactions between TIM-3⁺ T cells and galectin-9⁺ microglia/macrophages, suggesting reduced activity of the galectin-9/TIM-3 immune checkpoint pathway in IDH-mutant astrocytic gliomas.

KEYWORDS

galectin-9, glioma, immune checkpoint, immunohistochemistry, isocitrate dehydrogenase, microglia, multiplex, TIM-3

This is an open access article under the terms of the Creative Commons Attribution-NonCommercial License, which permits use, distribution and reproduction in any medium, provided the original work is properly cited and is not used for commercial purposes.

© 2020 The Authors. *Brain Pathology* published by John Wiley & Sons Ltd on behalf of International Society of Neuropathology

1 | INTRODUCTION

Somatic mutations in the genes *isocitrate dehydrogenase (IDH) 1* or *2* are found in ~80% of patients with WHO grade II–III diffuse gliomas (1–4). These mutations most frequently occur at codon R132 in *IDH1* or at the homologous residues R172 or R140 in *IDH2*, and are considered early events in gliomagenesis (5–7). IDH mutations were first reported in gliomas in 2008 (2) and have since been discovered in other cancers including acute leukemia (8, 9), angioimmunoblastic T cell lymphoma (10), chondrosarcoma (11, 12), melanoma (13), cholangiocarcinoma (14, 15), and prostate cancer (16). IDH1 is located in the cytoplasm and peroxisomes, whereas IDH2 is found in the mitochondrial matrix, however, both enzymes play important roles in several cellular functions, including glucose sensing, glutamine metabolism, lipogenesis, and regulation of cellular redox balance, especially in the human brain (6, 17). IDH active site mutations result in a neomorphic enzymatic activity generating the oncometabolite D-2-hydroxyglutarate instead of α -ketoglutarate, with concomitant consumption of NADPH to NADP⁺ (5–7). In IDH-mutant gliomas, D-2-hydroxyglutarate accumulates intra- and extracellularly up to concentrations that are 100-fold higher than in IDH-wildtype gliomas (5, 18, 19). D-2-hydroxyglutarate modifies the cellular energetics and epigenetics, including promotion of a DNA hypermethylation phenotype (5–7, 20–23).

Increasing data indicate that IDH mutation and D-2-hydroxyglutarate may modulate the tumor microenvironment and its nonneoplastic cells. Reportedly, IDH-mutant gliomas show suppressed antithrombotic and anticoagulant pathways (24, 25) and have a distinct vascular gene expression signature (26) compared to IDH-wildtype tumors. In addition, mutation in the *IDH* genes has been shown to impact the glioma-associated immune landscape. Generally, the immune microenvironment in gliomas is considered “cold” (27), lymphocyte-depleted/immunological quiet (28), and immunosuppressive because of tumor extrinsic and intrinsic mechanisms (27, 29, 30). IDH mutation and the consecutive expression of the D-2-hydroxyglutarate have been reported to alter the level of immune cell infiltration (20, 28, 31–37), immune activation/response (20, 22, 31, 33, 34, 37–41), and immune checkpoint systems (32–34, 42–44), overall hampering the immunosurveillance and immune-mediated destruction enabling development of “cold” tumors.

Immune responses are tightly regulated by an immune checkpoint system that adjusts the duration and amplitude preventing autoimmunity and tissue damage. Stimulatory checkpoint pathways promote activation of T cells, while inhibitory pathways confine the threshold for T cell activation and regulate resolution of inflammation, tolerance, and homeostasis. In malignancies, the inhibitory checkpoints can be

exploited by the cancer cells to escape immune surveillance. Immunotherapy targeting co-inhibitory immune checkpoints, especially cytotoxic T lymphocyte antigen 4 (CTLA-4) and programmed death receptor 1 (PD-1), has proven effective in several cancers including melanoma and non-small cell lung carcinoma, with combination therapies that target two co-inhibitory receptors/pathways showing increased antitumor efficacy (45–47). Another inhibitory checkpoint system of increasing interest in cancer immunotherapy is the galectin-9 (Gal-9)/T cell immunoglobulin and mucin-domain containing-3 (TIM-3) pathway. TIM-3 is expressed by different subsets of T cells and promotes T cell tolerance when interacting with its ligands including Gal-9. Additionally, TIM-3 has been linked to T cell exhaustion and dysfunction, especially when co-expressed with PD-1 (45, 48–51). Reportedly, TIM-3 is also expressed by cancer cells and cells of the myeloid lineage including macrophages in both non-cancerous and cancerous tissues, and TIM-3 has been shown to regulate immune responses in these cell types as well (48, 52–54). In glioma, Gal-9 (55–57) and TIM-3 (56, 58, 59) have been correlated to tumor aggressiveness, however, little knowledge exists about (a) the protein expression patterns of Gal-9 and TIM-3 at a cell type-specific level in glioma tissue and (b) the association between IDH mutation and expression/activation of the Gal-9/TIM-3 checkpoint system.

The aim of this study was to determine whether protein expression of the Gal-9/TIM-3 checkpoint pathway is affected by IDH mutation status in diffuse astrocytic glioma. Therefore, we investigated glioma tissue samples from a patient cohort with WHO grade III or IV astrocytic gliomas stratified according to IDH status using a novel brightfield multiplex chromogenic immunohistochemistry panel consisting of antibodies against Gal-9, TIM-3, and oligodendrocyte transcription factor 2 (OLIG2). OLIG2 was included in the panel as a glial marker that is commonly expressed in tumor cells of astrocytic gliomas (60, 61) and was used to identify the potential expression of Gal-9 and/or TIM-3 by glial tumor cells. This multiplexing approach facilitated that specific cell subpopulations including co-localization and interaction patterns could be identified within the same tissue slide.

2 | MATERIAL AND METHODS

2.1 | Patient tissue

Formalin-fixed, paraffin-embedded tissue samples from 72 adult glioma patients were used for the multiplex chromogenic immunohistochemistry part of the study. All patients underwent initial surgery between 1997 and 2017 at the Department of Neurosurgery, Odense University Hospital, Odense, Denmark, or at the Department of

Neurosurgery, Heinrich Heine University, Düsseldorf, Germany. The tumor samples were classified according to the WHO Classification 2016 (62). The 72 samples included: 23 IDH-mutant anaplastic astrocytomas, WHO grade III; 16 IDH-wildtype anaplastic astrocytomas, WHO grade III; 14 IDH-mutant glioblastomas, WHO grade IV; and 19 IDH-wildtype glioblastomas, WHO grade IV. IDH status was determined by immunohistochemistry or DNA sequencing as previously described (37, 63). The cohort has been used previously (37), and immunostaining results for CD4, CD8, and FOXP3 from the study were used for correlation analyses in the present study. For the present study, the cohort was additionally immunostained with antibodies against ionized calcium-binding adaptor molecule 1 (IBA-1) and CD204.

A tissue array containing eight to nine IDH-wild-type glioblastoma specimens was included for the double immunofluorescence part of the study to investigate the co-expression patterns of Gal-9/TIM-3, Gal-9/OLIG2, Gal-9/IBA-1, TIM-3/OLIG2, TIM-3/IBA-1, and TIM-3/CD3. In addition, four IDH1 R132H-mutant grade III–IV astrocytic gliomas were selected for double immunofluorescence stainings to examine the co-expression patterns of Gal-9/IDH1 R132H and TIM-3/IDH1 R132H.

2.2 | Multiplex chromogenic immunohistochemistry

A multiplex chromogenic immunohistochemistry panel (Figure 1) was implemented on the Discovery Ultra autostainer (Ventana Medical Systems, Tucson, AZ, USA) by sequential application of unconjugated primary antibodies with heat deactivation steps in between each sequence for elution purposes. Appropriate staining controls were performed during the panel development

to check for possible cross-reactivity related to the detection systems.

Three μm sections from formalin-fixed, paraffin-embedded tissue blocks were mounted on FLEX IHC slides (Dako, Glostrup, Denmark). The tissue sections were subjected to a standard immunostaining protocol including deparaffinization, epitope retrieval in Cell Conditioning 1 buffer (CC1, #950-500, Ventana) for 32 min and blockade of endogenous peroxidase activity. Following the incubation and detection steps described in Table 1, the tissue slides were counterstained with Hematoxylin II (#790-2208, Ventana) and Bluing Reagent (#760-2037, Ventana), dehydrated and cleared. Coverslips were mounted using Pertex® Mounting Medium (#00811, Histolab Products AB, Gothenburg, Sweden). Slides were digitized using a Hamamatsu Digital Slide Scanner (Hamamatsu, Japan).

2.3 | Stereological-based cell counting

Stereological-based image analysis was performed in the Visiopharm software module Stereology (Visiopharm, Hørsholm, Denmark). Vital tumor areas were manually outlined as regions of interest, guided by representative adjacent hematoxylin-eosin stains. Normal brain tissue and areas of tumor infiltration as well as larger areas of necrosis and blood vessels were excluded. Sample images were acquired using systematic uniform random sampling (meander: number of samples-based) at 20 \times magnification. The sampling algorithm was optimized to achieve accurate cell counting. Ultimately, the number of sample images was set at 10 images per tumor. Cell counting was done using a 2 \times 2 counting frame that covered 10% of the sampled image area. Reproducibility was tested by independently performing random sampling

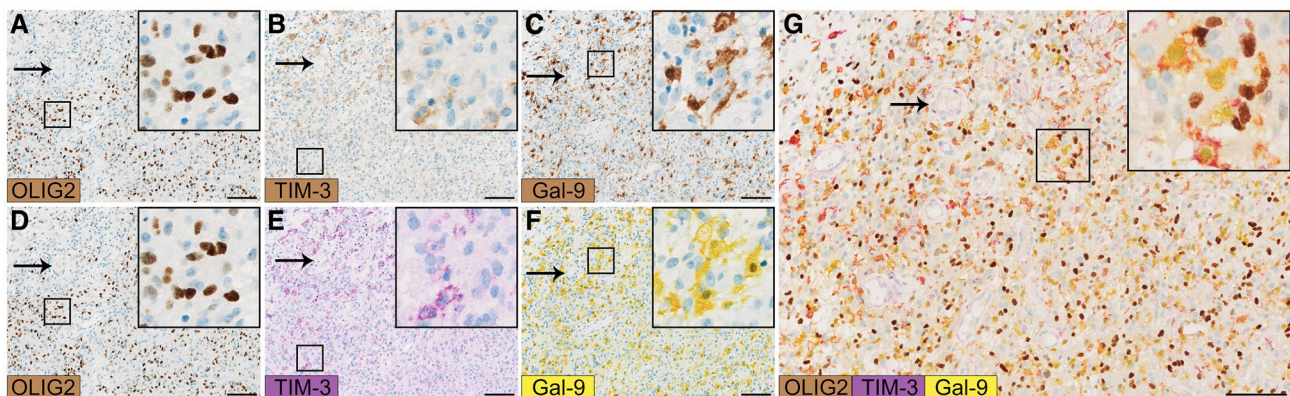


FIGURE 1 Design of the multiplex chromogenic immunohistochemistry panel. The multiplex immunohistochemistry assay was designed after implementing the antibodies by conventional DAB staining (A–C). Chromogens were then assigned for each antibody; brown for the nuclear OLIG2 (D), purple for the membranous/cytoplasmic TIM-3 (E), and yellow for the cytoplasmic Gal-9 (F). For each marker, the staining pattern of the individual DAB-stained slides was comparable to the matched single colored chromogen slide. The multiplexed staining obtained with the panel is shown in G. The use of translucent chromogens (purple and yellow) produced color changes at sites of chromogenic co-localization (red) allowing easy and reliable identification of co-expressing cells, that is, TIM-3⁺ Gal-9⁺ cells. No color mixing was observed between OLIG2 (brown) and TIM-3 (purple) or Gal-9 (yellow) as OLIG2 is expressed in the nuclei. Scale bar 100 μm

OLIG2/TIM-3/Gal-9 multiplex panel	
Pretreatment	Cell Conditioning 1 (CC1, #950-500) 32 min 100°C
Inhibitor	Inhibitor CM (#760-4307) 8 min
Primary Ab #1	Anti-OLIG2 rabbit polyclonal Ab (Immuno-Biological Laboratories, #18953) 1:200, 32 min 36°C
Detection	Anti-Rabbit-HQ (#760-4815) 20 min + anti-HQ-HRP (#760-4820) 20 min
Amplification	No
Chromogen	ChromoMap DAB kit (#760-159) 4 + 8 min
Elution	Cell Conditioning 2 (CC2, #950-123) 8 min 100°C
Primary Ab #2	Anti-TIM-3 rabbit monoclonal Ab (Cell Signaling Technology, clone D5D5R) 1:25, 60 min 36°C
Detection	Anti-Rabbit-HQ (#760-4815) 16 min + anti-HQ-HRP (#760-4820) 16 min
Amplification	No
Chromogen	Purple kit (#760-229) 32 min
Elution	CC2 8 min 100°C
Primary Ab #3	Anti-Gal-9 rabbit monoclonal Ab (Cell Signaling Technology, clone D9R4A) 1:100, 48 min 36°C
Detection	Anti-Rabbit-NP (#760-4817) 12 min + anti-NP-AP (#760-4827) 12 min
Amplification	No
Chromogen	Yellow kit (#760-239) 44 min

TABLE 1 Summary of technical conditions used for the multiplex chromogenic immunohistochemistry panel

Note: Apart from the antibodies, the slides were colored using #Ventana reagents. Prior to the development of the multiplex panel, all antibodies were implemented as conventional immunohistochemistry DAB stainings using OptiView (Ventana) as detection system and then tested with the Discovery HQ-HRP detection system (anti-Rabbit-HQ 20 min + anti-HQ-HRP 20 min) using DAB as chromogen.

Abbreviations: Ab, antibody; AP, alkaline phosphatase; HRP, horseradish peroxidase; NP, nitroprazole.

and cell counting twice on a training set of seven glioblastomas ($r_s = 0.91$, $p < 0.001$).

Eight different cell populations were counted. Tumor cells were defined as OLIG2⁺ cells. Tumor-associated microglia/macrophages (TAMs) were defined as OLIG2⁻ cells with expression of Gal-9 and/or TIM-3 with microglial/macrophage-like morphology (i.e., larger cells that were amoeboid, elongated, or ramified in shape with evident cytoplasm). T cells were defined as OLIG2⁻ Gal-9⁻ TIM-3⁺ cells with lymphocyte morphology (i.e., smaller round-shaped cells with prominent nuclei and sparse cytoplasm). Endothelial cells were not counted. The number of cells in the following cell populations was quantified:

- (i) Negative cells (OLIG2⁻ TIM-3⁻ Gal-9⁻ cells)
- (ii) TIM-3⁻ and Gal-9⁻ tumor cells (OLIG2⁺ TIM-3⁻ Gal-9⁻ cells)
- (iii) TIM-3⁻ and Gal-9⁺ tumor cells (OLIG2⁺ TIM-3⁻ Gal-9⁺ cells)
- (iv) TIM-3⁺ and Gal-9⁺ tumor cells (OLIG2⁺ TIM-3⁺ Gal-9⁺ cells)
- (v) Gal-9⁺ TAMs (OLIG2⁻ TIM-3⁻ Gal-9⁺ cells)
- (vi) TIM-3⁺ and Gal-9⁺ TAMs (OLIG2⁻ TIM-3⁺ Gal-9⁺ cells)

- (vii) TIM-3⁺ TAMs (OLIG2⁻ TIM-3⁺ Gal-9⁻ cells with microglial/macrophage-like morphology)
- (viii) TIM-3⁺ T cells (OLIG2⁻ TIM-3⁺ Gal-9⁻ cells with lymphocyte morphology)

Additionally, the number of interactions between TIM-3⁺ T cells and Gal-9⁺ cells was assessed. To count as an interaction, a TIM-3⁺ T cell had to be in direct contact with a Gal-9⁺ cell, with no other cell type residing in between the two cells. The interaction rate was estimated by dividing the interaction count with the TIM-3⁺ T cell count. Cells fractions were calculated for the specific cell population based on the total cell count as well as on the total number of tumor cells for the tumor cell population and the total number of TAMs for the TAM cell population. All fractions were converted to percentages by multiplying by 100.

2.4 | Conventional immunohistochemistry and automated quantitative image analysis

Formalin-fixed, paraffin-embedded tissue specimens were processed as described above. The tissue sections were stained according to a standard immunostaining

protocol including deparaffinization, epitope retrieval in CC1 (Ventana) for 32 min at 100°C, and blockade of endogenous peroxidase activity. Sections were then incubated with primary antibodies against IBA-1 (cat. no. 019-19741, Wako Pure Chemical Ind., Ltd., dilution 1:2000) and CD204 (clone SRA-E5, Cosmo Bio Co. LTD, dilution 1:600) for 16 and 32 min, respectively, at 36°C. Detection was performed using the OptiView DAB IHC Detection Kit (#760-700, Ventana). The processes of counterstaining, coverslipping, and slide digitization were performed as described above. Automated digital image analysis and quantification were done in the Visiopharm APP author module as previously described (64, 65). Output variables were percentages of positive area, defined as the area of positive expression divided by the total area of interest multiplied by 100.

2.5 | Double immunofluorescence and automated quantitative image analysis

Three μm sections from a formalin-fixed, paraffin-embedded tissue microarray were mounted onto FLEX IHC slides (Dako) and stained on the DISCOVERY Ultra autostainer (Ventana) (Table S1). Following deparaffinization, epitope retrieval was performed in CC1 buffer for 32 or 48 min at 100°C, and endogenous peroxidase activity was inhibited with Inhibitor CM. Slides were then incubated with primary antibody #1 (Gal-9, TIM-3, or IDH1 R132H) followed by detection with DISCOVERY OmniMap anti-Rabbit or anti-Mouse HRP (#760-4311)/DISCOVERY Cyanine 5 Kit (#760-238) system. Next, heat denaturation was performed in Cell Conditioning 2 buffer for 8 min at 100°C followed by incubation with primary antibody #2 (OLIG2, IBA-1, CD3, Gal-9, or TIM-3). The antigen-antibody complex was detected with the DISCOVERY OmniMap anti-Rabbit HRP/DISCOVERY FAM kit (#760-243) system. Slides were coverslipped with VECTASHIELD[®] Mounting Media containing 4,6-diamidino-2-phenylindole (DAPI) (VWR International, Radnor, PA, USA).

Super images were generated at 1.25 \times magnification using brightfield settings and the Visiopharm integrated microscope and software module connected to a Leica DM 6000B microscope with Olympus DP72 camera (Olympus, Ballerup, Denmark) and a Ludl motorized stage. Sample images were obtained as described above. Images were analyzed by generating pixel- and threshold-based algorithms in the Visiopharm APP author module as described previously (65). Output variables were percentages of double-positive area, defined as the area of double-positive expression divided by the total area of respective area of interest multiplied by 100.

2.6 | TCGA patient data set analyses

The mRNA expression levels of *OLIG2*, *TIM-3* (also known as Hepatitis A virus cellular receptor 2, *HAVCR2*), and *Gal-9* (*LGALS9*) as well as *CD4*, *CD8A*, *CD8B*, *FOXP3*, allograft inflammatory factor 1 (*AIFI*, also known as IBA-1), macrophage scavenger receptor 1 (*MSRI*, also known as CD204), secreted phosphoprotein 1 (*SPPI*, also known as osteopontin), interleukin-1 β (*IL1B*), *IL6*, *IL18*, C–C motif chemokine ligand 2 (*CCL2*), and Toll-like receptor (*TLR*)-1, 2, and 8 were examined in data sets of WHO grade III–IV astrocytomas included in The Cancer Genome Atlas (TCGA) database using GlioVis (<http://gliovis.bioinfo.cnio.es/>, data exported June or October 2020) (66). mRNA data were available for 255 tumors with known IDH status and without 1p/19q codeletion (67). The 255 tumors included 42 IDH-wild-type anaplastic astrocytomas, WHO grade III; 72 IDH-mutant anaplastic astrocytomas, WHO grade III; 133 IDH-wild-type glioblastomas, WHO grade IV; and eight IDH-mutant glioblastomas, WHO grade IV. Additionally, mRNA expression levels of some of the same genes were investigated in a data set of 160 WHO grade II and III gliomas with known IDH status with or without 1p/19q codeletion (67). These 160 tumors included 65 IDH-mutant and 1p/19q-codeleted oligodendrogliomas, WHO grade II; 43 IDH-mutant and 1p/19q-codeleted anaplastic oligodendrogliomas, WHO grade III; 43 IDH-mutant (1p/19q-non-codeleted) diffuse astrocytomas, WHO grade II; and 9 IDH-wild-type (1p/19q-non-codeleted) diffuse astrocytomas, WHO grade II. Differential expression analysis was done using the TCGA Agilent-4502A glioblastoma data set (68) to explore quantitative changes in mRNA expression levels of 17,811 genes between the groups of glioblastomas with the highest ($n = 122$) and lowest ($n = 120$) mRNA expression level of TIM-3. Kyoto Encyclopedia of Genes and Genomes (KEGG) and Gene Ontology (GO) enrichment analyses were performed for the differentially regulated genes using the GlioVis explore module with the following input parameters: p -value: 0.05; q -value: 0.05; and log₂ fold change (FC): 2.

2.7 | Statistical analyses

Mann–Whitney U -test or Student's unpaired t -test was used to investigate the difference in protein or mRNA expression levels between IDH-mutant and IDH-wild-type tumors. One-way ANOVA with Bonferroni's Multiple Comparison Test or Kruskal–Wallis test with Dunn's Multiple Comparison Test was used when comparing more than two groups. Correlation analyses were done using Spearman's correlation test. Statistical analyses were performed in Prism (Version 5, GraphPad Software Inc., San Diego, CA, USA). $p < 0.05$ was considered significant.

3 | RESULTS

3.1 | Cellular expression patterns of Gal-9 and TIM-3

In all tumor specimens, most Gal-9⁺ and/or TIM-3⁺ cells morphologically resembled microglia/macrophages (Figure 1). TIM-3 was primarily located in the membrane, while Gal-9 showed a cytoplasmic expression pattern. The expression of Gal-9 and TIM-3 by IBA-1⁺ microglia/macrophages was confirmed using double immunofluorescence as ~80% of the Gal-9 and TIM-3

area co-expressed IBA-1, whereas only ~30% and ~20% of the IBA-1 signal co-localized with Gal-9 and TIM-3 signals, respectively (Figure 2A–D). Most TIM-3⁺ cells co-expressed Gal-9, while many of Gal-9⁺ cells lacked expression of TIM-3 (Figures 1 and 3), and this was validated with double immunofluorescence (Figure 2E,F). Very few TIM-3⁺ Gal-9⁻ cells were observed, and these cells either resembled T cells or microglia/macrophages (Figure 3). T cell expression of TIM-3 was confirmed by double immunofluorescence showing that ~10% of CD3⁺ T cells co-expressed TIM-3 (Figure 2G,H).

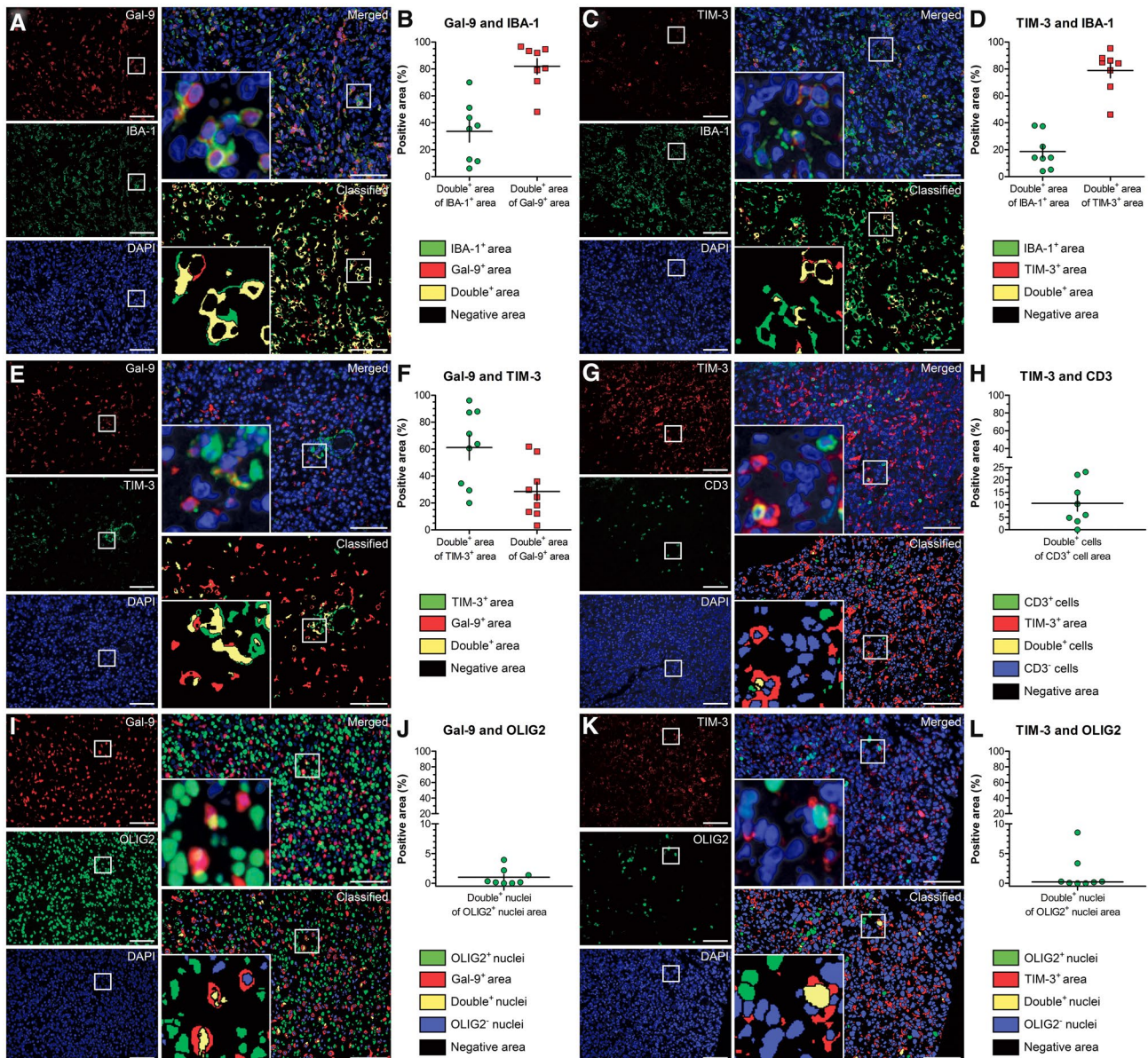


FIGURE 2 Co-expression patterns of Gal-9 and TIM-3 in glioblastoma. (A–D) Gal-9 and TIM-3 often co-localized with IBA-1, while the majority of the IBA-1⁺ cells lacked Gal-9 and TIM-3 expression. (E–F) TIM-3 was frequently co-expressed with Gal-9, while most Gal-9⁺ cells lacked TIM-3 expression. (G–H) Only a small population of CD3⁺ T cells expressed TIM-3. (I–L) Most OLIG2⁺ cells neither expressed Gal-9 nor TIM-3. Scale bar 100 μ M

3.2 | Association between IDH status and Gal-9 and/or TIM-3 expression in tumor cells

OLIG2⁺ tumor cells were observed in nearly all specimens and accounted for ~45%–50% of the cells in both

IDH-mutant and IDH-wild-type tumors (Figure 3A,B), and no significant IDH-dependent difference was detected ($p = 0.58$) (Figure 4A and Table 2). Irrespective of IDH status, most OLIG2⁺ cells did not exhibit membranous TIM-3 or cytoplasmic Gal-9 expression

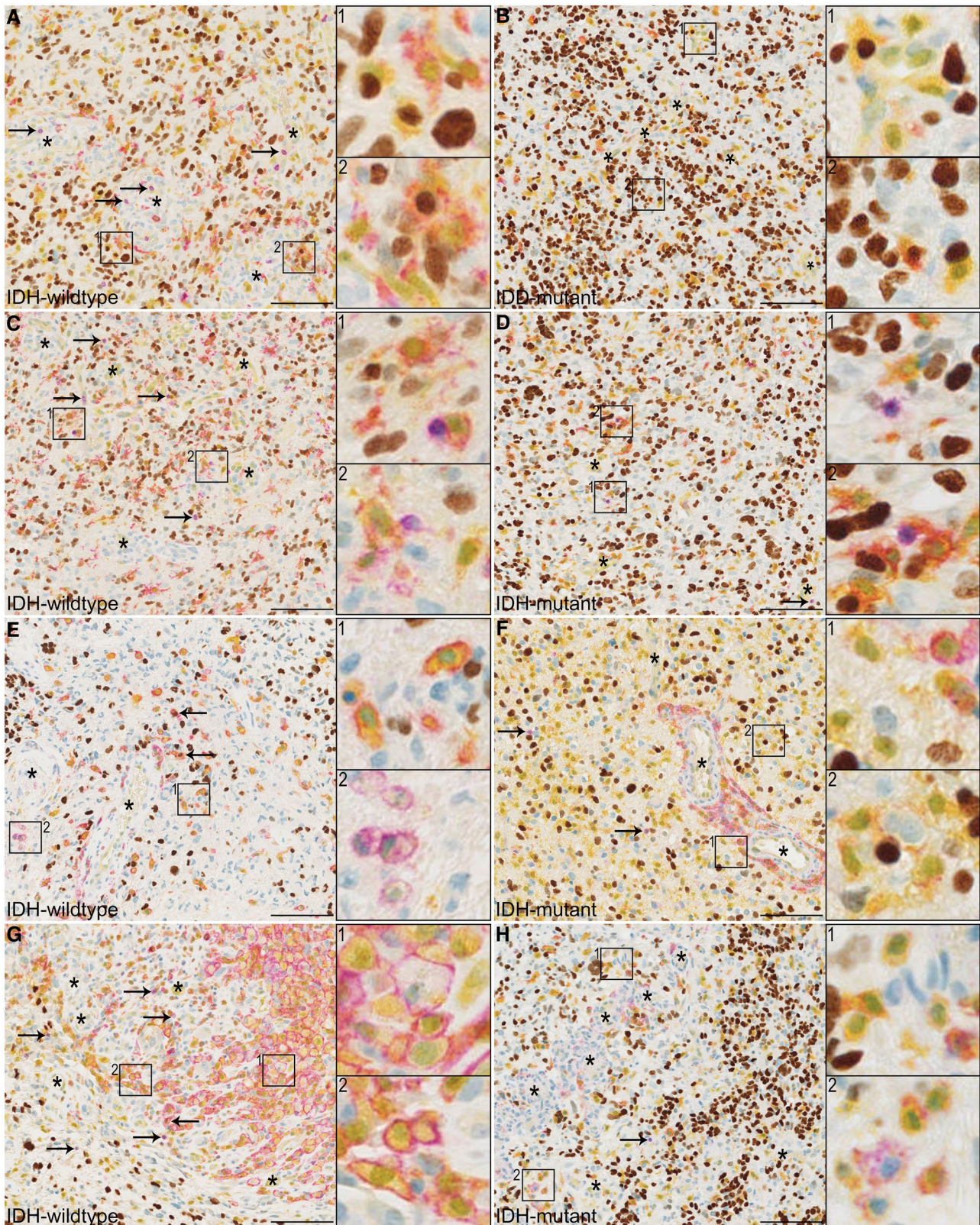


FIGURE 3 Expression patterns of Gal-9, TIM-3, and OLIG2 in IDH-wild-type and IDH-mutant astrocytic gliomas of WHO grades III and IV. (A–B) OLIG2 and Gal-9 were widely expressed in most tumors regardless of IDH mutation status. A weak Gal-9 expression was observed in vascular structures (indicated by *asterisk*). Few TIM-3⁺ cells were observed, but often resembled either microglia/macrophages or T cells (indicated by *rightward arrows*) with the latter often located in or proximate to vascular structures. Gal-9⁺ tumor cells (*insert 1*) and Gal-9⁺ TIM-3⁺ tumor cells (*insert 2*) were found in both IDH-wild-type and IDH-mutant tumors, although in sparse numbers. (C–D) The percentage of TIM-3⁺ T cells and the interactions between TIM-3⁺ T cells and Gal-9⁺ TAMs (inserts) appeared higher in IDH-wild-type compared to IDH-mutant tumors. (E–H) TIM-3⁺ cells were more dispersed in IDH-wild-type tumors, while they were more concentrated around blood vessels in IDH-mutant tumors (*asterisks*). Gal-9⁺ TIM-3⁺ microglia/macrophages and Gal-9⁻ TIM-3⁺ microglia/macrophages appeared to be more prevalent in IDH-wild-type tumors compared to IDH-mutant tumors. *Scale bar* 100 μ M. *Asterisk* indicates blood vessels. *Rightward arrows* in (A,C,D,F–H) indicate TIM-3⁺ T cells. *Leftward arrows* in (E,G) indicate Gal-9⁺ TIM-3⁺ tumor cells. *Chromogen colors* brown (OLIG2), purple (TIM-3), yellow (Gal-9), and red (TIM-3 and Gal-9 color mixing)

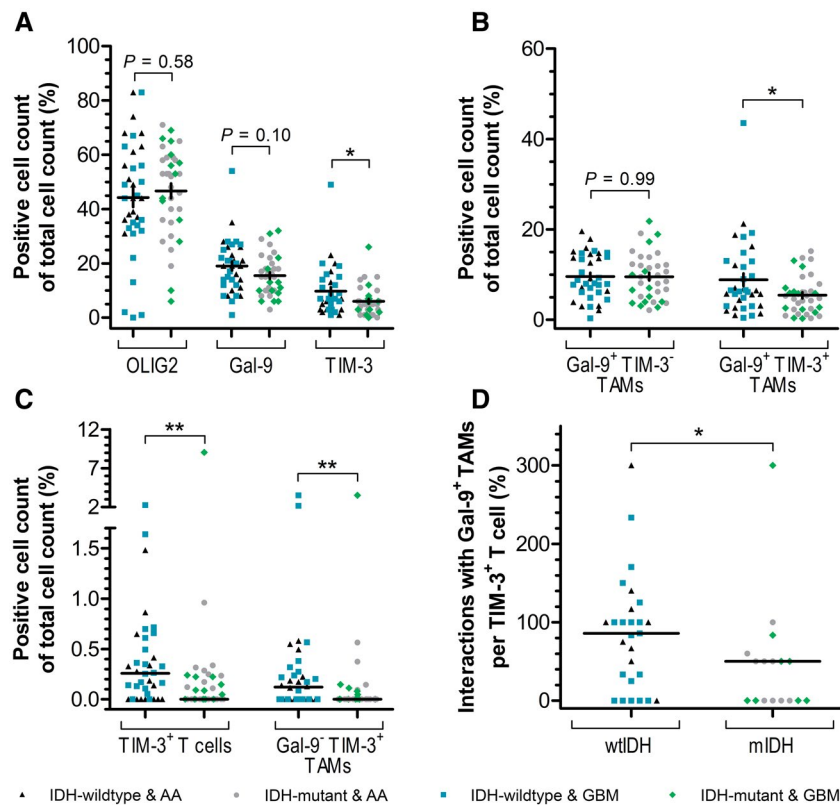


FIGURE 4 Associations between IDH mutation and protein expression of Gal-9, TIM-3, and OLIG2. (A) The percentage of TIM-3⁺ cells was significantly lower in IDH-mutant tumors compared to IDH-wild-type tumors, while expression levels of OLIG2 and Gal-9 was IDH-independent. (B) The percentage of Gal-9⁺ TIM-3⁺ TAMs was lower in IDH-mutant tumors than in IDH-wild-type tumors. (C) The percentages of TIM-3⁺ T cells and Gal-9⁻ TIM-3⁺ TAMs were decreased in IDH-mutant tumors compared to IDH-wild-type tumors. (D) The interaction rate between TIM-3⁺ T cells and Gal-9⁺ TAMs was lower in IDH-mutant tumors than in IDH-wild-type tumors. *Horizontal lines* indicate mean (A,B) or median (C,D). *Vertical lines* indicate \pm standard error of the mean (SEM) (A, B). *indicates $p < 0.05$; ** $p < 0.01$

(mean \pm SEM (%): 98.9 ± 0.15 and 98.8 ± 0.20 for IDH-mutant and IDH-wild-type tumors, respectively, $p = 0.73$) (Table 3). About 1% of the OLIG2⁺ cells expressed Gal-9 in both IDH-mutant and IDH-wild-type tumors (mean \pm SEM (%): 0.83 ± 0.14 and 1.04 ± 0.19 , respectively, $p = 0.77$) (Figure 3A,B and Table 3), and generally Gal-9⁺ tumor cells only accounted for $\sim 0.50\%$ of the total cell population (Table 2). TIM-3 was rarely expressed by OLIG2⁺ cells and only seen when co-expressed with Gal-9 (Figure 3A,B). The presence of TIM-3⁺ tumor cells was independent of the IDH status (mean \pm SEM (%): 0.31 ± 0.08 and 0.19 ± 0.05 for IDH-mutant and

IDH-wild-type tumors, respectively, $p = 0.34$) (Table 3). Overall, TIM-3⁺ tumor cells only comprised $\sim 0.10\%$ of the total cell population (Table 2). Similar results were found when separately analyzing the immunopositivity in the groups of anaplastic astrocytomas and glioblastomas (Table 2 and Table 3). The low expression levels of Gal-9 and TIM-3 in OLIG2⁺ cells and astrocytic tumor cells in general were confirmed using double immunofluorescence with OLIG2 (Figure 2I–L) or IDH1 R132H (Figure S1). Correlation analyses showed that OLIG2 was negatively correlated with both TIM-3 ($r_s = -0.45$, $p < 0.05$) and Gal-9 ($r_s = -0.54$, $p < 0.01$) (Figure S2A)

TABLE 2 Summary of the immunostaining results for all cell populations

	Anaplastic astrocytoma		Glioblastoma		All astrocytic gliomas	
	WHO grade III		WHO grade IV		WHO grade III-IV	
	wtIDH	mIDH	wtIDH	mIDH	wtIDH	mIDH
	<i>n</i> = 16	<i>n</i> = 23	<i>n</i> = 19	<i>n</i> = 14	<i>n</i> = 35	<i>n</i> = 37
Total OLIG2 ⁺ cells						
Mean ± SEM (%)	52.6 ± 3.87	47.3 ± 2.86	37.6 ± 5.02	45.6 ± 5.71	44.3 ± 3.47	46.7 ± 2.71
Median (%)	50.0	52.0	35.5	53.0	44.0	52.5
<i>p</i> -value		0.27 ^a		0.31 ^a		0.58 ^a
Total Gal-9 ⁺ cells						
Mean ± SEM (%)	19.0 ± 1.92	16.1 ± 1.34	19.0 ± 2.55	14.4 ± 2.47	19.0 ± 1.63	15.5 ± 1.22
Median (%)	19.0	16.0	18.5	11.0	19.0	15.0
<i>p</i> -value		0.21 ^a		0.19 ^b		0.10 ^b
Total TIM-3 ⁺ cells						
Mean ± SEM	8.13 ± 1.65	5.83 ± 0.93	11.0 ± 2.36	6.31 ± 1.86	9.69 ± 1.50	6.00 ± 0.88
Median	6.50	5.00	8.00	6.00	7.00	5.00
<i>p</i> -value		0.20 ^a		0.061 ^b		0.024^b
Gal-9 ⁻ TIM-3 ⁻ tumor cells						
Mean ± SEM (%)	51.8 ± 3.74	46.8 ± 2.82	37.0 ± 4.95	45.1 ± 5.65	43.6 ± 3.40	46.2 ± 2.67
Median (%)	49.5	51.0	35.1	52.4	43.2	51.6
<i>p</i> -value		0.43 ^a		0.30 ^a		0.55 ^a
Gal-9 ⁺ TIM-3 ⁻ tumor cells						
Mean ± SEM (%)	0.64 ± 0.16	0.41 ± 0.09	0.44 ± 0.13	0.35 ± 0.11	0.53 ± 0.10	0.39 ± 0.07
Median	0.46	0.30	0.17	0.24	0.24	0.29
<i>p</i> -value		0.50 ^b		0.97 ^b		0.73 ^b
Gal-9 ⁺ TIM-3 ⁺ tumor cells						
Mean ± SEM (%)	0.10 ± 0.05	0.11 ± 0.04	0.09 ± 0.03	0.15 ± 0.04	0.09 ± 0.03	0.13 ± 0.03
Median (%)	0.00	0.00	0.00	0.15	0.00	0.04
<i>p</i> -value		0.73 ^b		0.16 ^b		0.33 ^b
Gal-9 ⁺ TIM-3 ⁻ TAMs						
Mean ± SEM (%)	10.7 ± 1.45	9.91 ± 0.87	8.57 ± 0.93	8.81 ± 1.81	9.54 ± 0.83	9.51 ± 0.84
Median (%)	13.08	9.85	7.92	6.55	8.40	9.36
<i>p</i> -value		0.60 ^a		0.90 ^a		0.99 ^a
Gal-9 ⁺ TIM-3 ⁺ TAMs						
Mean ± SEM (%)	7.48 ± 1.57	5.61 ± 0.89	9.89 ± 2.15	5.02 ± 1.11	8.82 ± 1.38	5.40 ± 0.69
Median (%)	5.71	4.75	6.82	5.79	6.35	5.00
<i>p</i> -value		0.32 ^b		0.068 ^b		0.044^b
Gal-9 ⁻ TIM-3 ⁺ TAMs						
Mean ± SEM	0.16 ± 0.05	0.05 ± 0.03	0.41 ± 0.20	0.30 ± 0.27	0.30 ± 0.11	0.14 ± 0.10
Median	0.12	0.00	0.13	0.00	0.12	0.00
<i>p</i> -value		0.014^b		0.16 ^b		0.004^b
TIM-3 ⁺ T cells						
Mean ± SEM (%)	0.29 ± 0.10	0.12 ± 0.05	0.47 ± 0.13	0.77 ± 0.69	0.39 ± 0.28	0.36 ± 0.25
Median (%)	0.16	0.00	0.29	0.10	0.26	0.00
<i>p</i> -value		0.13 ^b		0.014^b		0.002^b
Interactions with Gal-9 ⁺ tumor cell per TIM-3 ⁺ T cell						
Mean ± SEM	2.22 ± 2.22	11.1 ± 11.1	6.48 ± 5.58	0.00 ± 0.00	5.06 ± 3.77	5.88 ± 5.88

(Continues)

TABLE 2 (Continued)

	Anaplastic astrocytoma		Glioblastoma		All astrocytic gliomas	
	WHO grade III		WHO grade IV		WHO grade III-IV	
	wtIDH	mIDH	wtIDH	mIDH	wtIDH	mIDH
	<i>n</i> = 16	<i>n</i> = 23	<i>n</i> = 19	<i>n</i> = 14	<i>n</i> = 35	<i>n</i> = 37
Median	0.00	0.00	0.00	0.00	0.00	0.00
<i>p</i> -value		1.00 ^b		–		0.61 ^b
Interactions with Gal-9 ⁺ TAMs per TIM-3 ⁺ T cell						
Mean ± SEM	105 ± 27.8	34.4 ± 12.0	74.4 ± 16.1	60.4 ± 36.0	84.7 ± 14.2	46.7 ± 17.8
Median	100	50.0	84.5	25.0	85.7	50.0
<i>p</i> -value		0.017^b		0.28 ^b		0.025^b

Bold values indicate that the difference is significant ($p < 0.05$).

Abbreviations: mIDH, IDH-mutant; TAMs, tumor-associated microglia/macrophages; wtIDH, IDH-wild-type.

^aStudent's *t*-test.

^bMann–Whitney *U*-test.

suggesting that the tumor cell density was lower in tumors and/or tumor areas with high levels of TIM-3 and Gal-9 expression.

3.3 | Association between IDH status and expression of Gal-9 and/or TIM-3

Gal-9 was widely distributed in all tumors and also weakly expressed by most blood vessels (Figure 3A–D). The overall percentage of Gal-9⁺ cells tended to be lower in IDH-mutant than in IDH-wild-type tumors ($p = 0.10$) accounting for ~15% and ~20% of all cells, respectively (Figure 4A and Table 2). TIM-3⁺ cells were often found around vascular structures in IDH-mutant tumors (Figure 3F,H), while they were detected both perivascularly as well as in a more dispersed manner in IDH-wild-type tumors (Figure 3E,G). The TIM-3⁺ cell population was significantly lower in IDH-mutant than in IDH-wild-type tumors ($p = 0.024$) contributing with ~6% and ~10% of the total cell count, respectively. Spearman's correlation analysis showed a strong positive correlation between the percentages of Gal-9⁺ and TIM-3⁺ cells ($r_s = 0.73$, $p < 0.0001$) (Figure S2A,B).

3.4 | Association between IDH status and expression of Gal-9 and/or TIM-3 in tumor-associated immune cells

Gal-9⁺ TIM-3[−] TAMs comprised ~10% of the cells in both IDH-mutant and IDH-wild-type tumors ($p = 0.99$), whereas the percentage of Gal-9⁺ TIM-3⁺ TAMs was lower in IDH-mutant tumors compared to IDH-wild-type tumors (~5% vs. 9%, respectively, $p = 0.044$) (Figure 4B and Table 2). The presence of Gal-9[−] TIM-3⁺ TAMs were generally low irrespective of the IDH status, however, the percentage was significantly lower in IDH-mutant tumors (~0.15% vs. 0.30%, $p = 0.004$) (Figure 4C and Table 2). Similarly, TIM-3⁺ T cells were rarely found, but

the median percentage was significantly lower in IDH-mutant tumors (0.00% vs. 0.26%, $p = 0.002$) (Figure 4C and Table 2). Almost none of the TIM-3⁺ T cells interacted with Gal-9⁺ tumor cells. In contrast, ~85%–100% of TIM-3⁺ T cells interacted with Gal-9⁺ TAMs in IDH-wild-type tumors, whereas a 50% interaction rate was found in IDH-mutant tumors ($p = 0.025$) (Figures 3C,D, 4D and Table 2). Similar outcomes/tendencies were obtained when stratifying according to WHO grade and IDH status.

Looking only at the population of TAMs, the percentage of Gal-9⁺ TIM-3⁺ TAMs was significantly lower in IDH-mutant compared to IDH-wild-type tumors (mean ± SEM (%): 34.7 ± 3.12 and 44.1 ± 3.49, $p = 0.048$) (Table 3). TIM-3⁺ TAMs often appeared amoeboid and had a large cytoplasm that expressed Gal-9 to varying extents (Figure 3E–H). Inversely, the percentage of Gal-9⁺ TIM-3[−] TAMs was significantly higher in IDH-mutant compared to IDH-wild-type tumors (mean ± SEM (%): 64.6 ± 3.14 and 54.4 ± 3.49, respectively, $p = 0.033$). Few Gal-9[−] and TIM-3⁺ TAMs were seen, accounting for <1% of the TAM population, but the actual percentage was significantly lower in IDH-mutant tumors ($p = 0.012$) (Table 3). Similar results/tendencies were found stratifying based on WHO grade and IDH status (Table 3).

Next, we investigated the association between Gal-9/TIM-3 expression and the different T cell populations by performing correlation analyses using the CD4, CD8, and FOXP3 immunostaining results from our previous study (37). Both Gal-9 and TIM-3 positively correlated with all three T cell markers (CD4: $r_s = 0.51$ and $r_s = 0.53$, $p < 0.001$; CD8: $r_s = 0.58$ and $r_s = 0.52$, $p < 0.001$; and FOXP3: $r_s = 0.42$ and $r_s = 0.49$, $p < 0.001$) (Figure S2A).

3.5 | In silico analyses of TCGA data sets

To explore the impact of IDH status on the expression levels of *Gal-9* and *TIM-3* at the transcriptional level, we

TABLE 3 Summary of the immunostaining results for tumor cells and TAMs

	Anaplastic astrocytoma		Glioblastoma		All astrocytic gliomas	
	WHO grade III		WHO grade IV		WHO grade III-IV	
	wtIDH	mIDH	wtIDH	mIDH	wtIDH	mIDH
	n = 16	n = 23	n = 19	n = 14	n = 35	n = 37
<i>Tumor cells^a</i>						
Gal-9 ⁻ and TIM-3 ⁻						
Mean ± SEM	98.8 ± 0.28	98.9 ± 0.17	98.8 ± 0.29	98.9 ± 0.29	98.8 ± 0.20	98.9 ± 0.15
Median	98.7	99.0	99.3	99.1	99.1	99.1
p-value		0.97 ^b		0.89 ^a		0.73 ^a
Gal-9 ⁺ and TIM-3 ⁻						
Mean ± SEM	1.09 ± 0.25	0.88 ± 0.18	0.99 ± 0.28	0.75 ± 0.20	1.04 ± 0.19	0.83 ± 0.14
Median	1.09	0.74	0.48	0.50	0.60	0.64
p-value		0.63 ^b		0.99 ^b		0.77 ^b
Gal-9 ⁺ and TIM-3 ⁺						
Mean ± SEM	0.16 ± 0.07	0.26 ± 0.10	0.21 ± 0.07	0.39 ± 0.14	0.19 ± 0.05	0.31 ± 0.08
Median	0.00	0.00	0.00	0.28	0.00	0.07
p-value		0.65 ^b		0.21 ^b		0.34 ^b
<i>TAMs^d</i>						
Gal-9 ⁺ and TIM-3 ⁻						
Mean ± SEM	59.2 ± 6.16	66.5 ± 3.88	50.6 ± 3.83	61.3 ± 5.40	54.4 ± 3.49	64.6 ± 3.14
Median	65.7	68.2	52.9	57.9	54.6	64.0
p-value		0.30 ^a		0.11 ^a		0.033^a
Gal-9 ⁺ and TIM-3 ⁺						
Mean ± SEM	39.9 ± 6.11	33.1 ± 3.92	47.5 ± 3.93	37.5 ± 5.28	44.1 ± 3.49	34.7 ± 3.12
Median	34.3	31.8	44.9	39.7	43.0	36.0
p-value		0.33 ^a		0.13 ^a		0.048^a
Gal-9 ⁻ and TIM-3 ⁺						
Mean ± SEM	0.92 ± 0.26	0.44 ± 0.28	1.94 ± 0.79	1.17 ± 0.78	1.49 ± 0.46	0.70 ± 0.34
Median	0.68	0.00	0.57	0.00	0.67	0.00
p-value		0.021^b		0.39 ^b		0.012^b

Bold values indicate that the difference is significant ($p < 0.05$).

Abbreviations: mIDH, IDH-mutant; TAMs, tumor-associated microglia/macrophages; wtIDH, IDH-wild-type.

^aStudent's *t*-test.

^bMann-Whitney *U*-test.

^cTumor cells were defined as OLIG2⁺ cells.

^dTAMs were defined as OLIG2⁻, Gal-9^{+/+} and TIM-3^{-/+} cells with microglial/macrophage-like morphology.

performed *in silico* analyses based on data provided in the TCGA database (<http://gliovis.bioinfo.cnio.es/>). In line with our immunohistochemical findings, IDH-mutant astrocytic gliomas of WHO grade III and IV showed a lower *TIM-3* mRNA expression compared to corresponding IDH-wild-type astrocytic gliomas ($p = 0.013$). A similar tendency was seen for *Gal-9* expression levels ($p = 0.074$). Similar to the protein data, a strong positive correlation was found between *Gal-9* and *TIM-3* mRNA expression levels ($r_s = 0.88$, $p < 0.0001$). Furthermore, *Gal-9* and *TIM-3* mRNA levels were positively correlated to mRNA expression levels of *CD4* ($r_s = 0.85$ and $r_s = 0.87$, respectively, $p < 0.001$), *CD8A* ($r_s = 0.36$ and

$r_s = 0.40$, respectively, $p < 0.001$), *CD8B* ($r_s = 0.43$ and $r_s = 0.44$, respectively, $p < 0.001$), and *FOXP3* ($r_s = 0.32$ and $r_s = 0.23$, respectively, $p < 0.001$). (Figure S2C,D). In contrast to the protein data, *OLIG2* mRNA expression was significantly higher in IDH-mutant than in IDH-wild-type tumors (Figure 5A), and like the protein data, *OLIG2* mRNA levels showed a weak to moderate negative correlation with mRNA expression levels of *Gal-9*, *TIM-3* and the T cell markers (Figure S2C).

To further investigate the influence of IDH mutation on the immune landscape in glioma, we included IDH-mutant and IDH-wild-type diffuse astrocytomas, WHO grade II, as well as IDH-mutant and 1p/19q-codeleted

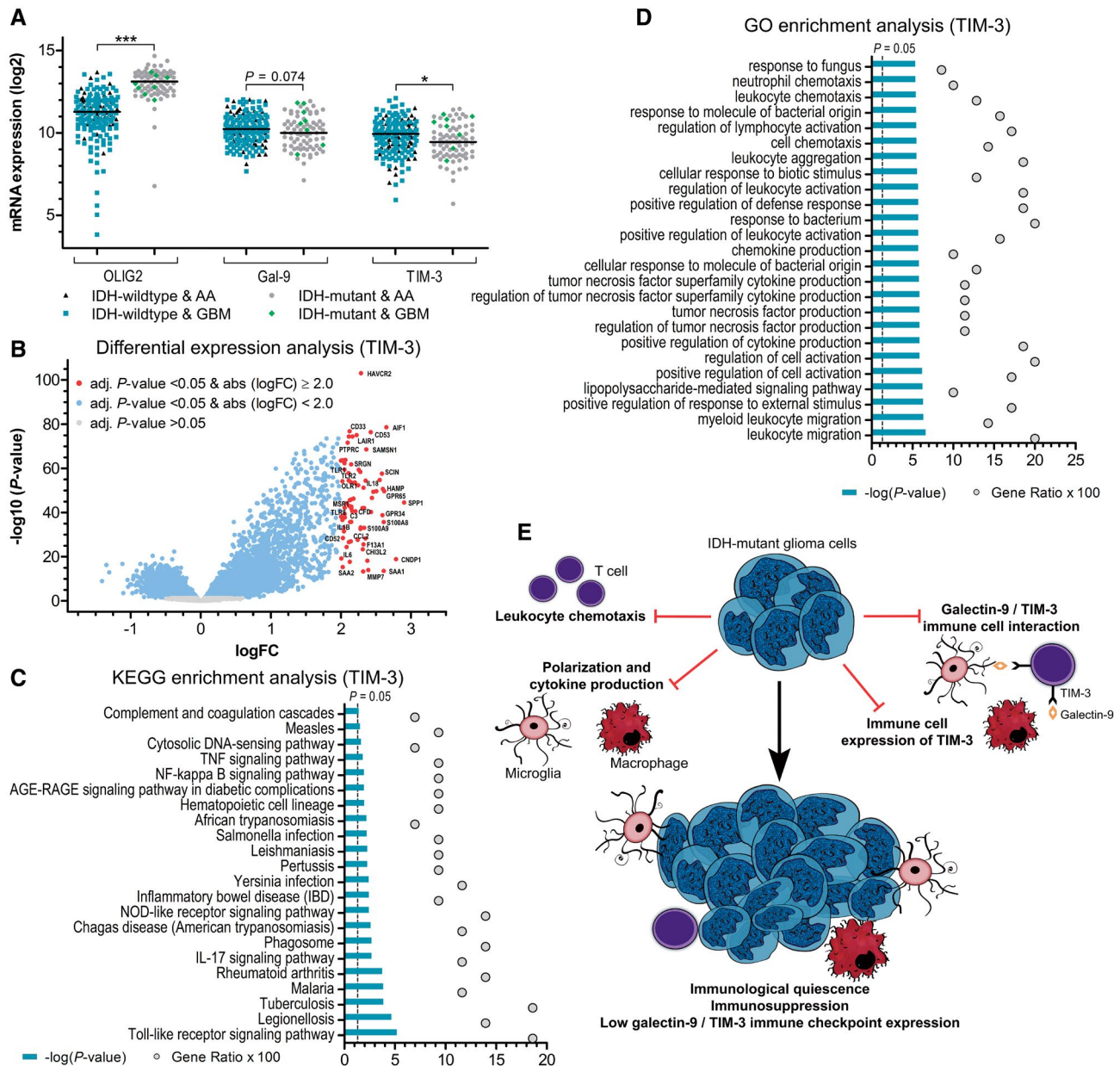


FIGURE 5 TCGA, differential expression analyses, and pathway enrichment analyses. (A) Association between IDH mutation status and *OLIG2*, *Gal-9*, and *TIM-3* expression levels in the TCGA data set. (B) Volcano plot illustrating the 75 genes (red dots) that were significantly upregulated ≥ 2.00 -fold threshold in *TIM-3*^{HIGH} versus *TIM-3*^{LOW} glioblastoma samples. (C,D) The upregulated genes were hierarchically classified according to biological processes and pathways using the Kyoto Encyclopedia of Genes and Genomes (KEGG) (C) and Gene Ontology (GO) term (D) enrichment analyses. (E) Schematic illustration of the possible immunomodulatory of IDH mutation in glioma. IDH mutation and its oncometabolite D-2-hydroxyglutarate may cause suppression of leukocyte chemotaxis and microglia/macrophage polarization as well as cytokine production thereby reducing the expression and activity of the galectin-9/TIM-3 immune checkpoint pathway. Horizontal lines indicate median (A). *indicates $p < 0.05$; *** $p < 0.001$

oligodendrogliomas, WHO grade II and III, in our *in silico* analyses. Oligodendrogliomas, WHO grade II, overall exhibited the lowest mRNA expression level of both *Gal-9* and *TIM-3* ($p < 0.001$) among the glioma subtypes. Interestingly, no significant difference was observed between IDH-wild-type WHO grade II or III astrocytomas and WHO grade IV glioblastoma for either *Gal-9* or *TIM-3*, while IDH-mutant WHO grade II and III astrocytomas had significantly lower mRNA expression levels of *Gal-9* ($p < 0.05$) and *TIM-3* ($p < 0.001$) compared to

IDH-wild-type glioblastoma of WHO grade IV (Figure S3A,B). We also examined the mRNA expression levels of the T cell markers *CD4*, *CD8A/B*, and *FOXP3* among the different glioma subtypes. WHO grade II–III oligodendroglial tumors had significantly lower *CD4* levels compared to the astrocytic tumors ($p < 0.001$) independent of IDH status. Among the astrocytic gliomas, IDH-mutant WHO grade II and III tumors had lower *CD4* levels compared to IDH-wild-type glioblastomas ($p < 0.05$) (Figure S3C). Oligodendroglial tumors as well

as IDH-mutant astrocytic gliomas including glioblastomas had significantly lower *CD8A/B* expression levels compared to IDH-wild-type astrocytic tumors (Figure S3D,E). In contrast, *FOXP3* expression levels were highest in oligodendroglial tumors, followed by IDH-wild-type astrocytomas/glioblastomas (Figure S3F). As our double immunofluorescence stainings showed that most Gal-9⁺ and TIM-3⁺ co-expressed IBA-1, we explored the association between glioma subtype including IDH status and *IBA-1* mRNA expression. We found that oligodendroglial tumors had significantly lower *IBA-1* levels than astrocytic tumors, irrespective of IDH status and WHO grade ($p < 0.001$), while no significant differences were observed among the astrocytic subgroups (Figure S4A) despite the fact that *IBA-1* was positively correlated to both mRNA *Gal-9* ($r_s = 0.88$, $p < 0.001$) and mRNA *TIM-3* ($r_s = 0.92$, $p < 0.001$) in glioma (Figure S4B,C).

As *TIM-3* mRNA expression was consistently lower in IDH-mutant gliomas, we employed the TCGA data set to screen for changes in mRNA levels of 17,811 genes between the glioblastomas with the highest and lowest *TIM-3* mRNA levels. A total of 75 genes were found to be differentially upregulated (FC ≥ 2.00) in glioblastomas with the highest *TIM-3* mRNA level (Figure 5B and Table S2), while no genes were differentially downregulated with a twofold change threshold. Several of the upregulated genes were related to microglia/macrophage migration, chemotaxis, and/or polarization (69–73), including *SPPI*, *IBA-1*, *CD204*, *IL1B*, *IL6*, *IL18*, and *CCL2* as well as *TLR1*, *TLR2*, and *TLR8*. Exploratory analyses showed that the mRNA expression of these microglial/macrophage genes, except *IBA-1*, was significantly lower in WHO grade III and IV IDH-mutant astrocytic gliomas compared to their IDH-wild-type counterparts (Figure S5), and the mRNA results were validated for *IBA-1* and *CD204* at a protein level using immunohistochemistry (Figure S5). KEGG and GO enrichment analyses were used to generate a biological and functional profile of the differentially regulated genes. The differentially upregulated genes were significantly enriched in the signaling pathways of TLR, IL17, nucleotide-binding oligomerization domain-like (NOD-like) receptor, nuclear factor-kappa B (NF κ B), and TNF as well as in the phagosome pathway and various inflammatory/infectious diseases (Figure 5C and Table S3). Further, the upregulated genes were involved in biological processes such as leukocyte migration, regulation and aggregation as well as regulation of cell activation and production of cytokines including the tumor necrosis factor (TNF) superfamily (Figure 5D and Table S4).

4 | DISCUSSION

This study reports that IDH mutation is related to overall decreased expression levels of TIM-3 and fewer TIM-3⁺ immune cells in human astrocytoma tissues.

Furthermore, a significantly lower interaction rate between TIM-3⁺ T cells and Gal-9⁺ TAMs was detected in IDH-mutant anaplastic astrocytomas and glioblastomas, suggesting that the Gal-9/TIM-3 checkpoint pathway could be suppressed to a higher degree compared to IDH-wildtype tumors.

TIM-3 is a type I transmembrane glycoprotein that contains a variable immunoglobulin domain and a mucin-like domain. It was initially identified on differentiated CD4⁺ T helper type 1 cells (74), and is also expressed by other subtypes of lymphoid cells, monocytes/macrophages, dendritic cells, and distinct types of cancer cells. TIM-3 expression is upregulated when stimulated by antigens and in response to pro-inflammatory cytokines. TIM-3 negatively regulates T cell activation, is involved in T cell exhaustion along with PD-1, and contributes to tumor-induced immune suppression by binding to its ligand Gal-9 (45, 48). Combined targeting of TIM-3 and PD-1 was able to restore tumor-infiltrating lymphocyte (TIL) function (51). In myeloid cells, TIM-3 has been shown to regulate cytokine production, cell activation, and capture of apoptotic bodies (52).

We found that IDH mutation was associated with fewer TIM-3⁺ cells in astrocytic gliomas and lower *TIM-3* mRNA levels in gliomas. Using the TCGA data set, glioblastomas with high *TIM-3* mRNA levels showed upregulation of a distinct gene set including genes encoding macrophage/immune-related markers, such as *IBA-1*, *CD204*, *SPPI*, *CCL2*, *IL6*, *IL18*, and *IL1B* as well as *TLR1*, *TLR2*, and *TLR8*. The upregulated genes were involved in regulation of biological processes of the immunocyte including migration, activation, chemotaxis, and cytokine/chemokine production. KEGG enrichment analyses of upregulated genes showed categories such as the TNF and NF κ B signaling pathways which have been associated with shaping of the extracellular matrix and tumor invasiveness in glioblastoma (73, 75). Additionally, the TLR and IL17 signaling pathways were enriched in glioblastomas with high *TIM-3* expression. Dependent on the stimulated receptor, the cell type, and the microenvironment, these pathways can exhibit both pro- and antitumor properties either by facilitating antigen presentation and stimulating innate and adaptive immunity or by promoting an immunosuppressive tumor microenvironment, respectively (76–79). These findings are in agreement with analyses performed on RNA-seq data from patients with glioma where *TIM-3* was associated with IDH-wild-type tumors, mesenchymal glioblastoma, poorer performance status, and shorter survival (56, 58, 59). Investigating the TIM-3 expression on peripheral innate immune cells, Li et al. found that monocytes and natural killer (NK) cells had higher TIM-3 expression in glioma patients compared to healthy controls, despite the fact that the overall level of circulating NK cells was reduced in patients. In glioma patients, the TIM-3⁺ NK cells showed a diminished ability to secrete their antitumor effector molecule interferon- γ (IFN γ),

while the TIM-3⁺ monocytes exhibited a pro-tumorigenic M2-like phenotype compared to healthy controls (59). In a recent meta-analysis that included seven studies on carcinomas, high TIM-3 expression was found to be significantly associated with shorter overall survival and more advanced tumor stage (80). Overall, these results indicate that TIM-3 could facilitate tumor progression and aggressiveness.

We observed that the frequency of Gal-9⁺ cells was not significantly affected by IDH status in WHO grade III and IV astrocytic gliomas. However, we observed a trend toward a lower percentage of Gal-9⁺ cells in IDH-mutant tumors. Using data from three RNA-seq cohorts, Liang et al. reported that *Gal-9* expression was downregulated in high-grade gliomas with mutant IDH, while no significant IDH-dependent difference was seen in low-grade gliomas (55). This inconsistency in results could be explained by the inclusion of IDH-mutant and 1p/19q-codeleted oligodendroglial tumors in the study by Liang et al. as these tumors are more immunologically quiet than IDH-mutant noncodeleted astrocytic tumors (28, 65, 81), and in our *in silico* TCGA analyses we found that oligodendroglial tumors had the lower expression levels of *Gal-9* compared to astrocytic gliomas. Consistent with studies by Liang et al. (55) and Liu et al. (56), we observed a strong positive correlation between Gal-9 and TIM-3 immunoreactivity. Like TIM-3, Gal-9 has been linked to poorer prognosis and the aggressive mesenchymal subtype of glioblastoma (55, 57). In contrast, OLIG2 has been associated with the proneural subtype of high-grade gliomas (61, 82, 83), and thus, IDH mutations (83, 84). Surprisingly, no association between OLIG2 and IDH mutation was found at the protein level, while IDH-mutant anaplastic astrocytomas and glioblastomas expressed higher *OLIG2* mRNA levels compared to the respective IDH-wildtype tumors in the TCGA data set. The observed discrepancy between protein and mRNA results could be explained by translational regulation (85, 86), and can also be attributed to the sensitivity of OLIG2 antibody used in our study. Further, only the number of OLIG2⁺ cells was evaluated, but not the staining intensity which could also contribute to the overall OLIG2 expression level in the tissue.

We analyzed an immune checkpoint pathway using a new emerging method for detection of multiple biomarkers within a single tissue section (87–90). Using this brightfield multiplex chromogenic immunohistochemistry methodology; we were able to decipher three dyes while preserving tissue morphology and architecture without any loss of antigenicity and only limited steric interference and cross-reactivity. We validated the reliability of the chromogenic color mixing using double immunofluorescence. The present study, however, had some limitations. The quantification was done using a stereological approach as digital automated quantification was not feasible because of the overlap of the chromogenic spectra and the detail level that would

be acquired by our image analysis. Also, stereology is often a very time-consuming process limiting the usability of chromogenic multiplexing in clinical pathology. Moreover, our choice for selected markers was limited when developing the multiplex panel because of both technical and antigen-specific aspects. Thus, while chromogenic multiplexing can be a valuable tool, the ability to multiplex beyond three targets/antigens is limited in practice (90). Most studies performing multiplexed imaging to examine the tumor immune microenvironment use multiplex immunofluorescence (91, 92) which allows for combining up to 12 fluorophores (90). However, cellular morphology and tissue context are often more difficult to evaluate in fluorescent stains compared to chromogenic stains, presenting a disadvantage in using fluorescent multiplexing.

In our study, most Gal-9⁺ and TIM-3⁺ cells morphologically resembled microglia/macrophages, while a weak expression also was observed in vascular structures. Reportedly, Gal-9 expression can be induced by IFNG or IL1B in various cells such as endothelial cells, T cells, astrocytes, and neurons (93–97), while ischemia was found to induce TIM-3 expression by astrocytes (98). In our study, cells were denoted as microglia/macrophages based on morphological features. This presents a possible drawback as microglia and reactive astrocytes as well as ameboid macrophages and gemistocytic tumor cells, respectively, can be difficult to discriminate morphologically. To address this aspect, we performed double immunofluorescence and confirmed that on average 80% of Gal-9⁺ and TIM-3⁺ area co-expressed the microglial/macrophage marker IBA-1. Gal-9 expression in glioma cells was reported by Liu et al. (56), however, we observed very few Gal-9 expressing tumor cells, and even fewer tumor cells that expressed TIM-3. Our findings were validated by double immunofluorescence as only ~1% and ~0.1% of the OLIG2⁺ tumor cells co-expressed Gal-9 and TIM-3, respectively. We used OLIG2 to denote tumor cells instead of, for example, glial fibrillary acidic protein (GFAP) because of its nuclear localization and distinct expression making it feasible to perform chromogenic multiplexing with the cytoplasmic Gal-9 and membranous TIM-3. OLIG2 is expressed in most gliomas and glioblastomas, but only in a subset of tumor cells thus introducing a caveat in our study, as the level of Gal-9 and/or TIM-3 expressing tumor cells may be underestimated. To address this limitation, we performed double immunofluorescence with an antibody against the tumor cell-specific IDH1 R132H mutant protein. These stainings supported our finding, demonstrating that Gal-9 and TIM-3 expression is rare in glioma cells.

Similarly to Gal-9⁺ cells, most TIM-3⁺ cells had microglial/macrophage-like morphology, and TIM-3 was almost consistently co-expressed with Gal-9. A few cells expressed TIM-3 only, and these cells resembled either lymphocytes or microglia/macrophages. Less than 0.5% of cells were TIM-3⁺ T cells, and only ~10% of the CD3⁺

T cell population in glioblastoma expressed TIM-3. This is in agreement with work performed by others (49, 56, 99–101). Using flow cytometry, Han et al reported that CD3⁺ T cells were a rare population in glioblastomas accounting for less than 0.25% of the cells (100). Among the T cell populations ~ 6%–12% and ~ 4%–6% of the CD8⁺ and CD4⁺ TILs were found to express TIM-3, respectively (56, 99, 101). Despite their rarity in glioma, TIM-3⁺ TILs could play an important part in the immunosuppressive microenvironment in glioma. Reportedly, TIM-3 expression has been shown to contribute to an immune signature of exhaustion in TILs (51), also in glioblastoma patients (49, 101), and together with PD-1 expression was found to increase over time in murine gliomas (102) suggesting that TIM-3 may be upregulated during gliomagenesis representing an immunosuppressive adaptation. Additionally, TIM-3⁺ T cells correlated with increased tumor grade and poorer performance status (49, 99), overall suggesting an association with tumor aggressiveness. Further, TIM-3 blockade combined with PD-1 blockade and radiation was demonstrated to improve survival in murine glioma compared with dual or monotherapy, and combination therapy was able to restore the anti-tumorigenic functions of T cells (102). In the clinical setting, a phase I trial (NCT03961971) has been scheduled in recurrent glioblastoma, combining the anti-TIM-3 inhibitor MBG453 with the PD-1 inhibitor spartalizumab and stereotactic radiosurgery (47).

We observed significantly lower percentages of Gal-9^{+/−} TIM-3⁺ TAMs and TIM-3⁺ T cells in WHO grade III anaplastic astrocytomas and WHO grade IV glioblastomas with IDH mutation compared to their IDH-wild-type counterparts. Interestingly, we found that most TIM-3⁺ cells resembled TAMs. Almost half of the Gal-9⁺ TAMs co-expressed TIM-3 in WHO grade III–IV IDH-wild-type astrocytic gliomas, while only a third of the Gal-9⁺ TAMs co-expressed TIM-3 in WHO grade III–IV IDH-mutant astrocytic gliomas. Co-expression of Gal-9 and TIM-3 has also been observed in human acute myeloid leukemia cells (103, 104) and human breast cancer cells (105), possibly forming an autocrine loop that promotes self-renewal and immune evasion. In monocytes and macrophages, the specific association of Gal-9 with TIM-3 was reported to differentially regulate TLR activation, IL12/IL23 production, and Gal-9/TIM-3 surface expression depending on whether TIM-3 was expressed by other cells (*trans*) or on the monocyte/macrophage itself (*cis*) (106). This suggests that our observed Gal-9 and TIM-3 expression pattern by microglia/macrophages could constitute an intricate autocrine and paracrine signaling loop which may ultimately impact the general activity level of the immune checkpoint pathway. Also, we found a reduced interaction rate between TIM-3⁺ T cells and Gal-9⁺ TAMs in IDH-mutant compared to IDH-wild-type astrocytic gliomas. Overall, our findings suggest that the expression and possibly activation of the Gal-9/TIM-3 immune checkpoint pathway may be

compromised in astrocytic gliomas that carry an IDH mutation. It is unknown whether this is specifically because of the fewer number of TIM-3⁺ T cells and/or microglia/macrophages or is a result of an overall reduced level of these immune cells in IDH-mutant tumors. We attempted to address this aspect by correlating protein and/or mRNA expression levels of TIM-3 and Gal-9 to the T cell markers, CD4 (T helper cells), CD8 (cytotoxic T cells), and FOXP3 (regulatory T cells) as well as the microglial/macrophage marker IBA-1. Gal-9 and TIM-3 expression were only weakly to moderately correlated with T cell levels, but showed strong positive correlation with microglia/macrophage levels. This suggests that the decrease in TIM-3⁺ cells in IDH-mutant tumors could be because of a lower level of especially microglia/macrophages as the majority of TIM-3⁺ cells co-expressed IBA-1. However, as opposed to T cell levels, mRNA and protein IBA-1 expression did not depend on IDH mutation status in astrocytic gliomas, overall indicating that the regulation of the Gal-9/TIM-3 checkpoint pathway is complex and multifactorial. In contrast to IBA-1, genes related to both M1- and M2 polarization, for example, CD204 were significantly lower in IDH-mutant astrocytic gliomas (69–73), suggesting innate immune activation is suppressed in tumors carrying an IDH mutation.

Several studies have reported on the immunomodulating effects of IDH mutation and its oncometabolite D-2-hydroxyglutarate functioning as an intercellular inhibitor of both the innate and adaptive immune systems. Recently, D-2-hydroxyglutarate was found to inhibit the activation of complement in both the classical and the alternative pathways and also shown to compromise the activity of T cells. Furthermore, IDH-mutant WHO grade III–IV astrocytic gliomas generally contained fewer CD4⁺ TILs, CD8⁺ TILs, and regulatory TILs compared to their IDH-wild-type counterparts (37). Similar results on TILs have been reported by others (20, 28, 31–33, 35). Studies have also shown that the expression of the immunosuppressive molecule and immune checkpoint marker programmed death protein ligand 1 (PD-L1) is diminished in IDH-mutant gliomas relative to IDH-wild-type gliomas, possibly because of epigenetic regulation and suppression mediated by D-2-hydroxyglutarate (32, 42). Further, in a study by Gao et al. immunophenotyping showed that WHO grade II gliomas, which predominantly harbored an IDH mutation, had an immunophenogram that was different from glioblastomas and correlated with poorer response to checkpoint inhibition (34, 107). Bunse et al. demonstrated that oral administration of an IDH inhibitor in combination with R132H peptide vaccination, adoptive T lymphocyte immunotherapy, or PD-1 blockade had synergistic effects and resulted in increased overall survival in a syngeneic orthotopic IDH-mutant mouse model (33), suggesting that combining immunotherapy with IDH inhibition could have clinical relevance. IDH-mutant glioma cells were also reported to resist NK cell-mediated lysis by silencing expression of

NK group 2D ligands through D-2-hydroxyglutarate-induced hypermethylation (41). IDH mutation status may also affect the presence and function of microglia/macrophages in gliomas as lower quantities were found in IDH-mutant gliomas, especially oligodendrogliomas (20, 31, 81). Interestingly, α -ketoglutarate, the normal product from the IDH-catalyzed reaction, was found to prevent M1 activation and enhance M2 polarization in macrophages thereby facilitating tumor progression and development (38). A decline in α -ketoglutarate and indirectly an increase in D2-hydroxyglutarate levels in IDH-mutant gliomas may thus favor anti-tumorigenic M1 activation in microglia/macrophages. Overall, these data indicate that the tumor microenvironment is more immunosuppressive in gliomas harboring an IDH mutation compared to their wildtype counterparts. This seems somewhat counterintuitive as IDH mutation has been associated with a survival benefit in patients with glioma. In a recent study by Unruh et al. (22), the patterns of DNA methylation and transcriptome profiles were investigated in IDH-mutant cancers including glioma. The IDH mutation-induced hypermethylation was found to be more pronounced in gliomas compared to other cancers, and gene set enrichment analyses of IDH-mutant versus IDH-wildtype gliomas revealed downregulation of multiple biological processes in IDH-mutant gliomas; the most notable processes were tissue development, immune response, angiogenesis, and cell proliferation which are all considered to contribute to tumor aggressiveness (40, 67, 82, 83). Taken together, research indicates that IDH mutation promotes an immunosuppressive tumor microenvironment.

5 | CONCLUSION

The success of immunotherapy in glioma faces several obstacles including a lymphocyte-depleted and immunosuppressive tumor microenvironment as well as the limitations of effectively generating an immune response in the central nervous system. Increasing evidence suggests that mutations in IDH play an essential role in glioma-associated immune suppression. The neomorphic activity of mutant IDH results in accumulation of D-2-hydroxyglutarate which has been implicated in DNA hypermethylation, ultimately promoting global repression of several genes including those involved in stimulating antitumor immune responses. Reportedly, the activity of the innate and adaptive immune system including the checkpoint systems is reduced in gliomas harboring an IDH mutation. Our results demonstrate that the Gal-9/TIM-3 checkpoint pathway is affected by IDH mutation as the overall level of TIM-3 expression was diminished in IDH-mutant astrocytic gliomas. Additionally, fewer receptor-ligand interactions was observed as the interaction rate between TIM-3⁺ T cells and Gal-9⁺ microglia/macrophages were less frequent in IDH-mutant tumors (Figure 5E). Collectively, these

results indicate that IDH mutation could convey a resistance to checkpoint inhibition; however, so far no clinical data confirm this hypothesis. A better understanding on the regulatory factors of the immune system and tumor microenvironment is vital. Additional characterization of the composition and biological functions of immune infiltrates and their association with mutational tumor burden could constitute an important approach to select patients more likely to benefit from immunotherapy including immune checkpoint inhibition.

ACKNOWLEDGMENTS

We gratefully acknowledge the excellent laboratory work done by technicians Helle Wohlleben and Lone Christiansen. Parts of this study were based on data generated by the TCGA Research Network, and we thankfully acknowledge all tissue donors and workers involved in this project. This work was supported by grants from Danish Council for Independent Research (4183-00183), Fabrikant Einar Willumsens Mindefond, Familien Erichsens Mindefond, Købmand M. Kristjan Kjær og Hustru Margrethe Kjær, Født la Cour-Holmes Fond, Oda og Hans Svenningsens Fond, Thora og Viggo Groves Mindelegat, Harboefonden, A.J. Andersen og Hustrus Fond, Torben og Alice Frimodts Fond, Marie og Børge Kroghs Fond, and Arkitekt Holger Hjortenbergs og Hustru Dagmar Hjortenbergs Fond.

ETHICS APPROVAL AND CONSENT TO PARTICIPATE

The study was approved by the Institutional Review Board of the Medical Faculty, Heinrich Heine University, Düsseldorf, Germany (Study No.5848R), the official Danish ethical review board named the Regional Scientific Ethical Committee of the Region of Southern Denmark (Project-ID: S-20150148), and the official Danish data registration authority (the Data Protection Authority, file number: 16/11065). The study was completed in agreement with the Declaration of Helsinki. The use of tissue was allowed by all patients in the Danish Tissue Application Register.

CONFLICT OF INTEREST

All authors declare that they have no conflicts of interest.

AUTHOR CONTRIBUTIONS

MDS and BWK conceived the study. MDS and ON designed the experiments. MDS and GR collected the data. MDS assembled the data and analyzed and interpreted the results. GR and BWK contributed with the reagents/materials/analysis tools. MDS drafted and edited the manuscript. All authors have read and approved the final manuscript.

DATA AVAILABILITY STATEMENT

The data that support the findings of this study are available from the corresponding author upon reasonable request.



REFERENCES

- Hartmann C, Meyer J, Bals J, Capper D, Mueller W, Christians A, et al. Type and frequency of IDH1 and IDH2 mutations are related to astrocytic and oligodendroglial differentiation and age: a study of 1,010 diffuse gliomas. *Acta Neuropathol.* 2009;118:469–74.
- Parsons DW, Jones S, Zhang X, Lin JC, Leary RJ, Angenendt P, et al. An integrated genomic analysis of human glioblastoma multiforme. *Science.* 2008;321:1807–12.
- Yan H, Parsons DW, Jin G, McLendon R, Rasheed BA, Yuan W, et al. IDH1 and IDH2 mutations in gliomas. *N Eng J Med.* 2009;360:765–73.
- Zhang C, Moore LM, Li X, Yung WK, Zhang W. IDH1/2 mutations target a key hallmark of cancer by deregulating cellular metabolism in glioma. *Neuro-Oncology.* 2013;15:1114–26.
- Cairns RA, Mak TW. Oncogenic isocitrate dehydrogenase mutations: mechanisms, models, and clinical opportunities. *Cancer Discov.* 2013;3:730–41.
- Horbinski C. What do we know about IDH1/2 mutations so far, and how do we use it? *Acta Neuropathol.* 2013;125:621–36.
- Waitkus MS, DiPlas BH, Yan H. Isocitrate dehydrogenase mutations in gliomas. *Neuro-Oncology.* 2016;18:16–26.
- Mardis ER, Ding L, Dooling DJ, Larson DE, McLellan MD, Chen K, et al. Recurring mutations found by sequencing an acute myeloid leukemia genome. *N Eng J Med.* 2009;361:1058–66.
- Tang JY, Chang CC, Lin PC, Chang JG. Isocitrate dehydrogenase mutation hot spots in acute lymphoblastic leukemia and oral cancer. *Kaohsiung J Med Sci.* 2012;28:138–44.
- Cairns RA, Iqbal J, Lemonnier F, Kucuk C, de Leval L, Jais JP, et al. IDH2 mutations are frequent in angioimmunoblastic T-cell lymphoma. *Blood.* 2012;119:1901–3.
- Amary MF, Bacci K, Maggiani F, Damato S, Halai D, Berisha F, et al. IDH1 and IDH2 mutations are frequent events in central chondrosarcoma and central and periosteal chondromas but not in other mesenchymal tumours. *J Pathol.* 2011;224:334–43.
- Damato S, Alorjani M, Bonar F, McCarthy SW, Cannon SR, O'Donnell P, et al. IDH1 mutations are not found in cartilaginous tumours other than central and periosteal chondrosarcomas and enchondromas. *Histopathology.* 2012;60:363–5.
- Lopez GY, Reitman ZJ, Solomon D, Waldman T, Bigner DD, McLendon RE, et al. IDH1(R132) mutation identified in one human melanoma metastasis, but not correlated with metastases to the brain. *Biochem Biophys Res Commun.* 2010;398:585–7.
- Borger DR, Tanabe KK, Fan KC, Lopez HU, Fantin VR, Straley KS, et al. Frequent mutation of isocitrate dehydrogenase (IDH1) and IDH2 in cholangiocarcinoma identified through broad-based tumor genotyping. *Oncologist.* 2012;17:72–9.
- Wang P, Dong Q, Zhang C, Kuan PF, Liu Y, Jeck WR, et al. Mutations in isocitrate dehydrogenase 1 and 2 occur frequently in intrahepatic cholangiocarcinomas and share hypermethylation targets with glioblastomas. *Oncogene.* 2013;32:3091–100.
- Ghiam AF, Cairns RA, Thoms J, Dal Pra A, Ahmed O, Meng A, et al. IDH mutation status in prostate cancer. *Oncogene.* 2012;31:3826.
- Bleeker FE, Atai NA, Lamba S, Jonker A, Rijkeboer D, Bosch KS, et al. The prognostic IDH1(R132) mutation is associated with reduced NADP⁺-dependent IDH activity in glioblastoma. *Acta Neuropathol.* 2010;119:487–94.
- Dang L, White DW, Gross S, Bennett BD, Bittinger MA, Driggers EM, et al. Cancer-associated IDH1 mutations produce 2-hydroxyglutarate. *Nature.* 2009;462:739–44.
- Jin G, Reitman ZJ, Spasojevic I, Batinic-Haberle I, Yang J, Schmidt-Kittler O, et al. 2-hydroxyglutarate production, but not dominant negative function, is conferred by glioma-derived NADP-dependent isocitrate dehydrogenase mutations. *PLoS One.* 2011;6:e16812.
- Luoto S, Hermelo I, Vuorinen EM, Hannus P, Kesseli J, Nykter M, et al. Computational characterization of suppressive immune microenvironments in glioblastoma. *Cancer Res.* 2018;78:5574–85.
- Turcan S, Rohle D, Goenka A, Walsh LA, Fang F, Yilmaz E, et al. IDH1 mutation is sufficient to establish the glioma hypermethylator phenotype. *Nature.* 2012;483:479–83.
- Unruh D, Zewde M, Buss A, Drumm MR, Tran AN, Scholtens DM, et al. Methylation and transcription patterns are distinct in IDH mutant gliomas compared to other IDH mutant cancers. *Sci Rep.* 2019;9:8946.
- Yang M, Soga T, Pollard PJ. Oncometabolites: linking altered metabolism with cancer. *J Clin Invest.* 2013;123:3652–8.
- Unruh D, Mirkov S, Wray B, Drumm M, Lamano J, Li YD, et al. Methylation-dependent tissue factor suppression contributes to the reduced malignancy of IDH1-mutant gliomas. *Clin Cancer Res.* 2019;25:747–59.
- Unruh D, Schwarze SR, Khoury L, Thomas C, Wu M, Chen L, et al. Mutant IDH1 and thrombosis in gliomas. *Acta Neuropathol.* 2016;132:917–30.
- Zhang L, He L, Lugano R, Roodakker K, Bergqvist M, Smits A, et al. IDH mutation status is associated with distinct vascular gene expression signatures in lower-grade gliomas. *Neuro-Oncology.* 2018;20:1505–16.
- Tomaszewski W, Sanchez-Perez L, Gajewski TF, Sampson JH. Brain tumor microenvironment and host state: implications for immunotherapy. *Clin Cancer Res.* 2019;25:4202–10.
- Thorsson V, Gibbs DL, Brown SD, Wolf D, Bortone DS, Ou Yang TH, et al. The immune landscape of cancer. *Immunity.* 2018;48:812–30.e14.
- Binnewies M, Roberts EW, Kersten K, Chan V, Fearon DF, Merad M, et al. Understanding the tumor immune microenvironment (TIME) for effective therapy. *Nat Med.* 2018;24:541–50.
- Hodges TR, Ott M, Xiu J, Gatalica Z, Swensen J, Zhou S, et al. Mutational burden, immune checkpoint expression, and mismatch repair in glioma: implications for immune checkpoint immunotherapy. *Neuro-Oncology.* 2017;19:1047–57.
- Amankulor NM, Kim Y, Arora S, Kargl J, Szulzewsky F, Hanke M, et al. Mutant IDH1 regulates the tumor-associated immune system in gliomas. *Genes Dev.* 2017;31:774–86.
- Berghoff AS, Kiesel B, Widhalm G, Wilhelm D, Rajky O, Kurscheid S, et al. Correlation of immune phenotype with IDH mutation in diffuse glioma. *Neuro-Oncology.* 2017;19:1460–8.
- Bunse L, Pusch S, Bunse T, Sahn F, Sanghvi K, Friedrich M, et al. Suppression of antitumor T cell immunity by the oncometabolite (R)-2-hydroxyglutarate. *Nature Med.* 2018;24:1192–203.
- Gao Y, Weenink B, van den Bent MJ, Erdem-Eraslan L, Kros JM, Sillevs Smitt P, et al. Expression-based intrinsic glioma subtypes are prognostic in low-grade gliomas of the EORTC22033-26033 clinical trial. *Eur J Cancer.* 2018;94:168–78.
- Kohanbash G, Carrera DA, Shrivastav S, Ahn BJ, Jahan N, Mazar T, et al. Isocitrate dehydrogenase mutations suppress STAT1 and CD8⁺ T cell accumulation in gliomas. *J Clin Invest.* 2017;127:1425–37.
- Poon CC, Gordon PMK, Liu K, Yang R, Sarkar S, Mirzaei R, et al. Differential microglia and macrophage profiles in human IDH-mutant and -wild type glioblastoma. *Oncotarget.* 2019;10:3129–43.
- Zhang L, Sorensen MD, Kristensen BW, Reifenger G, McIntyre TM, Lin F. D-2-Hydroxyglutarate is an intercellular mediator in IDH-mutant gliomas inhibiting complement and T cells. *Clin Cancer Res.* 2018;24:5381–91.
- Liu PS, Wang H, Li X, Chao T, Teav T, Christen S, et al. Alpha-ketoglutarate orchestrates macrophage activation through metabolic and epigenetic reprogramming. *Nat Immunol.* 2017;18:985–94.

39. Liu S, Zhang C, Maimela NR, Yang L, Zhang Z, Ping Y, et al. Molecular and clinical characterization of CD163 expression via large-scale analysis in glioma. *Oncoimmunology*. 2019;8:e1601478.
40. Yuan Y, Zhao Q, Zhao S, Zhang P, Zhao H, Li Z, et al. Characterization of transcriptome profile and clinical features of a novel immunotherapy target CD204 in diffuse glioma. *Cancer Med*. 2019;8:3811–21.
41. Zhang X, Rao A, Sette P, Deibert C, Pomerantz A, Kim WJ, et al. IDH mutant gliomas escape natural killer cell immune surveillance by downregulation of NKG2D ligand expression. *Neuro-Oncology*. 2016;18:1402–12.
42. Mu L, Long Y, Yang C, Jin L, Tao H, Ge H, et al. The IDH1 mutation-induced oncometabolite, 2-hydroxyglutarate, may affect DNA methylation and expression of PD-L1 in gliomas. *Front Mol Neurosci*. 2018;11:82.
43. Wang Z, Wang Z, Zhang C, Liu X, Li G, Liu S, et al. Genetic and clinical characterization of B7–H3 (CD276) expression and epigenetic regulation in diffuse brain glioma. *Cancer Sci*. 2018;109:2697–705.
44. Zhang C, Zhang Z, Li F, Shen Z, Qiao Y, Li L, et al. Large-scale analysis reveals the specific clinical and immune features of B7–H3 in glioma. *Oncoimmunology*. 2018;7:e1461304.
45. Baumeister SH, Freeman GJ, Dranoff G, Sharpe AH. Coinhibitory pathways in immunotherapy for cancer. *Ann Rev Immunol*. 2016;34:539–73.
46. Koyama S, Akbay EA, Li YY, Herter-Sprie GS, Buczkowski KA, Richards WG, et al. Adaptive resistance to therapeutic PD-1 blockade is associated with upregulation of alternative immune checkpoints. *Nat Commun*. 2016;7:10501.
47. Qin S, Xu L, Yi M, Yu S, Wu K, Luo S. Novel immune checkpoint targets: moving beyond PD-1 and CTLA-4. *Mol Cancer*. 2019;18:155.
48. Du W, Yang M, Turner A, Xu C, Ferris RL, Huang J, et al. TIM-3 as a target for cancer immunotherapy and mechanisms of action. *Int J Mol Sci*. 2017;18:645.
49. Goods BA, Hernandez AL, Lowther DE, Lucca LE, Lerner BA, Gunel M, et al. Functional differences between PD-1+ and PD-1-CD4+ effector T cells in healthy donors and patients with glioblastoma multiforme. *PLoS One*. 2017;12:e0181538.
50. Lowther DE, Goods BA, Lucca LE, Lerner BA, Raddassi K, van Dijk D, et al. PD-1 marks dysfunctional regulatory T cells in malignant gliomas. *JCI Insight*. 2016;1:e85935.
51. Sakuishi K, Apetoh L, Sullivan JM, Blazar BR, Kuchroo VK, Anderson AC. Targeting Tim-3 and PD-1 pathways to reverse T cell exhaustion and restore anti-tumor immunity. *J Exp Med*. 2010;207:2187–94.
52. Oceana-Guzman R, Torre-Bouscoulet L, Sada-Ovalle I. TIM-3 regulates distinct functions in macrophages. *Front Immunol*. 2016;7:229.
53. Yan W, Liu X, Ma H, Zhang H, Song X, Gao L, et al. Tim-3 fosters HCC development by enhancing TGF-beta-mediated alternative activation of macrophages. *Gut*. 2015;64:1593–604.
54. Yang X, Jiang X, Chen G, Xiao Y, Geng S, Kang C, et al. T cell Ig Mucin-3 promotes homeostasis of sepsis by negatively regulating the TLR response. *J Immunol*. 2013;190:2068–79.
55. Liang T, Wang X, Wang F, Feng E, You G. Galectin-9: a predictive biomarker negatively regulating immune response in glioma patients. *World Neurosurg*. 2019;9:e455–e462.
56. Liu Z, Han H, He X, Li S, Wu C, Yu C, et al. Expression of the galectin-9-Tim-3 pathway in glioma tissues is associated with the clinical manifestations of glioma. *Oncol Lett*. 2016;11:1829–34.
57. Yuan F, Ming H, Wang Y, Yang Y, Yi L, Li T, et al. Molecular and clinical characterization of Galectin-9 in glioma through 1,027 samples. *J Cell Physiol*. 2019;235:4326–34.
58. Li G, Wang Z, Zhang C, Liu X, Cai J, Wang Z, et al. Molecular and clinical characterization of TIM-3 in glioma through 1,024 samples. *Oncoimmunology*. 2017;6:e1328339.
59. Li X, Wang B, Gu L, Zhang J, Li X, Gao L, et al. Tim-3 expression predicts the abnormal innate immune status and poor prognosis of glioma patients. *Clin Chim Acta*. 2018;476:178–84.
60. Ligon KL, Alberta JA, Kho AT, Weiss J, Kwaan MR, Nutt CL, et al. The oligodendroglial lineage marker OLIG2 is universally expressed in diffuse gliomas. *J Neuropathol Exp Neurol*. 2004;63:499–509.
61. Popova SN, Bergqvist M, Dimberg A, Edqvist PH, Ekman S, Hesselager G, et al. Subtyping of gliomas of various WHO grades by the application of immunohistochemistry. *Histopathology*. 2014;64:365–79.
62. Louis DN, Ohgaki H, Wiestler OD, Cavenee WK, Ellison DW, Figarella-Branger D, et al. WHO classification of tumours of the central nervous system, Revised, 4th ed. Lyon: International Agency for Research on Cancer (IARC); 2016.
63. Dahlrot RH, Kristensen BW, Hjelmborg J, Herrstedt J, Hansen S. A population-based study of low-grade gliomas and mutated isocitrate dehydrogenase 1 (IDH1). *J Neuro-Oncol*. 2013;114:309–17.
64. Petterson SA, Sørensen MD, Kristensen BW. Expression profiling of primary and recurrent glioblastomas reveals a reduced level of pentraxin 3 in recurrent glioblastomas. *J Neuropathol Exp Neurol*. 2020;79:975–85.
65. Sorensen MD, Dahlrot RH, Boldt HB, Hansen S, Kristensen BW. Tumour-associated microglia/macrophages predict poor prognosis in high-grade gliomas and correlate with an aggressive tumour subtype. *Neuropathol Appl Neurobiol*. 2018;44:185–206.
66. Bowman RL, Wang Q, Carro A, Verhaak RG, Squatrito M. GlioVis data portal for visualization and analysis of brain tumor expression datasets. *Neuro-Oncology*. 2017;19:139–41.
67. Ceccarelli M, Barthel FP, Malta TM, Sabedot TS, Salama SR, Murray BA, et al. Molecular profiling reveals biologically discrete subsets and pathways of progression in diffuse glioma. *Cell*. 2016;164:550–63.
68. The Cancer Genome Atlas Research Network. Comprehensive genomic characterization defines human glioblastoma genes and core pathways. *Nature*. 2008;455:1061–8.
69. Hao N-B, Lü M-H, Fan Y-H, Cao Y-L, Zhang Z-R, Yang S-M. Macrophages in tumor microenvironments and the progression of tumors. *Clin Dev Immunol*. 2012;2012:948098.
70. Li W, Graeber MB. The molecular profile of microglia under the influence of glioma. *Neuro-Oncology*. 2012;14:958–78.
71. Mantovani A, Sica A, Sozzani S, Allavena P, Vecchi A, Locati M. The chemokine system in diverse forms of macrophage activation and polarization. *Trends Immunol*. 2004;25:677–86.
72. Rabenstein M, Vay SU, Flitsch LJ, Fink GR, Schroeter M, Rueger MA. Osteopontin directly modulates cytokine expression of primary microglia and increases their survival. *J Neuroimmunol*. 2016;299:130–8.
73. Szulzewsky F, Pelz A, Feng X, Synowitz M, Markovic D, Langmann T, et al. Glioma-associated microglia/macrophages display an expression profile different from M1 and M2 polarization and highly express Gpnmb and Sppl. *PLoS One*. 2015;10:e0116644.
74. Monney L, Sabatos CA, Gaglia JL, Ryu A, Waldner H, Chernova T, et al. Th1-specific cell surface protein Tim-3 regulates macrophage activation and severity of an autoimmune disease. *Nature*. 2002;415:536–41.
75. Velasquez C, Mansouri S, Mora C, Nassiri F, Suppiah S, Martino J, et al. Molecular and clinical insights into the invasive capacity of glioblastoma cells. *J Oncol*. 2019;2019:1740763.
76. Cai J, Zhang W, Yang P, Wang Y, Li M, Zhang C, et al. Identification of a 6-cytokine prognostic signature in patients with primary glioblastoma harboring M2 microglia/macrophage phenotype relevance. *PLoS One*. 2015;10:e0126022.
77. Deng S, Zhu S, Qiao Y, Liu YJ, Chen W, Zhao G, et al. Recent advances in the role of toll-like receptors and TLR agonists in immunotherapy for human glioma. *Protein Cell*. 2014;5:899–911.

78. Liang H, Yi L, Wang X, Zhou C, Xu L. Interleukin-17 facilitates the immune suppressor capacity of high-grade glioma-derived CD4 (+) CD25 (+) Foxp3 (+) T cells via releasing transforming growth factor beta. *Scand J Immunol.* 2014;80:144–50.
79. Parajuli P, Mittal S. Role of IL-17 in glioma progression. *J Spine Neurosurg.* 2013;(Suppl 1). <https://doi.org/10.4172/2325-9701.S1-004>.
80. Zhang Y, Cai P, Liang T, Wang L, Hu L. TIM-3 is a potential prognostic marker for patients with solid tumors: a systematic review and meta-analysis. *Oncotarget.* 2017;8:31705–13.
81. Venteicher AS, Tirosch I, Hebert C, Yizhak K, Neftel C, Filbin MG, et al. Decoupling genetics, lineages, and microenvironment in IDH-mutant gliomas by single-cell RNA-seq. *Science.* 2017;355:eaai8478.
82. Phillips HS, Kharbanda S, Chen R, Forrest WF, Soriano RH, Wu TD, et al. Molecular subclasses of high-grade glioma predict prognosis, delineate a pattern of disease progression, and resemble stages in neurogenesis. *Cancer Cell.* 2006;9:157–73.
83. Verhaak RGW, Hoadley KA, Purdom E, Wang V, Qi Y, Wilkerson MD, et al. An integrated genomic analysis identifies clinically relevant subtypes of glioblastoma characterized by abnormalities in PDGFRA, IDH1, EGFR and NF1. *Cancer Cell.* 2010;17:98–110.
84. Noushmehr H, Weisenberger DJ, Diefes K, Phillips HS, Pujara K, Berman BP, et al. Identification of a CpG island methylator phenotype that defines a distinct subgroup of glioma. *Cancer Cell.* 2010;17:510–22.
85. Helmy K, Halliday J, Fomchenko E, Setty M, Pitter K, Hafemeister C, et al. Identification of global alteration of transcriptional regulation in glioma in vivo. *PLoS One.* 2012;7:e46965.
86. Vogel C, Marcotte EM. Insights into the regulation of protein abundance from proteomic and transcriptomic analyses. *Nat Rev Genet.* 2012;13:227–32.
87. Ilie M, Beaulande M, Ben Hadj S, Chamorey E, Schiappa R, Long-Mira E, et al. Chromogenic multiplex immunohistochemistry reveals modulation of the immune microenvironment associated with survival in elderly patients with lung adenocarcinoma. *Cancers.* 2018;10:326.
88. Ilie M, Beaulande M, Hamila M, Erb G, Hofman V, Hofman P. Automated chromogenic multiplexed immunohistochemistry assay for diagnosis and predictive biomarker testing in non-small cell lung cancer. *Lung Cancer.* 2018;124:90–4.
89. Rakae M, Busund L-TR, Jamaly S, Paulsen E-E, Richardsen E, Andersen S, et al. Prognostic value of macrophage phenotypes in resectable non-small cell lung cancer assessed by multiplex immunohistochemistry. *Neoplasia.* 2019;21:282–93.
90. Stack EC, Wang C, Roman KA, Hoyt CC. Multiplexed immunohistochemistry, imaging, and quantitation: a review, with an assessment of Tyramide signal amplification, multispectral imaging and multiplex analysis. *Methods.* 2014;70:46–58.
91. Giraldo NA, Nguyen P, Engle EL, Kaunitz GJ, Cottrell TR, Berry S, et al. Multidimensional, quantitative assessment of PD-1/PD-L1 expression in patients with Merkel cell carcinoma and association with response to pembrolizumab. *J Immunother Cancer.* 2018;6:99.
92. Saylor J, Ma Z, Goodridge HS, Huang F, Cress AE, Pandol SJ, et al. Spatial mapping of myeloid cells and macrophages by multiplexed tissue staining. *Front Immunol.* 2018;9:2925.
93. Hirashima M, Kashio Y, Nishi N, Yamauchi A, Imaizumi TA, Kageshita T, et al. Galectin-9 in physiological and pathological conditions. *Glycoconj J.* 2002;19:593–600.
94. John S, Mishra R. Galectin-9: From cell biology to complex disease dynamics. *J Biosci.* 2016;41:507–34.
95. Steelman AJ, Li J. Astrocyte galectin-9 potentiates microglial TNF secretion. *J Neuroinflammation.* 2014;11:144.
96. Steelman AJ, Smith R 3rd, Welsh CJ, Li J. Galectin-9 protein is up-regulated in astrocytes by tumor necrosis factor and promotes encephalitogenic T-cell apoptosis. *J Biol Chem.* 2013;288:23776–87.
97. Thijssen VL, Hulsmans S, Griffioen AW. The galectin profile of the endothelium: altered expression and localization in activated and tumor endothelial cells. *Am J Pathol.* 2008;172:545–53.
98. Kim Y, Park J, Choi YK. The role of astrocytes in the central nervous system focused on bk channel and heme oxygenase metabolites: a review. *Antioxidants (Basel).* 2019;8:121.
99. Han S, Feng S, Xu L, Shi W, Wang X, Wang H, et al. Tim-3 on peripheral CD4(+) and CD8(+) T cells is involved in the development of glioma. *DNA Cell Biol.* 2014;33:245–50.
100. Han S, Ma E, Wang X, Yu C, Dong T, Zhan W, et al. Rescuing defective tumor-infiltrating T-cell proliferation in glioblastoma patients. *Oncol Lett.* 2016;12:2924–9.
101. Mohme M, Schliffke S, Maire CL, Runger A, Glau L, Mende KC, et al. Immunophenotyping of newly diagnosed and recurrent glioblastoma defines distinct immune exhaustion profiles in peripheral and tumor-infiltrating lymphocytes. *Clin Cancer Res.* 2018;24:4187–200.
102. Kim JE, Patel MA, Mangraviti A, Kim ES, Theodoros D, Velarde E, et al. Combination therapy with anti-PD-1, anti-TIM-3, and focal radiation results in regression of murine gliomas. *Clin Cancer Res.* 2017;23:124–36.
103. Goncalves Silva I, Yasinska IM, Sakhnevych SS, Fiedler W, Wellbrock J, Bardelli M, et al. The Tim-3-galectin-9 secretory pathway is involved in the immune escape of human acute myeloid leukemia cells. *EBioMedicine.* 2017;22:44–57.
104. Kikushige Y, Miyamoto T, Yuda J, Jabbarzadeh-Tabrizi S, Shima T, Takayanagi S-i, et al. A TIM-3/Gal-9 autocrine stimulatory loop drives self-renewal of human myeloid leukemia stem cells and leukemic progression. *Cell Stem Cell.* 2015;17:341–52.
105. Yasinska IM, Sakhnevych SS, Pavlova L, Teo Hansen Selno A, Teuscher Abeleira AM, Benlaouer O, et al. The Tim-3-Galectin-9 pathway and its regulatory mechanisms in human breast cancer. *Front Immunol.* 2019;10:1594.
106. Ma CJ, Li GY, Cheng YQ, Wang JM, Ying RS, Shi L, et al. Cis association of Galectin-9 with Tim-3 differentially regulates IL-12/IL-23 expressions in monocytes via TLR signaling. *PLoS One.* 2013;8:e72488.
107. Charoentong P, Finotello F, Angelova M, Mayer C, Efremova M, Rieder D, et al. Pan-cancer immunogenomic analyses reveal genotype-immunophenotype relationships and predictors of response to checkpoint blockade. *Cell Rep.* 2017;18:248–62.

SUPPORTING INFORMATION

Additional supporting information may be found online in the Supporting Information section.

FIGURE S1 Co-expression patterns of Gal-9 and TIM-3 in IDH1 R132H-mutant WHO III-IV astrocytic gliomas. IDH1 R132-mutant glial tumor cells rarely expressed Gal-9 (A,B) and TIM-3 (C,D). *Scale bar 100 μM*

FIGURE S2 Correlation analyses in WHO grade III and IV astrocytic gliomas. (A,B) A positive correlation was found between total Gal-9 cell count (in %) and total TIM-3 cell count (in %) in the astrocytoma cohort used for the multiplex chromogenic immunohistochemistry study. Additionally, positive correlations were found among Gal-9, TIM-3 and T cell markers CD4, CD8, and FOXP3, while OLIG2 was negatively correlated with Gal-9, TIM-3 as well as CD4 and CD8. (C,D) Gal-9 mRNA expression was positively correlated with TIM-3 mRNA levels in the TCGA dataset. Both TIM-3

and *Gal-9* showed a moderate-strong correlation with mRNA levels of the T cell markers *CD4*, *CD8A/B* and *FOXP3*, while *OLIG2* mRNA levels were negatively correlated with *TIM-3*, *Gal-9* and the T cell markers to a weak-moderate degree

FIGURE S3 Association between glioma subtype and mRNA expression levels in the TCGA dataset. (A,B) OD had the lowest *Gal-9* (A) and *TIM-3* (B) mRNA expression level compared to other five glioma subtypes, while GBM, WHO grade IV, and IDH-wildtype diffuse and anaplastic astrocytomas, WHO grade II and III, appeared to have the highest expression levels. (C) OD and AOD had the lowest mRNA expression level of *CD4* compared to the four astrocytic subtypes. Further, IDH-wildtype GBM had higher *CD4* levels than IDH-mutant astrocytomas of WHO grades II and III. (D,E) *CD8A* and *CD8B* mRNA expression levels were lower in oligodendroglial tumors and IDH-mutant astrocytomas compared IDH-wildtype astrocytomas. (F) Oligodendroglial tumors and IDH-wildtype astrocytoma, WHO grade II- III and IV, had the highest mRNA expression level of *FOXP3*. *Horizontal lines* indicate mean (A,C,D) or median (B,E,F). *Vertical lines* indicate \pm standard error of the mean (SEM) (A,C,D). * $p < 0.05$; ** $p < 0.01$; *** $p < 0.001$. AA, anaplastic astrocytoma; AOD, anaplastic oligodendrogloma; DA, diffuse astrocytoma; GBM, glioblastoma; IDH, isocitrate dehydrogenase; mIDH, IDH-mutant; OD, oligodendrogloma; wtIDH, IDH-wildtype

FIGURE S4 *IBA-1* mRNA expression in the TCGA dataset. (A) OD and AOD had lower *IBA-1* mRNA expression level compared to the four astrocytic tumor groups, while no differences in mRNA levels were observed among the astrocytic groups. (B,C) *IBA-1* mRNA expression levels were positively correlated to mRNA expression of *Gal-9* (B) and *TIM-3* (C). *Horizontal and vertical lines* indicate mean and \pm standard error of the mean (SEM), respectively. *** $p < 0.001$. AA, anaplastic astrocytoma; AOD, anaplastic oligodendrogloma; DA, diffuse astrocytoma; GBM, glioblastoma; IDH,

isocitrate dehydrogenase; mIDH, IDH-mutant; OD, oligodendrogloma; wtIDH, IDH-wildtype

FIGURE S5 Expression levels of microglia/macrophage-related markers in IDH-mutant vs. IDH-wildtype astrocytic gliomas of WHO grade III and IV. (A,B) Expression of mRNA *IBA-1* and protein IBA-1 did not differ between IDH-mutant and IDH-wildtype tumors. (C,D). In contrast, expression of the M2-related CD204 was significantly lower in IDH-mutant tumors at both the mRNA and the protein levels. (E-G) mRNA levels of the M2-related markers *IL6* (E), *TLR1* (F), and *TLR8* (G) were decreased in IDH-mutant tumors compared to IDH-wildtype tumors. (H-K) mRNA expression of the M1-related markers *IL1B* (H), *IL18* (I), *TLR2* (J), and *CCL2* (K) was diminished in IDH-mutant tumors compared to IDH-wildtype tumors. (L) *SPPI* mRNA levels were significantly lower in IDH-mutant tumors. *Horizontal lines* indicate the mean (A,C,F,G,I-L) or the median (B,D,E,H). *Vertical lines* indicate \pm standard error of the mean (SEM). AA, anaplastic astrocytoma; AOD, anaplastic oligodendrogloma; DA, diffuse astrocytoma; GBM, glioblastoma; IDH, isocitrate dehydrogenase; mIDH, IDH-mutant; OD, oligodendrogloma; wtIDH, IDH-wildtype

TABLE S1 Antibodies and detection systems used for double immunofluorescence

TABLE S2 Differentially upregulated genes in TIM-3 enriched glioblastomas in the TCGA dataset

TABLE S3 KEGG enrichment analysis

TABLE S4 Gene Ontology enrichment analysis (biological processes)

How to cite this article: D. Sørensen M, Nielsen O, Reifenberger G, W. Kristensen B. The presence of TIM-3 positive cells in WHO grade III and IV astrocytic gliomas correlates with isocitrate dehydrogenase mutation status. *Brain Pathology*. 2021;31:e12921. <https://doi.org/10.1111/bpa.12921>

BRAIN PATHOLOGY

THE PRESENCE OF TIM-3 POSITIVE CELLS IN WHO GRADE III AND IV ASTROCYTIC GLIOMAS CORRELATES WITH ISOCITRATE DEHYDROGENASE MUTATION STATUS

Mia D. Sørensen^{1,2}, Ole Nielsen¹, Guido Reifenberger^{2,5}, Bjarne W. Kristensen^{1,2,3,4}

Affiliations:

¹ Department of Pathology, Odense University Hospital, Odense, Denmark

² Department of Clinical Research, University of Southern Denmark, Odense, Denmark

³ Department of Pathology, Rigshospitalet, Copenhagen University Hospital, Copenhagen, Denmark

⁴ Department of Clinical Medicine and Biotech Research and Innovation Center (BRIC), University of Copenhagen, Copenhagen, Denmark.

⁵ Institute of Neuropathology, Heinrich Heine University, Düsseldorf, and German Cancer Consortium (DKT), partner site Essen/Düsseldorf, Germany

Corresponding author: mia.soerensen@rsyd.dk

Supplemental figures 1-5

+

Supplemental tables 1-4

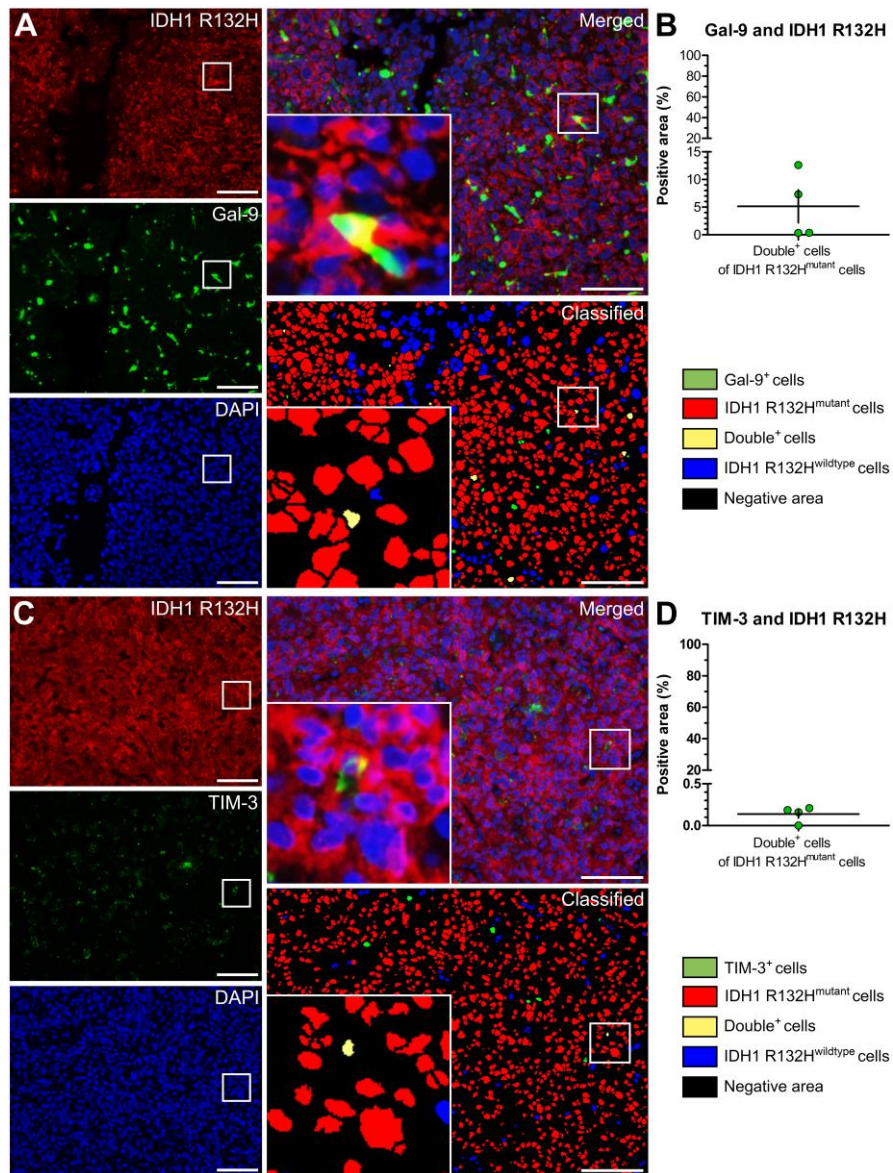


Figure S1. Co-expression patterns of Gal-9 and TIM-3 in IDH1 R132H-mutant WHO III-IV astrocytic gliomas. IDH1 R132-mutant glial tumor cells rarely expressed Gal-9 (A-B) and TIM-3 (C-D). Scale bar 100 μ M.

A

	Gal-9	TIM-3	CD4	CD8	FOXP3	OLIG2
Gal-9		0.73***	0.51***	0.58***	0.42***	-0.54***
TIM-3	0.73***		0.53***	0.52***	0.49***	-0.45***
CD4	0.51***	0.53***		0.59***	0.63***	-0.34**
CD8	0.58***	0.52***	0.59***		0.65***	-0.24*
FOXP3	0.42***	0.49***	0.63***	0.65***		-0.16
OLIG2	-0.54**	-0.45*	-0.34**	-0.24*	-0.16	

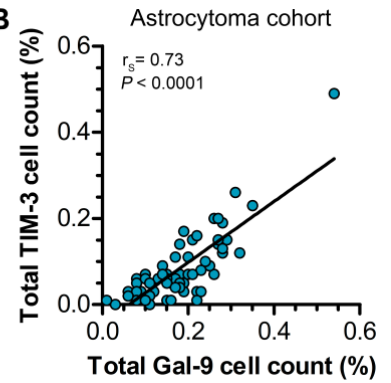
Spearman's ρ 1 0 -1 *** P -value < 0.001 ** P -value < 0.01 * P -value < 0.05

C

	Gal-9	TIM-3	CD4	CD8A	CD8B	FOXP3	OLIG2
Gal-9		0.88***	0.85***	0.36***	0.43***	0.32***	-0.27***
TIM-3	0.88***		0.87***	0.40***	0.44***	0.23***	-0.38***
CD4	0.85***	0.87***		0.37***	0.42***	0.31***	-0.34***
CD8A	0.36***	0.40***	0.37***		0.67***	0.26***	-0.47***
CD8B	0.43***	0.44***	0.42***	0.67***		0.28***	-0.32***
FOXP3	0.32***	0.23***	0.31***	0.26***	0.28***		-0.38***
OLIG2	-0.27***	-0.38***	-0.34***	-0.47***	-0.32***	-0.38***	

Spearman's ρ 1 0 -1 *** P -value < 0.001 ** P -value < 0.01 * P -value < 0.05

B



D

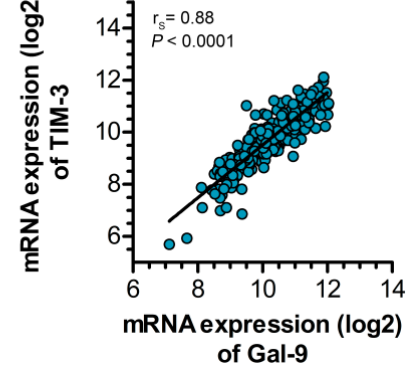


Figure S2. Correlation analyses in WHO grade III and IV astrocytic gliomas. **(A, B)** A positive correlation was found between total Gal-9 cell count (in %) and total TIM-3 cell count (in %) in the astrocytoma cohort used for the multiplex chromogenic immunohistochemistry study. Additionally, positive correlations were found among Gal-9, TIM-3 and T cell markers CD4, CD8, and FOXP3, while OLIG2 was negatively correlated with Gal-9, TIM-3 as well as CD4 and CD8. **(C, D)** *Gal-9* mRNA expression was positively correlated with *TIM-3* mRNA levels in the TCGA dataset. Both *TIM-3* and *Gal-9* showed a moderate-strong correlation with mRNA levels of the T cell markers *CD4*, *CD8A/B* and *FOXP3*, while *OLIG2* mRNA levels were negatively correlated with *TIM-3*, *Gal-9* and the T cell markers to a weak-moderate degree.

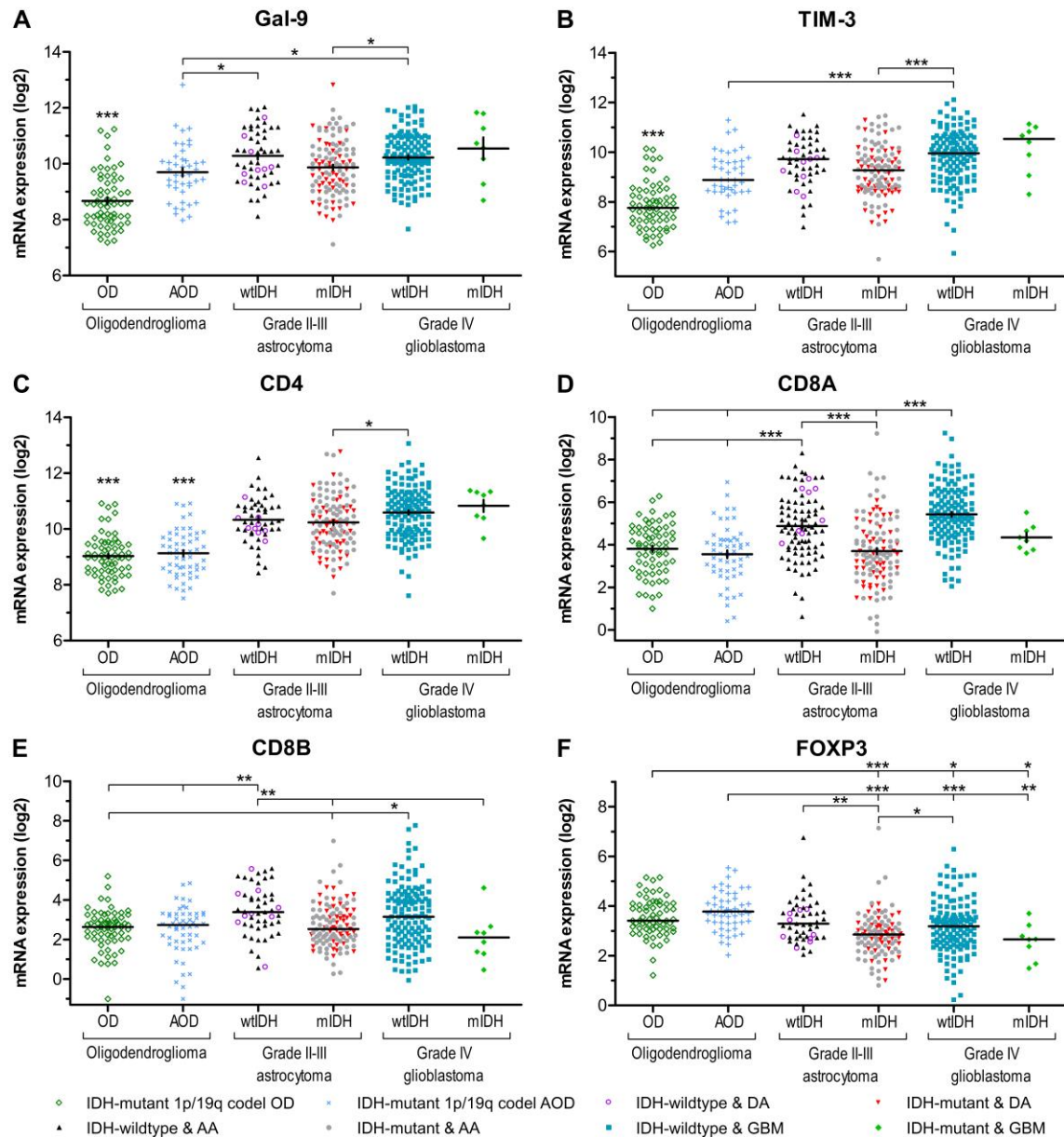


Figure S3. Association between glioma subtype and mRNA expression levels in the TCGA dataset. **(A, B)** OD had the lowest *Gal-9* **(A)** and *TIM-3* **(B)** mRNA expression level compared to other five glioma subtypes, while GBM, WHO grade IV, and IDH-wildtype diffuse and anaplastic astrocytomas, WHO grade II and III, appeared to have the highest expression levels. **(C)** OD and AOD had the lowest mRNA expression level of *CD4* compared to the four astrocytic subtypes. Further, IDH-wildtype GBM had higher *CD4* levels than IDH-mutant astrocytomas of WHO grades II and III. **(D, E)** *CD8A* and *CD8B* mRNA expression levels were lower in oligodendroglial tumors and IDH-mutant astrocytomas compared IDH-wildtype astrocytomas. **(F)** Oligodendroglial tumors and IDH-wildtype astrocytoma, WHO grade II-III and IV, had the highest mRNA expression level of *FOXP3*.

Horizontal lines indicate mean (A, C, D) or median (B, E, F). Vertical lines indicate \pm standard error of the mean (SEM) (A, C, D).

* indicates $P < 0.05$; ** $P < 0.01$; *** $P < 0.001$.

Abbreviations: AA, anaplastic astrocytoma; AOD, anaplastic oligodendroglioma; DA, diffuse astrocytoma; GBM, glioblastoma; IDH, isocitrate dehydrogenase; mIDH, IDH-mutant; OD, oligodendroglioma; wtIDH, IDH-wildtype.

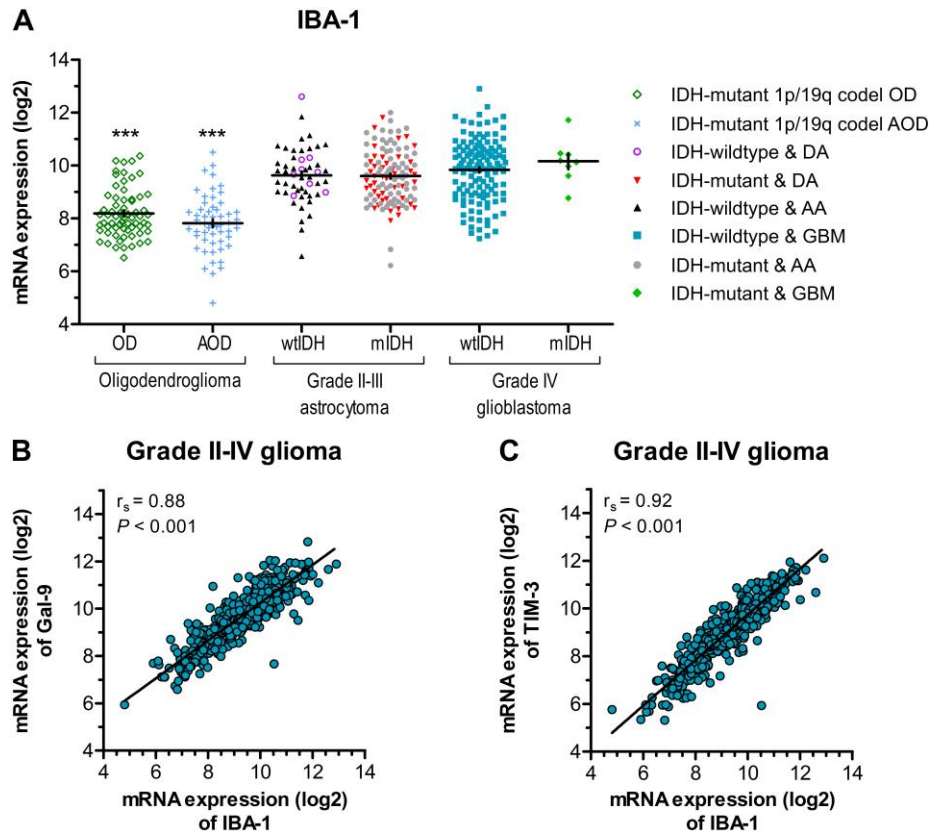


Figure S4. *IBA-1* mRNA expression in the TCGA dataset. (A) OD and AOD had lower *IBA-1* mRNA expression level compared to the four astrocytic tumor groups, while no differences in mRNA levels were observed among the astrocytic groups. (B, C) *IBA-1* mRNA expression levels were positively correlated to mRNA expression of Gal-9 (B) and TIM-3 (C).

Horizontal and vertical lines indicate mean and \pm standard error of the mean (SEM), respectively. *** indicates $P < 0.001$.

Abbreviations: AA, anaplastic astrocytoma; AOD, anaplastic oligodendroglioma; DA, diffuse astrocytoma; GBM, glioblastoma; IDH, isocitrate dehydrogenase; mIDH, IDH-mutant; OD, oligodendroglioma; wtIDH, IDH-wildtype.

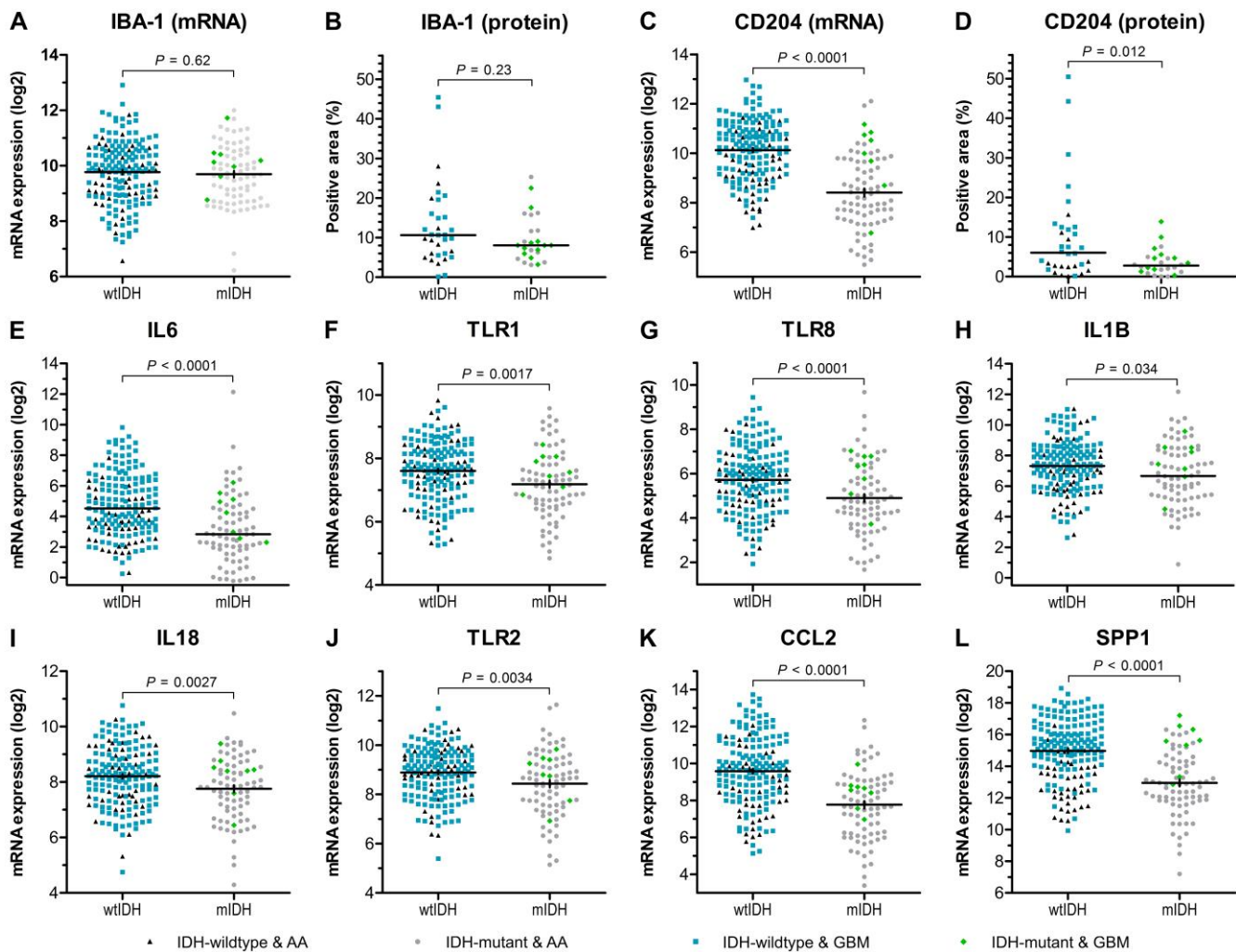


Figure S5. Expression levels of microglia/macrophage-related markers in IDH-mutant vs. IDH-wildtype astrocytic gliomas of WHO grade III and IV. (A, B) Expression of mRNA *IBA-1* and protein IBA-1 did not differ between IDH-mutant and IDH-wildtype tumors. (C, D). In contrast, expression of the M2-related CD204 was significantly lower in IDH-mutant tumors at both the mRNA and the protein levels. (E-G) mRNA levels of the M2-related markers *IL6* (E), *TLR1* (F), and *TLR8* (G) were decreased in IDH-mutant tumors compared to IDH-wildtype tumors. (H-K) mRNA expression of the M1-related markers *IL1B* (H), *IL18* (I), *TLR2* (J), and *CCL2* (K) was diminished in IDH-mutant tumors compared to IDH-wildtype tumors. (L) *SPP1* mRNA levels were significantly lower in IDH-mutant tumors. Horizontal lines indicate the mean (A, C, F, G, I-L) or the median (B, D, E, H). Vertical lines indicate ± standard error of the mean (SEM). Abbreviations: AA, anaplastic astrocytoma; AOD, anaplastic oligodendroglioma; DA, diffuse astrocytoma; GBM, glioblastoma; IDH, isocitrate dehydrogenase; mIDH, IDH-mutant; OD, oligodendroglioma; wtIDH, IDH-wildtype.

Table S1 Antibodies and detection systems used for double immunofluorescence.

Antibody	Vendor	Species / clonality	Clone / catalog no.	Dilution	Incubation (min / Tp)	Detection
CD3	Ventana Medical Systems	Rb / mono	2GV6	RTU	8 / 36 °C	OmniMap-FAM (8-8)
Gal-9	Cell signaling technology	Rb / mono	D9R4A	1:100	32 / 36 °C	OmniMap -Cy5 (20-12)
Gal-9	Cell signaling technology	Rb / mono	D9R4A	1:100	32 / 36 °C	OmniMap -FAM (12-12)
IBA-1	Wako Pure Chemical Industries, Ltd.	Rb / poly	019-19741	1:2000	16 / 36 °C	OmniMap -FAM (12-4)
IDH1 R132H	Dianova	Ms / mono	H09	1:100	32 / 36 °C	OmniMap -Cy5 (20-20)
OLIG2	Immuno-Biological Laboratories	Rb / poly	18953	1:200	32 / 36 °C	OmniMap -FAM (12-8)
TIM-3	Cell signaling technology	Rb / mono	D5D5R	1:25	60 / 36 °C	OmniMap -Cy5 (12-16)
TIM-3	Cell signaling technology	Rb / mono	D5D5R	1:25	60 / 36 °C	OmniMap -FAM (12-8)

Table S2 Differentially upregulated genes in TIM-3 enriched glioblastomas in the TCGA dataset

Gene ID	logFC	Average expression	t	P-value	adj. P-value
<i>SPP1</i>	2.90	3.64	18.10	3.09E-47	3.20E-45
<i>CNDP1</i>	2.79	3.94	10.33	4.84E-21	1.29E-19
<i>AIF1</i>	2.65	1.86	29.60	2.68E-83	2.39E-79
<i>GPR65</i>	2.62	4.33	19.66	1.76E-52	2.57E-50
<i>SAA1</i>	2.61	1.68	8.51	1.71E-15	2.91E-14
<i>SI00A8</i>	2.61	2.50	15.46	3.47E-38	2.21E-36
<i>HAMP</i>	2.60	0.55	19.98	1.45E-53	2.39E-51
<i>GPR34</i>	2.59	5.49	16.38	2.27E-41	1.68E-39
<i>SCIN</i>	2.59	4.01	22.17	9.76E-61	2.71E-58
<i>MNDA</i>	2.55	3.62	21.26	8.61E-58	1.97E-55
<i>MS4A4A</i>	2.50	0.53	19.68	1.51E-52	2.28E-50
<i>RNASE2</i>	2.46	2.18	19.60	2.85E-52	4.10E-50
<i>CSTA</i>	2.44	0.85	18.73	2.30E-49	2.76E-47
<i>ANKRD22</i>	2.43	2.78	16.82	7.09E-43	5.72E-41
<i>CD53</i>	2.43	1.06	28.70	9.64E-81	4.29E-77
<i>MMP7</i>	2.39	3.07	8.64	6.95E-16	1.22E-14
<i>TMEM125</i>	2.38	-0.28	10.09	2.89E-20	7.35E-19
<i>SAMSN1</i>	2.36	-0.91	25.86	2.50E-72	2.62E-69
<i>IL18</i>	2.35	1.05	21.17	1.77E-57	3.79E-55
<i>AQP9</i>	2.35	3.02	13.25	1.17E-30	5.17E-29
<i>SI00A9</i>	2.33	2.20	14.68	1.58E-35	8.58E-34
<i>CD69</i>	2.33	-2.31	17.36	1.06E-44	9.45E-43
<i>RGS18</i>	2.32	3.46	20.17	3.59E-54	6.14E-52
<i>F13A1</i>	2.32	3.63	12.42	7.14E-28	2.72E-26
<i>LTF</i>	2.32	2.62	8.43	2.86E-15	4.77E-14
<i>CHI3L2</i>	2.31	2.65	11.72	1.51E-25	5.15E-24
<i>EBI2</i>	2.31	3.01	17.35	1.13E-44	1.01E-42
<i>HAVCR2</i>	2.29	1.75	39.12	5.16E-108	9.19E-104
<i>GLDN</i>	2.28	3.27	14.73	1.07E-35	5.89E-34
<i>P2RY12</i>	2.28	3.40	14.53	5.27E-35	2.80E-33
<i>APOC2</i>	2.28	0.90	22.44	1.28E-61	3.99E-59
<i>BATF</i>	2.25	-1.21	22.74	1.43E-62	4.63E-60
<i>APOC1</i>	2.25	1.73	20.50	2.79E-55	5.23E-53
<i>CCL2</i>	2.24	2.68	13.06	5.27E-30	2.23E-28
<i>LAIR1</i>	2.22	1.37	28.20	2.83E-79	1.01E-75
<i>CFD</i>	2.21	-0.32	16.90	3.83E-43	3.17E-41
<i>NLRC4</i>	2.20	3.31	20.92	1.19E-56	2.40E-54
<i>BCL2A1</i>	2.18	-0.11	18.64	4.64E-49	5.43E-47
<i>PLEK</i>	2.16	2.12	27.93	1.68E-78	4.28E-75
<i>C3</i>	2.16	0.76	16.94	2.82E-43	2.35E-41

<i>CD74</i>	2.15	3.18	17.30	1.74E-44	1.54E-42
<i>ALOX5AP</i>	2.15	3.75	17.55	2.35E-45	2.19E-43
<i>EVI2A</i>	2.15	0.30	15.48	2.93E-38	1.90E-36
<i>SRGN</i>	2.15	1.87	23.55	3.64E-65	1.63E-62
<i>OLR1</i>	2.14	2.11	20.93	1.04E-56	2.12E-54
<i>TNFSF13B</i>	2.14	3.37	18.53	1.12E-48	1.27E-46
<i>FCGR2B</i>	2.14	2.91	12.83	3.01E-29	1.21E-27
<i>CD48</i>	2.13	0.62	15.47	3.05E-38	1.97E-36
<i>VNN2</i>	2.13	2.20	18.43	2.50E-48	2.75E-46
<i>MOG</i>	2.13	2.65	9.94	8.52E-20	2.09E-18
<i>CD33</i>	2.12	-0.36	28.89	2.76E-81	1.64E-77
<i>PGDS</i>	2.12	3.87	17.65	1.09E-45	1.04E-43
<i>CH25H</i>	2.11	2.13	12.73	6.97E-29	2.78E-27
<i>LAPTM5</i>	2.11	1.70	27.96	1.35E-78	4.02E-75
<i>IFI30</i>	2.11	0.82	21.18	1.58E-57	3.43E-55
<i>TLR2</i>	2.11	3.94	22.26	5.09E-61	1.49E-58
<i>PTPRC</i>	2.10	0.52	26.93	1.50E-75	2.67E-72
<i>GPNMB</i>	2.08	0.04	12.05	1.23E-26	4.33E-25
<i>MSR1</i>	2.08	3.46	17.98	7.85E-47	7.72E-45
<i>FYB</i>	2.06	0.81	24.23	2.69E-67	1.70E-64
<i>CD2</i>	2.06	1.07	16.07	2.70E-40	1.92E-38
<i>TLR8</i>	2.05	2.42	16.56	5.60E-42	4.34E-40
<i>MAP3K8</i>	2.05	0.42	17.39	8.28E-45	7.45E-43
<i>CYBB</i>	2.05	1.76	23.73	1.02E-65	4.93E-63
<i>TLR1</i>	2.05	2.31	22.76	1.24E-62	4.09E-60
<i>PKD2L1</i>	2.04	2.59	14.19	7.26E-34	3.72E-32
<i>IL1B</i>	2.04	1.30	14.69	1.52E-35	8.32E-34
<i>CD52</i>	2.03	-0.64	13.29	8.46E-31	3.76E-29
<i>SAA2</i>	2.02	1.65	9.14	2.42E-17	4.87E-16
<i>LY86</i>	2.02	2.25	24.18	3.81E-67	2.26E-64
<i>FAM26F</i>	2.02	0.09	15.74	3.82E-39	2.59E-37
<i>MS4A6A</i>	2.02	2.98	21.08	3.51E-57	7.36E-55
<i>IL6</i>	2.01	-0.18	10.42	2.53E-21	6.86E-20
<i>LY96</i>	2.00	1.56	16.18	1.16E-40	8.36E-39
<i>APBB1IP</i>	2.00	1.60	24.11	6.21E-67	3.46E-64

Table S3 KEGG enrichment analysis

ID	Description	GeneRatio	BgRatio	P-value	adj. P-value	q-value	geneID
hsa04620	Toll-like receptor signaling pathway	8/43	104/7915	6.71E-08	6.51E-06	4.45E-06	<i>IL1B / IL6 / LY96 / MAP3K8 / SPPI / TLR1 / TLR2 / TLR8</i>
hsa05134	Legionellosis	6/43	56/7915	4.75E-07	2.30E-05	1.58E-05	<i>C3 / IL18 / IL1B / IL6 / NLRC4 / TLR2</i>
hsa05152	Tuberculosis	8/43	179/7915	4.31E-06	1.40E-04	9.54E-05	<i>C3 / CD74 / FCGR2B / IL18 / IL1B / IL6 / TLR1 / TLR2</i>
hsa05144	Malaria	5/43	49/7915	5.95E-06	1.44E-04	9.87E-05	<i>CCL2 / IL18 / IL1B / IL6 / TLR2</i>
hsa05323	Rheumatoid arthritis	6/43	93/7915	9.61E-06	1.86E-04	1.27E-04	<i>CCL2 / IL18 / IL1B / IL6 / TLR2 / TNFSF13B</i>
hsa04657	IL17 signaling pathway	5/43	93/7915	1.36E-04	2.14E-03	1.46E-03	<i>CCL2 / IL1B / IL6 / SI00A8 / SI00A9</i>
hsa04145	Phagosome	6/43	152/7915	1.54E-04	2.14E-03	1.46E-03	<i>C3 / CYBB / FCGR2B / MSRI / OLR1 / TLR2</i>
hsa05142	Chagas disease (American trypanosomiasis)	5/43	102/7915	2.10E-04	2.55E-03	1.74E-03	<i>C3 / CCL2 / IL1B / IL6 / TLR2</i>
hsa04621	NOD-like receptor signaling pathway	6/43	181/7915	3.97E-04	3.90E-03	2.67E-03	<i>CCL2 / CYBB / IL18 / IL1B / IL6 / NLRC4</i>
hsa05321	Inflammatory bowel disease (IBD)	4/43	65/7915	4.02E-04	3.90E-03	2.67E-03	<i>IL18 / IL1B / IL6 / TLR2</i>
hsa05135	Yersinia infection	5/43	120/7915	4.48E-04	3.95E-03	2.70E-03	<i>CCL2 / FYB / IL18 / IL1B / IL6</i>
hsa05133	Pertussis	4/43	76/7915	7.30E-04	5.44E-03	3.72E-03	<i>C3 / IL1B / IL6 / LY96</i>
hsa05140	Leishmaniasis	4/43	76/7915	7.30E-04	5.44E-03	3.72E-03	<i>C3 / CYBB / IL1B / TLR2</i>
hsa05132	Salmonella infection	4/43	80/7915	8.85E-04	6.13E-03	4.19E-03	<i>IL18 / IL1B / IL6 / NLRC4</i>
hsa05143	African trypanosomiasis	3/43	37/7915	1.02E-03	6.60E-03	4.51E-03	<i>IL18 / IL1B / IL6</i>
hsa04640	Hematopoietic cell lineage	4/43	98/7915	1.88E-03	1.14E-02	7.81E-03	<i>CD2 / CD33 / IL1B / IL6</i>
hsa04933	AGE-RAGE signaling pathway in diabetic complications	4/43	100/7915	2.03E-03	1.16E-02	7.92E-03	<i>CCL2 / CYBB / IL1B / IL6</i>
hsa04064	NF-kappa B signaling pathway	4/43	102/7915	2.18E-03	1.18E-02	8.04E-03	<i>BCL2A1 / IL1B / LY96 / TNFSF13B</i>
hsa04668	TNF signaling pathway	4/43	112/7915	3.07E-03	1.57E-02	1.07E-02	<i>CCL2 / IL1B / IL6 / MAP3K8</i>
hsa04623	Cytosolic DNA-sensing pathway	3/43	63/7915	4.73E-03	2.29E-02	1.57E-02	<i>IL18 / IL1B / IL6</i>
hsa05162	Measles	4/43	138/7915	6.45E-03	2.98E-02	2.04E-02	<i>FCGR2B / IL1B / IL6 / TLR2</i>
hsa04610	Complement and coagulation cascades	3/43	79/7915	8.87E-03	3.91E-02	2.67E-02	<i>C3 / CFD / FI3A1</i>

Table S4 Gene Ontology enrichment analysis (biological processes)

ID	Description	GeneRatio	BgRatio	P-value	adj. P-value	q-value	geneID
GO:0050900	leukocyte migration	14 / 70	342 / 16536	1.37E-10	2.44E-07	1.60E-07	AIF1 / CCL2 / CD2 / CD48 / CD74 / IL1B / IL6 / OLRI / P2RY12 / S100A8 / S100A9 / SAA1 / SPP1 / TLR2
GO:0097529	myeloid leukocyte migration	10 / 70	146 / 16536	5.33E-10	4.76E-07	3.12E-07	AIF1 / CCL2 / CD74 / IL1B / IL6 / P2RY12 / S100A8 / S100A9 / SAA1 / SPP1
GO:0032103	positive regulation of response to external stimulus	12 / 70	261 / 16536	8.77E-10	5.23E-07	3.43E-07	AIF1 / C3 / CCL2 / CD74 / IL18 / IL1B / IL6 / LY86 / LY96 / S100A8 / S100A9 / TLR2
GO:0031663	lipopolysaccharide-mediated signaling pathway	7 / 70	49 / 16536	1.34E-09	5.97E-07	3.91E-07	CCL2 / IL18 / IL1B / LTF / LY86 / LY96 / TLR2
GO:0050867	positive regulation of cell activation	12 / 70	279 / 16536	1.87E-09	6.69E-07	4.39E-07	AIF1 / CCL2 / CD2 / CD74 / HAMP / IL18 / IL1B / IL6 / MAP3K8 / PLEK / PTPRC / TNFSF13B
GO:0050865	regulation of cell activation	14 / 70	452 / 16536	5.08E-09	1.39E-06	9.08E-07	AIF1 / CCL2 / CD2 / CD74 / HAMP / IL18 / IL1B / IL6 / MAP3K8 / MNDA / PLEK / PTPRC / SAMSNI / TNFSF13B
GO:0001819	positive regulation of cytokine production	13 / 70	381 / 16536	6.09E-09	1.39E-06	9.08E-07	C3 / CCL2 / CD2 / CD74 / HAVCR2 / IL18 / IL1B / IL6 / LY96 / SAA1 / TLR1 / TLR2 / TLR8
GO:0032680	regulation of tumor necrosis factor production	8 / 70	95 / 16536	6.20E-09	1.39E-06	9.08E-07	CCL2 / CD2 / GPNMB / HAVCR2 / LTF / LY96 / TLR1 / TLR2
GO:0032640	tumor necrosis factor production	8 / 70	97 / 16536	7.32E-09	1.42E-06	9.31E-07	CCL2 / CD2 / GPNMB / HAVCR2 / LTF / LY96 / TLR1 / TLR2
GO:1903555	regulation of tumor necrosis factor superfamily cytokine production	8 / 70	98 / 16536	7.95E-09	1.42E-06	9.31E-07	CCL2 / CD2 / GPNMB / HAVCR2 / LTF / LY96 / TLR1 / TLR2
GO:0071706	tumor necrosis factor superfamily cytokine production	8 / 70	102 / 16536	1.09E-08	1.66E-06	1.09E-06	CCL2 / CD2 / GPNMB / HAVCR2 / LTF / LY96 / TLR1 / TLR2
GO:0071219	cellular response to molecule of bacterial origin	9 / 70	147 / 16536	1.11E-08	1.66E-06	1.09E-06	CCL2 / IL18 / IL1B / IL6 / LTF / LY86 / LY96 / TLR1 / TLR2
GO:0032602	chemokine production	7 / 70	68 / 16536	1.42E-08	1.94E-06	1.27E-06	CD74 / IL18 / IL1B / IL6 / S100A8 / S100A9 / TLR2
GO:0002696	positive regulation of leukocyte activation	11 / 70	270 / 16536	1.66E-08	1.94E-06	1.27E-06	AIF1 / CCL2 / CD2 / CD74 / HAMP / IL18 / IL1B / IL6 / MAP3K8 / PTPRC / TNFSF13B
GO:0009617	response to bacterium	14 / 70	497 / 16536	1.69E-08	1.94E-06	1.27E-06	CCL2 / HAMP / IL18 / IL1B / IL6 / LTF / LY86 / LY96 / MMP7 / NLR4 / S100A8 / S100A9 / TLR1 / TLR2
GO:0031349	positive regulation of defense response	13 / 70	416 / 16536	1.73E-08	1.94E-06	1.27E-06	C3 / IL18 / IL1B / IL6 / LTF / LY96 / MAP3K8 / NLR4 / S100A8 / S100A9 / TLR1 / TLR2 / TLR8
GO:0002694	regulation of leukocyte activation	13 / 70	421 / 16536	2.00E-08	2.10E-06	1.38E-06	AIF1 / CCL2 / CD2 / CD74 / HAMP / IL18 / IL1B / IL6 / MAP3K8 / MNDA / PTPRC / SAMSNI / TNFSF13B
GO:0071216	cellular response to biotic stimulus	9 / 70	164 / 16536	2.89E-08	2.87E-06	1.88E-06	CCL2 / IL18 / IL1B / IL6 / LTF / LY86 / LY96 / TLR1 / TLR2
GO:0070486	leukocyte aggregation	13 / 70	441 / 16536	3.45E-08	3.23E-06	2.12E-06	AIF1 / BATF / CCL2 / CD2 / CD74 / IL18 / IL1B / IL6 / MAP3K8 / PTPRC / S100A8 / S100A9 / TNFSF13B
GO:0060326	cell chemotaxis	10 / 70	226 / 16536	3.61E-08	3.23E-06	2.12E-06	AIF1 / CCL2 / CD74 / IL1B / IL6 / S100A8 / S100A9 / SAA1 / SAA2 / SPP1
GO:0051249	regulation of lymphocyte activation	12 / 70	367 / 16536	3.99E-08	3.40E-06	2.23E-06	AIF1 / CCL2 / CD2 / CD74 / IL18 / IL1B / IL6 / MAP3K8 / MNDA / PTPRC / SAMSNI / TNFSF13B

GO:0002237	response to molecule of bacterial origin	11 / 70	297 / 16536	4.40E-08	3.58E-06	2.35E-06	CCL2 / IL18 / IL1B / IL6 / LTF / LY86 / LY96 / S100A8 / S100A9 / TLR1 / TLR2
GO:0030595	leukocyte chemotaxis	9 / 70	175 / 16536	5.06E-08	3.93E-06	2.58E-06	AIF1 / CCL2 / CD74 / IL1B / IL6 / S100A8 / S100A9 / SAA1 / SPP1
GO:0030593	neutrophil chemotaxis	7 / 70	83 / 16536	5.76E-08	4.29E-06	2.81E-06	CCL2 / CD74 / IL1B / S100A8 / S100A9 / SAA1 / SPP1
GO:0009620	response to fungus	6 / 70	50 / 16536	6.35E-08	4.54E-06	2.97E-06	HAMP / IL6 / LTF / S100A8 / S100A9 / TLR2